

# $\Omega^-$ and $\bar{\Omega}^+$ Analysis Note

Feng Zhao

## 1 Data in the Run10 and Run11 RHIC Beam Energy Scan Program

In Run10 and Run11, STAR took Au+Au collision data at 7.7, 11.5, 19.6, 27 and 39 GeV in the RHIC beam energy scan program. In this analysis, we use data of all the five energies to study the Omega production. The Table 1 lists the events selection for the analysis. The Figure 1 shows the multiplicity distribution in the five energies. The centrality is defined with the "StRefMultCorr" class.

Table 1: Event Selection

Energy	Year	Trigger ID	Vertex Z Cut	Vertex Radius Cut	Number of Events
7.7 GeV	2010	290001 290004	$\leq \pm 70$ cm	$\leq 2$ cm	3.1 M (0-60%)
11.5 GeV	2010	310014	$\leq \pm 50$ cm	$\leq 2$ cm	8.4 M (0-60%)
19.6 GeV	2011	340001 340011 340021	$\leq \pm 50$ cm	$\leq 2$ cm	19.5 M (0-60%)
27 GeV	2011	360001	$\leq \pm 50$ cm	$\leq 2$ cm	37.9 M (0-60%)
39 GeV	2010	280001	$\leq \pm 40$ cm	$\leq 2$ cm	126.8 M (0-80%)

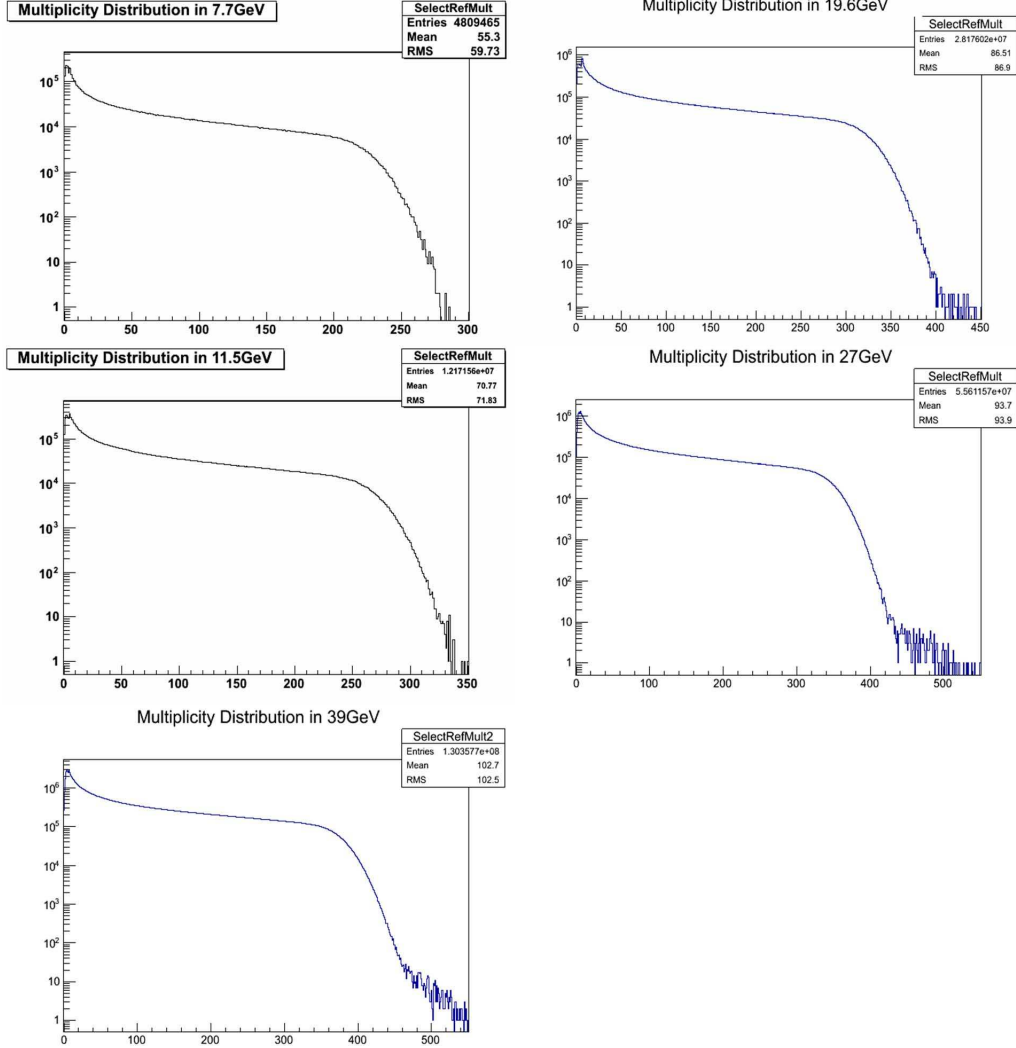


Figure 1: The multiplicity distribution for all the five energies.

## 2 $\Omega^-$ and $\bar{\Omega}^+$ Signal Reconstruction and Rotational Background

The  $\Omega^-$  and  $\bar{\Omega}^+$  signals are reconstructed through their weak decay channels, which are listed in Table 2.

Table 2: Weak Decay Channels of Strange  $\Omega^-$  and  $\bar{\Omega}^+$ 

$\Omega^- \rightarrow \Lambda K^-$	67.8%,	$\Lambda \rightarrow p\pi^-$	63.9%
$\bar{\Omega}^+ \rightarrow \bar{\Lambda} K^+$	67.8%,	$\bar{\Lambda} \rightarrow \bar{p}\pi^+$	63.9%

The decay daughters proton, pion and kaons are identified with the TPC, with the cuts in the Table 3.

Table 3: Decay Daughter Identification

p and $\bar{p}$	$n\sigma_p \leq 3.0$	Nhits>15	$p_T \geq 0.15 \text{ GeV}/c$
$\pi^-$ and $\pi^+$	$n\sigma_\pi \leq 4.0$	Nhits>15	$p_T \geq 0.15 \text{ GeV}/c$
$K^-$ and $K^+$	$n\sigma_K \leq 4.0$	Nhits>15	$p_T \geq 0.15 \text{ GeV}/c$

As there is an issue in the Run11 27 GeV data calibration, the  $n\sigma$  is twice of the real value. So for 27 GeV analysis, the cuts are the half of other energies', that is  $n\sigma_p \leq 1.5$  for proton and anti-proton identification,  $n\sigma_\pi \leq 2.0$  for pion identification, and  $n\sigma_K \leq 2.0$  for kaon identification.

We firstly reconstruct  $\Lambda$  and  $\bar{\Lambda}$  with proton and pion, and then select pure  $\Lambda$  and  $\bar{\Lambda}$  with a mass window cut ( $|M_\Lambda - M_{PDG}| < 6 \text{ MeV}$ ) to reconstruct  $\Omega^-$  and  $\bar{\Omega}^+$ . The  $\Omega$  decay topology is shown in Figure 2. The topological cuts we use in the signal reconstruction are also shown in the figure. The  $\Xi$  has a similar decay topology with  $\Omega$ , and in the  $p_T > 0.6 \text{ GeV}/c$  range, kaon  $dE/dx$  band merges with pion band. In this case, the  $\Xi$  contributes a lot to the background in the reconstructed  $\Omega$  signal. So we change the mass of the bachelor particle (kaon in the  $\Omega$  decay, and pion in the  $\Xi$  decay) to be the mass of pion instead of kaon, and calculated the invariant mass of parent. If the mass falls in the mass window around the  $\Xi$  mass ( $|M_\Xi - M_{PDG}| < 10 \text{ MeV}$ ), we exclude this  $\Omega$  candidate to reduce the background from  $\Xi$ . The overall  $\Omega^-$  and  $\bar{\Omega}^+$  signals at each beam energy are shown in Figure 3.

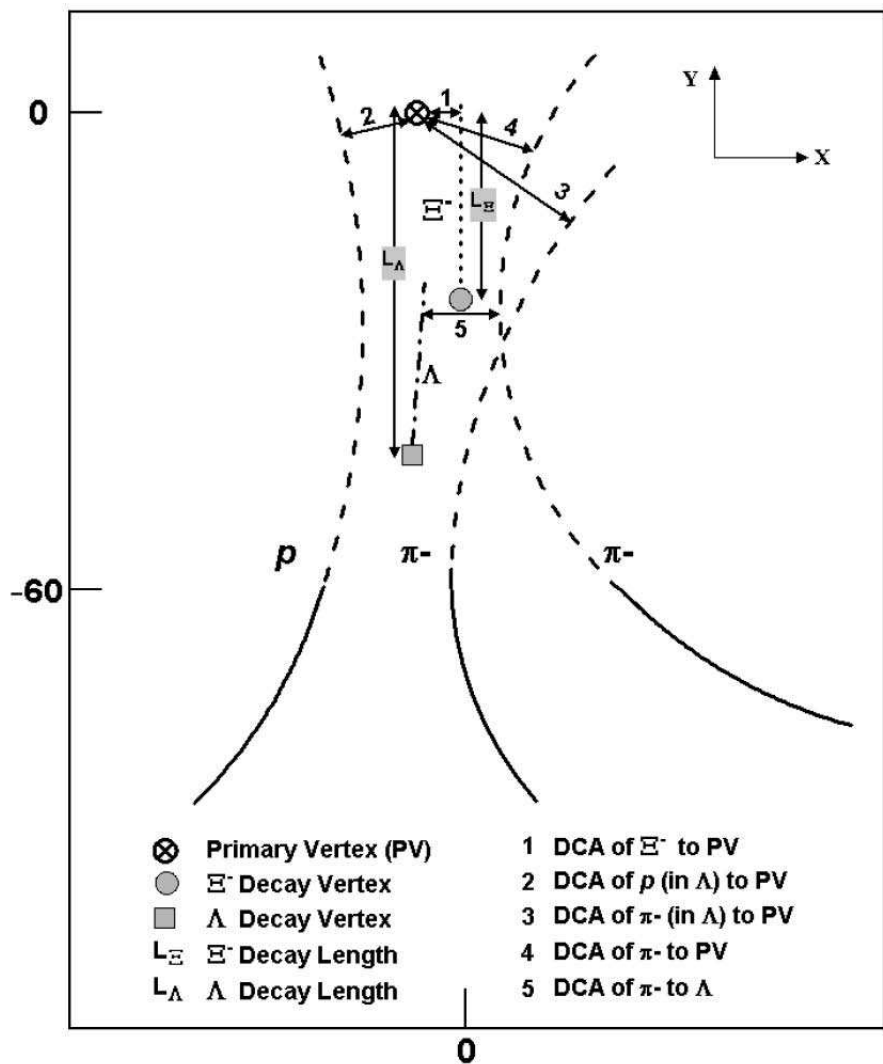


Figure 2: The  $\Xi$  decay topology. Replace the second  $\pi$  with  $K$  for  $\Omega$ . The solid line is detectable by the TPC anode sector 60 cm away from the beam line. The dash line is extrapolated from the solid line or reconstructed  $\Lambda$  and  $\Omega$ . The topological cuts are shown in the plot. The plot is from Hai Jiang's thesis.

Table 4:  $\Omega^-$  and  $\bar{\Omega}^+$  Topological Cuts

Energy (GeV)	7.7	11.5	19.6	27	39
Particle	$\Omega^-$	$\Omega^-$	$\Omega^-$	$\Omega^-$	$\Omega^-$
$ y $ of $\Omega^-$	<0.5	<0.5	<0.5	<0.5	<0.5
DCA p to PV	>0.6 cm				
DCA $\pi$ to PV	>2.0 cm				
DCA K to PV	>1.0 cm				
DCA $\pi$ to p	<0.7 cm				
DCA k to $\Lambda$	<0.7 cm				
DCA $\Lambda$ to PV	>0.3 cm	>0.4 cm	>0.4 cm	>0.4 cm	>0.4 cm
DCA $\Omega$ to PV	<0.4 cm	<0.4 cm	<0.5 cm	<0.4 cm	<0.4 cm
$\Lambda$ Decay Length ( $L_\Lambda$ )	>4.0 cm	>5.0 cm	>5.0 cm	>5.0 cm	>5.0 cm
$\Omega$ Decay Length ( $L_\Omega$ )	>2.0 cm	>3.0 cm	>3.0 cm	>3.0 cm	>3.0 cm
$L_\Lambda > L_\Omega$	yes	yes	yes	yes	yes
$(\vec{r}_\Lambda - \vec{r}_\Omega) \cdot \vec{p}_\Lambda$	>0	>0	>0	>0	>0
$(\vec{r}_\Omega - \vec{r}_{PV}) \cdot \vec{p}_\Omega$	>0	>0	>0	>0	>0
$ (\vec{r}_\Omega - \vec{r}_{PV}) \times \vec{p}_\Omega  /  (\vec{r}_\Omega - \vec{r}_{PV})  /  \vec{p}_\Omega $	>0.15	>0.15	>0.12	>0.12	>0.12
Particle	$\bar{\Omega}^+$	$\bar{\Omega}^+$	$\bar{\Omega}^+$	$\bar{\Omega}^+$	$\bar{\Omega}^+$
$ y $ of $\bar{\Omega}^+$	<0.5	<0.5	<0.5	<0.5	<0.5
DCA p to PV	>0.6 cm				
DCA $\pi$ to PV	>2.0 cm				
DCA K to PV	>1.0 cm				
DCA $\pi$ to p	<1.0 cm	<0.7 cm	<0.7 cm	<0.7 cm	<0.7 cm
DCA k to $\Lambda$	<1.0 cm	<0.7 cm	<0.7 cm	<0.7 cm	<0.7 cm
DCA $\Lambda$ to PV	>0.3 cm	>0.4 cm	>0.4 cm	>0.4 cm	>0.4 cm
DCA $\Omega$ to PV	<0.6 cm	<0.4 cm	<0.5 cm	<0.5 cm	<0.4 cm
$\Lambda$ Decay Length ( $L_\Lambda$ )	>4.0 cm	>4.0 cm	>5.0 cm	>5.0 cm	>5.0 cm
$\Omega$ Decay Length ( $L_\Omega$ )	>2.0 cm	>2.0 cm	>3.0 cm	>3.0 cm	>3.0 cm
$L_\Lambda > L_\Omega$	yes	yes	yes	yes	yes
$(\vec{r}_\Lambda - \vec{r}_\Omega) \cdot \vec{p}_\Lambda$	>0	>0	>0	>0	>0
$(\vec{r}_\Omega - \vec{r}_{PV}) \cdot \vec{p}_\Omega$	>0	>0	>0	>0	>0
$ (\vec{r}_\Omega - \vec{r}_{PV}) \times \vec{p}_\Omega  /  (\vec{r}_\Omega - \vec{r}_{PV})  /  \vec{p}_\Omega $	>0.15	>0.15	>0.12	>0.12	>0.12

The background in the invariant mass distribution is studied with the rotational background. With  $\Lambda$  unchanged, we rotate kaon tracks in the x-y plane with an angle. Theoretically, with rotated tracks, the signal is destroyed, while

the combinatorial background is simulated. The rotational background have good match with the real background not only the shape, but also the amplitude. We rotate five angles to increase statistics, which are  $\pi/3$ ,  $2\pi/3$ ,  $\pi$ ,  $4\pi/3$  and  $5\pi/3$ . The overall rotational backgrounds for each energy are shown in Figure 3, which have good match with the real background.

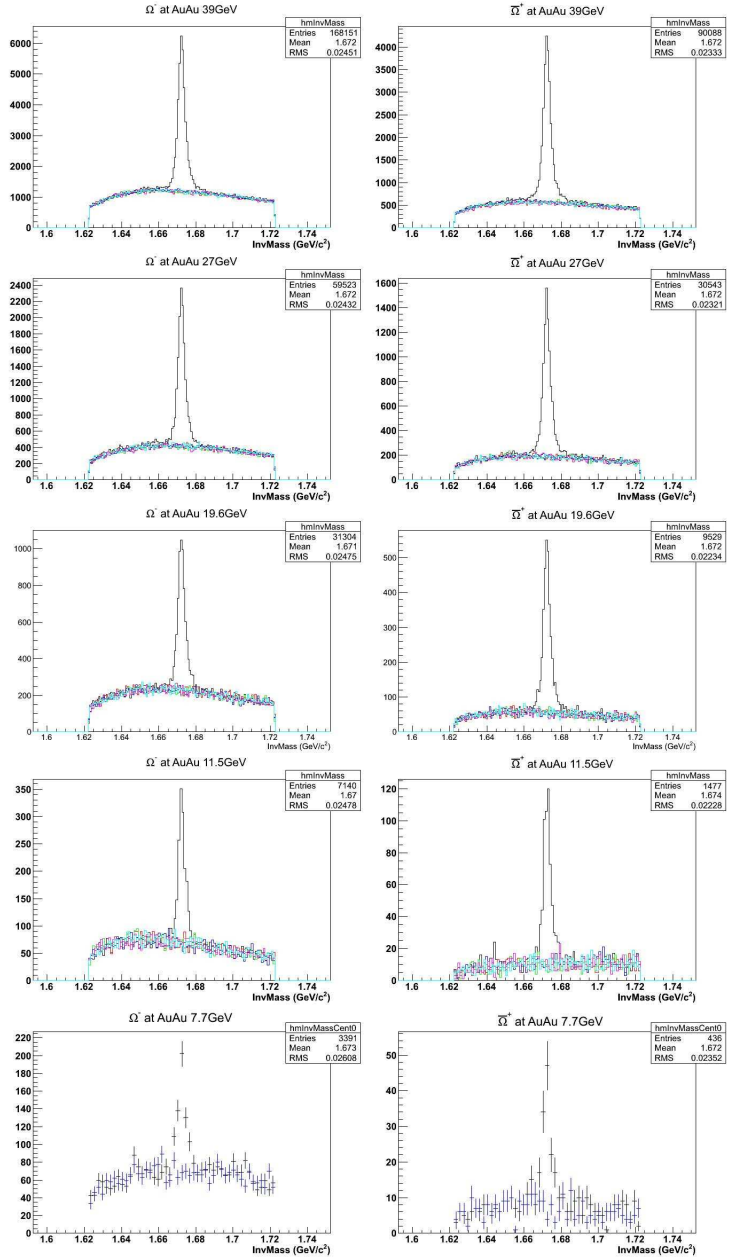


Figure 3: The black curves or points are the real signal. The rotational background method is used in AuAu collisions from 11.5 to 39 GeV. The red, green, blue, magenta and cyan curves are the rotational backgrounds with rotation angles  $\pi/3$ ,  $2\pi/3$ ,  $\pi$ ,  $4\pi/3$  and  $5\pi/3$  separately. We only rotate  $\pi$  angle for 7.7 GeV.

The raw yield of  $\Omega$  is extracted from the invariant mass distribution and rotational background of each  $p_T$  and centrality bin at different energies. The rotational backgrounds of all five rotation angles are added together, and then scaled by 1/5. The combined rotational background at higher energies, such as 19.6 GeV, 27 GeV and 39 GeV, is a little lower than the real background especially at higher  $p_T$  range. That could be due to the stronger particle correlations at higher energies. So we need to normalize the combined rotational background. The normalization mass window is  $(1.625 \text{ GeV}/c^2, 1.655 \text{ GeV}/c^2)$  and  $(1.69 \text{ GeV}/c^2, 1.72 \text{ GeV}/c^2)$ . While for lower energies, such as 7.7 and 11.5 GeV, the combined rotational background matches the real background well, and the normalization factor is around 1. So we make the rotational background without normalization. We subtract the normalized rotational background from the signal, and set a counting mass window of  $(1.66 \text{ GeV}/c^2, 1.685 \text{ GeV}/c^2)$ , and use bin counting method to count the raw yield of the signal. The signals of all the  $p_T$  and centrality bins at all the energies are in the appendix of this file. The mass window efficiency is studied by comparison of the real signal and embedding signal. Figure 4 show an example. We calculate the mass window efficiency with the embedding signal. The width of signal at a fixed  $p_T$  has little dependence of the centrality, so we combined signal at each  $p_T$  bin of all the centrality bins to increase the statistics. The efficiency is the percentage of embedding signals fall in our mass window to the total number of embedding signals. The raw yields of signal is then corrected by the mass window efficiency. For 7.7 GeV data, we only use the rotational background with a rotation angle equals to  $\pi$ , and use the same counting mass window as other energies.

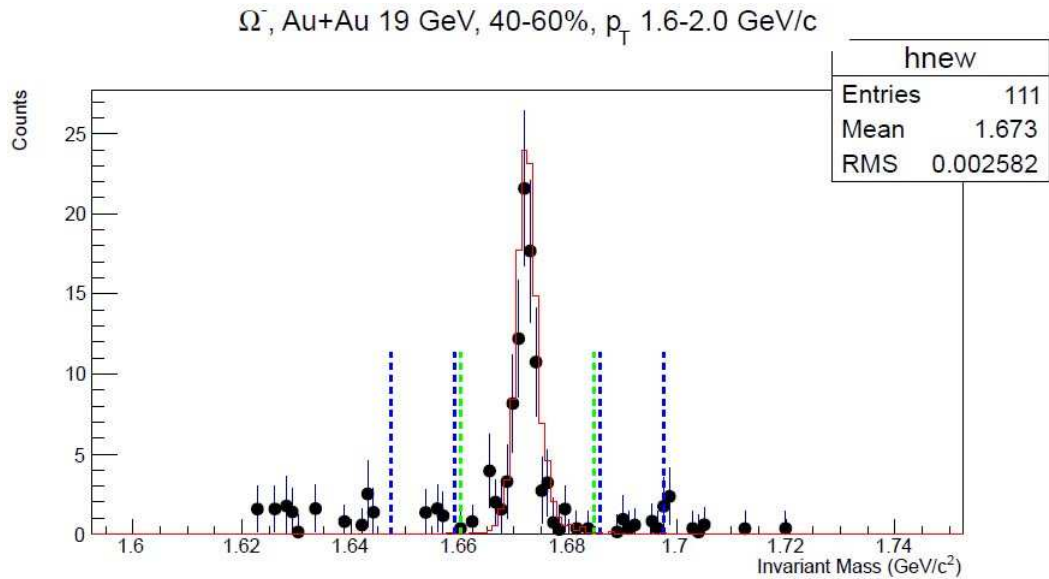


Figure 4: The black points are the real signal after rotational background subtraction. The red curve is the normalized embedding signal at the same  $p_T$  bin.

### 3 Raw Spectra

After getting the raw yields of  $\Omega^-$  and  $\bar{\Omega}^+$  at all the five energies, we are able to calculate the raw spectra of them. The figures from 5 to 9 show the  $\Omega^-$  and  $\bar{\Omega}^+$  at the five energies.

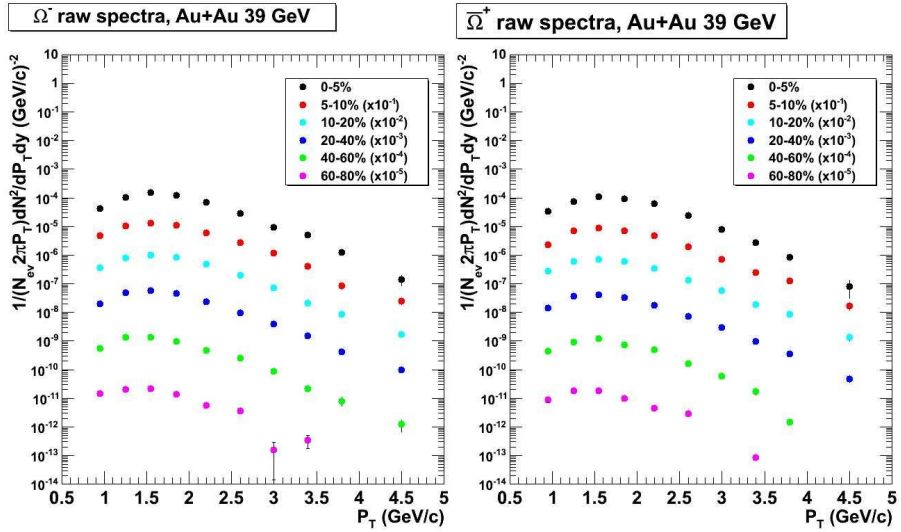


Figure 5: The raw spectra of  $\Omega^-$  and  $\bar{\Omega}^+$  at 39 GeV.

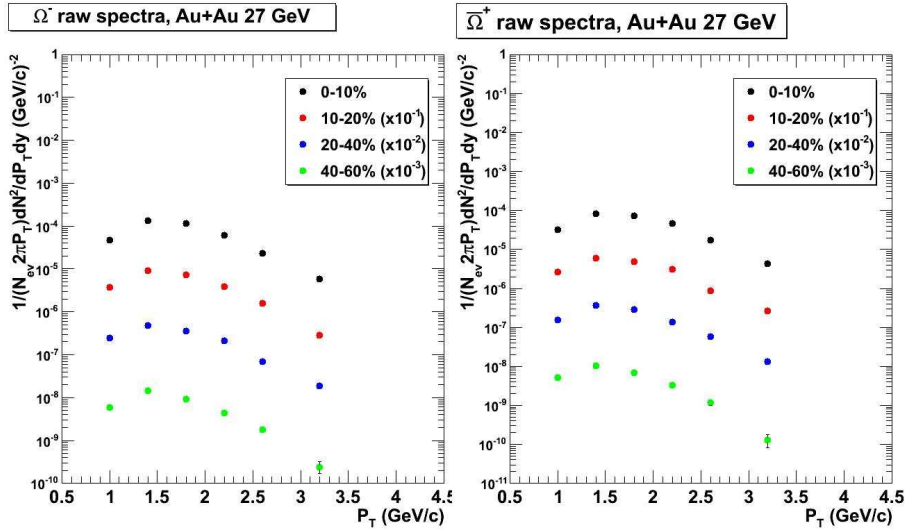


Figure 6: The raw spectra of  $\Omega^-$  and  $\bar{\Omega}^+$  at 27 GeV.

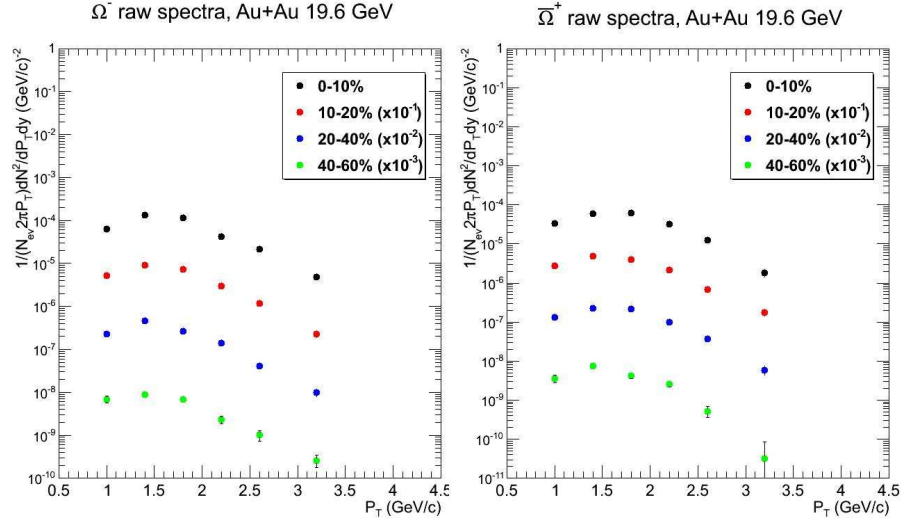


Figure 7: The raw spectra of  $\Omega^-$  and  $\bar{\Omega}^+$  at 19.6 GeV.

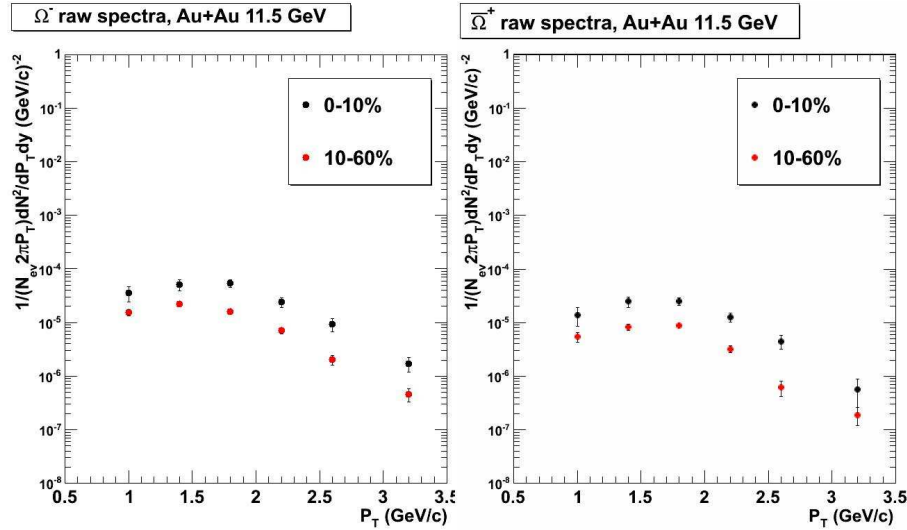


Figure 8: The raw spectra of  $\Omega^-$  and  $\bar{\Omega}^+$  at 11.5 GeV.

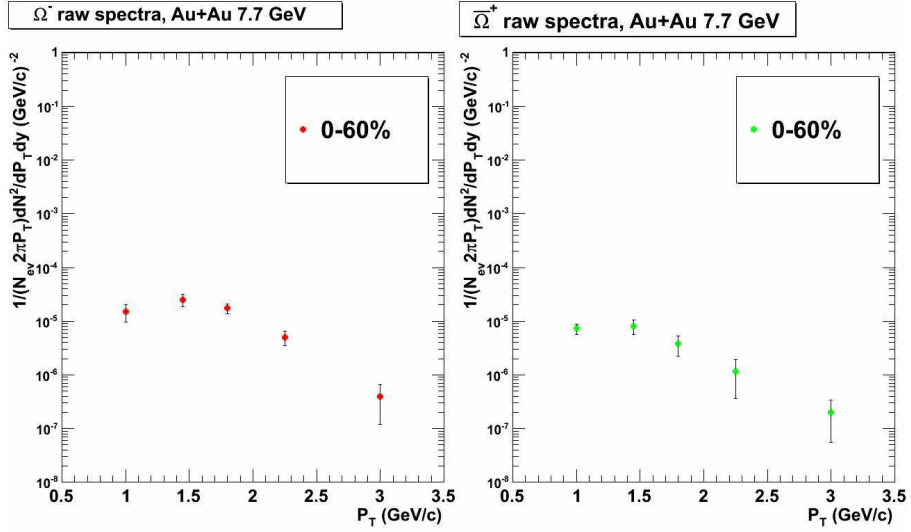


Figure 9: The raw spectra of  $\Omega^-$  and  $\bar{\Omega}^+$  at 7.7 GeV.

## 4 Efficiency

The signal reconstruction efficiency is studied with the embedding data by applying the same topological cuts as the real signal reconstruction. The plots of efficiency as a function of  $p_T$  are shown in Figure 10 to Figure 14.

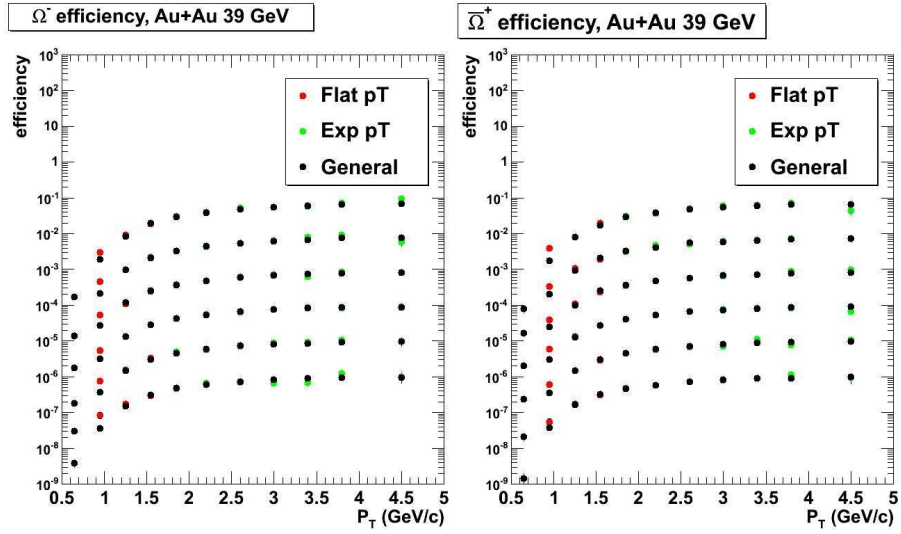


Figure 10: The reconstruction efficiency of  $\Omega^-$  and  $\bar{\Omega}^+$  at 39 GeV. The efficiency trends are from different centralities, from up to down they are  $0 - 5\%$ ,  $5 - 10\% \times 10^{-1}$ ,  $10 - 20\% \times 10^{-2}$ ,  $20 - 40\% \times 10^{-3}$ ,  $40 - 60\% \times 10^{-4}$  and  $60 - 80\% \times 10^{-5}$  separately.

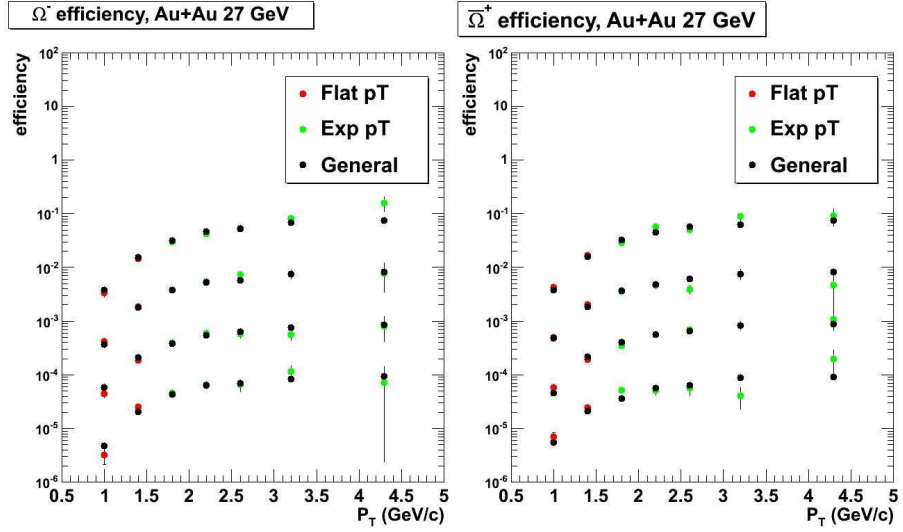


Figure 11: The reconstruction efficiency of  $\Omega^-$  and  $\bar{\Omega}^+$  at 27 GeV. The efficiency trends are from different centralities, from up to down they are  $0 - 10\%$ ,  $10 - 20\% \times 10^{-1}$ ,  $20 - 40\% \times 10^{-2}$  and  $40 - 60\% \times 10^{-3}$  separately.

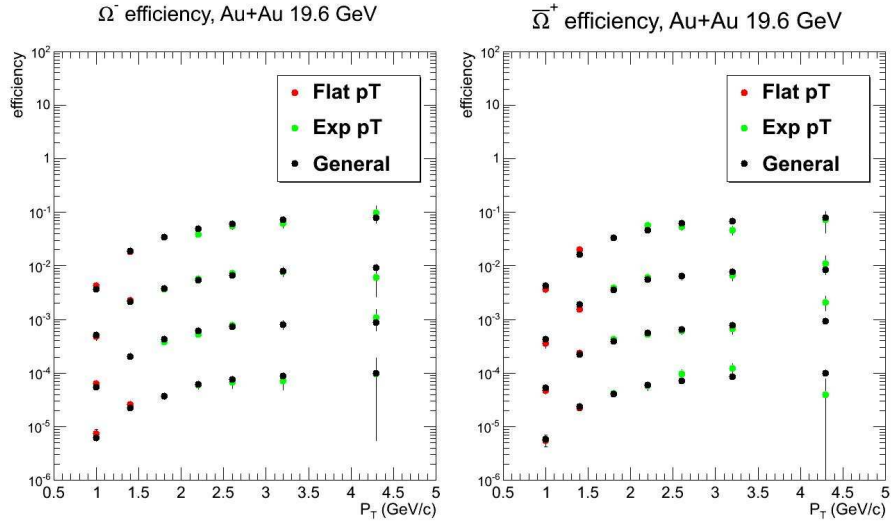


Figure 12: The reconstruction efficiency of  $\Omega^-$  and  $\bar{\Omega}^+$  at 19.6 GeV. The efficiency trends are from different centralities, from up to down they are  $0 - 10\%$ ,  $10 - 20\% \times 10^{-1}$ ,  $20 - 40\% \times 10^{-2}$  and  $40 - 60\% \times 10^{-3}$  separately.

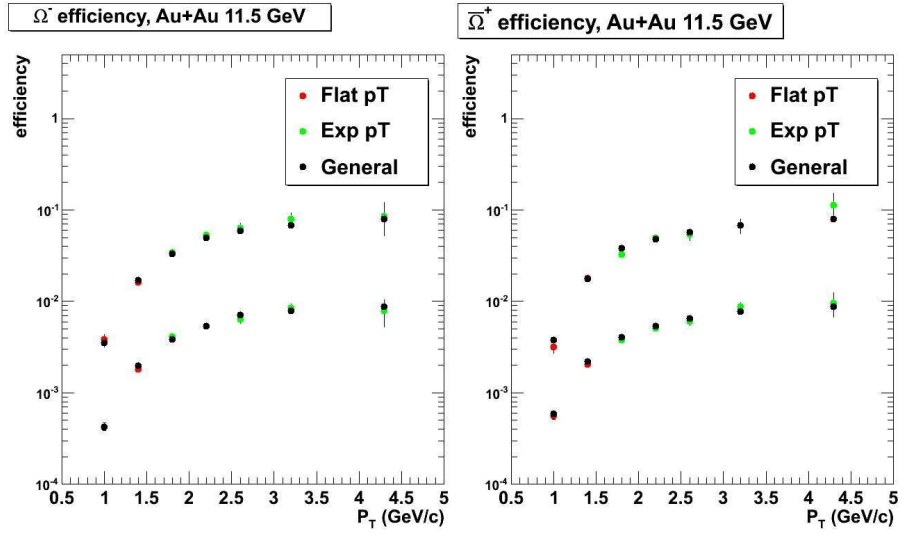


Figure 13: The reconstruction efficiency of  $\Omega^-$  and  $\bar{\Omega}^+$  at 11.5 GeV. The efficiency trends are from different centralities, from up to down they are 0 – 10% and  $10 - 60\% \times 10^{-1}$  separately.

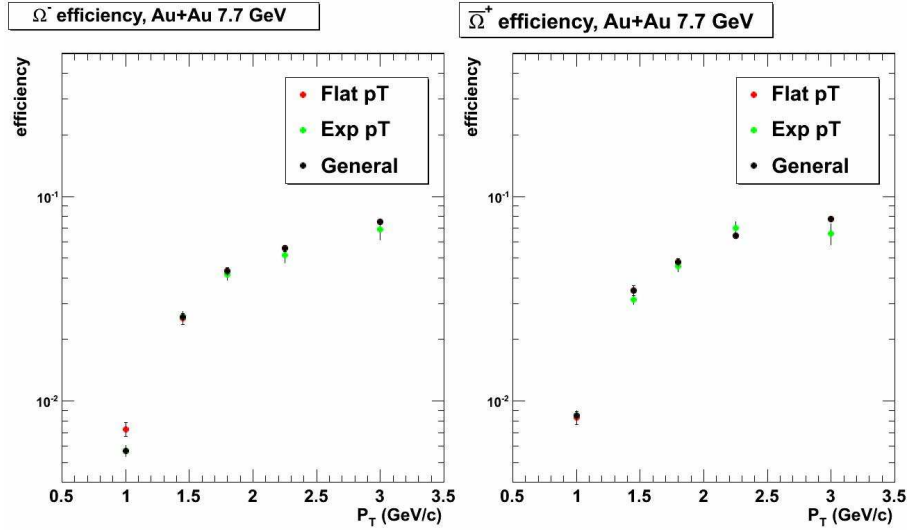


Figure 14: The reconstruction efficiency of  $\Omega^-$  and  $\bar{\Omega}^+$  at 0 – 60% centrality at 7.7 GeV.

## 5 Corrected Spectra

With the efficiency correction, we can get the  $p_T$  spectra of  $\Omega^-$  and  $\bar{\Omega}^+$ . The  $p_T$  value of each bin is not at the center of the bin, but is shifted with the method in the reference [1], with the Levy function as the default fitting function. The data points are shown in the Table 165 to 173 in the summary section. The Figure 15 to Figure 24 show the  $\Omega^-$  and  $\bar{\Omega}^+$   $p_T$  spectra of the five energies from 39 GeV to 7.7 GeV.

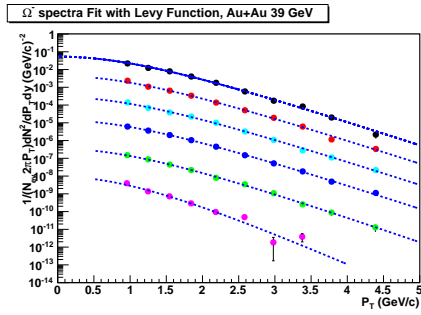


Figure 15: The corrected  $\Omega^-$   $p_T$  spectra at 39 GeV fitted with Levy function. From up to down they are 0 – 5%,  $5 - 10\% \times 10^{-1}$ ,  $10 - 20\% \times 10^{-2}$ , 5%,  $5 - 10\% \times 10^{-1}$ ,  $10 - 20\% \times 10^{-2}$ ,  $20 - 40\% \times 10^{-3}$ ,  $40 - 60\% \times 10^{-4}$  and  $60 - 80\% \times 10^{-5}$  separately.

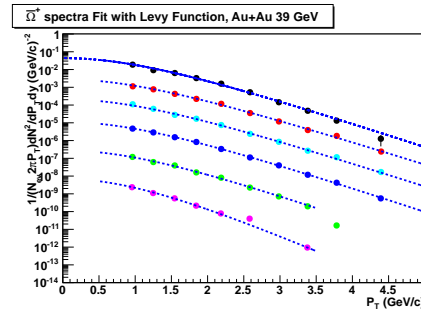


Figure 16: The corrected  $\bar{\Omega}^+$   $p_T$  spectra at 39 GeV fitted with Levy function. From up to down they are 0 – 5%,  $5 - 10\% \times 10^{-1}$ ,  $10 - 20\% \times 10^{-2}$ , 5%,  $5 - 10\% \times 10^{-1}$ ,  $10 - 20\% \times 10^{-2}$ ,  $20 - 40\% \times 10^{-3}$ ,  $40 - 60\% \times 10^{-4}$  and  $60 - 80\% \times 10^{-5}$  separately.

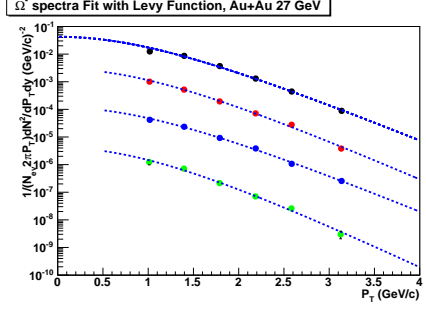


Figure 17: The corrected  $\Omega^-$   $p_T$  spectra at 27 GeV fitted with Levy function. From up to down they are 0–10%, 10–20%  $\times 10^{-1}$ , 20–40%  $\times 10^{-2}$  and 40–60%  $\times 10^{-3}$  separately.

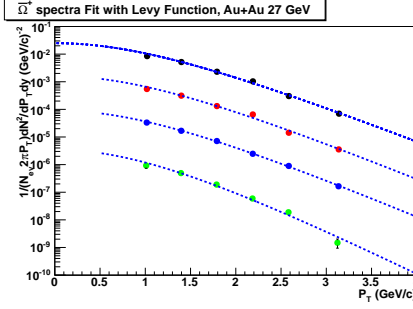


Figure 18: The corrected  $\bar{\Omega}^+$   $p_T$  spectra at 27 GeV fitted with Levy function. From up to down they are 0–10%, 10–20%  $\times 10^{-1}$ , 20–40%  $\times 10^{-2}$  and 40–60%  $\times 10^{-3}$  separately.

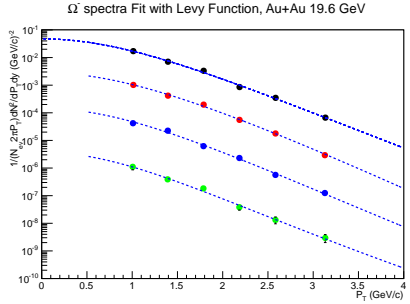


Figure 19: The corrected  $\Omega^-$   $p_T$  spectra at 19.6 GeV fitted with Levy function. From up to down they are 0–10%, 10–20%  $\times 10^{-1}$ , 20–40%  $\times 10^{-2}$  and 40–60%  $\times 10^{-3}$  separately.

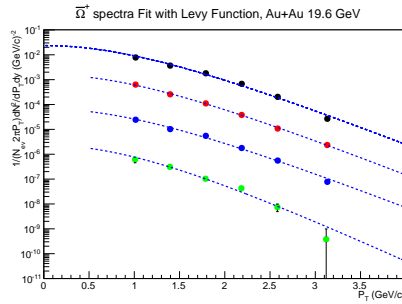


Figure 20: The corrected  $\bar{\Omega}^+$   $p_T$  spectra at 19.6 GeV fitted with Levy function. From up to down they are 0–10%, 10–20%  $\times 10^{-1}$ , 20–40%  $\times 10^{-2}$  and 40–60%  $\times 10^{-3}$  separately.

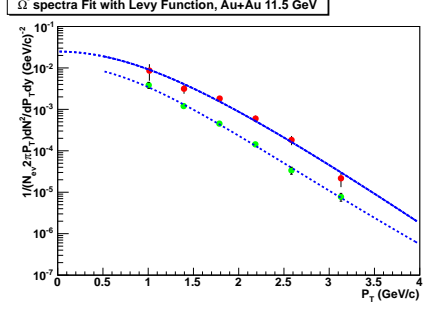


Figure 21: The corrected  $\Omega^-$   $p_T$  spectra at 11.5 GeV fitted with Levy function. From up to down they are 0 – 10% and 10 – 60% separately.

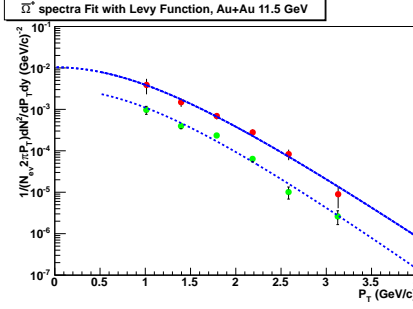


Figure 22: The corrected  $\bar{\Omega}^+$   $p_T$  spectra at 11.5 GeV fitted with Levy function. From up to down they are 0 – 10% and 10 – 60% separately.

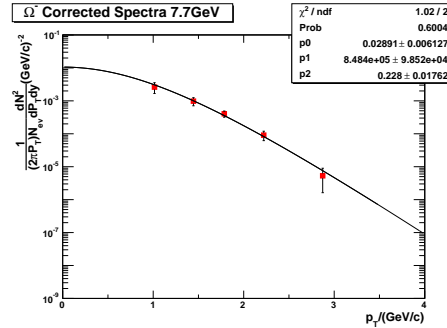


Figure 23: The corrected  $\Omega^-$   $p_T$  spectra at 7.7 GeV fitted with Levy function. The spectrum is 0 – 60% centrality.

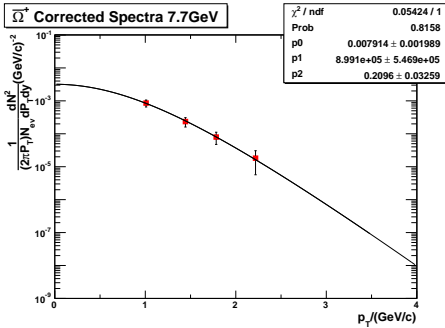


Figure 24: The corrected  $\bar{\Omega}^+$   $p_T$  spectra at 7.7 GeV fitted with Levy function. The spectrum is 0 – 60% centrality.

## 6 Systematic Error

The systematic error of the spectra and  $dN/dy$  analysis, consists of several parts. One is the systematic error of the reconstruction efficiency, which is related with the topological cuts. We change the topological cuts a little bit, and compare the difference between the corrected spectra with different cuts, to study the systematic error of this part. Another part is the systematic error of signal extraction. We set a mass window of counting raw yield, and correct the efficiency. We change the mass window a little bit, and compared the difference between

the corrected spectra with different mass windows, to study the systematic error of this part. The third part of systematic error is the uncertainty of unmeasured  $p_T$  range of the spectra for the  $dN/dy$  analysis. We use Levy function, Boltzmann function and exponential function to fit the spectra separately. We use Levy function as default function to calculate the  $dN/dy$  of unmeasured  $p_T$  range, and use the difference among the  $dN/dy$  calculated with the three functions as the systematic error for the  $dN/dy$  of unmeasured  $p_T$  range.

## 6.1 Systematic Error of Reconstruction Efficiency and Signal Extraction

The systematic error of reconstruction efficiency is related with the topological cuts. We change the topological cuts a little bit to two directions, and compare the difference between the corrected spectra with different cuts. In details, we calculate the ratio of spectra with changed cuts to the spectra with default cuts, and get the deviation of the ratio from 1. We take the larger deviation of the ratios (because we change the cuts to two directions, so we can get another two corrected spectra) as the systematic error for that  $p_T$  bin. In the end, we quadratically sum the systematic errors from different cuts for each  $p_T$  and centrality bin. As Ifspectra convenors suggested, we combine different centralities for reconstruction efficiency systematic error study. Because there is little centrality dependence of the systematic error of reconstruction efficiency, but combining all the centralities will help us reduce the statistical fluctuation. But for signal extraction systematic error, is related with signal at each  $p_T$  and centrality bin, so we leave it unmerged for each centrality.

### 6.1.1 $\Omega^-$ at 39GeV

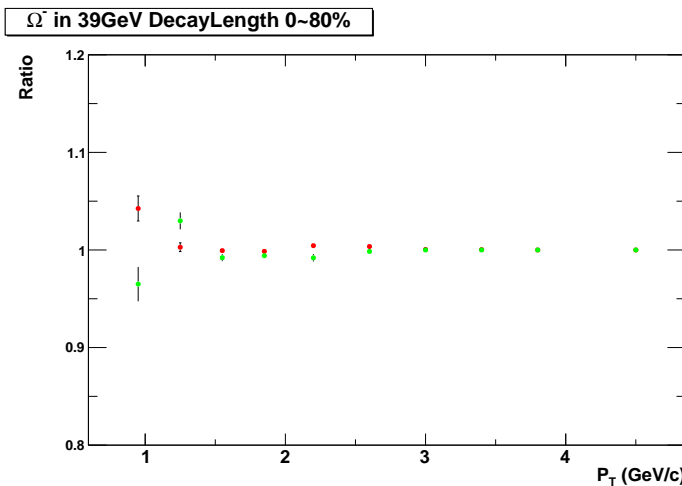
**Decay Length** The cuts are in Table 5. The systematic errors for each  $p_T$  bin are listed in Table 6. The Figure 25 shows the comparison of different cuts.

Table 5: Decay Length Cut of  $\Omega^-$  at 39GeV

Default	$L_\Lambda > 5.0 \text{ cm}$	$L_\Omega > 3.0 \text{ cm}$
Red	$L_\Lambda > 4.5 \text{ cm}$	$L_\Omega > 2.5 \text{ cm}$
Green	$L_\Lambda > 5.5 \text{ cm}$	$L_\Omega > 3.5 \text{ cm}$

Table 6: Decay Length Systematic Error of  $\Omega^-$  at 39GeV

$p_T$ bin (GeV/c)	Systematic Error
0.8-1.1	0.0425
1.1-1.4	0.02984
1.4-1.7	0.007871
1.7-2.0	0.005866
2.0-2.4	0.008059
2.4-2.8	0.00353
2.8-3.2	0.00054
3.2-3.6	0.00038
3.6-4.0	0
4.0-5.0	0


 Figure 25: The comparison of Decay Length cuts for  $\Omega^-$  at 39 GeV.

**Invariant Mass of  $\Lambda$  and  $\Xi$**  The cuts are in Table 7. The systematic errors for each  $p_T$  bin are listed in Table 8. The Figure 26 shows the comparison of different cuts.

Table 7: Invariant Mass Cut of  $\Lambda$  and  $\Xi$  for  $\Omega^-$  at 39GeV

Default	$ V0 - pdg  < 6 \text{ MeV}$	$ Xi - pdg  > 10 \text{ MeV}$
Red	$ V0 - pdg  < 5 \text{ MeV}$	$ Xi - pdg  > 12 \text{ MeV}$
Green	$ V0 - pdg  < 7 \text{ MeV}$	$ Xi - pdg  > 8 \text{ MeV}$

Table 8: Invariant Mass of  $\Lambda$  and  $\Xi$  Systematic Error of  $\Omega^-$  at 39GeV

$p_T$ bin (GeV/c)	Systematic Error
0.8-1.1	0.00976
1.1-1.4	0.015975
1.4-1.7	0.004364
1.7-2.0	0.009404
2.0-2.4	0.012889
2.4-2.8	0.00082
2.8-3.2	0.013596
3.2-3.6	0.033106
3.6-4.0	0.03035
4.0-5.0	0.05788

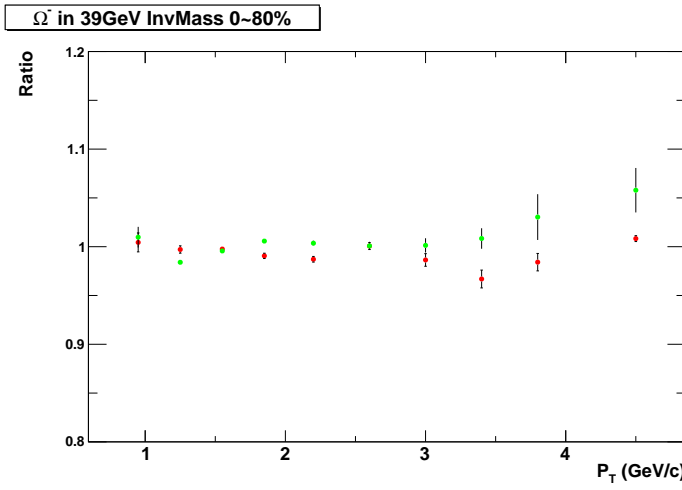


Figure 26: The comparison of cuts of  $\Lambda$  and  $\Xi$  invariant mass for  $\Omega^-$  at 39 GeV.

**DCA of  $\Omega$  and  $\Lambda$  to PV** The cuts are in Table 9. The systematic errors for each  $p_T$  bin are listed in Table 10. The Figure 27 shows the comparison of

different cuts.

Table 9: DCA of  $\Omega$  and  $\Lambda$  Cut of  $\Omega^-$  at 39GeV

Default	$DCA_{\Omega}PV < 0.4\text{ cm}$	$DCA_{\Lambda}PV > 0.4\text{ cm}$
Red	$DCA_{\Omega}PV < 0.35\text{ cm}$	$DCA_{\Lambda}PV > 0.45\text{ cm}$
Green	$DCA_{\Omega}PV < 0.45\text{ cm}$	$DCA_{\Lambda}PV > 0.35\text{ cm}$

Table 10: DCA of  $\Omega$  and  $\Lambda$  Systematic Error of  $\Omega^-$  at 39GeV

$p_T$ bin (GeV/c)	Systematic Error
0.8-1.1	0.027932
1.1-1.4	0.005653
1.4-1.7	0.01103
1.7-2.0	0.013352
2.0-2.4	0.02507
2.4-2.8	0.02255
2.8-3.2	0.022773
3.2-3.6	0.000394
3.6-4.0	0.043798
4.0-5.0	0.10328

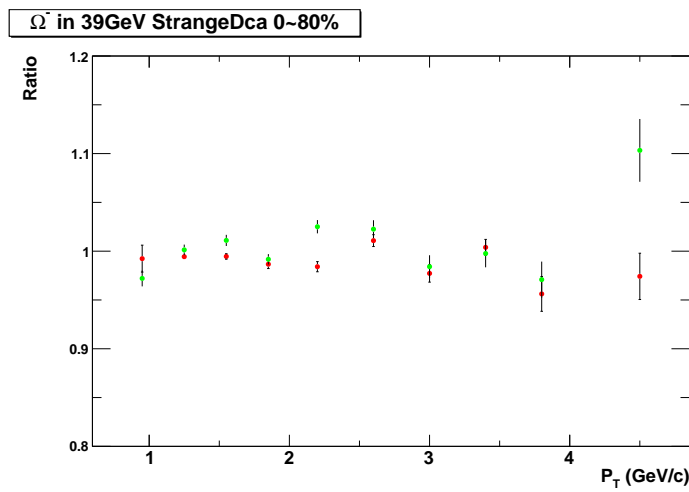


Figure 27: The comparison of DCA of  $\Omega$  and  $\Lambda$  cuts for  $\Omega^-$  at 39 GeV.

**DCA of  $K\Lambda$  and  $\pi$ -proton** The cuts are in Table 11. The systematic errors for each  $p_T$  bin are listed in Table 12. The Figure 28 shows the comparison of different cuts.

Table 11: DCA of  $K\Lambda$  and  $\pi$ -proton Cut of  $\Omega^-$  at 39GeV

Default	$DCA_{\pi\text{-proton}} < 0.7 \text{ cm}$	$DCA_{K\Lambda} < 0.7 \text{ cm}$
Red	$DCA_{\pi\text{-proton}} < 0.6 \text{ cm}$	$DCA_{K\Lambda} < 0.6 \text{ cm}$
Green	$DCA_{\pi\text{-proton}} < 0.8 \text{ cm}$	$DCA_{K\Lambda} < 0.8 \text{ cm}$

Table 12: DCA of  $K\Lambda$  and  $\pi$ -proton Systematic Error of  $\Omega^-$  at 39GeV

$p_T$ bin (GeV/c)	Systematic Error
0.8-1.1	0.023571
1.1-1.4	0.007211
1.4-1.7	0.01964
1.7-2.0	0.040063
2.0-2.4	0.020269
2.4-2.8	0.00515
2.8-3.2	0.009542
3.2-3.6	0.037315
3.6-4.0	0.009513
4.0-5.0	0.025002

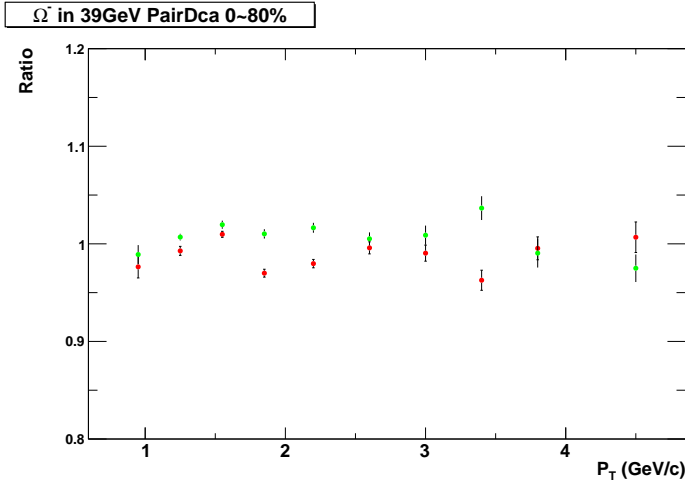


Figure 28: The comparison of DCA of  $K_{\Lambda}$  and  $\pi_{-}$ proton cuts for  $\Omega^-$  at 39 GeV.

**DCA of Decay Daughters to PV** The cuts are in Table 13. The systematic errors for each  $p_T$  bin are listed in Table 14. The Figure 29 shows the comparison of different cuts.

Table 13: DCA of Decay Daughters to PV Cut of  $\Omega^-$  at 39GeV

Default	$DCA_{p\_PV} > 0.6 \text{ cm}$	$DCA_{\pi\_PV} > 2.0 \text{ cm}$	$DCA_{K\_PV} > 1.0 \text{ cm}$
Red	$DCA_{p\_PV} > 0.5 \text{ cm}$	$DCA_{\pi\_PV} > 1.6 \text{ cm}$	$DCA_{K\_PV} > 0.8 \text{ cm}$
Green	$DCA_{p\_PV} > 0.7 \text{ cm}$	$DCA_{\pi\_PV} > 2.4 \text{ cm}$	$DCA_{K\_PV} > 1.2 \text{ cm}$

Table 14: DCA of Decay Daughters to PV Systematic Error of  $\Omega^-$  at 39GeV

$p_T$ bin (GeV/c)	Systematic Error
0.8-1.1	0.01386
1.1-1.4	0.03355
1.4-1.7	0.01766
1.7-2.0	0.014743
2.0-2.4	0.014248
2.4-2.8	0.042566
2.8-3.2	0.04478
3.2-3.6	0.0082
3.6-4.0	0.090788
4.0-5.0	0.04645

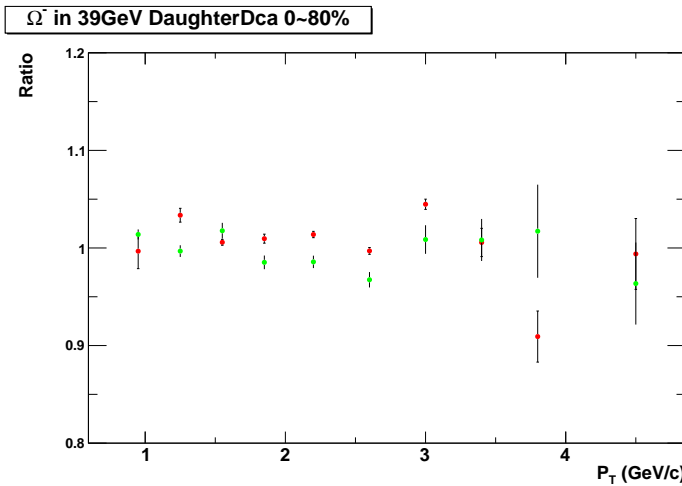


Figure 29: The comparison of DCA of Decay Daughters to PV cuts for  $\Omega^-$  at 39 GeV.

**Number of Track nHits** The cuts are in Table 15. The systematic errors for each  $p_T$  bin are listed in Table 16. The Figure 30 shows the comparison of different cuts.

Table 15: Number of Track nHits Cut of  $\Omega^-$  at 39GeV

Default	$nHits > 15$
Red	$nHits > 17$
Green	$nHits > 20$

Table 16: Number of Track nHits Systematic Error of  $\Omega^-$  at 39GeV

$p_T$ bin (GeV/c)	Systematic Error
0.8-1.1	0.037188
1.1-1.4	0.007255
1.4-1.7	0.040024
1.7-2.0	0.032994
2.0-2.4	0.048813
2.4-2.8	0.044682
2.8-3.2	0.037474
3.2-3.6	0.086721
3.6-4.0	0.0107
4.0-5.0	0.003398

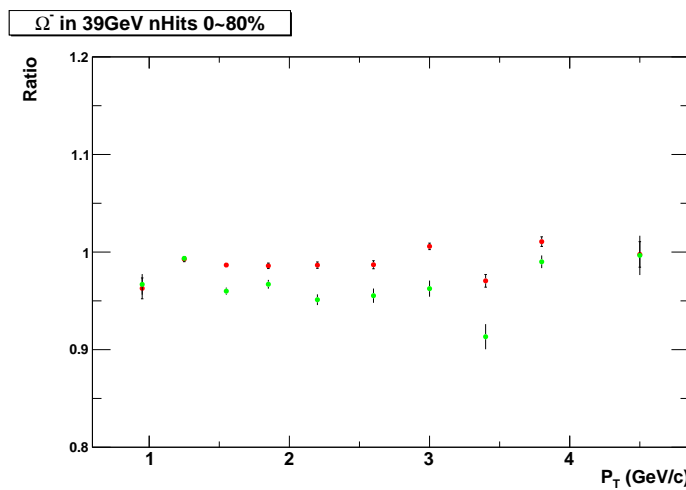


Figure 30: The comparison of Number of Track nHits cuts for  $\Omega^-$  at 39 GeV.

**Signal Extraction** The cuts are in Table 17. The systematic errors for each  $p_T$  bin are listed in Table 18. The Figure 31 shows the comparison of different cuts.

Table 17: Mass Window of Signal Extraction of  $\Omega^-$  at 39GeV

Default	(1.66-1.685) $GeV/c^2$
Red	(1.6575-1.6875) $GeV/c^2$
Green	(1.6625-1.6825) $GeV/c^2$

Table 18: Mass Window of Signal Extraction Systematic Error of  $\Omega^-$  at 39GeV

$p_T$ bin ( $GeV/c$ )	Systematic Error						
	0-5%	5-10%	10-20%	20-40%	40-60%	60-80%	0-10%
0.8-1.1	0.086537	0.02904	0.00845	0.03701	0.03181	0.020189	0.045017
1.1-1.4	0.020237	0.01772	0.01466	0.006614	0.012448	0.0056	0.00732
1.4-1.7	0.045527	0.04327	0.001943	0.00643	0.00852	0.028816	0.02927
1.7-2.0	0.01119	0.033214	0.035306	0.00769	0.01452	0.02692	0.021762
2.0-2.4	0.027933	0.019373	0.018338	0.008315	0.00912	0.01481	0.019568
2.4-2.8	0.016263	0.054167	0.019305	0.008757	0.035933	0.049491	0.026052
2.8-3.2	0.027392	0.020434	0.02301	0.01592	0.043828	0.16305	0.023915
3.2-3.6	0.056746	0.043122	0.03904	0.03133	0.038963	0.01033	0.043555
3.6-4.0	0.01278	0.00191	0.08431	0.053241	0.012811	0	0.00701
4.0-5.0	0.132118	0.05681	0.066231	0.019	0.01899	0	0.017842

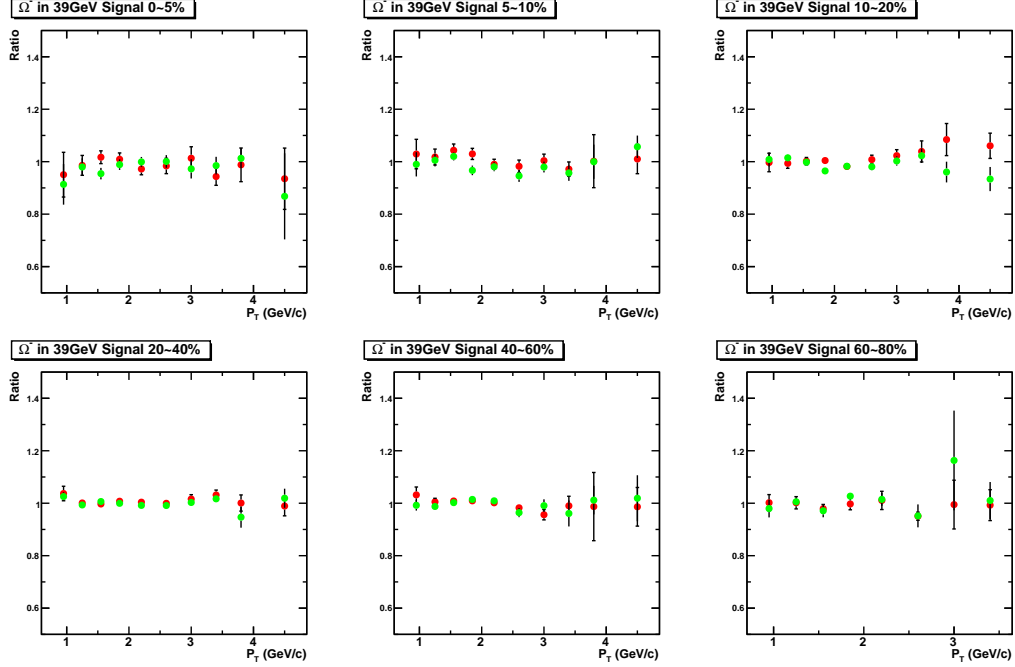


Figure 31: The comparison of Mass Window Cut of Signal Extraction for  $\Omega^-$  at 39 GeV.

#### Overall Systematic Error from Reconstruction and Signal Extraction

The overall relative systematic error from the reconstruction efficiency and signal extraction is quadratically summed up for each  $p_T$  and centrality bin. The Table 19 shows you the systematic error for  $\Omega^-$  at 39 GeV.

Table 19: The Overall Systematic Error of  $\Omega^-$  at 39GeV

$p_T$ bin (GeV/c)	Systematic Error						
	0-5%	5-10%	10-20%	20-40%	40-60%	60-80%	0-10%
0.8-1.1	0.11091	0.0752042	0.0698838	0.0786262	0.0763166	0.0722491	0.08269
1.1-1.4	0.0530788	0.052171	0.0512126	0.0495133	0.0506238	0.049388	0.04961
1.4-1.7	0.0676622	0.0661398	0.0500596	0.0504334	0.0507439	0.0577282	0.05795
1.7-2.0	0.0513428	0.0601168	0.0612975	0.0506952	0.0521699	0.0568819	0.05463
2.0-2.4	0.068091	0.0650495	0.0647488	0.0626519	0.0627638	0.0638393	0.06510
2.4-2.8	0.0622067	0.0808629	0.0630703	0.0606784	0.069974	0.0778109	0.06545
2.8-3.2	0.0703894	0.0679846	0.0688027	0.0667667	0.0782639	0.17547	0.06911
3.2-3.6	0.115377	0.109322	0.107777	0.10523	0.10775	0.100988	0.10949
3.6-4.0	0.107005	0.106257	0.135628	0.118834	0.107009	0.10624	0.10647
4.0-5.0	0.182859	0.138598	0.142719	0.12784	0.127839	0.12642	0.12767

### 6.1.2 $\bar{\Omega}^+$ at 39GeV

**Decay Length** The cuts are in Table 20. The systematic errors for each  $p_T$  bin are listed in Table 21. The Figure 32 shows the comparison of different cuts.

 Table 20: Decay Length Cut of  $\bar{\Omega}^+$  at 39GeV

	$L_\Lambda > 5.0 \text{ cm}$	$L_\Omega > 3.0 \text{ cm}$
Default	$L_\Lambda > 5.0 \text{ cm}$	$L_\Omega > 3.0 \text{ cm}$
Red	$L_\Lambda > 4.5 \text{ cm}$	$L_\Omega > 2.5 \text{ cm}$
Green	$L_\Lambda > 5.5 \text{ cm}$	$L_\Omega > 3.5 \text{ cm}$

Table 21: Decay Length Systematic Error of  $\bar{\Omega}^+$  at 39GeV

$p_T$ bin (GeV/c)	Systematic Error
0.8-1.1	0.0216
1.1-1.4	0.003692
1.4-1.7	0.013318
1.7-2.0	0.00549
2.0-2.4	0.00692
2.4-2.8	0.00185
2.8-3.2	0.002163
3.2-3.6	0.002518
3.6-4.0	0.000672
4.0-5.0	0

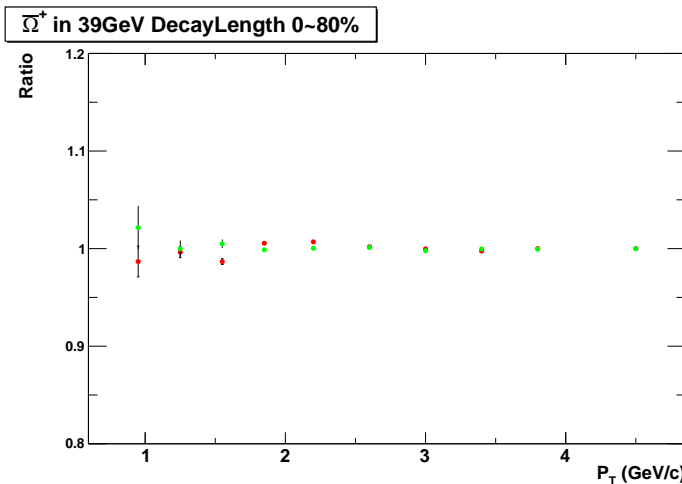


Figure 32: The comparison of Decay Length cuts for  $\bar{\Omega}^+$  at 39 GeV.

**Invariant Mass of  $\Lambda$  and  $\Xi$**  The cuts are in Table 22. The systematic errors for each  $p_T$  bin are listed in Table 23. The Figure 33 shows the comparison of different cuts.

Table 22: Invariant Mass Cut of  $\Lambda$  and  $\Xi$  for  $\bar{\Omega}^+$  at 39GeV

Default	$ V0 - pdg  < 6 \text{ MeV}$	$ Xi - pdg  > 10 \text{ MeV}$
Red	$ V0 - pdg  < 5 \text{ MeV}$	$ Xi - pdg  > 12 \text{ MeV}$
Green	$ V0 - pdg  < 7 \text{ MeV}$	$ Xi - pdg  > 8 \text{ MeV}$

Table 23: Invariant Mass of  $\Lambda$  and  $\Xi$  Systematic Error of  $\bar{\Omega}^+$  at 39GeV

$p_T$ bin (GeV/c)	Systematic Error
0.8-1.1	0.01463
1.1-1.4	0.00372
1.4-1.7	0.009675
1.7-2.0	0.004226
2.0-2.4	0.01152
2.4-2.8	0.017689
2.8-3.2	0.005267
3.2-3.6	0.00805
3.6-4.0	0.0037113
4.0-5.0	0.0303

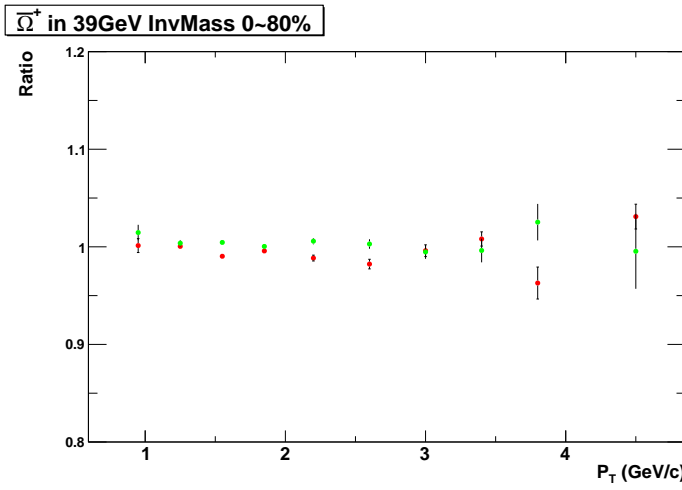


Figure 33: The comparison of cuts of  $\Lambda$  and  $\Xi$  invariant mass for  $\bar{\Omega}^+$  at 39 GeV.

**DCA of  $\Omega$  and  $\Lambda$  to PV** The cuts are in Table 24. The systematic errors for each  $p_T$  bin are listed in Table 25. The Figure 34 shows the comparison of

different cuts.

Table 24: DCA of  $\Omega$  and  $\Lambda$  Cut of  $\bar{\Omega}^+$  at 39GeV

Default	$DCA_{\Omega}PV < 0.4\text{ cm}$	$DCA_{\Lambda}PV > 0.4\text{ cm}$
Red	$DCA_{\Omega}PV < 0.35\text{ cm}$	$DCA_{\Lambda}PV > 0.45\text{ cm}$
Green	$DCA_{\Omega}PV < 0.45\text{ cm}$	$DCA_{\Lambda}PV > 0.35\text{ cm}$

Table 25: DCA of  $\Omega$  and  $\Lambda$  Systematic Error of  $\bar{\Omega}^+$  at 39GeV

$p_T$ bin (GeV/c)	Systematic Error
0.8-1.1	0.02382
1.1-1.4	0.011899
1.4-1.7	0.023494
1.7-2.0	0.00982
2.0-2.4	0.02524
2.4-2.8	0.05392
2.8-3.2	0.05088
3.2-3.6	0.06981
3.6-4.0	0.00398
4.0-5.0	0.03925

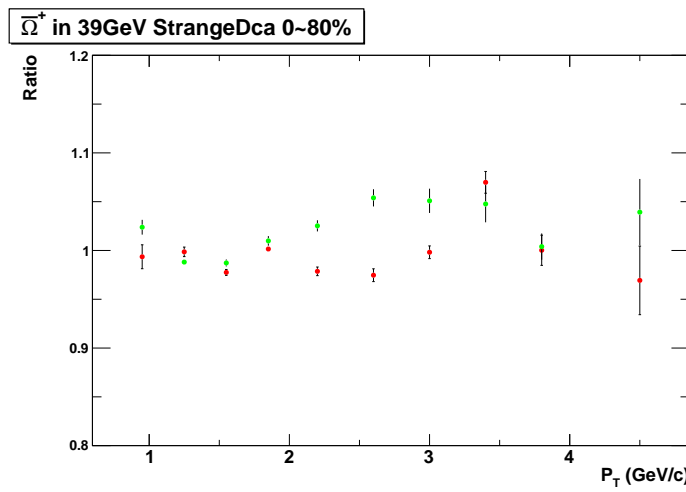


Figure 34: The comparison of DCA of  $\Omega$  and  $\Lambda$  cuts for  $\bar{\Omega}^+$  at 39 GeV.

**DCA of  $K\Lambda$  and  $\pi$ -proton** The cuts are in Table 26. The systematic errors for each  $p_T$  bin are listed in Table 27. The Figure 35 shows the comparison of different cuts.

Table 26: DCA of  $K\Lambda$  and  $\pi$ -proton Cut of  $\bar{\Omega}^+$  at 39GeV

Default	$DCA_{\pi\text{-proton}} < 0.7 \text{ cm}$	$DCA_{K\Lambda} < 0.7 \text{ cm}$
Red	$DCA_{\pi\text{-proton}} < 0.6 \text{ cm}$	$DCA_{K\Lambda} < 0.6 \text{ cm}$
Green	$DCA_{\pi\text{-proton}} < 0.8 \text{ cm}$	$DCA_{K\Lambda} < 0.8 \text{ cm}$

Table 27: DCA of  $K\Lambda$  and  $\pi$ -proton Systematic Error of  $\bar{\Omega}^+$  at 39GeV

$p_T$ bin (GeV/c)	Systematic Error
0.8-1.1	0.040773
1.1-1.4	0.00817
1.4-1.7	0.009045
1.7-2.0	0.00661
2.0-2.4	0.017675
2.4-2.8	0.00233
2.8-3.2	0.03346
3.2-3.6	0.00974
3.6-4.0	0.020929
4.0-5.0	0.0594

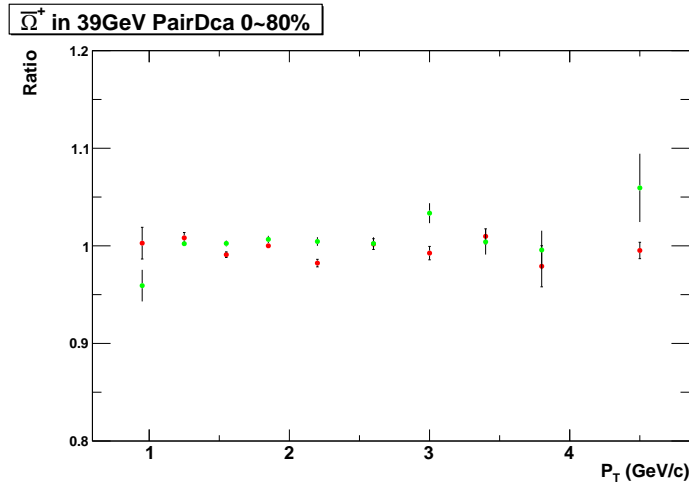


Figure 35: The comparison of DCA of  $K\Lambda$  and  $\pi$ -*proton* cuts for  $\bar{\Omega}^+$  at 39 GeV.

**DCA of Decay Daughters to PV** The cuts are in Table 28. The systematic errors for each  $p_T$  bin are listed in Table 29. The Figure 36 shows the comparison of different cuts.

Table 28: DCA of Decay Daughters to PV Cut of  $\bar{\Omega}^+$  at 39GeV

Default	$DCA.p.PV > 0.6 \text{ cm}$	$DCA.\pi.PV > 2.0 \text{ cm}$	$DCA.K.PV > 1.0 \text{ cm}$
Red	$DCA.p.PV > 0.5 \text{ cm}$	$DCA.\pi.PV > 1.6 \text{ cm}$	$DCA.K.PV > 0.8 \text{ cm}$
Green	$DCA.p.PV > 0.7 \text{ cm}$	$DCA.\pi.PV > 2.4 \text{ cm}$	$DCA.K.PV > 1.2 \text{ cm}$

Table 29: DCA of Decay Daughters to PV Systematic Error of  $\bar{\Omega}^+$  at 39GeV

$p_T$ bin (GeV/c)	Systematic Error
0.8-1.1	0.036408
1.1-1.4	0.013605
1.4-1.7	0.011102
1.7-2.0	0.034
2.0-2.4	0.02593
2.4-2.8	0.04686
2.8-3.2	0.0164
3.2-3.6	0.054357
3.6-4.0	0.12322
4.0-5.0	0.03519

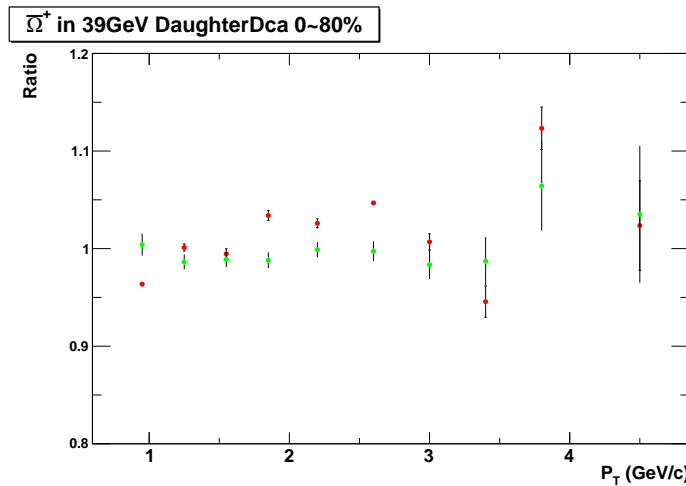


Figure 36: The comparison of DCA of Decay Daughters to PV cuts for  $\bar{\Omega}^+$  at 39 GeV.

**Number of Track nHits** The cuts are in Table 30. The systematic errors for each  $p_T$  bin are listed in Table 31. The Figure 37 shows the comparison of different cuts.

Table 30: Number of Track nHits Cut of  $\bar{\Omega}^+$  at 39GeV

Default	$nHits > 15$
Red	$nHits > 17$
Green	$nHits > 20$

Table 31: Number of Track nHits Systematic Error of  $\bar{\Omega}^+$  at 39GeV

$p_T$ bin (GeV/c)	Systematic Error
0.8-1.1	0.014801
1.1-1.4	0.027858
1.4-1.7	0.024333
1.7-2.0	0.03536
2.0-2.4	0.042758
2.4-2.8	0.046215
2.8-3.2	0.008634
3.2-3.6	0.050712
3.6-4.0	0.001519
4.0-5.0	0.05921

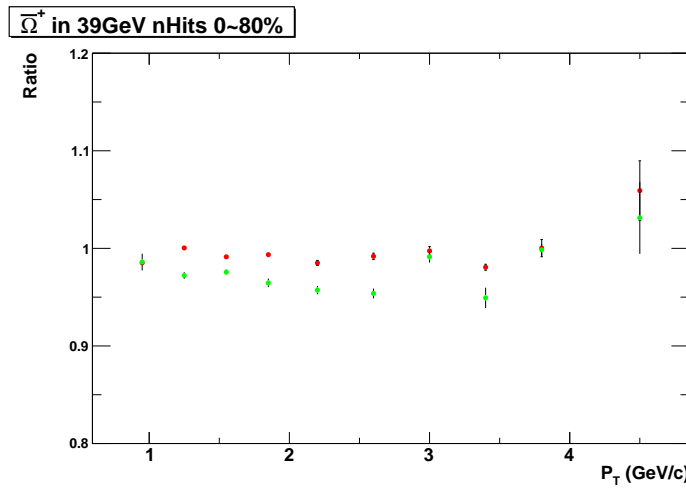


Figure 37: The comparison of Number of Track nHits cuts for  $\bar{\Omega}^+$  at 39 GeV.

**Signal Extraction** The cuts are in Table 32. The systematic errors for each  $p_T$  bin are listed in Table 33. The Figure 38 shows the comparison of different cuts.

Table 32: Mass Window of Signal Extraction of  $\bar{\Omega}^+$  at 39GeV

Default	(1.66-1.685) $GeV/c^2$
Red	(1.6575-1.6875) $GeV/c^2$
Green	(1.6625-1.6825) $GeV/c^2$

Table 33: Mass Window of Signal Extraction Systematic Error of  $\bar{\Omega}^+$  at 39GeV

$p_T$ bin ( $GeV/c$ )	Systematic Error						
	0-5%	5-10%	10-20%	20-40%	40-60%	60-80%	0-10%
0.8-1.1	0.05072	0.02441	0.04176	0.0185	0.01463	0.03532	0.0233
1.1-1.4	0.026483	0.029313	0.011372	0.00492	0.02083	0.04158	0.027857
1.4-1.7	0.04871	0.015811	0.03232	0.00902	0.008479	0.04696	0.03325
1.7-2.0	0.04608	0.02822	0.00861	0.01026	0.00634	0.008958	0.03834
2.0-2.4	0.037088	0.027107	0.00369	0.01727	0.01346	0.031937	0.032645
2.4-2.8	0.018573	0.021615	0.008042	0.01216	0.00779	0.03235	0.19897
2.8-3.2	0.11682	0.01208	0.03247	0.01661	0.047504	0	0.06943
3.2-3.6	0.051945	0.04456	0.04913	0.0179	0.01145	0.01145	0.00733
3.6-4.0	0.17523	0.017003	0.060339	0.00668	0.48579	0	0.06266
4.0-5.0	0.25704	0.03484	0.10819	0.0901	0	0	0.09397

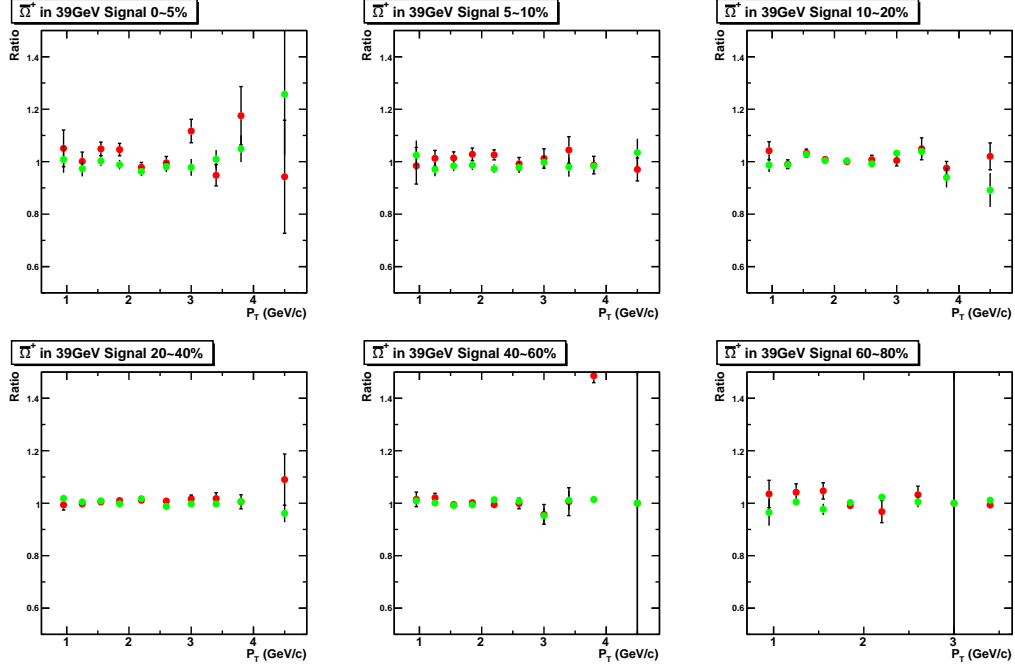


Figure 38: The comparison of Mass Window Cut of Signal Extraction for  $\bar{\Omega}^+$  at 39 GeV.

#### Overall Systematic Error from Reconstruction and Signal Extraction

The overall relative systematic error from the reconstruction efficiency and signal extraction is quadratically summed up for each  $p_T$  and centrality bin. The Table 34 shows you the systematic error for  $\bar{\Omega}^+$  at 39 GeV.

Table 34: The Overall Systematic Error of  $\bar{\Omega}^+$  at 39GeV

$p_T$ bin (GeV/c)	Systematic Error						
	0-5%	5-10%	10-20%	20-40%	40-60%	60-80%	0-10%
0.8-1.1	0.0838305	0.0710696	0.0787333	0.0692625	0.0683306	0.0755152	0.07069
1.1-1.4	0.0435697	0.0453456	0.0364183	0.0349453	0.0403839	0.0540913	0.04441
1.4-1.7	0.0628234	0.0427095	0.0511732	0.0406875	0.040571	0.0614765	0.05176
1.7-2.0	0.0686864	0.0582308	0.0516584	0.0519588	0.0513288	0.0517175	0.06375
2.0-2.4	0.0707544	0.0660716	0.0603679	0.0626811	0.0617401	0.0681956	0.0685
2.4-2.8	0.0889143	0.0895992	0.087324	0.087799	0.0873011	0.0927757	0.08920
2.8-3.2	0.133158	0.06504	0.0716838	0.0660315	0.0796298	0.0639083	0.09436
3.2-3.6	0.11517	0.112033	0.113928	0.104337	0.103426	0.103426	0.10298
3.6-4.0	0.218455	0.131553	0.143729	0.130621	0.503	0.13045	0.14471
4.0-5.0	0.277204	0.109481	0.149924	0.137442	0.103789	0.103789	0.14000

### 6.1.3 $\Omega^-$ at 27GeV

**Decay Length** The cuts are in Table 35. The systematic errors for each  $p_T$  bin are listed in Table 36. The Figure 39 shows the comparison of different cuts.

 Table 35: Decay Length Cut of  $\Omega^-$  at 27GeV

Default	$L_\Lambda > 5.0 \text{ cm}$	$L_\Omega > 3.0 \text{ cm}$
Red	$L_\Lambda > 4.5 \text{ cm}$	$L_\Omega > 2.5 \text{ cm}$
Green	$L_\Lambda > 5.5 \text{ cm}$	$L_\Omega > 3.5 \text{ cm}$

 Table 36: Decay Length Systematic Error of  $\Omega^-$  at 27GeV

$p_T$ bin (GeV/c)	Systematic Error
0.8-1.2	0.03424
1.2-1.6	0.01474
1.6-2.0	0.02996
2.0-2.4	0.009767
2.4-2.8	0.00516
2.8-3.6	0.00304

Table 37: Invariant Mass Cut of  $\Lambda$  and  $\Xi$  for  $\Omega^-$  at 27GeV

Default	$ V0 - pdg  < 6 \text{ MeV}$	$ Xi - pdg  > 10 \text{ MeV}$
Red	$ V0 - pdg  < 5 \text{ MeV}$	$ Xi - pdg  > 12 \text{ MeV}$
Green	$ V0 - pdg  < 7 \text{ MeV}$	$ Xi - pdg  > 8 \text{ MeV}$

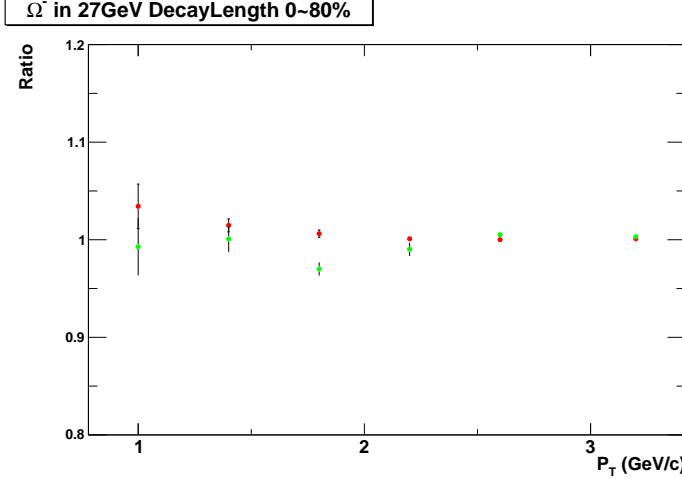


Figure 39: The comparison of Decay Length cuts for  $\Omega^-$  at 27 GeV.

**Invariant Mass of  $\Lambda$  and  $\Xi$**  The cuts are in Table 37. The systematic errors for each  $p_T$  bin are listed in Table 38. The Figure 40 shows the comparison of different cuts.

Table 38: Invariant Mass of  $\Lambda$  and  $\Xi$  Systematic Error of  $\Omega^-$  at 27GeV

$p_T$ bin (GeV/c)	Systematic Error
0.8-1.2	0.00969
1.2-1.6	0.001703
1.6-2.0	0.019856
2.0-2.4	0.020684
2.4-2.8	0.01006
2.8-3.6	0.009625

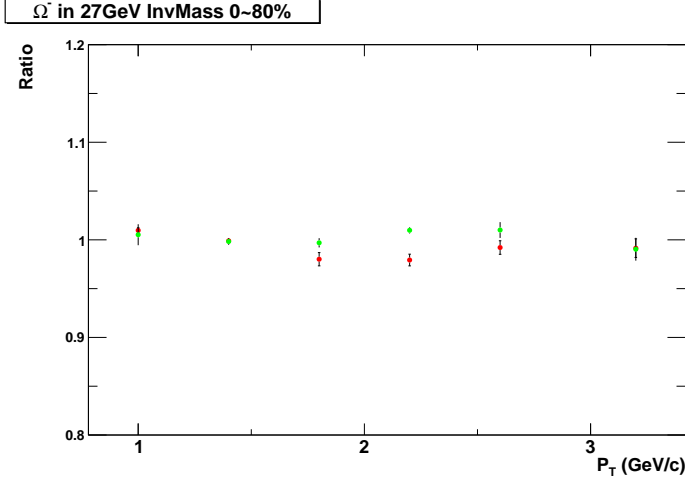


Figure 40: The comparison of cuts of  $\Lambda$  and  $\Xi$  invariant mass for  $\Omega^-$  at 27 GeV.

**DCA of  $\Omega$  and  $\Lambda$  to PV** The cuts are in Table 39. The systematic errors for each  $p_T$  bin are listed in Table 40. The Figure 41 shows the comparison of different cuts.

Table 39: DCA of  $\Omega$  and  $\Lambda$  Cut of  $\Omega^-$  at 27GeV

Default	$DCA_{\Omega}PV < 0.4 \text{ cm}$	$DCA_{\Lambda}PV > 0.4 \text{ cm}$
Red	$DCA_{\Omega}PV < 0.35 \text{ cm}$	$DCA_{\Lambda}PV > 0.45 \text{ cm}$
Green	$DCA_{\Omega}PV < 0.45 \text{ cm}$	$DCA_{\Lambda}PV > 0.35 \text{ cm}$

Table 40: DCA of  $\Omega$  and  $\Lambda$  Systematic Error of  $\Omega^-$  at 27GeV

$p_T$ bin (GeV/c)	Systematic Error
0.8-1.2	0.0474
1.2-1.6	0.024807
1.6-2.0	0.02765
2.0-2.4	0.027341
2.4-2.8	0.07201
2.8-3.6	0.00365

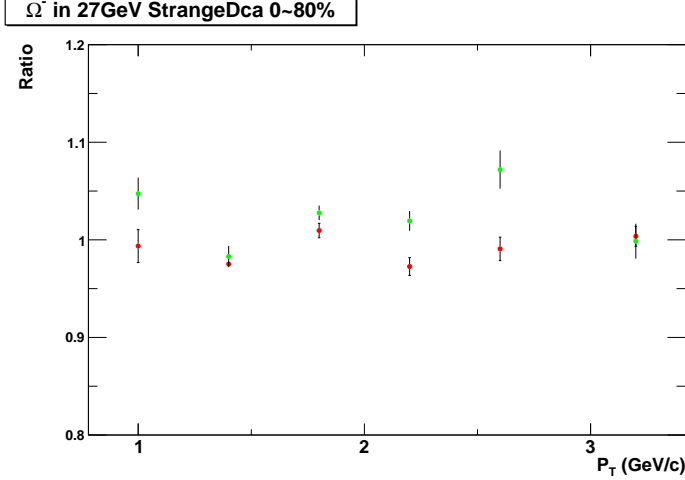


Figure 41: The comparison of DCA of  $\Omega$  and  $\Lambda$  cuts for  $\Omega^-$  at 27 GeV.

**DCA of  $K\Lambda$  and  $\pi$ -proton** The cuts are in Table 41. The systematic errors for each  $p_T$  bin are listed in Table 42. The Figure 42 shows the comparison of different cuts.

Table 41: DCA of  $K\Lambda$  and  $\pi$ -proton Cut of  $\Omega^-$  at 27GeV

Default	$DCA_{\pi\text{-proton}} < 0.7 \text{ cm}$	$DCA_{K\Lambda} < 0.7 \text{ cm}$
Red	$DCA_{\pi\text{-proton}} < 0.6 \text{ cm}$	$DCA_{K\Lambda} < 0.6 \text{ cm}$
Green	$DCA_{\pi\text{-proton}} < 0.8 \text{ cm}$	$DCA_{K\Lambda} < 0.8 \text{ cm}$

Table 42: DCA of  $K\Lambda$  and  $\pi$ -proton Systematic Error of  $\Omega^-$  at 27GeV

$p_T$ bin (GeV/c)	Systematic Error
0.8-1.2	0.07123
1.2-1.6	0.020523
1.6-2.0	0.02209
2.0-2.4	0.024539
2.4-2.8	0.0218
2.8-3.6	0.043734

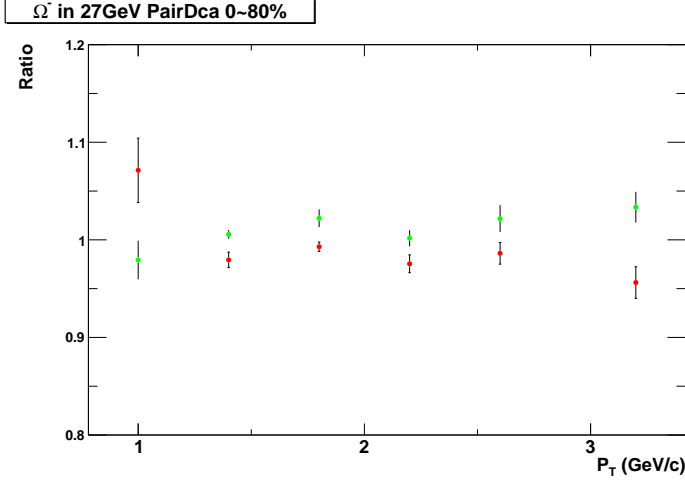


Figure 42: The comparison of DCA of  $K\Lambda$  and  $\pi$ -proton cuts for  $\Omega^-$  at 27 GeV.

**DCA of Decay Daughters to PV** The cuts are in Table 43. The systematic errors for each  $p_T$  bin are listed in Table 44. The Figure 43 shows the comparison of different cuts.

Table 43: DCA of Decay Daughters to PV Cut of  $\Omega^-$  at 27GeV

Default	$DCA_{p-PV} > 0.6 \text{ cm}$	$DCA_{\pi-PV} > 2.0 \text{ cm}$	$DCA_{K-PV} > 1.0 \text{ cm}$
Red	$DCA_{p-PV} > 0.5 \text{ cm}$	$DCA_{\pi-PV} > 1.6 \text{ cm}$	$DCA_{K-PV} > 0.8 \text{ cm}$
Green	$DCA_{p-PV} > 0.7 \text{ cm}$	$DCA_{\pi-PV} > 2.4 \text{ cm}$	$DCA_{K-PV} > 1.2 \text{ cm}$

Table 44: DCA of Decay Daughters to PV Systematic Error of  $\Omega^-$  at 27GeV

$p_T$ bin (GeV/c)	Systematic Error
0.8-1.2	0.042577
1.2-1.6	0.00605
1.6-2.0	0.01968
2.0-2.4	0.074188
2.4-2.8	0.02935
2.8-3.6	0.091947

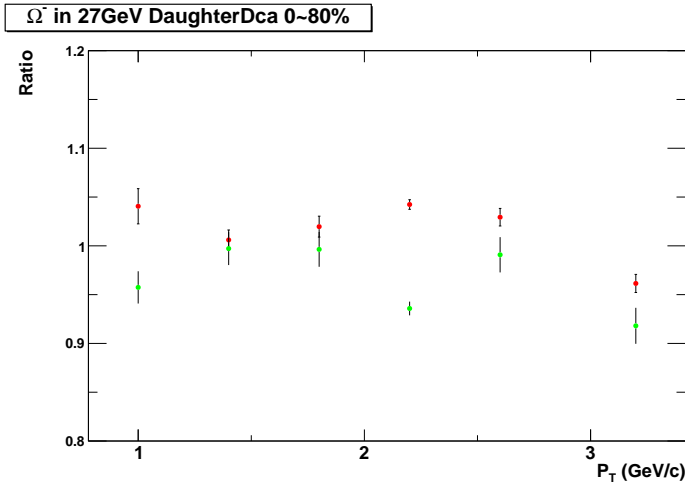


Figure 43: The comparison of DCA of Decay Daughters to PV cuts for  $\Omega^-$  at 27 GeV.

**Number of Track nHits** The cuts are in Table 45. The systematic errors for each  $p_T$  bin are listed in Table 46. The Figure 44 shows the comparison of different cuts.

Table 45: Number of Track nHits Cut of  $\Omega^-$  at 27GeV

Default	$nHits > 15$
Red	$nHits > 17$
Green	$nHits > 20$

Table 46: Number of Track nHits Systematic Error of  $\Omega^-$  at 27GeV

$p_T$ bin (GeV/c)	Systematic Error
0.8-1.2	0.03803
1.2-1.6	0.055915
1.6-2.0	0.026387
2.0-2.4	0.072741
2.4-2.8	0.021119
2.8-3.6	0.06507

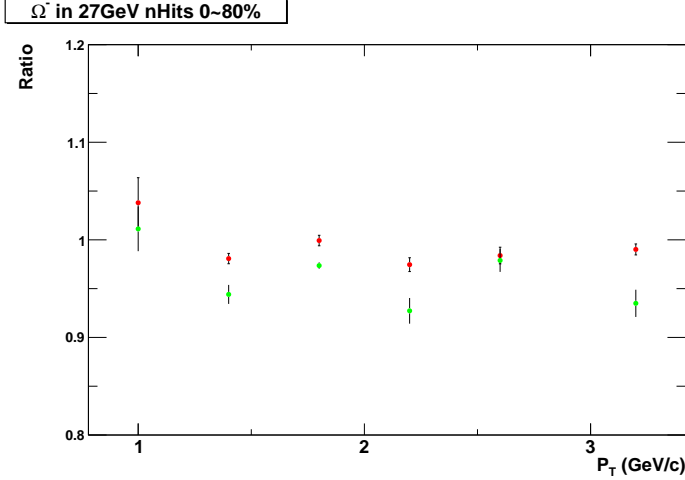


Figure 44: The comparison of Number of Track nHits cuts for  $\Omega^-$  at 27 GeV.

**Signal Extraction** The cuts are in Table 47. The systematic errors for each  $p_T$  bin are listed in Table 48. The Figure 45 shows the comparison of different cuts.

Table 47: Mass Window of Signal Extraction of  $\Omega^-$  at 27GeV

Default	(1.66-1.685) $GeV/c^2$
Red	(1.6575-1.6875) $GeV/c^2$
Green	(1.6625-1.6825) $GeV/c^2$

Table 48: Mass Window of Signal Extraction Systematic Error of  $\Omega^-$  at 27GeV

$p_T$ bin ( $GeV/c$ )	Systematic Error			
	0-10%	10-20%	20-40%	40-60%
0.8-1.2	0.02573	0.07106	0.037205	0.04049
1.2-1.6	0.039061	0.02258	0.007657	0.011739
1.6-2.0	0.08221	0.01809	0.01998	0.02013
2.0-2.4	0.07497	0.06392	0.01802	0.01571
2.4-2.8	0.046749	0.015011	0.01418	0.01537
2.8-3.6	0.0504	0.05376	0.062807	0.07037

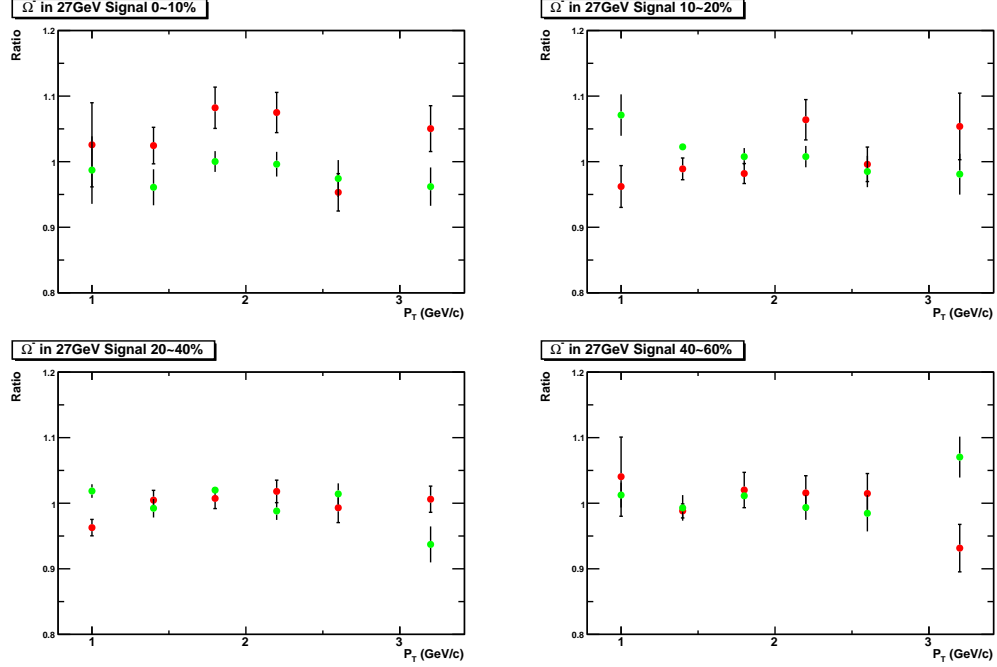


Figure 45: The comparison of Mass Window Cut of Signal Extraction for  $\Omega^-$  at 27 GeV.

#### Overall Systematic Error from Reconstruction and Signal Extraction

The overall relative systematic error from the reconstruction efficiency and signal extraction is quadratically summed up for each  $p_T$  and centrality bin. The Table 49 shows you the systematic error for  $\Omega^-$  at 27 GeV.

Table 49: The Overall Systematic Error of  $\Omega^-$  at 27 GeV

$p_T$ bin (GeV/c)	Systematic Error			
	0-10%	10-20%	20-40%	40-60%
0.8-1.2	0.111839	0.129982	0.115022	0.116126
1.2-1.6	0.0771077	0.0702118	0.0669214	0.0675103
1.6-2.0	0.101914	0.0628902	0.0634597	0.0635071
2.0-2.4	0.130018	0.123976	0.107745	0.107383
2.4-2.8	0.0963401	0.0855644	0.0854226	0.0856282
2.8-3.6	0.124569	0.125966	0.130085	0.1339

### 6.1.4 $\bar{\Omega}^+$ at 27GeV

**Decay Length** The cuts are in Table 50. The systematic errors for each  $p_T$  bin are listed in Table 51. The Figure 46 shows the comparison of different cuts.

Table 50: Decay Length Cut of  $\bar{\Omega}^+$  at 27GeV

Default	$L_\Lambda > 5.0 \text{ cm}$	$L_\Omega > 3.0 \text{ cm}$
Red	$L_\Lambda > 4.5 \text{ cm}$	$L_\Omega > 2.5 \text{ cm}$
Green	$L_\Lambda > 5.5 \text{ cm}$	$L_\Omega > 3.5 \text{ cm}$

Table 51: Decay Length Systematic Error of  $\bar{\Omega}^+$  at 27GeV

$p_T$ bin (GeV/c)	Systematic Error
0.8-1.2	0.00551
1.2-1.6	0.02235
1.6-2.0	0.02691
2.0-2.4	0.006366
2.4-2.8	0.00287
2.8-3.6	0.004885

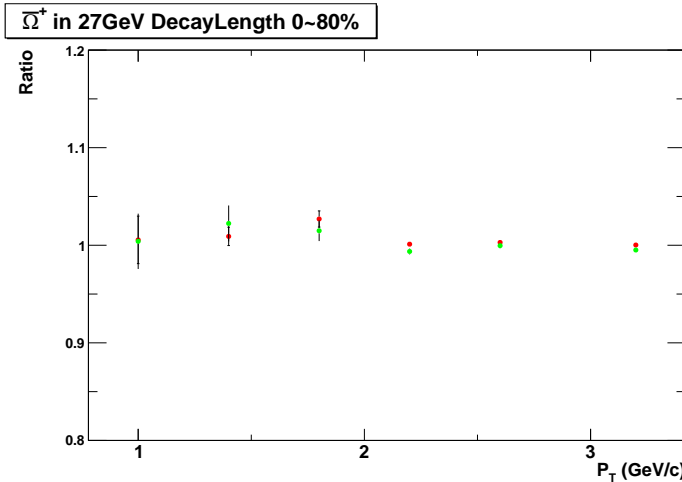


Figure 46: The comparison of Decay Length cuts for  $\bar{\Omega}^+$  at 27 GeV.

Table 52: Invariant Mass Cut of  $\Lambda$  and  $\Xi$  for  $\bar{\Omega}^+$  at 27GeV

Default	$ V0 - pdg  < 6 \text{ MeV}$	$ Xi - pdg  > 10 \text{ MeV}$
Red	$ V0 - pdg  < 5 \text{ MeV}$	$ Xi - pdg  > 12 \text{ MeV}$
Green	$ V0 - pdg  < 7 \text{ MeV}$	$ Xi - pdg  > 8 \text{ MeV}$

**Invariant Mass of  $\Lambda$  and  $\Xi$**  The cuts are in Table 52. The systematic errors for each  $p_T$  bin are listed in Table 53. The Figure 47 shows the comparison of different cuts.

Table 53: Invariant Mass of  $\Lambda$  and  $\Xi$  Systematic Error of  $\bar{\Omega}^+$  at 27GeV

$p_T$ bin (GeV/c)	Systematic Error
0.8-1.2	0.018602
1.2-1.6	0.007057
1.6-2.0	0.003933
2.0-2.4	0.02477
2.4-2.8	0.002788
2.8-3.6	0.043486

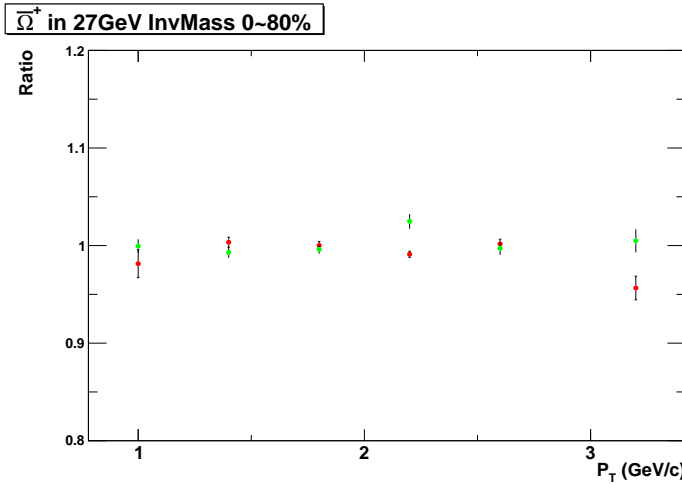


Figure 47: The comparison of cuts of  $\Lambda$  and  $\Xi$  invariant mass for  $\bar{\Omega}^+$  at 27 GeV.

**DCA of  $\Omega$  and  $\Lambda$  to PV** The cuts are in Table 54. The systematic errors for each  $p_T$  bin are listed in Table 55. The Figure 48 shows the comparison of

different cuts.

Table 54: DCA of  $\Omega$  and  $\Lambda$  Cut of  $\bar{\Omega}^+$  at 27GeV

Default	$DCA_{\Omega}PV < 0.5\text{ cm}$	$DCA_{\Lambda}PV > 0.4\text{ cm}$
Red	$DCA_{\Omega}PV < 0.45\text{ cm}$	$DCA_{\Lambda}PV > 0.45\text{ cm}$
Green	$DCA_{\Omega}PV < 0.55\text{ cm}$	$DCA_{\Lambda}PV > 0.35\text{ cm}$

Table 55: DCA of  $\Omega$  and  $\Lambda$  Systematic Error of  $\bar{\Omega}^+$  at 27GeV

$p_T$ bin (GeV/c)	Systematic Error
0.8-1.2	0.025801
1.2-1.6	0.02042
1.6-2.0	0.000947
2.0-2.4	0.04856
2.4-2.8	0.024965
2.8-3.6	0.037697

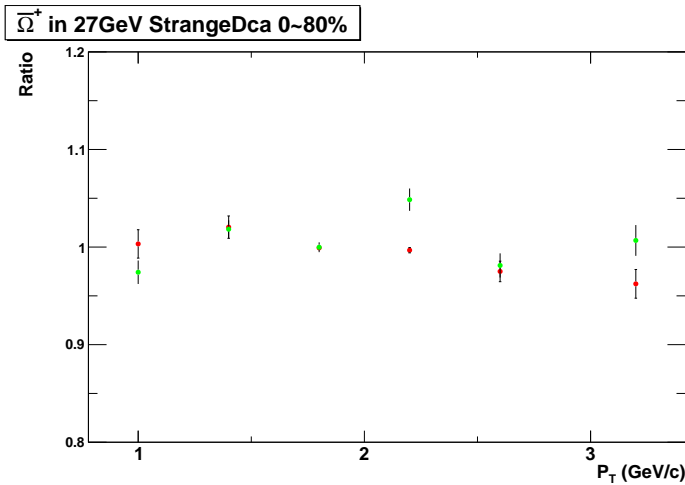


Figure 48: The comparison of DCA of  $\Omega$  and  $\Lambda$  cuts for  $\bar{\Omega}^+$  at 27 GeV.

**DCA of  $K_{\Lambda}$  and  $\pi_{-}$ proton** The cuts are in Table 56. The systematic errors for each  $p_T$  bin are listed in Table 57. The Figure 49 shows the comparison of different cuts.

Table 56: DCA of  $K\Lambda$  and  $\pi$ -proton Cut of  $\bar{\Omega}^+$  at 27GeV

Default	$DCA_{\pi\text{-proton}} < 0.7 \text{ cm}$	$DCA_{K\Lambda} < 0.7 \text{ cm}$
Red	$DCA_{\pi\text{-proton}} < 0.6 \text{ cm}$	$DCA_{K\Lambda} < 0.6 \text{ cm}$
Green	$DCA_{\pi\text{-proton}} < 0.8 \text{ cm}$	$DCA_{K\Lambda} < 0.8 \text{ cm}$

Table 57: DCA of  $K\Lambda$  and  $\pi$ -proton Systematic Error of  $\bar{\Omega}^+$  at 27GeV

$p_T$ bin (GeV/c)	Systematic Error
0.8-1.2	0.05528
1.2-1.6	0.02339
1.6-2.0	0.01251
2.0-2.4	0.017298
2.4-2.8	0.01455
2.8-3.6	0.019264

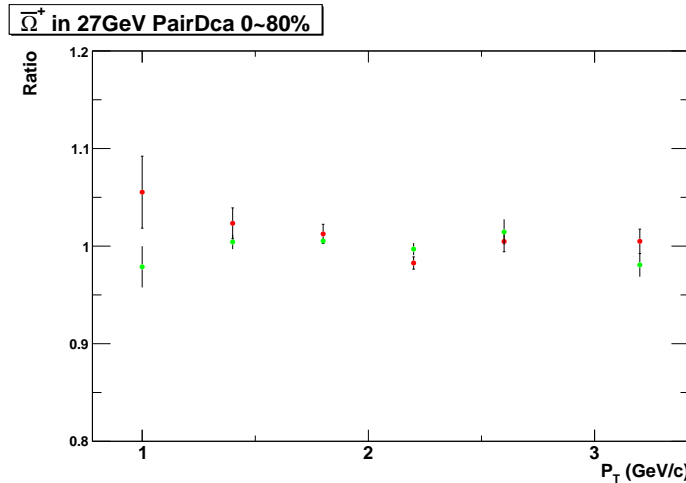


Figure 49: The comparison of DCA of  $K\Lambda$  and  $\pi$ -proton cuts for  $\bar{\Omega}^+$  at 27 GeV.

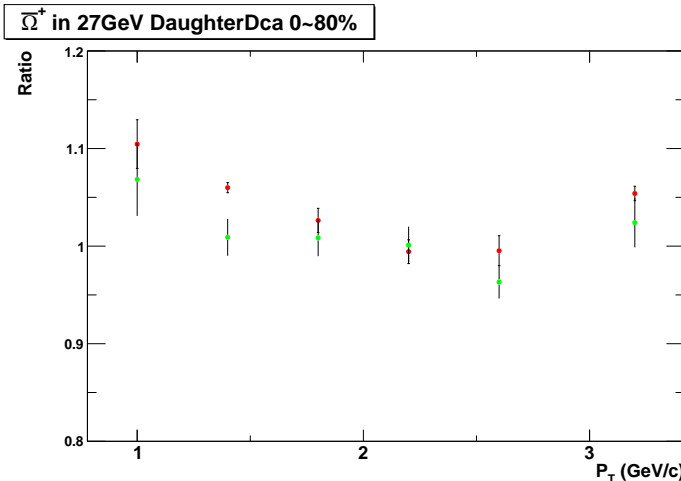
**DCA of Decay Daughters to PV** The cuts are in Table 58. The systematic errors for each  $p_T$  bin are listed in Table 59. The Figure 50 shows the comparison of different cuts.

Table 58: DCA of Decay Daughters to PV Cut of  $\bar{\Omega}^+$  at 27GeV

Default	$DCA\_p\_PV > 0.6 \text{ cm}$	$DCA\_{\pi}\_PV > 2.0 \text{ cm}$	$DCA\_{K}\_PV > 1.0 \text{ cm}$
Red	$DCA\_p\_PV > 0.5 \text{ cm}$	$DCA\_{\pi}\_PV > 1.6 \text{ cm}$	$DCA\_{K}\_PV > 0.8 \text{ cm}$
Green	$DCA\_p\_PV > 0.7 \text{ cm}$	$DCA\_{\pi}\_PV > 2.4 \text{ cm}$	$DCA\_{K}\_PV > 1.2 \text{ cm}$

 Table 59: DCA of Decay Daughters to PV Systematic Error of  $\bar{\Omega}^+$  at 27GeV

$p_T$ bin (GeV/c)	Systematic Error
0.8-1.2	0.10456
1.2-1.6	0.05992
1.6-2.0	0.02634
2.0-2.4	0.005692
2.4-2.8	0.036832
2.8-3.6	0.05394


 Figure 50: The comparison of DCA of Decay Daughters to PV cuts for  $\bar{\Omega}^+$  at 27 GeV.

**Number of Track nHits** The cuts are in Table 60. The systematic errors for each  $p_T$  bin are listed in Table 61. The Figure 51 shows the comparison of different cuts.

Table 60: Number of Track nHits Cut of  $\bar{\Omega}^+$  at 27GeV

Default	$nHits > 15$
Red	$nHits > 17$
Green	$nHits > 20$

Table 61: Number of Track nHits Systematic Error of  $\bar{\Omega}^+$  at 27GeV

$p_T$ bin (GeV/c)	Systematic Error
0.8-1.2	0.039014
1.2-1.6	0.032837
1.6-2.0	0.031947
2.0-2.4	0.047855
2.4-2.8	0.050791
2.8-3.6	0.042367

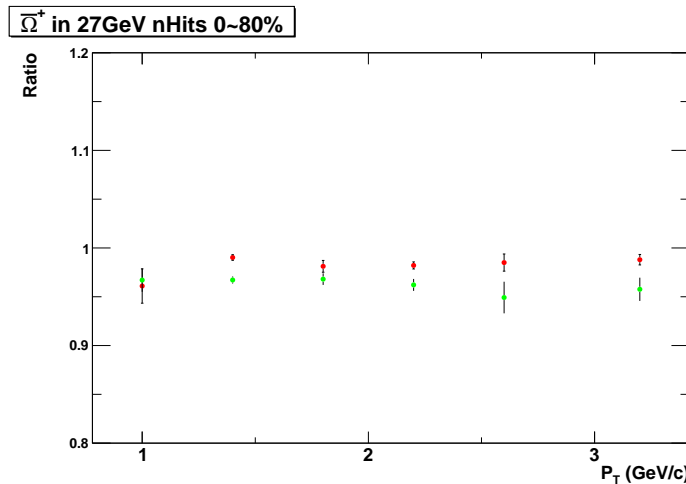


Figure 51: The comparison of Number of Track nHits cuts for  $\bar{\Omega}^+$  at 27 GeV.

**Signal Extraction** The cuts are in Table 62. The systematic errors for each  $p_T$  bin are listed in Table 63. The Figure 52 shows the comparison of different cuts.

Table 62: Mass Window of Signal Extraction of  $\bar{\Omega}^+$  at 27GeV

Default	(1.66-1.685) $GeV/c^2$
Red	(1.6575-1.6875) $GeV/c^2$
Green	(1.6625-1.6825) $GeV/c^2$

 Table 63: Mass Window of Signal Extraction Systematic Error of  $\bar{\Omega}^+$  at 27GeV

$p_T$ bin ( $GeV/c$ )	Systematic Error			
	0-10%	10-20%	20-40%	40-60%
0.8-1.2	0.072027	0.04942	0.06809	0.02807
1.2-1.6	0.01495	0.007364	0.01369	0.005483
1.6-2.0	0.00875	0.02632	0.008235	0.016066
2.0-2.4	0.0161	0.03022	0.023348	0.026496
2.4-2.8	0.058121	0.04501	0.02636	0.022999
2.8-3.6	0.07853	0.0266	0.029788	0.09473

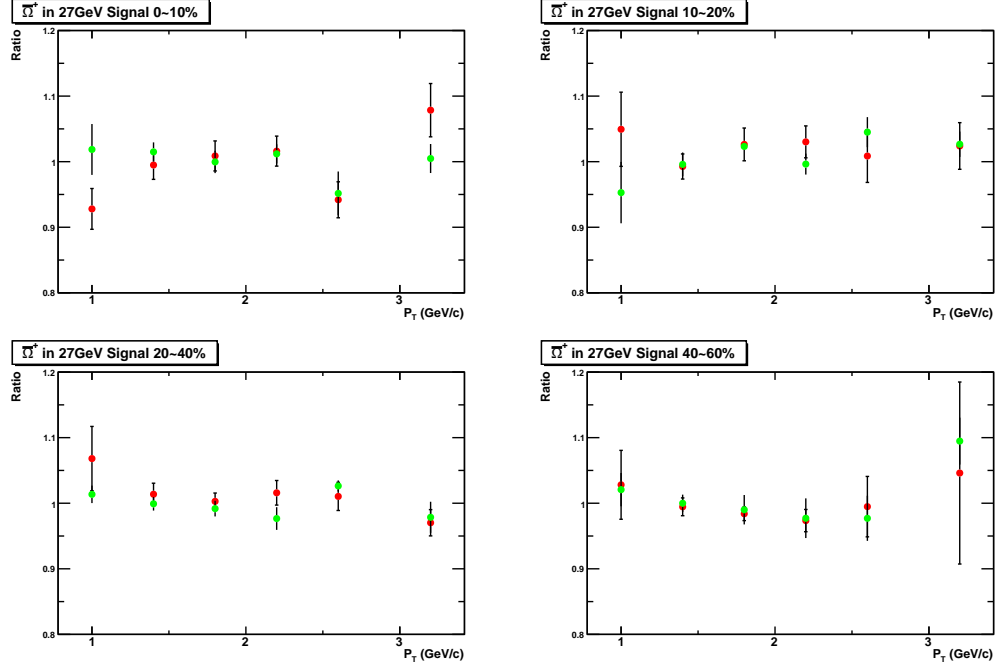


Figure 52: The comparison of Mass Window Cut of Signal Extraction for  $\bar{\Omega}^+$  at 27 GeV.

#### Overall Systematic Error from Reconstruction and Signal Extraction

The overall relative systematic error from the reconstruction efficiency and signal extraction is quadratically summed up for each  $p_T$  and centrality bin. The Table 64 shows you the systematic error for  $\bar{\Omega}^+$  at 27 GeV.

Table 64: The Overall Systematic Error of  $\bar{\Omega}^+$  at 27GeV

$p_T$ bin (GeV/c)	Systematic Error			
	0-10%	10-20%	20-40%	40-60%
0.8-1.2	0.147447	0.137823	0.145565	0.131684
1.2-1.6	0.0800348	0.0789702	0.079809	0.0788171
1.6-2.0	0.051844	0.0574803	0.0517596	0.0535644
2.0-2.4	0.0709647	0.0754322	0.0729514	0.074019
2.4-2.8	0.0903622	0.082542	0.0740414	0.0729125
2.8-3.6	0.120741	0.095494	0.0964307	0.131853

### 6.1.5 $\Omega^-$ at 19.6 GeV

**Decay Length** The cuts are in Table 65. The systematic errors for each  $p_T$  bin are listed in Table 66. The Figure 53 shows the comparison of different cuts.

Table 65: Decay Length Cut of  $\Omega^-$  at 19.6 GeV

Default	$L_\Lambda > 5.0 \text{ cm}$	$L_\Omega > 3.0 \text{ cm}$
Red	$L_\Lambda > 4.5 \text{ cm}$	$L_\Omega > 2.5 \text{ cm}$
Green	$L_\Lambda > 5.5 \text{ cm}$	$L_\Omega > 3.5 \text{ cm}$

Table 66: Decay Length Systematic Error of  $\Omega^-$  at 19.6 GeV

$p_T$ bin (GeV/c)	Systematic Error
0.8-1.2	0.117479
1.2-1.6	0.027019
1.6-2.0	0.023481
2.0-2.4	0.01743
2.4-2.8	0.011571
2.8-3.6	0.001539

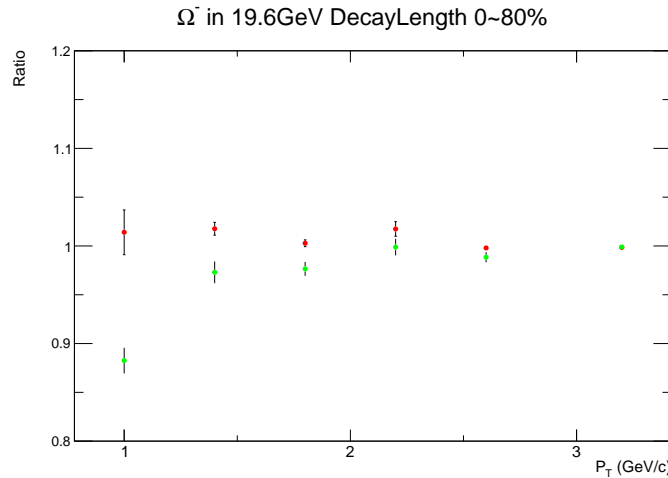


Figure 53: The comparison of Decay Length cuts for  $\Omega^-$  at 19.6 GeV.

Table 67: Invariant Mass Cut of  $\Lambda$  and  $\Xi$  for  $\Omega^-$  at 19.6 GeV

Default	$ V0 - pdg  < 6 \text{ MeV}$	$ Xi - pdg  > 10 \text{ MeV}$
Red	$ V0 - pdg  < 5 \text{ MeV}$	$ Xi - pdg  > 12 \text{ MeV}$
Green	$ V0 - pdg  < 7 \text{ MeV}$	$ Xi - pdg  > 8 \text{ MeV}$

**Invariant Mass of  $\Lambda$  and  $\Xi$**  The cuts are in Table 67. The systematic errors for each  $p_T$  bin are listed in Table 68. The Figure 54 shows the comparison of different cuts.

Table 68: Invariant Mass of  $\Lambda$  and  $\Xi$  Systematic Error of  $\Omega^-$  at 19.6 GeV

$p_T$ bin (GeV/c)	Systematic Error
0.8-1.2	0.0068
1.2-1.6	0.00908
1.6-2.0	0.0045
2.0-2.4	0.016074
2.4-2.8	0.04218
2.8-3.6	0.02073

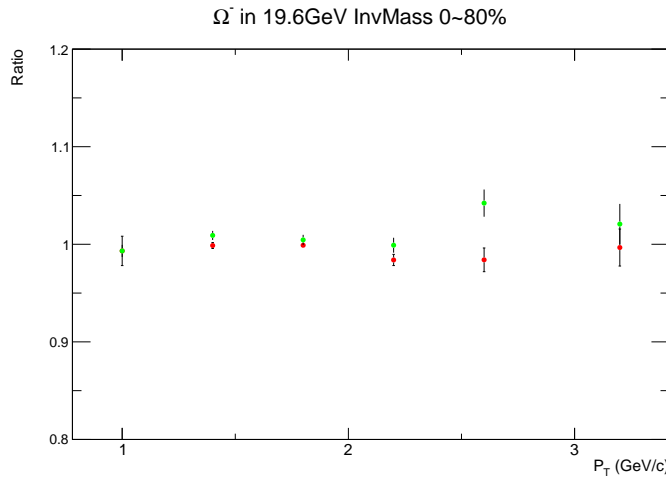


Figure 54: The comparison of cuts of  $\Lambda$  and  $\Xi$  invariant mass for  $\Omega^-$  at 19.6 GeV.

**DCA of  $\Omega$  and  $\Lambda$  to PV** The cuts are in Table 69. The systematic errors for each  $p_T$  bin are listed in Table 70. The Figure 55 shows the comparison of

different cuts.

Table 69: DCA of  $\Omega$  and  $\Lambda$  Cut of  $\Omega^-$  at 19.6 GeV

Default	$DCA_{\Omega}PV < 0.5 \text{ cm}$	$DCA_{\Lambda}PV > 0.4 \text{ cm}$
Red	$DCA_{\Omega}PV < 0.45 \text{ cm}$	$DCA_{\Lambda}PV > 0.45 \text{ cm}$
Green	$DCA_{\Omega}PV < 0.55 \text{ cm}$	$DCA_{\Lambda}PV > 0.35 \text{ cm}$

Table 70: DCA of  $\Omega$  and  $\Lambda$  Systematic Error of  $\Omega^-$  at 19.6 GeV

$p_T$ bin (GeV/c)	Systematic Error
0.8-1.2	0.018712
1.2-1.6	0.026384
1.6-2.0	0.027803
2.0-2.4	0.02636
2.4-2.8	0.11102
2.8-3.6	0.03266

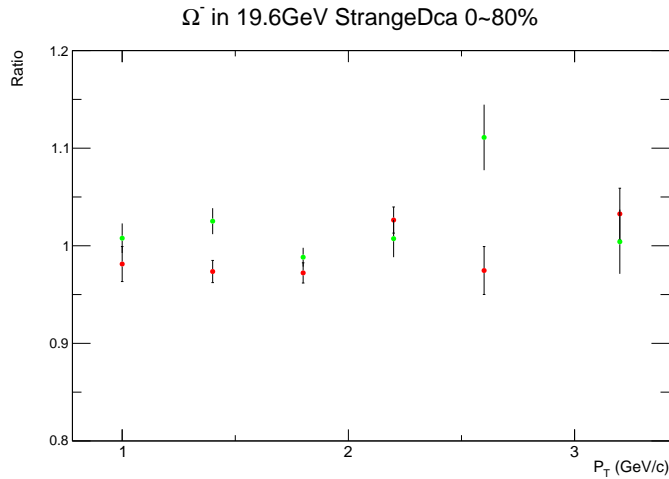


Figure 55: The comparison of DCA of  $\Omega$  and  $\Lambda$  cuts for  $\Omega^-$  at 19.6 GeV.

**DCA of  $K_{\Lambda}$  and  $\pi_{-proton}$**  The cuts are in Table 71. The systematic errors for each  $p_T$  bin are listed in Table 72. The Figure 56 shows the comparison of different cuts.

Table 71: DCA of  $K\Lambda$  and  $\pi$ -proton Cut of  $\Omega^-$  at 19.6 GeV

Default	$DCA_{\pi\text{-}proton} < 0.7 \text{ cm}$	$DCA_{K\Lambda} < 0.7 \text{ cm}$
Red	$DCA_{\pi\text{-}proton} < 0.6 \text{ cm}$	$DCA_{K\Lambda} < 0.6 \text{ cm}$
Green	$DCA_{\pi\text{-}proton} < 0.8 \text{ cm}$	$DCA_{K\Lambda} < 0.8 \text{ cm}$

Table 72: DCA of  $K\Lambda$  and  $\pi$ -proton Systematic Error of  $\Omega^-$  at 19.6 GeV

$p_T$ bin (GeV/c)	Systematic Error
0.8-1.2	0.0581131
1.2-1.6	0.013096
1.6-2.0	0.01541
2.0-2.4	0.04191
2.4-2.8	0.01961
2.8-3.6	0.0438081

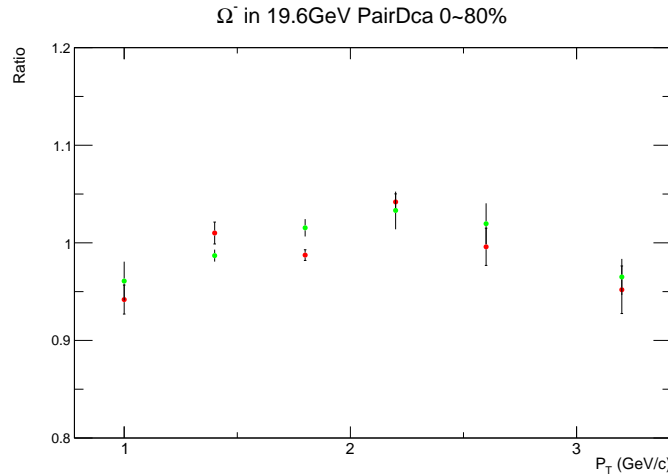


Figure 56: The comparison of DCA of  $K\Lambda$  and  $\pi$ -proton cuts for  $\Omega^-$  at 19.6 GeV.

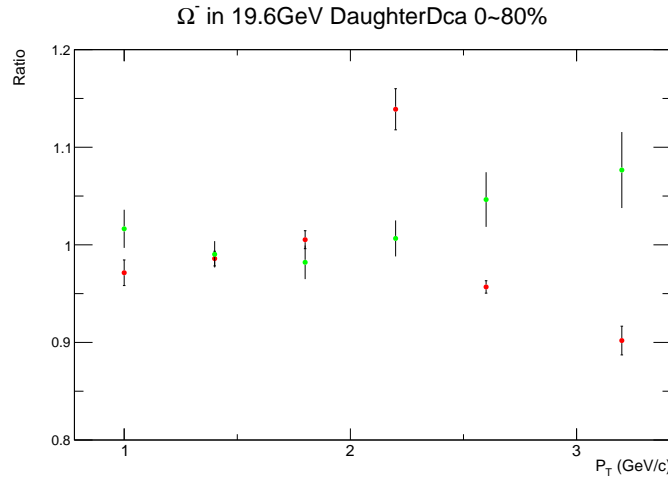
**DCA of Decay Daughters to PV** The cuts are in Table 73. The systematic errors for each  $p_T$  bin are listed in Table 74. The Figure 57 shows the comparison of different cuts.

Table 73: DCA of Decay Daughters to PV Cut of  $\Omega^-$  at 19.6 GeV

Default	$DCA_{p\_PV} > 0.6 \text{ cm}$	$DCA_{\pi\_PV} > 2.0 \text{ cm}$	$DCA_{K\_PV} > 1.0 \text{ cm}$
Red	$DCA_{p\_PV} > 0.5 \text{ cm}$	$DCA_{\pi\_PV} > 1.6 \text{ cm}$	$DCA_{K\_PV} > 0.8 \text{ cm}$
Green	$DCA_{p\_PV} > 0.7 \text{ cm}$	$DCA_{\pi\_PV} > 2.4 \text{ cm}$	$DCA_{K\_PV} > 1.2 \text{ cm}$

 Table 74: DCA of Decay Daughters to PV Systematic Error of  $\Omega^-$  at 19.6 GeV

$p_T$ bin (GeV/c)	Systematic Error
0.8-1.2	0.02861
1.2-1.6	0.014093
1.6-2.0	0.017926
2.0-2.4	0.13893
2.4-2.8	0.04641
2.8-3.6	0.098089


 Figure 57: The comparison of DCA of Decay Daughters to PV cuts for  $\Omega^-$  at 19.6 GeV.

**Number of Track nHits** The cuts are in Table 75. The systematic errors for each  $p_T$  bin are listed in Table 76. The Figure 58 shows the comparison of different cuts.

Table 75: Number of Track nHits Cut of  $\Omega^-$  at 19.6 GeV

Default	$nHits > 15$
Red	$nHits > 17$
Green	$nHits > 20$

Table 76: Number of Track nHits Systematic Error of  $\Omega^-$  at 19.6 GeV

$p_T$ bin (GeV/c)	Systematic Error
0.8-1.2	0.042775
1.2-1.6	0.065958
1.6-2.0	0.055598
2.0-2.4	0.040661
2.4-2.8	0.066792
2.8-3.6	0.049857

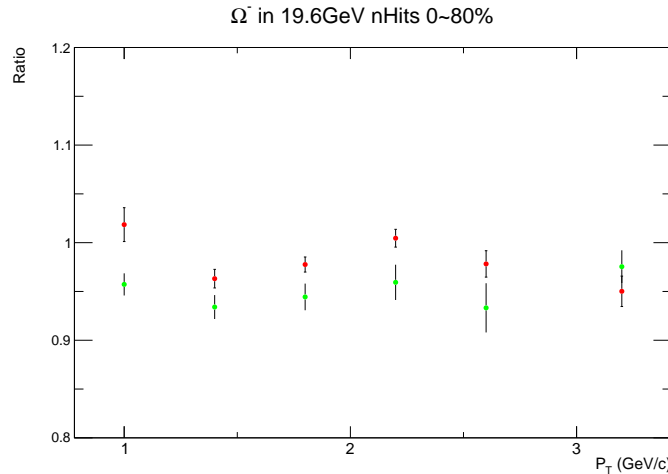


Figure 58: The comparison of Number of Track nHits cuts for  $\Omega^-$  at 19.6 GeV.

**Signal Extraction** The cuts are in Table 77. The systematic errors for each  $p_T$  bin are listed in Table 78. The Figure 59 shows the comparison of different cuts.

Table 77: Mass Window of Signal Extraction of  $\Omega^-$  at 19.6 GeV

Default	$(1.66-1.685) \text{ GeV}/c^2$
Red	$(1.6575-1.6875) \text{ GeV}/c^2$
Green	$(1.6625-1.6825) \text{ GeV}/c^2$

 Table 78: Mass Window of Signal Extraction Systematic Error of  $\Omega^-$  at 19.6 GeV

$p_T$ bin (GeV/c)	Systematic Error			
	0-10%	10-20%	20-40%	40-60%
0.8-1.2	0.039103	0.028193	0.056431	0.11868
1.2-1.6	0.010364	0.073274	0.01549	0.03457
1.6-2.0	0.020681	0.012187	0.04625	0.033035
2.0-2.4	0.11011	0.03323	0.016425	0.03809
2.4-2.8	0.06664	0.05534	0.047424	0.09059
2.8-3.6	0.13356	0.06782	0.06691	0.133353

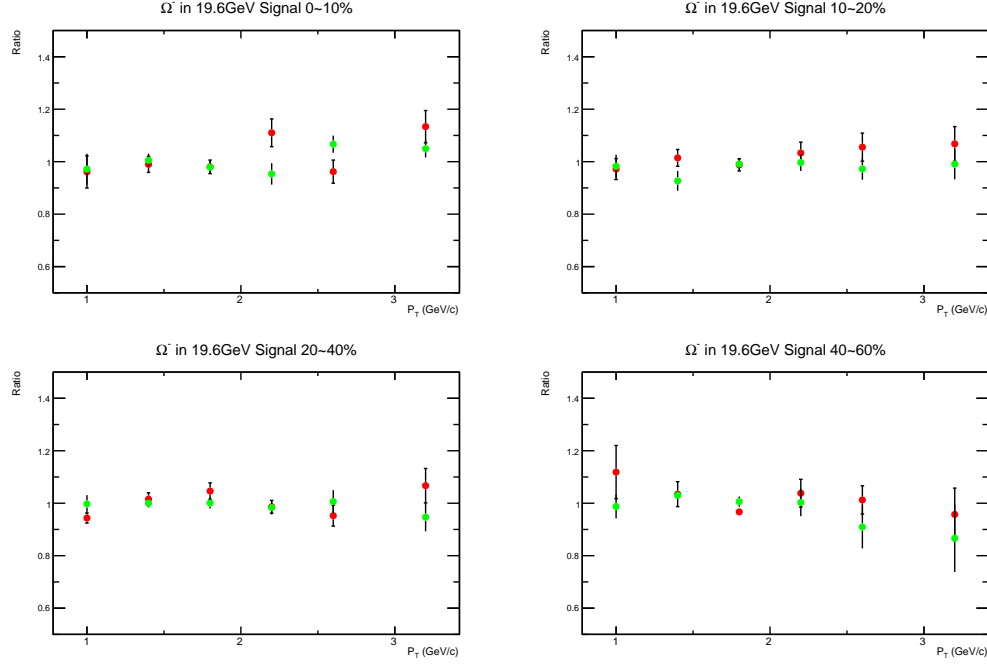


Figure 59: The comparison of Mass Window Cut of Signal Extraction for  $\Omega^-$  at 19.6 GeV.

#### Overall Systematic Error from Reconstruction and Signal Extraction

The overall relative systematic error from the reconstruction efficiency and signal extraction is quadratically summed up for each  $p_T$  and centrality bin. The Table 79 shows you the systematic error for  $\Omega^-$  at 19.6 GeV.

Table 79: The Overall Systematic Error of  $\Omega^-$  at 19.6 GeV

$p_T$ bin (GeV/c)	Systematic Error			
	0-10%	10-20%	20-40%	40-60%
0.8-1.2	0.147493	0.144983	0.153002	0.18523
1.2-1.6	0.0796026	0.107695	0.0804307	0.0861641
1.6-2.0	0.073636	0.0717153	0.0844608	0.078012
2.0-2.4	0.18998	0.158343	0.155686	0.159434
2.4-2.8	0.160247	0.155887	0.153255	0.171594
2.8-3.6	0.183728	0.143239	0.14281	0.183578

### 6.1.6 $\bar{\Omega}^+$ at 19.6 GeV

**Decay Length** The cuts are in Table 80. The systematic errors for each  $p_T$  bin are listed in Table 81. The Figure 60 shows the comparison of different cuts.

Table 80: Decay Length Cut of  $\bar{\Omega}^+$  at 19.6 GeV

Default	$L_\Lambda > 5.0 \text{ cm}$	$L_\Omega > 3.0 \text{ cm}$
Red	$L_\Lambda > 4.5 \text{ cm}$	$L_\Omega > 2.5 \text{ cm}$
Green	$L_\Lambda > 5.5 \text{ cm}$	$L_\Omega > 3.5 \text{ cm}$

Table 81: Decay Length Systematic Error of  $\bar{\Omega}^+$  at 19.6 GeV

$p_T$ bin (GeV/c)	Systematic Error
0.8-1.2	0.037425
1.2-1.6	0.00801
1.6-2.0	0.002121
2.0-2.4	0.00503
2.4-2.8	0.0135
2.8-3.6	0.00789

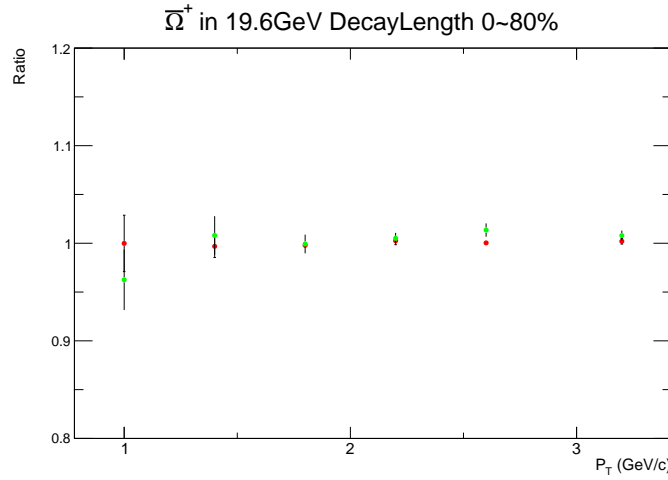


Figure 60: The comparison of Decay Length cuts for  $\bar{\Omega}^+$  at 19.6 GeV.

Table 82: Invariant Mass Cut of  $\Lambda$  and  $\Xi$  for  $\bar{\Omega}^+$  at 19.6 GeV

Default	$ V0 - pdg  < 6 \text{ MeV}$	$ Xi - pdg  > 10 \text{ MeV}$
Red	$ V0 - pdg  < 5 \text{ MeV}$	$ Xi - pdg  > 12 \text{ MeV}$
Green	$ V0 - pdg  < 7 \text{ MeV}$	$ Xi - pdg  > 8 \text{ MeV}$

**Invariant Mass of  $\Lambda$  and  $\Xi$**  The cuts are in Table 82. The systematic errors for each  $p_T$  bin are listed in Table 83. The Figure 61 shows the comparison of different cuts.

Table 83: Invariant Mass of  $\Lambda$  and  $\Xi$  Systematic Error of  $\bar{\Omega}^+$  at 19.6 GeV

$p_T$ bin (GeV/c)	Systematic Error
0.8-1.2	0.012118
1.2-1.6	0.01378
1.6-2.0	0.006688
2.0-2.4	0.01636
2.4-2.8	0.01272
2.8-3.6	0.03492

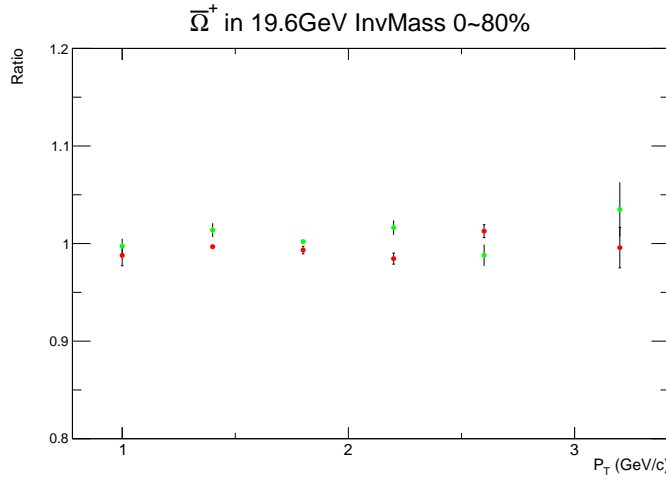


Figure 61: The comparison of cuts of  $\Lambda$  and  $\Xi$  invariant mass for  $\bar{\Omega}^+$  at 19.6 GeV.

**DCA of  $\Omega$  and  $\Lambda$  to PV** The cuts are in Table 84. The systematic errors for each  $p_T$  bin are listed in Table 85. The Figure 62 shows the comparison of

different cuts.

Table 84: DCA of  $\Omega$  and  $\Lambda$  Cut of  $\bar{\Omega}^+$  at 19.6 GeV

Default	$DCA_{\Omega}PV < 0.5 \text{ cm}$	$DCA_{\Lambda}PV > 0.4 \text{ cm}$
Red	$DCA_{\Omega}PV < 0.45 \text{ cm}$	$DCA_{\Lambda}PV > 0.45 \text{ cm}$
Green	$DCA_{\Omega}PV < 0.55 \text{ cm}$	$DCA_{\Lambda}PV > 0.35 \text{ cm}$

Table 85: DCA of  $\Omega$  and  $\Lambda$  Systematic Error of  $\bar{\Omega}^+$  at 19.6 GeV

$p_T$ bin (GeV/c)	Systematic Error
0.8-1.2	0.025128
1.2-1.6	0.036802
1.6-2.0	0.025672
2.0-2.4	0.016581
2.4-2.8	0.07778
2.8-3.6	0.058666

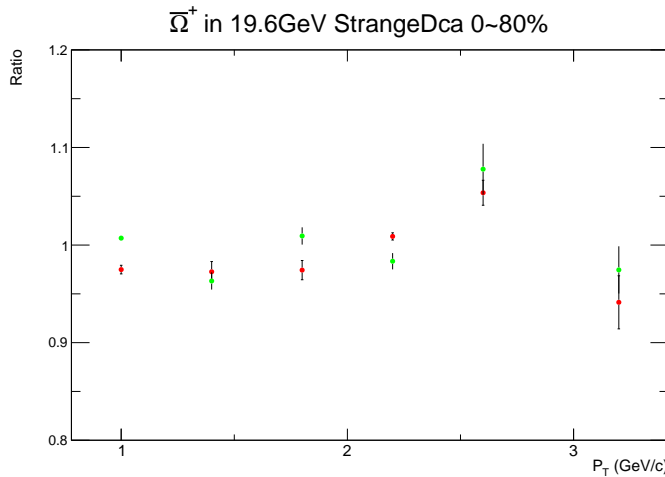


Figure 62: The comparison of DCA of  $\Omega$  and  $\Lambda$  cuts for  $\bar{\Omega}^+$  at 19.6 GeV.

**DCA of  $K_{\Lambda}$  and  $\pi_{-}$ proton** The cuts are in Table 86. The systematic errors for each  $p_T$  bin are listed in Table 87. The Figure 63 shows the comparison of different cuts.

Table 86: DCA of  $K_{\Lambda}$  and  $\pi$ -proton Cut of  $\bar{\Omega}^+$  at 19.6 GeV

Default	$DCA_{\pi\text{-proton}} < 0.7 \text{ cm}$	$DCA_{K_{\Lambda}} < 0.7 \text{ cm}$
Red	$DCA_{\pi\text{-proton}} < 0.6 \text{ cm}$	$DCA_{K_{\Lambda}} < 0.6 \text{ cm}$
Green	$DCA_{\pi\text{-proton}} < 0.8 \text{ cm}$	$DCA_{K_{\Lambda}} < 0.8 \text{ cm}$

Table 87: DCA of  $K_{\Lambda}$  and  $\pi$ -proton Systematic Error of  $\bar{\Omega}^+$  at 19.6 GeV

$p_T$ bin (GeV/c)	Systematic Error
0.8-1.2	0.02891
1.2-1.6	0.03586
1.6-2.0	0.00603
2.0-2.4	0.010782
2.4-2.8	0.04168
2.8-3.6	0.036583

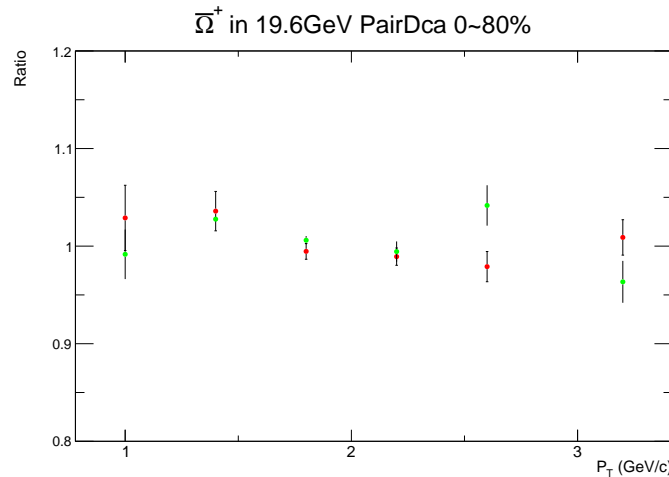


Figure 63: The comparison of DCA of  $K_{\Lambda}$  and  $\pi$ -proton cuts for  $\bar{\Omega}^+$  at 19.6 GeV.

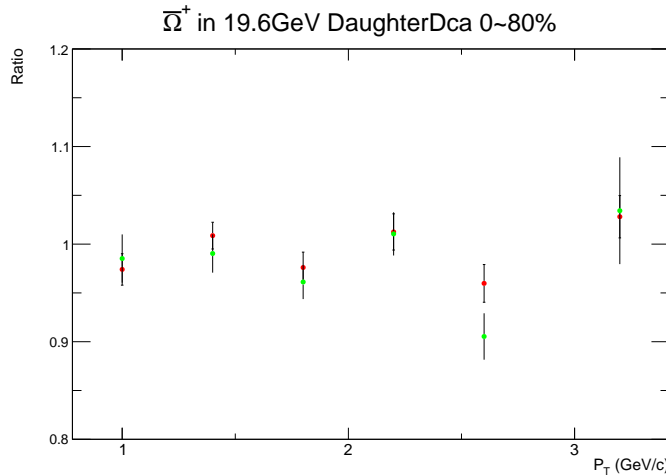
**DCA of Decay Daughters to PV** The cuts are in Table 88. The systematic errors for each  $p_T$  bin are listed in Table 89. The Figure 64 shows the comparison of different cuts.

Table 88: DCA of Decay Daughters to PV Cut of  $\bar{\Omega}^+$  at 19.6 GeV

Default	$DCA_{p\_PV} > 0.6 \text{ cm}$	$DCA_{\pi\_PV} > 2.0 \text{ cm}$	$DCA_{K\_PV} > 1.0 \text{ cm}$
Red	$DCA_{p\_PV} > 0.5 \text{ cm}$	$DCA_{\pi\_PV} > 1.6 \text{ cm}$	$DCA_{K\_PV} > 0.8 \text{ cm}$
Green	$DCA_{p\_PV} > 0.7 \text{ cm}$	$DCA_{\pi\_PV} > 2.4 \text{ cm}$	$DCA_{K\_PV} > 1.2 \text{ cm}$

 Table 89: DCA of Decay Daughters to PV Systematic Error of  $\bar{\Omega}^+$  at 19.6 GeV

$p_T$ bin (GeV/c)	Systematic Error
0.8-1.2	0.025929
1.2-1.6	0.009618
1.6-2.0	0.038783
2.0-2.4	0.01249
2.4-2.8	0.094549
2.8-3.6	0.03425


 Figure 64: The comparison of DCA of Decay Daughters to PV cuts for  $\bar{\Omega}^+$  at 19.6 GeV.

**Number of Track nHits** The cuts are in Table 90. The systematic errors for each  $p_T$  bin are listed in Table 91. The Figure 65 shows the comparison of different cuts.

Table 90: Number of Track nHits Cut of  $\bar{\Omega}^+$  at 19.6 GeV

Default	$nHits > 15$
Red	$nHits > 17$
Green	$nHits > 20$

Table 91: Number of Track nHits Systematic Error of  $\bar{\Omega}^+$  at 19.6 GeV

$p_T$ bin (GeV/c)	Systematic Error
0.8-1.2	0.02312
1.2-1.6	0.019288
1.6-2.0	0.059517
2.0-2.4	0.026215
2.4-2.8	0.029291
2.8-3.6	0.012019

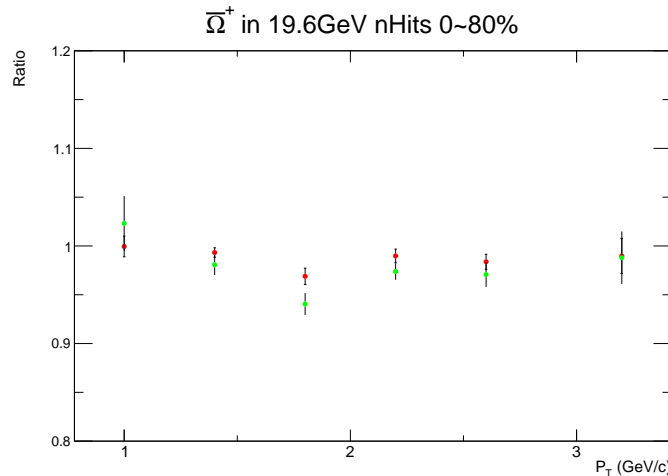


Figure 65: The comparison of Number of Track nHits cuts for  $\bar{\Omega}^+$  at 19.6 GeV.

**Signal Extraction** The cuts are in Table 92. The systematic errors for each  $p_T$  bin are listed in Table 93. The Figure 66 shows the comparison of different cuts.

Table 92: Mass Window of Signal Extraction of  $\bar{\Omega}^+$  at 19.6 GeV

Default	$(1.66-1.685) \text{ GeV}/c^2$
Red	$(1.6575-1.6875) \text{ GeV}/c^2$
Green	$(1.6625-1.6825) \text{ GeV}/c^2$

 Table 93: Mass Window of Signal Extraction Systematic Error of  $\bar{\Omega}^+$  at 19.6 GeV

$p_T$ bin (GeV/c)	Systematic Error			
	0-10%	10-20%	20-40%	40-60%
0.8-1.2	0.025447	0.10876	0.05473	0.040869
1.2-1.6	0.04507	0.02954	0.008301	0.05337
1.6-2.0	0.03605	0.02798	0.00872	0.03114
2.0-2.4	0.008988	0.053661	0.03037	0.01349
2.4-2.8	0.02558	0.05136	0.028053	0.09854
2.8-3.6	0.23117	0.03666	0.029143	0.00962

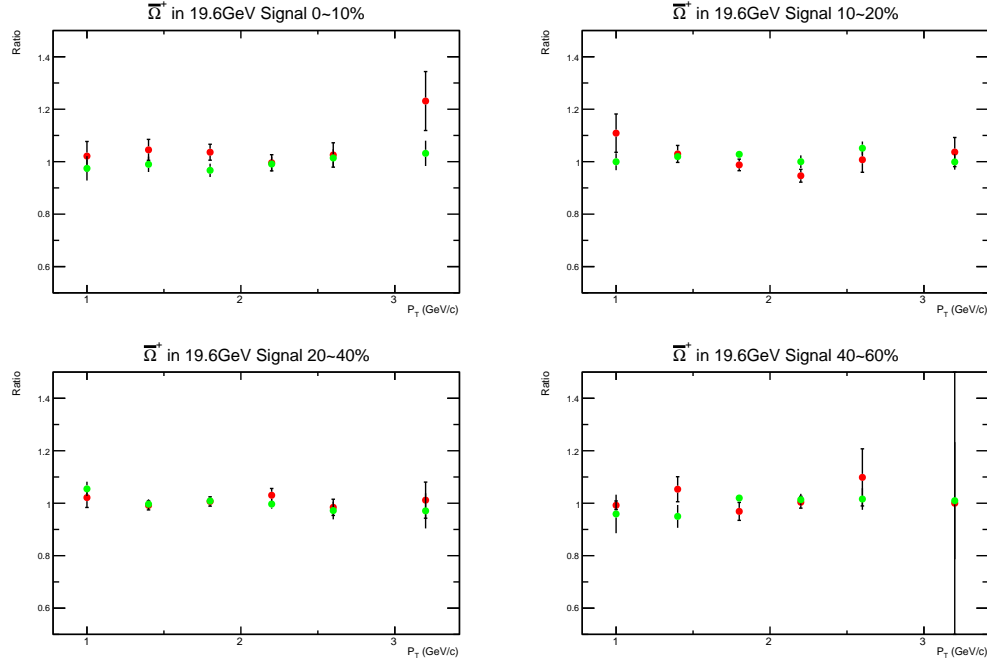


Figure 66: The comparison of Mass Window Cut of Signal Extraction for  $\bar{\Omega}^+$  at 19.6 GeV.

#### Overall Systematic Error from Reconstruction and Signal Extraction

The overall relative systematic error from the reconstruction efficiency and signal extraction is quadratically summed up for each  $p_T$  and centrality bin. The Table 94 shows you the systematic error for  $\bar{\Omega}^+$  at 219.6 GeV.

Table 94: The Overall Systematic Error of  $\bar{\Omega}^+$  at 19.6 GeV

$p_T$ bin (GeV/c)	Systematic Error			
	0-10%	10-20%	20-40%	40-60%
0.8-1.2	0.0697788	0.12669	0.0849523	0.0767581
1.2-1.6	0.0734181	0.0650501	0.0585475	0.0787862
1.6-2.0	0.0842059	0.0810797	0.0765968	0.0822237
2.0-2.4	0.0401016	0.0663842	0.0494944	0.0413441
2.4-2.8	0.136388	0.143476	0.136874	0.166306
2.8-3.6	0.246615	0.0933978	0.0907111	0.0864392

### 6.1.7 $\Omega^-$ at 11.5 GeV

The convenors of lfspectra group suggested to use high statistics 39 GeV data to study the systematic error of 11.5 GeV  $\Omega$  to reduce the statistical fluctuation, the convenors claim that the systematic error has little energy dependence due to previous analysis. Here, we use 39 GeV data and apply the same topological cuts as 11.5 GeV.

**Decay Length** The cuts are in Table 95. The systematic errors for each  $p_T$  bin are listed in Table 96. The Figure 67 shows the comparison of different cuts.

Table 95: Decay Length Cut of  $\Omega^-$  at 11.5 GeV

Default	$L_\Lambda > 5.0 \text{ cm}$	$L_\Omega > 3.0 \text{ cm}$
Red	$L_\Lambda > 4.5 \text{ cm}$	$L_\Omega > 2.5 \text{ cm}$
Green	$L_\Lambda > 5.5 \text{ cm}$	$L_\Omega > 3.5 \text{ cm}$

Table 96: Decay Length Systematic Error of  $\Omega^-$  at 11.5 GeV

$p_T$ bin (GeV/c)	Systematic Error
0.8-1.2	0.016194
1.2-1.6	0.0236
1.6-2.0	0.008695
2.0-2.4	0.006652
2.4-2.8	0.00361
2.8-3.6	0.00059

Table 97: Invariant Mass Cut of  $\Lambda$  and  $\Xi$  for  $\Omega^-$  at 11.5 GeV

Default	$ V0 - pdg  < 6 \text{ MeV}$	$ Xi - pdg  > 10 \text{ MeV}$
Red	$ V0 - pdg  < 5 \text{ MeV}$	$ Xi - pdg  > 12 \text{ MeV}$
Green	$ V0 - pdg  < 7 \text{ MeV}$	$ Xi - pdg  > 8 \text{ MeV}$

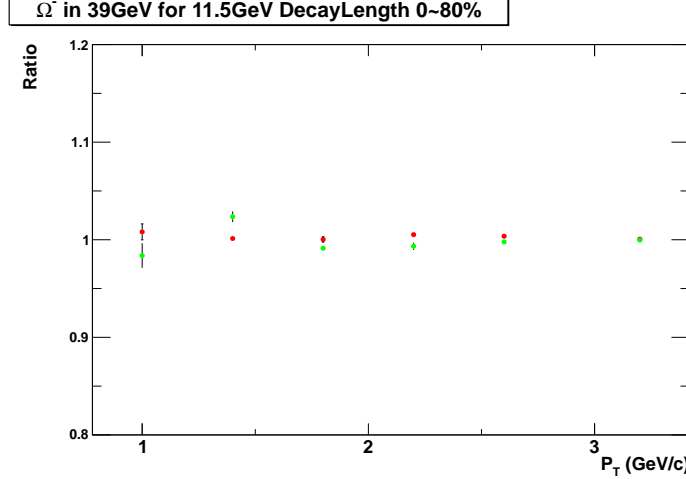


Figure 67: The comparison of Decay Length cuts for  $\Omega^-$  at 11.5 GeV.

**Invariant Mass of  $\Lambda$  and  $\Xi$**  The cuts are in Table 97. The systematic errors for each  $p_T$  bin are listed in Table 98. The Figure 68 shows the comparison of different cuts.

Table 98: Invariant Mass of  $\Lambda$  and  $\Xi$  Systematic Error of  $\Omega^-$  at 11.5 GeV

$p_T$ bin (GeV/c)	Systematic Error
0.8-1.2	0.00603
1.2-1.6	0.010566
1.6-2.0	0.005176
2.0-2.4	0.013054
2.4-2.8	0.00086
2.8-3.6	0.019656

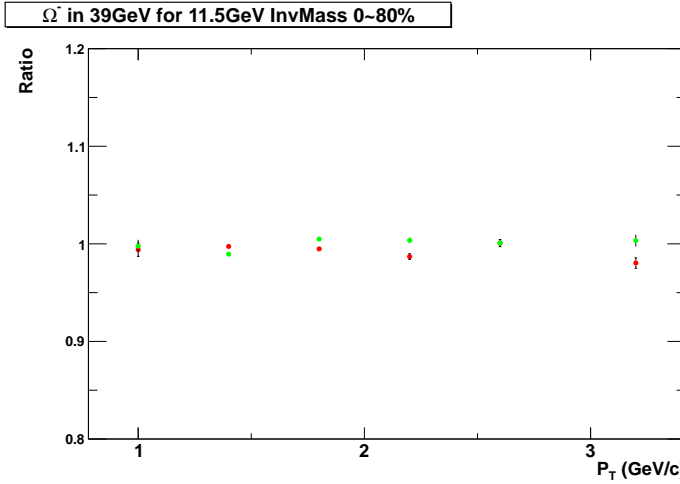


Figure 68: The comparison of cuts of  $\Lambda$  and  $\Xi$  invariant mass for  $\Omega^-$  at 11.5 GeV.

**DCA of  $\Omega$  and  $\Lambda$  to PV** The cuts are in Table 99. The systematic errors for each  $p_T$  bin are listed in Table 100. The Figure 69 shows the comparison of different cuts.

Table 99: DCA of  $\Omega$  and  $\Lambda$  Cut of  $\Omega^-$  at 11.5 GeV

Default	$DCA_{\Omega\_PV} < 0.4 \text{ cm}$	$DCA_{\Lambda\_PV} > 0.4 \text{ cm}$
Red	$DCA_{\Omega\_PV} < 0.35 \text{ cm}$	$DCA_{\Lambda\_PV} > 0.45 \text{ cm}$
Green	$DCA_{\Omega\_PV} < 0.45 \text{ cm}$	$DCA_{\Lambda\_PV} > 0.35 \text{ cm}$

Table 100: DCA of  $\Omega$  and  $\Lambda$  Systematic Error of  $\Omega^-$  at 11.5 GeV

$p_T$ bin (GeV/c)	Systematic Error
0.8-1.2	0.035675
1.2-1.6	0.01431
1.6-2.0	0.013501
2.0-2.4	0.02308
2.4-2.8	0.02073
2.8-3.6	0.01493

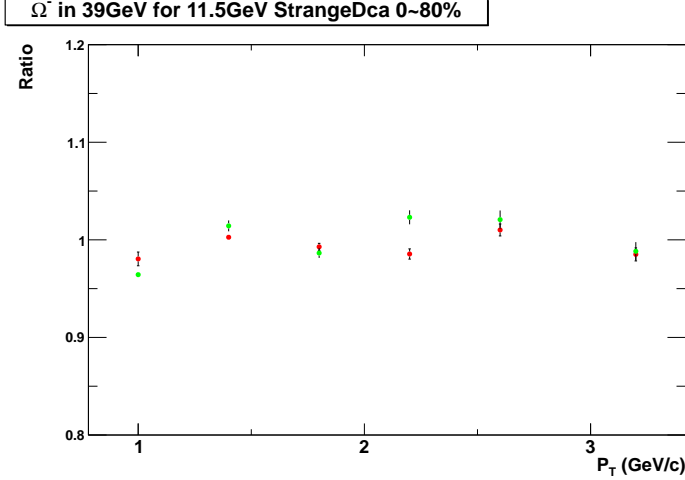


Figure 69: The comparison of DCA of  $\Omega$  and  $\Lambda$  cuts for  $\Omega^-$  at 11.5 GeV.

**DCA of  $K\Lambda$  and  $\pi$ -proton** The cuts are in Table 101. The systematic errors for each  $p_T$  bin are listed in Table 102. The Figure 70 shows the comparison of different cuts.

Table 101: DCA of  $K\Lambda$  and  $\pi$ -proton Cut of  $\Omega^-$  at 11.5 GeV

Default	$DCA_{\pi\text{-proton}} < 0.7 \text{ cm}$	$DCA_{K\Lambda} < 0.7 \text{ cm}$
Red	$DCA_{\pi\text{-proton}} < 0.6 \text{ cm}$	$DCA_{K\Lambda} < 0.6 \text{ cm}$
Green	$DCA_{\pi\text{-proton}} < 0.8 \text{ cm}$	$DCA_{K\Lambda} < 0.8 \text{ cm}$

Table 102: DCA of  $K\Lambda$  and  $\pi$ -proton Systematic Error of  $\Omega^-$  at 11.5 GeV

$p_T$ bin (GeV/c)	Systematic Error
0.8-1.2	0.013962
1.2-1.6	0.01824
1.6-2.0	0.018524
2.0-2.4	0.019504
2.4-2.8	0.00558
2.8-3.6	0.017397

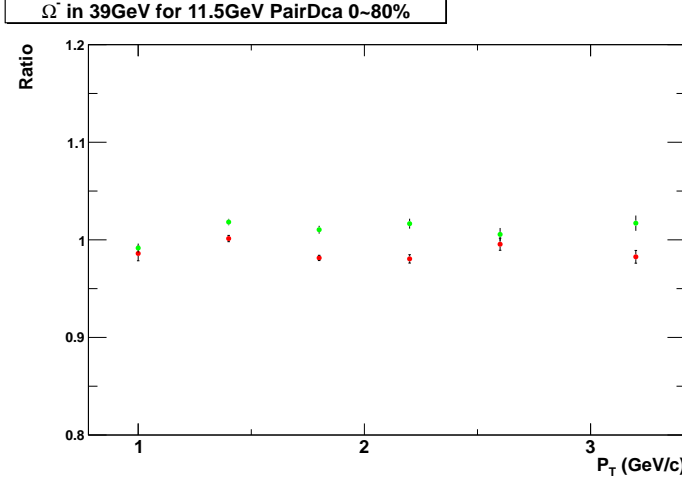


Figure 70: The comparison of DCA of  $K\Lambda$  and  $\pi$ -proton cuts for  $\Omega^-$  at 11.5 GeV.

**DCA of Decay Daughters to PV** The cuts are in Table 103. The systematic errors for each  $p_T$  bin are listed in Table 104. The Figure 71 shows the comparison of different cuts.

Table 103: DCA of Decay Daughters to PV Cut of  $\Omega^-$  at 11.5 GeV

Default	$DCA_{p\_PV} > 0.6 \text{ cm}$	$DCA_{\pi\_PV} > 2.0 \text{ cm}$	$DCA_{K\_PV} > 1.0 \text{ cm}$
Red	$DCA_{p\_PV} > 0.5 \text{ cm}$	$DCA_{\pi\_PV} > 1.6 \text{ cm}$	$DCA_{K\_PV} > 0.8 \text{ cm}$
Green	$DCA_{p\_PV} > 0.7 \text{ cm}$	$DCA_{\pi\_PV} > 2.4 \text{ cm}$	$DCA_{K\_PV} > 1.2 \text{ cm}$

Table 104: DCA of Decay Daughters to PV Systematic Error of  $\Omega^-$  at 11.5 GeV

$p_T$ bin (GeV/c)	Systematic Error
0.8-1.2	0.01041
1.2-1.6	0.0114
1.6-2.0	0.0151
2.0-2.4	0.01461
2.4-2.8	0.033462
2.8-3.6	0.03215

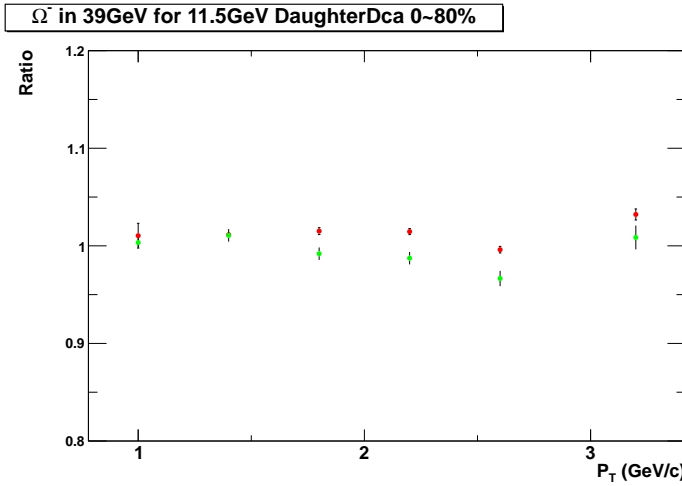


Figure 71: The comparison of DCA of Decay Daughters to PV cuts for  $\Omega^-$  at 11.5 GeV.

**Number of Track nHits** The cuts are in Table 105. The systematic errors for each  $p_T$  bin are listed in Table 106. The Figure 72 shows the comparison of different cuts.

Table 105: Number of Track nHits Cut of  $\Omega^-$  at 11.5 GeV

Default	$nHits > 15$
Red	$nHits > 17$
Green	$nHits > 20$

Table 106: Number of Track nHits Systematic Error of  $\Omega^-$  at 11.5 GeV

$p_T$ bin (GeV/c)	Systematic Error
0.8-1.2	0.028197
1.2-1.6	0.02209
1.6-2.0	0.032872
2.0-2.4	0.049027
2.4-2.8	0.044456
2.8-3.6	0.052363

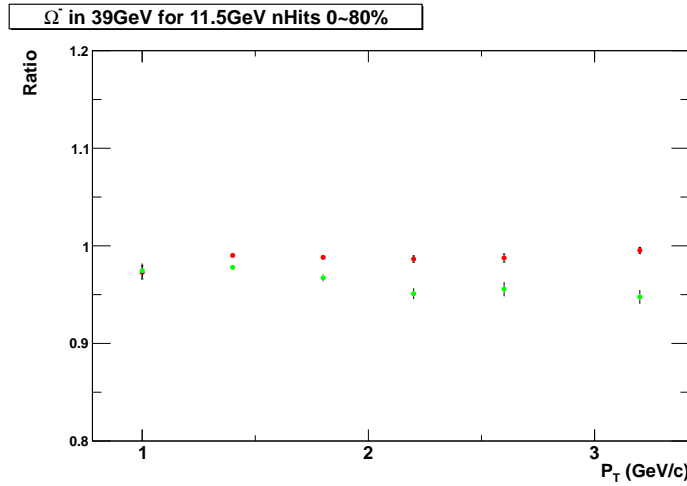


Figure 72: The comparison of Number of Track nHits cuts for  $\Omega^-$  at 11.5 GeV.

**Signal Extraction** The cuts are in Table 107. The systematic errors for each  $p_T$  bin are listed in Table 108. The Figure 73 shows the comparison of different cuts.

Table 107: Mass Window of Signal Extraction of  $\Omega^-$  at 11.5 GeV

Default	(1.66-1.685) $GeV/c^2$
Red	(1.6575-1.6875) $GeV/c^2$
Green	(1.6625-1.6825) $GeV/c^2$

Table 108: Mass Window of Signal Extraction Systematic Error of  $\Omega^-$  at 11.5 GeV

$p_T$ bin ( $GeV/c$ )	Systematic Error	
	0-10%	10-60%
0.8-1.2	0.12676	0.032673
1.2-1.6	0.05565	0.042044
1.6-2.0	0.04843	0.04816
2.0-2.4	0.06307	0.037842
2.4-2.8	0.05994	0.10092
2.8-3.6	0.12616	0.031665

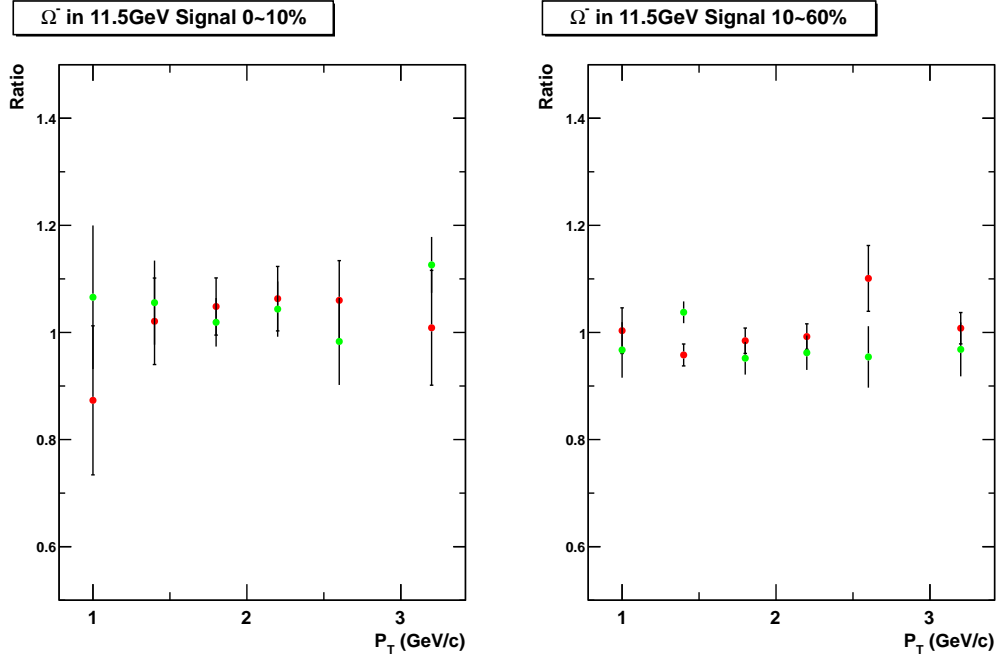


Figure 73: The comparison of Mass Window Cut of Signal Extraction for  $\Omega^-$  at 11.5 GeV.

#### Overall Systematic Error from Reconstruction and Signal Extraction

The overall relative systematic error from the reconstruction efficiency and signal extraction is quadratically summed up for each  $p_T$  and centrality bin. The Table 109 shows you the systematic error for  $\Omega^-$  at 11.5 GeV.

Table 109: The Overall Systematic Error of  $\Omega^-$  at 11.5 GeV

$p_T$ bin (GeV/c)	Systematic Error	
	0-10%	10-60%
0.8-1.2	0.136684	0.060678
1.2-1.6	0.0701493	0.0599308
1.6-2.0	0.0654359	0.0652363
2.0-2.4	0.0878787	0.0719504
2.4-2.8	0.0846374	0.117284
2.8-3.6	0.143541	0.075435

### 6.1.8 $\bar{\Omega}^+$ at 11.5 GeV

The convenors of lfspectra group suggested to use high statistics 39 GeV data to study the systematic error of 11.5 GeV  $\Omega$  to reduce the statistical fluctuation, the convenors claim that the systematic error has little energy dependence due to previous analysis. Here, we use 39 GeV data and apply the same topological cuts as 11.5 GeV.

**Decay Length** The cuts are in Table 110. The systematic errors for each  $p_T$  bin are listed in Table 111. The Figure 74 shows the comparison of different cuts.

Table 110: Decay Length Cut of  $\bar{\Omega}^+$  at 11.5 GeV

Default	$L_\Lambda > 4.0 \text{ cm}$	$L_\Omega > 2.0 \text{ cm}$
Red	$L_\Lambda > 3.5 \text{ cm}$	$L_\Omega > 1.5 \text{ cm}$
Green	$L_\Lambda > 4.5 \text{ cm}$	$L_\Omega > 2.5 \text{ cm}$

Table 111: Decay Length Systematic Error of  $\bar{\Omega}^+$  at 11.5 GeV

$p_T$ bin (GeV/c)	Systematic Error
0.8-1.2	0.03055
1.2-1.6	0.01036
1.6-2.0	0.00058
2.0-2.4	0.002021
2.4-2.8	0.000989
2.8-3.6	0

Table 112: Invariant Mass Cut of  $\Lambda$  and  $\Xi$  for  $\bar{\Omega}^+$  at 11.5 GeV

Default	$ V0 - pdg  < 6 \text{ MeV}$	$ Xi - pdg  > 10 \text{ MeV}$
Red	$ V0 - pdg  < 5 \text{ MeV}$	$ Xi - pdg  > 12 \text{ MeV}$
Green	$ V0 - pdg  < 7 \text{ MeV}$	$ Xi - pdg  > 8 \text{ MeV}$

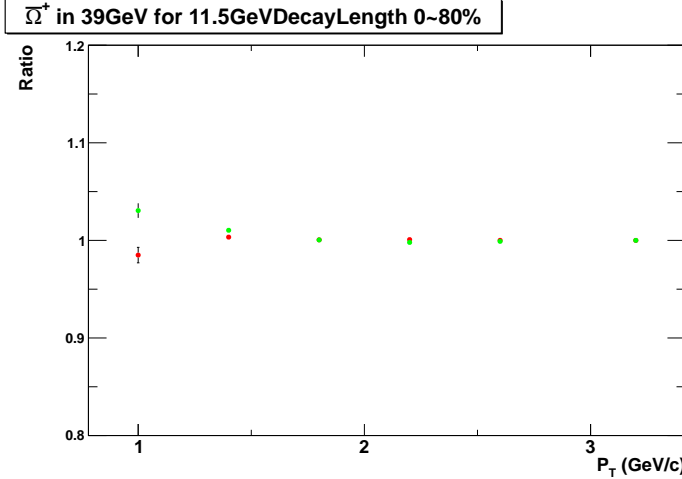


Figure 74: The comparison of Decay Length cuts for  $\bar{\Omega}^+$  at 11.5 GeV.

**Invariant Mass of  $\Lambda$  and  $\Xi$**  The cuts are in Table 112. The systematic errors for each  $p_T$  bin are listed in Table 113. The Figure 75 shows the comparison of different cuts.

Table 113: Invariant Mass of  $\Lambda$  and  $\Xi$  Systematic Error of  $\bar{\Omega}^+$  at 11.5 GeV

$p_T$ bin (GeV/c)	Systematic Error
0.8-1.2	0.00589
1.2-1.6	0.010276
1.6-2.0	0.00682
2.0-2.4	0.013057
2.4-2.8	0.017681
2.8-3.6	0.004586

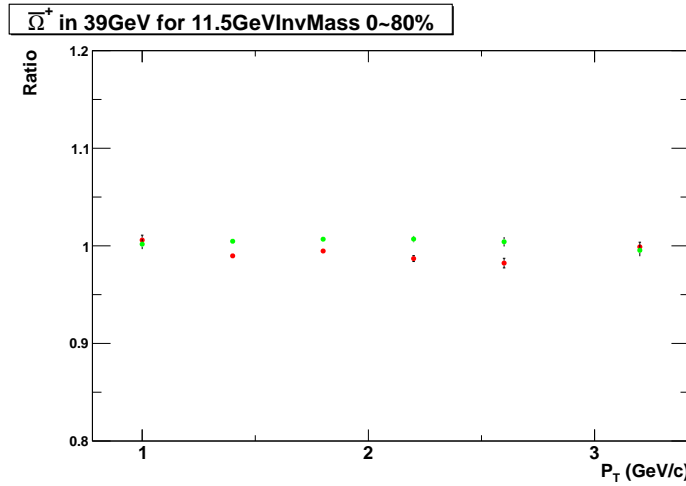


Figure 75: The comparison of cuts of  $\Lambda$  and  $\Xi$  invariant mass for  $\bar{\Omega}^+$  at 11.5 GeV.

**DCA of  $\Omega$  and  $\Lambda$  to PV** The cuts are in Table 114. The systematic errors for each  $p_T$  bin are listed in Table 115. The Figure 76 shows the comparison of different cuts.

Table 114: DCA of  $\Omega$  and  $\Lambda$  Cut of  $\bar{\Omega}^+$  at 11.5 GeV

Default	$DCA_{\Omega\_PV} < 0.4 \text{ cm}$	$DCA_{\Lambda\_PV} > 0.4 \text{ cm}$
Red	$DCA_{\Omega\_PV} < 0.35 \text{ cm}$	$DCA_{\Lambda\_PV} > 0.45 \text{ cm}$
Green	$DCA_{\Omega\_PV} < 0.45 \text{ cm}$	$DCA_{\Lambda\_PV} > 0.35 \text{ cm}$

Table 115: DCA of  $\Omega$  and  $\Lambda$  Systematic Error of  $\bar{\Omega}^+$  at 11.5 GeV

$p_T$ bin (GeV/c)	Systematic Error
0.8-1.2	0.0273
1.2-1.6	0.008209
1.6-2.0	0.00918
2.0-2.4	0.03039
2.4-2.8	0.0607
2.8-3.6	0.05306

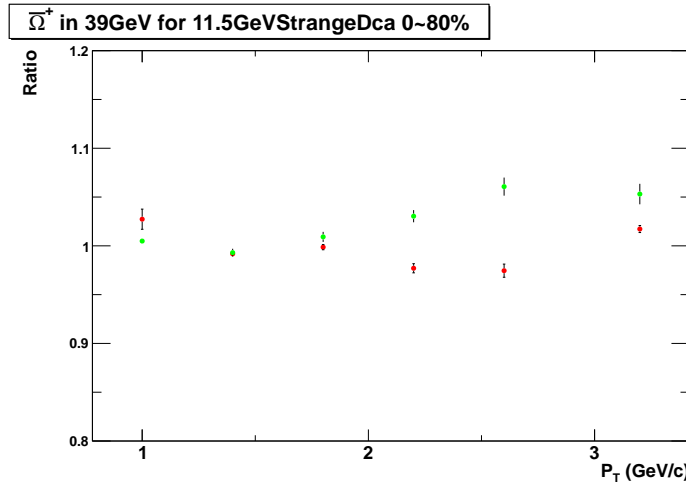


Figure 76: The comparison of DCA of  $\Omega$  and  $\Lambda$  cuts for  $\bar{\Omega}^+$  at 11.5 GeV.

**DCA of  $K\Lambda$  and  $\pi$ -proton** The cuts are in Table 116. The systematic errors for each  $p_T$  bin are listed in Table 117. The Figure 77 shows the comparison of different cuts.

Table 116: DCA of  $K\Lambda$  and  $\pi$ -proton Cut of  $\bar{\Omega}^+$  at 11.5 GeV

Default	$DCA_{\pi\text{-proton}} < 0.7 \text{ cm}$	$DCA_{K\Lambda} < 0.7 \text{ cm}$
Red	$DCA_{\pi\text{-proton}} < 0.6 \text{ cm}$	$DCA_{K\Lambda} < 0.6 \text{ cm}$
Green	$DCA_{\pi\text{-proton}} < 0.8 \text{ cm}$	$DCA_{K\Lambda} < 0.8 \text{ cm}$

Table 117: DCA of  $K\Lambda$  and  $\pi$ -proton Systematic Error of  $\bar{\Omega}^+$  at 11.5 GeV

$p_T$ bin (GeV/c)	Systematic Error
0.8-1.2	0.042829
1.2-1.6	0.00741
1.6-2.0	0.008478
2.0-2.4	0.01989
2.4-2.8	0.00341
2.8-3.6	0.02545

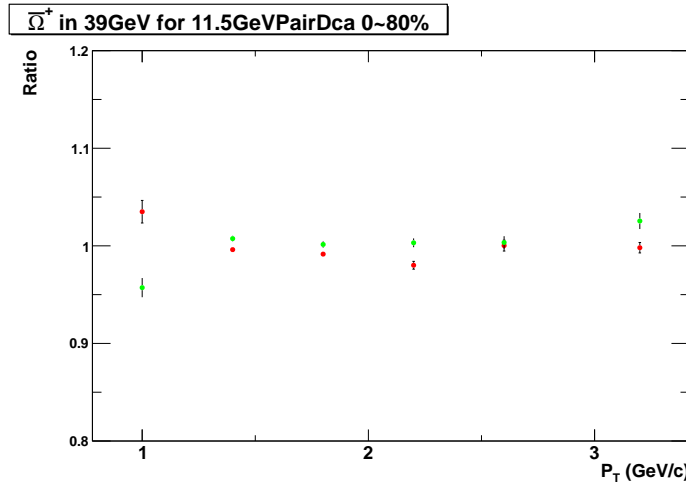


Figure 77: The comparison of DCA of  $K_{\Lambda}$  and  $\pi_{proton}$  cuts for  $\bar{\Omega}^+$  at 11.5 GeV.

**DCA of Decay Daughters to PV** The cuts are in Table 118. The systematic errors for each  $p_T$  bin are listed in Table 119. The Figure 78 shows the comparison of different cuts.

Table 118: DCA of Decay Daughters to PV Cut of  $\bar{\Omega}^+$  at 11.5 GeV

Default	$DCA.p\_PV > 0.6 \text{ cm}$	$DCA.\pi\_PV > 2.0 \text{ cm}$	$DCA.K\_PV > 1.0 \text{ cm}$
Red	$DCA.p\_PV > 0.5 \text{ cm}$	$DCA.\pi\_PV > 1.6 \text{ cm}$	$DCA.K\_PV > 0.8 \text{ cm}$
Green	$DCA.p\_PV > 0.7 \text{ cm}$	$DCA.\pi\_PV > 2.4 \text{ cm}$	$DCA.K\_PV > 1.2 \text{ cm}$

Table 119: DCA of Decay Daughters to PV Systematic Error of  $\bar{\Omega}^+$  at 11.5 GeV

$p_T$ bin (GeV/c)	Systematic Error
0.8-1.2	0.04711
1.2-1.6	0.006062
1.6-2.0	0.01862
2.0-2.4	0.0265
2.4-2.8	0.06116
2.8-3.6	0.01544

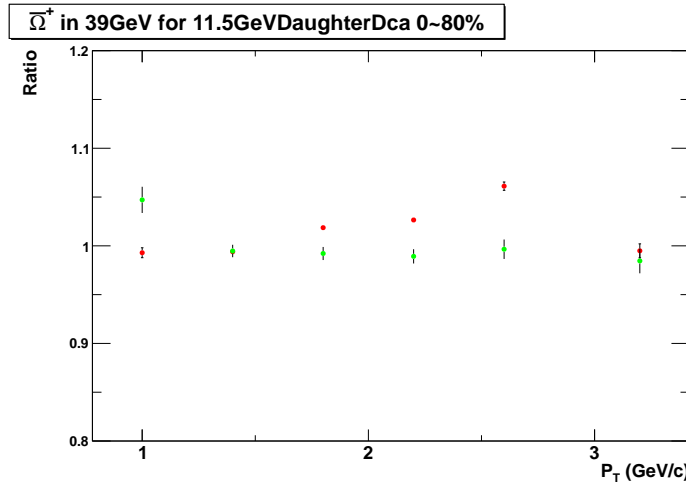


Figure 78: The comparison of DCA of Decay Daughters to PV cuts for  $\bar{\Omega}^+$  at 11.5 GeV.

**Number of Track nHits** The cuts are in Table 120. The systematic errors for each  $p_T$  bin are listed in Table 121. The Figure 79 shows the comparison of different cuts.

Table 120: Number of Track nHits Cut of  $\bar{\Omega}^+$  at 11.5 GeV

Default	$nHits > 15$
Red	$nHits > 17$
Green	$nHits > 20$

Table 121: Number of Track nHits Systematic Error of  $\bar{\Omega}^+$  at 11.5 GeV

$p_T$ bin (GeV/c)	Systematic Error
0.8-1.2	0.012981
1.2-1.6	0.028563
1.6-2.0	0.03302
2.0-2.4	0.040974
2.4-2.8	0.04773
2.8-3.6	0.019662

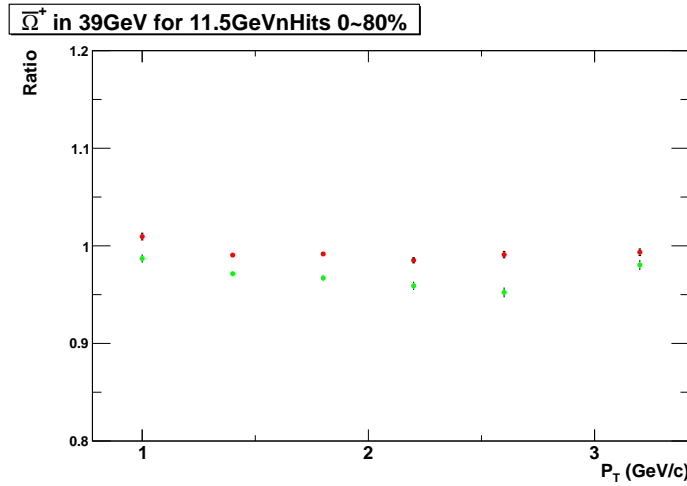


Figure 79: The comparison of Number of Track nHits cuts for  $\bar{\Omega}^+$  at 11.5 GeV.

**Signal Extraction** The cuts are in Table 122. The systematic errors for each  $p_T$  bin are listed in Table 123. The Figure 80 shows the comparison of different cuts.

Table 122: Mass Window of Signal Extraction of  $\bar{\Omega}^+$  at 11.5 GeV

Default	(1.66-1.685) $GeV/c^2$
Red	(1.6575-1.6875) $GeV/c^2$
Green	(1.6625-1.6825) $GeV/c^2$

Table 123: Mass Window of Signal Extraction Systematic Error of  $\bar{\Omega}^+$  at 11.5 GeV

$p_T$ bin ( $GeV/c$ )	Systematic Error	
	0-10%	10-60%
0.8-1.2	0.14563	0.174722
1.2-1.6	0.10756	0.0802877
1.6-2.0	0.03757	0.0392907
2.0-2.4	0.04661	0.0253192
2.4-2.8	0.032421	0.0584237
2.8-3.6	0.15264	0.0946911

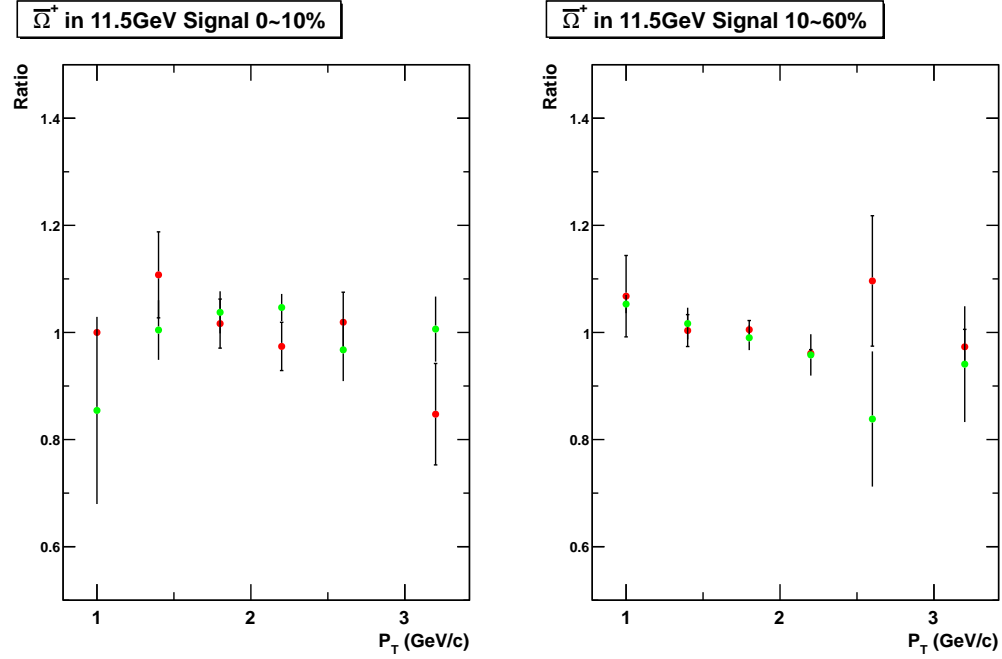


Figure 80: The comparison of Mass Window Cut of Signal Extraction for  $\bar{\Omega}^+$  at 11.5 GeV.

#### Overall Systematic Error from Reconstruction and Signal Extraction

The overall relative systematic error from the reconstruction efficiency and signal extraction is quadratically summed up for each  $p_T$  and centrality bin. The Table 124 shows you the systematic error for  $\bar{\Omega}^+$  at 11.5 GeV.

Table 124: The Overall Systematic Error of  $\bar{\Omega}^+$  at 11.5 GeV

$p_T$ bin (GeV/c)	Systematic Error	
	0-10%	10-60%
0.8-1.2	0.164753	0.102581
1.2-1.6	0.112947	0.0382454
1.6-2.0	0.0552406	0.0416916
2.0-2.4	0.077766	0.0750618
2.4-2.8	0.105259	0.190114
2.8-3.6	0.165554	0.0872499

### 6.1.9 $\Omega^-$ at 7.7 GeV

**Decay Length** The cuts are in Table 125. The systematic errors for each  $p_T$  bin are listed in Table 126. The Figure 81 shows the comparison of different cuts.

Table 125: Decay Length Cut of  $\Omega^-$  at 7.7 GeV

Default	$L_\Lambda > 4.0 \text{ cm}$	$L_\Omega > 2.0 \text{ cm}$
Red	$L_\Lambda > 3.5 \text{ cm}$	$L_\Omega > 1.5 \text{ cm}$
Green	$L_\Lambda > 4.5 \text{ cm}$	$L_\Omega > 2.5 \text{ cm}$

Table 126: Decay Length Systematic Error of  $\Omega^-$  at 7.7 GeV

$p_T$ bin (GeV/c)	Systematic Error
0.7-1.3	0.020857
1.3-1.6	0.00249
1.6-2.0	0.00651
2.0-2.5	0.001949

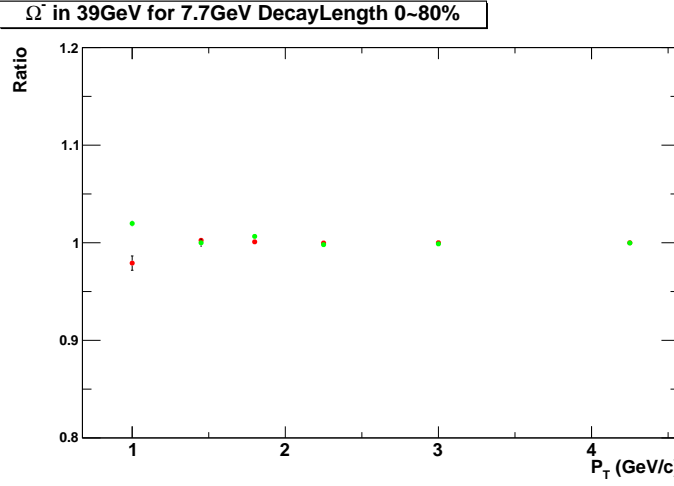


Figure 81: The comparison of Decay Length cuts for  $\Omega^-$  at 7.7 GeV.

**Invariant Mass of  $\Lambda$  and  $\Xi$**  The cuts are in Table 127. The systematic errors for each  $p_T$  bin are listed in Table 128. The Figure 82 shows the comparison of

Table 127: Invariant Mass Cut of  $\Lambda$  and  $\Xi$  for  $\Omega^-$  at 7.7 GeV

Default	$ V0 - pdg  < 6 \text{ MeV}$	$ Xi - pdg  > 10 \text{ MeV}$
Red	$ V0 - pdg  < 5 \text{ MeV}$	$ Xi - pdg  > 12 \text{ MeV}$
Green	$ V0 - pdg  < 7 \text{ MeV}$	$ Xi - pdg  > 8 \text{ MeV}$

different cuts.

Table 128: Invariant Mass of  $\Lambda$  and  $\Xi$  Systematic Error of  $\Omega^-$  at 7.7 GeV

$p_T$ bin (GeV/c)	Systematic Error
0.7-1.3	0.005732
1.3-1.6	0.009546
1.6-2.0	0.006814
2.0-2.5	0.009514

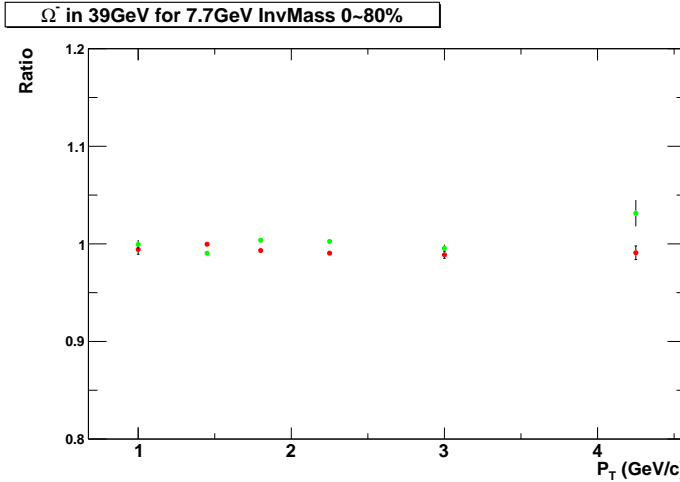


Figure 82: The comparison of cuts of  $\Lambda$  and  $\Xi$  invariant mass for  $\Omega^-$  at 7.7 GeV.

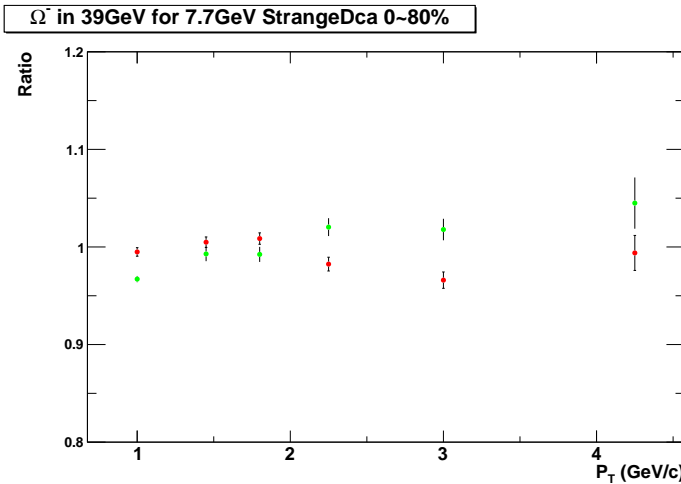
**DCA of  $\Omega$  and  $\Lambda$  to PV** The cuts are in Table 129. The systematic errors for each  $p_T$  bin are listed in Table 130. The Figure 83 shows the comparison of different cuts.

Table 129: DCA of  $\Omega$  and  $\Lambda$  Cut of  $\Omega^-$  at 7.7 GeV

Default	$DCA_{\Omega}PV < 0.4 \text{ cm}$	$DCA_{\Lambda}PV > 0.3 \text{ cm}$
Red	$DCA_{\Omega}PV < 0.35 \text{ cm}$	$DCA_{\Lambda}PV > 0.35 \text{ cm}$
Green	$DCA_{\Omega}PV < 0.45 \text{ cm}$	$DCA_{\Lambda}PV > 0.25 \text{ cm}$

 Table 130: DCA of  $\Omega$  and  $\Lambda$  Systematic Error of  $\Omega^-$  at 7.7 GeV

$p_T$ bin (GeV/c)	Systematic Error
0.7-1.3	0.032905
1.3-1.6	0.007137
1.6-2.0	0.00861
2.0-2.5	0.02033


 Figure 83: The comparison of DCA of  $\Omega$  and  $\Lambda$  cuts for  $\Omega^-$  at 7.7 GeV.

**DCA of  $K$ - $\Lambda$  and  $\pi$ -proton** The cuts are in Table 131. The systematic errors for each  $p_T$  bin are listed in Table 132. The Figure 84 shows the comparison of different cuts.

Table 131: DCA of  $K\Lambda$  and  $\pi$ -proton Cut of  $\Omega^-$  at 7.7 GeV

Default	$DCA_{\pi\text{-proton}} < 0.7 \text{ cm}$	$DCA_{K\Lambda} < 0.7 \text{ cm}$
Red	$DCA_{\pi\text{-proton}} < 0.6 \text{ cm}$	$DCA_{K\Lambda} < 0.6 \text{ cm}$
Green	$DCA_{\pi\text{-proton}} < 0.8 \text{ cm}$	$DCA_{K\Lambda} < 0.8 \text{ cm}$

Table 132: DCA of  $K\Lambda$  and  $\pi$ -proton Systematic Error of  $\Omega^-$  at 7.7 GeV

$p_T$ bin (GeV/c)	Systematic Error
0.7-1.3	0.026765
1.3-1.6	0.01433
1.6-2.0	0.01425
2.0-2.5	0.02479

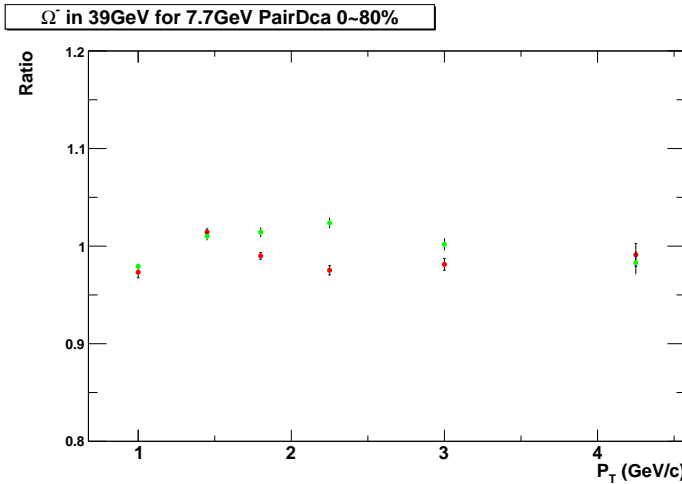


Figure 84: The comparison of DCA of  $K\Lambda$  and  $\pi$ -proton cuts for  $\Omega^-$  at 7.7 GeV.

**DCA of Decay Daughters to PV** The cuts are in Table 133. The systematic errors for each  $p_T$  bin are listed in Table 134. The Figure 85 shows the comparison of different cuts.

Table 133: DCA of Decay Daughters to PV Cut of  $\Omega^-$  at 7.7 GeV

Default	$DCA_p_{-}PV > 0.6\text{ cm}$	$DCA_{\pi_{-}}PV > 2.0\text{ cm}$	$DCA_{K_{-}}PV > 1.0\text{ cm}$
Red	$DCA_p_{-}PV > 0.5\text{ cm}$	$DCA_{\pi_{-}}PV > 1.6\text{ cm}$	$DCA_{K_{-}}PV > 0.8\text{ cm}$
Green	$DCA_p_{-}PV > 0.7\text{ cm}$	$DCA_{\pi_{-}}PV > 2.4\text{ cm}$	$DCA_{K_{-}}PV > 1.2\text{ cm}$

Table 134: DCA of Decay Daughters to PV Systematic Error of  $\Omega^-$  at 7.7 GeV

$p_T$ bin (GeV/c)	Systematic Error
0.7-1.3	0.00811
1.3-1.6	0.0115
1.6-2.0	0.02061
2.0-2.5	0.028222

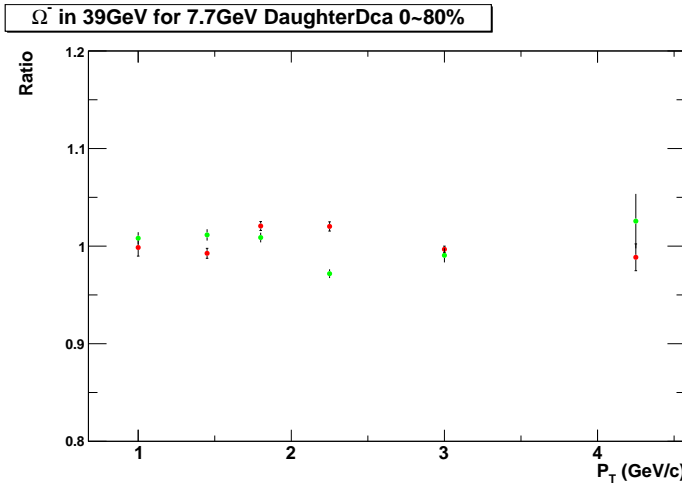


Figure 85: The comparison of DCA of Decay Daughters to PV cuts for  $\Omega^-$  at 7.7 GeV.

**Number of Track nHits** The cuts are in Table 135. The systematic errors for each  $p_T$  bin are listed in Table 136. The Figure 86 shows the comparison of different cuts.

Table 135: Number of Track nHits Cut of  $\Omega^-$  at 7.7 GeV

Default	$nHits > 15$
Red	$nHits > 17$
Green	$nHits > 20$

Table 136: Number of Track nHits Systematic Error of  $\Omega^-$  at 7.7 GeV

$p_T$ bin (GeV/c)	Systematic Error
0.7-1.3	0.02478
1.3-1.6	0.047808
1.6-2.0	0.032029
2.0-2.5	0.052546

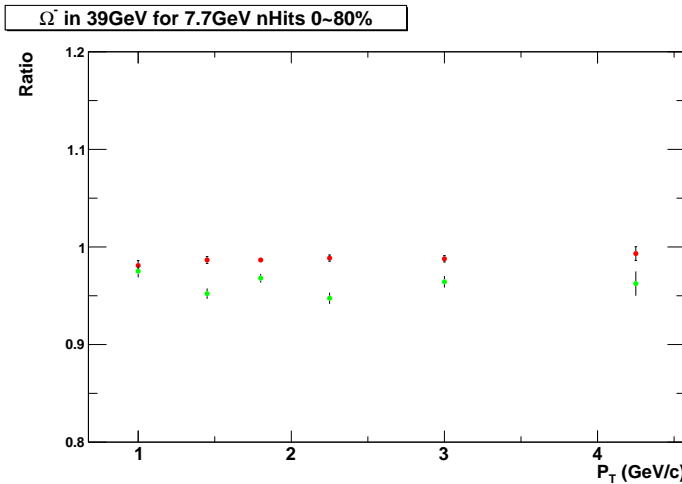


Figure 86: The comparison of Number of Track nHits cuts for  $\Omega^-$  at 7.7 GeV.

**Signal Extraction** The cuts are in Table 137. The systematic errors for each  $p_T$  bin are listed in Table 138. The Figure 87 shows the comparison of different cuts.

Table 137: Mass Window of Signal Extraction of  $\Omega^-$  at 7.7 GeV

Default	$(1.66-1.685) \text{ GeV}/c^2$
Red	$(1.6575-1.6875) \text{ GeV}/c^2$
Green	$(1.6625-1.6825) \text{ GeV}/c^2$

Table 138: Mass Window of Signal Extraction Systematic Error of  $\Omega^-$  at 7.7 GeV

$p_T$ bin ( $\text{GeV}/c$ )	Systematic Error
0.7-1.3	0.10626
1.3-1.6	0.16337
1.6-2.0	0.105058
2.0-2.5	0.14266

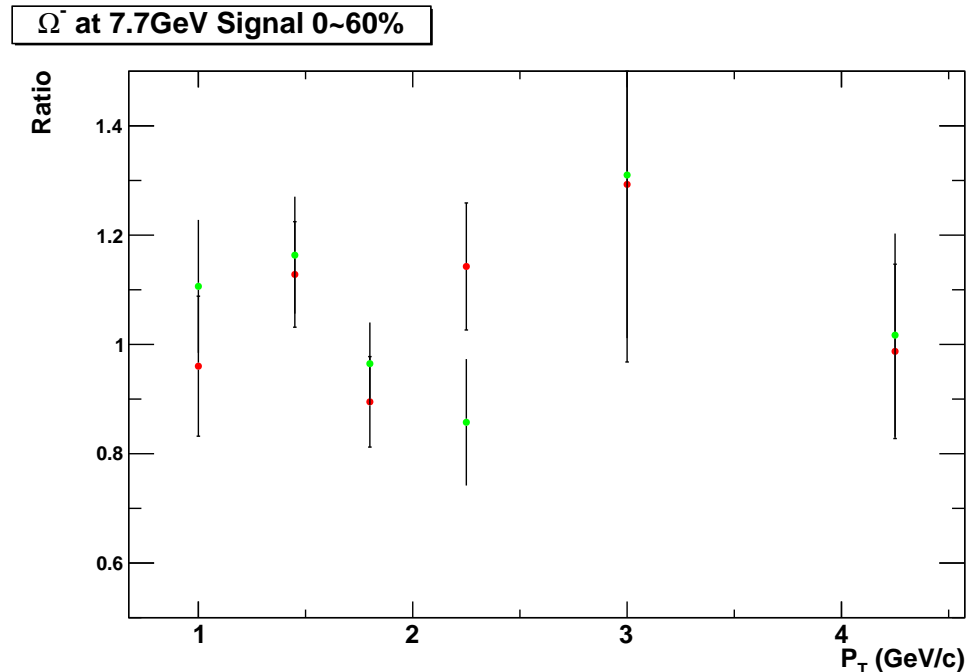


Figure 87: The comparison of Mass Window Cut of Signal Extraction for  $\Omega^-$  at 7.7 GeV.

### Overall Systematic Error from Reconstruction and Signal Extraction

The overall relative systematic error from the reconstruction efficiency and signal extraction is quadratically summed up for each  $p_T$  and centrality bin. The Table 139 shows you the systematic error for  $\Omega^-$  at 7.7 GeV.

Table 139: The Overall Systematic Error of  $\Omega^-$  at 7.7 GeV

$p_T$ bin (GeV/c)	Systematic Error
0.7-1.3	0.119323
1.3-1.6	0.171643
1.6-2.0	0.113375
2.0-2.5	0.158214

### 6.1.10 $\bar{\Omega}^+$ at 7.7 GeV

**Decay Length** The cuts are in Table 140. The systematic errors for each  $p_T$  bin are listed in Table 141. The Figure 88 shows the comparison of different cuts.

Table 140: Decay Length Cut of  $\bar{\Omega}^+$  at 7.7 GeV

Default	$L_\Lambda > 4.0 \text{ cm}$	$L_\Omega > 2.0 \text{ cm}$
Red	$L_\Lambda > 3.5 \text{ cm}$	$L_\Omega > 1.5 \text{ cm}$
Green	$L_\Lambda > 4.5 \text{ cm}$	$L_\Omega > 2.5 \text{ cm}$

Table 141: Decay Length Systematic Error of  $\bar{\Omega}^+$  at 7.7 GeV

$p_T$ bin (GeV/c)	Systematic Error
0.7-1.3	0.03014
1.3-1.6	0.001414
1.6-2.0	0.002902
2.0-2.5	0.002221

Table 142: Invariant Mass Cut of  $\Lambda$  and  $\Xi$  for  $\bar{\Omega}^+$  at 7.7 GeV

Default	$ V0 - pdg  < 6 \text{ MeV}$	$ Xi - pdg  > 10 \text{ MeV}$
Red	$ V0 - pdg  < 5 \text{ MeV}$	$ Xi - pdg  > 12 \text{ MeV}$
Green	$ V0 - pdg  < 7 \text{ MeV}$	$ Xi - pdg  > 8 \text{ MeV}$

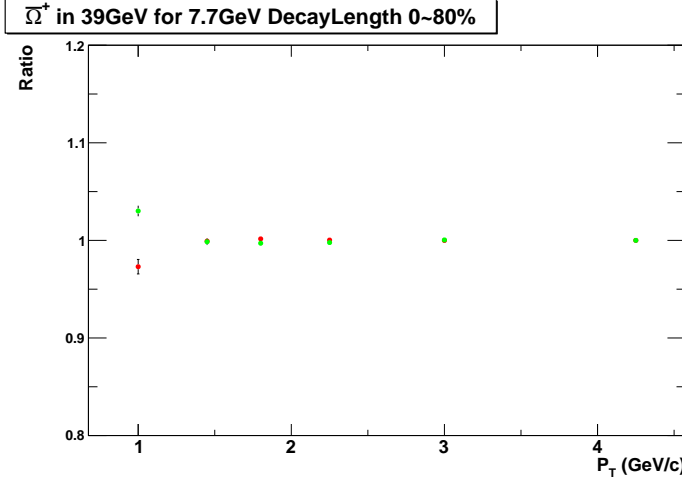


Figure 88: The comparison of Decay Length cuts for  $\bar{\Omega}^+$  at 7.7 GeV.

**Invariant Mass of  $\Lambda$  and  $\Xi$**  The cuts are in Table 142. The systematic errors for each  $p_T$  bin are listed in Table 143. The Figure 89 shows the comparison of different cuts.

Table 143: Invariant Mass of  $\Lambda$  and  $\Xi$  Systematic Error of  $\bar{\Omega}^+$  at 7.7 GeV

$p_T$ bin (GeV/c)	Systematic Error
0.7-1.3	0.00264
1.3-1.6	0.013716
1.6-2.0	0.014679
2.0-2.5	0.029149

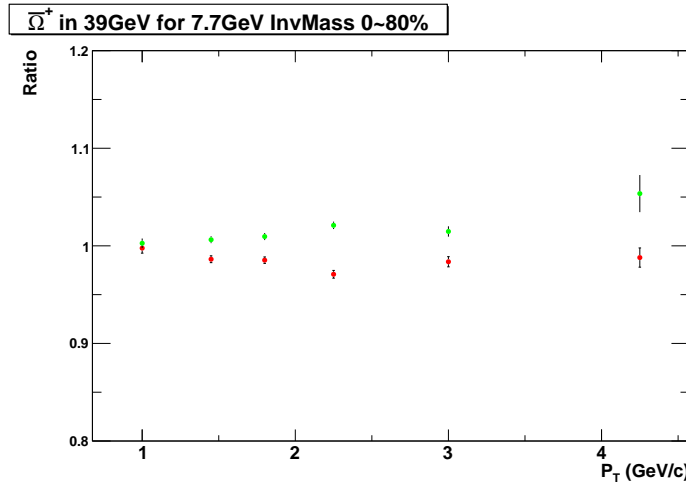


Figure 89: The comparison of cuts of  $\Lambda$  and  $\Xi$  invariant mass for  $\bar{\Omega}^+$  at 7.7 GeV.

**DCA of  $\Omega$  and  $\Lambda$  to PV** The cuts are in Table 144. The systematic errors for each  $p_T$  bin are listed in Table 145. The Figure 90 shows the comparison of different cuts.

Table 144: DCA of  $\Omega$  and  $\Lambda$  Cut of  $\bar{\Omega}^+$  at 7.7 GeV

Default	$DCA_{\Omega\_PV} < 0.6 \text{ cm}$	$DCA_{\Lambda\_PV} > 0.3 \text{ cm}$
Red	$DCA_{\Omega\_PV} < 0.55 \text{ cm}$	$DCA_{\Lambda\_PV} > 0.35 \text{ cm}$
Green	$DCA_{\Omega\_PV} < 0.65 \text{ cm}$	$DCA_{\Lambda\_PV} > 0.25 \text{ cm}$

Table 145: DCA of  $\Omega$  and  $\Lambda$  Systematic Error of  $\bar{\Omega}^+$  at 7.7 GeV

$p_T$ bin (GeV/c)	Systematic Error
0.7-1.3	0.00946
1.3-1.6	0.00739
1.6-2.0	0.02477
2.0-2.5	0.02222

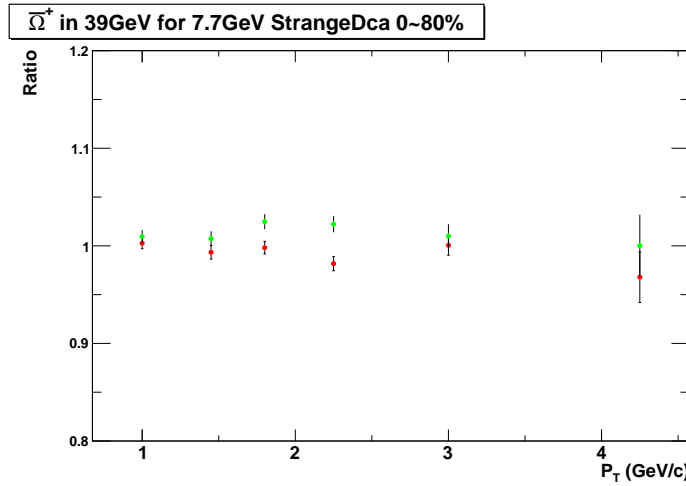


Figure 90: The comparison of DCA of  $\Omega$  and  $\Lambda$  cuts for  $\bar{\Omega}^+$  at 7.7 GeV.

**DCA of  $K\Lambda$  and  $\pi$ -proton** The cuts are in Table 146. The systematic errors for each  $p_T$  bin are listed in Table 147. The Figure 91 shows the comparison of different cuts.

Table 146: DCA of  $K\Lambda$  and  $\pi$ -proton Cut of  $\bar{\Omega}^+$  at 7.7 GeV

Default	$DCA_{\pi\text{-proton}} < 1.0 \text{ cm}$	$DCA_{K\Lambda} < 1.0 \text{ cm}$
Red	$DCA_{\pi\text{-proton}} < 0.9 \text{ cm}$	$DCA_{K\Lambda} < 0.9 \text{ cm}$
Green	$DCA_{\pi\text{-proton}} < 0.8 \text{ cm}$	$DCA_{K\Lambda} < 0.8 \text{ cm}$

Table 147: DCA of  $K\Lambda$  and  $\pi$ -proton Systematic Error of  $\bar{\Omega}^+$  at 7.7 GeV

$p_T$ bin (GeV/c)	Systematic Error
0.7-1.3	0.01109
1.3-1.6	0.01313
1.6-2.0	0.01606
2.0-2.5	0.021541

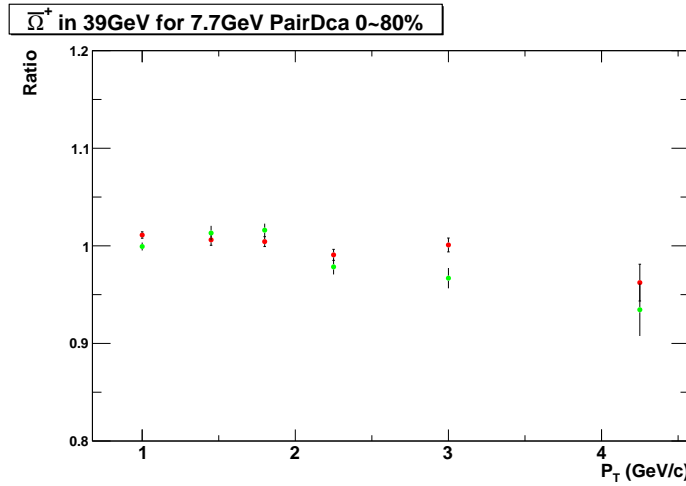


Figure 91: The comparison of DCA of  $K\Lambda$  and  $\pi$ -proton cuts for  $\bar{\Omega}^+$  at 7.7 GeV.

**DCA of Decay Daughters to PV** The cuts are in Table 148. The systematic errors for each  $p_T$  bin are listed in Table 149. The Figure 92 shows the comparison of different cuts.

Table 148: DCA of Decay Daughters to PV Cut of  $\bar{\Omega}^+$  at 7.7 GeV

Default	$DCA_{p-PV} > 0.6 \text{ cm}$	$DCA_{\pi-PV} > 2.0 \text{ cm}$	$DCA_{K-PV} > 1.0 \text{ cm}$
Red	$DCA_{p-PV} > 0.5 \text{ cm}$	$DCA_{\pi-PV} > 1.6 \text{ cm}$	$DCA_{K-PV} > 0.8 \text{ cm}$
Green	$DCA_{p-PV} > 0.7 \text{ cm}$	$DCA_{\pi-PV} > 2.4 \text{ cm}$	$DCA_{K-PV} > 1.2 \text{ cm}$

Table 149: DCA of Decay Daughters to PV Systematic Error of  $\bar{\Omega}^+$  at 7.7 GeV

$p_T$ bin (GeV/c)	Systematic Error
0.7-1.3	0.03156
1.3-1.6	0.02503
1.6-2.0	0.04119
2.0-2.5	0.04197

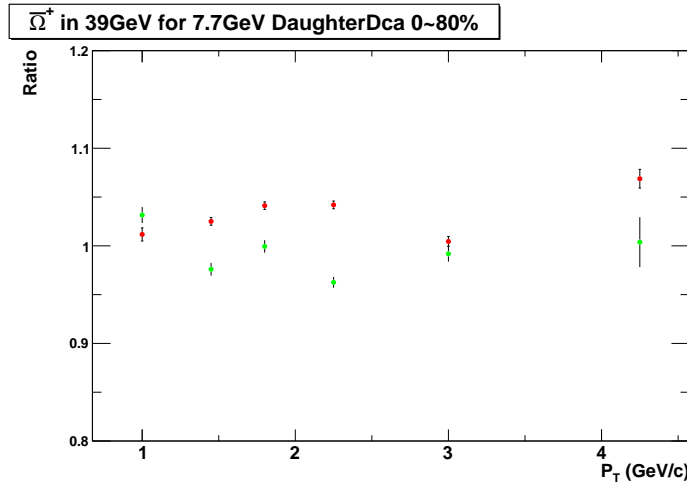


Figure 92: The comparison of DCA of Decay Daughters to PV cuts for  $\bar{\Omega}^+$  at 7.7 GeV.

**Number of Track nHits** The cuts are in Table 150. The systematic errors for each  $p_T$  bin are listed in Table 151. The Figure 93 shows the comparison of different cuts.

Table 150: Number of Track nHits Cut of  $\bar{\Omega}^+$  at 7.7 GeV

Default	$nHits > 15$
Red	$nHits > 17$
Green	$nHits > 20$

Table 151: Number of Track nHits Systematic Error of  $\bar{\Omega}^+$  at 7.7 GeV

$p_T$ bin (GeV/c)	Systematic Error
0.7-1.3	0.019744
1.3-1.6	0.033282
1.6-2.0	0.041227
2.0-2.5	0.04491

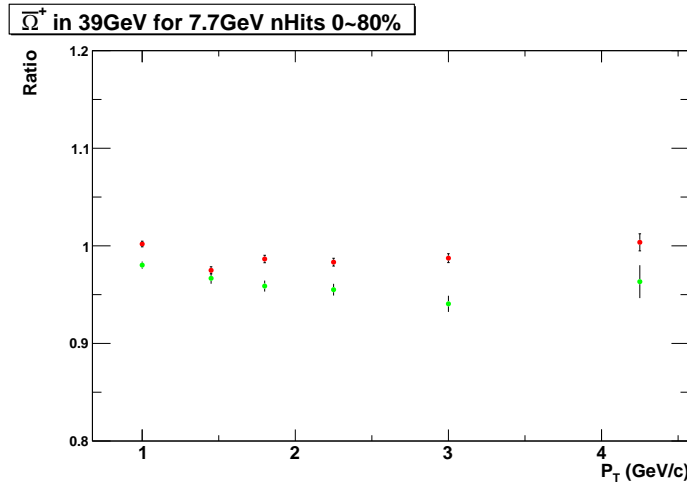


Figure 93: The comparison of Number of Track nHits cuts for  $\bar{\Omega}^+$  at 7.7 GeV.

**Signal Extraction** The cuts are in Table 152. The systematic errors for each  $p_T$  bin are listed in Table 153. The Figure 94 shows the comparison of different cuts.

Table 152: Mass Window of Signal Extraction of  $\bar{\Omega}^+$  at 7.7 GeV

Default	(1.66-1.685) $GeV/c^2$
Red	(1.6575-1.6875) $GeV/c^2$
Green	(1.6625-1.6825) $GeV/c^2$

Table 153: Mass Window of Signal Extraction Systematic Error of  $\bar{\Omega}^+$  at 7.7 GeV

$p_T$ bin ( $GeV/c$ )	Systematic Error
0.7-1.3	0.00168
1.3-1.6	0.09764
1.6-2.0	0.09189
2.0-2.5	0.4648

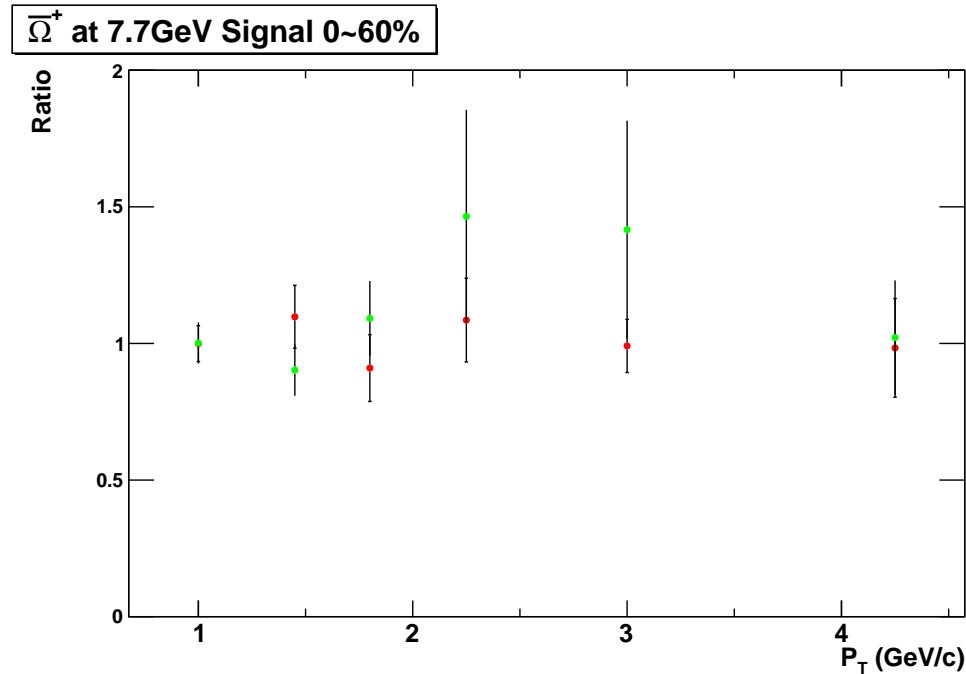


Figure 94: The comparison of Mass Window Cut of Signal Extraction for  $\bar{\Omega}^+$  at 7.7 GeV.

#### Overall Systematic Error from Reconstruction and Signal Extraction

The overall relative systematic error from the reconstruction efficiency and signal extraction is quadratically summed up for each  $p_T$  and centrality bin. The Table 154 shows you the systematic error for  $\bar{\Omega}^+$  at 7.7 GeV.

Table 154: The Overall Systematic Error of  $\bar{\Omega}^+$  at 7.7 GeV

$p_T$ bin (GeV/c)	Systematic Error
0.7-1.3	0.0501652
1.3-1.6	0.108097
1.6-2.0	0.113734
2.0-2.5	0.470786

## 6.2 Systematic Error of Unmeasured $p_T$ Range

The unmeasured  $p_T$  range of  $dN/dy$  is estimated by fitting function. We use Levy function as default fitting function to fit the  $p_T$  spectra, and integrated the function with unmeasured  $p_T$  range. We also use exponential function and Boltzmann function to fit spectra, and estimate  $dN/dy$  of unmeasured  $p_T$  range. We use the larger difference among the Levy, exponential and Boltzmann functions as the systematic error of the  $dN/dy$  of unmeasured  $p_T$  range. The statistical error of this part is difficult to estimate, we use the statistical error of the fitting  $dN/dy$  and quadratically subtract the statistical errors of  $dN/dy$  of measured range to get the statistical error of unmeasured  $p_T$  range. So in the end, when we calculate the  $dN/dy$  of full  $p_T$  range, the statistical error is the statistical error of the fitting parameter. So in this subsection, when we list the value of unmeasured  $dN/dy$ , we don't include the statistical error.

### 6.2.1 $\Omega^-$ at 39 GeV

The Figure 95 to 97 show you the fitting with Levy, Boltzmann and exponential functions. The Table 155 lists the value and systematic error of  $dN/dy$  of unmeasured  $p_T$  range.

Table 155: The  $dN/dy$  of Unmeasured  $p_T$  range of  $\Omega^-$  at 39 GeV

Centrality	Value	Systematic Error
0-5%	0.0809533	0.0065681
5-10%	0.0661111	0.0054094
10-20%	0.0425409	0.0031771
20-40%	0.0212926	0.0014578
40-60%	0.00511629	0.00033321
60-80%	0.00128558	6.475e-05

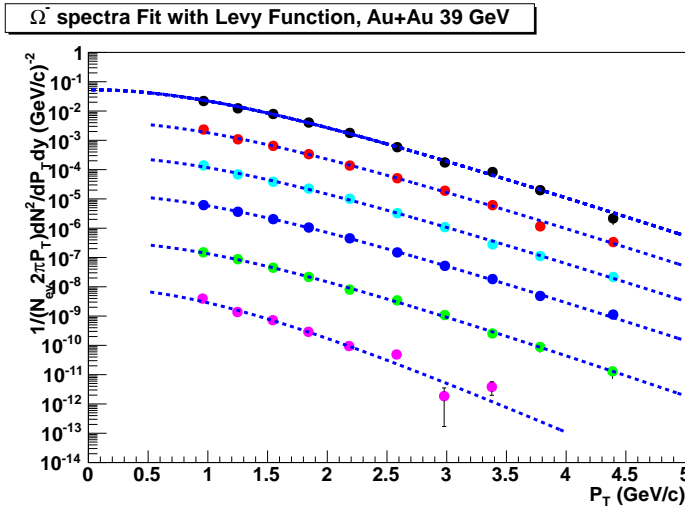


Figure 95: The Levy function fit of  $\Omega^-$  at 39 GeV.

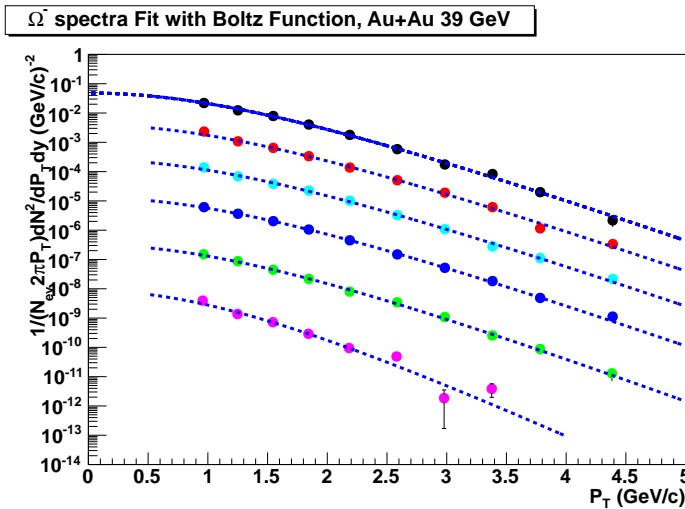


Figure 96: The Boltzmann function fit of  $\Omega^-$  at 39 GeV.

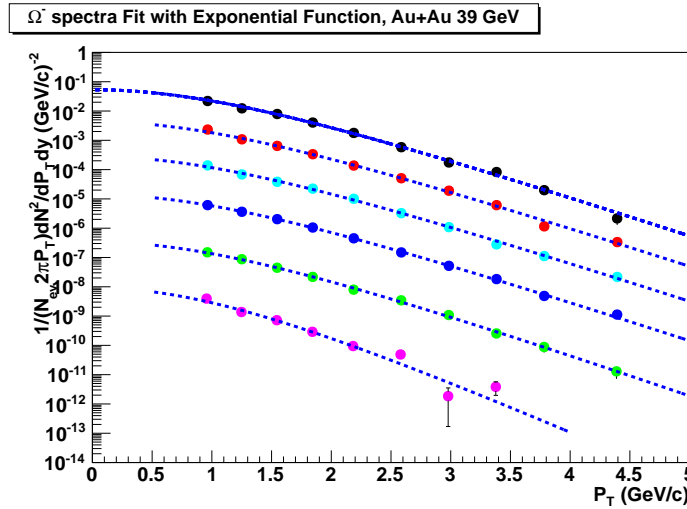


Figure 97: The Exponential function fit of  $\Omega^-$  at 39 GeV.

### 6.2.2 $\bar{\Omega}^+$ at 39 GeV

The Figure 98 to 100 show you the fitting with Levy, Boltzmann and exponential functions. The Table 156 lists the value and systematic error of  $dN/dy$  of unmeasured  $p_T$  range.

Table 156: The  $dN/dy$  of Unmeasured  $p_T$  range of  $\bar{\Omega}^+$  at 39 GeV

Centrality	Value	Systematic Error
0-5%	0.0667619	0.0051368
5-10%	0.0431551	0.0033206
10-20%	0.0322048	0.0023984
20-40%	0.0168927	0.0011435
40-60%	0.00415007	0.00023488
60-80%	0.000973871	6.8065e-05

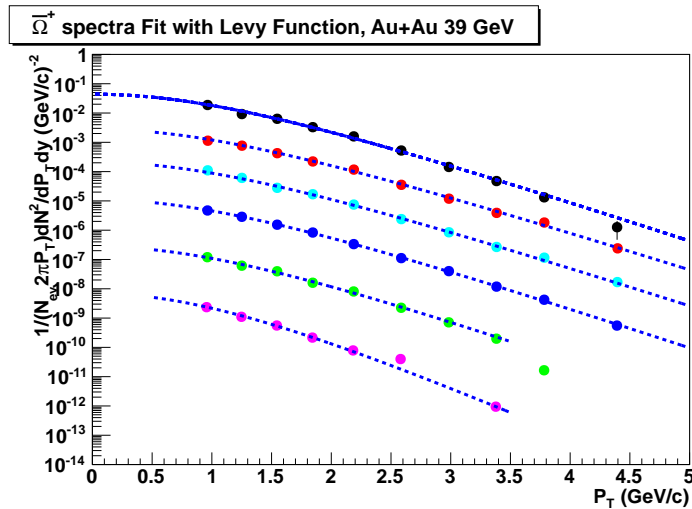


Figure 98: The Levy function fit of  $\bar{\Omega}^+$  at 39 GeV.

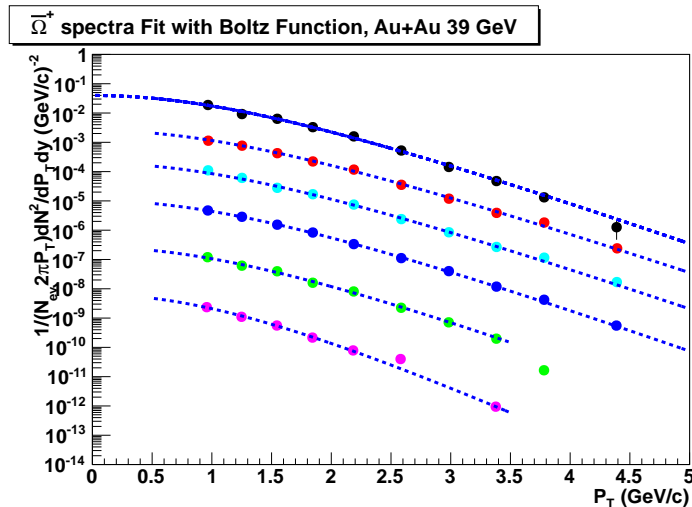


Figure 99: The Boltzmann function fit of  $\bar{\Omega}^+$  at 39 GeV.

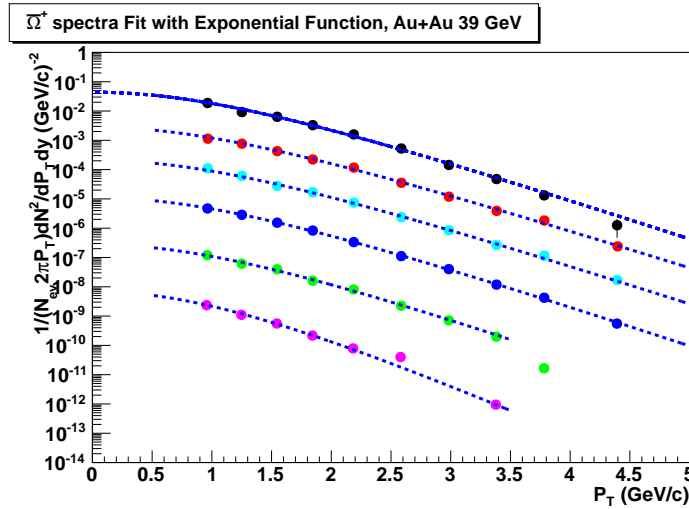


Figure 100: The Exponential function fit of  $\bar{\Omega}^+$  at 39 GeV.

### 6.2.3 $\Omega^-$ at 27 GeV

The Figure 101 to 103 show you the fitting with Levy, Boltzmann and exponential functions. The Table 157 lists the value and systematic error of  $dN/dy$  of unmeasured  $p_T$  range.

Table 157: The  $dN/dy$  of Unmeasured  $p_T$  range of  $\Omega^-$  at 27 GeV

Centrality	Value	Systematic Error
0-10%	0.0644382	0.0038771
10-20%	0.0439063	0.0028131
20-40%	0.0178705	0.001022
40-60%	0.00596206	0.00031885

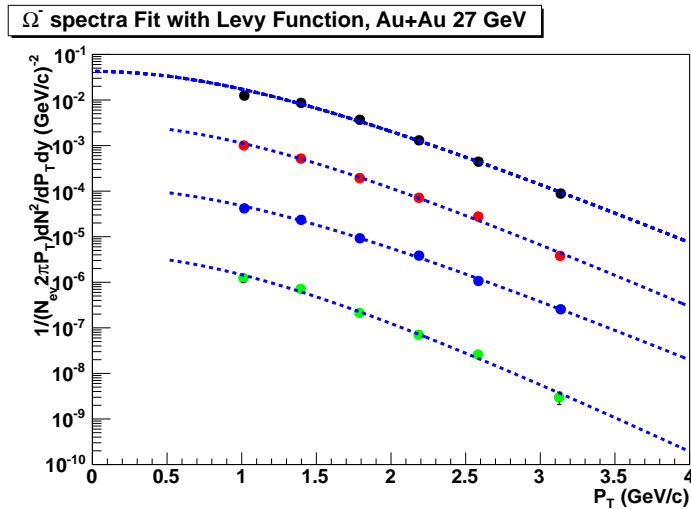


Figure 101: The Levy function fit of  $\Omega^-$  at 27 GeV.

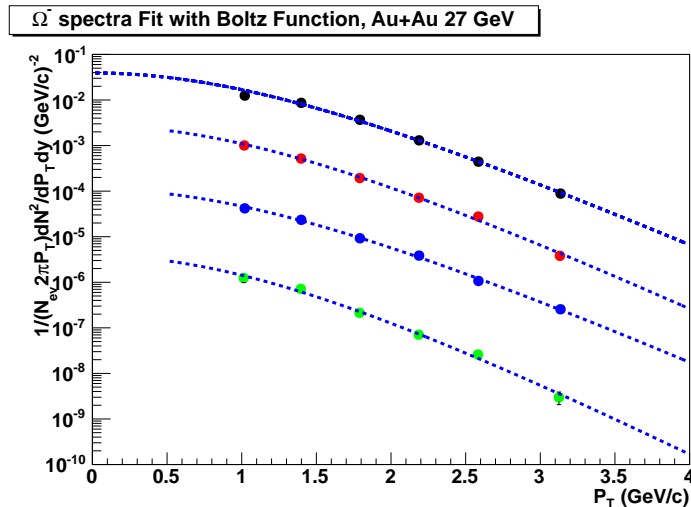


Figure 102: The Boltzmann function fit of  $\Omega^-$  at 27 GeV.

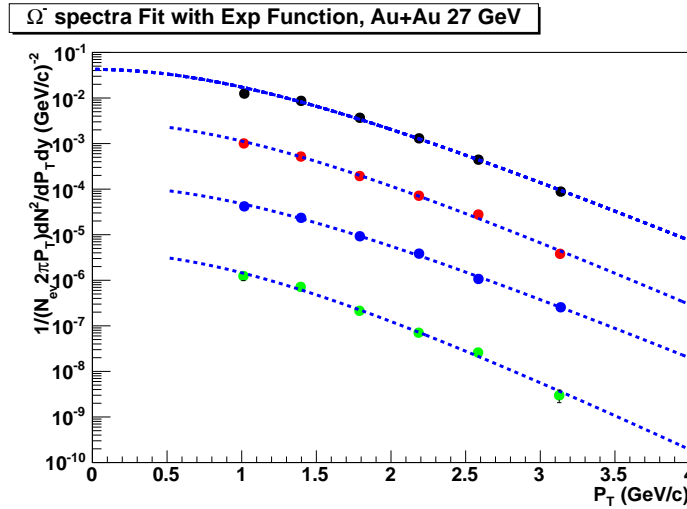


Figure 103: The Exponential function fit of  $\Omega^-$  at 27 GeV.

#### 6.2.4 $\bar{\Omega}^+$ at 27 GeV

The Figure 104 to 106 show you the fitting with Levy, Boltzmann and exponential functions. The Table 158 lists the value and systematic error of  $dN/dy$  of unmeasured  $p_T$  range.

Table 158: The  $dN/dy$  of Unmeasured  $p_T$  range of  $\bar{\Omega}^+$  at 27 GeV

Centrality	Value	Systematic Error
0-10%	0.0384045	0.0023232
10-20%	0.0245941	0.0013687
20-40%	0.0137972	0.000826
40-60%	0.00499526	0.00024549

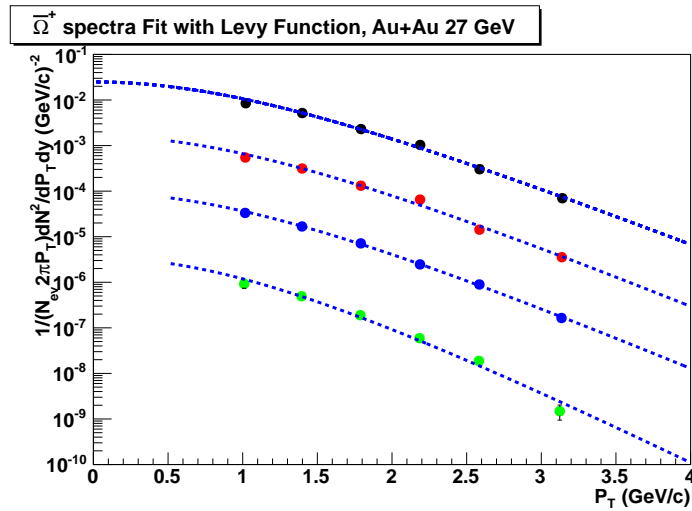


Figure 104: The Levy function fit of  $\bar{\Omega}^+$  at 27 GeV.

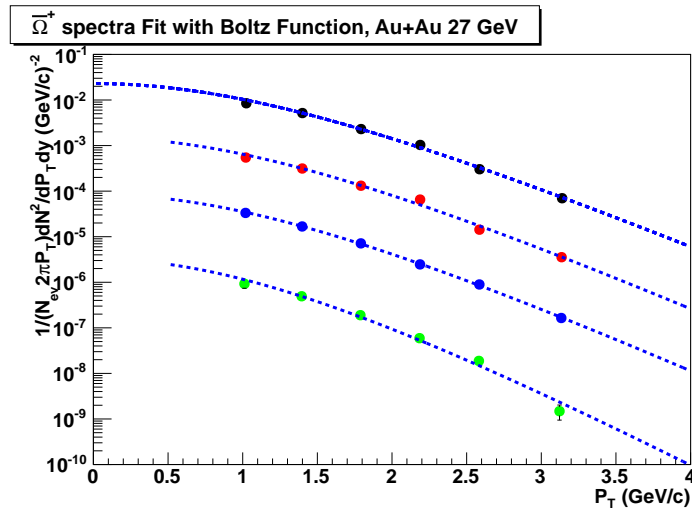


Figure 105: The Boltzmann function fit of  $\bar{\Omega}^+$  at 27 GeV.

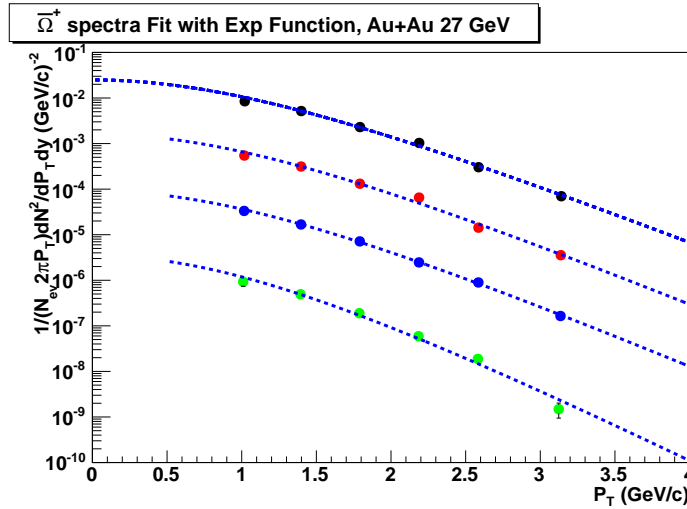


Figure 106: The Exponential function fit of  $\bar{\Omega}^+$  at 27 GeV.

### 6.2.5 $\Omega^-$ at 19.6 GeV

The Figure 107 to 109 show you the fitting with Levy, Boltzmann and exponential functions. The Table 159 lists the value and systematic error of  $dN/dy$  of unmeasured  $p_T$  range.

Table 159: The  $dN/dy$  of Unmeasured  $p_T$  range of  $\Omega^-$  at 19.6 GeV

Centrality	Value	Systematic Error
0-10%	0.0692283	0.009108
10-20%	0.0419856	0.0022503
20-40%	0.0205487	0.0024544
40-60%	0.00510458	0.00107262

$\Omega^-$  spectra Fit with Levy Function, Au+Au 19.6 GeV

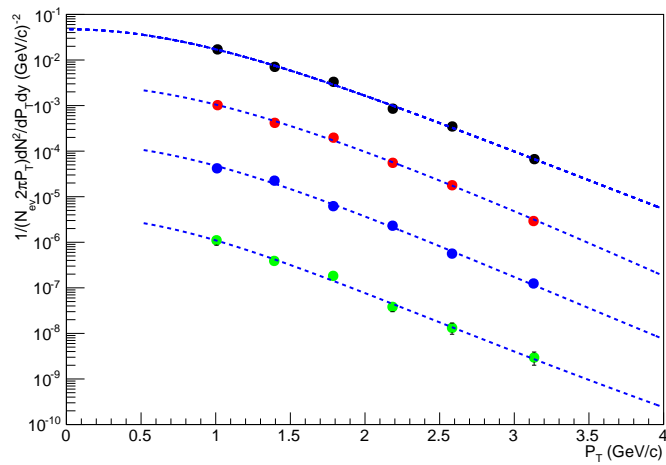


Figure 107: The Levy function fit of  $\Omega^-$  at 19.6 GeV.

$\Omega^-$  spectra Fit with Boltz Function, Au+Au 19.6 GeV

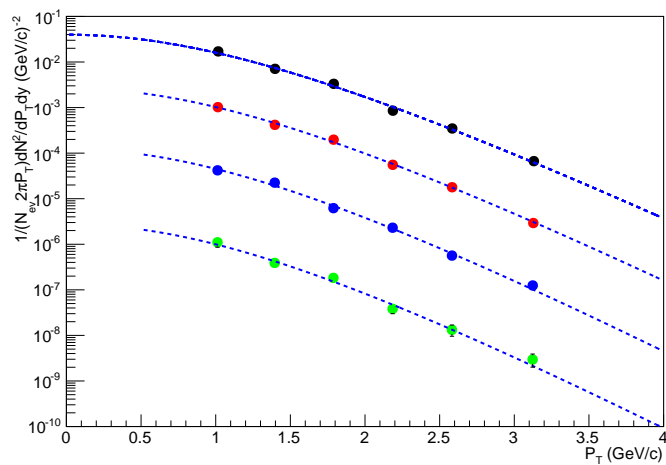


Figure 108: The Boltzmann function fit of  $\Omega^-$  at 19.6 GeV.

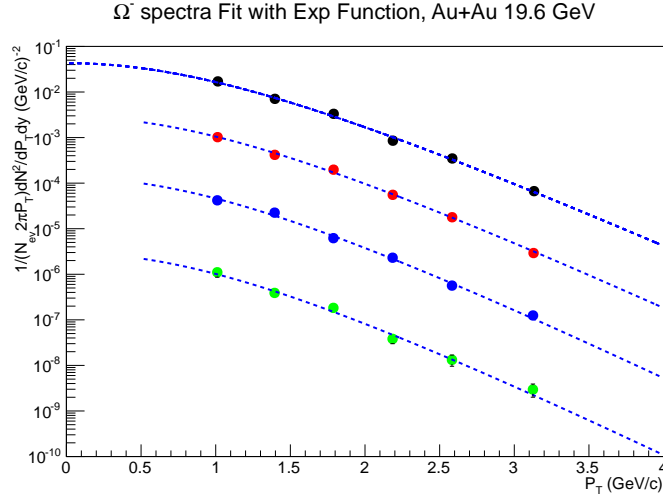


Figure 109: The Exponential function fit of  $\Omega^-$  at 19.6 GeV.

### 6.2.6 $\bar{\Omega}^+$ at 19.6 GeV

The Figure 110 to 112 show you the fitting with Levy, Boltzmann and exponential functions. The Table 160 lists the value and systematic error of  $dN/dy$  of unmeasured  $p_T$  range.

Table 160: The  $dN/dy$  of Unmeasured  $p_T$  range of  $\bar{\Omega}^+$  at 19.6 GeV

Centrality	Value	Systematic Error
0-10%	0.035067	0.0019289
10-20%	0.0237804	0.0013259
20-40%	0.00999176	0.00053153
40-60%	0.00331503	0.00015254

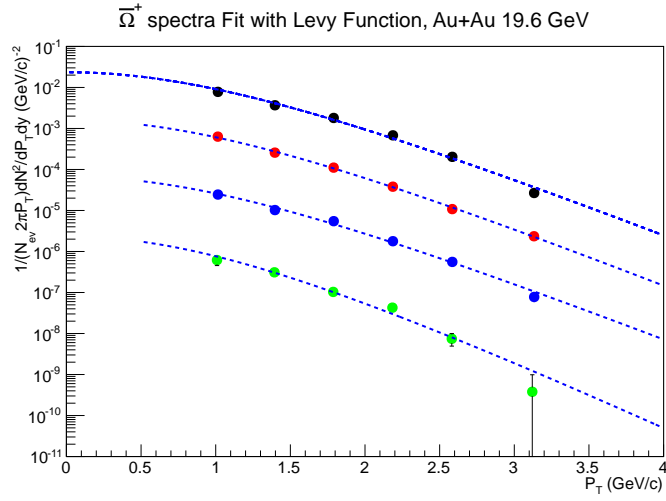


Figure 110: The Levy function fit of  $\bar{\Omega}^+$  at 19.6 GeV.

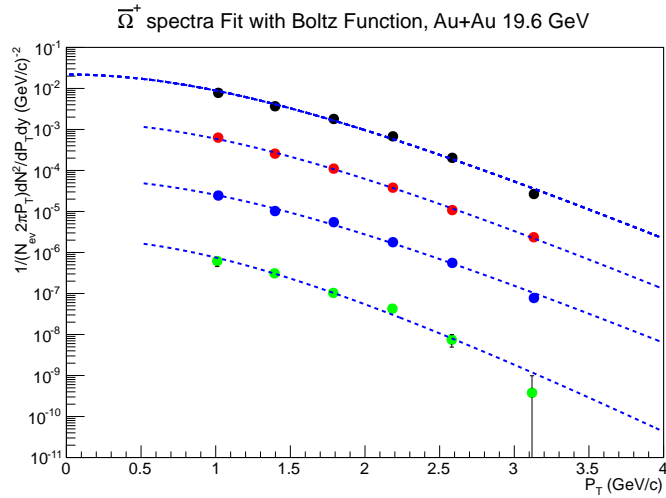


Figure 111: The Boltzmann function fit of  $\bar{\Omega}^+$  at 19.6 GeV.

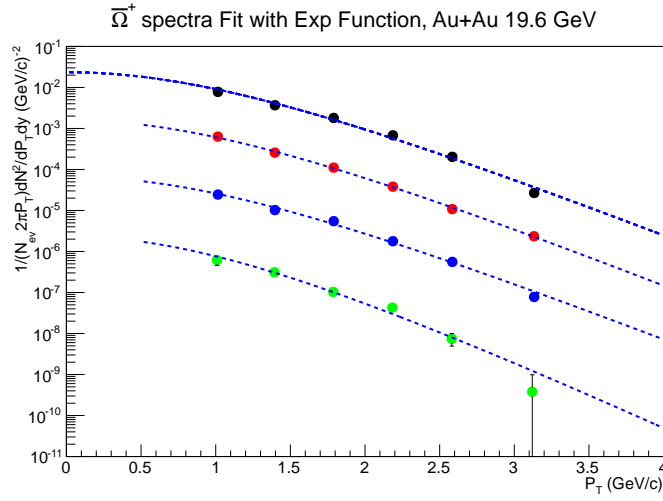


Figure 112: The Exponential function fit of  $\bar{\Omega}^+$  at 19.6 GeV.

### 6.2.7 $\Omega^-$ at 11.5 GeV

The Figure 113 to 115 show you the fitting with Levy, Boltzmann and exponential functions. The Table 161 lists the value and systematic error of  $dN/dy$  of unmeasured  $p_T$  range.

Table 161: The  $dN/dy$  of Unmeasured  $p_T$  range of  $\Omega^-$  at 11.5 GeV

Centrality	Value	Systematic Error
0-10%	0.0346324	0.0021592
10-60%	0.0150659	0.0032753

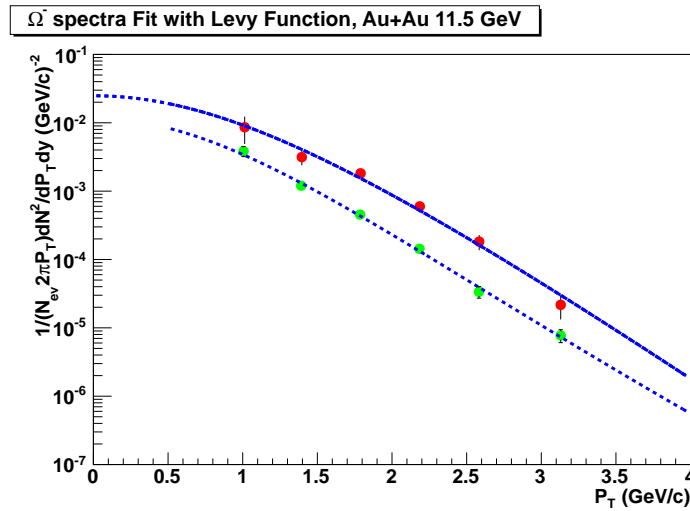


Figure 113: The Levy function fit of  $\Omega^-$  at 11.5 GeV.

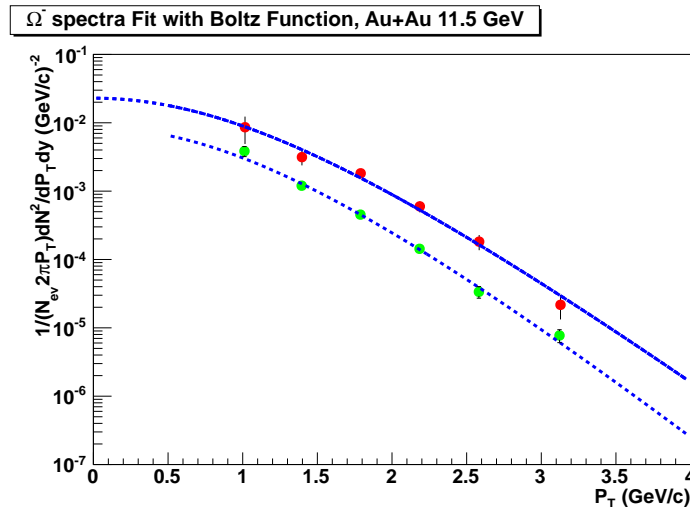


Figure 114: The Boltzmann function fit of  $\Omega^-$  at 11.5 GeV.

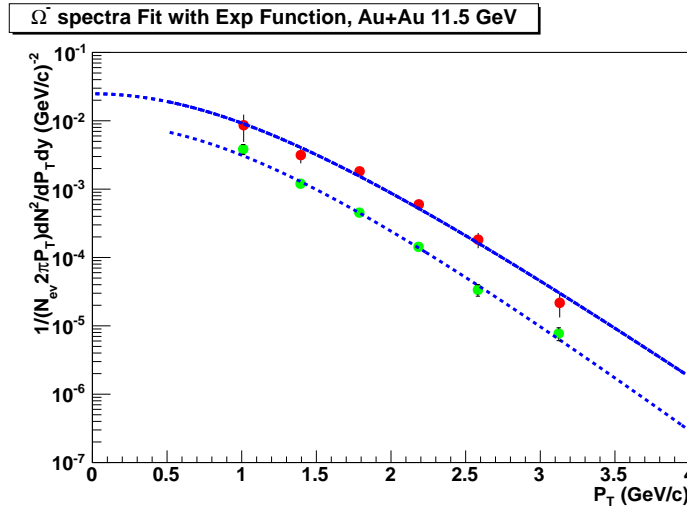


Figure 115: The Exponential function fit of  $\Omega^-$  at 11.5 GeV.

### 6.2.8 $\bar{\Omega}^+$ at 11.5 GeV

The Figure 116 to 118 show you the fitting with Levy, Boltzmann and exponential functions. The Table 162 lists the value and systematic error of  $dN/dy$  of unmeasured  $p_T$  range.

Table 162: The  $dN/dy$  of Unmeasured  $p_T$  range of  $\bar{\Omega}^+$  at 11.5 GeV

Centrality	Value	Systematic Error
0-10%	0.0145027	0.000898
10-60%	0.00428165	0.00020015

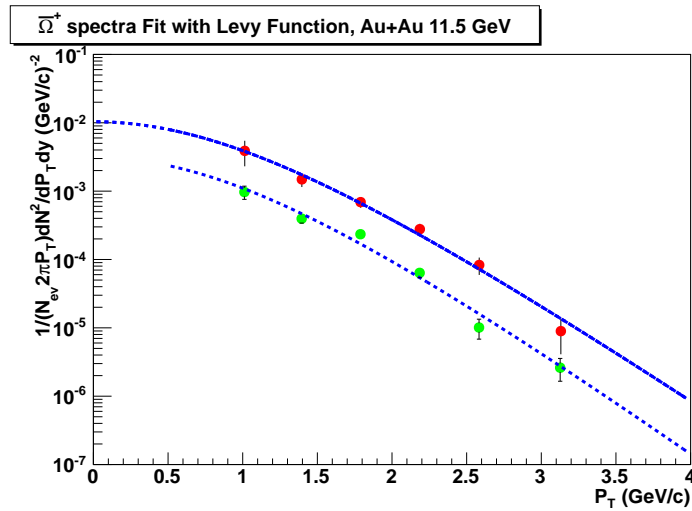


Figure 116: The Levy function fit of  $\bar{\Omega}^+$  at 11.5 GeV.

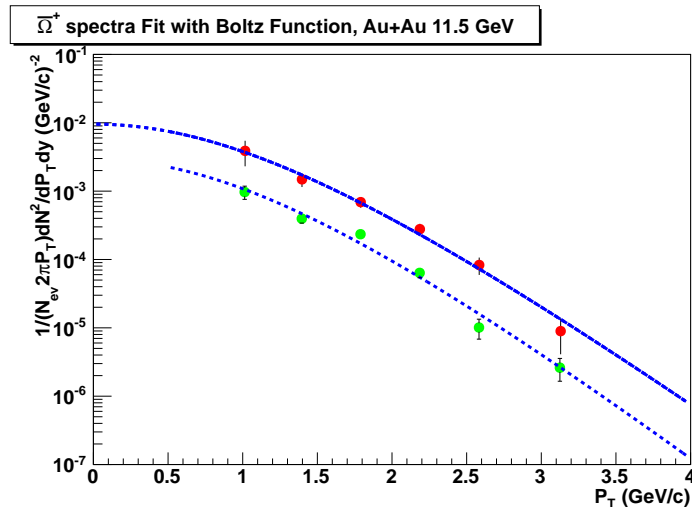


Figure 117: The Boltzmann function fit of  $\bar{\Omega}^+$  at 11.5 GeV.

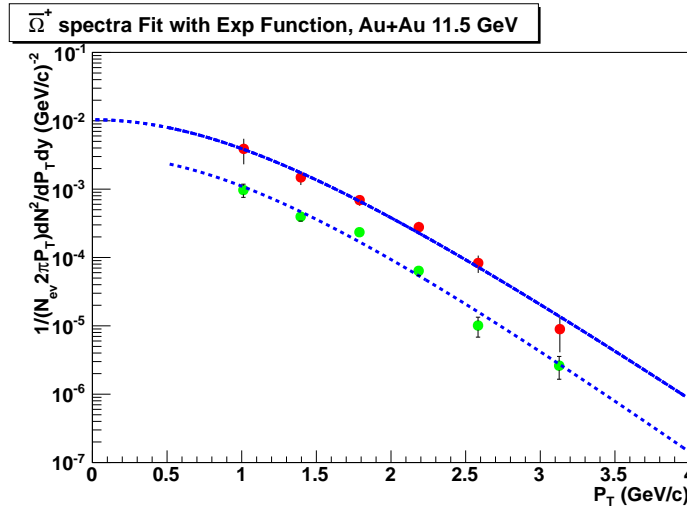


Figure 118: The Exponential function fit of  $\bar{\Omega}^+$  at 11.5 GeV.

### 6.2.9 $\Omega^-$ at 7.7 GeV

The Figure 119 to 121 show you the fitting with Levy, Boltzmann and exponential functions. The Table 163 lists the value and systematic error of  $dN/dy$  of unmeasured  $p_T$  range.

Table 163: The  $dN/dy$  of Unmeasured  $p_T$  range of  $\Omega^-$  at 7.7 GeV

Centrality	Value	Systematic Error
0-60%	0.0121545	0.0005302

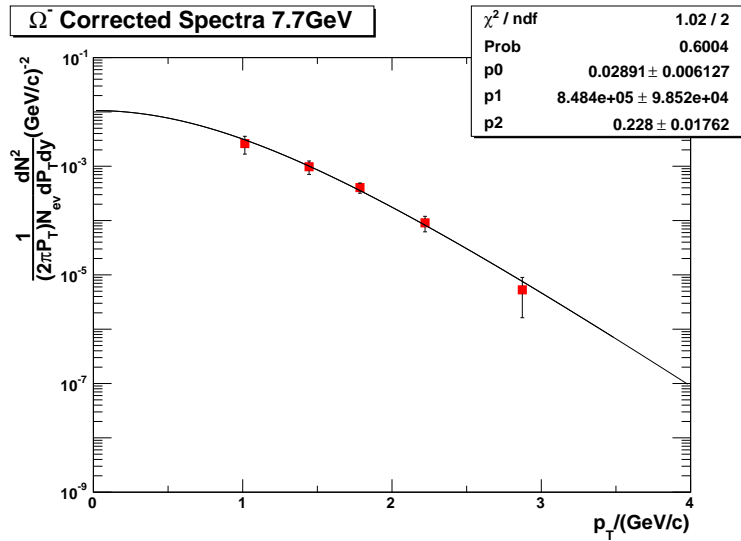


Figure 119: The Levy function fit of  $\Omega^-$  at 7.7 GeV.

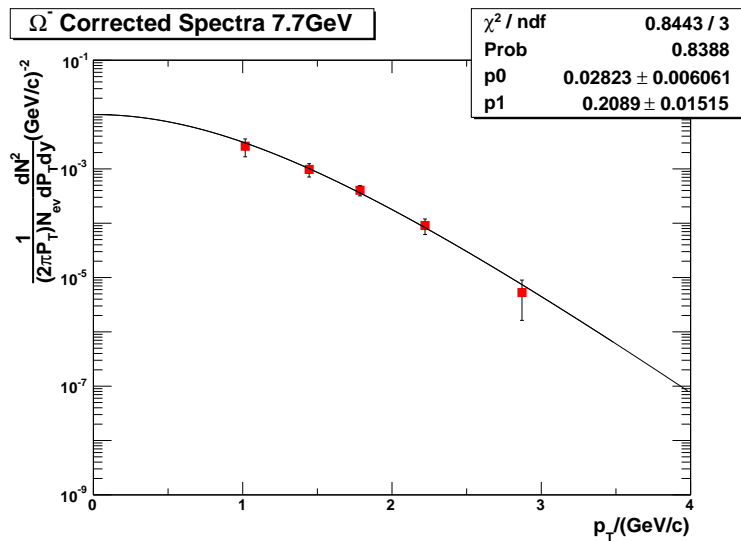


Figure 120: The Boltzmann function fit of  $\Omega^-$  at 7.7 GeV.

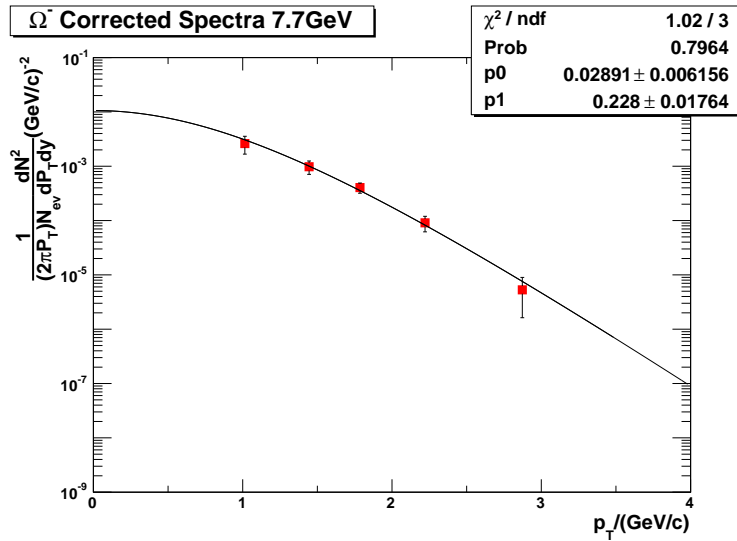


Figure 121: The Exponential function fit of  $\Omega^-$  at 7.7 GeV.

### 6.2.10 $\bar{\Omega}^+$ at 7.7 GeV

The Figure 122 to 124 show you the fitting with Levy, Boltzmann and exponential functions. The Table 164 lists the value and systematic error of  $dN/dy$  of unmeasured  $p_T$  range.

Table 164: The  $dN/dy$  of Unmeasured  $p_T$  range of  $\bar{\Omega}^+$  at 7.7 GeV

Centrality	Value	Systematic Error
0-60%	0.0035877	7.087e-05

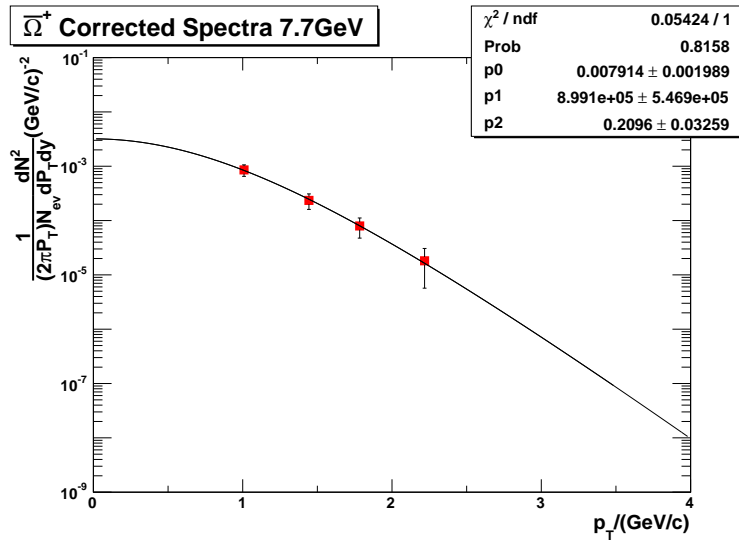


Figure 122: The Levy function fit of  $\bar{\Omega}^+$  at 7.7 GeV.

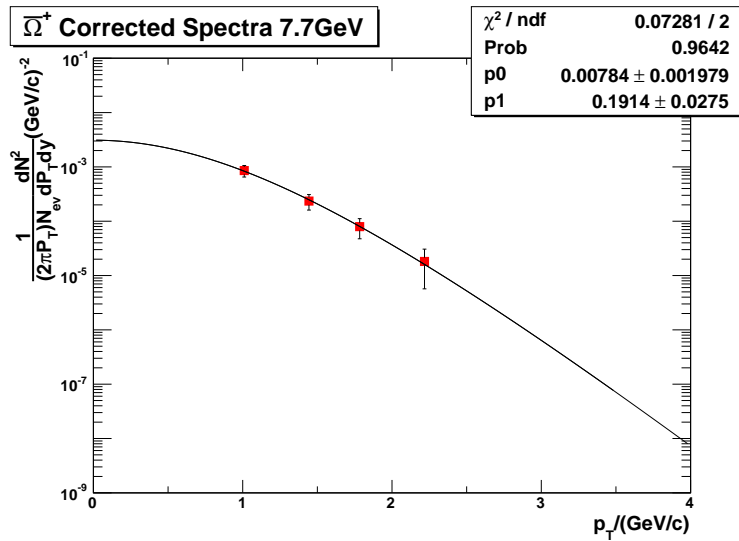


Figure 123: The Boltzmann function fit of  $\bar{\Omega}^+$  at 7.7 GeV.

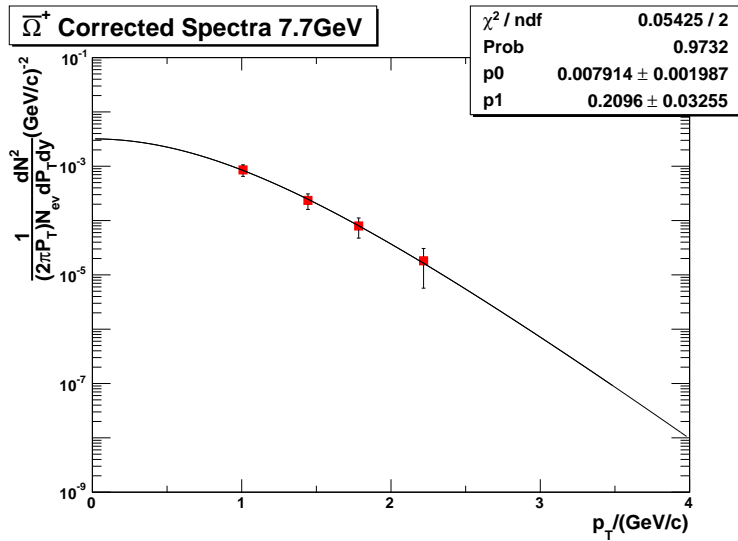


Figure 124: The Exponential function fit of  $\bar{\Omega}^+$  at 7.7 GeV.

## 7 Summary

In the previous sections, the steps how we get the  $p_T$  spectra and systematic errors are discussed. In the section, we'd like to summarize the data points of the spectra and the  $dN/dy$ . In the last section, the systematic error of each  $p_T$  bin is relative error. While in the following tables, when we mention the systematic errors, they are the absolute values.

## 7.1 $p_T$ Spectra

Table 165: The  $\Omega^- p_T$  spectra at 39 GeV

Centrality	$p_T$	$\frac{1}{2\pi} \frac{dN^2}{N p_T dp_T dy}$	Statistical Error	Systematic Error
0-5%	0.964511	0.0219906	0.00418377	0.00243898
	1.25135	0.0123583	0.00113967	0.000655964
	1.54719	0.00791966	0.000486096	0.000535862
	1.84496	0.00403859	0.00024748	0.000207353
	2.18823	0.00178677	0.000104579	0.000121663
	2.5861	0.000583055	4.46881e-05	3.62699e-05
	2.98469	0.000175305	1.95473e-05	1.23396e-05
	3.38367	8.2603e-05	9.707e-06	9.53049e-06
	3.78294	1.98664e-05	4.23158e-06	2.1258e-06
5-10%	0.964987	0.0233191	0.00321152	0.00175369
	1.25149	0.0108186	0.000829887	0.000564417
	1.5473	0.00645427	0.000384831	0.000426884
	1.84507	0.0033582	0.000191006	0.000201884
	2.18841	0.00137512	7.61259e-05	8.94509e-05
	2.5863	0.000508042	3.41342e-05	4.10817e-05
	2.98488	0.000190317	1.52775e-05	1.29386e-05
	3.38388	6.11445e-05	7.22466e-06	6.68444e-06
	3.78314	1.15512e-05	3.10767e-06	1.2274e-06
10-20%	0.964951	0.0139117	0.00130655	0.000972202
	1.25147	0.00685703	0.000373611	0.000351166
	1.5473	0.00383364	0.000166526	0.00019191
	1.84507	0.00224125	9.30772e-05	0.000137383
	2.1884	0.00101058	3.94607e-05	6.54338e-05
	2.58629	0.000326136	1.62243e-05	2.05695e-05
	2.98487	0.000108617	7.69933e-06	7.47314e-06
	3.38387	2.80399e-05	3.51073e-06	3.02206e-06
	3.78312	1.11986e-05	1.72558e-06	1.51884e-06
20-40%	0.964529	0.00613366	0.000464408	0.000482266
	1.25135	0.0036376	0.000152306	0.00018011
	1.54721	0.00203621	6.96722e-05	0.000102693
	1.84497	0.0010535	3.59518e-05	5.34074e-05
	2.18824	0.000451825	1.51067e-05	2.83077e-05
	2.58611	0.000149032	6.52618e-06	9.04302e-06
	2.9847	5.18299e-05	3.19059e-06	3.46051e-06
	3.38369	1.83105e-05	1.59193e-06	1.92681e-06
	3.78295	4.86789e-06	7.8599e-07	5.78471e-07
40-60%	0.962424	0.00150255	0.000168779	0.00011467
	1.25067	0.000873941	5.65913e-05	4.42422e-05
	1.54666	0.000446857	2.55647e-05	2.26753e-05
	1.84444	0.000217455	1.30817e-05	1.13446e-05
	2.18729	7.99036e-05	5.02446e-06	5.01505e-06
	2.58514	3.44753e-05	2.53849e-06	2.41237e-06
	2.9837	1.084e-05	1.25925e-06	8.48381e-07
	3.38267	2.55218e-06	5.25301e-07	2.74997e-07
	3.78295	0.000395057	7.6762e-05	2.85425e-05
60-80%	0.955978	0.000137647	1.8828e-05	6.79811e-06
	1.24767	7.23025e-05	8.64694e-06	4.17389e-06
	1.54398	2.90401e-05	3.93771e-06	1.65186e-06
	1.84177	9.48253e-06	1.63222e-06	6.05358e-07
	2.18244	4.88535e-06	8.93084e-07	3.80133e-07
	2.58013	1.23	0.00261536	0.0018894
	1.25144	0.0116259	0.000696369	0.00057679
	1.54726	0.00718977	0.00030896	0.000416692
	1.84503	0.00371336	0.000155729	0.000202861
0-10%	2.18835	0.00158573	6.42082e-05	0.000103244
	2.58624	0.000548248	2.80164e-05	3.58836e-05
	2.98481	0.000185027	1.23585e-05	1.27873e-05
	3.38381	7.20152e-05	6.01952e-06	7.88523e-06
	3.78307	1.54763e-05	2.60514e-06	1.64778e-06
	4.39417	2.85177e-06	5.86199e-07	3.64094e-07

Table 166: The  $\bar{\Omega}^+ p_T$  spectra at 39 GeV

Centrality	$p_T$	$\frac{1}{2\pi} \frac{dN^2}{N p_T dp_T dy}$	Statistical Error	Systematic Error
0-5%	0.964328	0.0187996	0.00298593	0.00157598
	1.25129	0.00922456	0.000818335	0.000401911
	1.54715	0.00635392	0.000404823	0.000399175
	1.84492	0.00329351	0.000194724	0.000226219
	2.18815	0.00159298	8.45269e-05	0.00011271
	2.58603	0.000525121	3.62808e-05	4.66908e-05
	2.98461	0.000144081	1.54141e-05	1.91855e-05
	3.3836	4.7635e-05	7.55315e-06	5.48612e-06
5-10%	3.78286	1.32325e-05	3.32735e-06	2.89071e-06
	0.966324	0.0113505	0.00203278	0.000806675
	1.25186	0.00767646	0.00062246	0.000348094
	1.54759	0.00425723	0.000276944	0.000181824
	1.84534	0.00222152	0.000144529	0.000129361
	2.1889	0.00117129	6.43318e-05	7.7389e-05
	2.58679	0.000354153	2.63332e-05	3.17318e-05
	2.98538	0.00011909	1.27636e-05	7.74561e-06
10-20%	3.38439	3.90352e-05	6.00599e-06	4.37323e-06
	3.78366	1.82734e-05	3.41554e-06	2.40392e-06
	0.965262	0.011051	0.00102827	0.000870082
	1.25157	0.00610198	0.000338657	0.000222224
	1.54737	0.00279582	0.00012737	0.000143071
	1.84512	0.00169046	7.37022e-05	8.73265e-05
	2.18852	0.000749598	3.14249e-05	4.52517e-05
	2.58641	0.000239253	1.36043e-05	2.08925e-05
20-40%	2.98499	8.48907e-05	6.28114e-06	6.08529e-06
	3.38399	2.67788e-05	3.25632e-06	3.05086e-06
	3.78326	1.15415e-05	1.72943e-06	1.65885e-06
	0.96387	0.00471022	0.000369886	0.000326242
	1.25114	0.0028673	0.000124328	0.000100199
	1.54704	0.00154131	5.69661e-05	6.27121e-05
	1.84481	0.000832524	3.06329e-05	4.32569e-05
	2.18796	0.000335101	1.22217e-05	2.10045e-05
40-60%	2.58583	0.000111427	5.33866e-06	9.78318e-06
	2.98441	4.0074e-05	2.62248e-06	2.64615e-06
	3.38339	1.18529e-05	1.28043e-06	1.2367e-06
	3.78265	4.22458e-06	6.95414e-07	5.51819e-07
	0.962204	0.00119804	0.000144036	8.18628e-05
	1.2506	0.000615025	4.45353e-05	2.48371e-05
	1.54659	0.000395916	2.33153e-05	1.60627e-05
	1.84437	0.000160727	1.03952e-05	8.24992e-06
60-80%	2.18716	8.10099e-05	4.85982e-06	5.00156e-06
	2.58502	2.24916e-05	2.08384e-06	1.96354e-06
	2.98358	7.14426e-06	9.85557e-07	5.68896e-07
	3.38255	1.98146e-06	4.71987e-07	2.04934e-07
	0.95607	0.000235876	5.39199e-05	1.78122e-05
	1.24772	0.000110506	1.52906e-05	5.97741e-06
	1.54404	5.57292e-05	6.99255e-06	3.42604e-06
	1.84181	2.15681e-05	3.28713e-06	1.11545e-06
0-10%	2.18253	7.85769e-06	1.50318e-06	5.3586e-07
	2.58023	3.99415e-06	7.9905e-07	3.7056e-07
	0.96528	0.0149123	0.00177317	0.00105424
	1.25157	0.00845682	0.00050982	0.000375638
	1.54737	0.00526321	0.000240271	0.000272453
	1.84514	0.00275424 <sup>124</sup>	0.000120584	0.00017559
	2.18853	0.00138275	5.2926e-05	9.47599e-05
	2.58641	0.000439269	2.22439e-05	3.91829e-05
	2.985	0.000131974	1.00023e-05	1.24538e-05
	3.384	4.34909e-05	4.81905e-06	4.47891e-06
	3.78326	1.60664e-05	2.40683e-06	2.3251e-06
	4.39523	1.90021e-06	5.22488e-07	2.66047e-07

Table 167: The  $\Omega^- p_T$  spectra at 27 GeV

Centrality	$p_T$	$\frac{1}{2\pi} \frac{dN^2}{N p_T dp_T dy}$	Statistical Error	Systematic Error
0-10%	1.01754	0.0124927	0.00204919	0.00139717
	1.39777	0.00865718	0.000767841	0.000667535
	1.79135	0.00368167	0.000269663	0.000375214
	2.18793	0.00130169	9.47594e-05	0.000169243
	2.5858	0.000442722	4.14181e-05	4.26519e-05
	3.1372	8.83589e-05	8.30889e-06	1.10068e-05
10-20%	1.01456	0.0100671	0.00162976	0.00130854
	1.39651	0.00518716	0.000480465	0.0003642
	1.79019	0.00193869	0.000154097	0.000121925
	2.18676	0.000716157	5.77449e-05	8.87863e-05
	2.5846	0.000277121	2.62264e-05	2.37117e-05
	3.13259	3.80716e-05	4.84698e-06	4.79573e-06
20-40%	1.01729	0.00418737	0.000483233	0.00048164
	1.39767	0.00234685	0.000183764	0.000157054
	1.79127	0.000924254	6.64142e-05	5.86529e-05
	2.18784	0.000384396	2.6126e-05	4.14167e-05
	2.58571	0.000106905	9.88205e-06	9.1321e-06
	3.13685	2.55497e-05	2.36213e-06	3.32363e-06
40-60%	1.01142	0.00124037	0.000256704	0.000144039
	1.39495	0.000715879	9.43549e-05	4.83292e-05
	1.78871	0.000213957	2.53438e-05	1.35878e-05
	2.18524	7.06493e-05	8.67516e-06	7.58653e-06
	2.58303	2.59733e-05	4.0219e-06	2.22405e-06
	3.12667	2.98132e-06	9.19676e-07	3.99199e-07

Table 168: The  $\bar{\Omega}^+ p_T$  spectra at 27 GeV

Centrality	$p_T$	$\frac{1}{2\pi} \frac{dN^2}{N p_T dp_T dy}$	Statistical Error	Systematic Error
0-10%	1.02033	0.00848074	0.00134475	0.00125046
	1.39879	0.00517073	0.000470267	0.000413838
	1.79225	0.0023014	0.000178634	0.000119314
	2.18884	0.00103122	7.52202e-05	7.31802e-05
	2.58672	0.000302677	2.95642e-05	2.73506e-05
	3.14075	6.99047e-05	7.09398e-06	8.44036e-06
10-20%	1.01778	0.00546324	0.000818779	0.00075296
	1.39787	0.00313816	0.000297686	0.000247821
	1.79144	0.00131549	0.000110281	7.56148e-05
	2.18802	0.000652817	5.33592e-05	4.92434e-05
	2.58589	0.00014271	1.73693e-05	1.17796e-05
	3.13753	3.55171e-05	4.39631e-06	3.39167e-06
20-40%	1.01628	0.00332534	0.000433737	0.000484053
	1.39726	0.00167727	0.000131418	0.000133861
	1.79089	0.000713622	5.03964e-05	3.69368e-05
	2.18746	0.000246654	1.84123e-05	1.79938e-05
	2.58532	8.94659e-05	8.27051e-06	6.62418e-06
	3.13536	1.64359e-05	1.79187e-06	1.58493e-06
40-60%	1.00999	0.00092586	0.000187503	0.000121921
	1.39415	0.000493195	6.73542e-05	3.88722e-05
	1.78793	0.000189466	2.54691e-05	1.0149e-05
	2.18443	5.93032e-05	8.29557e-06	4.38956e-06
	2.5822	1.8805e-05	3.56701e-06	1.37112e-06
	3.12355	1.4826e-06	5.38501e-07	1.95485e-07

Table 169: The  $\Omega^- p_T$  spectra at 19.6 GeV

Centrality	$p_T$	$\frac{1}{2\pi} \frac{dN^2}{N p_T dp_T dy}$	Statistical Error	Systematic Error
0-10%	1.01203	0.0170832	0.00296004	0.00251965
	1.39542	0.00707997	0.000674653	0.000563584
	1.78947	0.00331902	0.000280701	0.000244399
	2.18638	0.000854749	9.7949e-05	0.000162385
	2.58461	0.000347719	4.33678e-05	5.57209e-05
	3.13475	6.67558e-05	9.39822e-06	1.22649e-05
10-20%	1.0126	0.0102127	0.0015584	0.00148067
	1.39557	0.00417735	0.000424869	0.00044988
	1.78931	0.00197503	0.000179893	0.00014164
	2.18585	0.000554177	6.24609e-05	8.775e-05
	2.58366	0.000178461	2.58696e-05	2.78197e-05
	3.12905	2.92421e-05	5.69909e-06	4.18861e-06
20-40%	1.00867	0.00419571	0.000591435	0.000641952
	1.39357	0.00225078	0.000205111	0.000181032
	1.78775	0.000620339	5.69479e-05	5.23943e-05
	2.1847	0.000230813	2.30432e-05	3.59344e-05
	2.58295	5.64163e-05	8.88816e-06	8.64608e-06
	3.1289	1.24654e-05	2.394e-06	1.78018e-06
40-60%	1.00552	0.00110674	0.000245822	0.000205001
	1.39191	0.000389916	6.47817e-05	3.35968e-05
	1.78674	0.000183049	2.89577e-05	1.428e-05
	2.18432	3.82172e-05	8.25889e-06	6.09312e-06
	2.58322	1.32465e-05	3.65834e-06	2.27302e-06
	3.13297	2.9554e-06	9.48778e-07	5.42546e-07

Table 170: The  $\bar{\Omega}^+ p_T$  spectra at 19.6 GeV

Centrality	$p_T$	$\frac{1}{2\pi} \frac{dN^2}{N p_T dp_T dy}$	Statistical Error	Systematic Error
0-10%	1.01483	0.00780381	0.00125578	0.00054454
	1.39664	0.00367763	0.000399356	0.000270005
	1.79031	0.00180344	0.000158798	0.00015186
	2.18687	0.000679038	6.88774e-05	2.72305e-05
	2.58471	0.0002032	2.70923e-05	2.7714e-05
	3.13304	2.66992e-05	5.65005e-06	6.58442e-06
10-20%	1.01418	0.0063183	0.00105186	0.000800465
	1.39634	0.00257344	0.000281131	0.000167403
	1.79003	0.00110879	0.00011062	8.99004e-05
	2.18659	0.00038033	4.20205e-05	2.52479e-05
	2.58443	0.000108106	1.82675e-05	1.55106e-05
	3.13194	2.35251e-05	4.41111e-06	2.19719e-06
20-40%	1.01491	0.0024452	0.000367367	0.000207725
	1.39667	0.00102401	0.000104086	5.99532e-05
	1.79035	0.000548453	4.76946e-05	4.20097e-05
	2.18691	0.000178079	1.81421e-05	8.81391e-06
	2.58475	5.56916e-05	8.16267e-06	7.62273e-06
	3.13318	7.77912e-06	1.96016e-06	7.05653e-07
40-60%	1.00869	0.000617707	0.000164295	4.7414e-05
	1.39337	0.000310459	5.04858e-05	2.44599e-05
	1.78715	0.000103307	1.86916e-05	8.49428e-06
	2.18362	4.2699e-05	7.78225e-06	1.76535e-06
	2.58135	7.4499e-06	2.51914e-06	1.23896e-06

Table 171: The  $\Omega^- p_T$  spectra at 11.5 GeV

Centrality	$p_T$	$\frac{1}{2\pi} \frac{dN^2}{N p_T dp_T dy}$	Statistical Error	Systematic Error
0-10%	1.01313	0.00814011	0.00350706	0.00123738
	1.39583	0.00297549	0.000723081	0.000406702
	1.78956	0.00172435	0.000273602	0.000120962
	2.1861	0.000565869	0.000103202	3.70281e-05
	2.58393	0.000172394	4.3147e-05	1.51498e-05
	3.13005	2.05214e-05	7.97135e-06	1.73688e-06
10-60%	1.00563	0.00364036	0.00060951	0.00022089
	1.39186	0.00113642	0.000122437	6.81066e-05
	1.78653	0.000428949	4.17648e-05	2.7983e-05
	2.18393	0.00013559	1.6255e-05	9.75575e-06
	2.58266	3.18495e-05	6.14252e-06	3.73544e-06
	3.13015	7.31537e-06	1.5676e-06	5.51835e-07

Table 172: The  $\bar{\Omega}^+ p_T$  spectra at 11.5 GeV

Centrality	$p_T$	$\frac{1}{2\pi} \frac{dN^2}{N p_T dp_T dy}$	Statistical Error	Systematic Error
0-10%	1.01367	0.00367224	0.00148974	0.00369203
	1.3961	0.00140577	0.00031946	0.000231605
	1.7898	0.000653242	0.0001118	7.37817e-05
	2.18636	0.000262759	5.20221e-05	1.4515e-05
	2.58419	7.855e-05	2.23603e-05	6.10852e-06
	3.13102	8.46299e-06	4.5805e-06	8.90806e-07
10-60%	1.0113	0.000970335	0.000211822	9.95379e-05
	1.39489	0.000395753	5.50952e-05	1.51357e-05
	1.78865	0.000234294	2.50402e-05	9.76809e-06
	2.18517	6.37403e-05	9.66436e-06	4.78446e-06
	2.58297	1.01077e-05	3.27398e-06	1.92162e-06
	3.12641	2.61219e-06	9.57011e-07	2.27913e-07

Table 173: The  $\Omega^-$  and  $\bar{\Omega}^+$   $p_T$  spectra at 7.7 GeV

Centrality	$p_T$	$\frac{1}{2\pi} \frac{dN^2}{N p_T dp_T dy}$	Statistical Error	Systematic Error
$\Omega^-$	1.01427	0.00261527	0.000944016	0.000312062
	0-60%	0.000978677	0.000270339	0.000167983
	1.78541	0.000404759	8.62406e-05	4.58896e-05
	2.22129	9.08301e-05	2.88634e-05	1.43706e-05
$\bar{\Omega}^+$	1.0088	0.000855682	0.000204696	4.29255e-05
	0-60%	0.000234903	7.45194e-05	2.53923e-05
	1.78349	7.95117e-05	3.20239e-05	9.04318e-06
	2.21821	1.81605e-05	1.24703e-05	8.54971e-06

## 7.2 $dN/dy$

The  $dN/dy$  is calculated from the  $p_T$  spectra, with the sum of data points on measured  $p_T$  range and the unmeasured  $p_T$  range from Levy function estimate. The statistical error is the Levy function fitting error. The systematic error is the quadratical sum of data points on measured and unmeasured  $p_T$  range. The systematic error of each measured  $p_T$  bin, is discussed in section 6.1, and the systematic error of measured  $p_T$  range is discussed in section 6.2. The Table 174 summarizes the  $dN/dy$  of  $\Omega^-$  and  $\bar{\Omega}^+$  at all the energies.

 Table 174: The  $\Omega^-$  and  $\bar{\Omega}^+$   $dN/dy$ 

Energy	Centrality	$\Omega^-$			$\bar{\Omega}^+$		
		$dN/dy$	Stat_Err	Sys_Err	$dN/dy$	Stat_Err	Sys_Err
39 GeV	0-5%	0.20264	0.00900492	0.00825241	0.166105	0.00691071	0.00614294
	5-10%	0.177013	0.00684442	0.00657822	0.112017	0.00491252	0.00380827
	10-20%	0.111571	0.00312123	0.00380873	0.0871698	0.00260734	0.00296746
	20-40%	0.0545675	0.00131194	0.00179019	0.04253	0.00109382	0.00133382
	40-60%	0.0127127	0.000524924	0.000413617	0.010129	0.000448424	0.000289939
	60-80%	0.00271887	0.000258469	8.52111e-05	0.00196502	0.000166152	7.73212e-05
27 GeV	0-10%	0.154464	0.00991486	0.00606177	0.097128	0.00644993	0.00423082
	10-20%	0.102613	0.00705708	0.00457674	0.0604311	0.00407852	0.00253276
	20-40%	0.0440682	0.00247146	0.00171593	0.0334974	0.00197105	0.00155707
	40-60%	0.0131746	0.00140327	0.000517131	0.0103893	0.00107676	0.000419111
19.6 GeV	0-10%	0.160162	0.0196019	0.0113662	0.0812905	0.00611435	0.00265233
	10-20%	0.0959867	0.00752222	0.0047012	0.0569186	0.00482428	0.00251965
	20-40%	0.043665	0.00502187	0.00302201	0.0236951	0.0017385	0.000800428
	40-60%	0.0104316	0.00223982	0.00119814	0.00671811	0.000940283	0.00021567
11.5 GeV	0-10%	0.0824223	0.0130436	0.00386625	0.0356727	0.00591868	0.00197067
	10-60%	0.0329979	0.00547655	0.00352239	0.00987569	0.00105947	0.000336112
7.7 GeV	0-60%	0.0272618	0.00612652	0.00138937	0.00799258	0.00198897	0.0002044

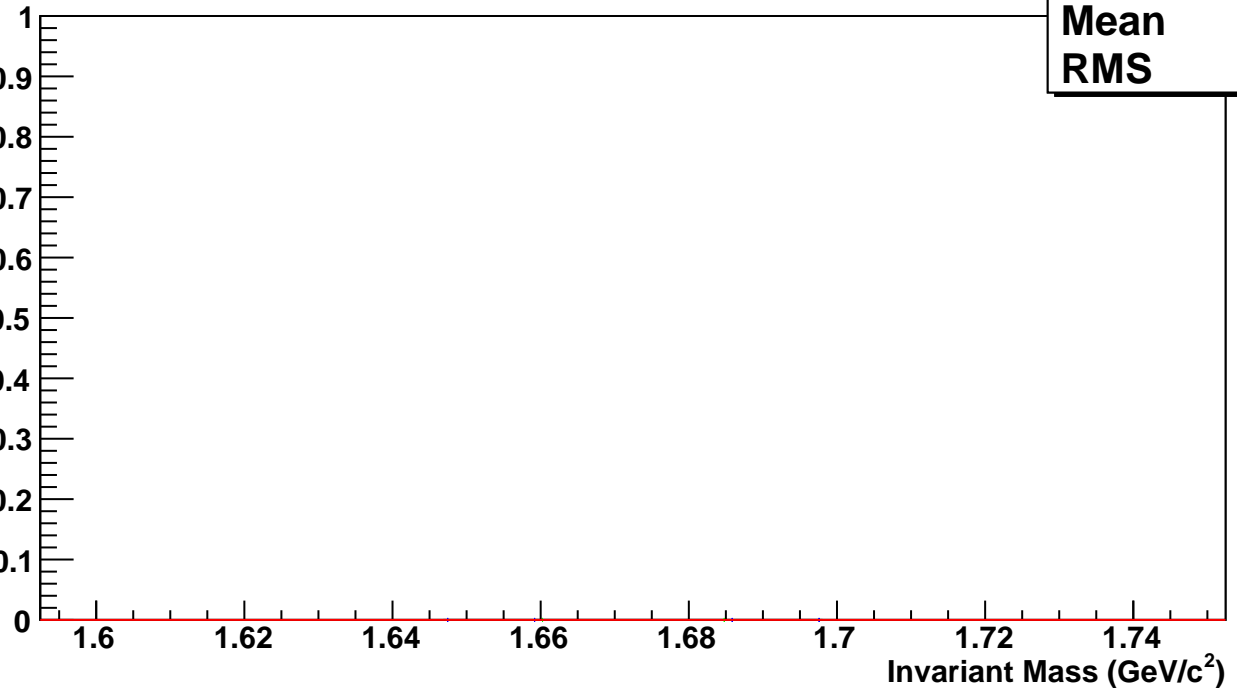
## References

- [1] G. D. Lafferty, T. R. Wyatt, "Where to Stick Your Data Points: The Treatment of Measurements Within Wide Bins", *Nucl. Instr. Meth. in Phys. Res. A* 355 (1995) 541

$\Omega^-$ , Au+Au 39 GeV, 60-80%,  $p_T$  0.2-0.5 GeV/c

Counts

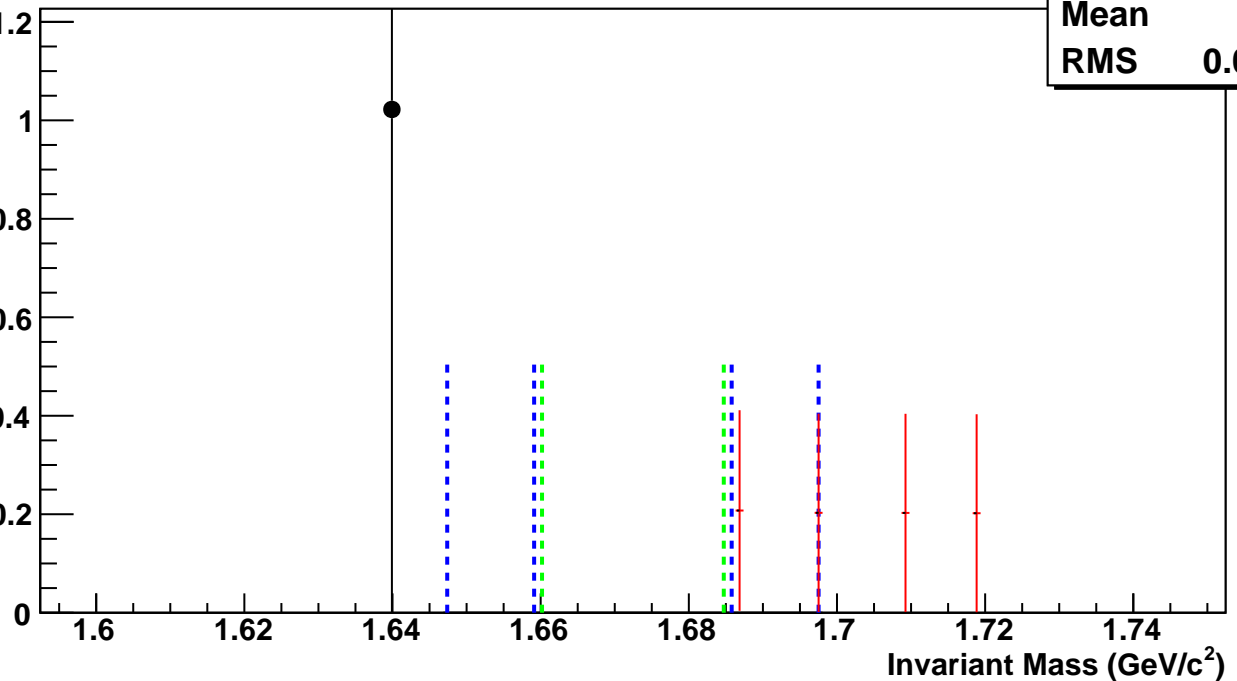
hmlInvMassBgCent0Pt0	
Entries	0
Mean	0
RMS	0



$\Omega^-$ , Au+Au 39 GeV, 40-60%,  $p_T$  0.2-0.5 GeV/c

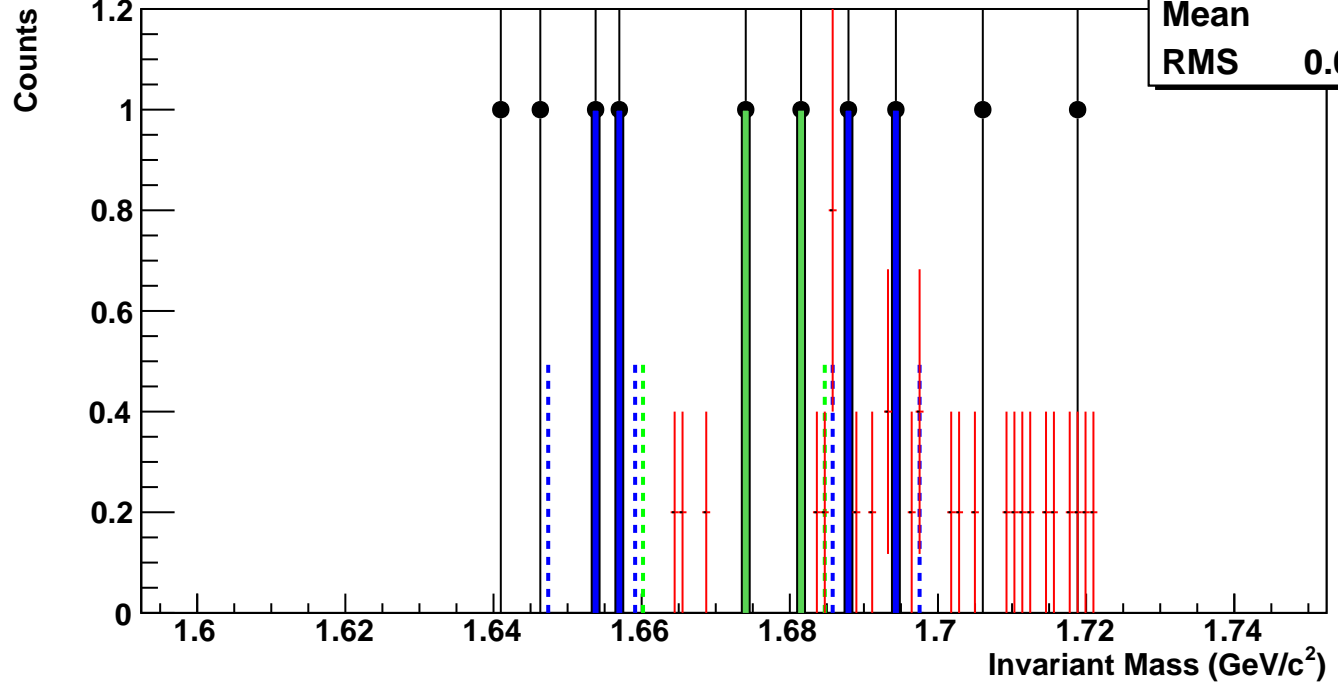
Counts

hmlInvMassBgCent1Pt0	
Entries	0
Mean	1.703
RMS	0.01208



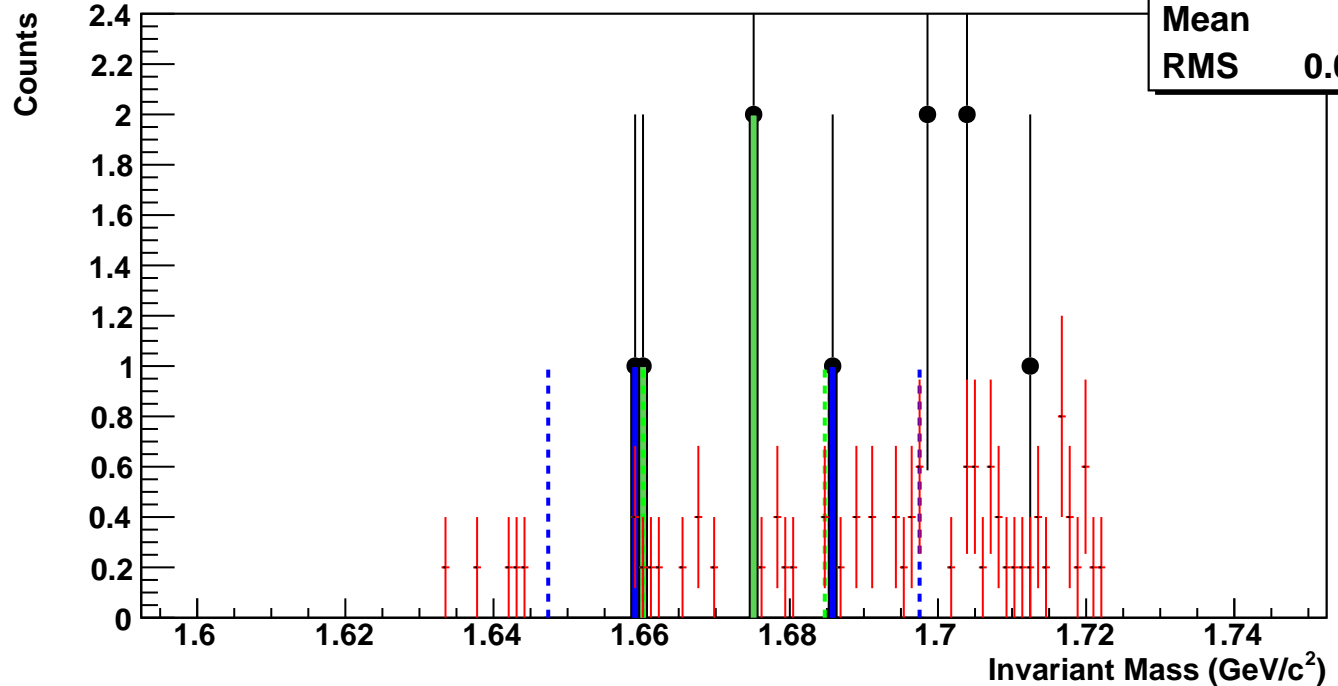
$\Omega^-$ , Au+Au 39 GeV, 20-40%,  $p_T$  0.2-0.5 GeV/c

hmlInvMassBgCent2Pt0	
Entries	1
Mean	1.698
RMS	0.01593



$\Omega^-$ , Au+Au 39 GeV, 10-20%,  $p_T$  0.2-0.5 GeV/c

hmlInvMassBgCent3Pt0	
Entries	2
Mean	1.693
RMS	0.02334



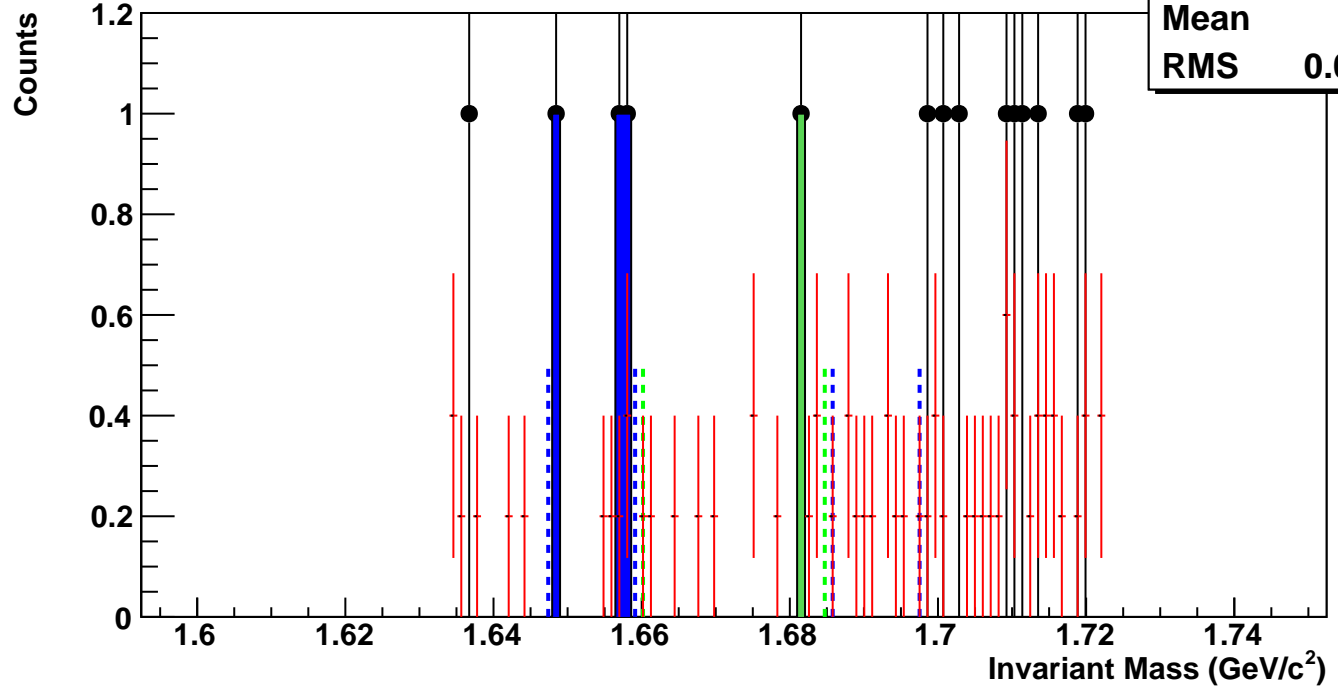
$\Omega^-$ , Au+Au 39 GeV, 5-10%,  $p_T$  0.2-0.5 GeV/c

hmlnvMassBgCent4Pt0

Entries 1

Mean 1.689

RMS 0.02547



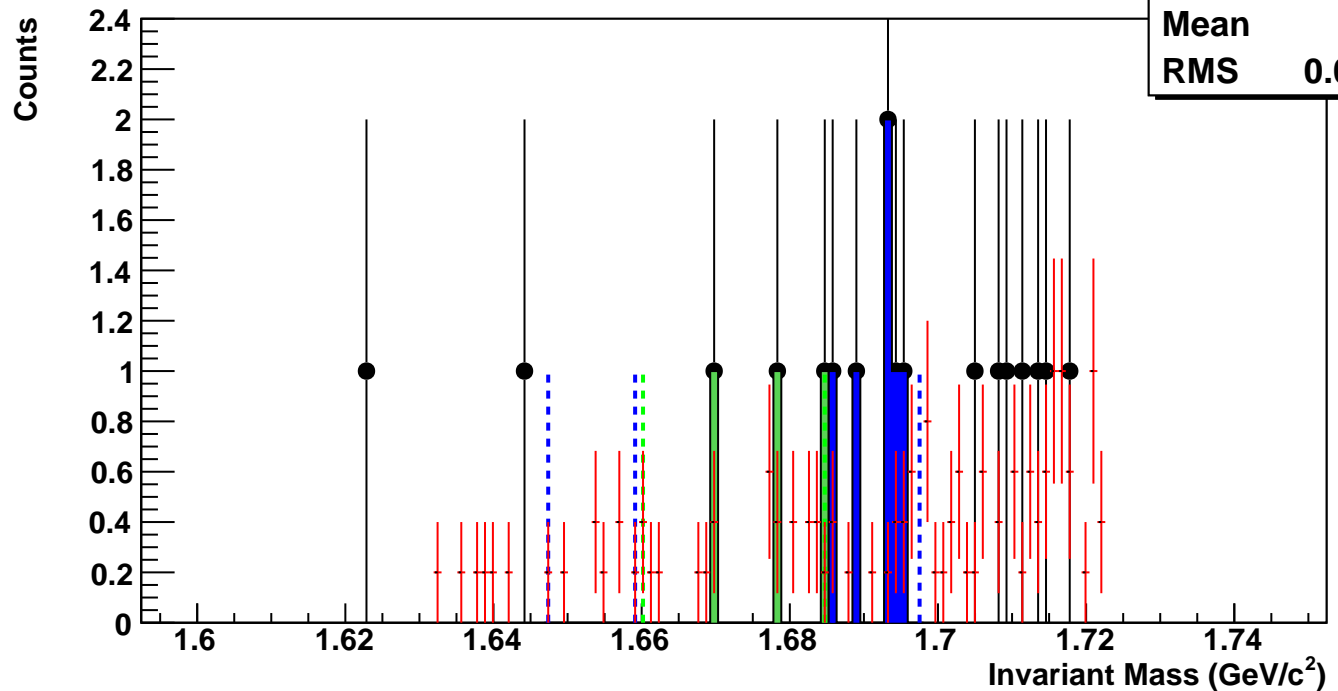
$\Omega^-$ , Au+Au 39 GeV, 0-5%,  $p_T$  0.2-0.5 GeV/c

hmlnvMassBgCent5Pt0

Entries 2

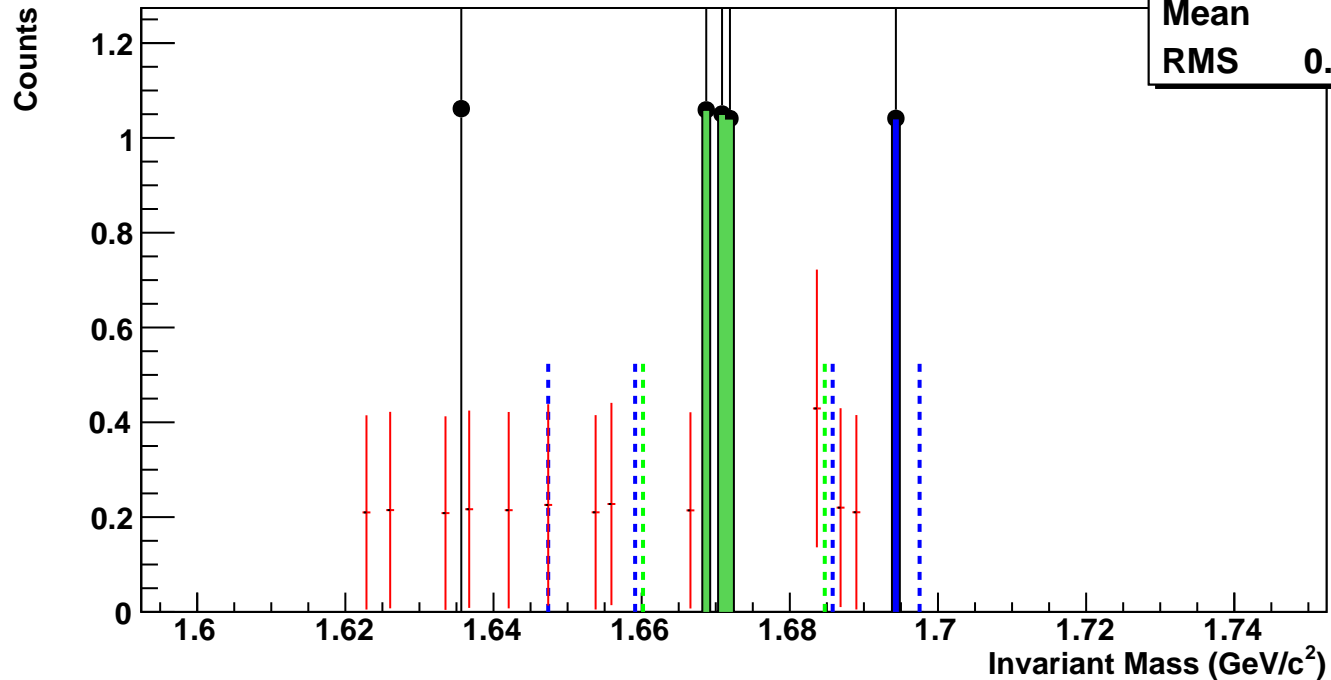
Mean 1.692

RMS 0.02469



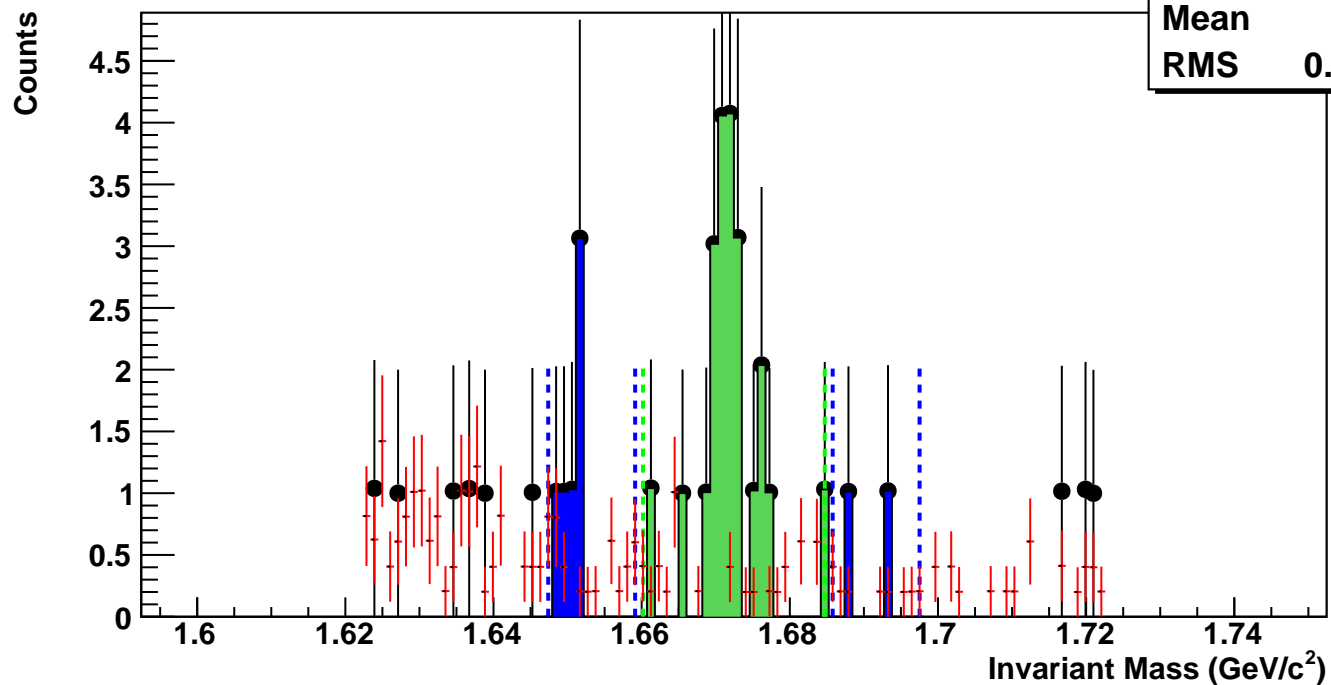
$\Omega^-$ , Au+Au 39 GeV, 60-80%,  $p_T$  0.5-0.8 GeV/c

hmlInvMassBgCent0Pt1	
Entries	0
Mean	1.656
RMS	0.02282



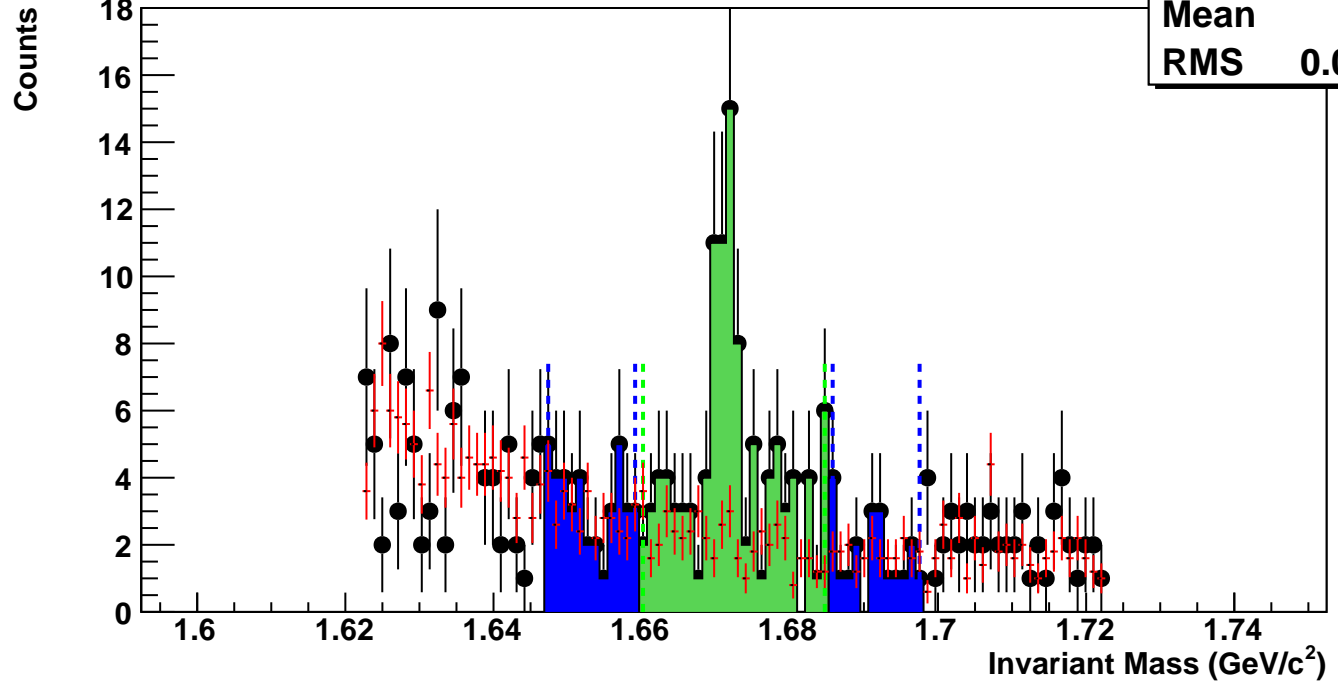
$\Omega^-$ , Au+Au 39 GeV, 40-60%,  $p_T$  0.5-0.8 GeV/c

hmlInvMassBgCent1Pt1	
Entries	4
Mean	1.656
RMS	0.02882



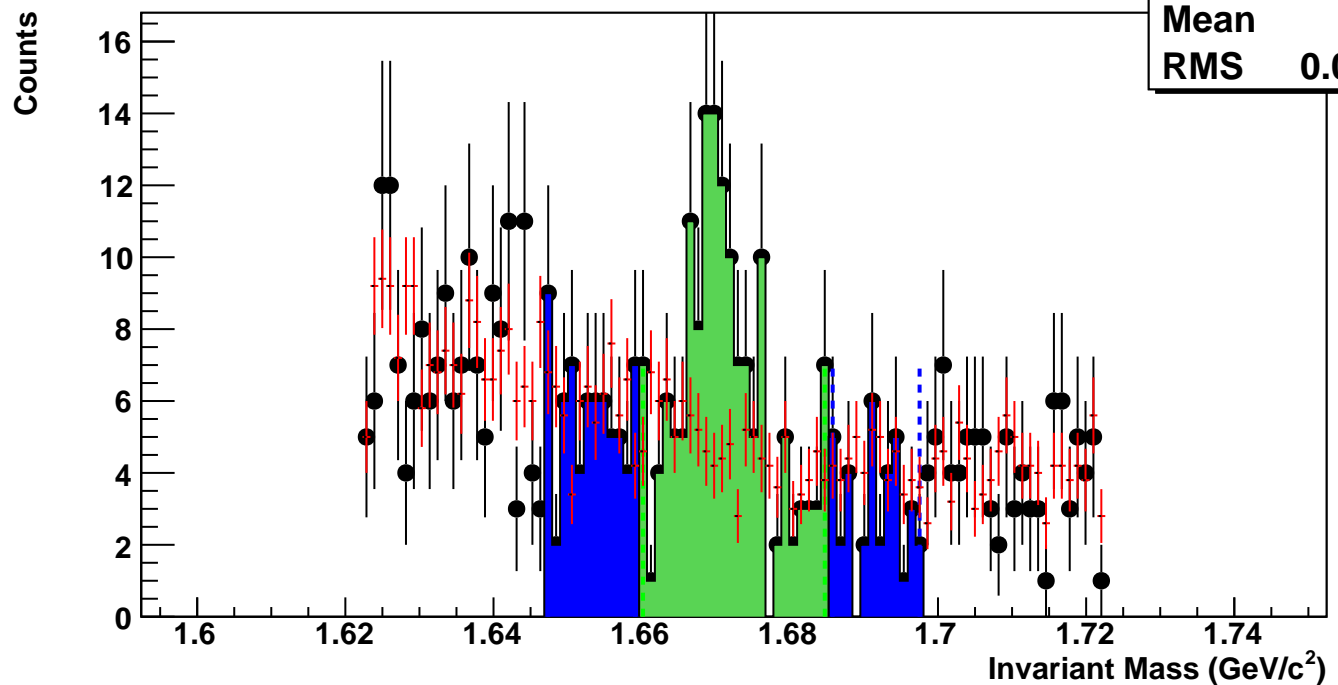
$\Omega^-$ , Au+Au 39 GeV, 20-40%,  $p_T$  0.5-0.8 GeV/c

hmlInvMassBgCent2Pt1	
Entries	31
Mean	1.661
RMS	0.02921



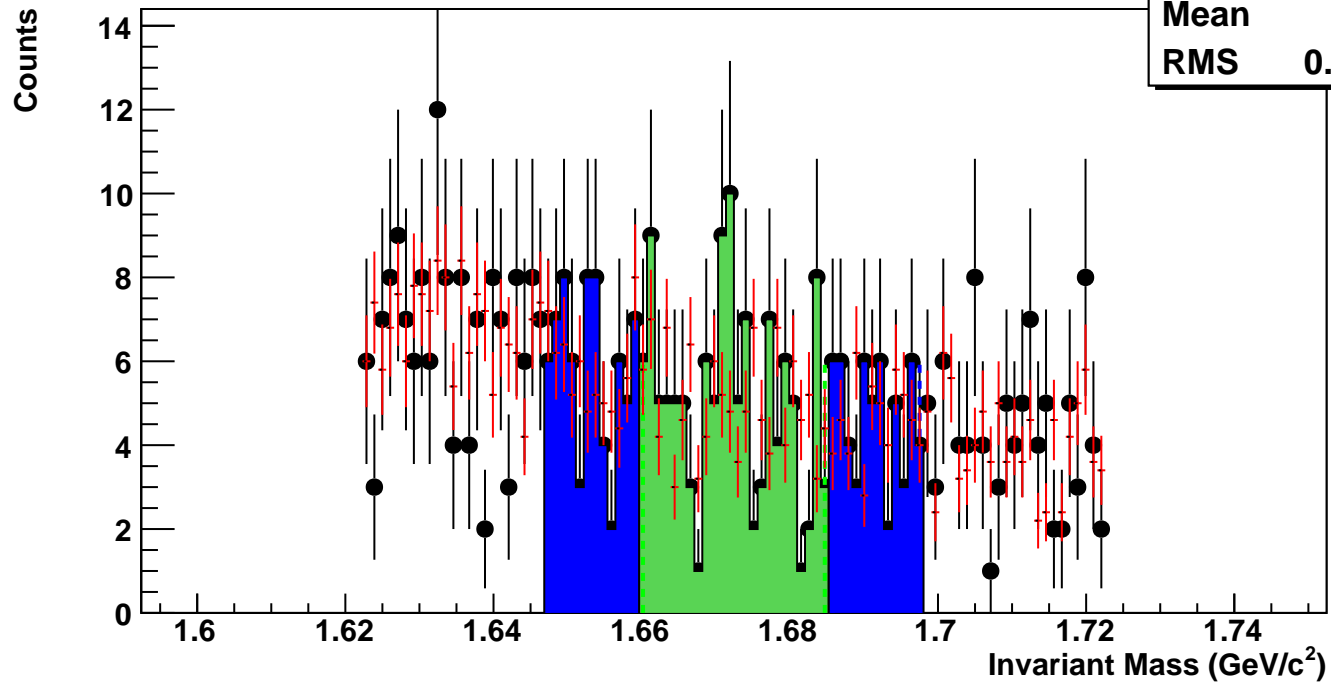
$\Omega^-$ , Au+Au 39 GeV, 10-20%,  $p_T$  0.5-0.8 GeV/c

hmlInvMassBgCent3Pt1	
Entries	61
Mean	1.665
RMS	0.02921



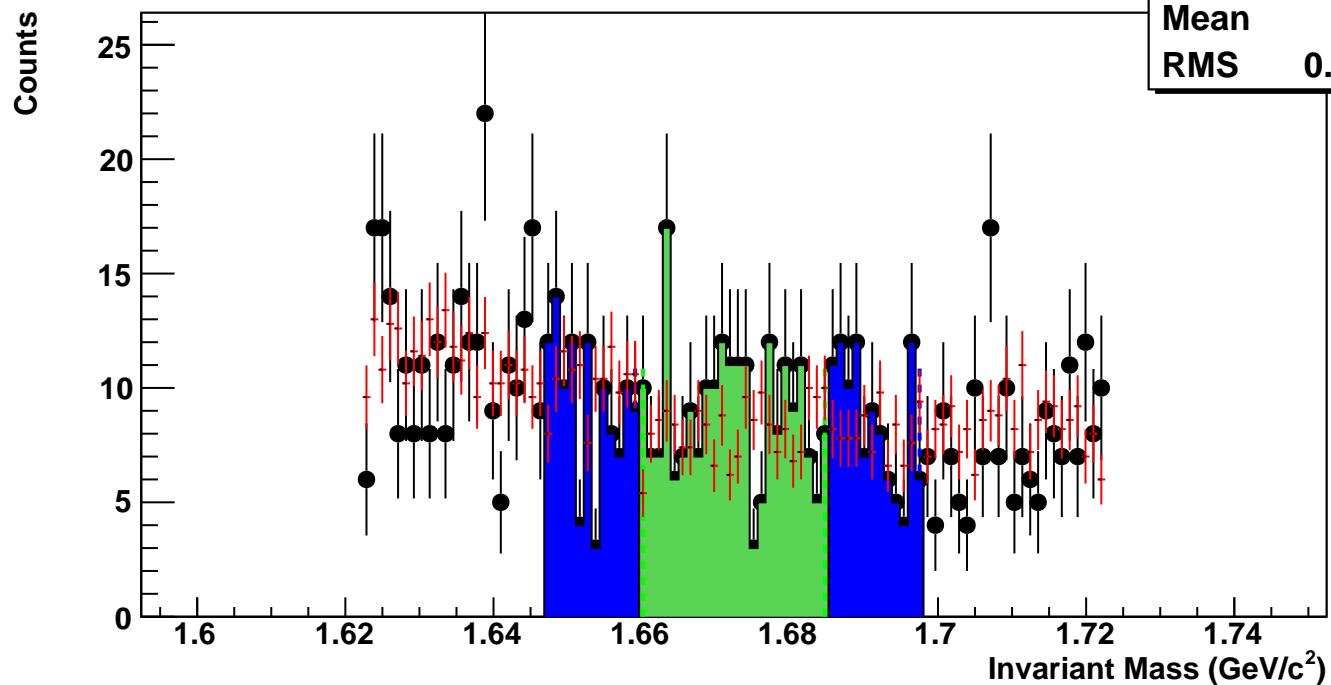
$\Omega^-$ , Au+Au 39 GeV, 5-10%,  $p_T$  0.5-0.8 GeV/c

hmlInvMassBgCent4Pt1  
Entries 60  
Mean 1.667  
RMS 0.02883



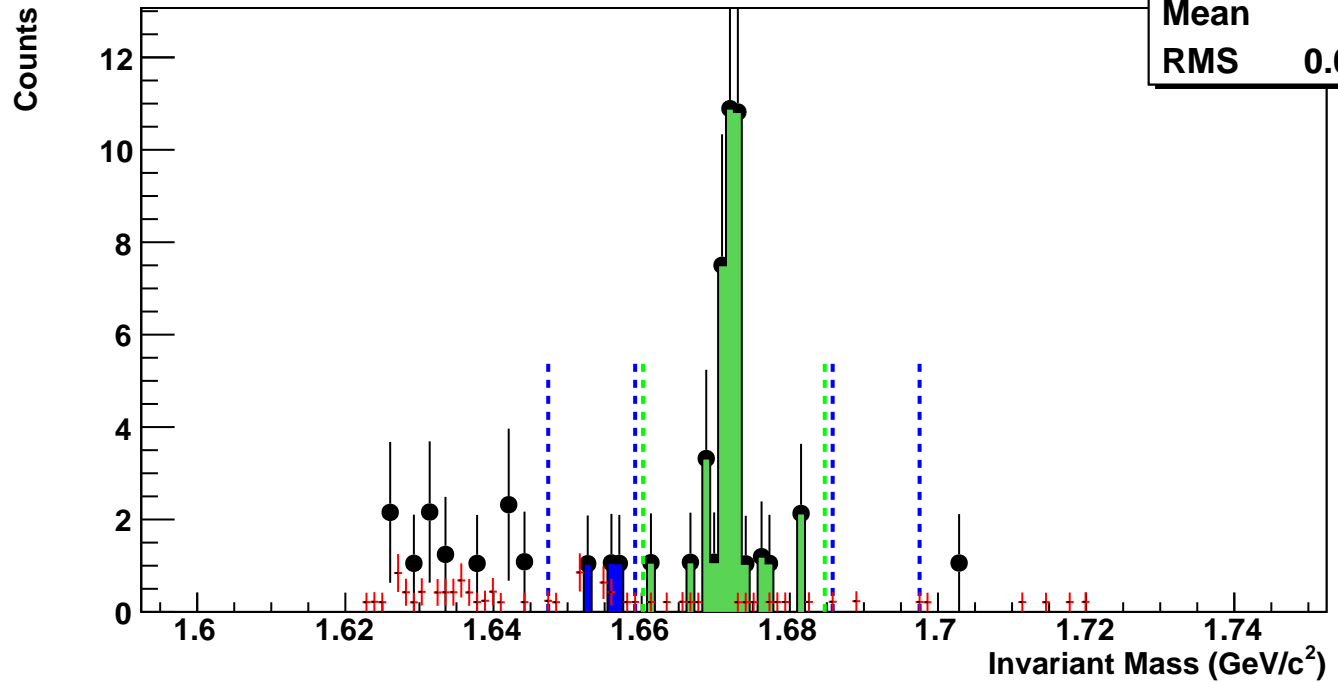
$\Omega^-$ , Au+Au 39 GeV, 0-5%,  $p_T$  0.5-0.8 GeV/c

hmlInvMassBgCent5Pt1  
Entries 106  
Mean 1.669  
RMS 0.02958



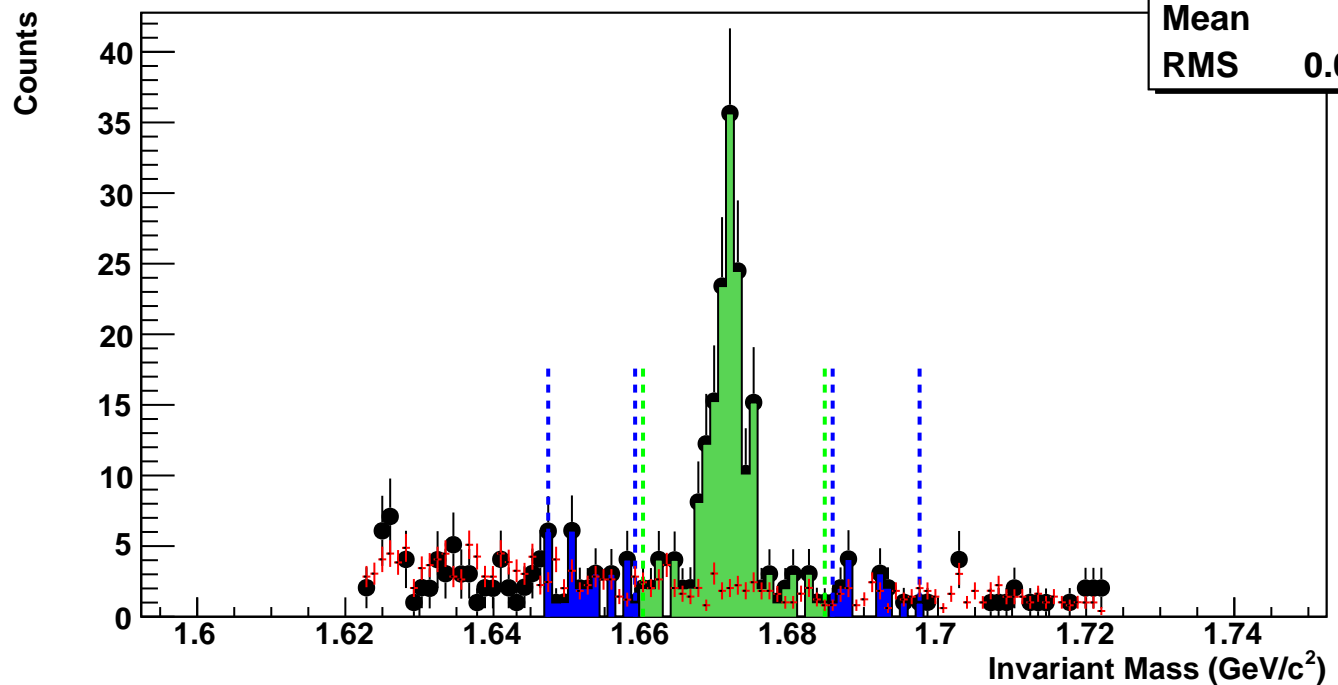
$\Omega^-$ , Au+Au 39 GeV, 60-80%,  $p_T$  0.8-1.1 GeV/c

hmlInvMassBgCent0Pt2	
Entries	2
Mean	1.654
RMS	0.02538



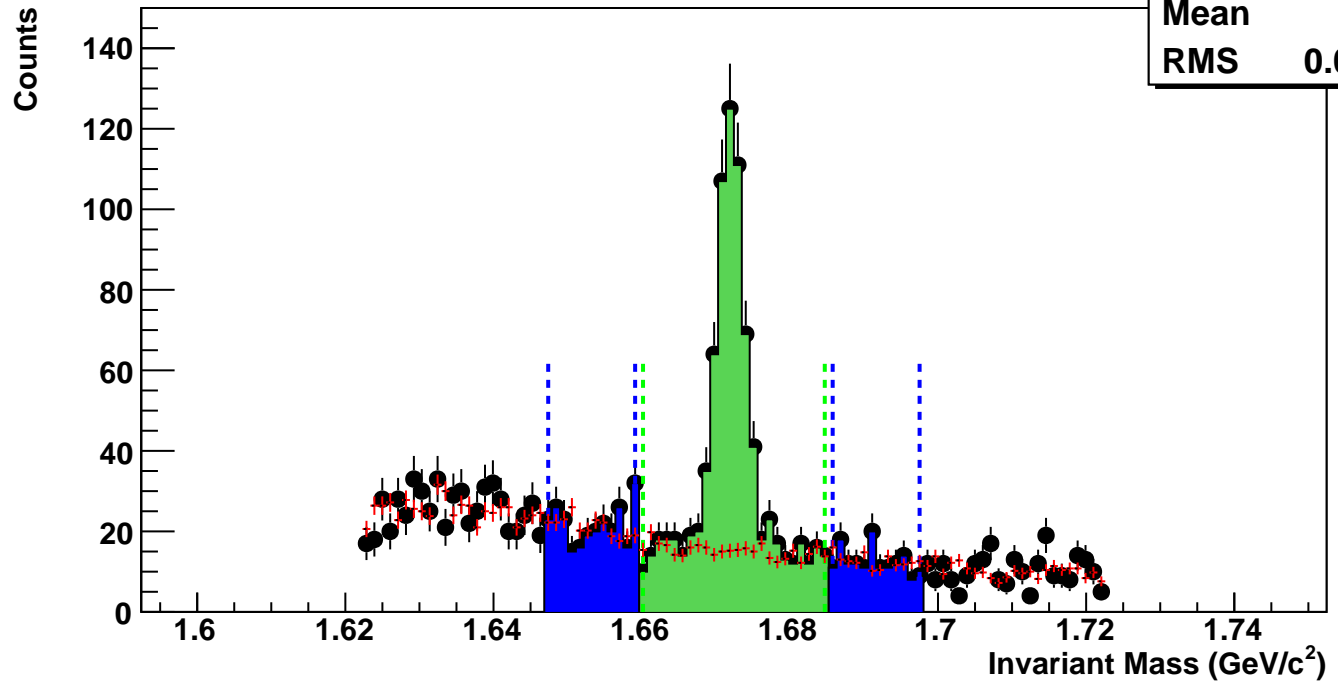
$\Omega^-$ , Au+Au 39 GeV, 40-60%,  $p_T$  0.8-1.1 GeV/c

hmlInvMassBgCent1Pt2	
Entries	25
Mean	1.661
RMS	0.02798



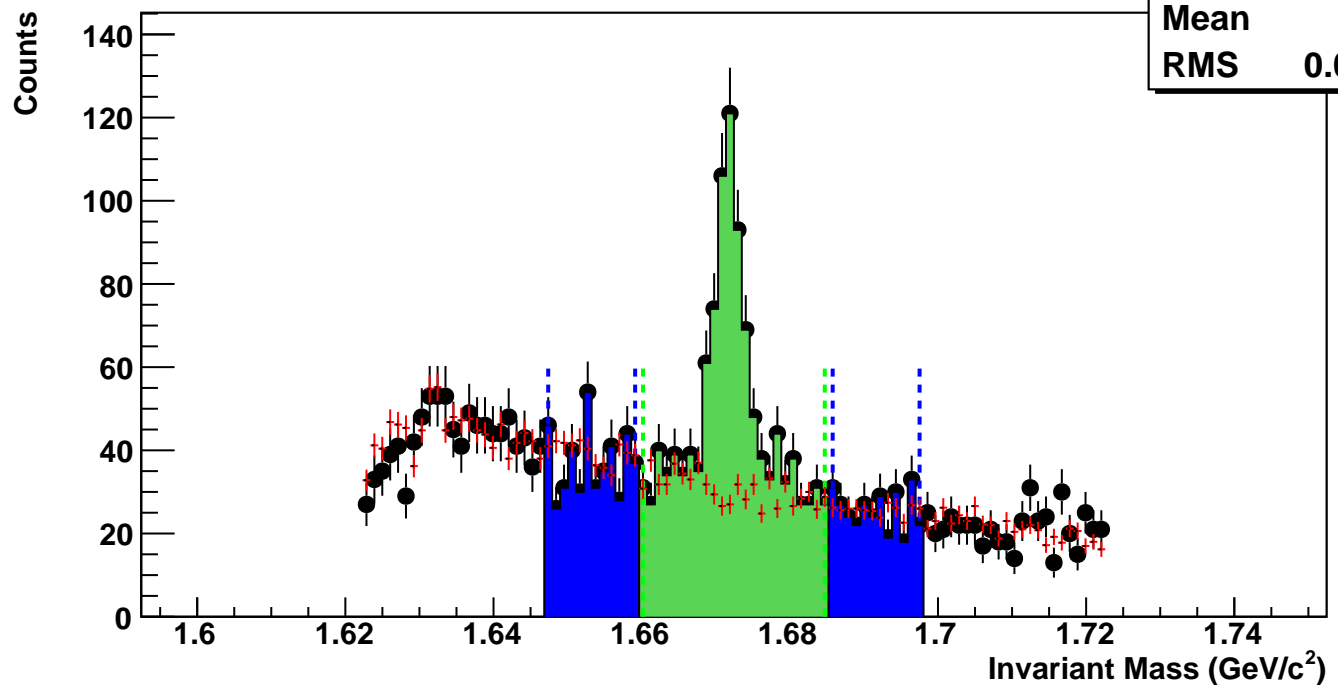
$\Omega^-$ , Au+Au 39 GeV, 20-40%,  $p_T$  0.8-1.1 GeV/c

hmlInvMassBgCent2Pt2	
Entries	193
Mean	1.663
RMS	0.02784



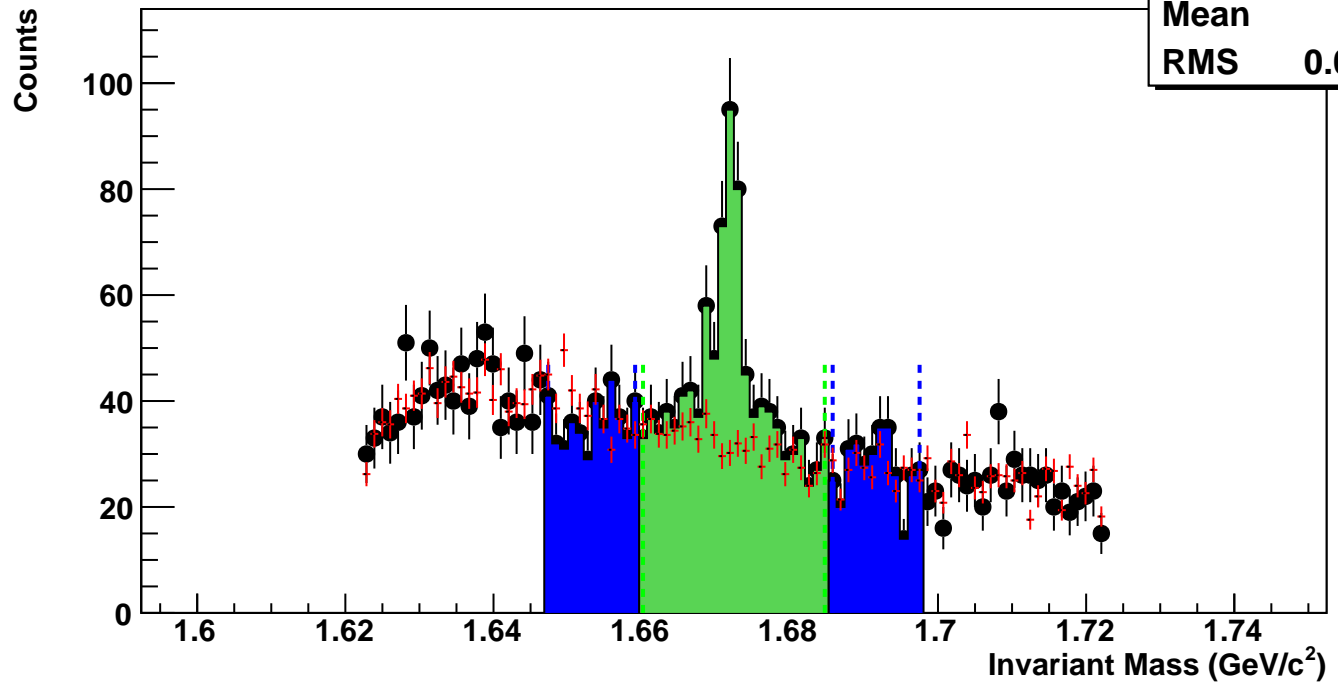
$\Omega^-$ , Au+Au 39 GeV, 10-20%,  $p_T$  0.8-1.1 GeV/c

hmlInvMassBgCent3Pt2	
Entries	367
Mean	1.665
RMS	0.02788



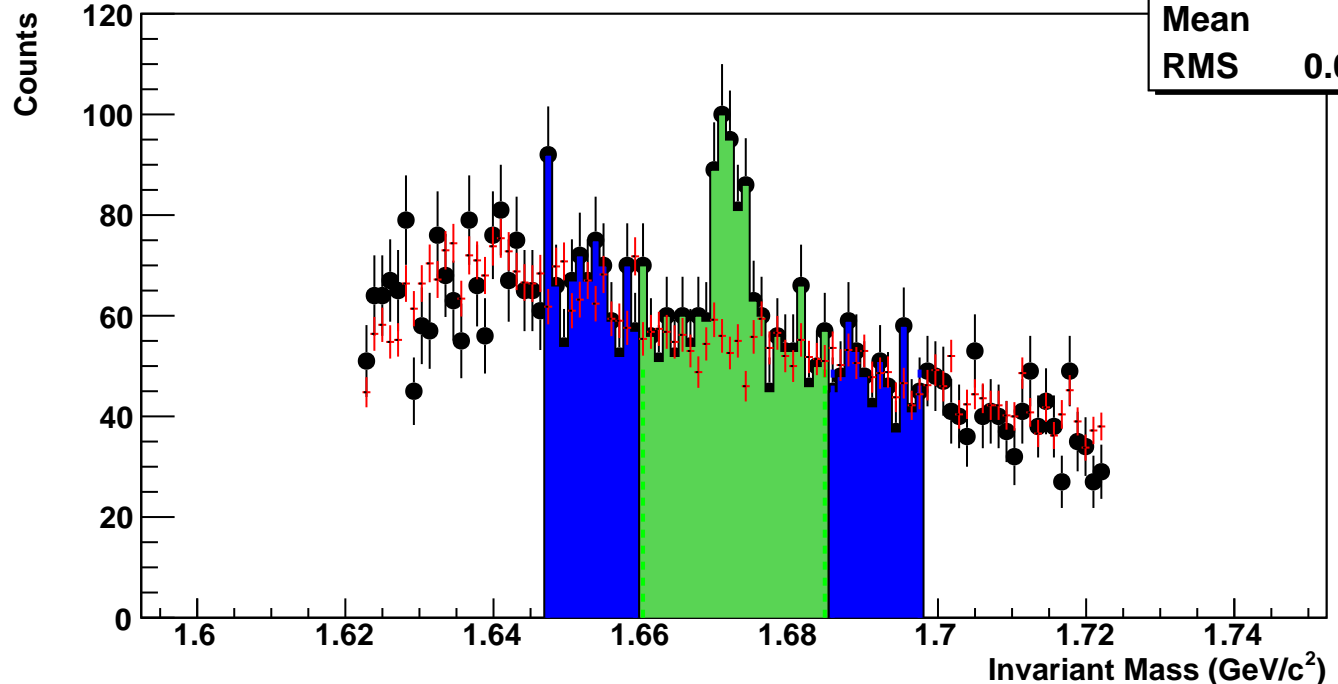
$\Omega^-$ , Au+Au 39 GeV, 5-10%,  $p_T$  0.8-1.1 GeV/c

hmlInvMassBgCent4Pt2	
Entries	372
Mean	1.667
RMS	0.02825



$\Omega^-$ , Au+Au 39 GeV, 0-5%,  $p_T$  0.8-1.1 GeV/c

hmlInvMassBgCent5Pt2	
Entries	626
Mean	1.668
RMS	0.02807



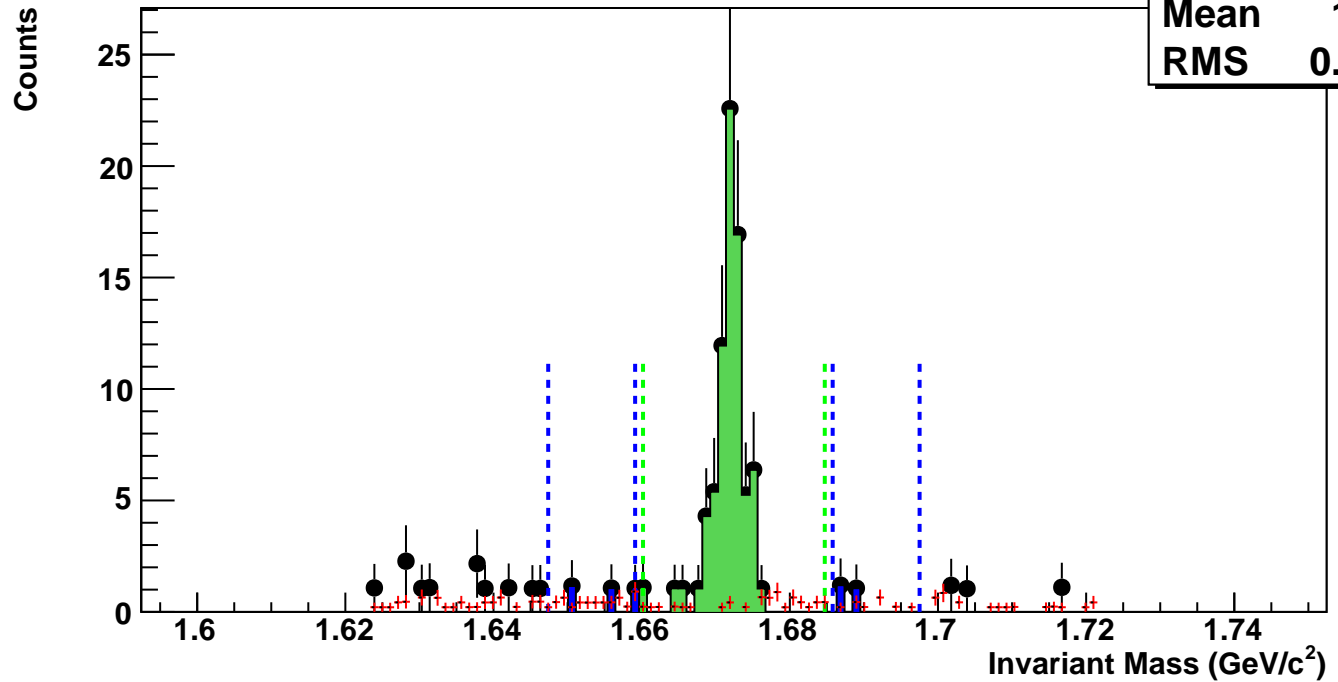
$\Omega^-$ , Au+Au 39 GeV, 60-80%,  $p_T$  1.1-1.4 GeV/c

hmlInvMassBgCent0Pt3

Entries 3

Mean 1.667

RMS 0.0262



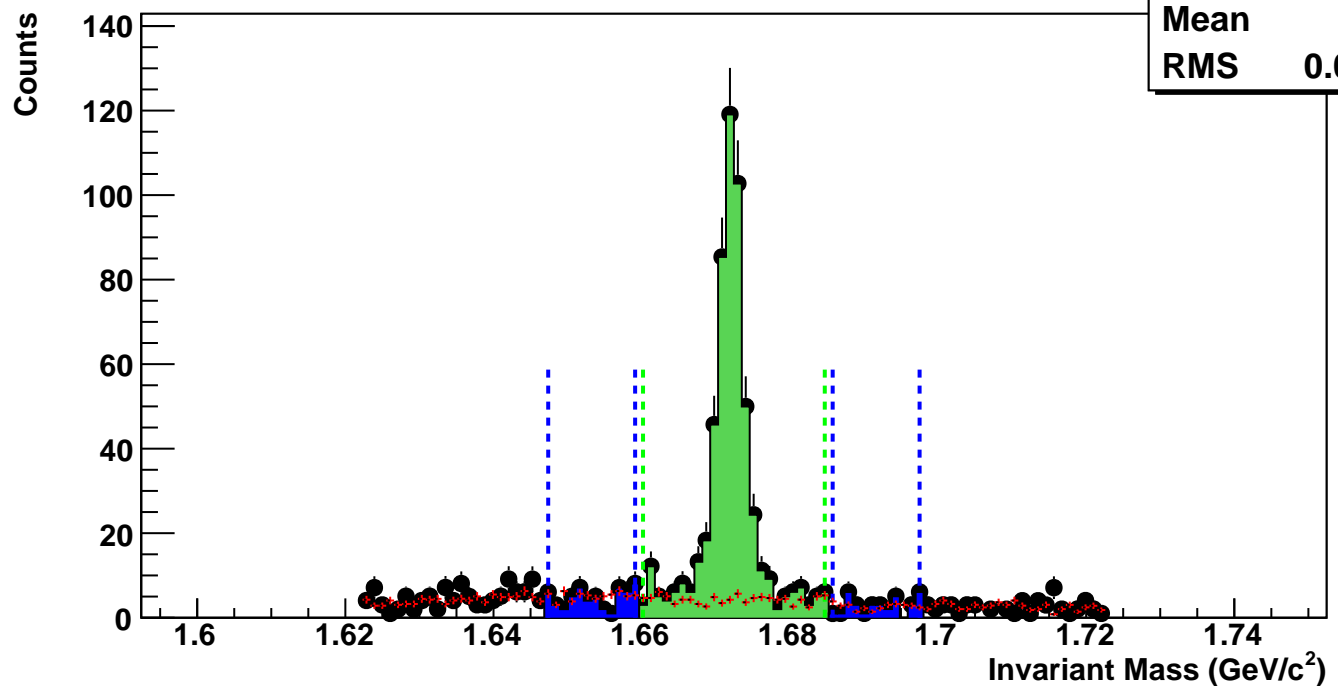
$\Omega^-$ , Au+Au 39 GeV, 40-60%,  $p_T$  1.1-1.4 GeV/c

hmlInvMassBgCent1Pt3

Entries 42

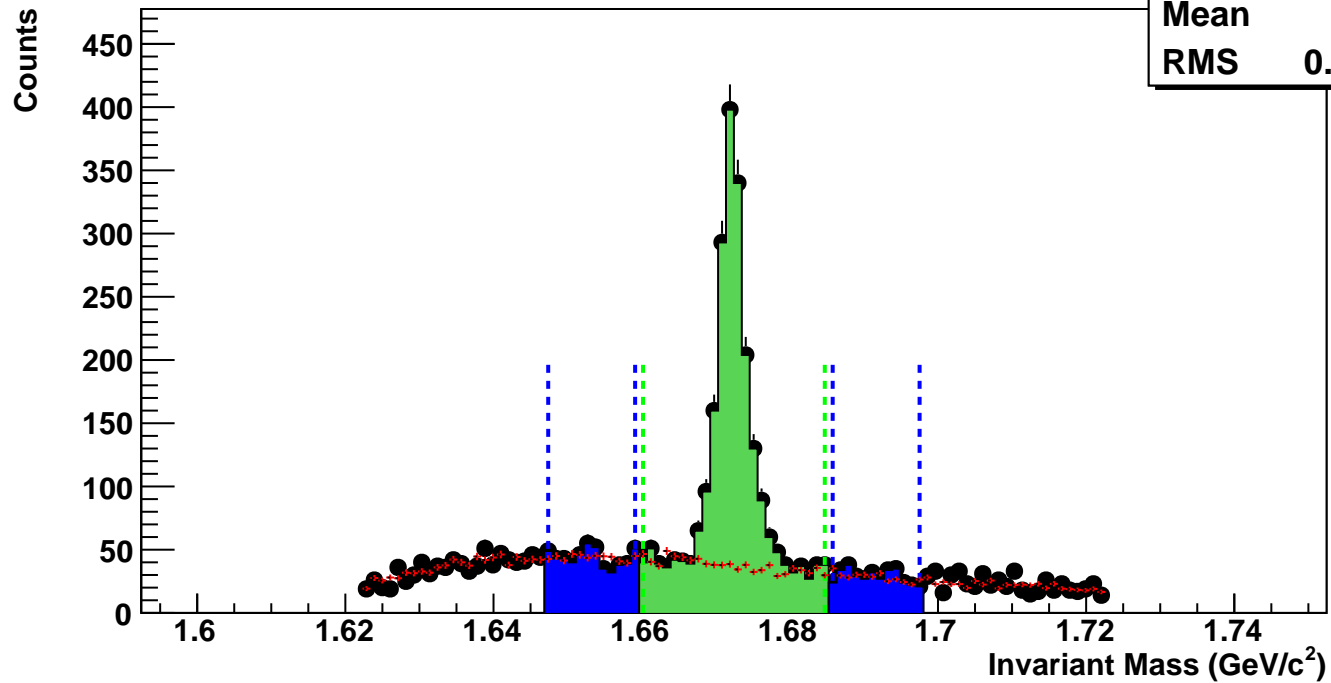
Mean 1.667

RMS 0.02674



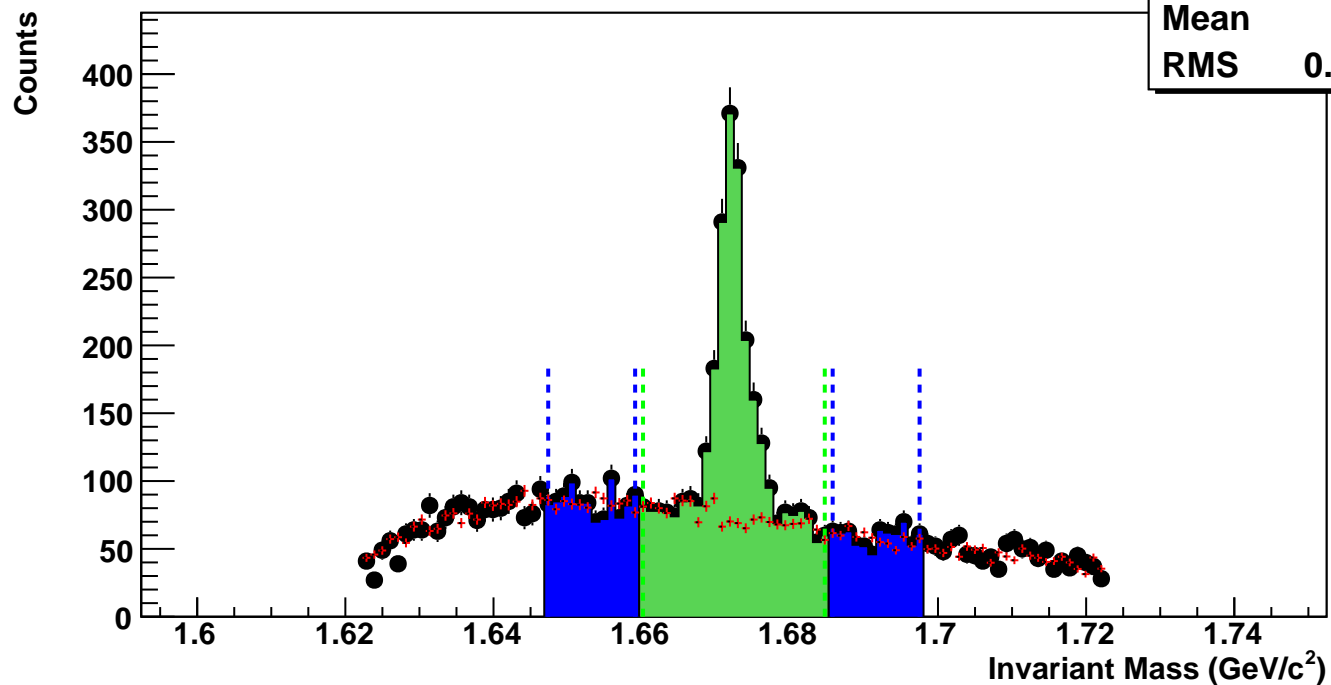
$\Omega^-$ , Au+Au 39 GeV, 20-40%,  $p_T$  1.1-1.4 GeV/c

hmlInvMassBgCent2Pt3	
Entries	377
Mean	1.667
RMS	0.02639



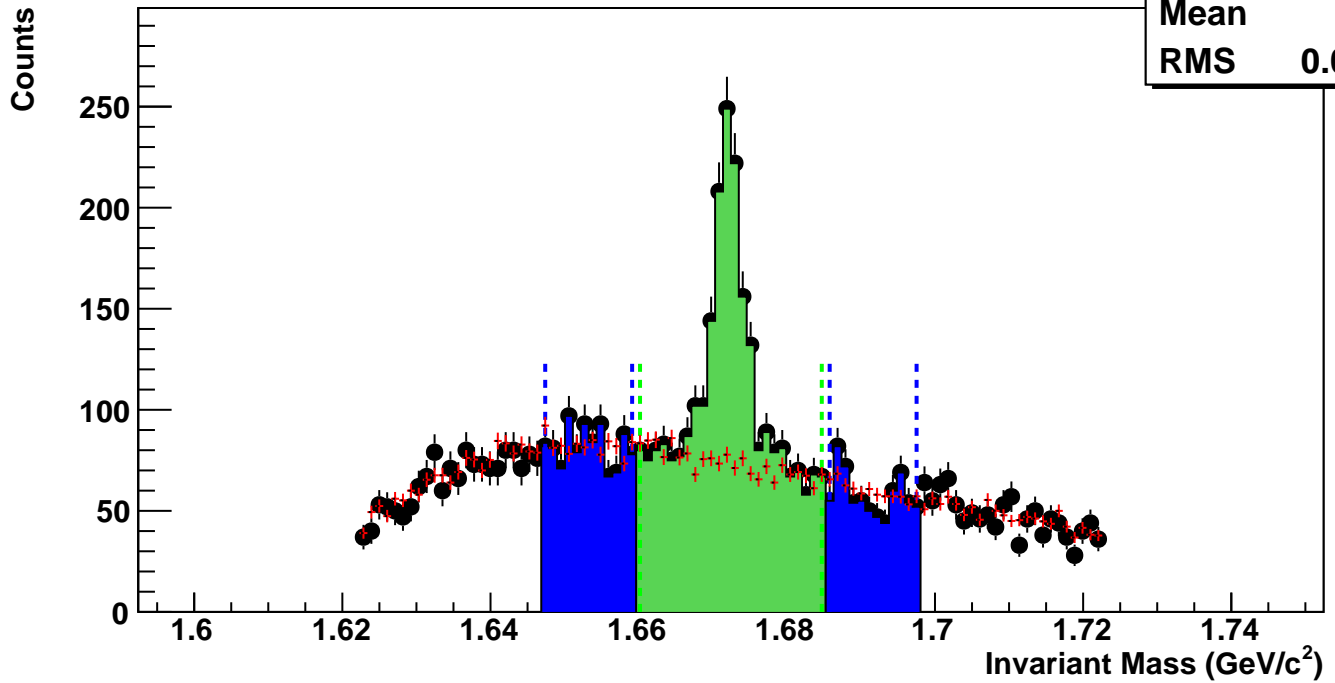
$\Omega^-$ , Au+Au 39 GeV, 10-20%,  $p_T$  1.1-1.4 GeV/c

hmlInvMassBgCent3Pt3	
Entries	744
Mean	1.668
RMS	0.02656



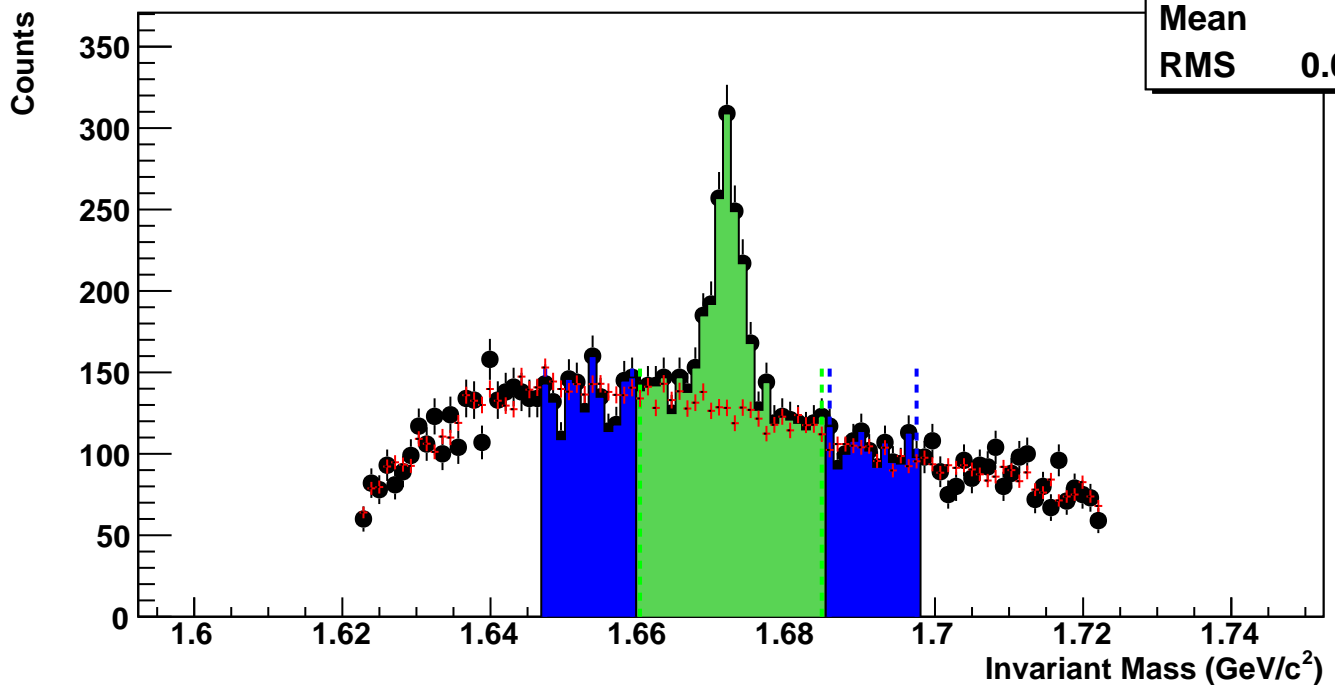
$\Omega^-$ , Au+Au 39 GeV, 5-10%,  $p_T$  1.1-1.4 GeV/c

hmlInvMassBgCent4Pt3	
Entries	743
Mean	1.669
RMS	0.02672



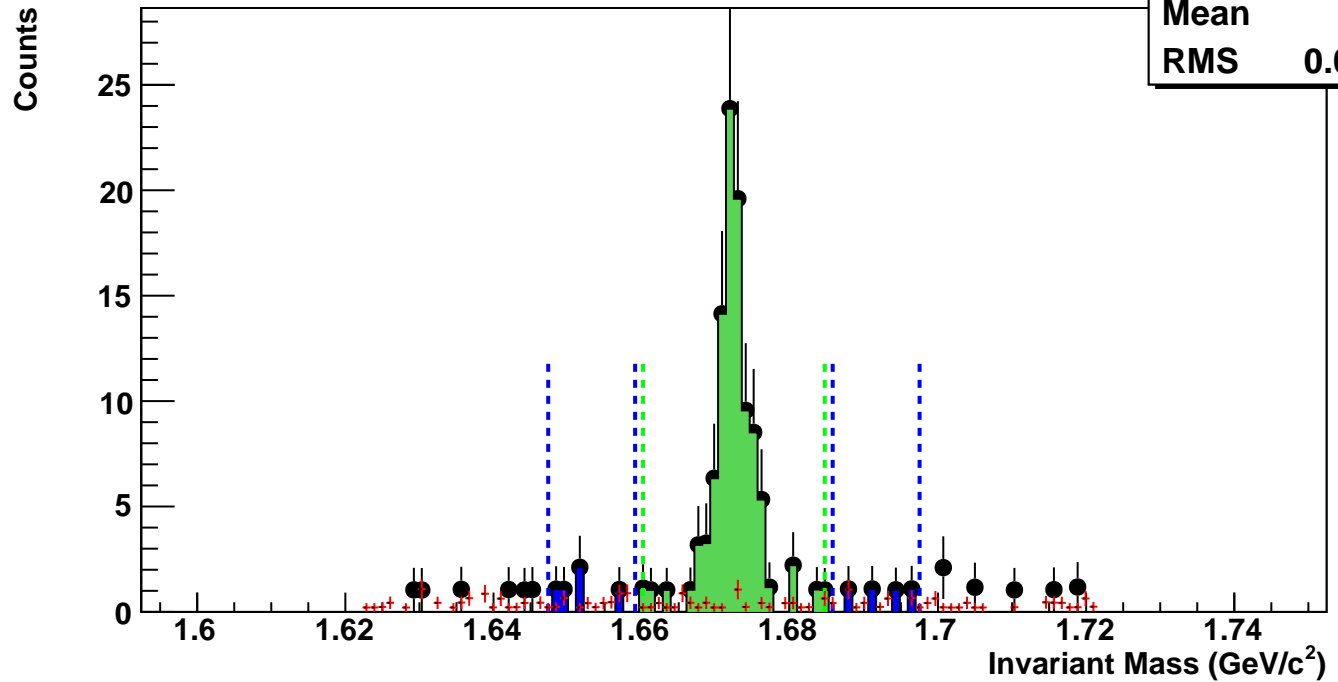
$\Omega^-$ , Au+Au 39 GeV, 0-5%,  $p_T$  1.1-1.4 GeV/c

hmlInvMassBgCent5Pt3	
Entries	1278
Mean	1.669
RMS	0.02685



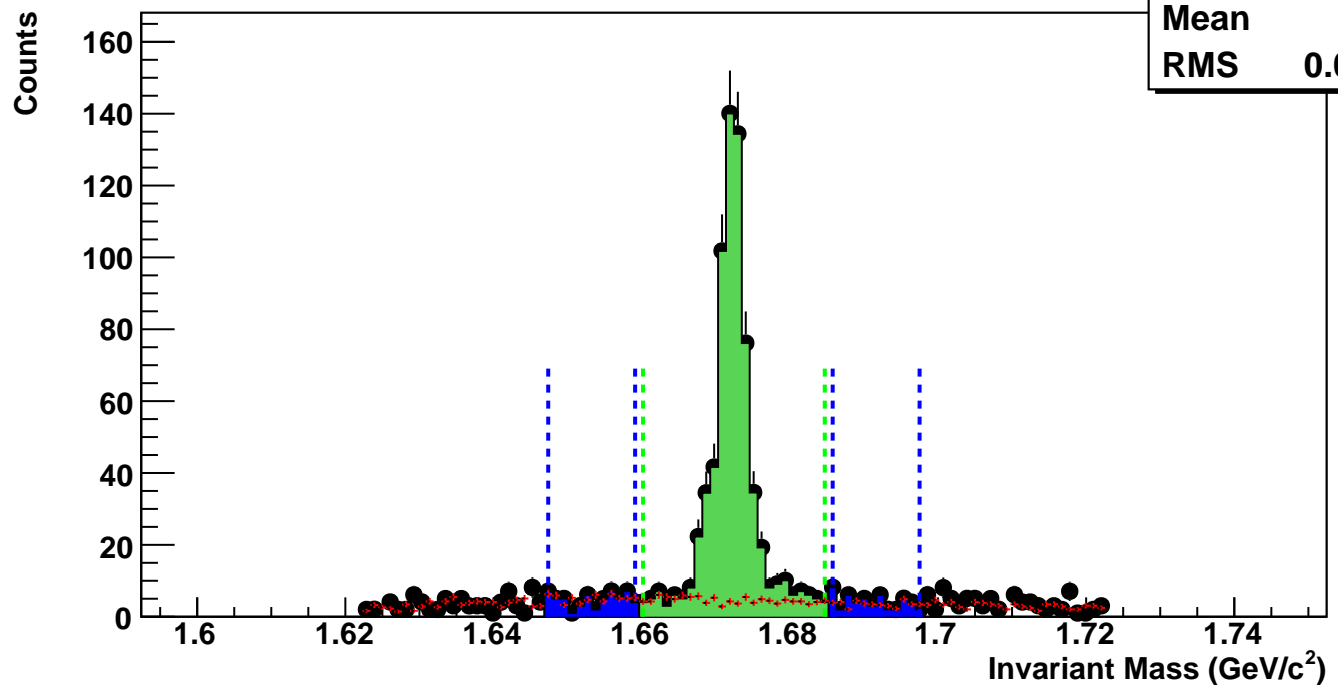
$\Omega^-$ , Au+Au 39 GeV, 60-80%,  $p_T$  1.4-1.7 GeV/c

hmlInvMassBgCent0Pt4	
Entries	3
Mean	1.67
RMS	0.02725



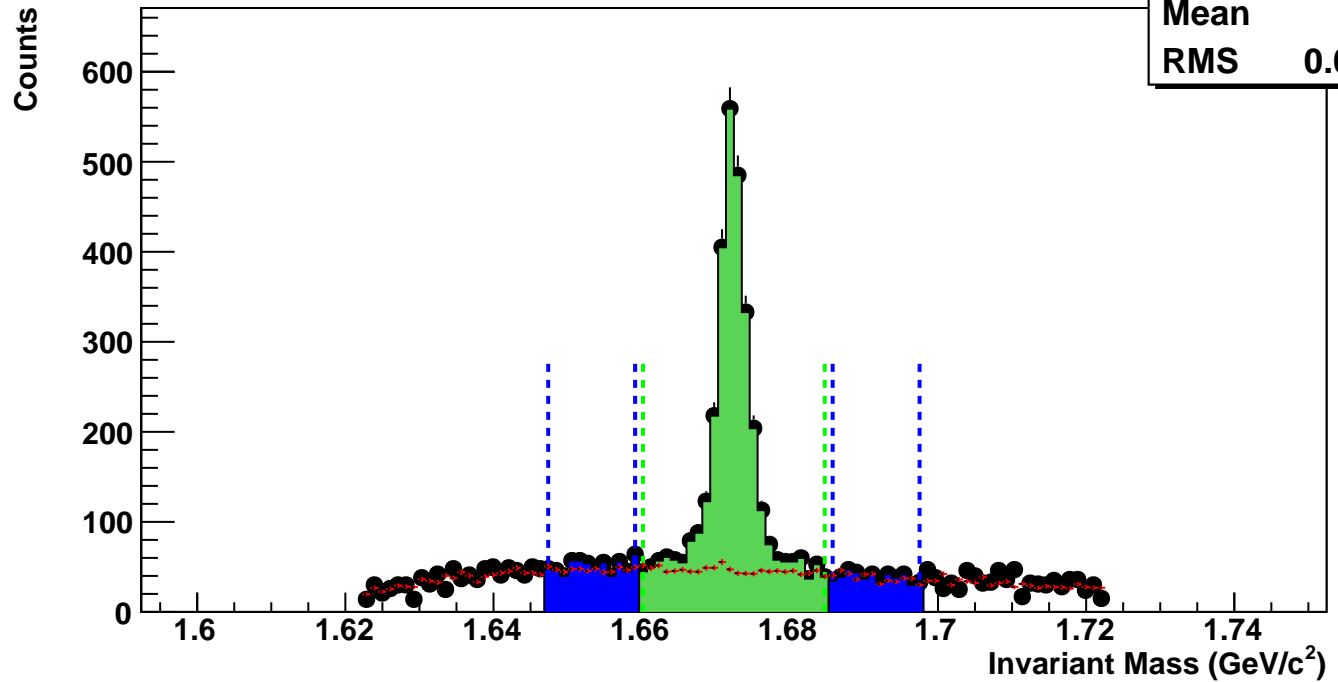
$\Omega^-$ , Au+Au 39 GeV, 40-60%,  $p_T$  1.4-1.7 GeV/c

hmlInvMassBgCent1Pt4	
Entries	43
Mean	1.67
RMS	0.02639



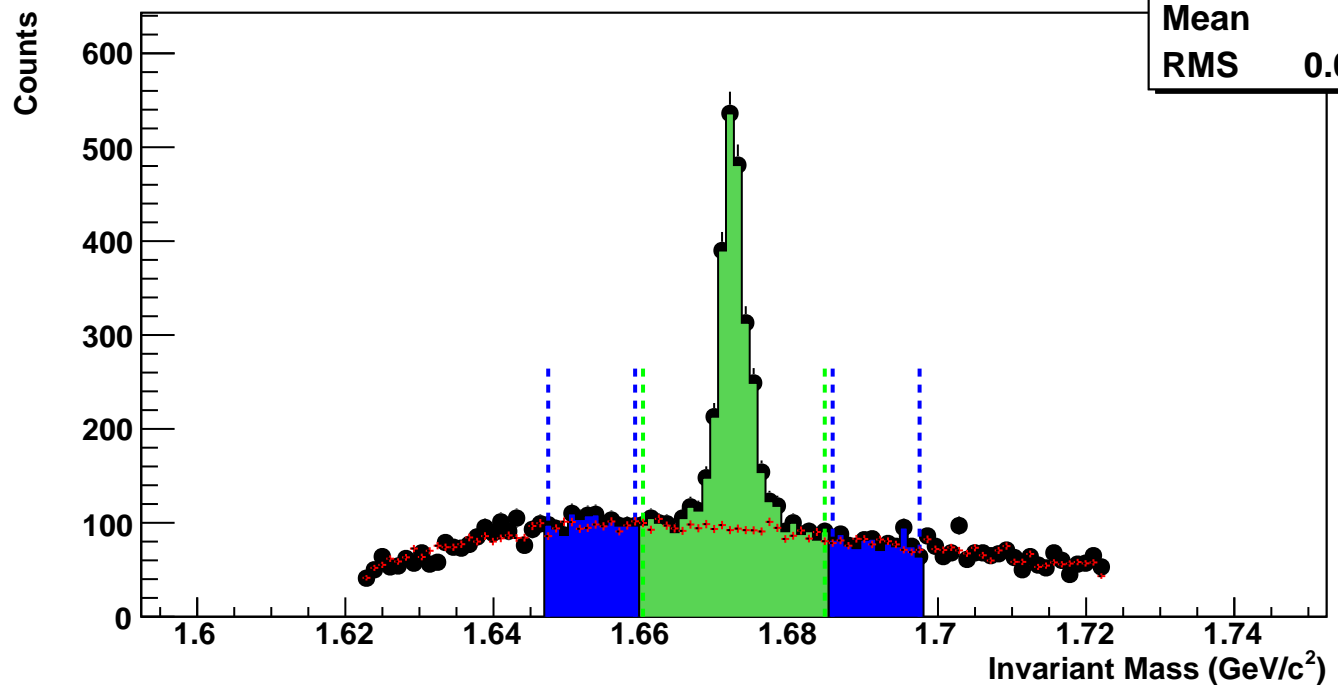
$\Omega^-$ , Au+Au 39 GeV, 20-40%,  $p_T$  1.4-1.7 GeV/c

hmlInvMassBgCent2Pt4	
Entries	446
Mean	1.671
RMS	0.02659



$\Omega^-$ , Au+Au 39 GeV, 10-20%,  $p_T$  1.4-1.7 GeV/c

hmlInvMassBgCent3Pt4	
Entries	912
Mean	1.671
RMS	0.02667



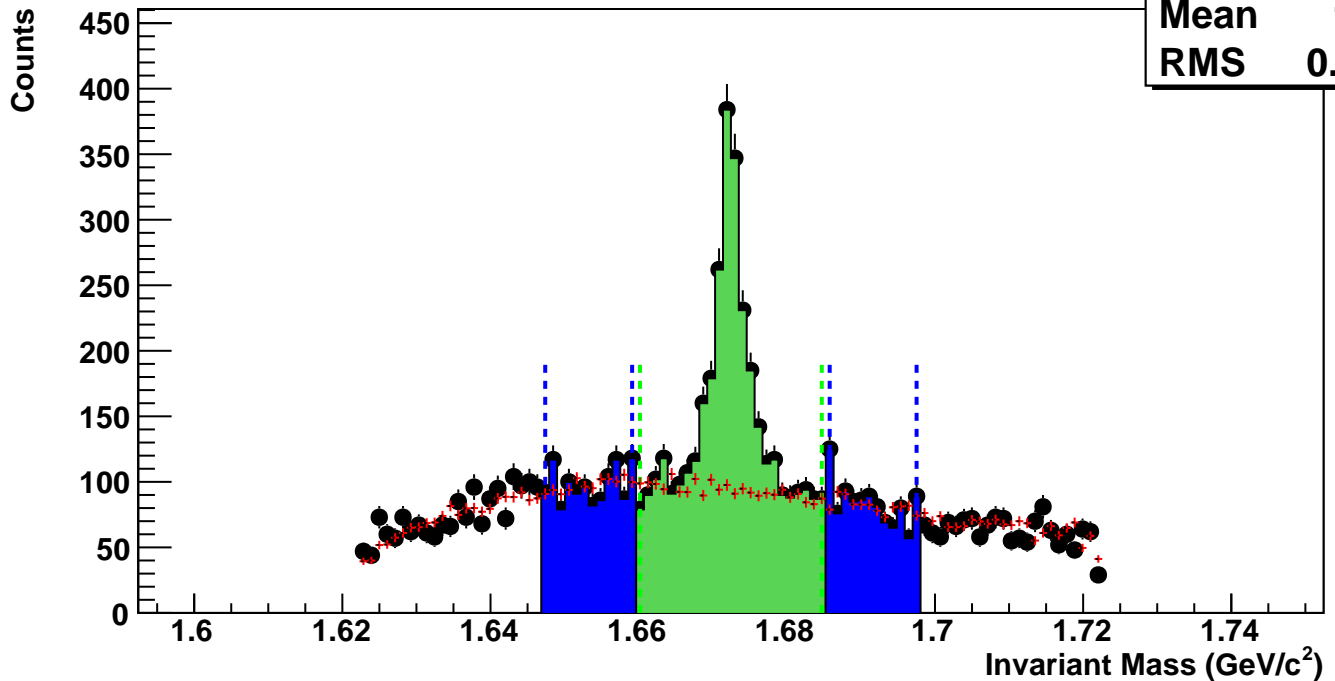
$\Omega^-$ , Au+Au 39 GeV, 5-10%,  $p_T$  1.4-1.7 GeV/c

hmlInvMassBgCent4Pt4

Entries 919

Mean 1.671

RMS 0.0266



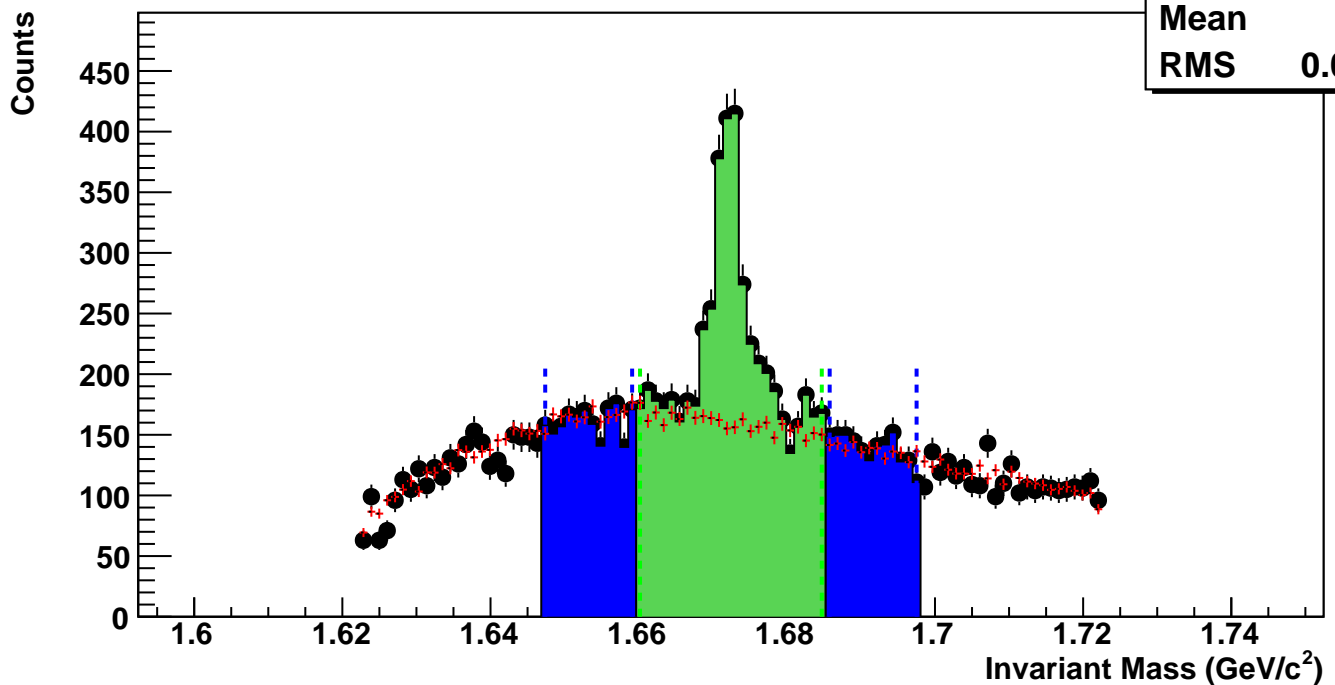
$\Omega^-$ , Au+Au 39 GeV, 0-5%,  $p_T$  1.4-1.7 GeV/c

hmlInvMassBgCent5Pt4

Entries 1571

Mean 1.671

RMS 0.02674



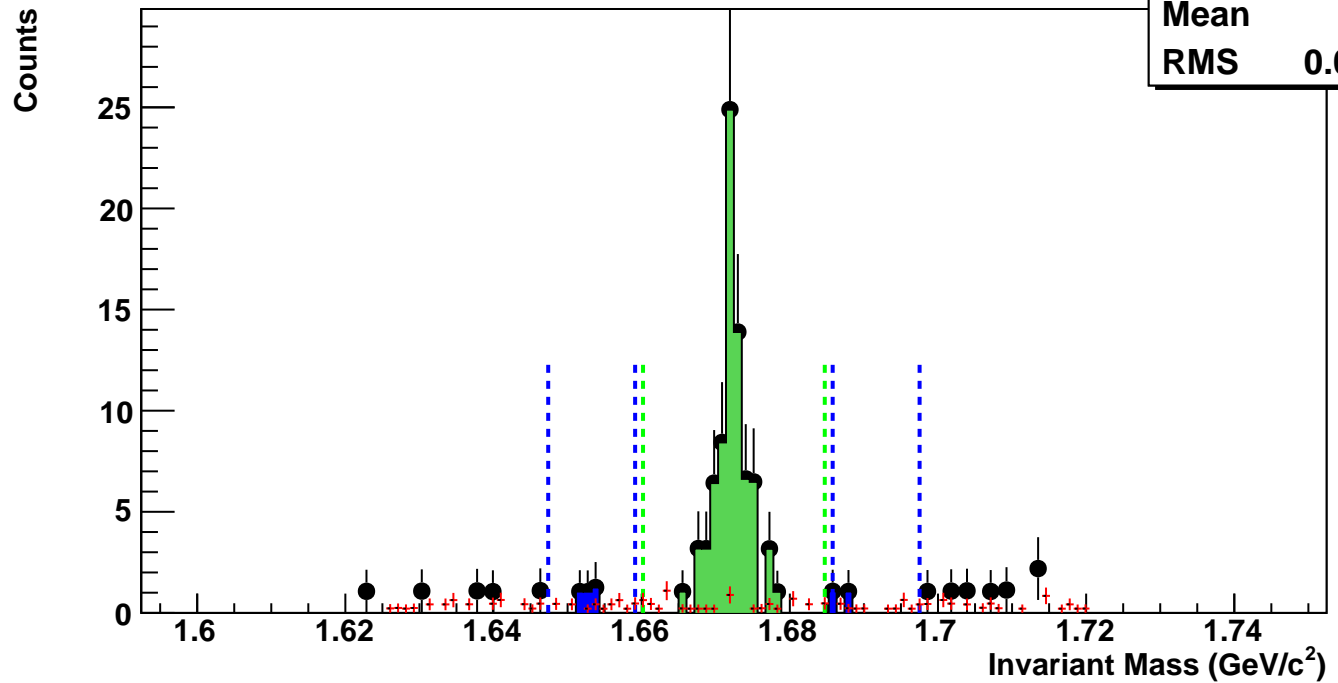
$\Omega^-$ , Au+Au 39 GeV, 60-80%,  $p_T$  1.7-2.0 GeV/c

hmlInvMassBgCent0Pt5

Entries 3

Mean 1.672

RMS 0.02635



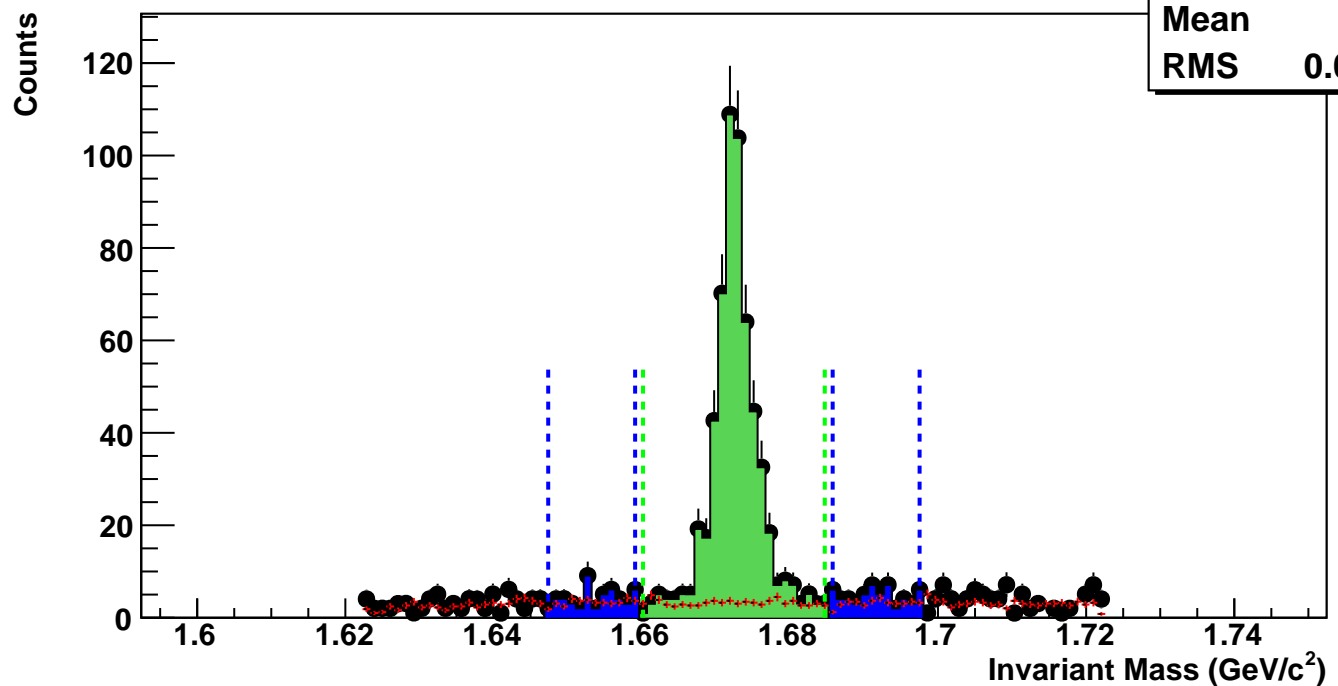
$\Omega^-$ , Au+Au 39 GeV, 40-60%,  $p_T$  1.7-2.0 GeV/c

hmlInvMassBgCent1Pt5

Entries 34

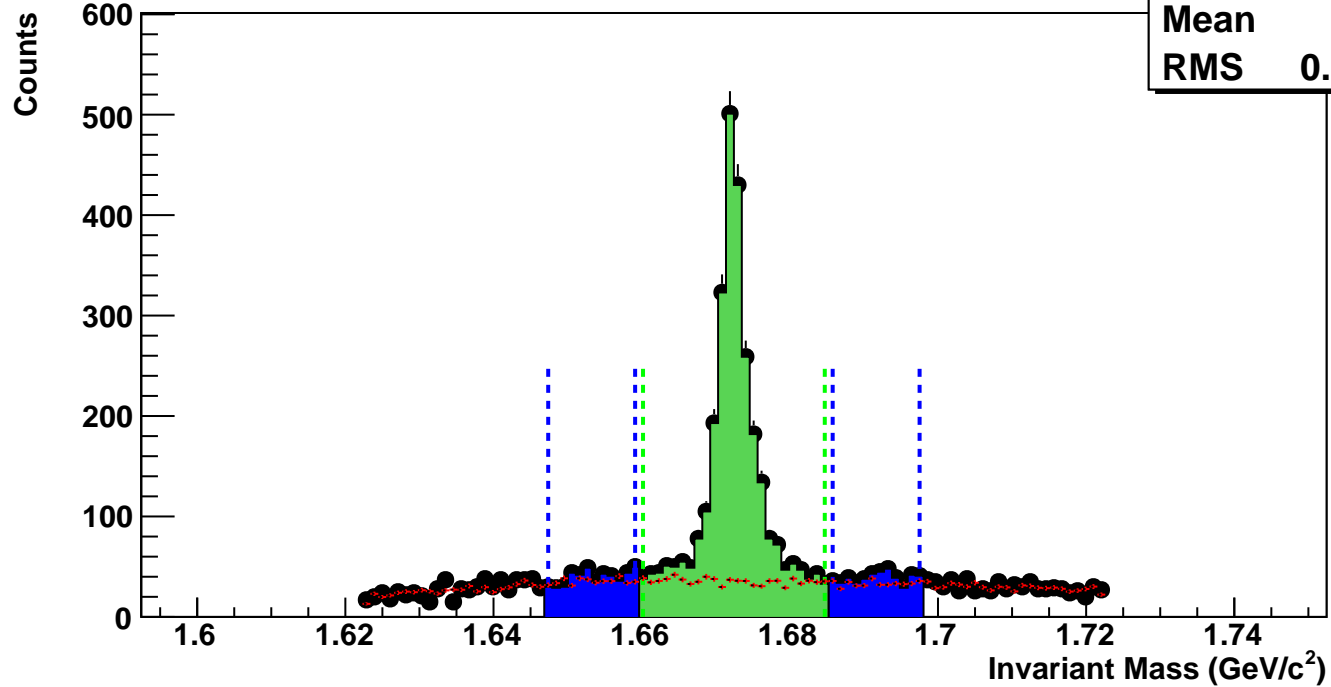
Mean 1.674

RMS 0.02742



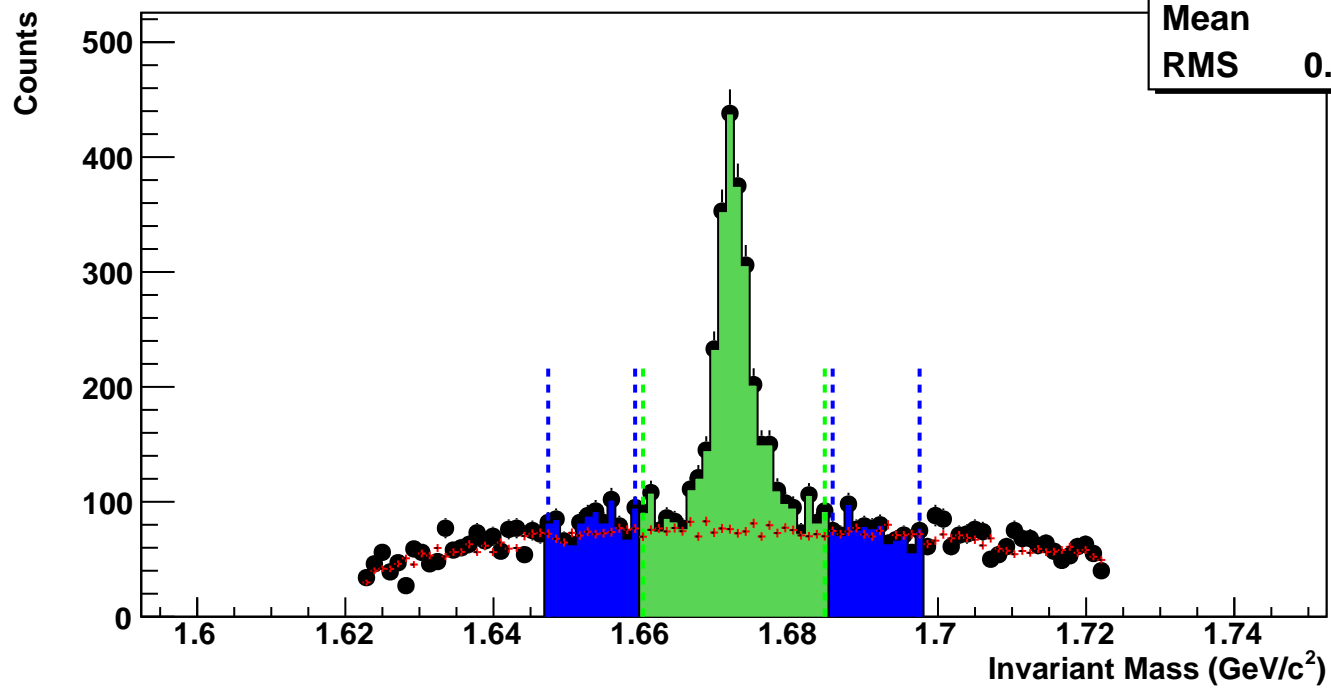
$\Omega^-$ , Au+Au 39 GeV, 20-40%,  $p_T$  1.7-2.0 GeV/c

hmlInvMassBgCent2Pt5  
Entries 360  
Mean 1.673  
RMS 0.02721



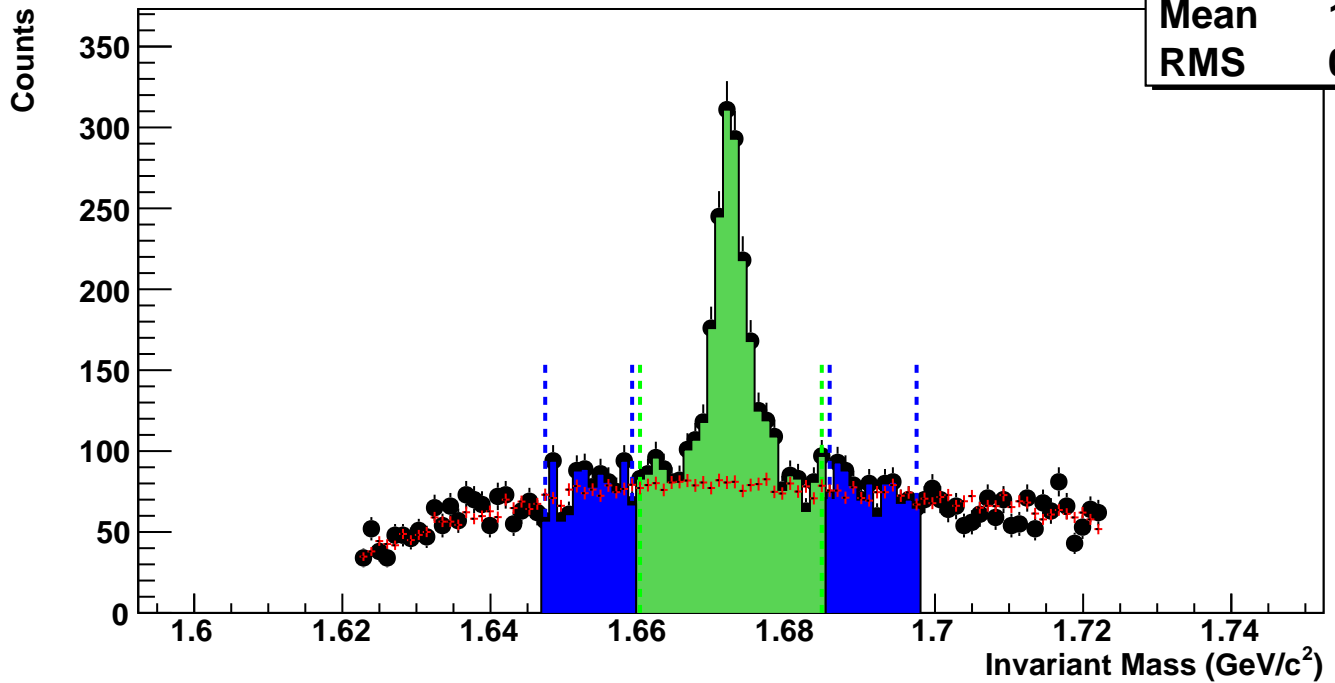
$\Omega^-$ , Au+Au 39 GeV, 10-20%,  $p_T$  1.7-2.0 GeV/c

hmlInvMassBgCent3Pt5  
Entries 757  
Mean 1.673  
RMS 0.02699



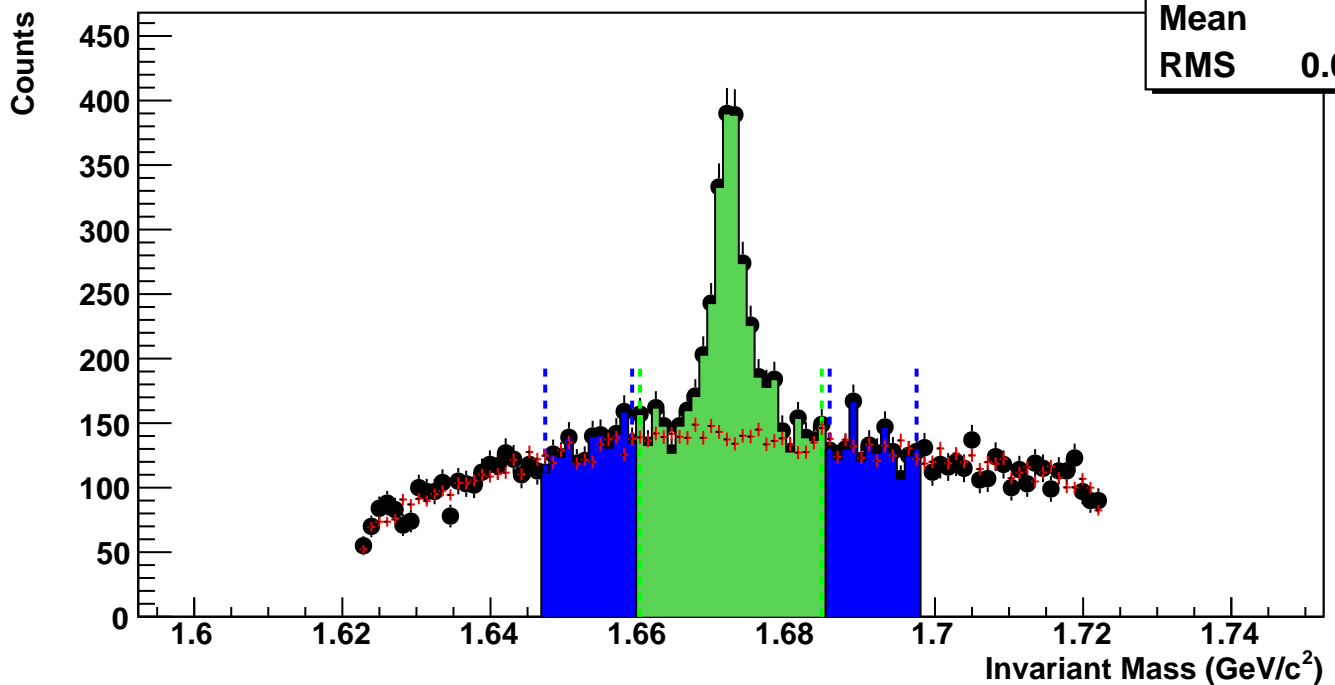
$\Omega^-$ , Au+Au 39 GeV, 5-10%,  $p_T$  1.7-2.0 GeV/c

hmlInvMassBgCent4Pt5	
Entries	783
Mean	1.674
RMS	0.027



$\Omega^-$ , Au+Au 39 GeV, 0-5%,  $p_T$  1.7-2.0 GeV/c

hmlInvMassBgCent5Pt5	
Entries	1372
Mean	1.674
RMS	0.02694



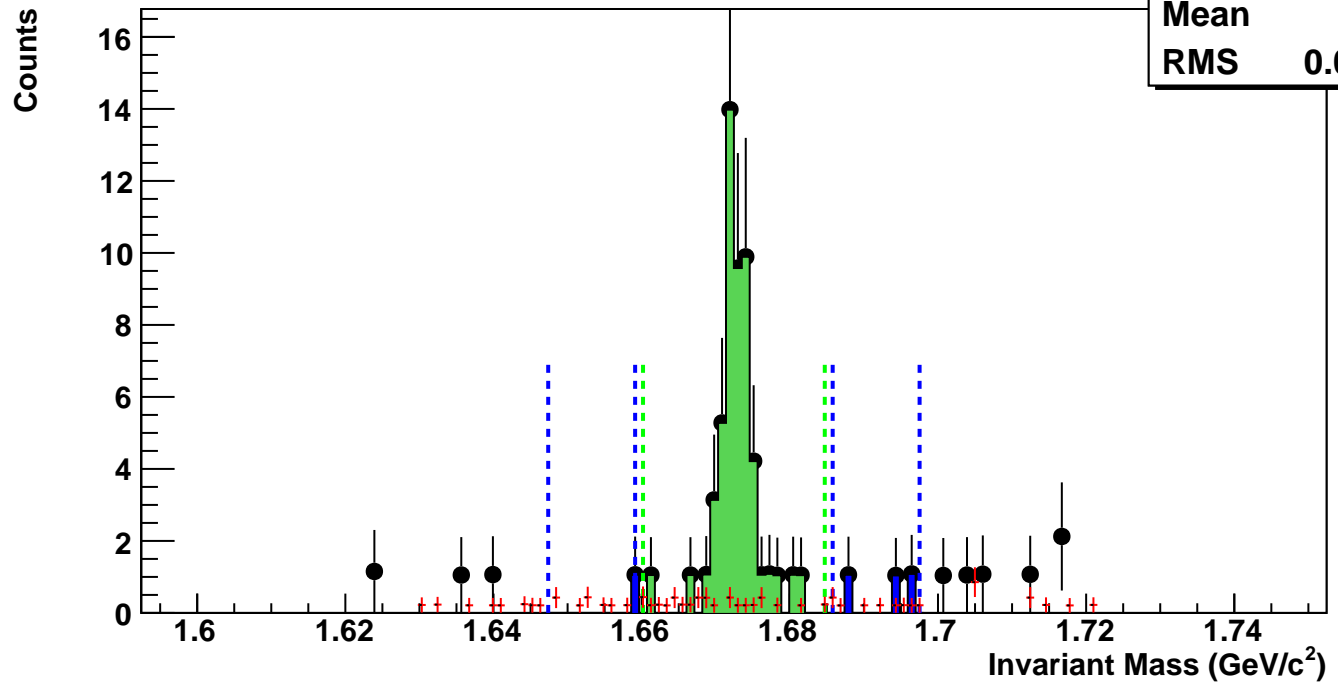
$\Omega^-$ , Au+Au 39 GeV, 60-80%,  $p_T$  2.0-2.4 GeV/c

hmlInvMassBgCent0Pt6

Entries 1

Mean 1.673

RMS 0.02292



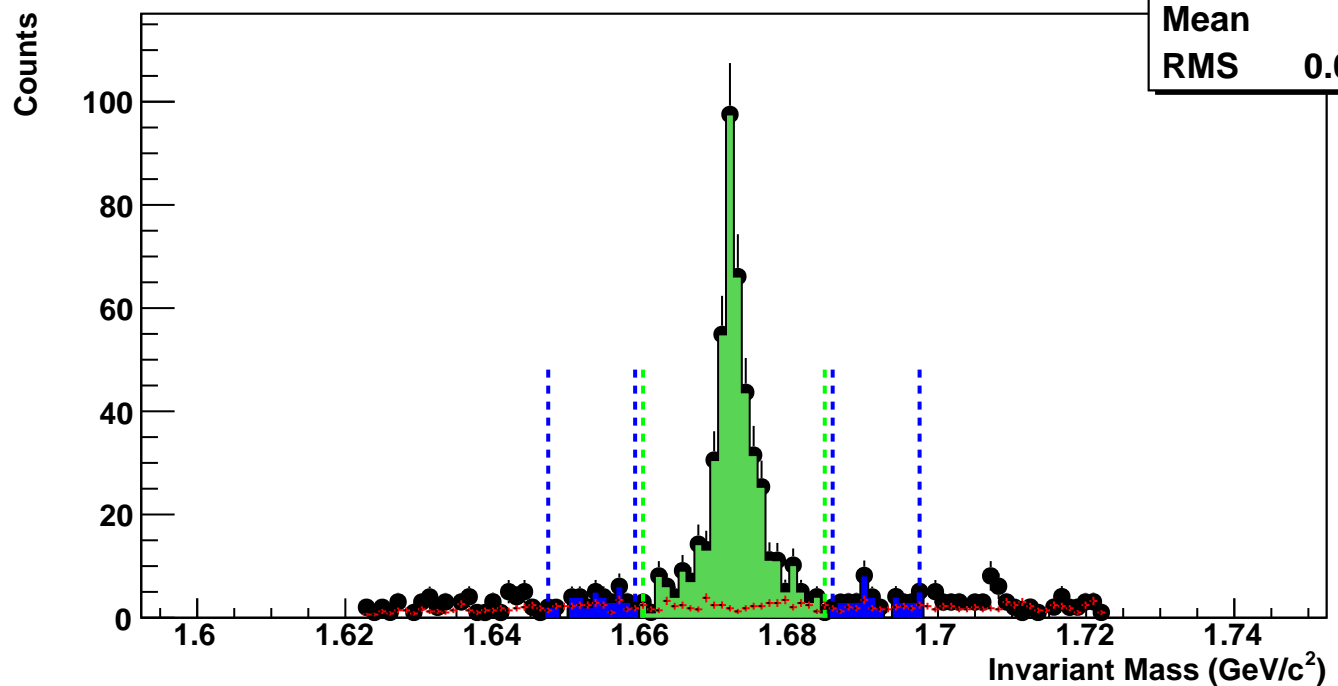
$\Omega^-$ , Au+Au 39 GeV, 40-60%,  $p_T$  2.0-2.4 GeV/c

hmlInvMassBgCent1Pt6

Entries 22

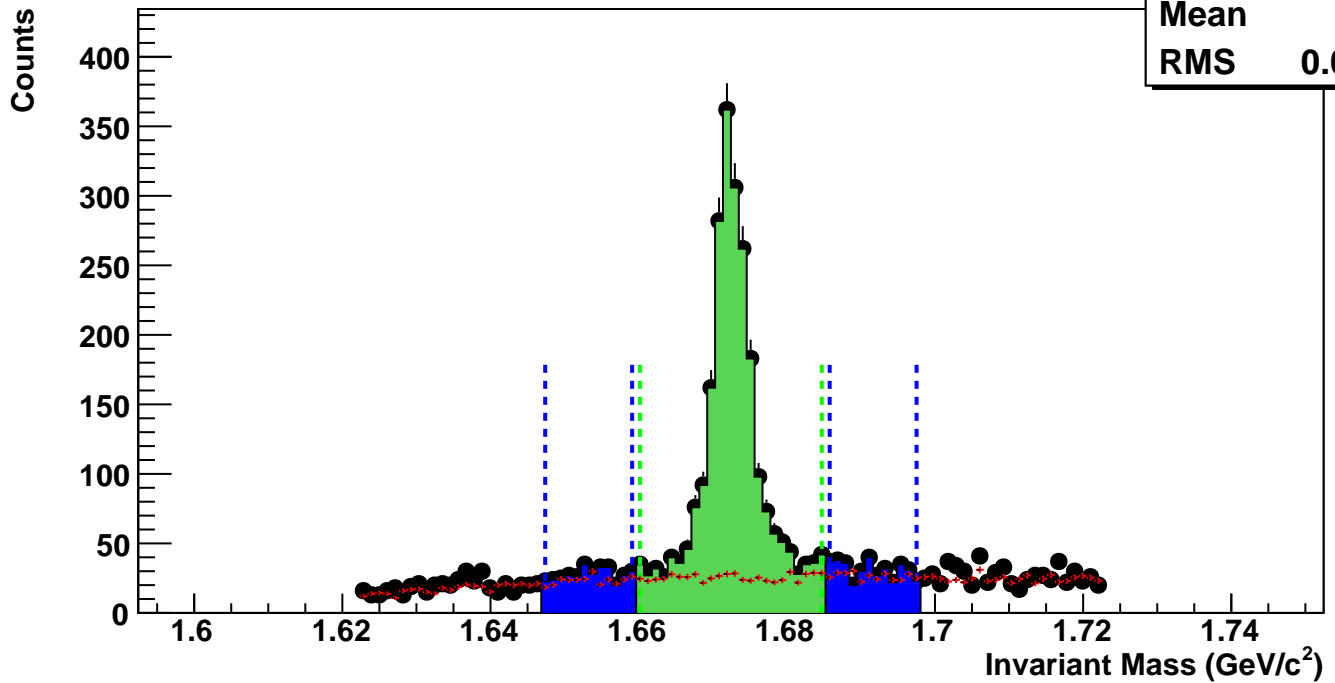
Mean 1.675

RMS 0.02694



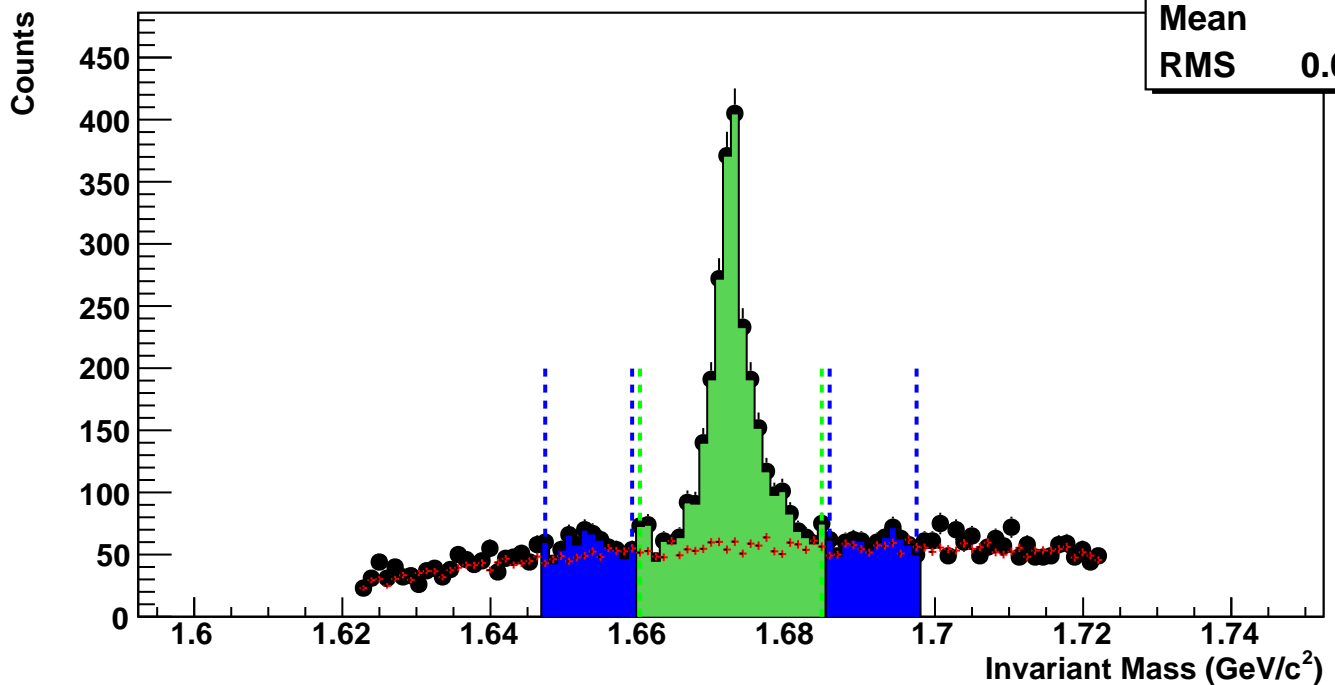
$\Omega^-$ , Au+Au 39 GeV, 20-40%,  $p_T$  2.0-2.4 GeV/c

hmlInvMassBgCent2Pt6	
Entries	264
Mean	1.676
RMS	0.02736



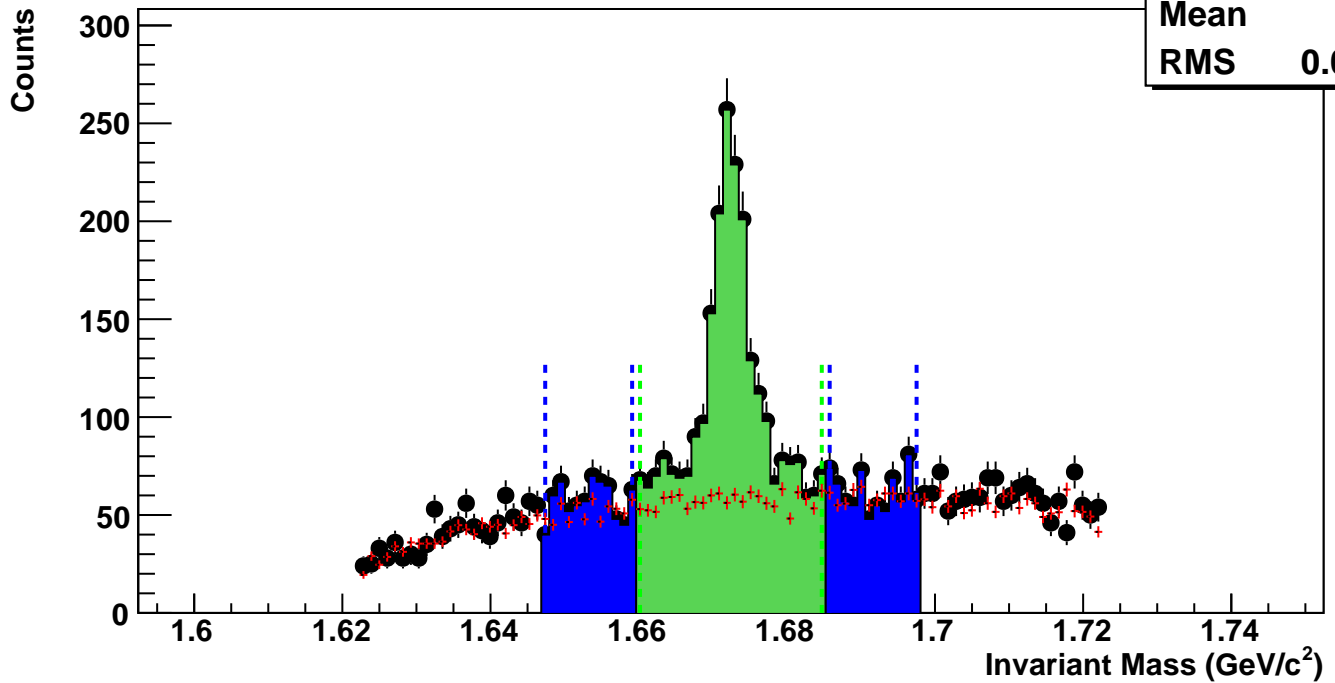
$\Omega^-$ , Au+Au 39 GeV, 10-20%,  $p_T$  2.0-2.4 GeV/c

hmlInvMassBgCent3Pt6	
Entries	568
Mean	1.676
RMS	0.02726



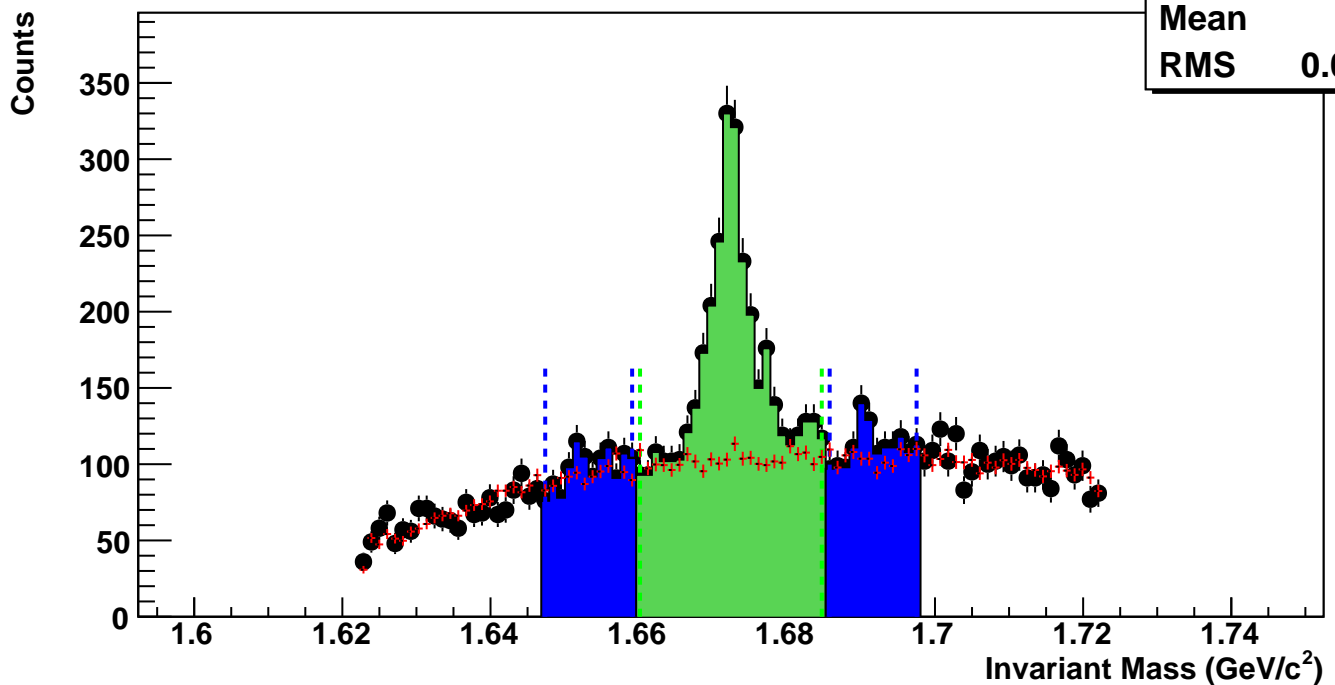
$\Omega^-$ , Au+Au 39 GeV, 5-10%,  $p_T$  2.0-2.4 GeV/c

hmlInvMassBgCent4Pt6	
Entries	591
Mean	1.676
RMS	0.02715



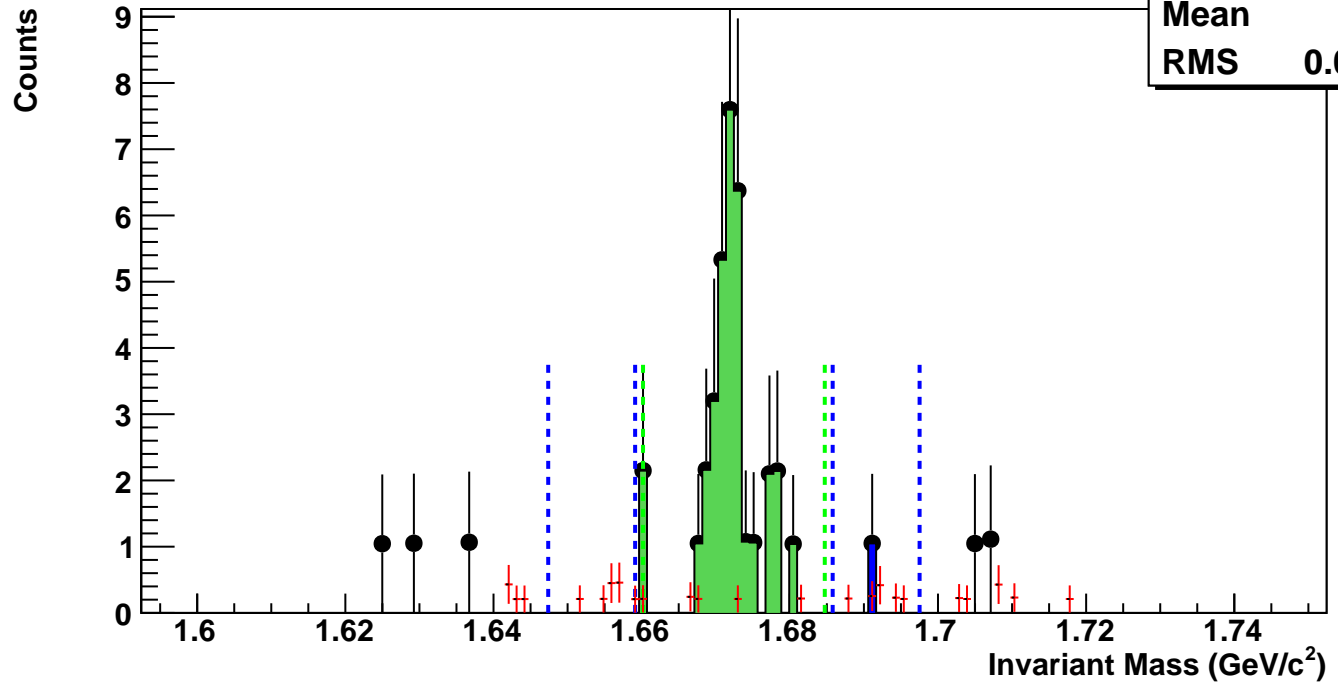
$\Omega^-$ , Au+Au 39 GeV, 0-5%,  $p_T$  2.0-2.4 GeV/c

hmlInvMassBgCent5Pt6	
Entries	1050
Mean	1.676
RMS	0.02704



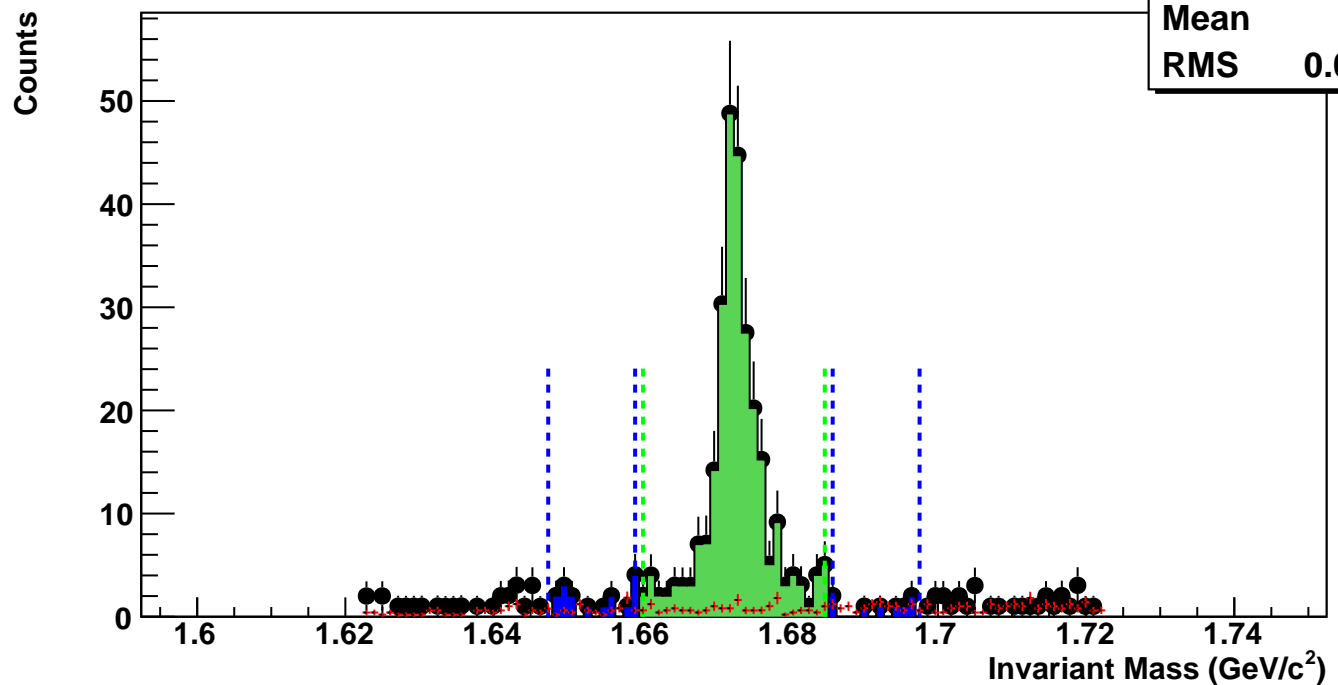
$\Omega^-$ , Au+Au 39 GeV, 60-80%,  $p_T$  2.4-2.8 GeV/c

hmlInvMassBgCent0Pt7	
Entries	1
Mean	1.676
RMS	0.02365



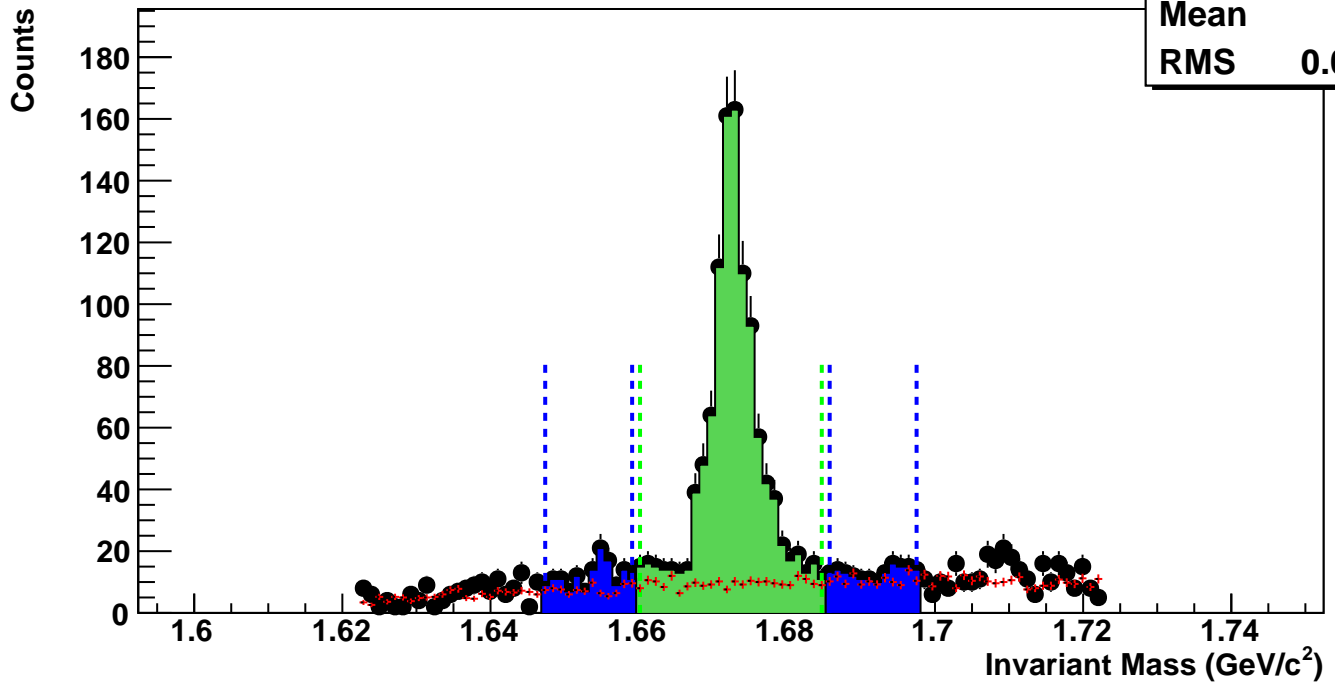
$\Omega^-$ , Au+Au 39 GeV, 40-60%,  $p_T$  2.4-2.8 GeV/c

hmlInvMassBgCent1Pt7	
Entries	8
Mean	1.68
RMS	0.02683



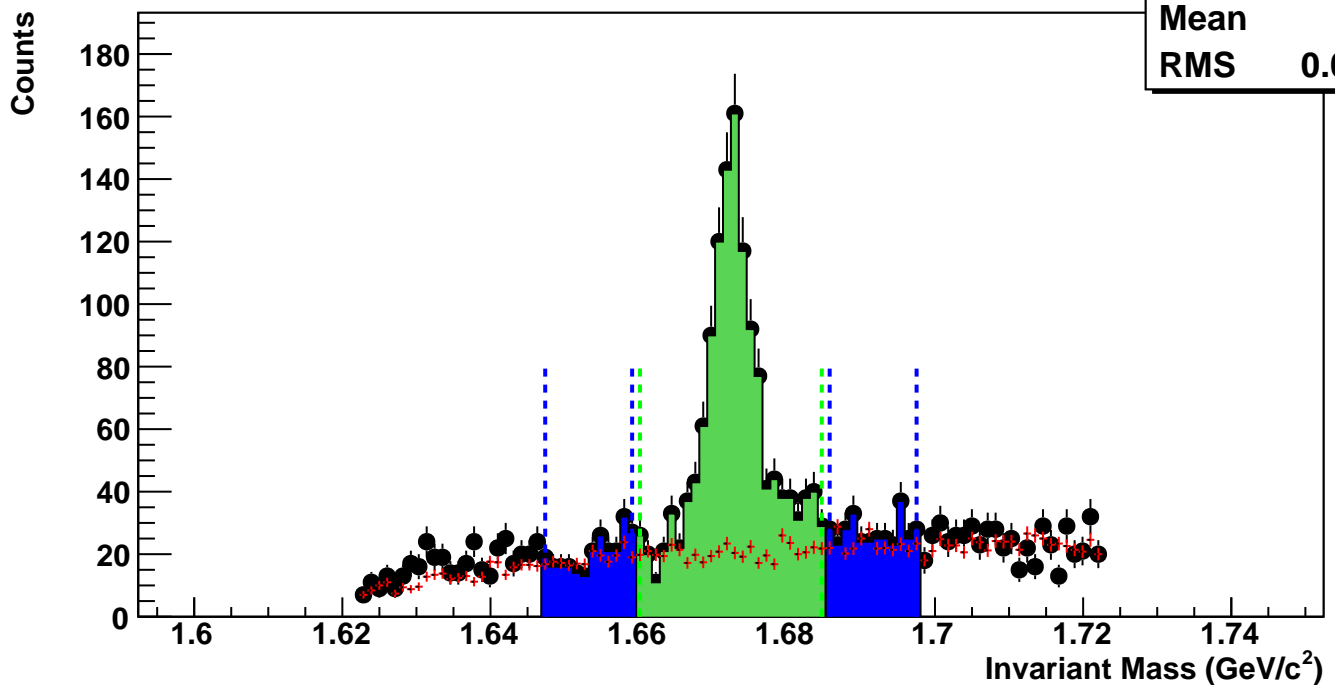
$\Omega^-$ , Au+Au 39 GeV, 20-40%,  $p_T$  2.4-2.8 GeV/c

hmlInvMassBgCent2Pt7	
Entries	98
Mean	1.679
RMS	0.02686



$\Omega^-$ , Au+Au 39 GeV, 10-20%,  $p_T$  2.4-2.8 GeV/c

hmlInvMassBgCent3Pt7	
Entries	220
Mean	1.678
RMS	0.02709



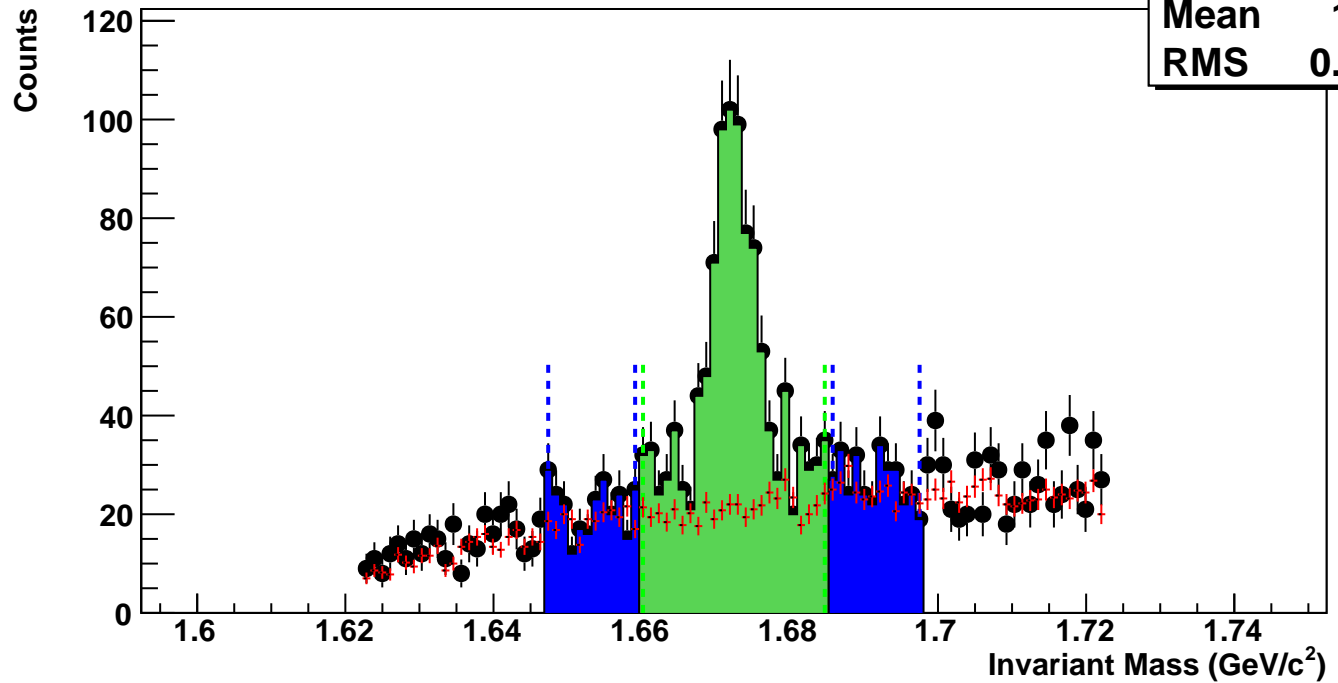
$\Omega^-$ , Au+Au 39 GeV, 5-10%,  $p_T$  2.4-2.8 GeV/c

hmlInvMassBgCent4Pt7

Entries 226

Mean 1.679

RMS 0.0269



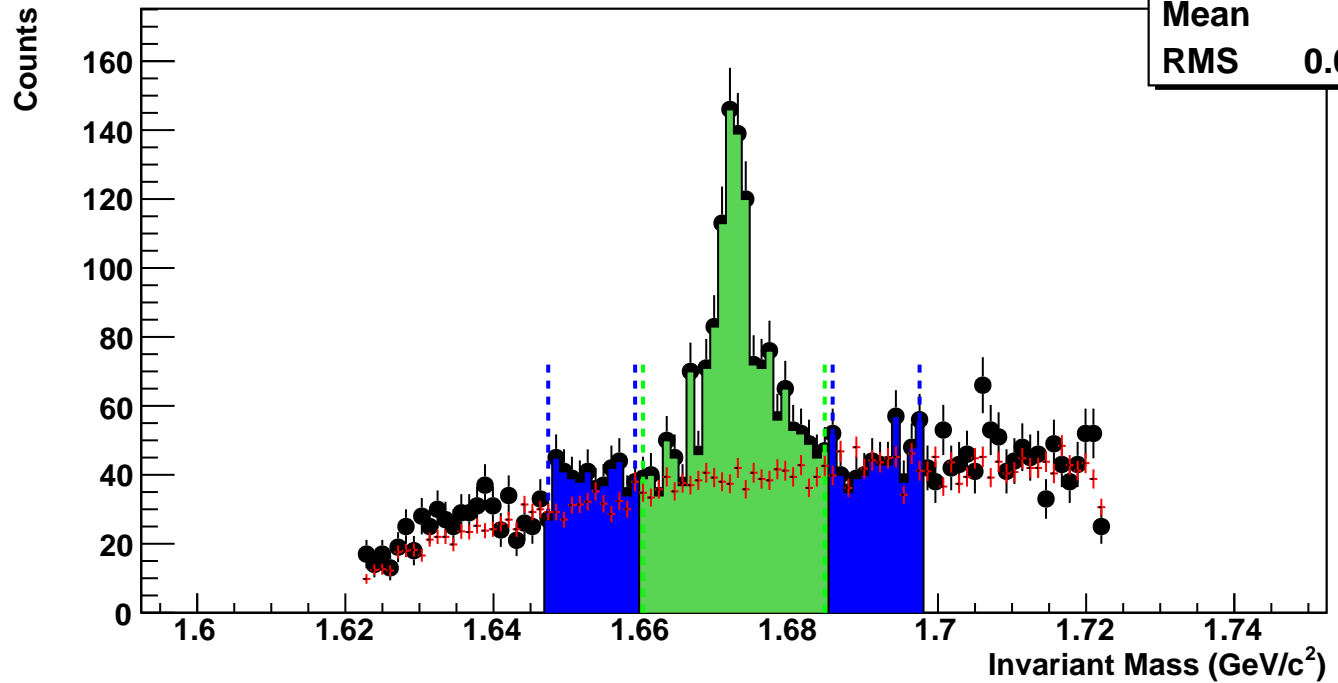
$\Omega^-$ , Au+Au 39 GeV, 0-5%,  $p_T$  2.4-2.8 GeV/c

hmlInvMassBgCent5Pt7

Entries 397

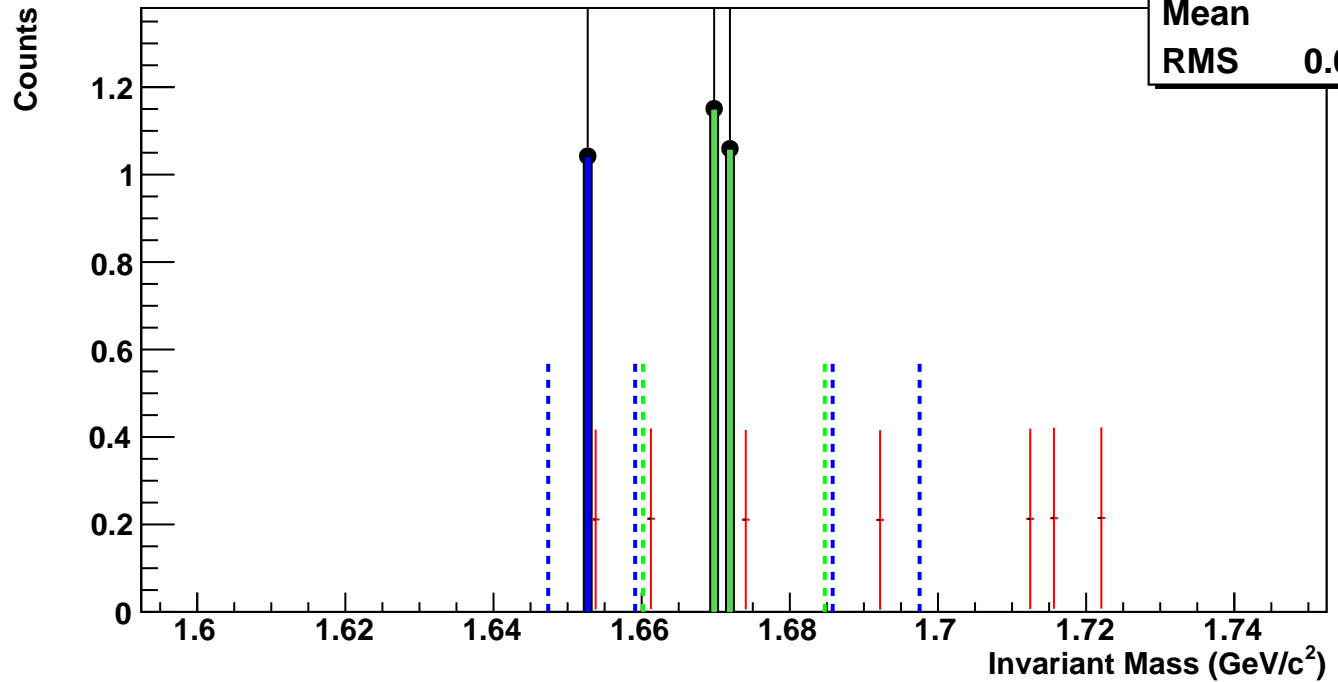
Mean 1.679

RMS 0.02665



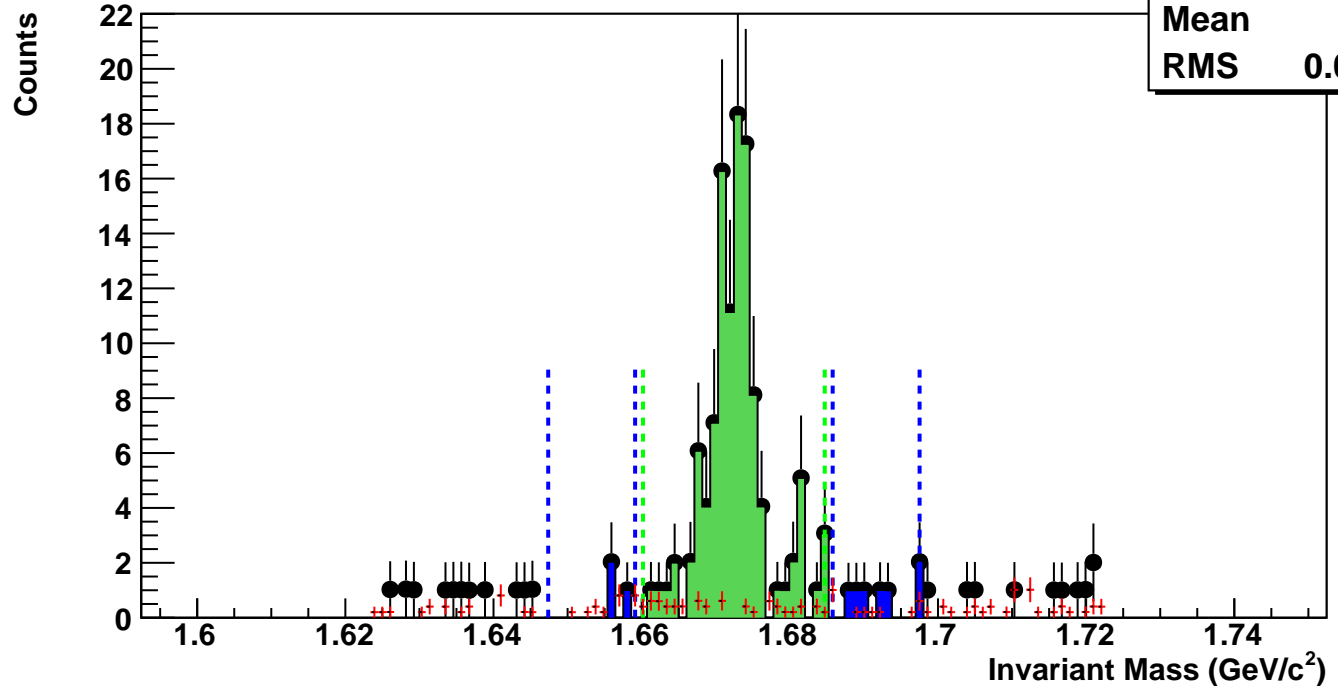
$\Omega^-$ , Au+Au 39 GeV, 60-80%,  $p_T$  2.8-3.2 GeV/c

hmlInvMassBgCent0Pt8	
Entries	0
Mean	1.69
RMS	0.02562



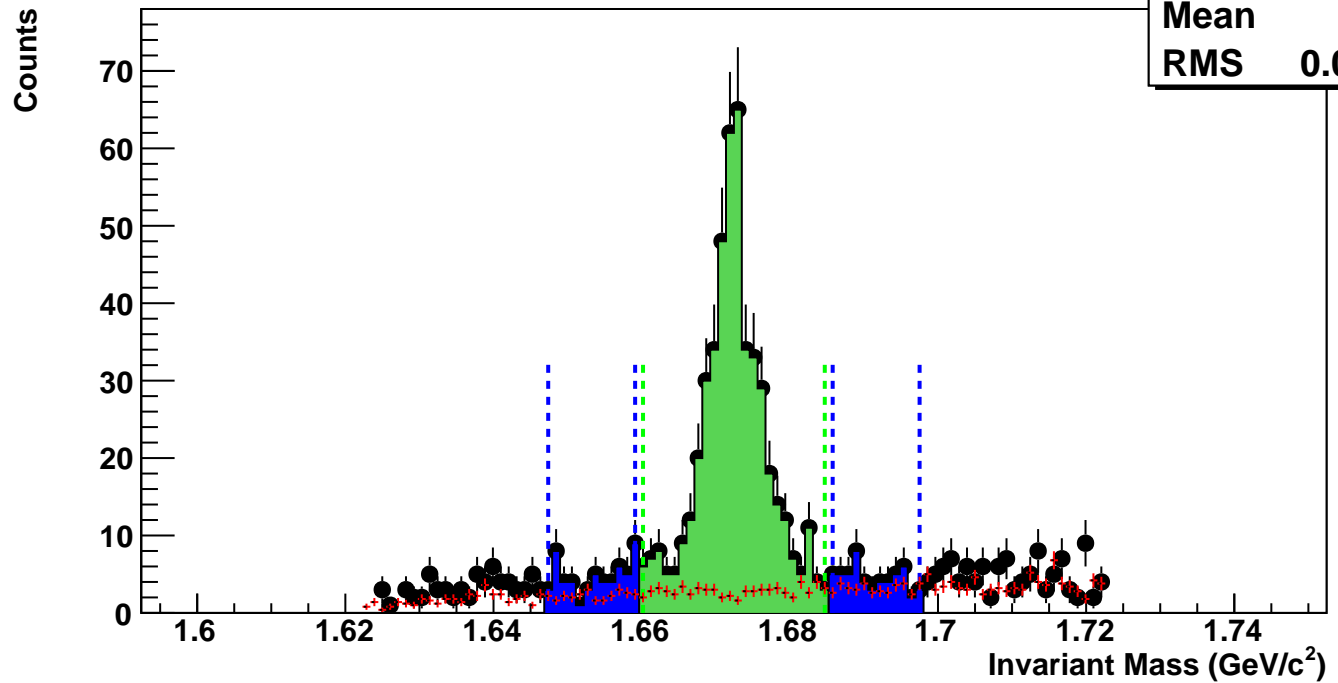
$\Omega^-$ , Au+Au 39 GeV, 40-60%,  $p_T$  2.8-3.2 GeV/c

hmlInvMassBgCent1Pt8	
Entries	3
Mean	1.677
RMS	0.02686



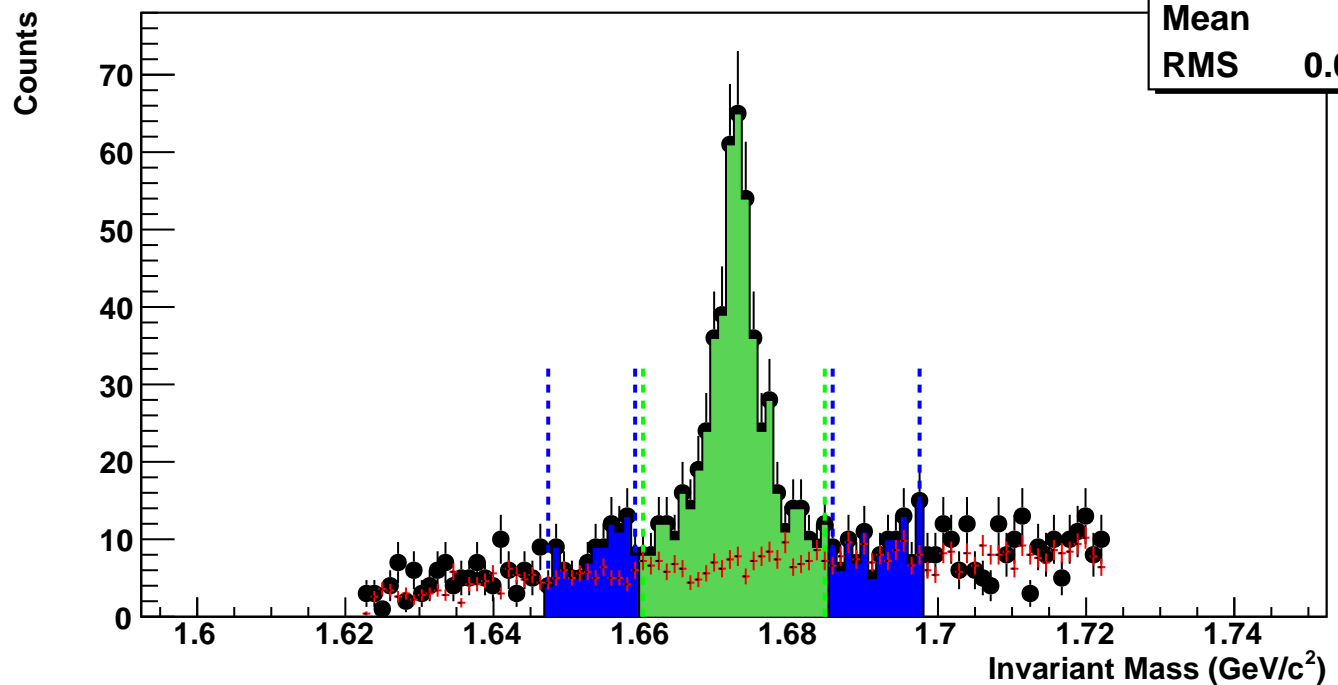
$\Omega^-$ , Au+Au 39 GeV, 20-40%,  $p_T$  2.8-3.2 GeV/c

hmlInvMassBgCent2Pt8	
Entries	31
Mean	1.68
RMS	0.02721



$\Omega^-$ , Au+Au 39 GeV, 10-20%,  $p_T$  2.8-3.2 GeV/c

hmlInvMassBgCent3Pt8	
Entries	72
Mean	1.68
RMS	0.02674



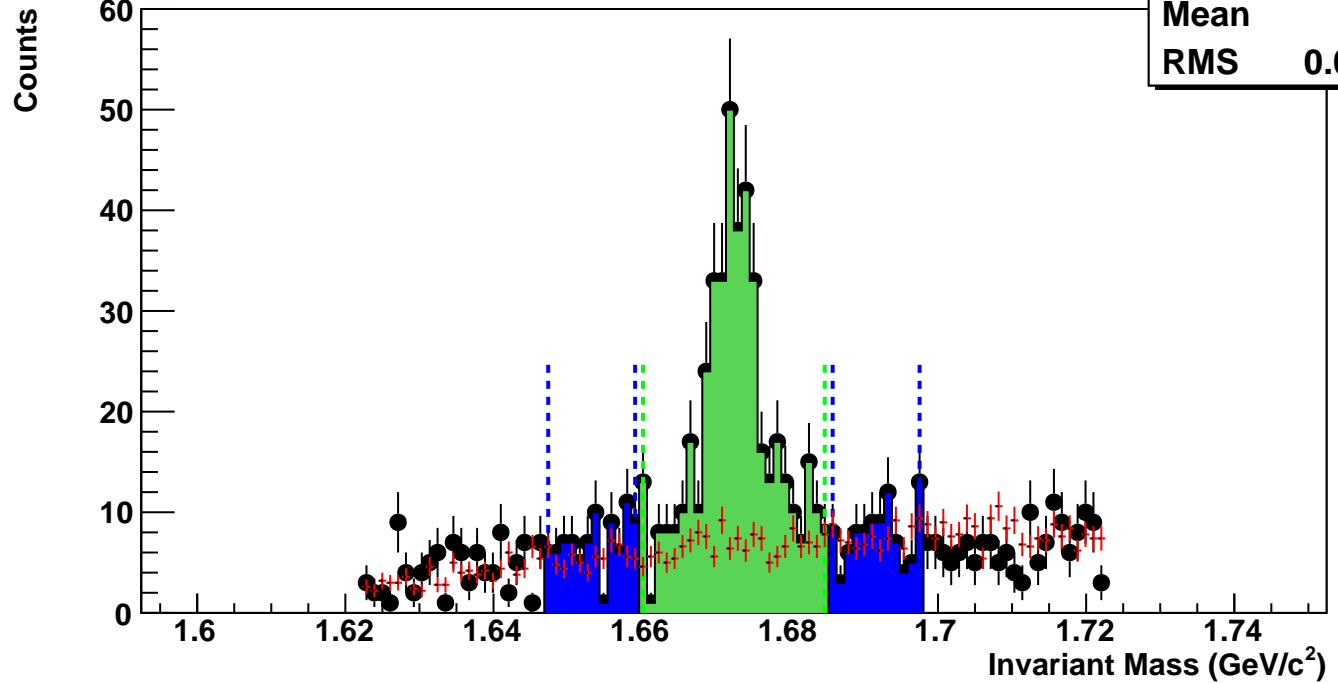
$\Omega^-$ , Au+Au 39 GeV, 5-10%,  $p_T$  2.8-3.2 GeV/c

hmlInvMassBgCent4Pt8

Entries 72

Mean 1.68

RMS 0.02687



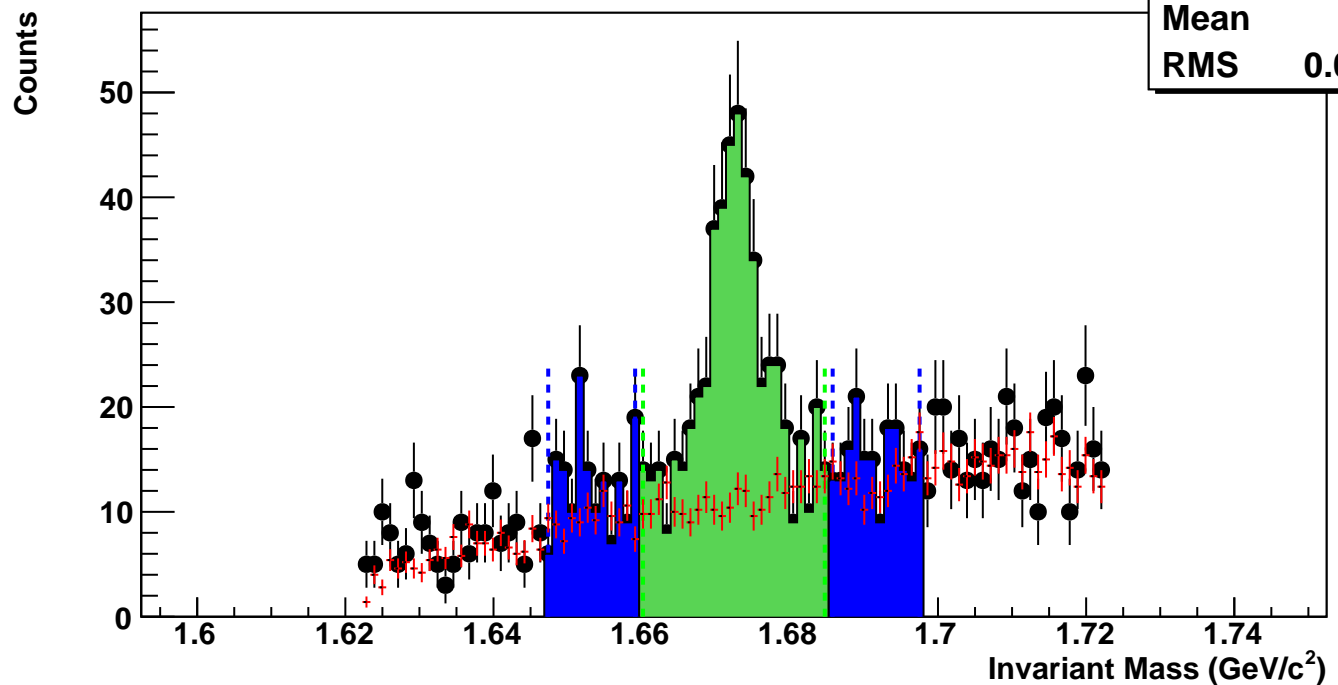
$\Omega^-$ , Au+Au 39 GeV, 0-5%,  $p_T$  2.8-3.2 GeV/c

hmlInvMassBgCent5Pt8

Entries 123

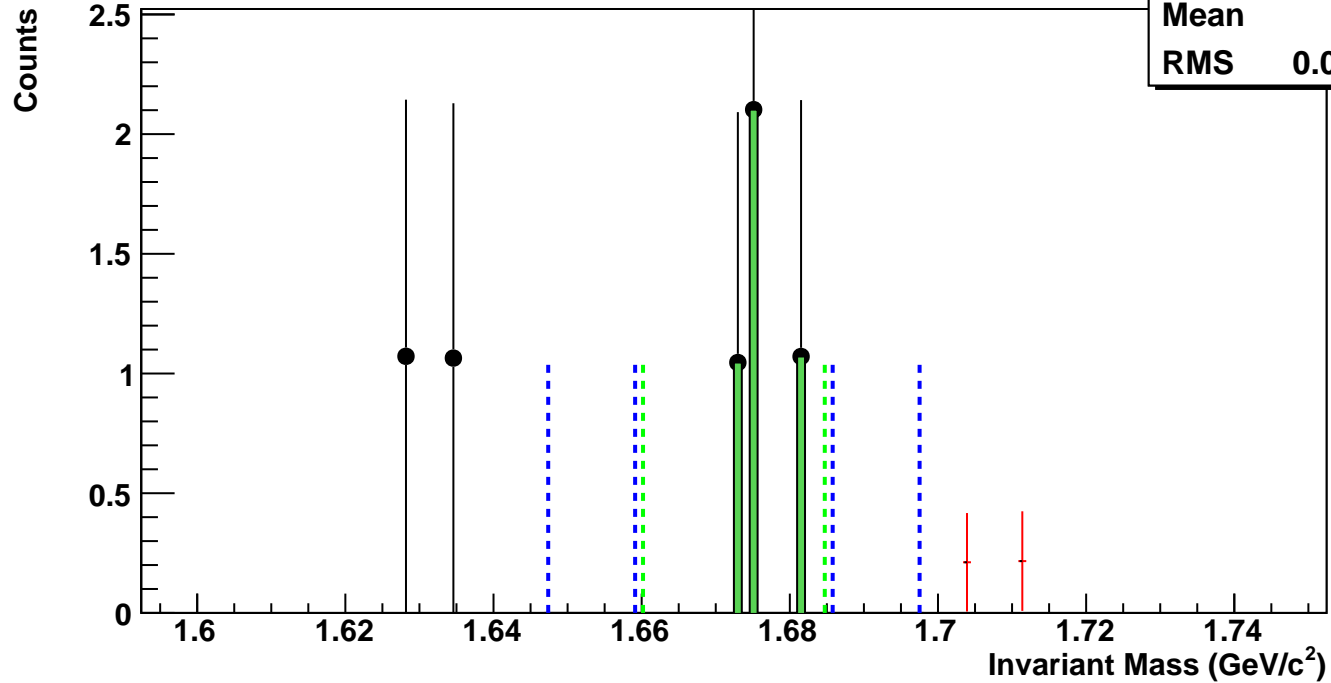
Mean 1.681

RMS 0.02668



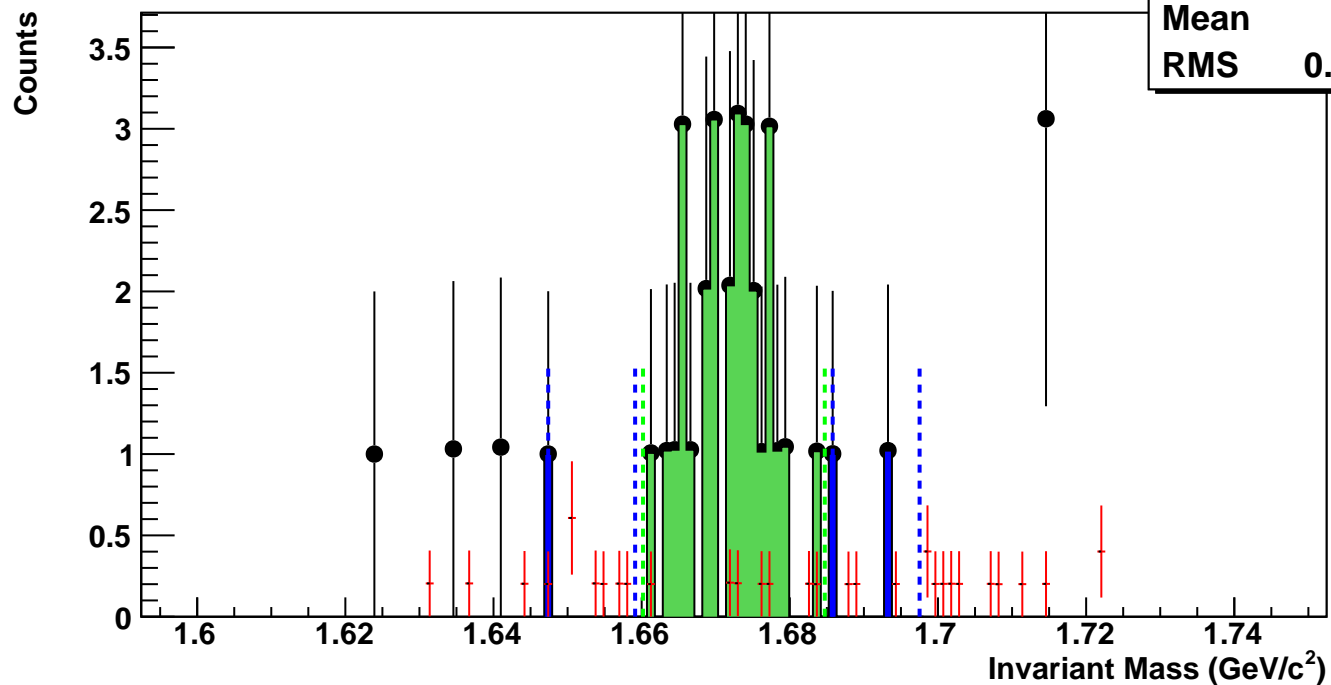
$\Omega^-$ , Au+Au 39 GeV, 60-80%,  $p_T$  3.2-3.6 GeV/c

hmlInvMassBgCent0Pt9	
Entries	0
Mean	1.708
RMS	0.003733



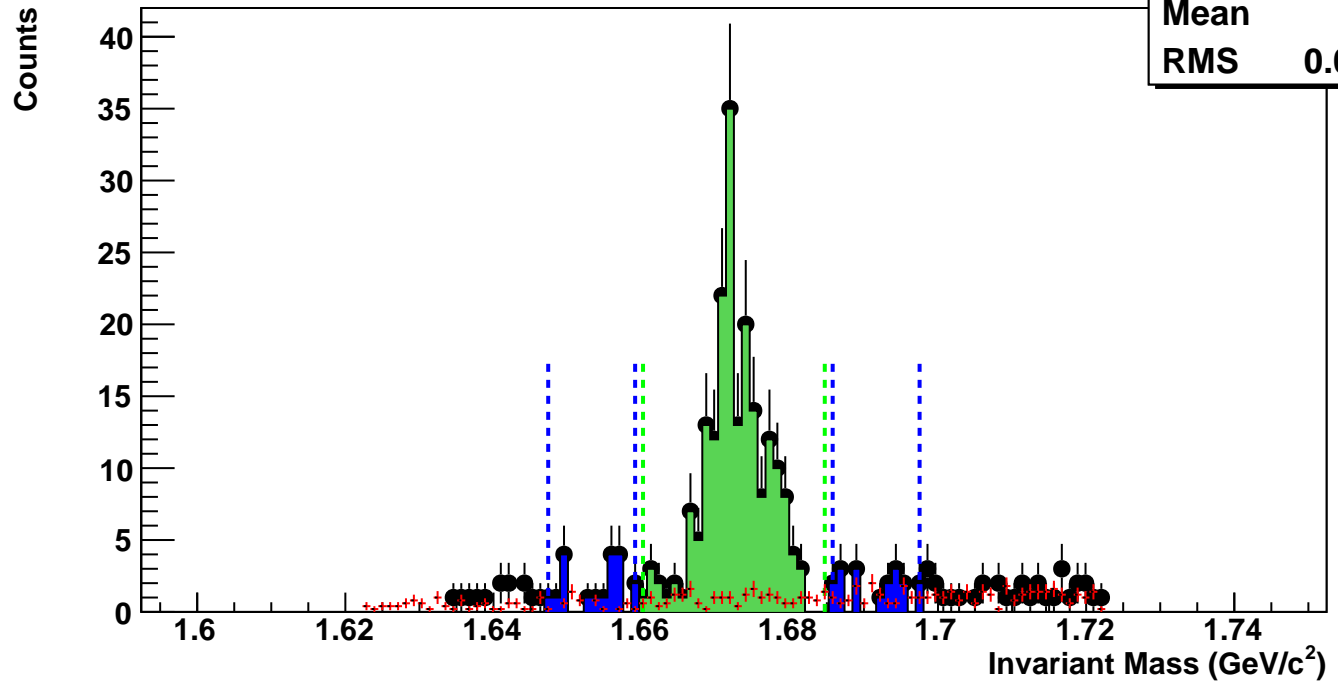
$\Omega^-$ , Au+Au 39 GeV, 40-60%,  $p_T$  3.2-3.6 GeV/c

hmlInvMassBgCent1Pt9	
Entries	1
Mean	1.679
RMS	0.02588



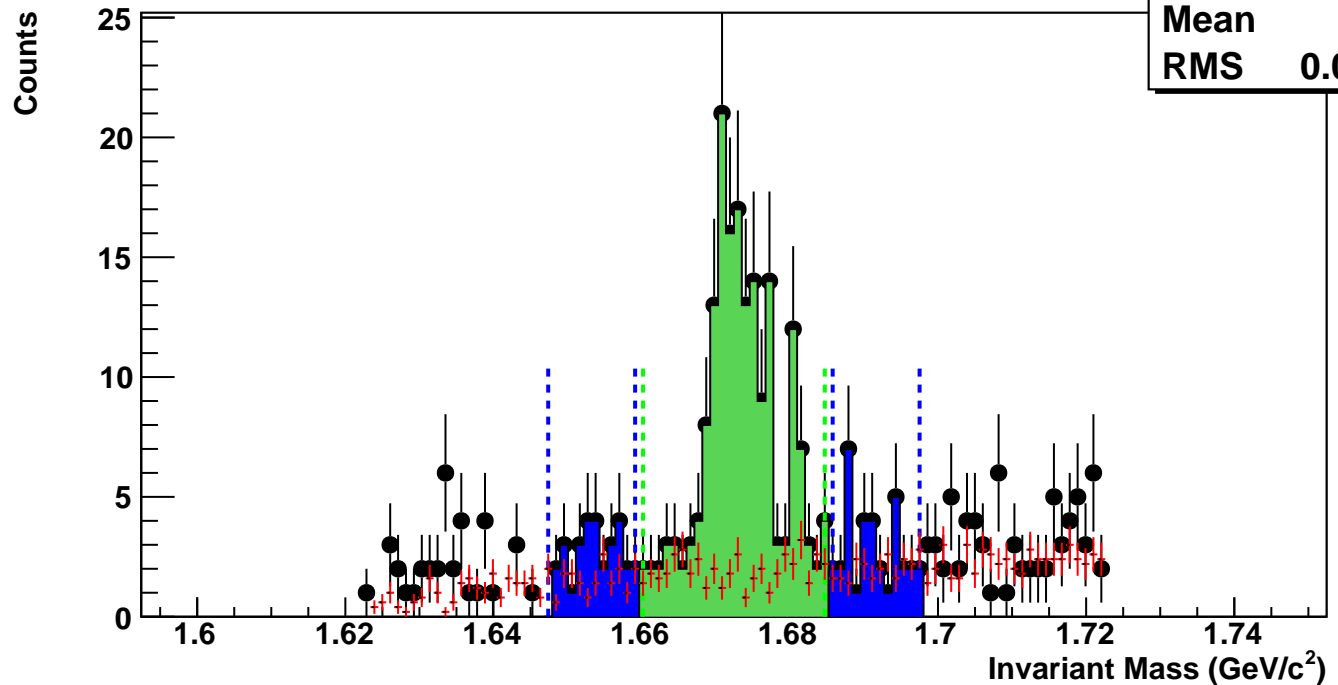
$\Omega^-$ , Au+Au 39 GeV, 20-40%,  $p_T$  3.2-3.6 GeV/c

hmlInvMassBgCent2Pt9	
Entries	9
Mean	1.682
RMS	0.02667



$\Omega^-$ , Au+Au 39 GeV, 10-20%,  $p_T$  3.2-3.6 GeV/c

hmlInvMassBgCent3Pt9	
Entries	20
Mean	1.681
RMS	0.02661



$\Omega^-$ , Au+Au 39 GeV, 5-10%,  $p_T$  3.2-3.6 GeV/c

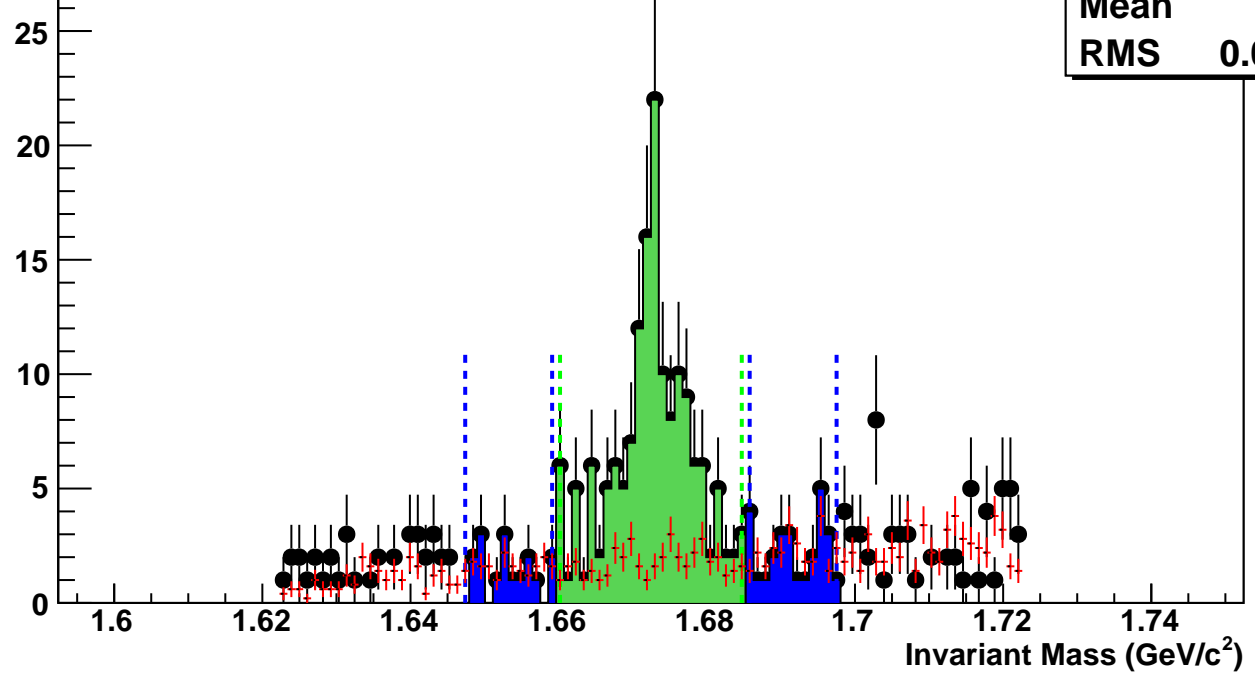
hmlInvMassBgCent4Pt9

Entries 20

Mean 1.681

RMS 0.02711

Counts



$\Omega^-$ , Au+Au 39 GeV, 0-5%,  $p_T$  3.2-3.6 GeV/c

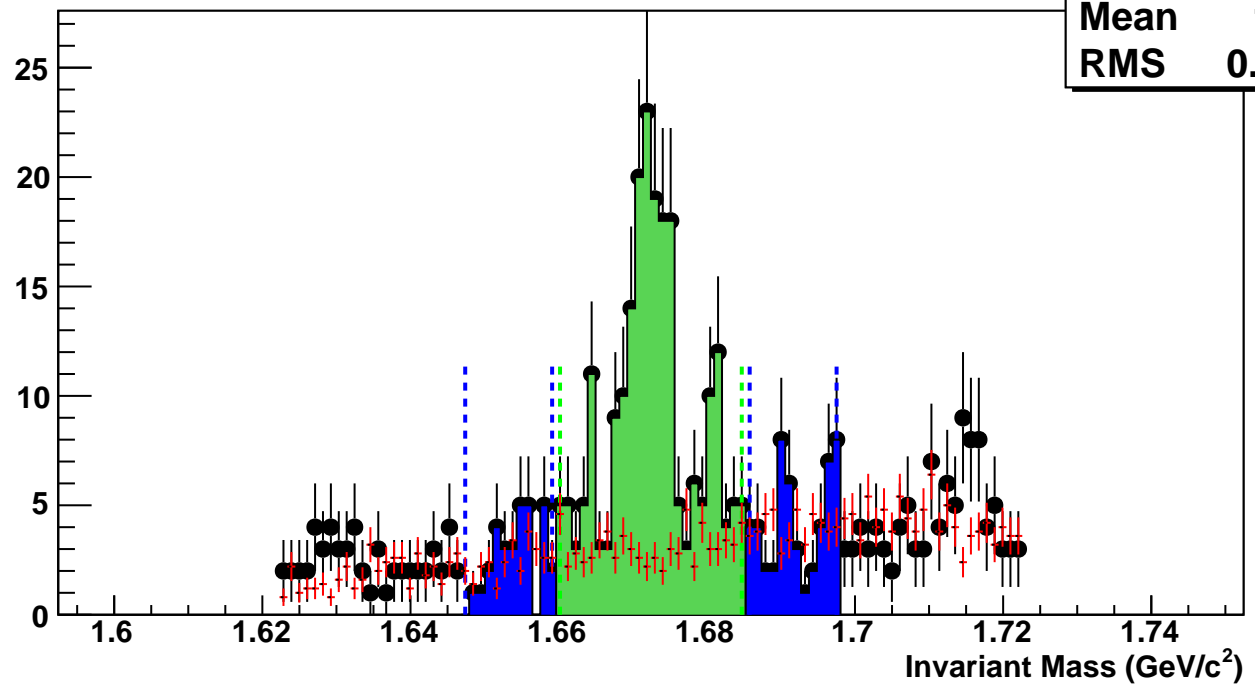
hmlInvMassBgCent5Pt9

Entries 35

Mean 1.681

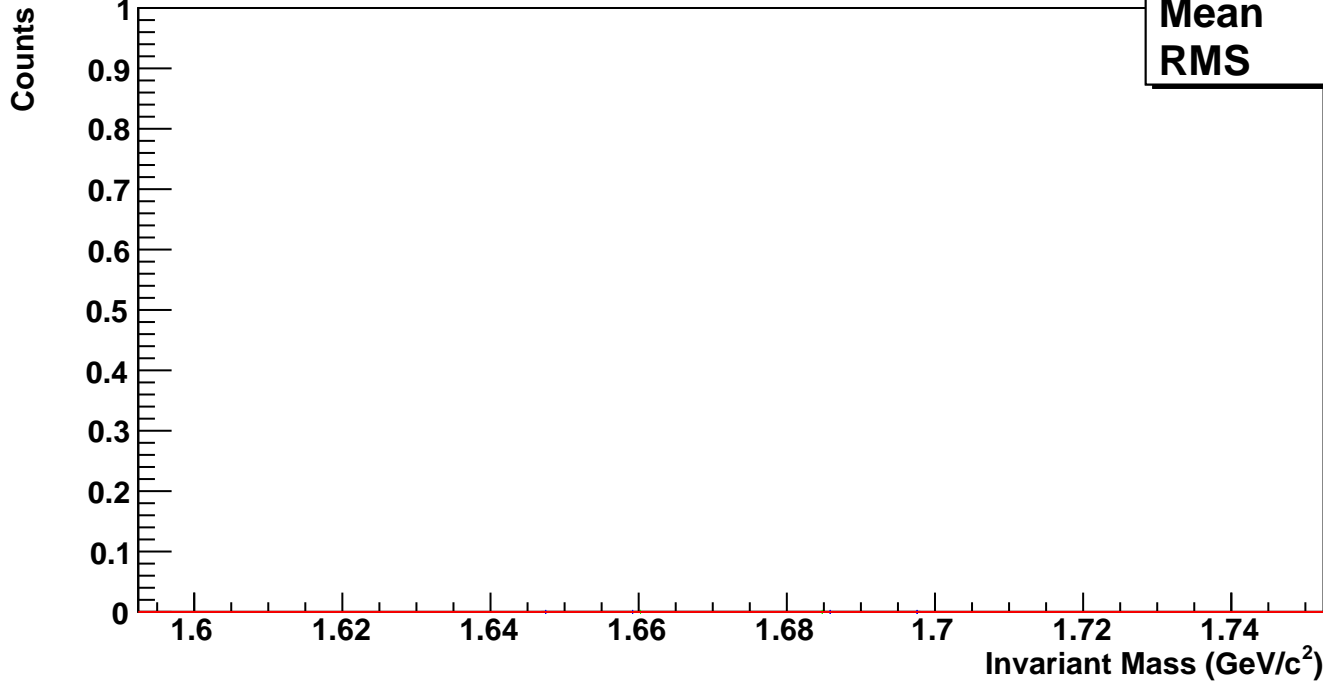
RMS 0.0269

Counts



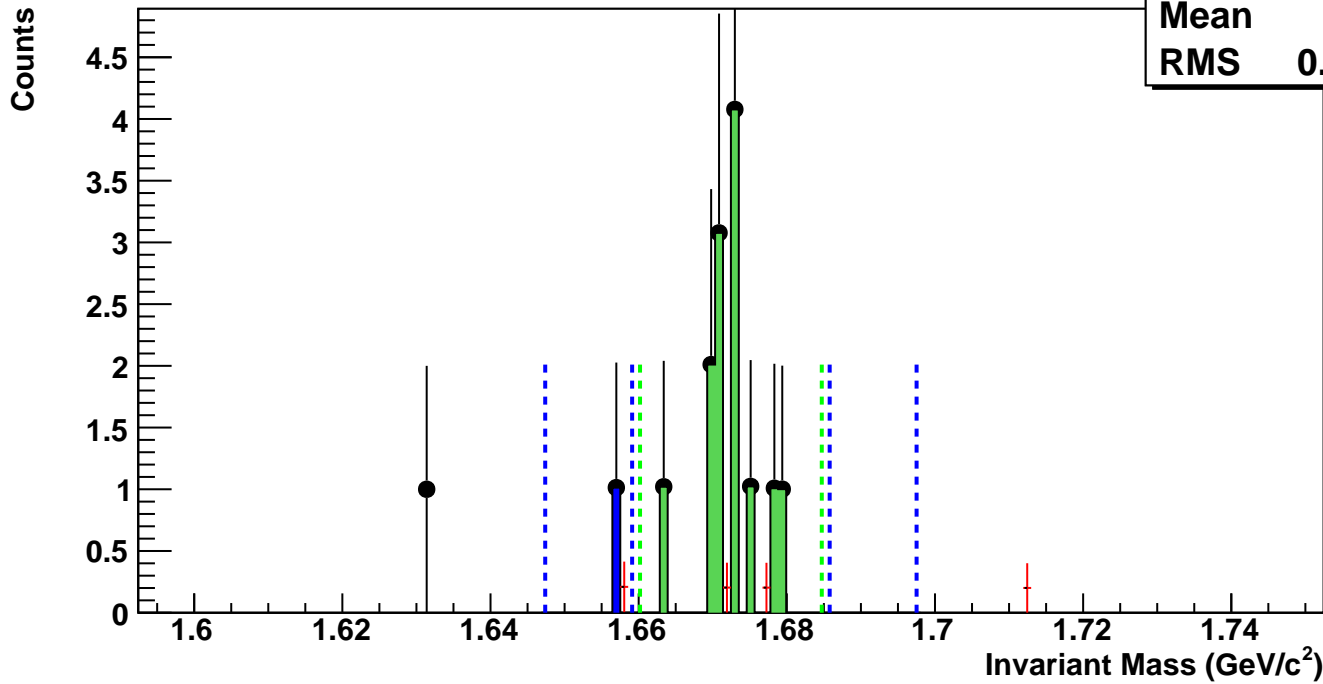
$\Omega^-$ , Au+Au 39 GeV, 60-80%,  $p_T$  3.6-4.0 GeV/c

hmlInvMassBgCent0Pt10
Entries 0
Mean 0
RMS 0



$\Omega^-$ , Au+Au 39 GeV, 40-60%,  $p_T$  3.6-4.0 GeV/c

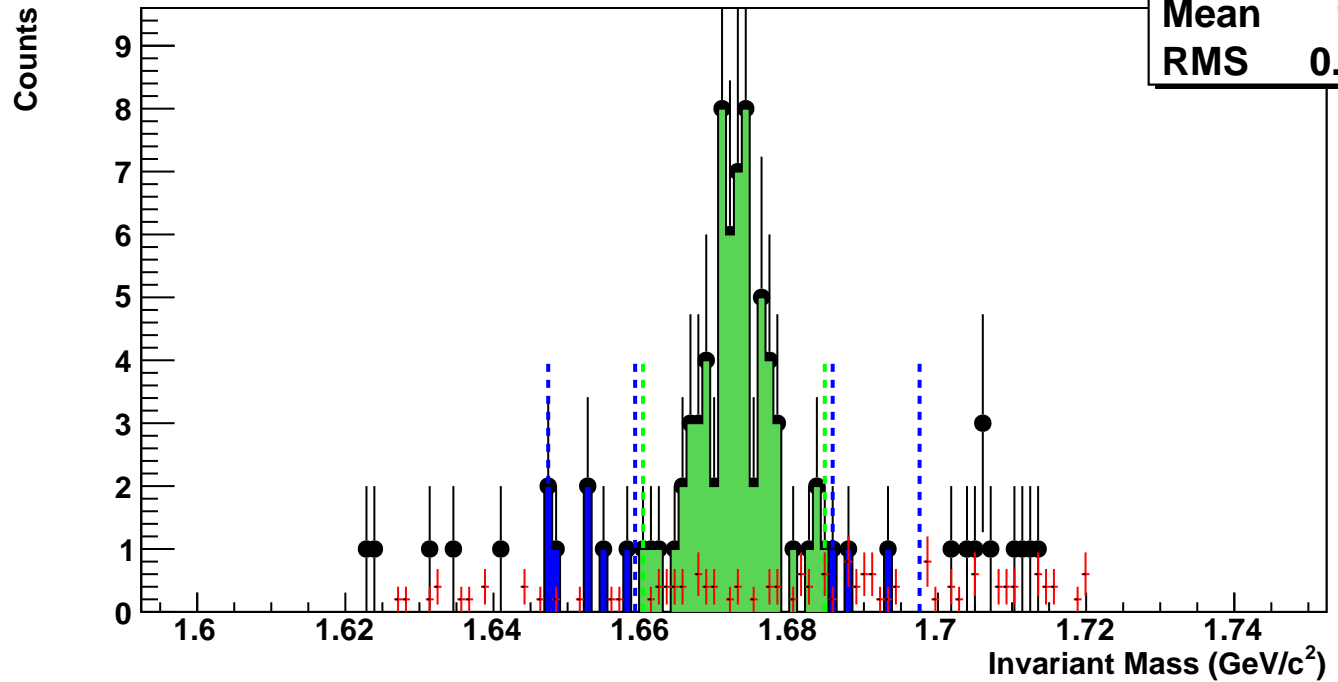
hmlInvMassBgCent1Pt10
Entries 0
Mean 1.68
RMS 0.02001



$\Omega^-$ , Au+Au 39 GeV, 20-40%,  $p_T$  3.6-4.0 GeV/c

hmlInvMassBgCent2Pt10

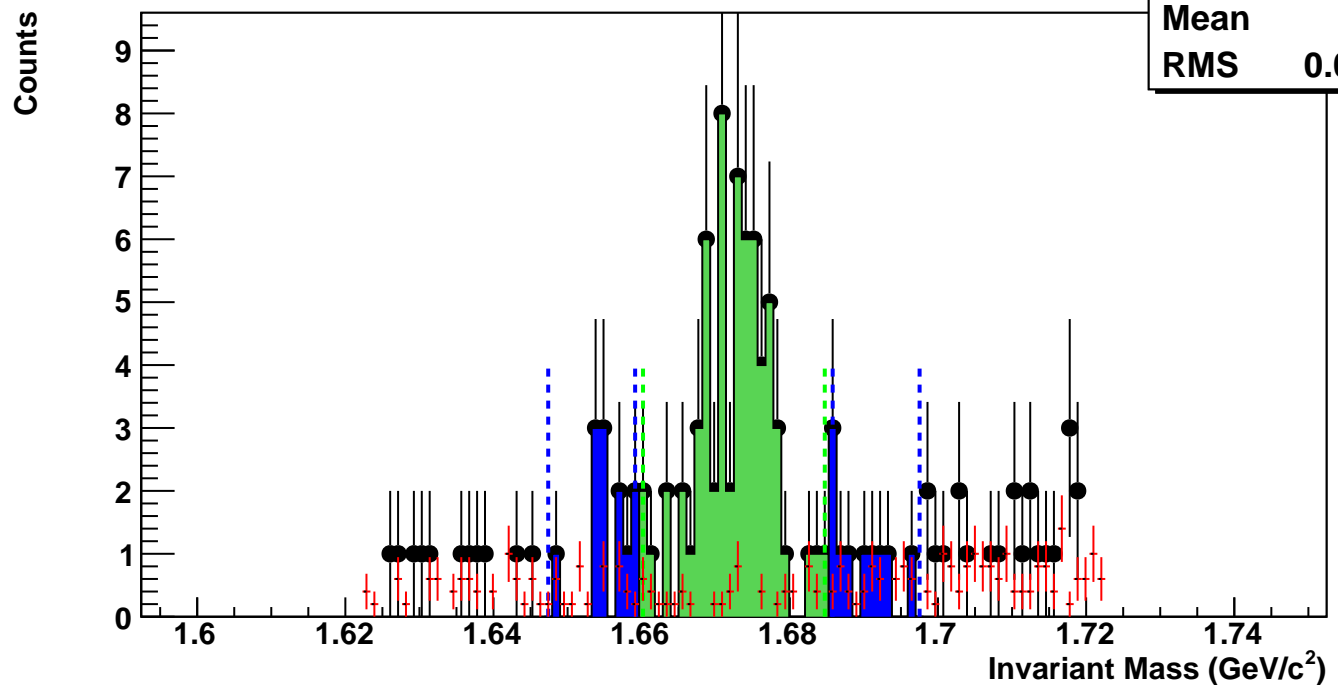
Entries 2  
Mean 1.681  
RMS 0.0245



$\Omega^-$ , Au+Au 39 GeV, 10-20%,  $p_T$  3.6-4.0 GeV/c

hmlInvMassBgCent3Pt10

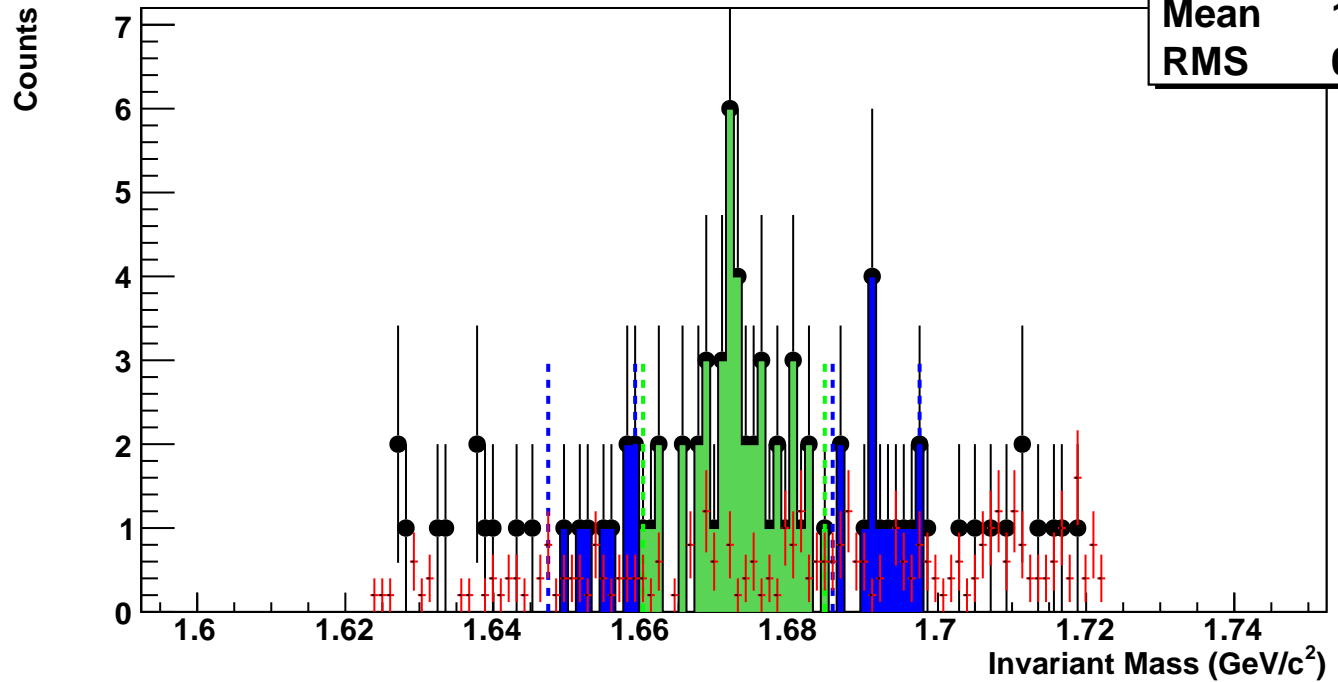
Entries 5  
Mean 1.681  
RMS 0.02967



$\Omega^-$ , Au+Au 39 GeV, 5-10%,  $p_T$  3.6-4.0 GeV/c

hmlInvMassBgCent4Pt10

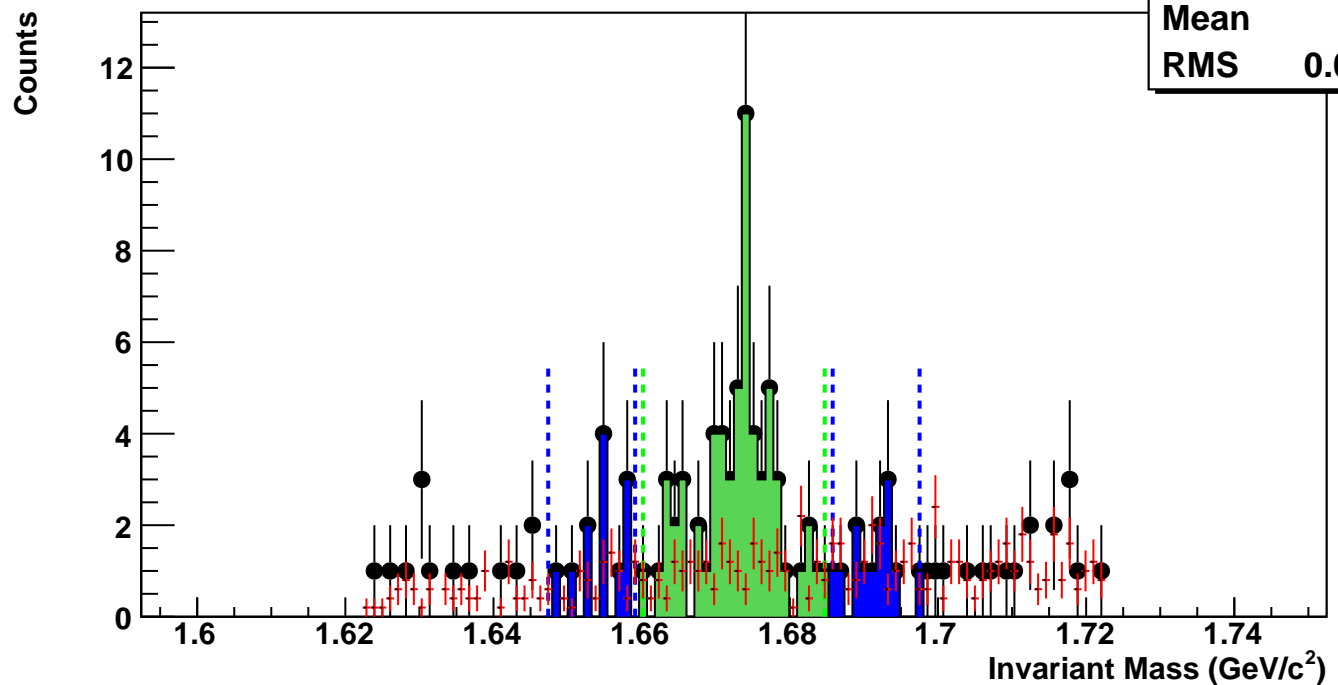
Entries 5  
Mean 1.684  
RMS 0.026



$\Omega^-$ , Au+Au 39 GeV, 0-5%,  $p_T$  3.6-4.0 GeV/c

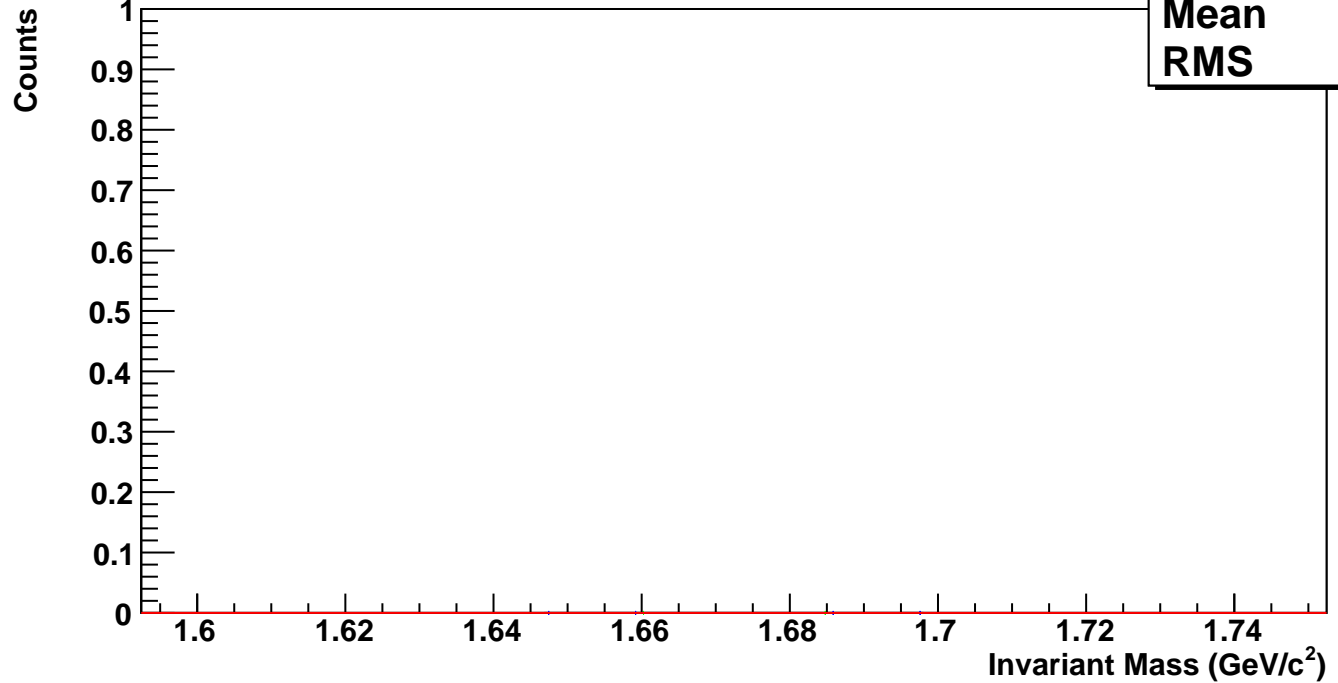
hmlInvMassBgCent5Pt10

Entries 10  
Mean 1.681  
RMS 0.02589



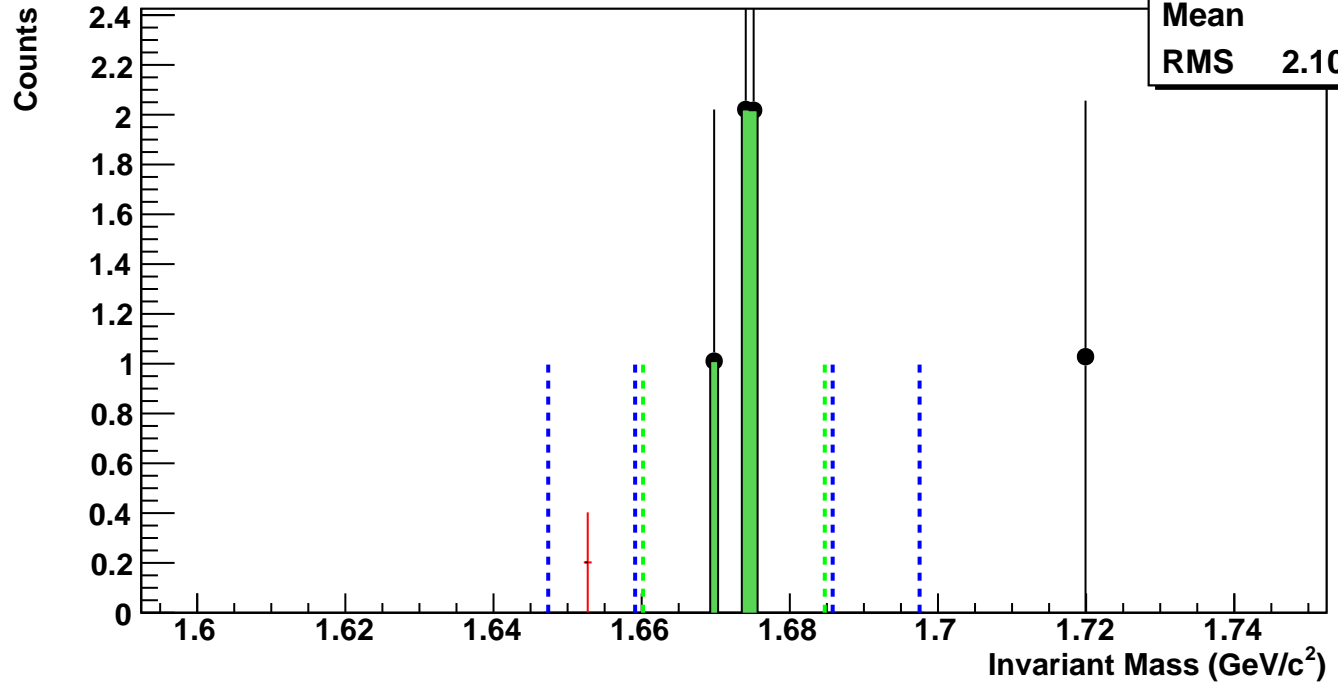
$\Omega^-$ , Au+Au 39 GeV, 60-80%,  $p_T$  4.0-5.0 GeV/c

hmlInvMassBgCent0Pt11	
Entries	0
Mean	0
RMS	0



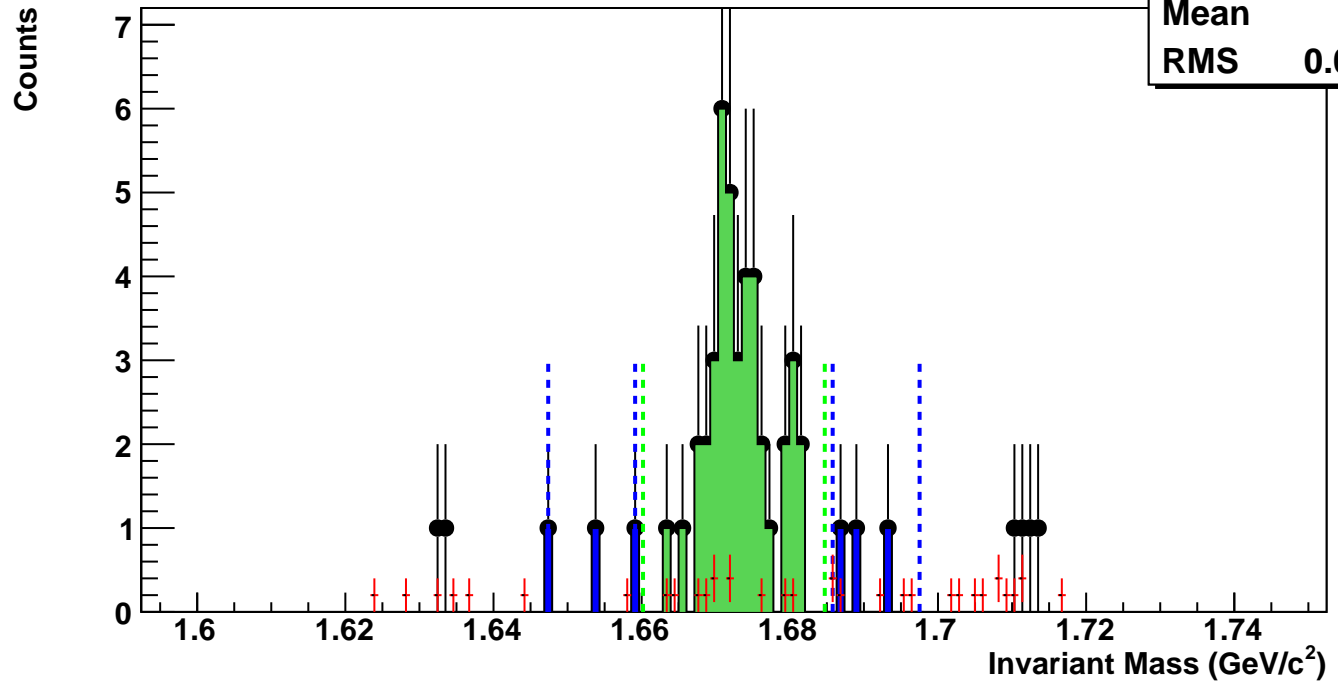
$\Omega^-$ , Au+Au 39 GeV, 40-60%,  $p_T$  4.0-5.0 GeV/c

hmlInvMassBgCent1Pt11	
Entries	0
Mean	1.653
RMS	2.107e-08



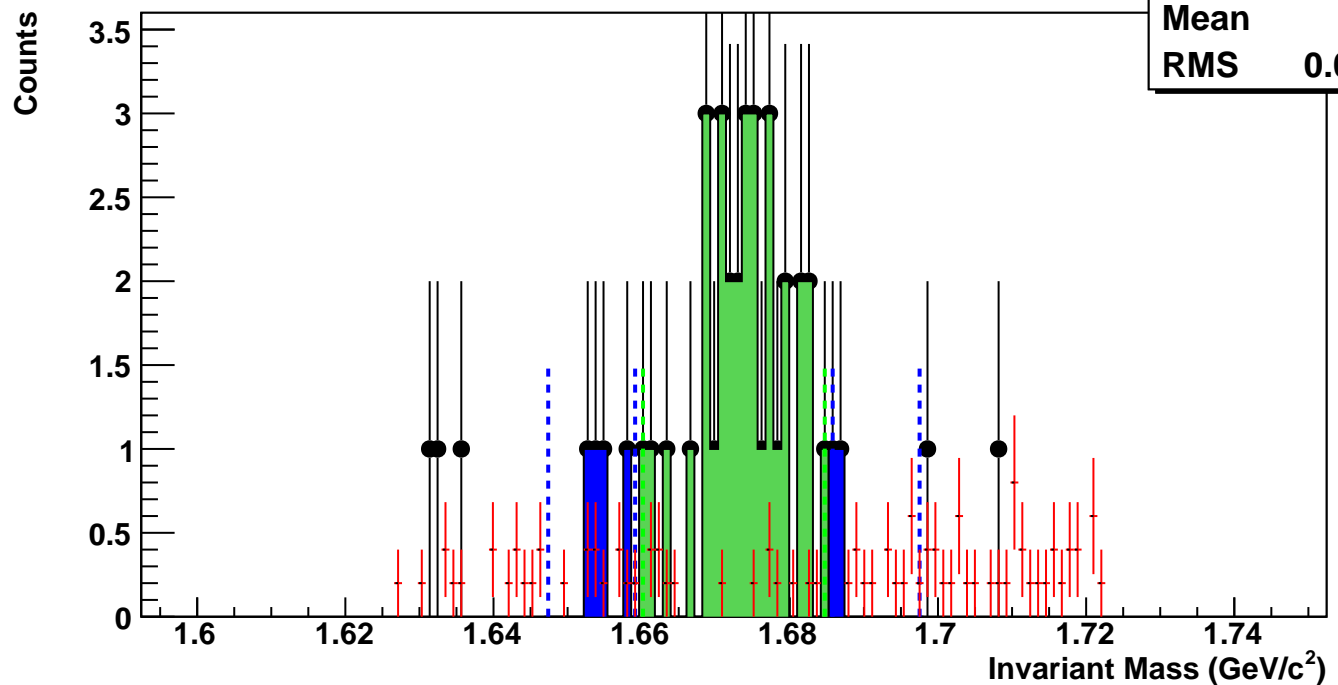
$\Omega^-$ , Au+Au 39 GeV, 20-40%,  $p_T$  4.0-5.0 GeV/c

hmlInvMassBgCent2Pt11	
Entries	1
Mean	1.679
RMS	0.02655



$\Omega^-$ , Au+Au 39 GeV, 10-20%,  $p_T$  4.0-5.0 GeV/c

hmlInvMassBgCent3Pt11	
Entries	2
Mean	1.683
RMS	0.02834



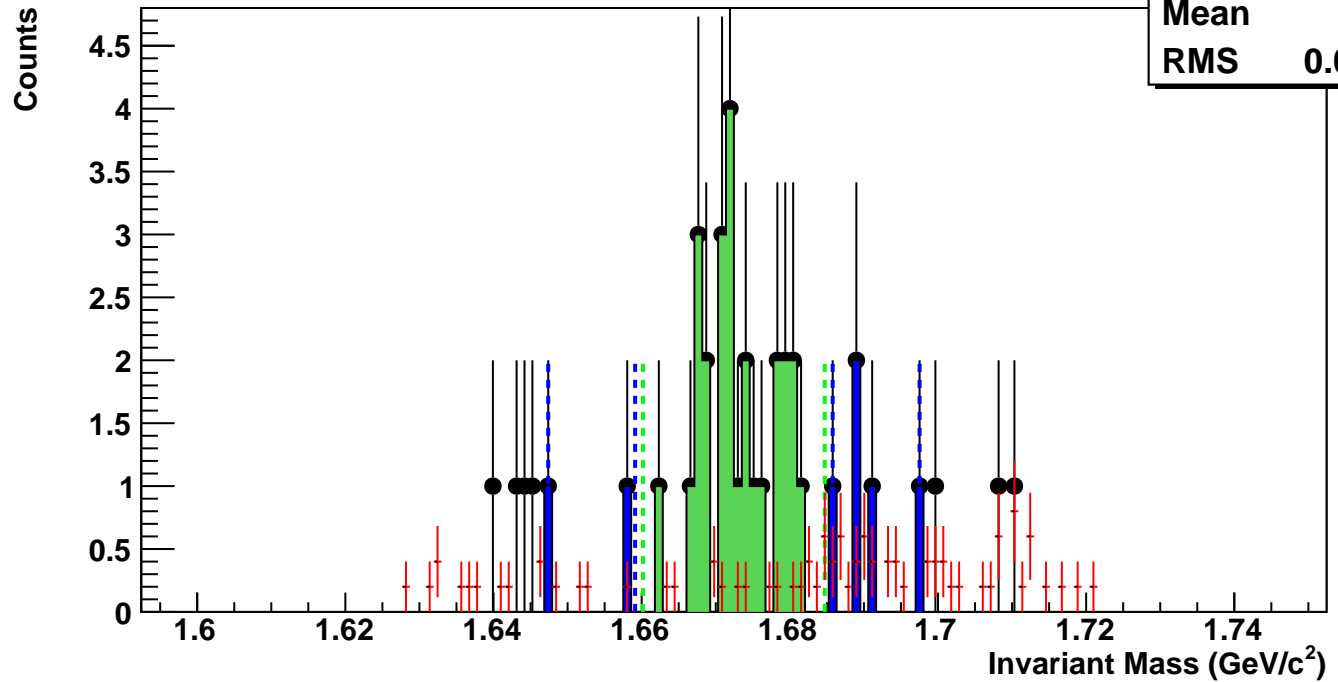
$\Omega^-$ , Au+Au 39 GeV, 5-10%,  $p_T$  4.0-5.0 GeV/c

hmlnMassBgCent4Pt11

Entries 2

Mean 1.683

RMS 0.02484



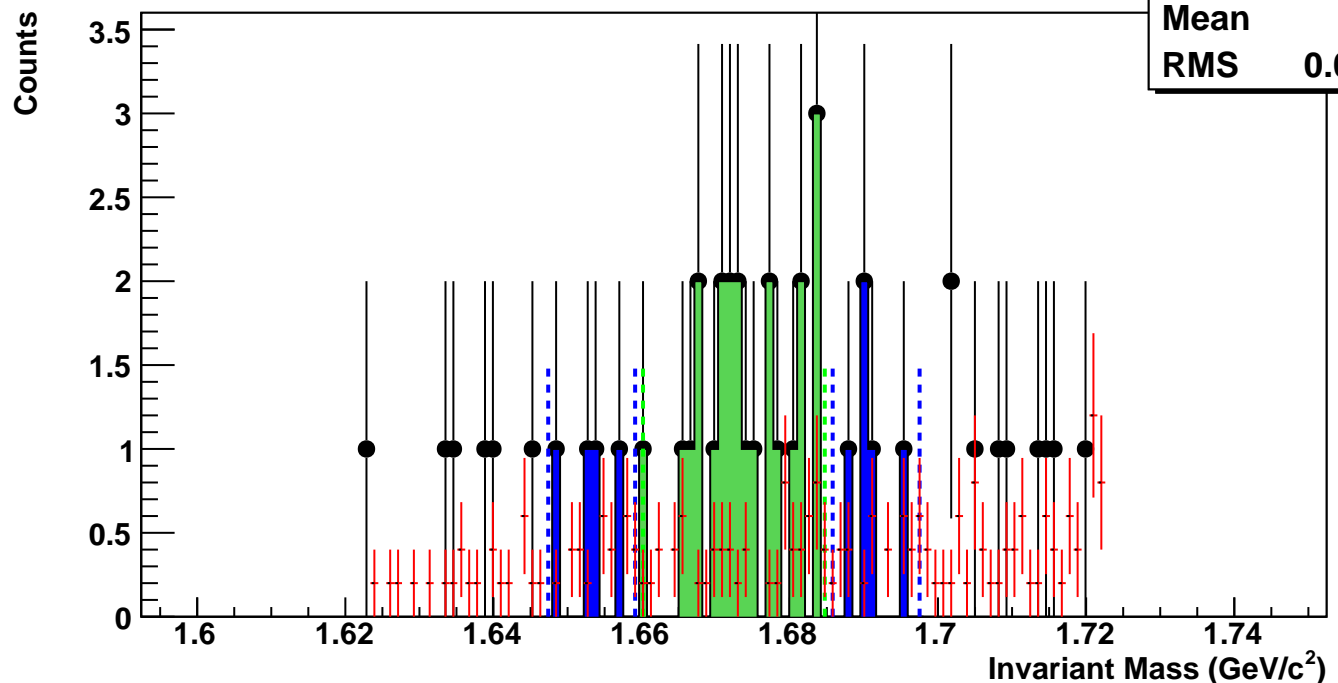
$\Omega^-$ , Au+Au 39 GeV, 0-5%,  $p_T$  4.0-5.0 GeV/c

hmlnMassBgCent5Pt11

Entries 3

Mean 1.682

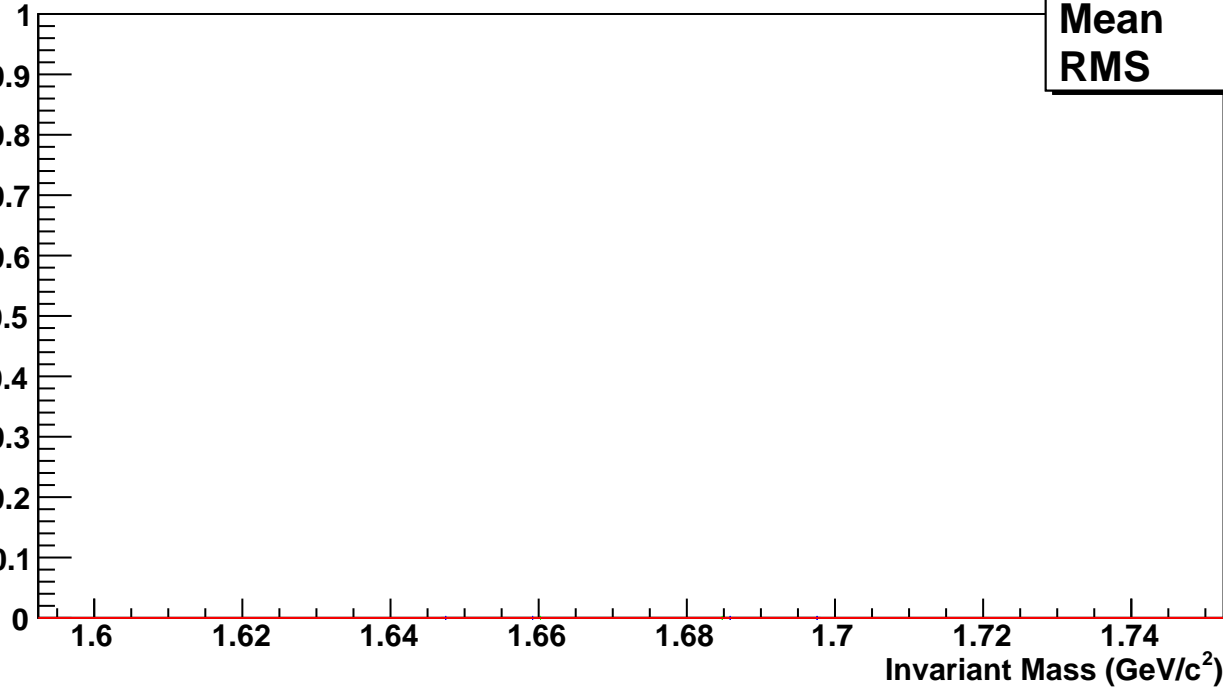
RMS 0.02727



$\Omega^-$ , Au+Au 39 GeV, 60-80%,  $p_T$  5.0-7.0 GeV/c

Counts

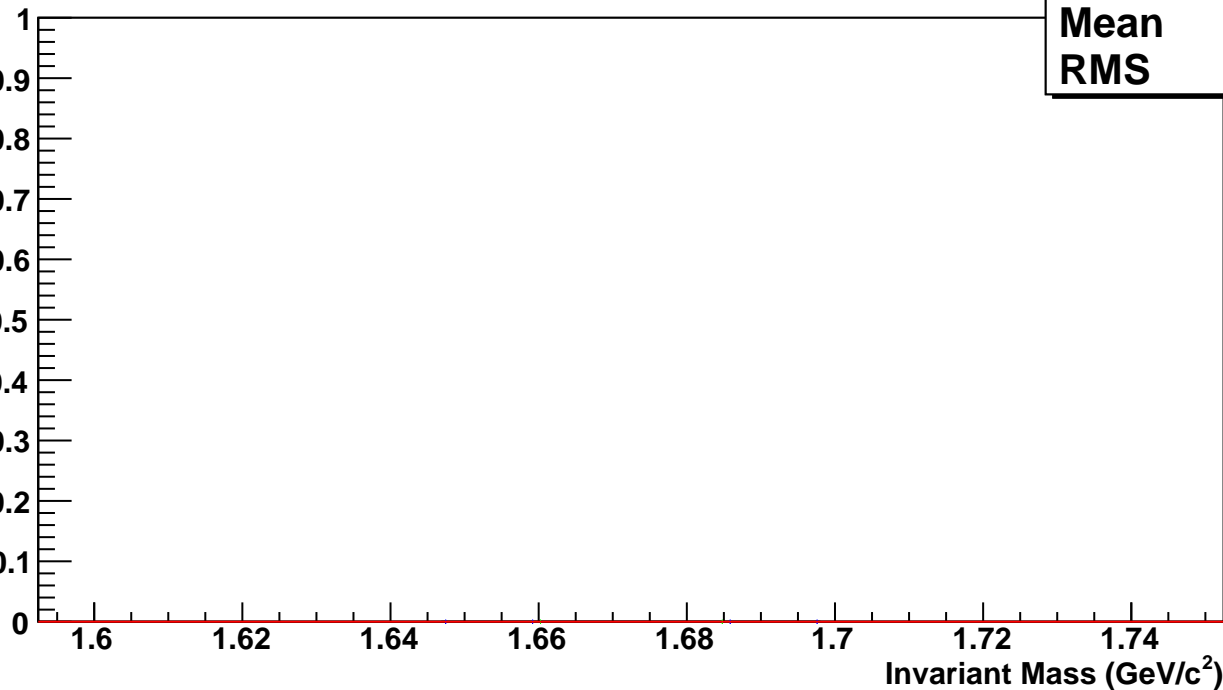
hmlInvMassBgCent0Pt12	
Entries	0
Mean	0
RMS	0



$\Omega^-$ , Au+Au 39 GeV, 40-60%,  $p_T$  5.0-7.0 GeV/c

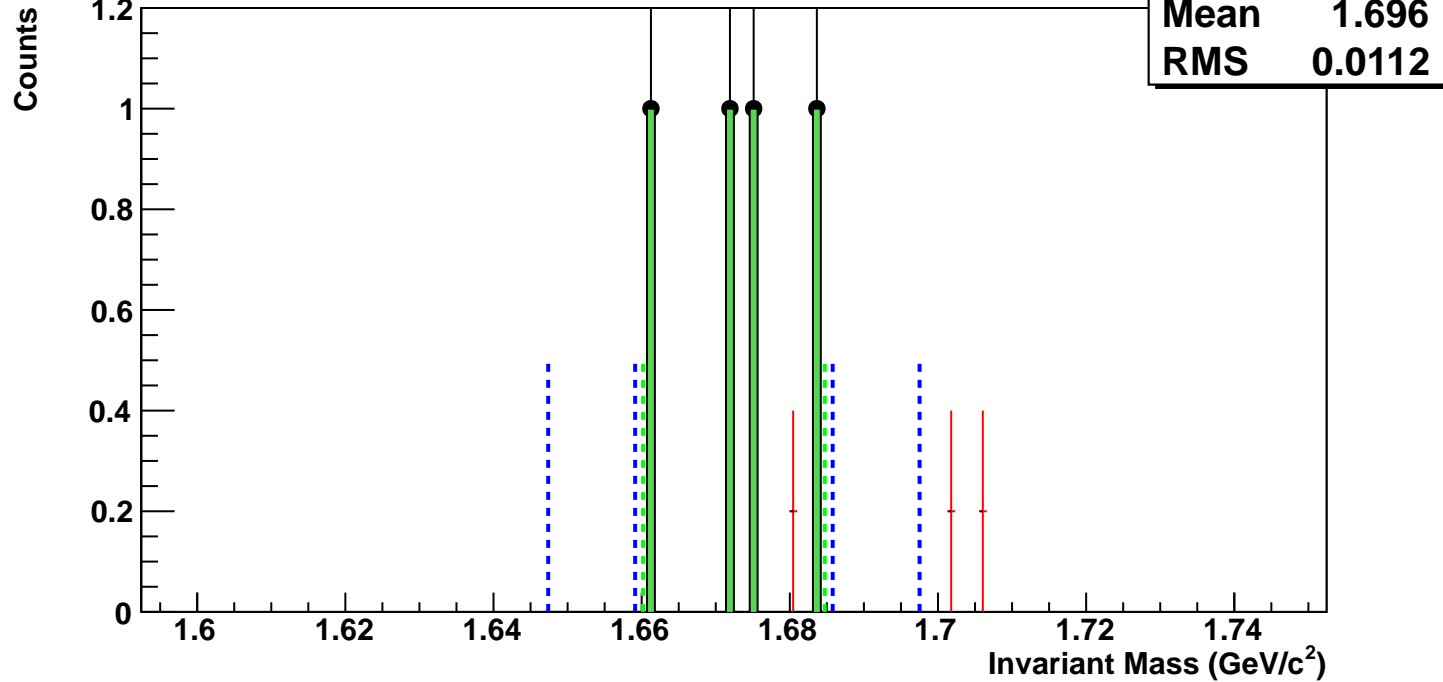
Counts

hmlInvMassBgCent1Pt12	
Entries	0
Mean	0
RMS	0



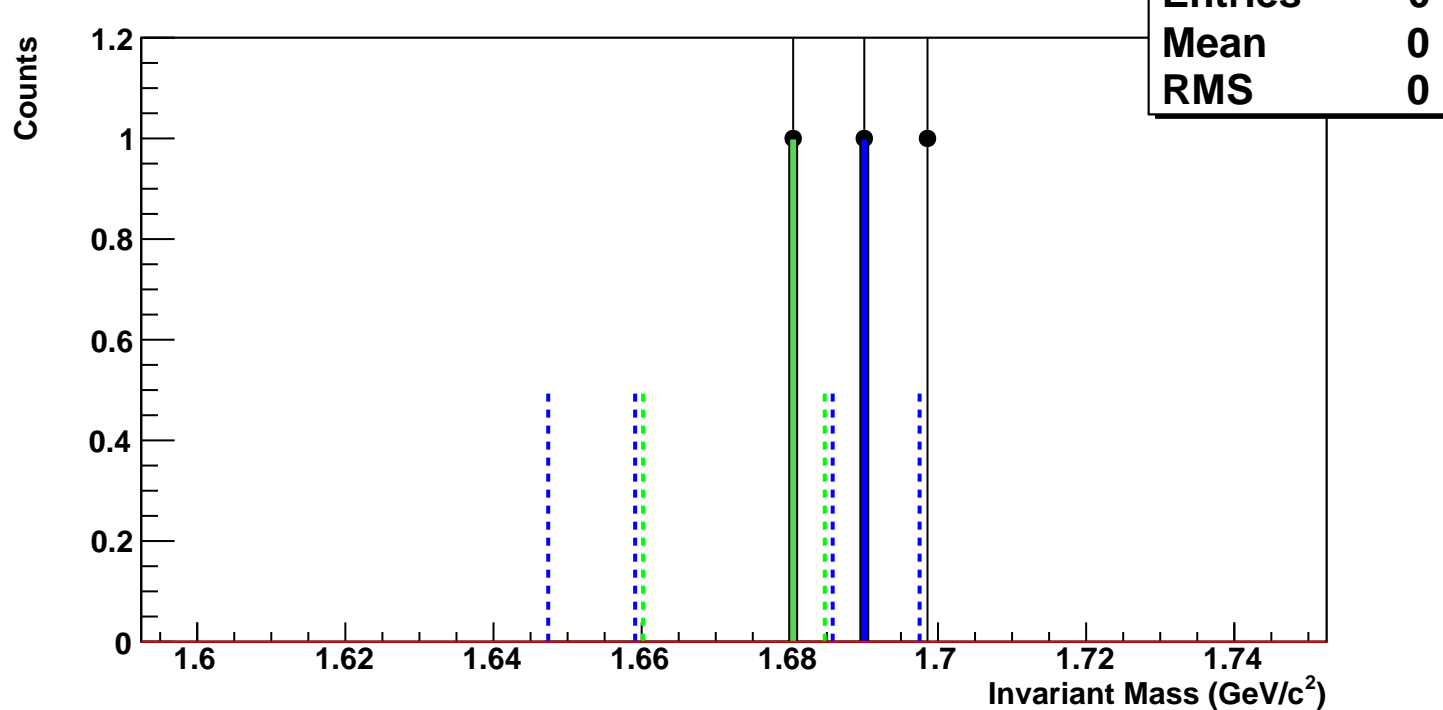
$\Omega^-$ , Au+Au 39 GeV, 20-40%,  $p_T$  5.0-7.0 GeV/c

hmlInvMassBgCent2Pt12



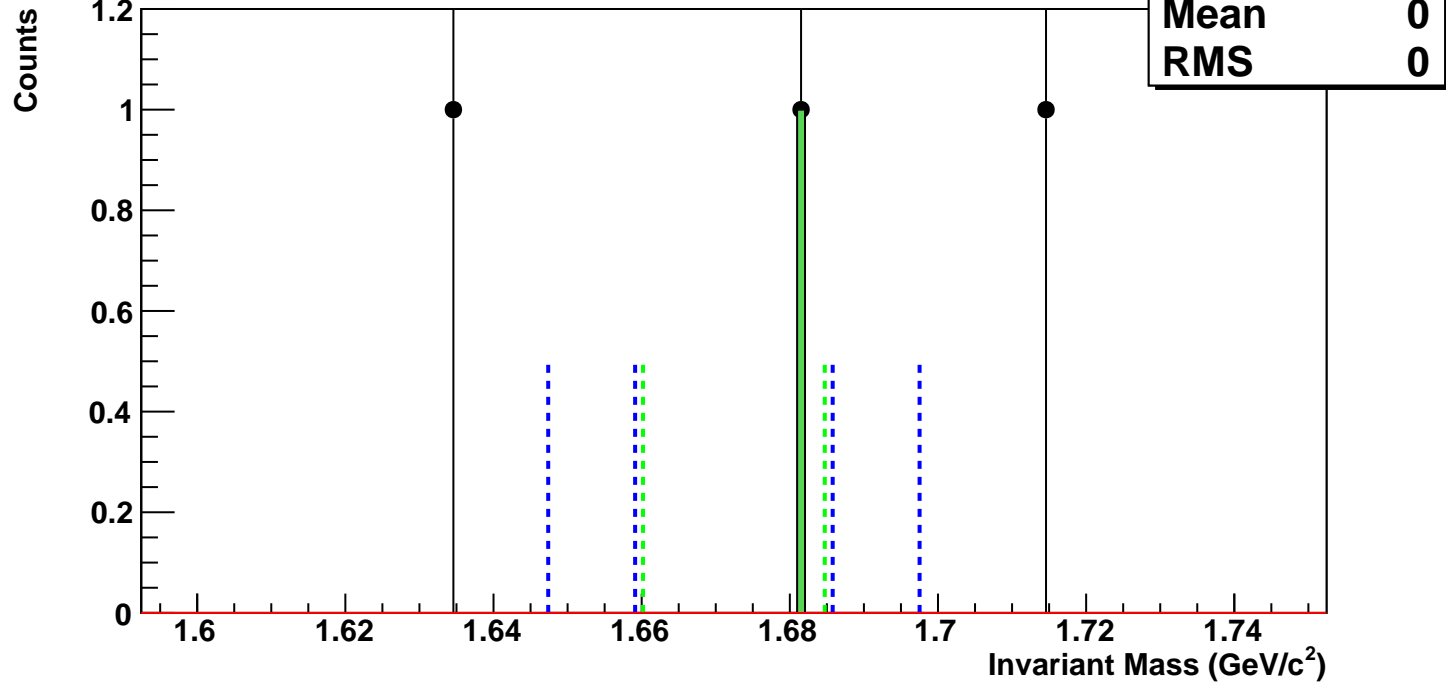
$\Omega^-$ , Au+Au 39 GeV, 10-20%,  $p_T$  5.0-7.0 GeV/c

hmlInvMassBgCent3Pt12



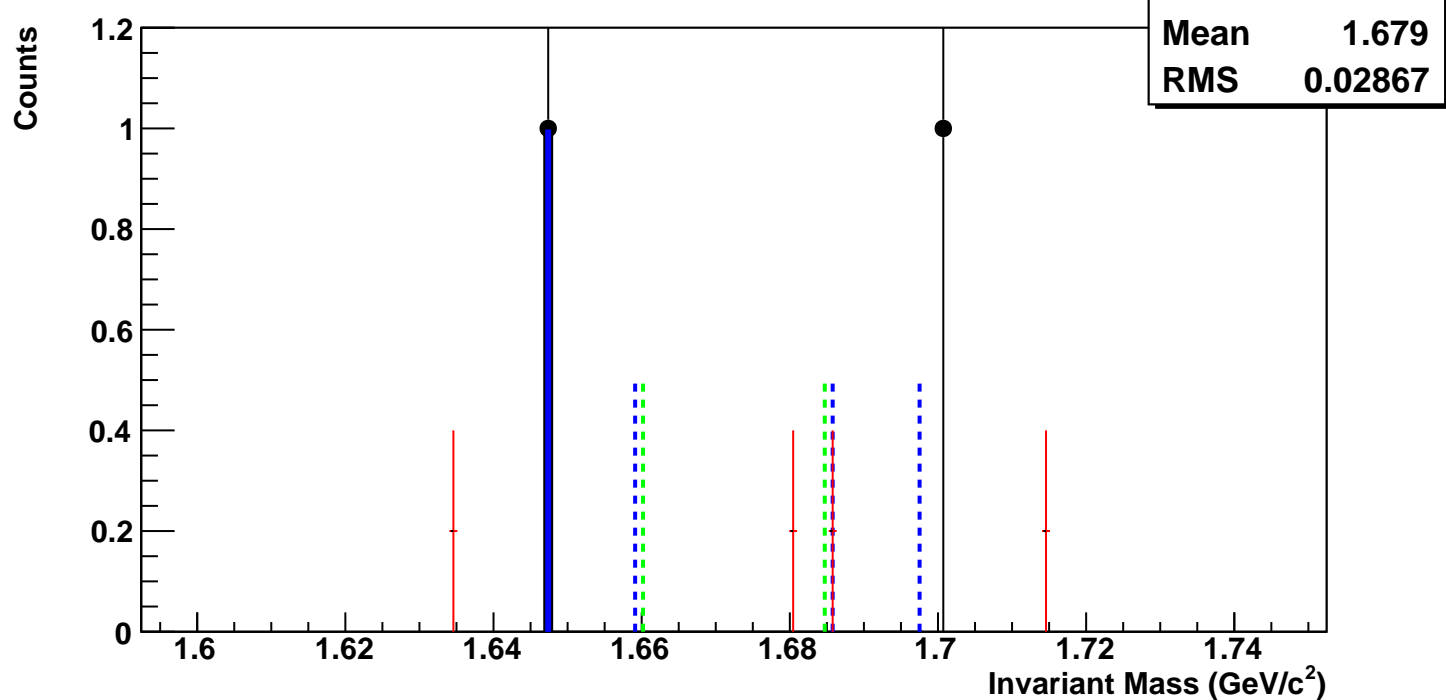
$\Omega^-$ , Au+Au 39 GeV, 5-10%,  $p_T$  5.0-7.0 GeV/c

hmlInvMassBgCent4Pt12

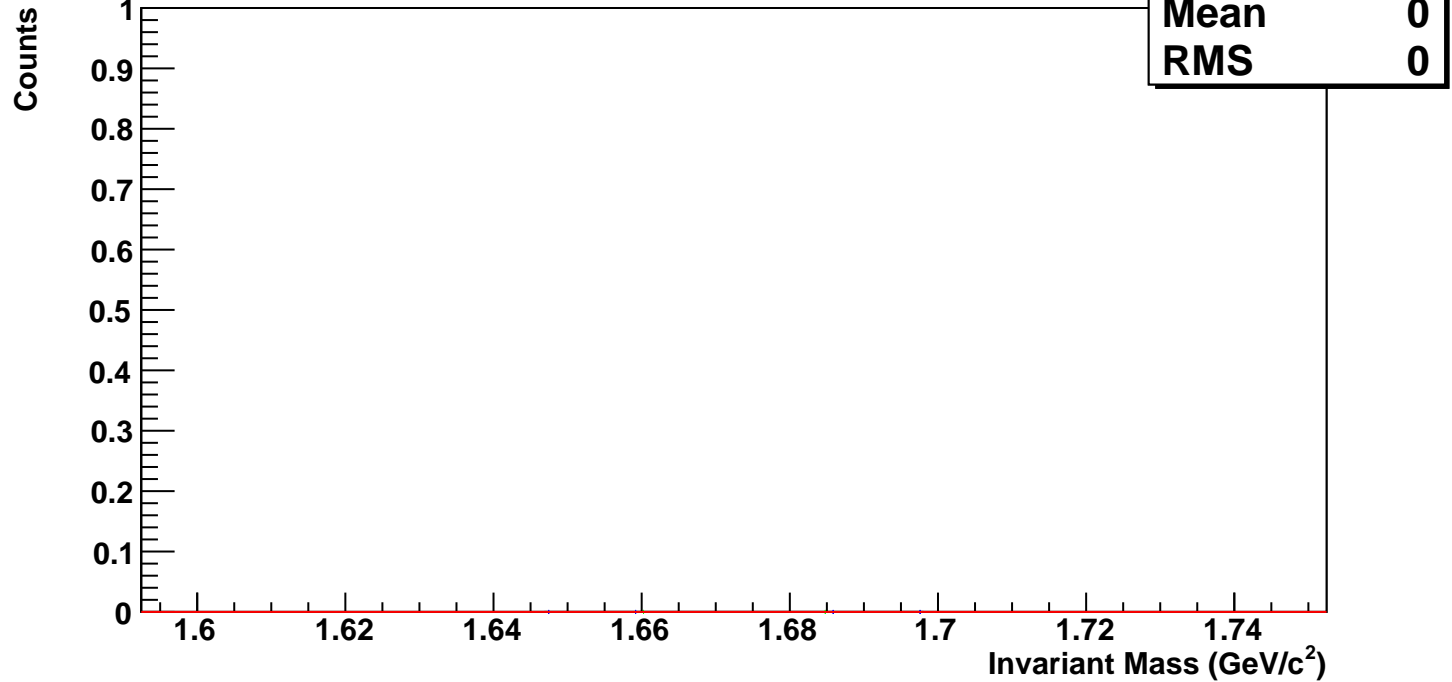


$\Omega^-$ , Au+Au 39 GeV, 0-5%,  $p_T$  5.0-7.0 GeV/c

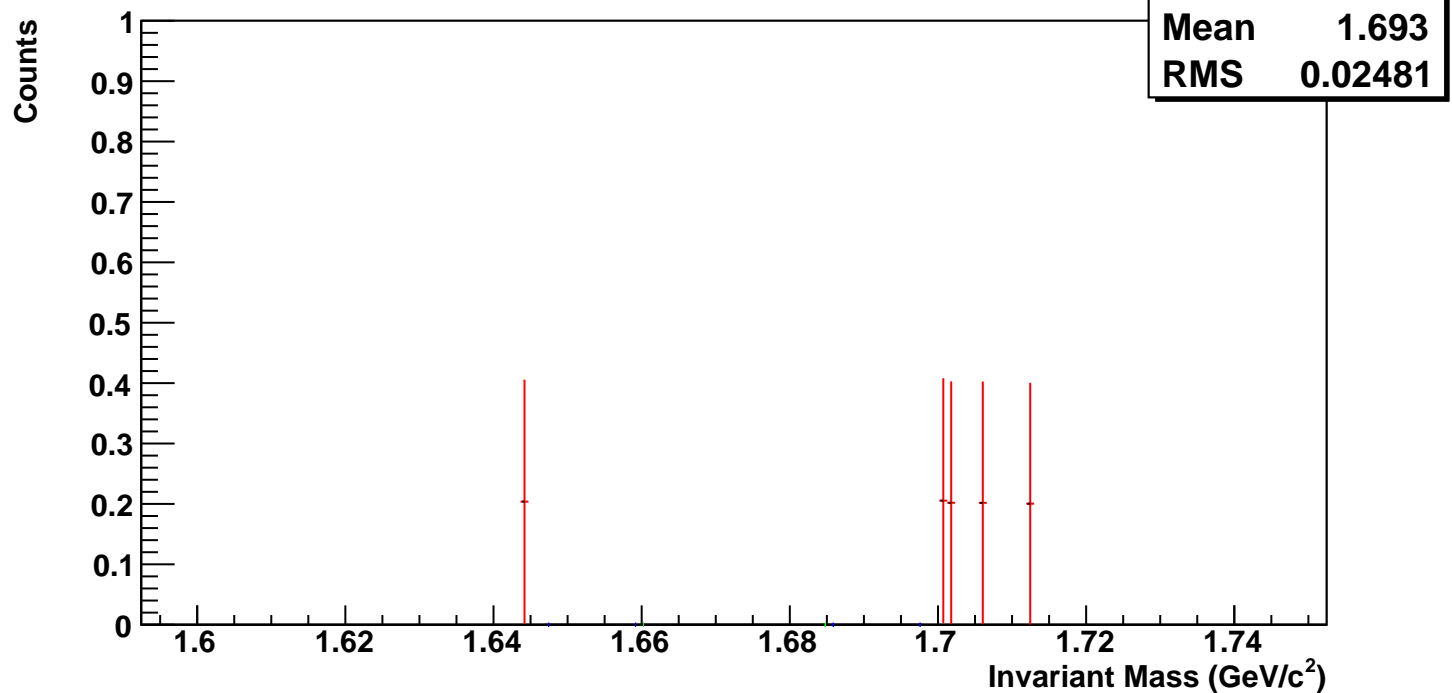
hmlInvMassBgCent5Pt12



$\bar{\Omega}^+$ , Au+Au 39 GeV, 60-80%,  $p_T$  0.2-0.5 GeV/c

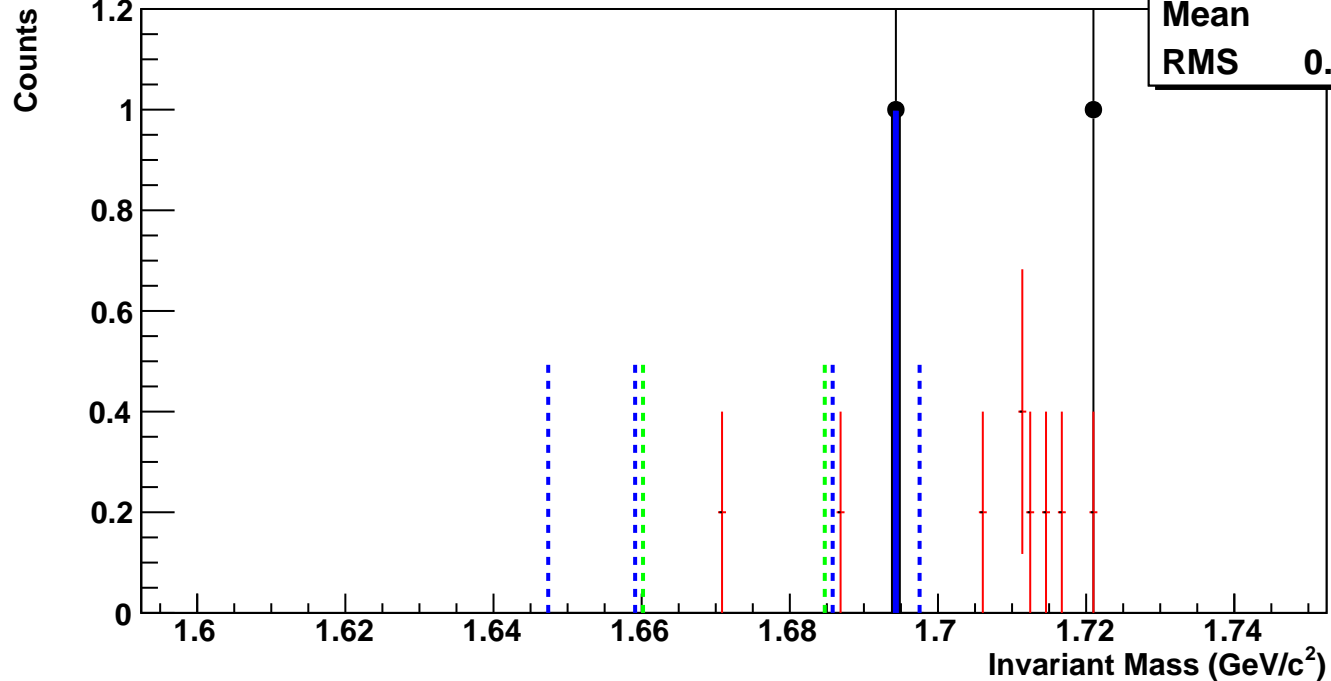


$\bar{\Omega}^+$ , Au+Au 39 GeV, 40-60%,  $p_T$  0.2-0.5 GeV/c



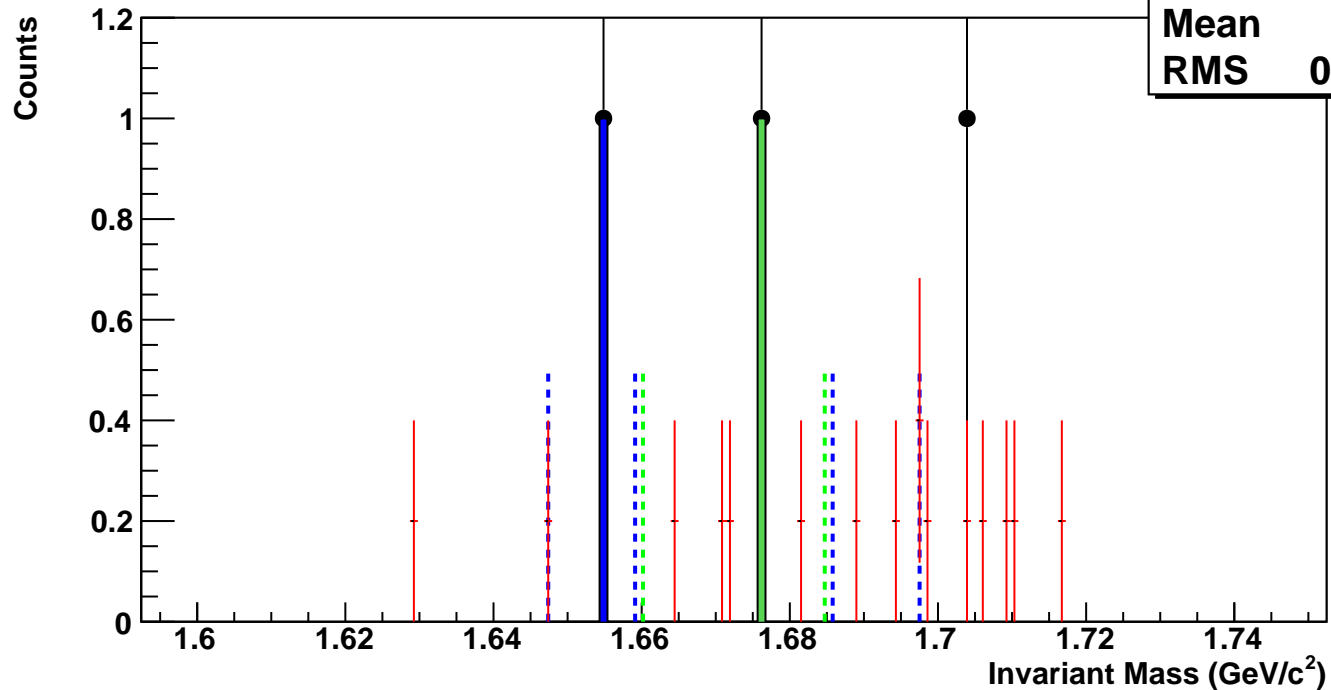
$\bar{\Omega}^+$ , Au+Au 39 GeV, 20-40%,  $p_T$  0.2-0.5 GeV/c

hmlInvMassBgCent2Pt0	
Entries	0
Mean	1.706
RMS	0.01533



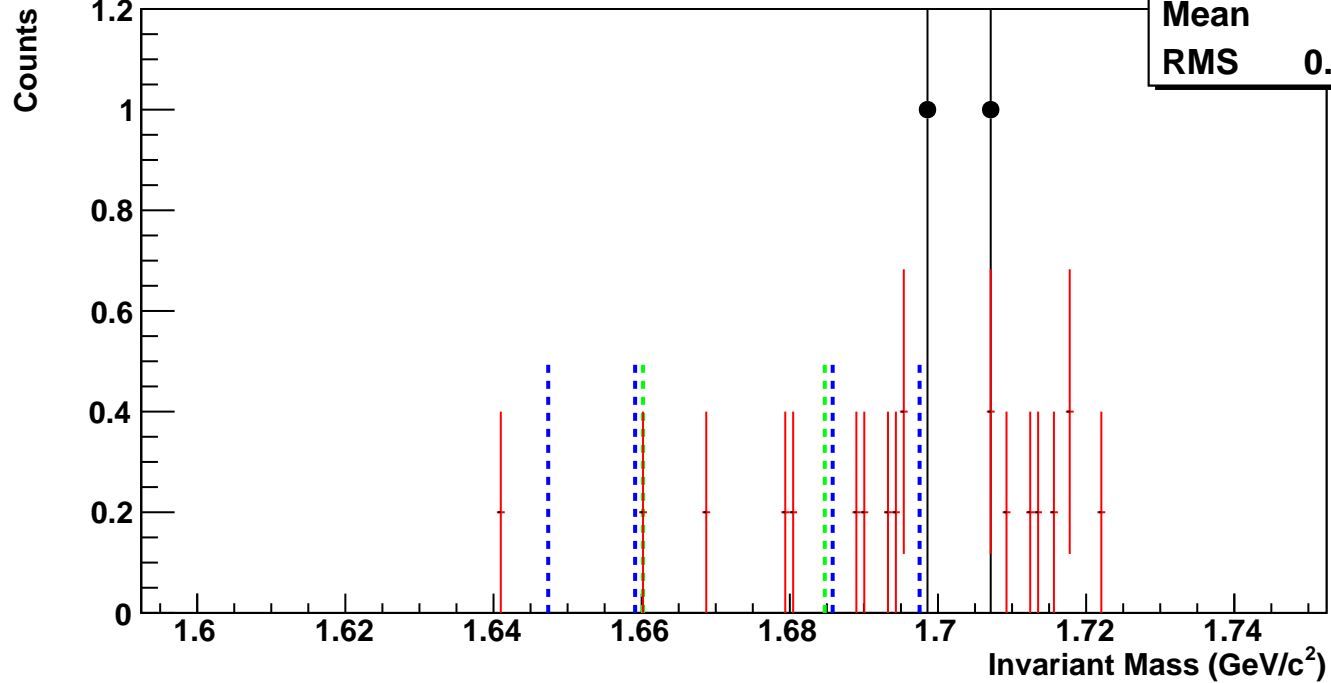
$\bar{\Omega}^+$ , Au+Au 39 GeV, 10-20%,  $p_T$  0.2-0.5 GeV/c

hmlInvMassBgCent3Pt0	
Entries	0
Mean	1.687
RMS	0.0236



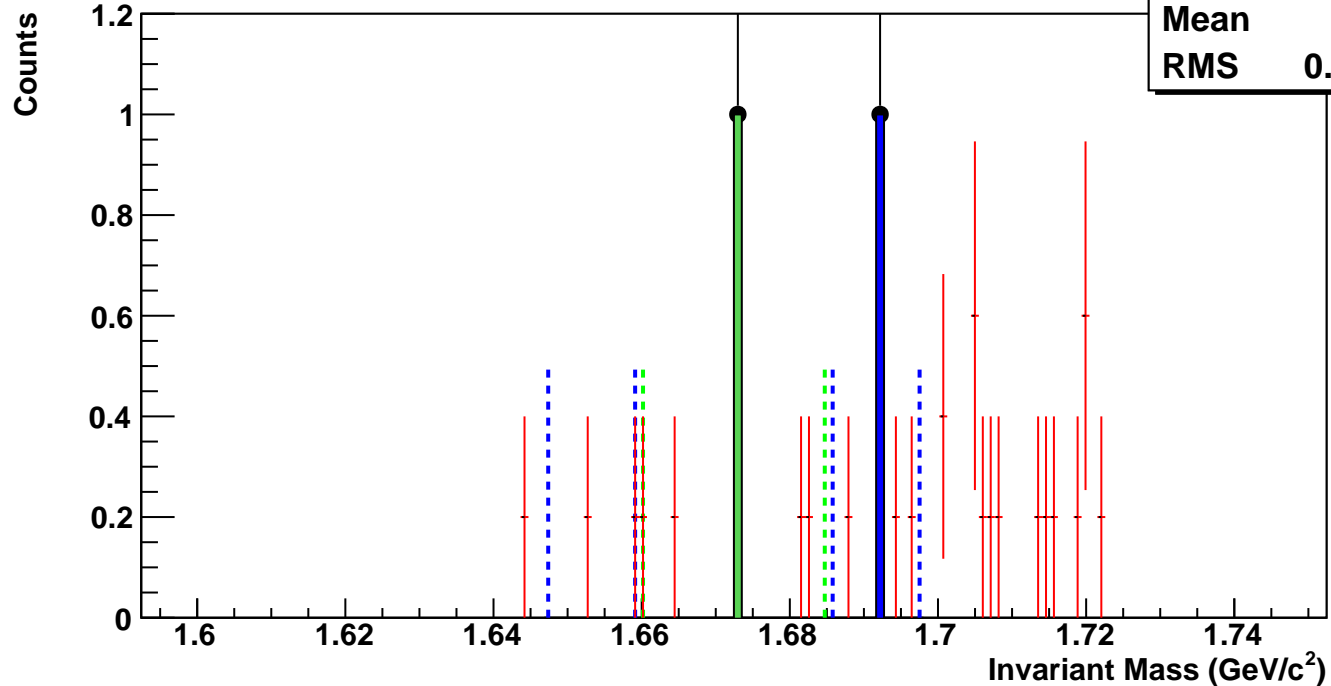
$\bar{\Omega}^+$ , Au+Au 39 GeV, 5-10%,  $p_T$  0.2-0.5 GeV/c

hmlInvMassBgCent4Pt0	
Entries	0
Mean	1.695
RMS	0.02083



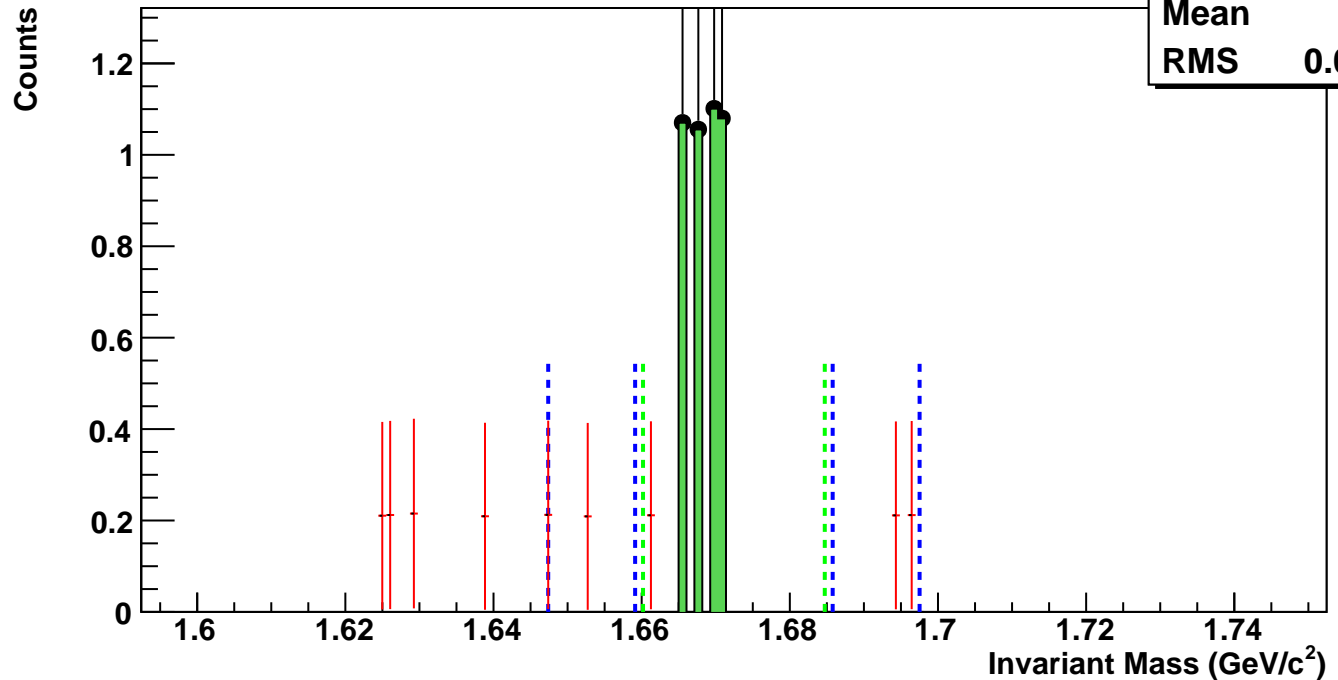
$\bar{\Omega}^+$ , Au+Au 39 GeV, 0-5%,  $p_T$  0.2-0.5 GeV/c

hmlInvMassBgCent5Pt0	
Entries	1
Mean	1.696
RMS	0.02259



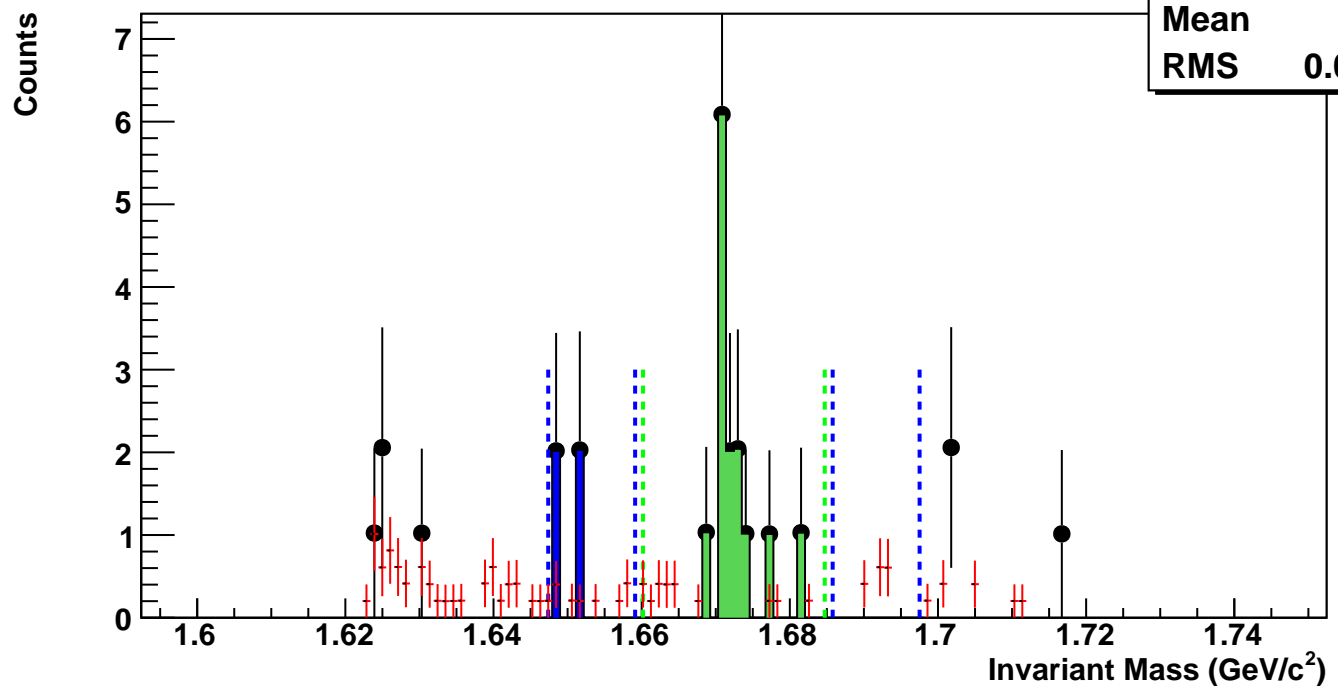
$\Omega^+$ , Au+Au 39 GeV, 60-80%,  $p_T$  0.5-0.8 GeV/c

hmlInvMassBgCent0Pt1	
Entries	0
Mean	1.652
RMS	0.02577



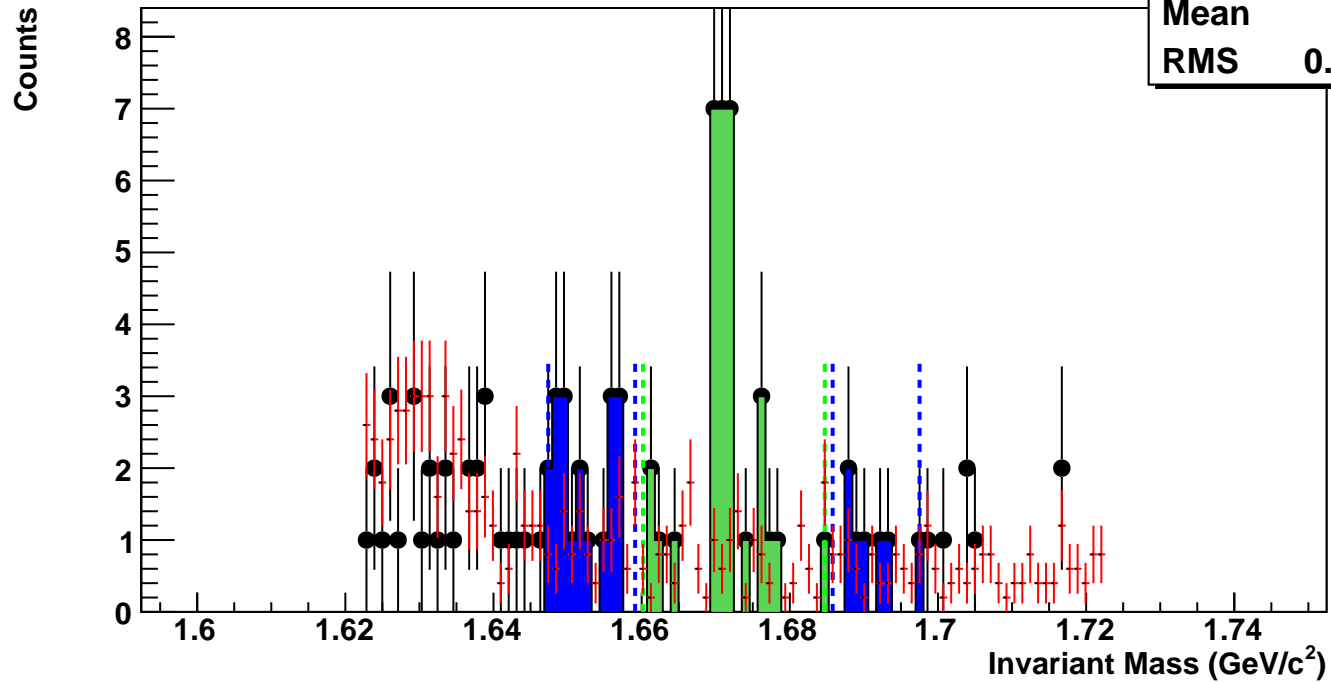
$\Omega^+$ , Au+Au 39 GeV, 40-60%,  $p_T$  0.5-0.8 GeV/c

hmlInvMassBgCent1Pt1	
Entries	2
Mean	1.653
RMS	0.02649



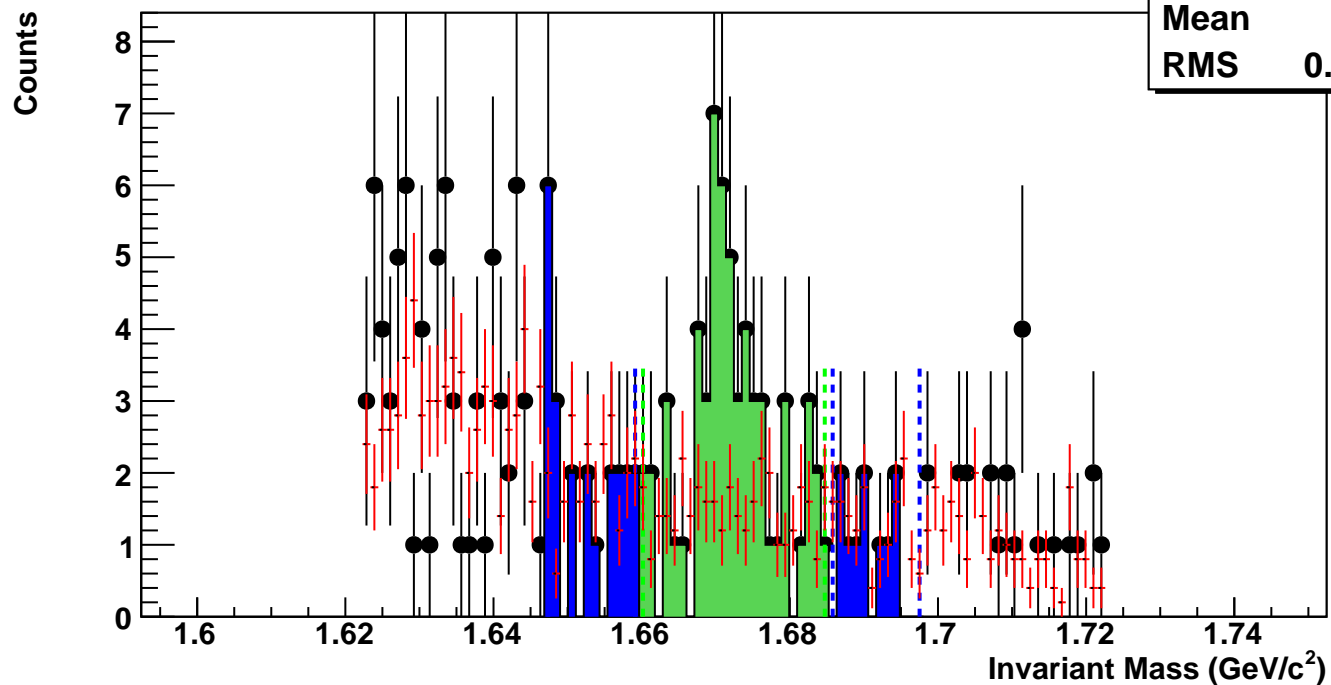
$\bar{\Omega}^+$ , Au+Au 39 GeV, 20-40%,  $p_T$  0.5-0.8 GeV/c

hmlInvMassBgCent2Pt1	
Entries	12
Mean	1.658
RMS	0.02932



$\bar{\Omega}^+$ , Au+Au 39 GeV, 10-20%,  $p_T$  0.5-0.8 GeV/c

hmlInvMassBgCent3Pt1	
Entries	20
Mean	1.661
RMS	0.02749



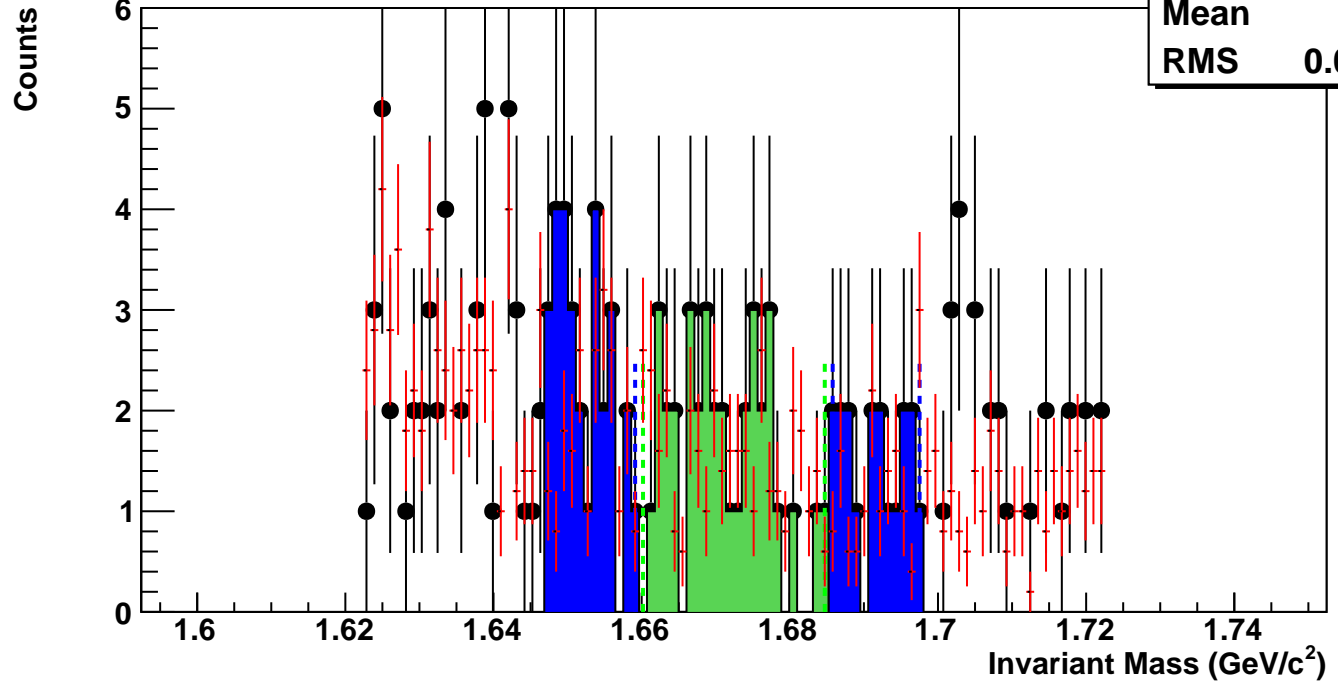
$\Omega^+$ , Au+Au 39 GeV, 5-10%,  $p_T$  0.5-0.8 GeV/c

hmlInvMassBgCent4Pt1

Entries 19

Mean 1.664

RMS 0.02915



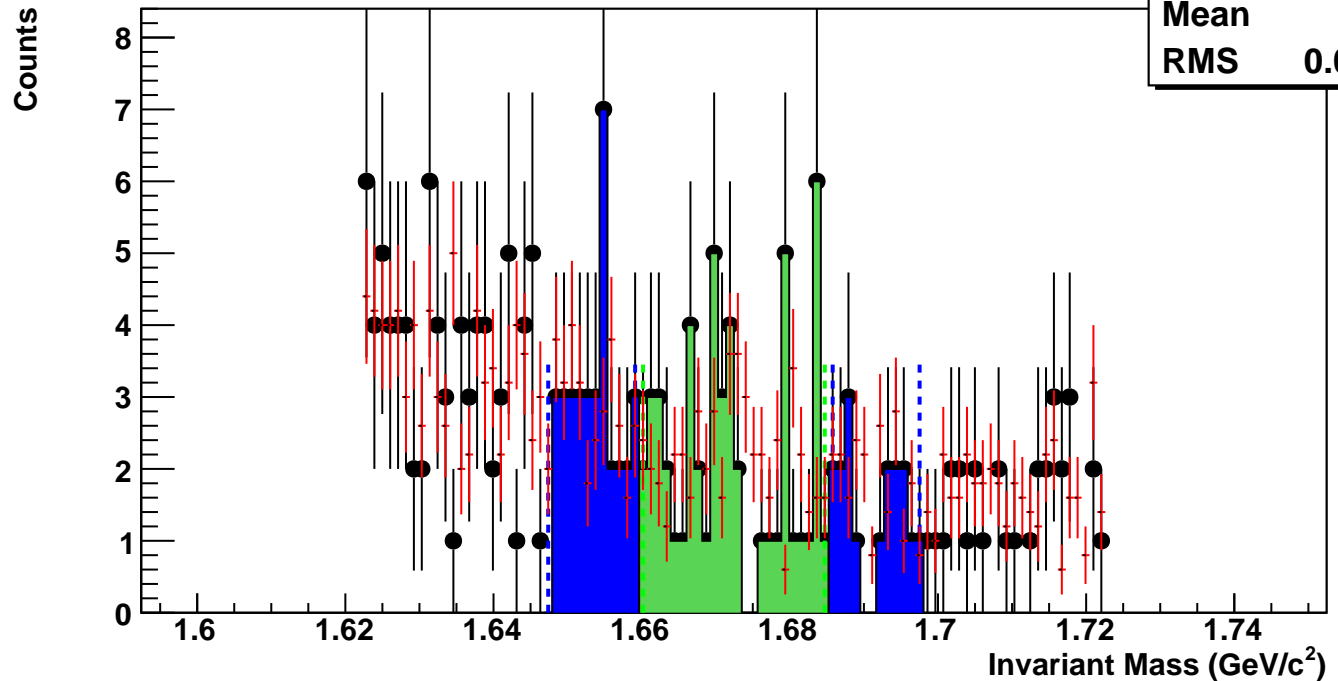
$\Omega^+$ , Au+Au 39 GeV, 0-5%,  $p_T$  0.5-0.8 GeV/c

hmlInvMassBgCent5Pt1

Entries 27

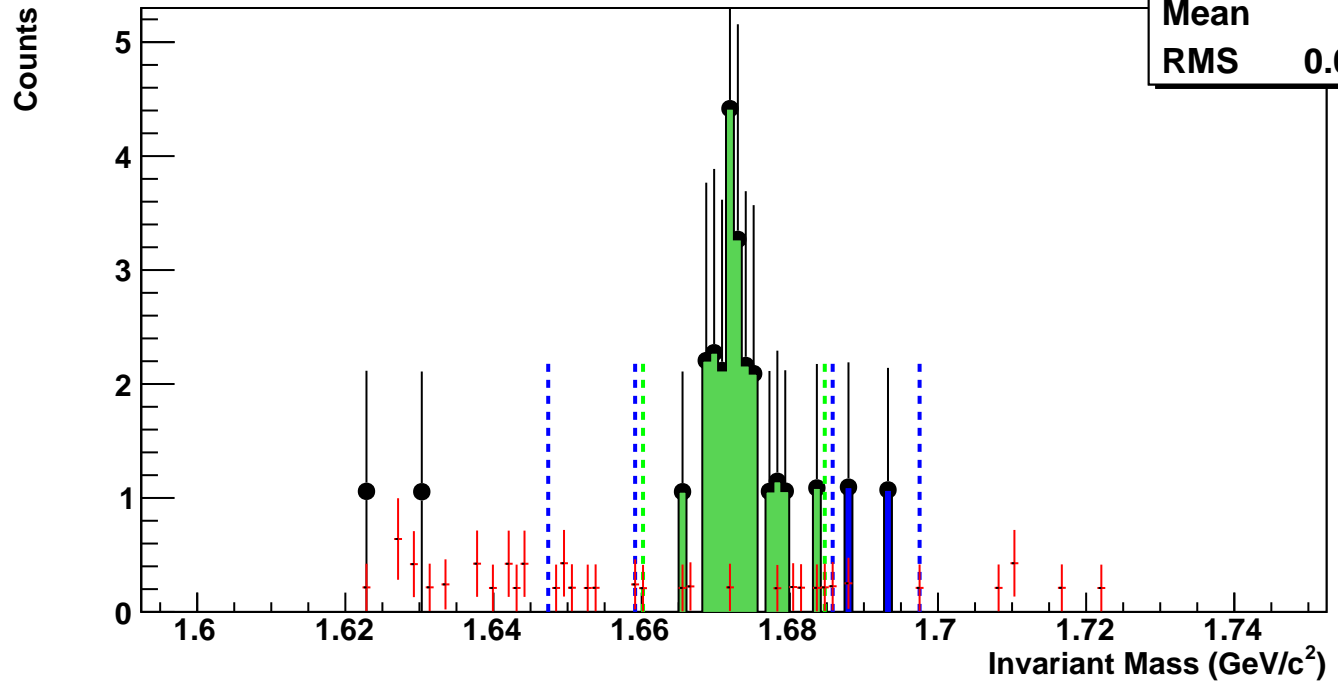
Mean 1.664

RMS 0.02883



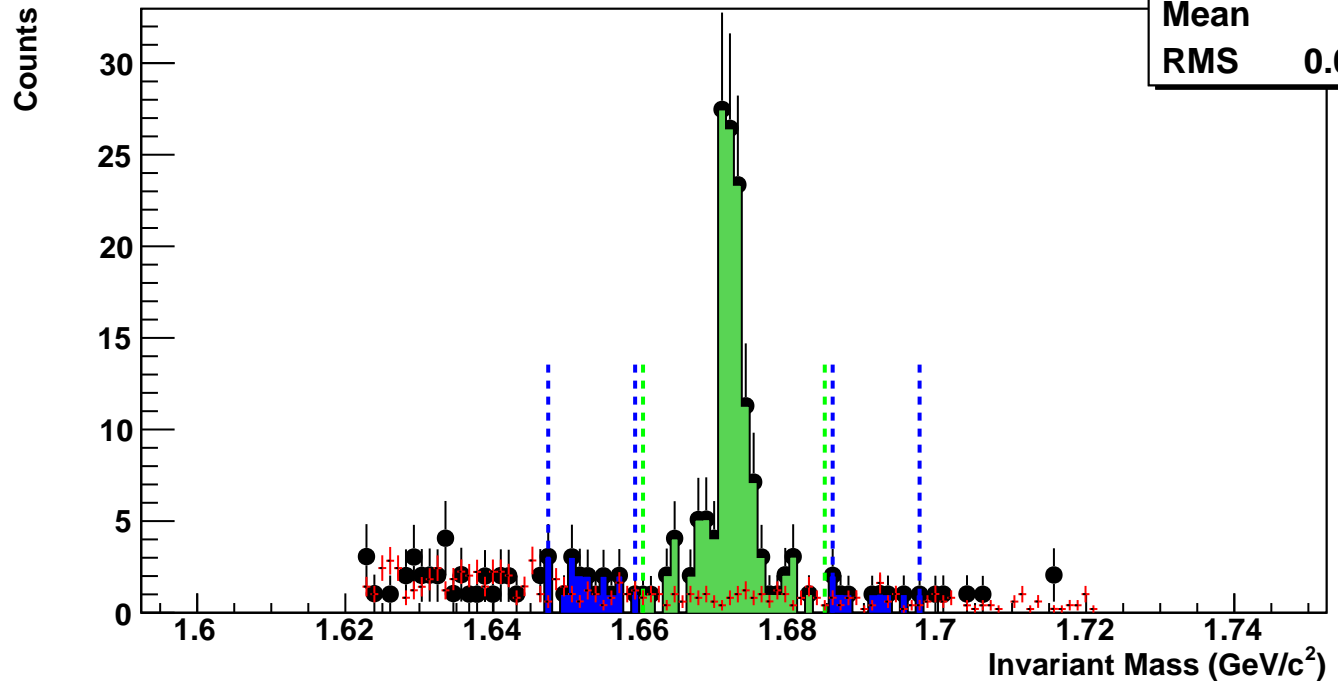
$\bar{\Omega}^+$ , Au+Au 39 GeV, 60-80%,  $p_T$  0.8-1.1 GeV/c

hmlInvMassBgCent0Pt2	
Entries	1
Mean	1.661
RMS	0.02789



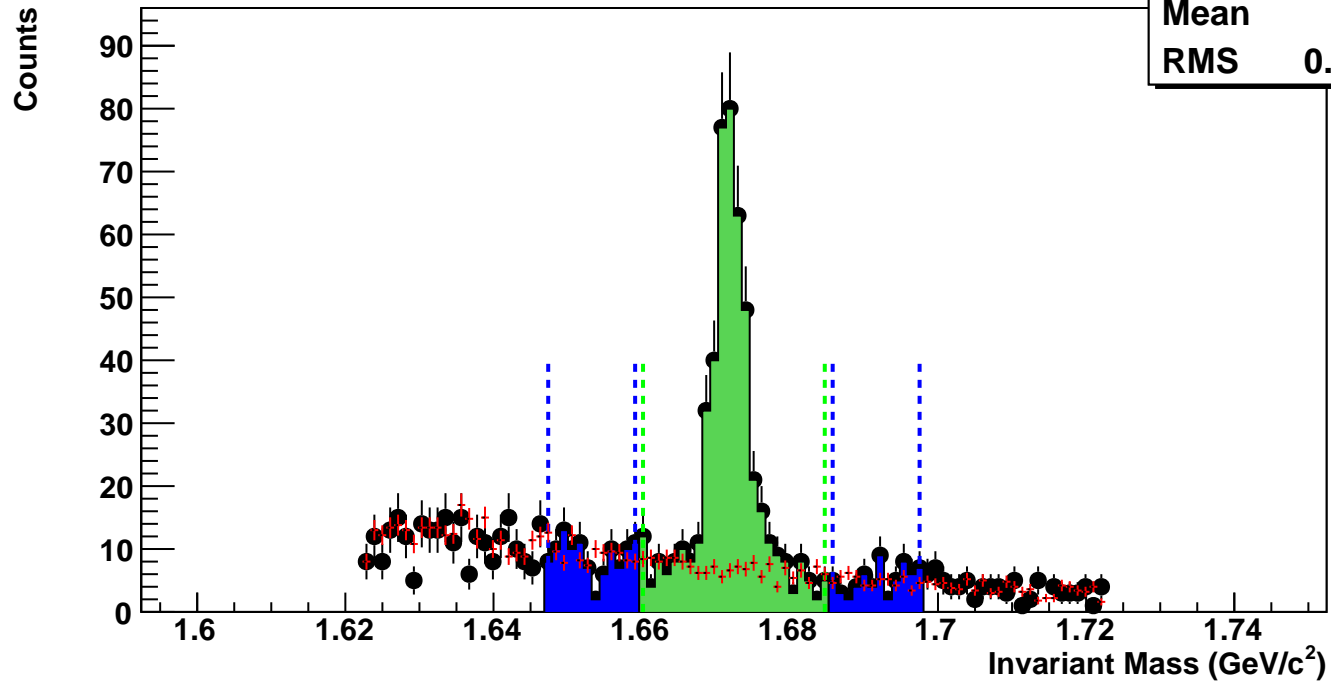
$\bar{\Omega}^+$ , Au+Au 39 GeV, 40-60%,  $p_T$  0.8-1.1 GeV/c

hmlInvMassBgCent1Pt2	
Entries	11
Mean	1.658
RMS	0.02648



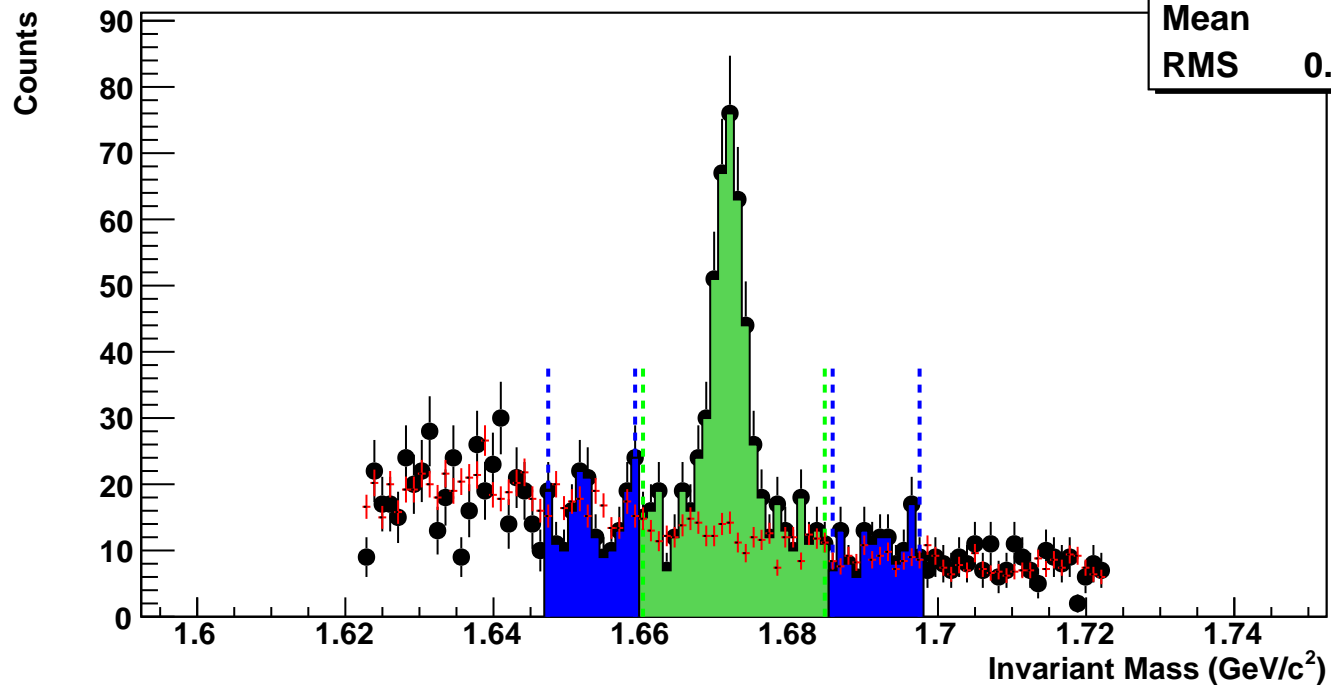
$\Omega^+$ , Au+Au 39 GeV, 20-40%,  $p_T$  0.8-1.1 GeV/c

hmlnvMassBgCent2Pt2	
Entries	85
Mean	1.66
RMS	0.02678



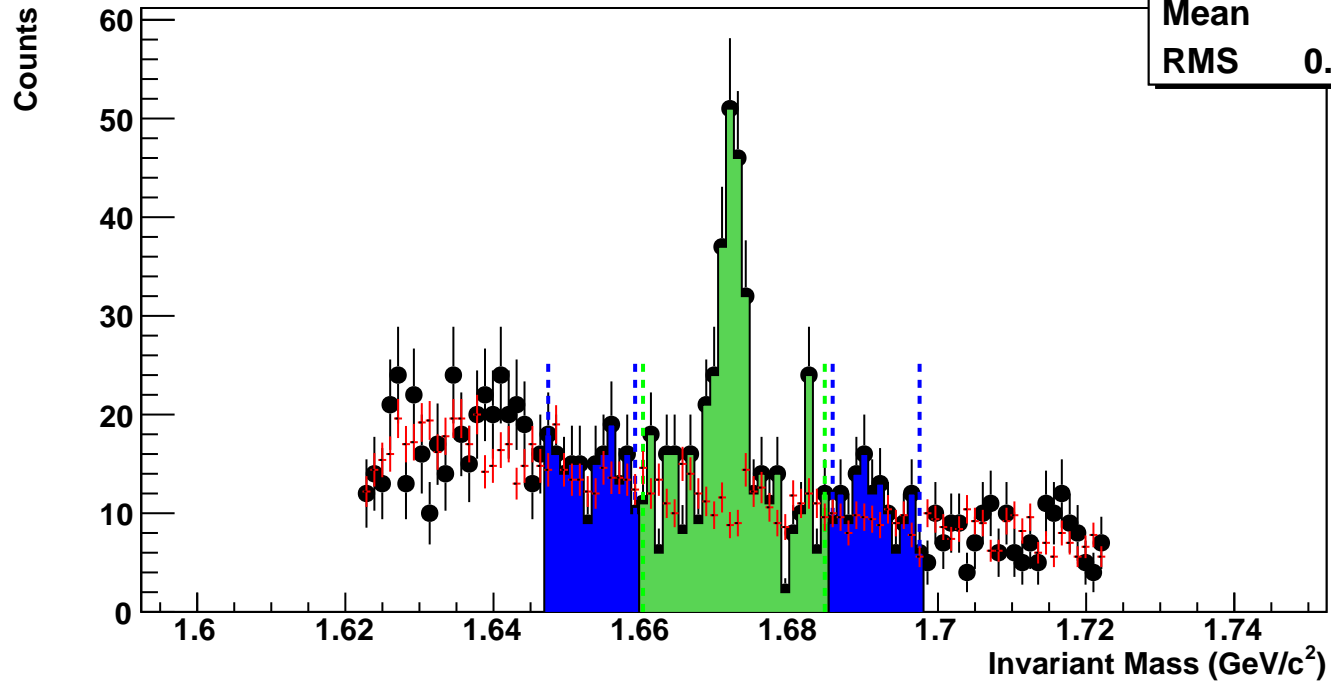
$\Omega^+$ , Au+Au 39 GeV, 10-20%,  $p_T$  0.8-1.1 GeV/c

hmlnvMassBgCent3Pt2	
Entries	148
Mean	1.662
RMS	0.02758



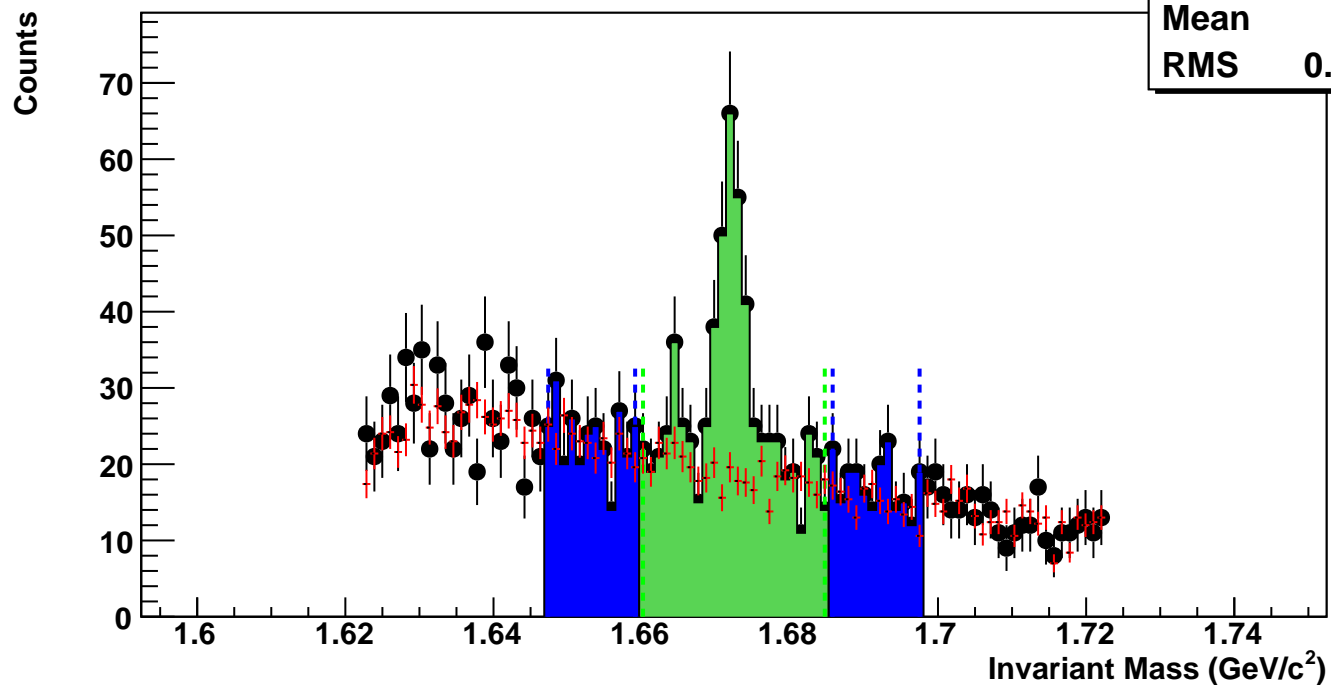
$\bar{\Omega}^+$ , Au+Au 39 GeV, 5-10%,  $p_T$  0.8-1.1 GeV/c

hmlInvMassBgCent4Pt2	
Entries	136
Mean	1.664
RMS	0.02797



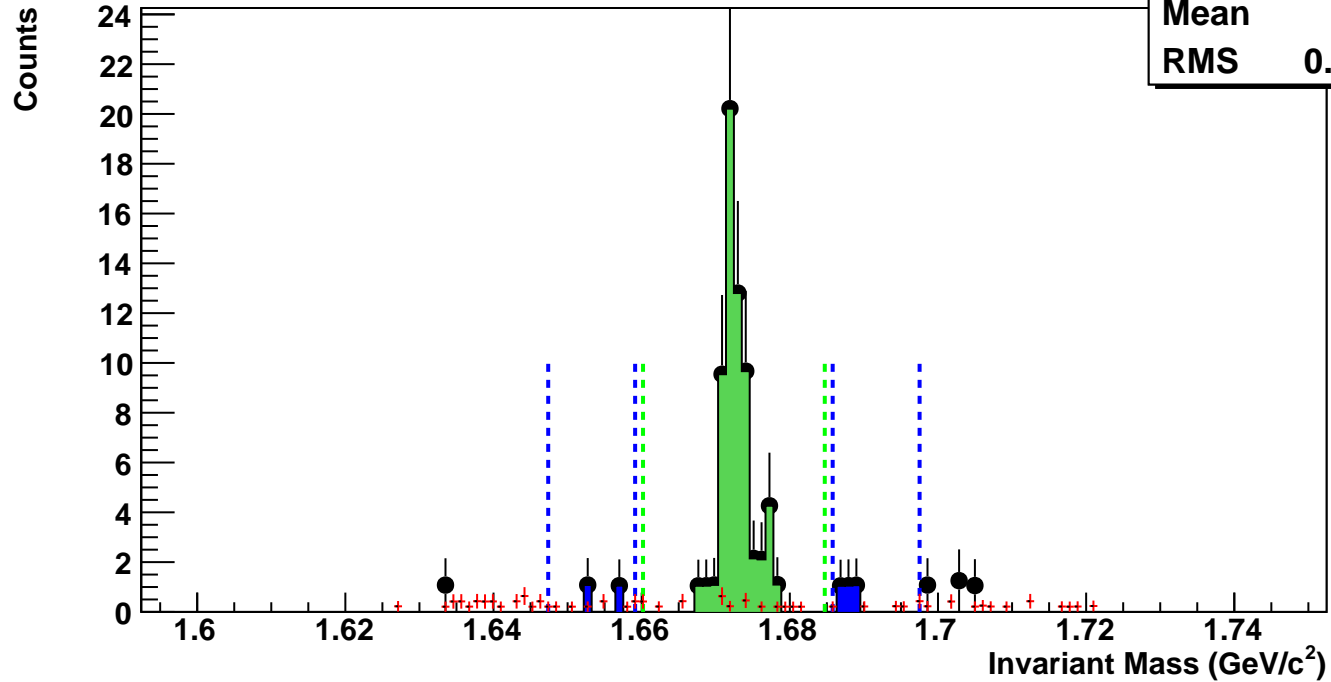
$\bar{\Omega}^+$ , Au+Au 39 GeV, 0-5%,  $p_T$  0.8-1.1 GeV/c

hmlInvMassBgCent5Pt2	
Entries	216
Mean	1.665
RMS	0.02784



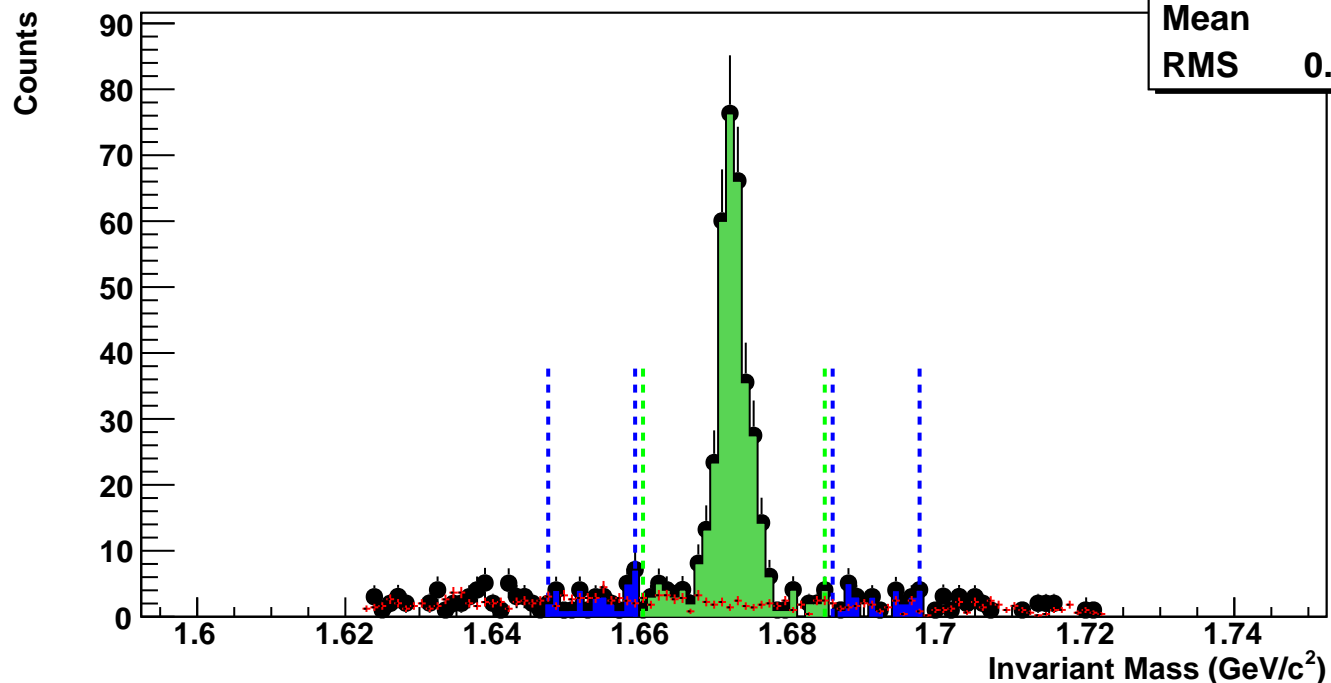
$\Omega^+$ , Au+Au 39 GeV, 60-80%,  $p_T$  1.1-1.4 GeV/c

hmlnvMassBgCent0Pt3	
Entries	2
Mean	1.668
RMS	0.02727



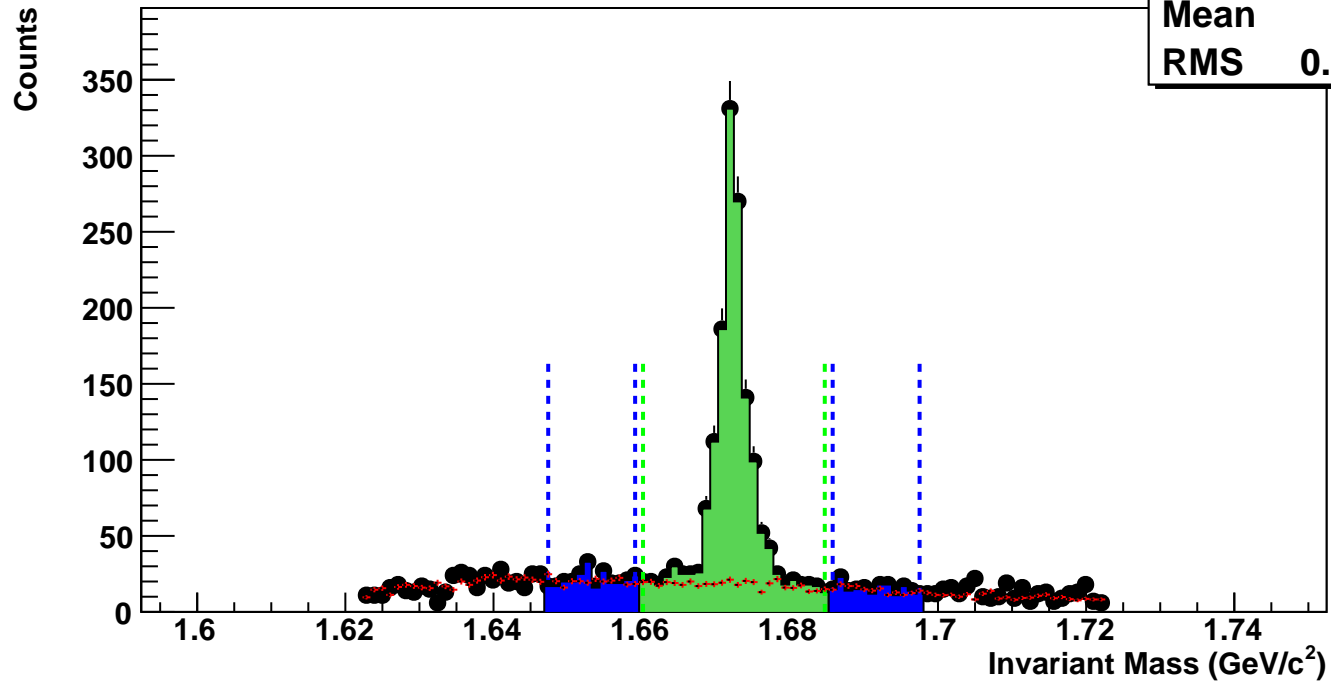
$\Omega^+$ , Au+Au 39 GeV, 40-60%,  $p_T$  1.1-1.4 GeV/c

hmlnvMassBgCent1Pt3	
Entries	21
Mean	1.666
RMS	0.02598



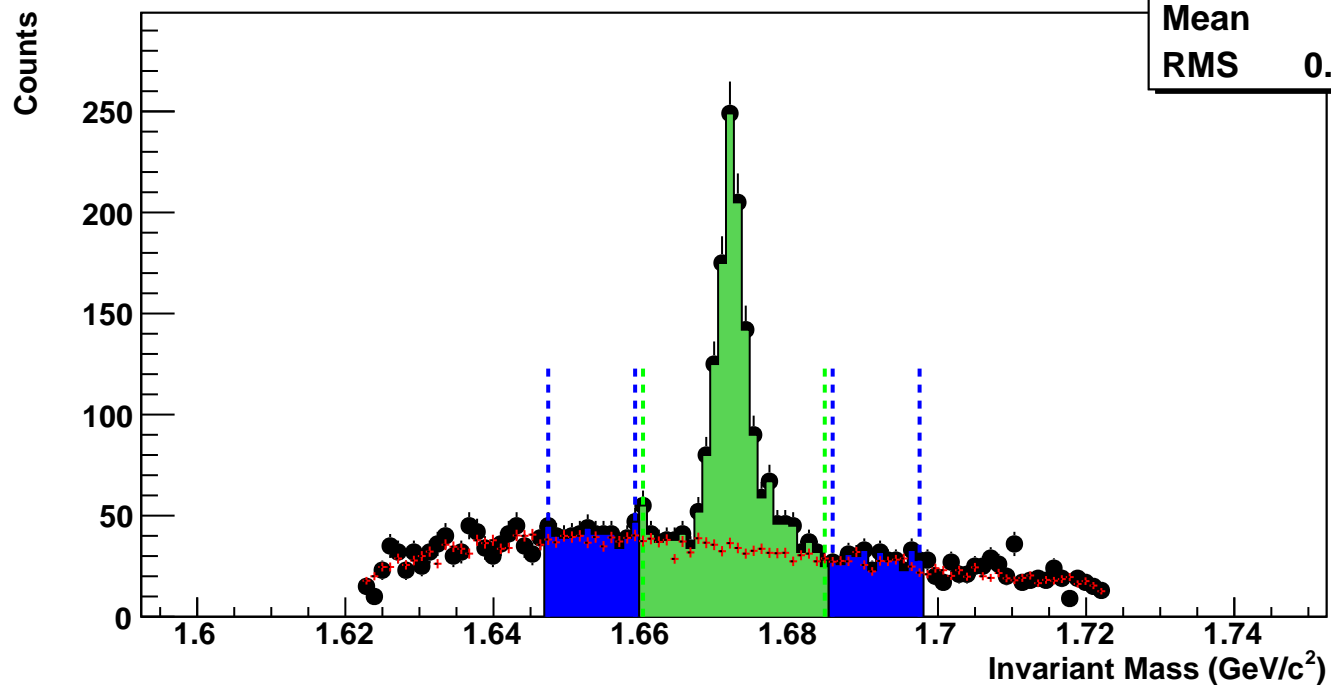
$\Omega^+$ , Au+Au 39 GeV, 20-40%,  $p_T$  1.1-1.4 GeV/c

hmlInvMassBgCent2Pt3	
Entries	182
Mean	1.667
RMS	0.02641



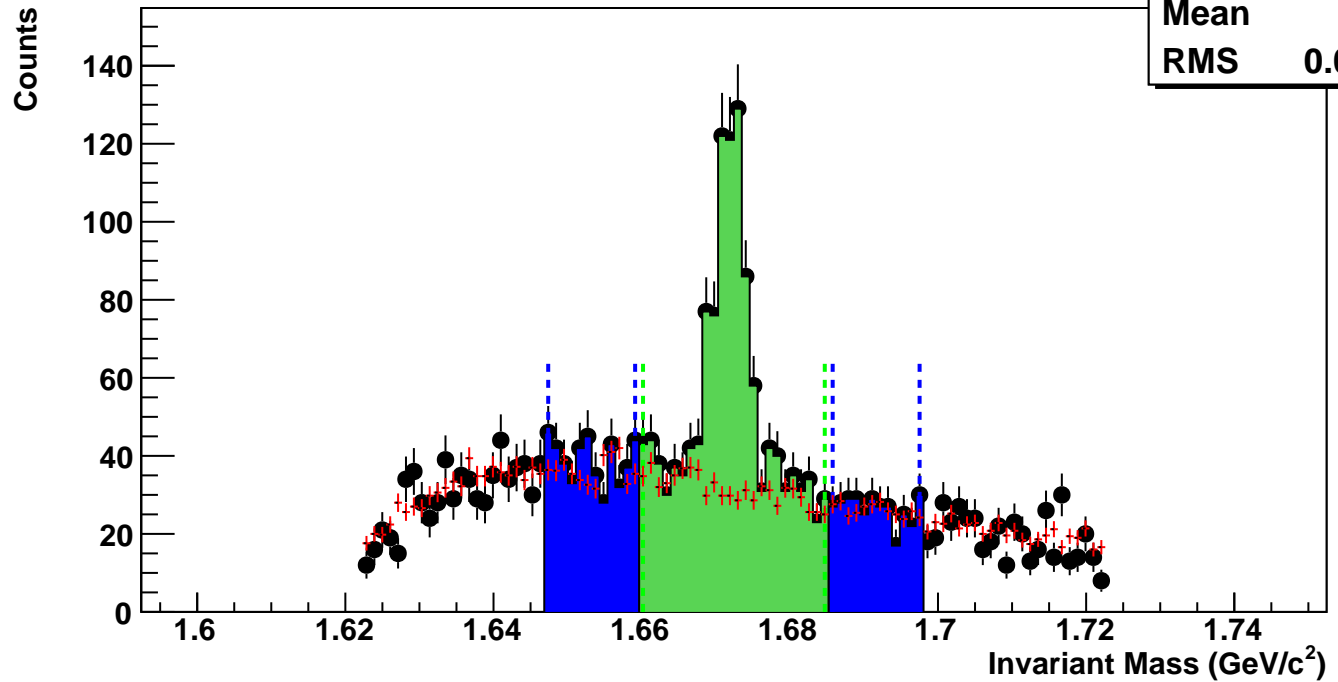
$\Omega^+$ , Au+Au 39 GeV, 10-20%,  $p_T$  1.1-1.4 GeV/c

hmlInvMassBgCent3Pt3	
Entries	336
Mean	1.668
RMS	0.02639



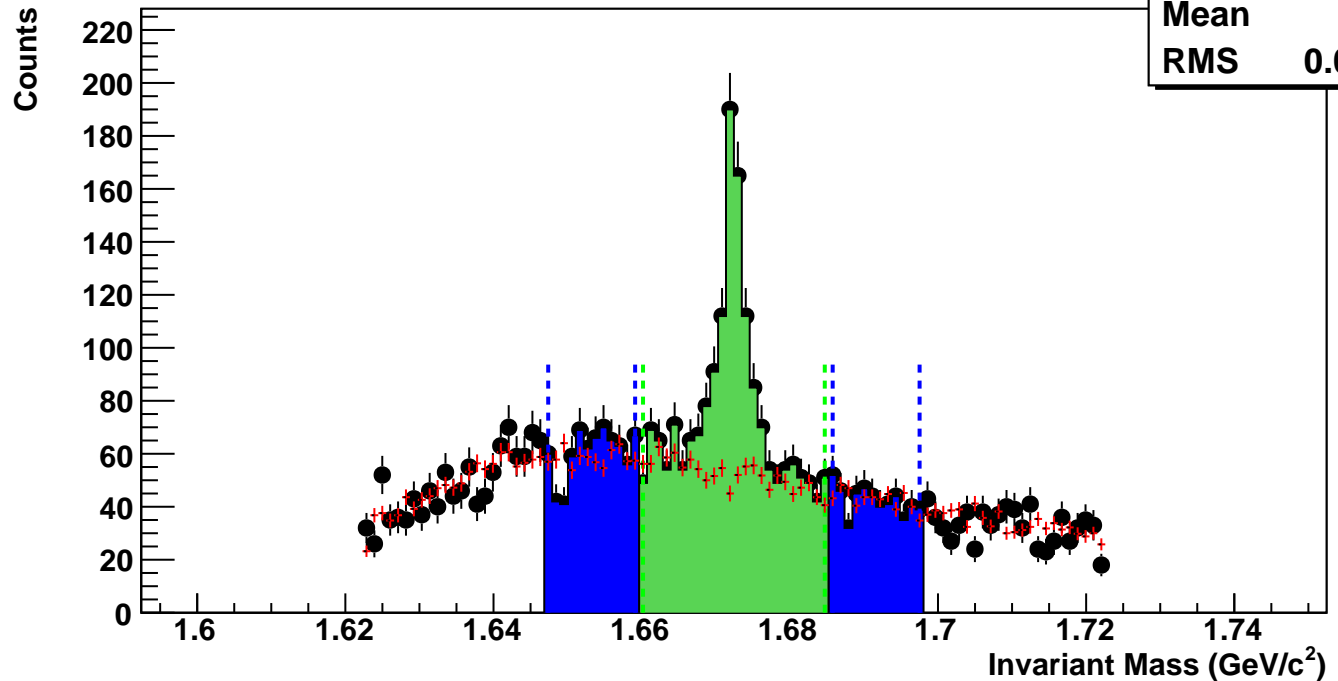
$\Omega^+$ , Au+Au 39 GeV, 5-10%,  $p_T$  1.1-1.4 GeV/c

hmlInvMassBgCent4Pt3	
Entries	326
Mean	1.668
RMS	0.02683



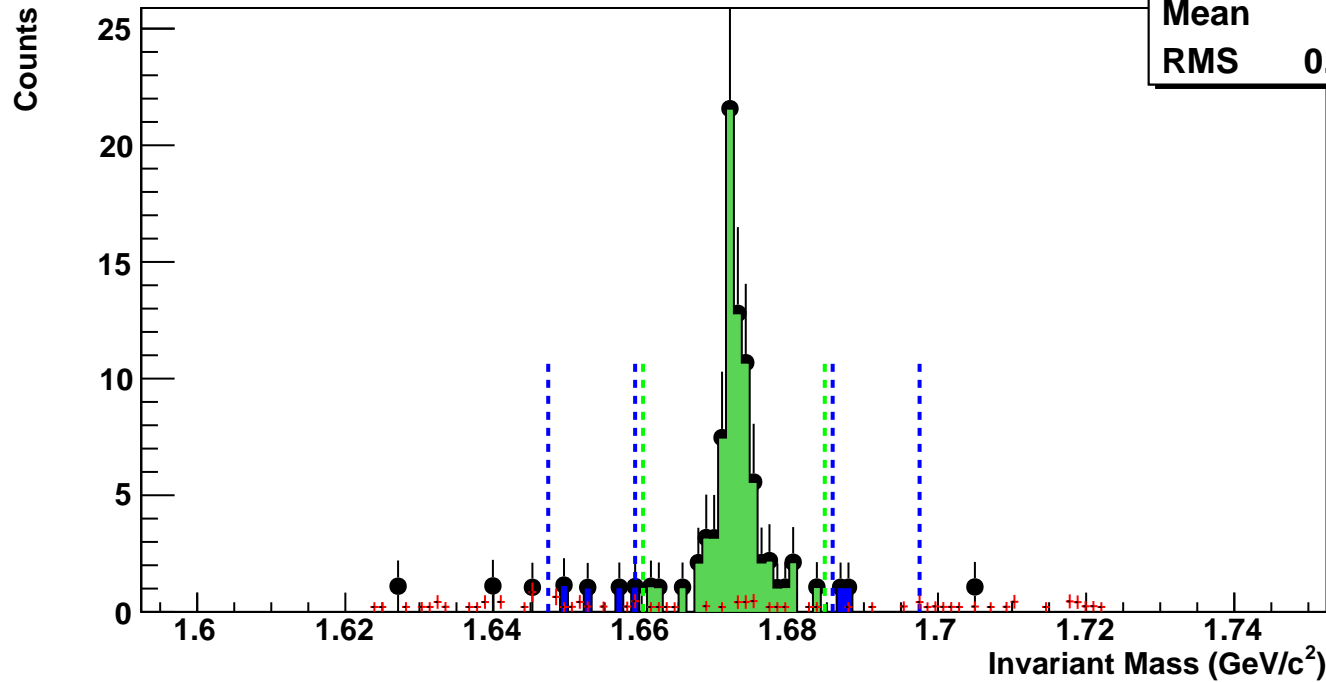
$\Omega^+$ , Au+Au 39 GeV, 0-5%,  $p_T$  1.1-1.4 GeV/c

hmlInvMassBgCent5Pt3	
Entries	529
Mean	1.669
RMS	0.02673



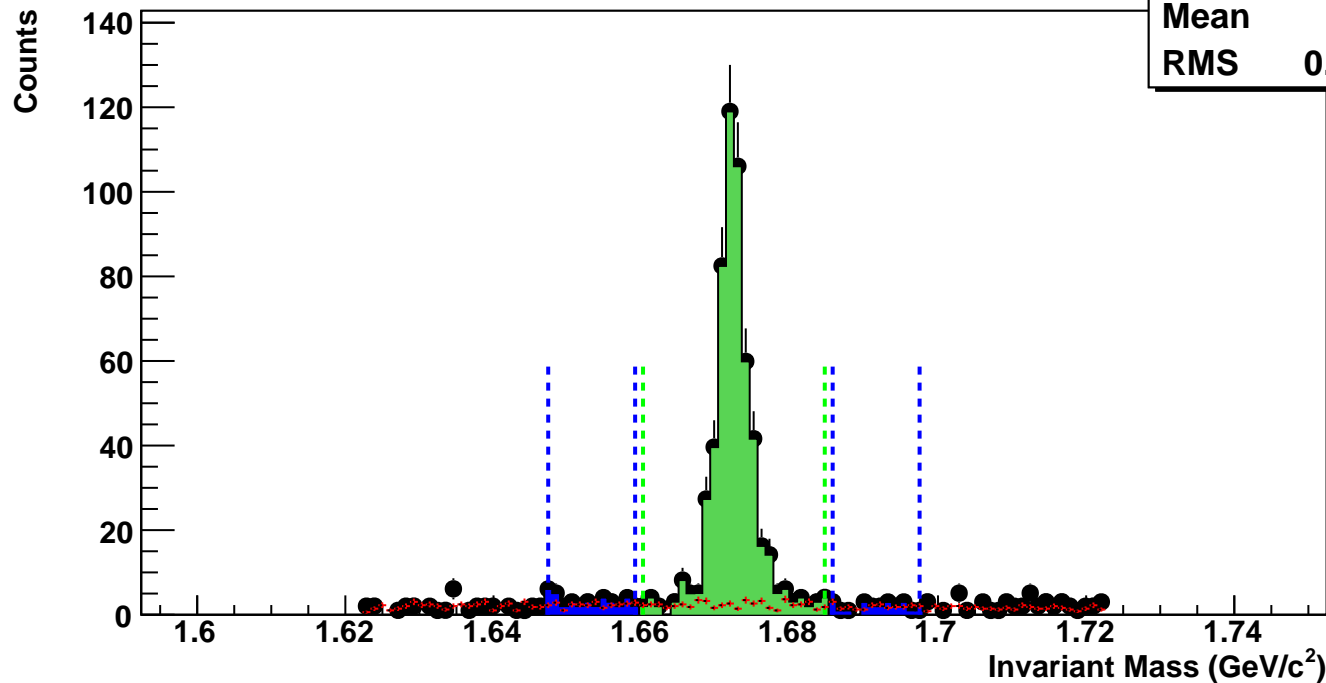
$\bar{\Omega}^+$ , Au+Au 39 GeV, 60-80%,  $p_T$  1.4-1.7 GeV/c

hmlInvMassBgCent0Pt4	
Entries	2
Mean	1.671
RMS	0.02928



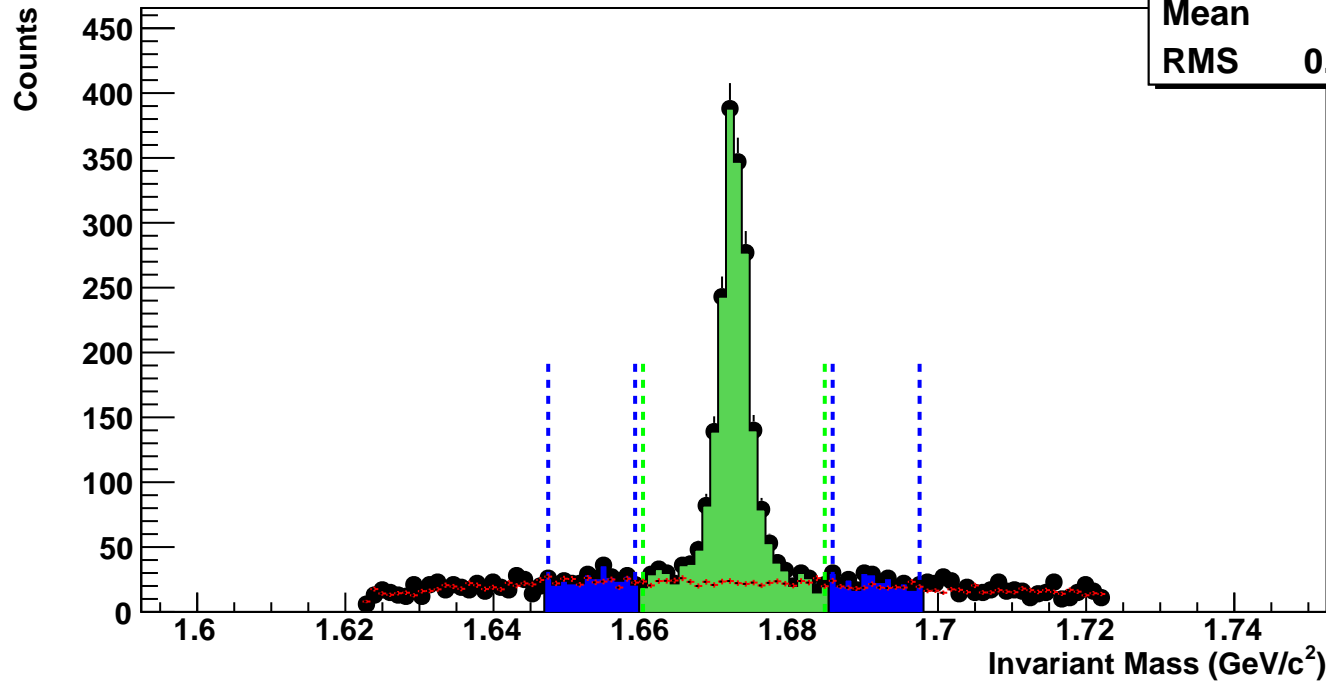
$\bar{\Omega}^+$ , Au+Au 39 GeV, 40-60%,  $p_T$  1.4-1.7 GeV/c

hmlInvMassBgCent1Pt4	
Entries	23
Mean	1.67
RMS	0.02714



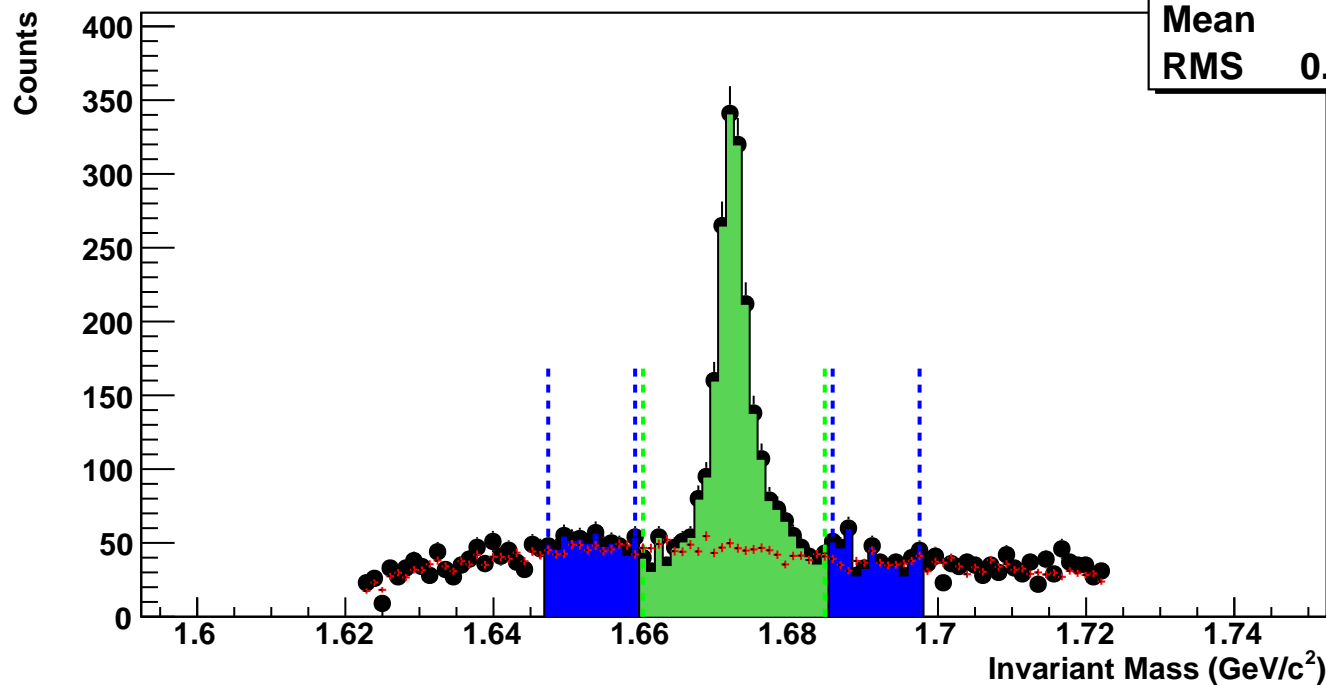
$\Omega^+$ , Au+Au 39 GeV, 20-40%,  $p_T$  1.4-1.7 GeV/c

hmlInvMassBgCent2Pt4	
Entries	225
Mean	1.671
RMS	0.02688



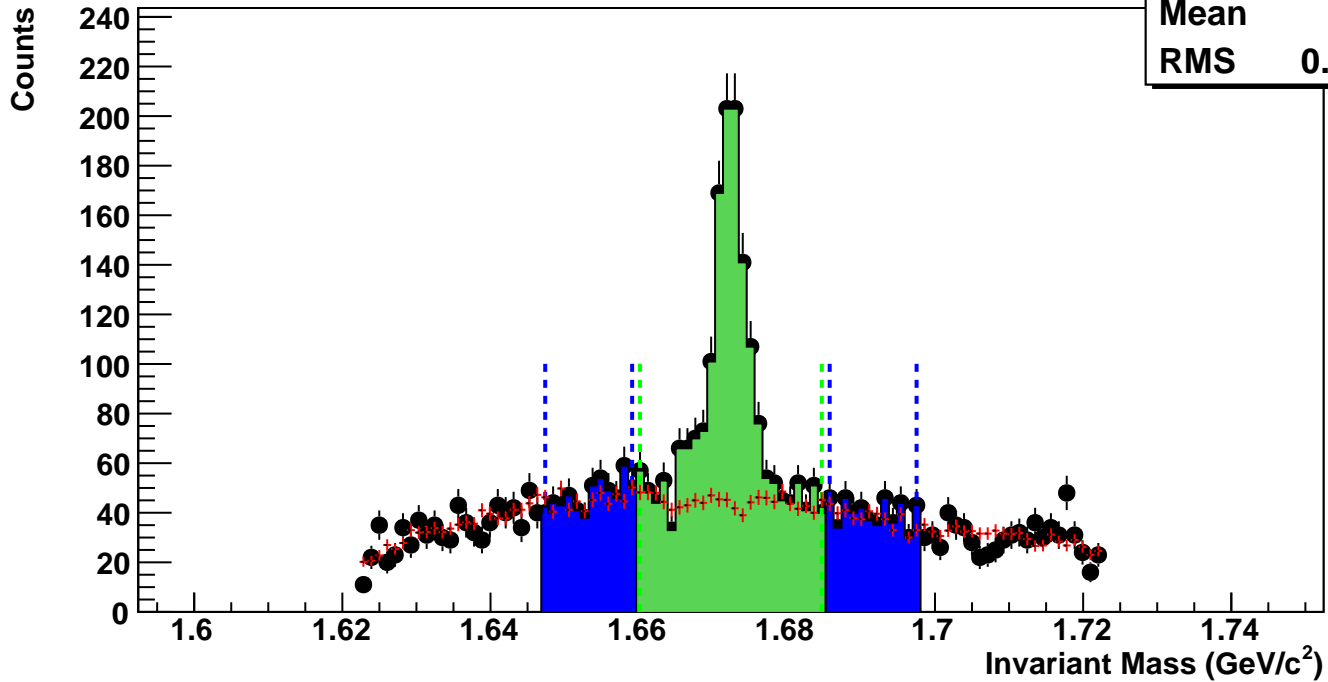
$\Omega^+$ , Au+Au 39 GeV, 10-20%,  $p_T$  1.4-1.7 GeV/c

hmlInvMassBgCent3Pt4	
Entries	438
Mean	1.671
RMS	0.02671



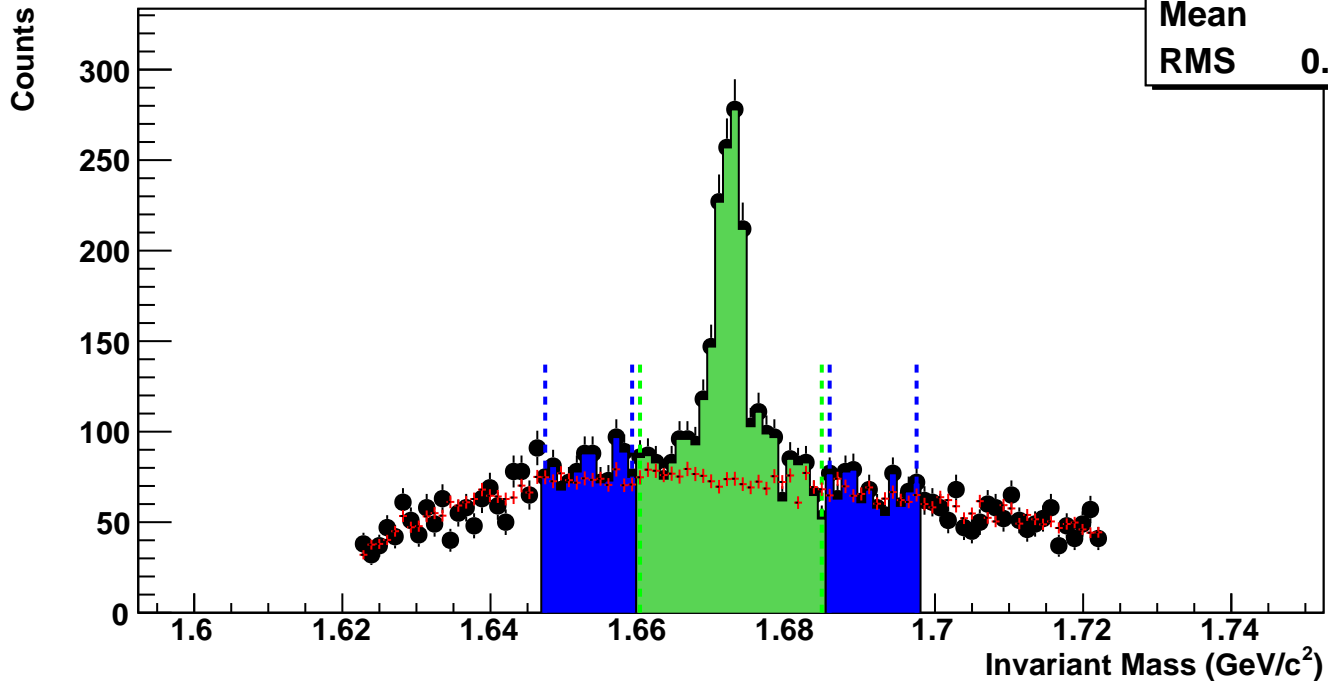
$\Omega^+$ , Au+Au 39 GeV, 5-10%,  $p_T$  1.4-1.7 GeV/c

hmlInvMassBgCent4Pt4	
Entries	431
Mean	1.671
RMS	0.02656



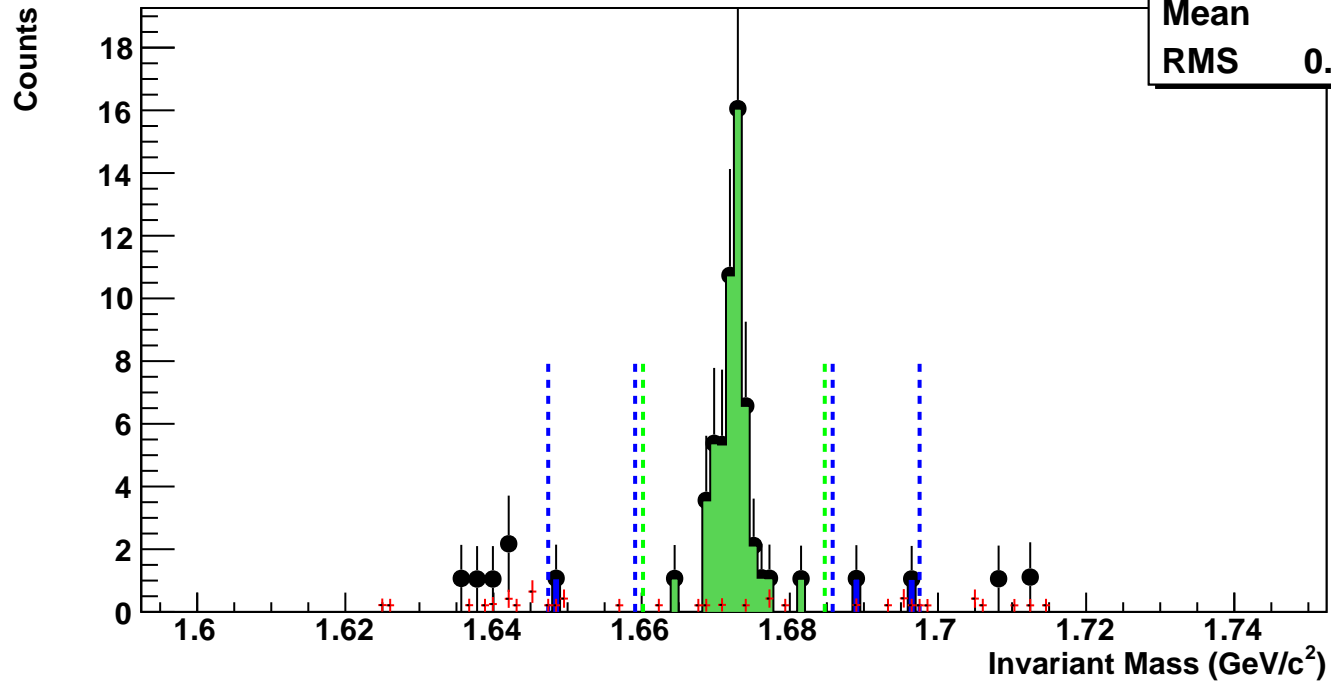
$\Omega^+$ , Au+Au 39 GeV, 0-5%,  $p_T$  1.4-1.7 GeV/c

hmlInvMassBgCent5Pt4	
Entries	724
Mean	1.672
RMS	0.02677



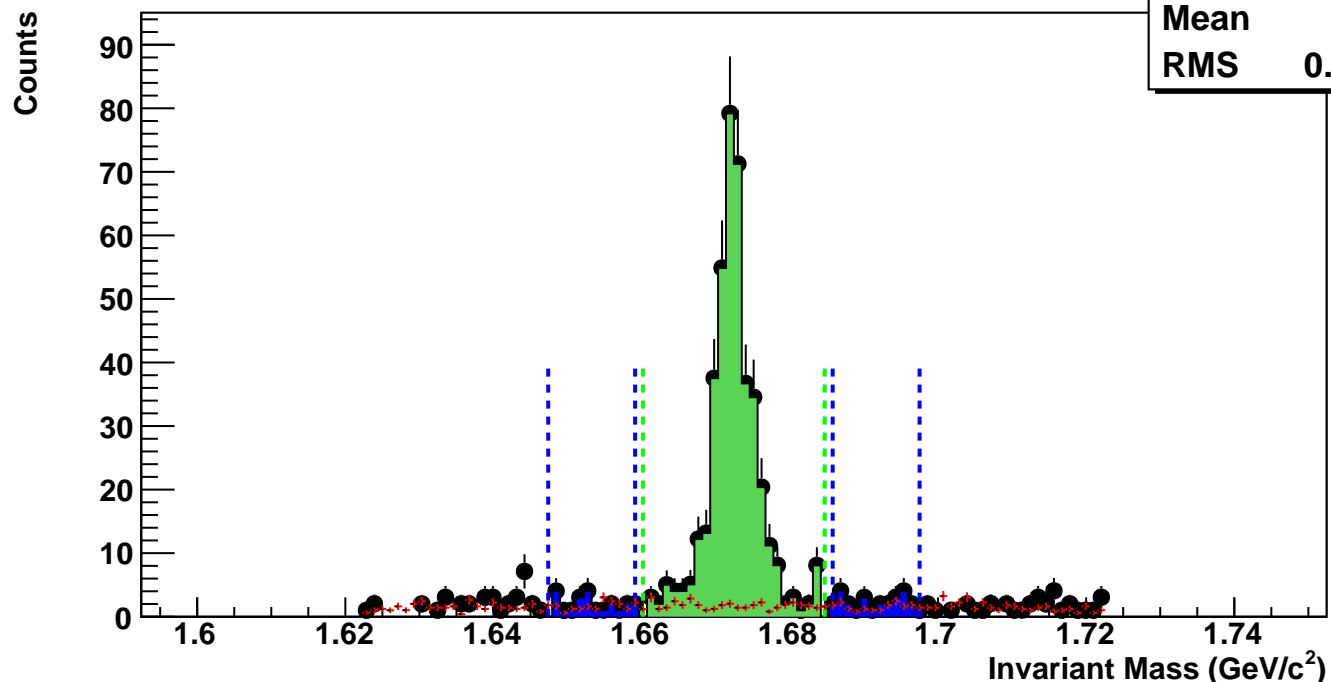
$\Omega^+$ , Au+Au 39 GeV, 60-80%,  $p_T$  1.7-2.0 GeV/c

hmlInvMassBgCent0Pt5	
Entries	1
Mean	1.669
RMS	0.02697



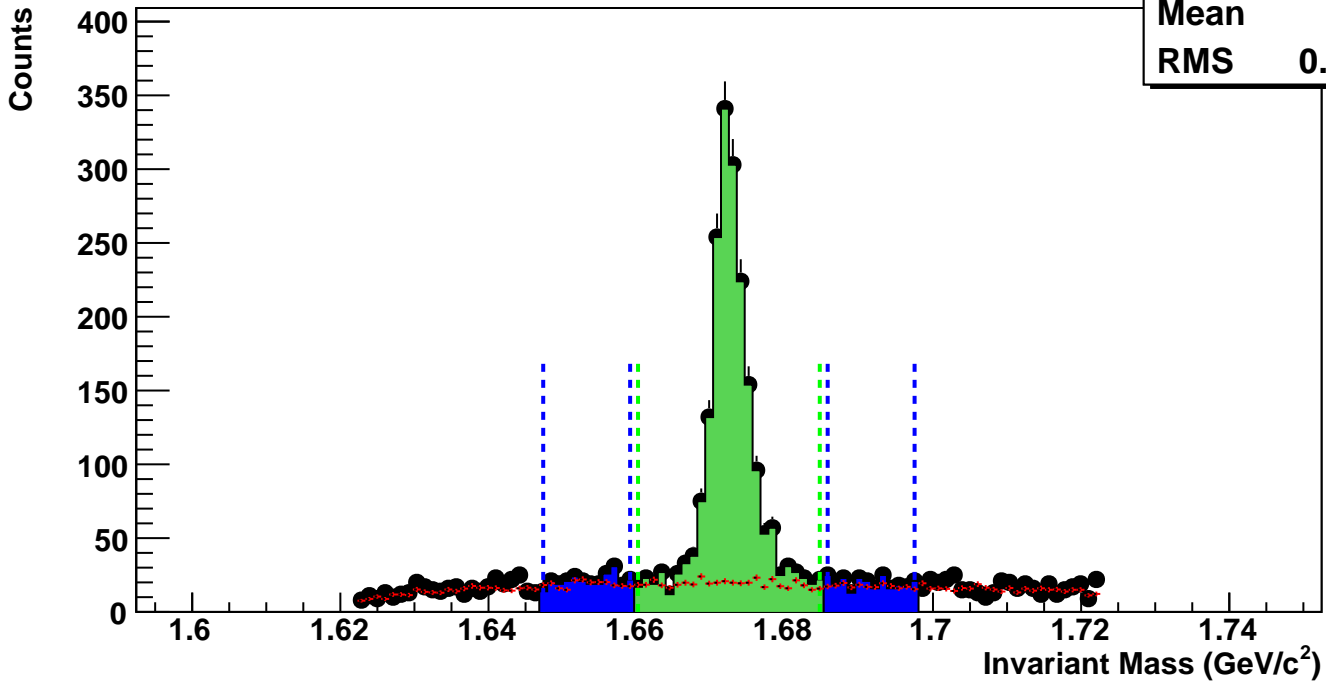
$\Omega^+$ , Au+Au 39 GeV, 40-60%,  $p_T$  1.7-2.0 GeV/c

hmlInvMassBgCent1Pt5	
Entries	18
Mean	1.672
RMS	0.02739



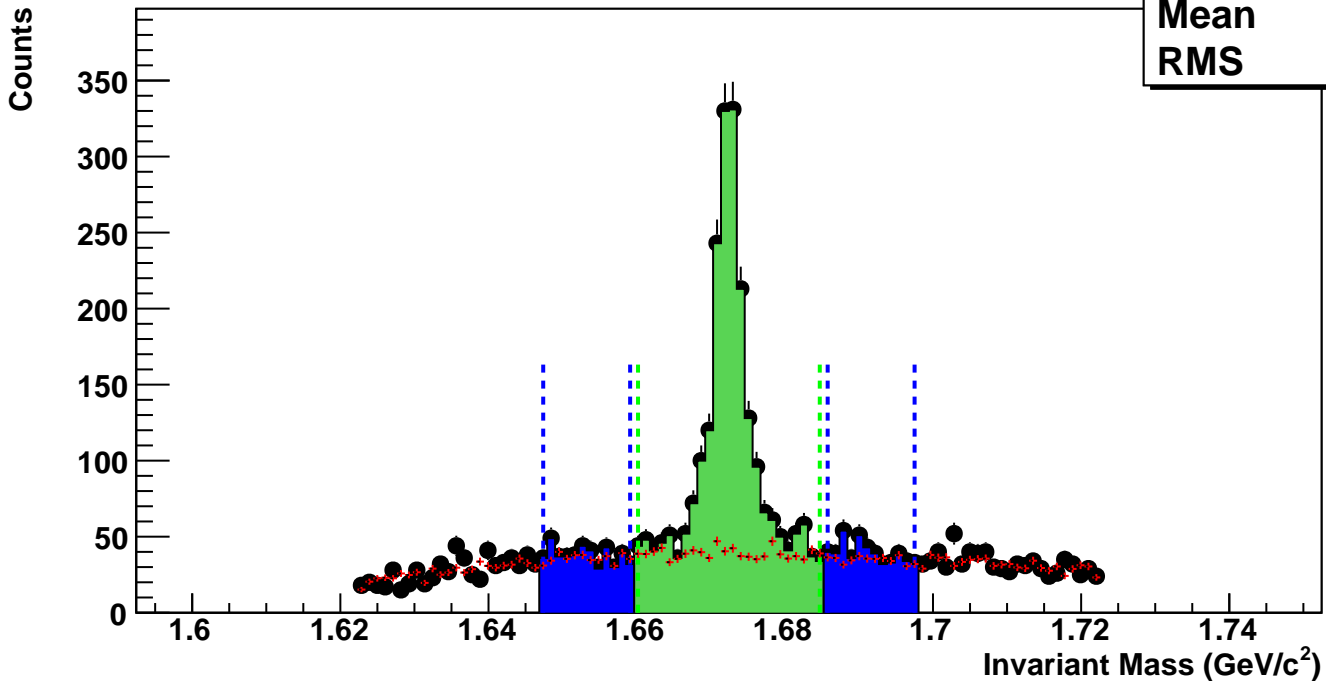
$\Omega^+$ , Au+Au 39 GeV, 20-40%,  $p_T$  1.7-2.0 GeV/c

hmlInvMassBgCent2Pt5
Entries 190
Mean 1.673
RMS 0.02694



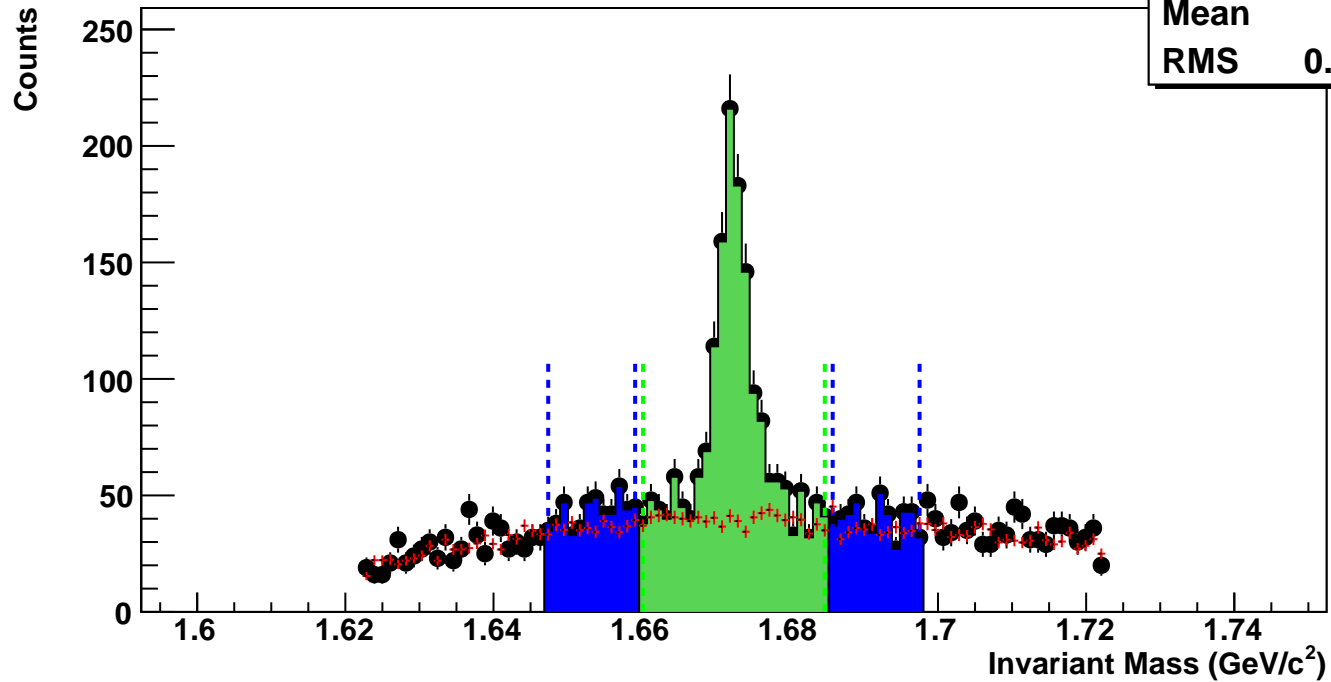
$\Omega^+$ , Au+Au 39 GeV, 10-20%,  $p_T$  1.7-2.0 GeV/c

hmlInvMassBgCent3Pt5
Entries 381
Mean 1.674
RMS 0.027



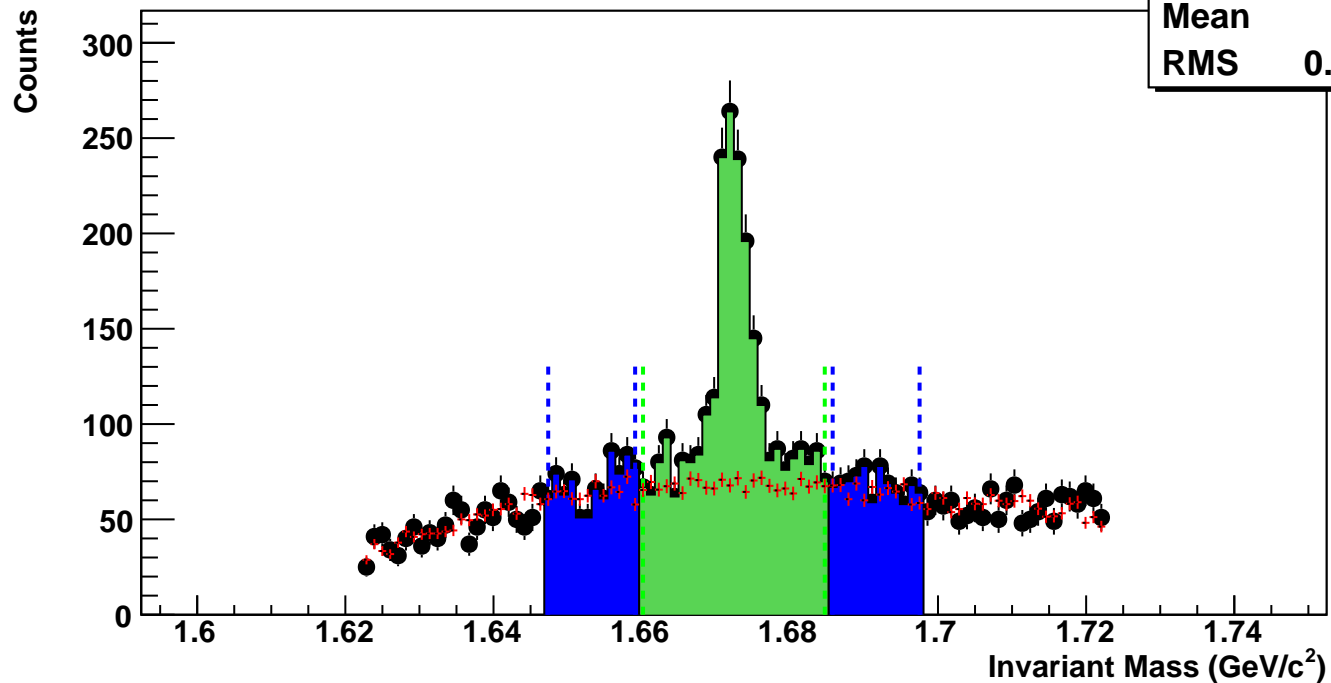
$\Omega^+$ , Au+Au 39 GeV, 5-10%,  $p_T$  1.7-2.0 GeV/c

hmlInvMassBgCent4Pt5	
Entries	387
Mean	1.674
RMS	0.02696



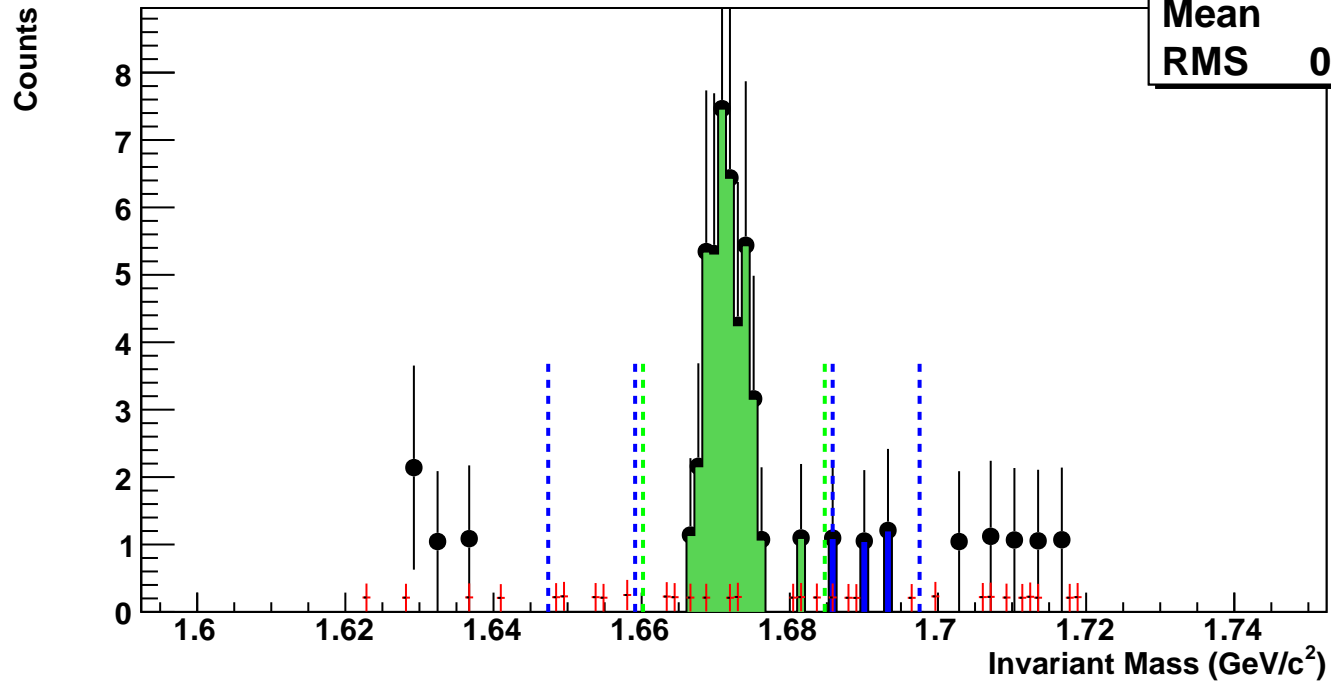
$\Omega^+$ , Au+Au 39 GeV, 0-5%,  $p_T$  1.7-2.0 GeV/c

hmlInvMassBgCent5Pt5	
Entries	677
Mean	1.674
RMS	0.02699



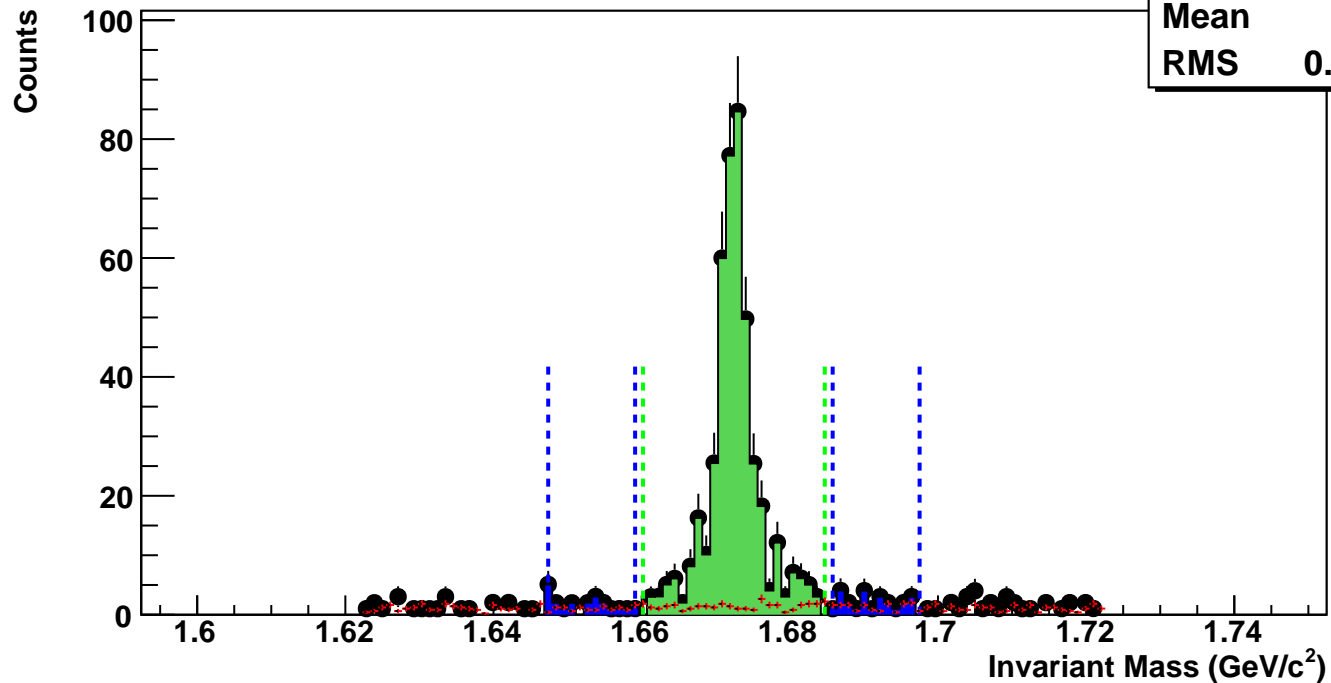
$\Omega^+$ , Au+Au 39 GeV, 60-80%,  $p_T$  2.0-2.4 GeV/c

hmlInvMassBgCent0Pt6	
Entries	1
Mean	1.677
RMS	0.0272



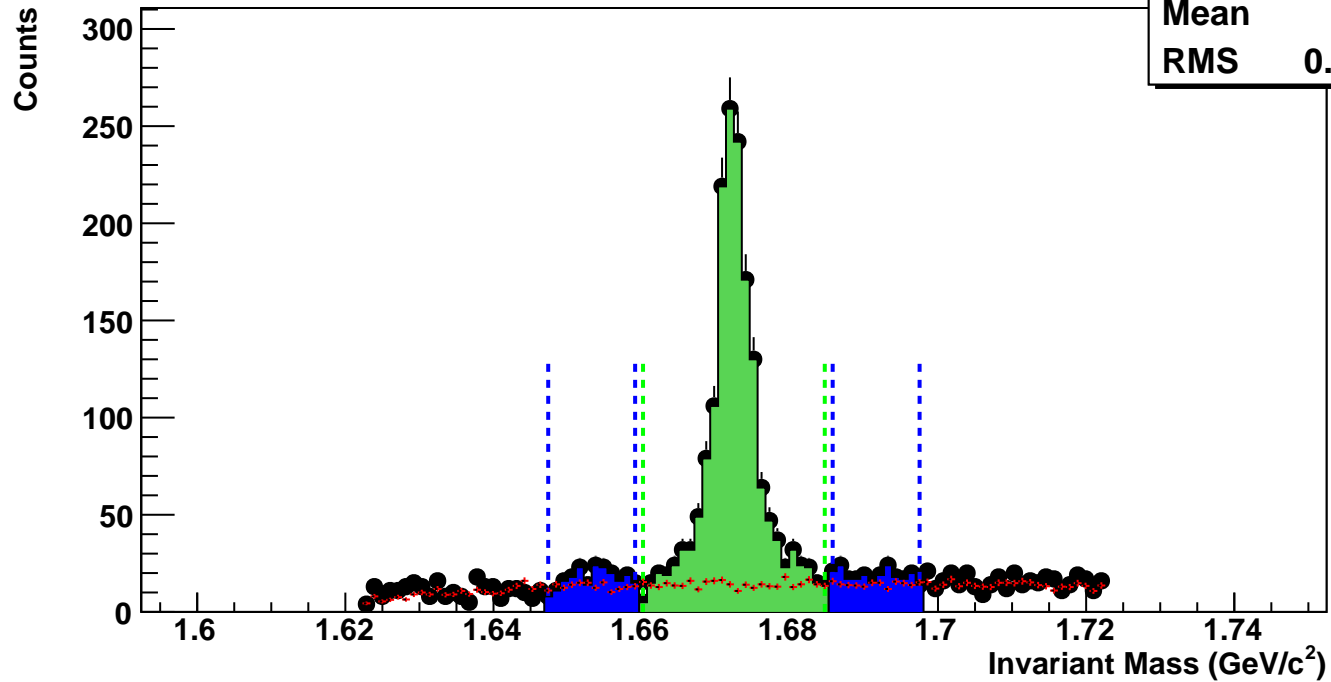
$\Omega^+$ , Au+Au 39 GeV, 40-60%,  $p_T$  2.0-2.4 GeV/c

hmlInvMassBgCent1Pt6	
Entries	13
Mean	1.673
RMS	0.02756



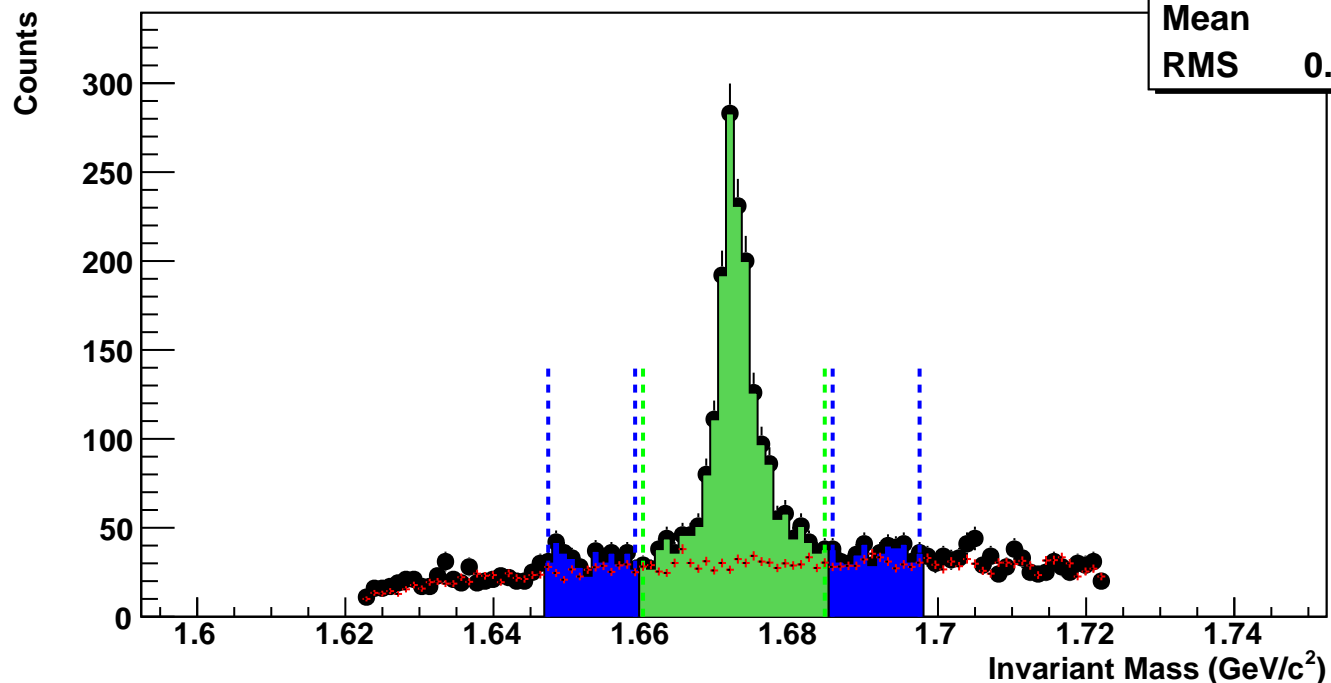
$\Omega^+$ , Au+Au 39 GeV, 20-40%,  $p_T$  2.0-2.4 GeV/c

hmlnvMassBgCent2Pt6	
Entries	148
Mean	1.676
RMS	0.02725



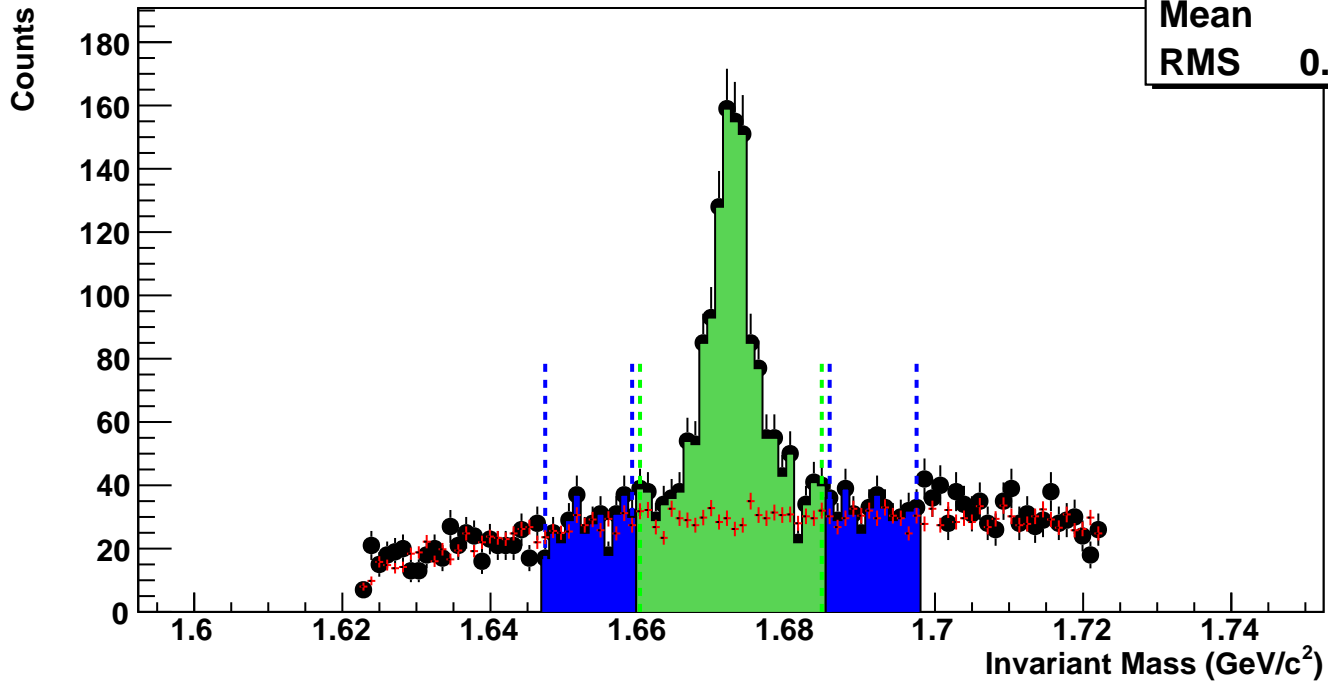
$\Omega^+$ , Au+Au 39 GeV, 10-20%,  $p_T$  2.0-2.4 GeV/c

hmlnvMassBgCent3Pt6	
Entries	302
Mean	1.676
RMS	0.02707



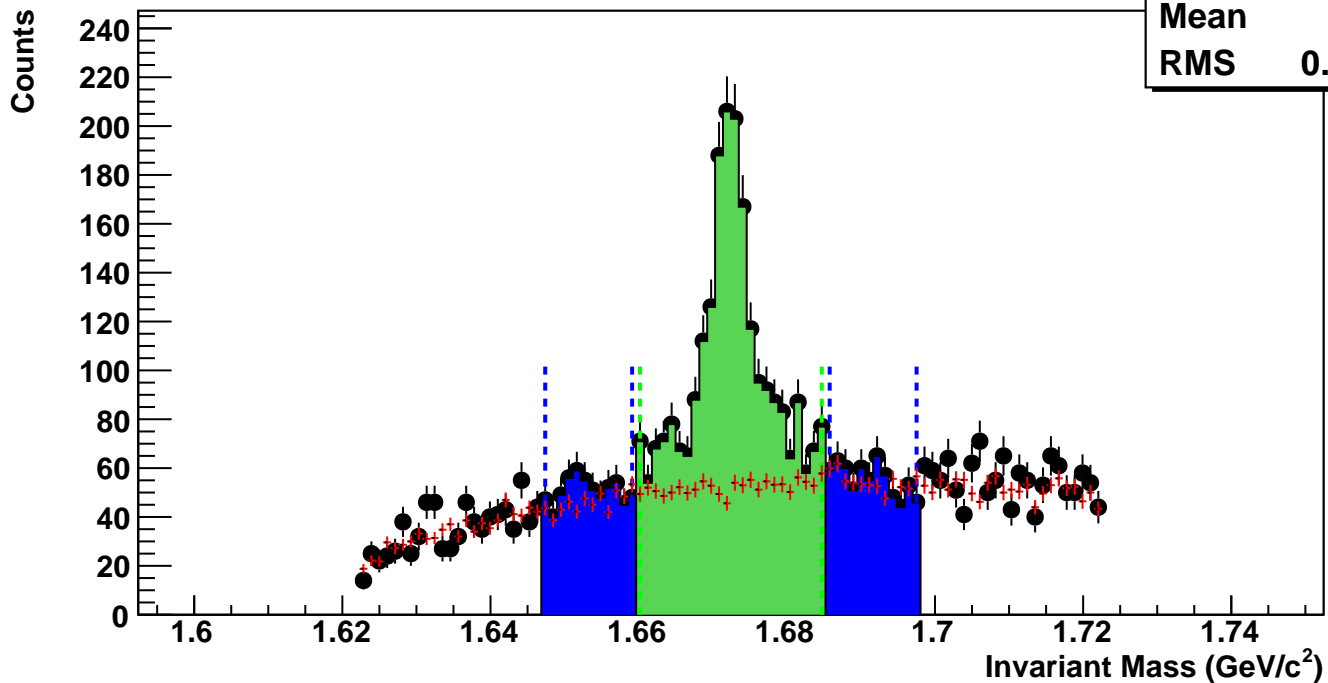
$\Omega^+$ , Au+Au 39 GeV, 5-10%,  $p_T$  2.0-2.4 GeV/c

hmlInvMassBgCent4Pt6	
Entries	307
Mean	1.676
RMS	0.02711



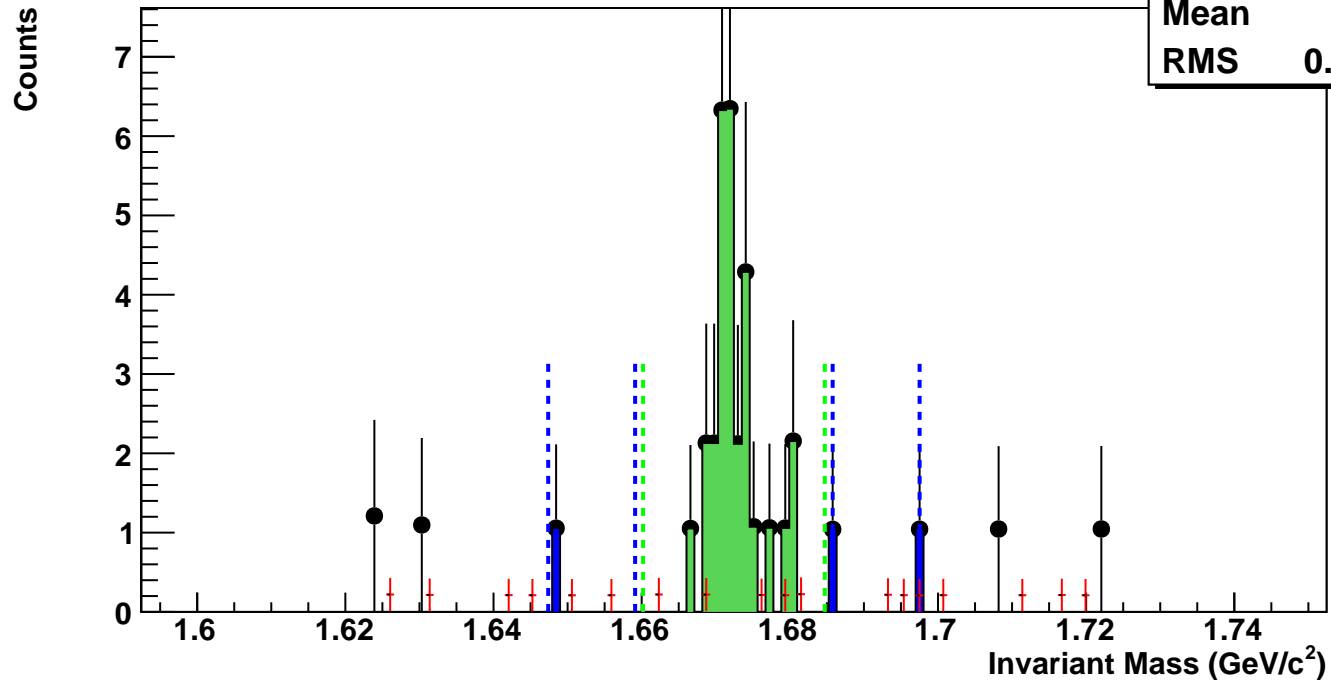
$\Omega^+$ , Au+Au 39 GeV, 0-5%,  $p_T$  2.0-2.4 GeV/c

hmlInvMassBgCent5Pt6	
Entries	538
Mean	1.677
RMS	0.02713



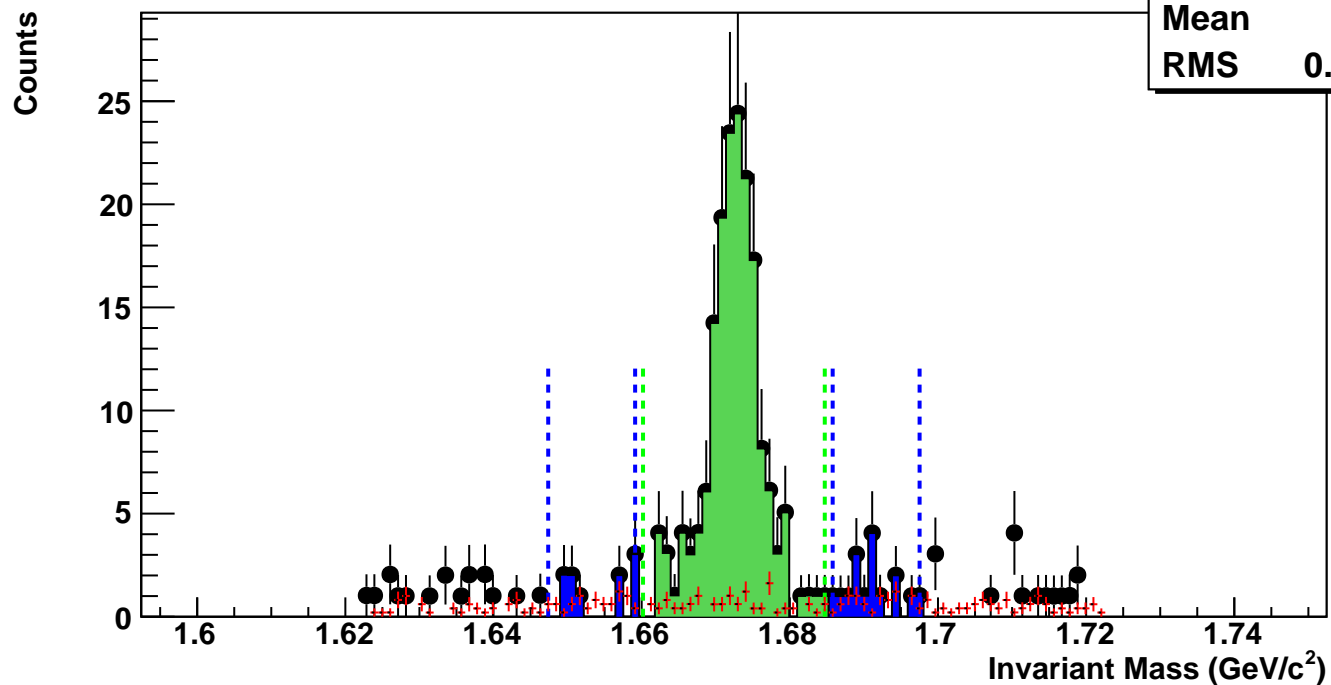
$\Omega^+$ , Au+Au 39 GeV, 60-80%,  $p_T$  2.4-2.8 GeV/c

hmlInvMassBgCent0Pt7	
Entries	0
Mean	1.675
RMS	0.02835



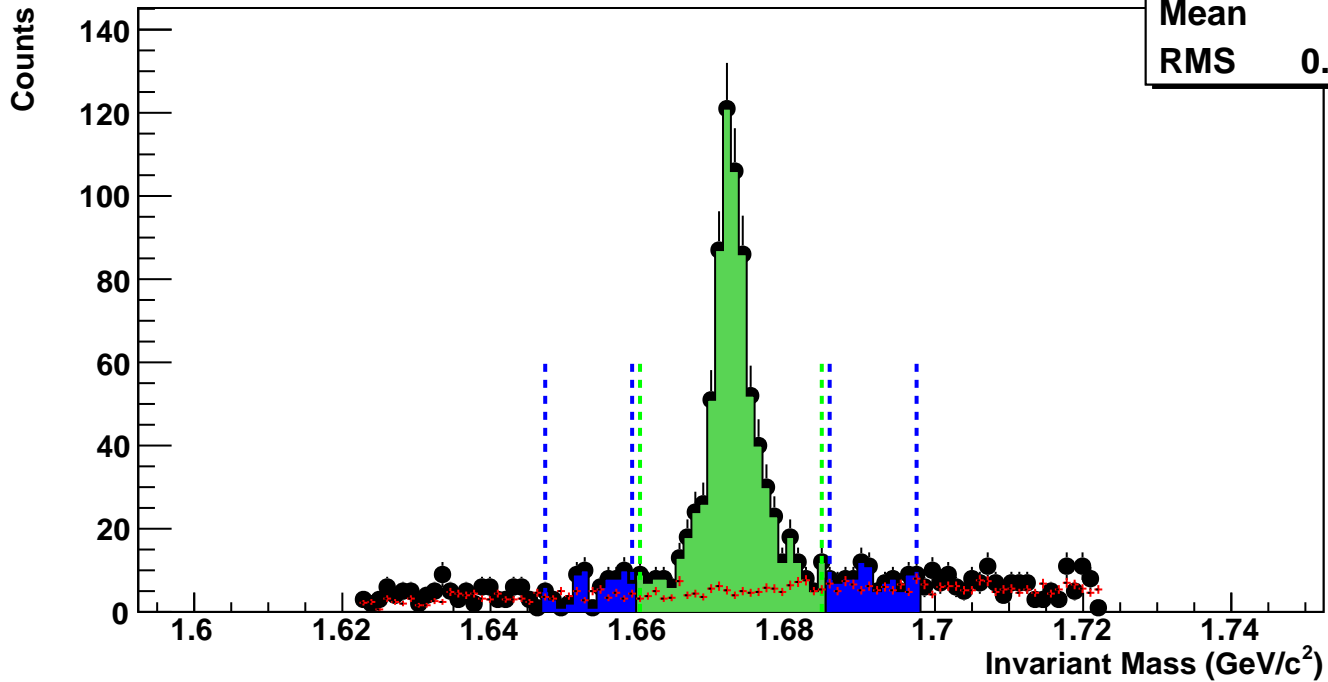
$\Omega^+$ , Au+Au 39 GeV, 40-60%,  $p_T$  2.4-2.8 GeV/c

hmlInvMassBgCent1Pt7	
Entries	6
Mean	1.675
RMS	0.02628



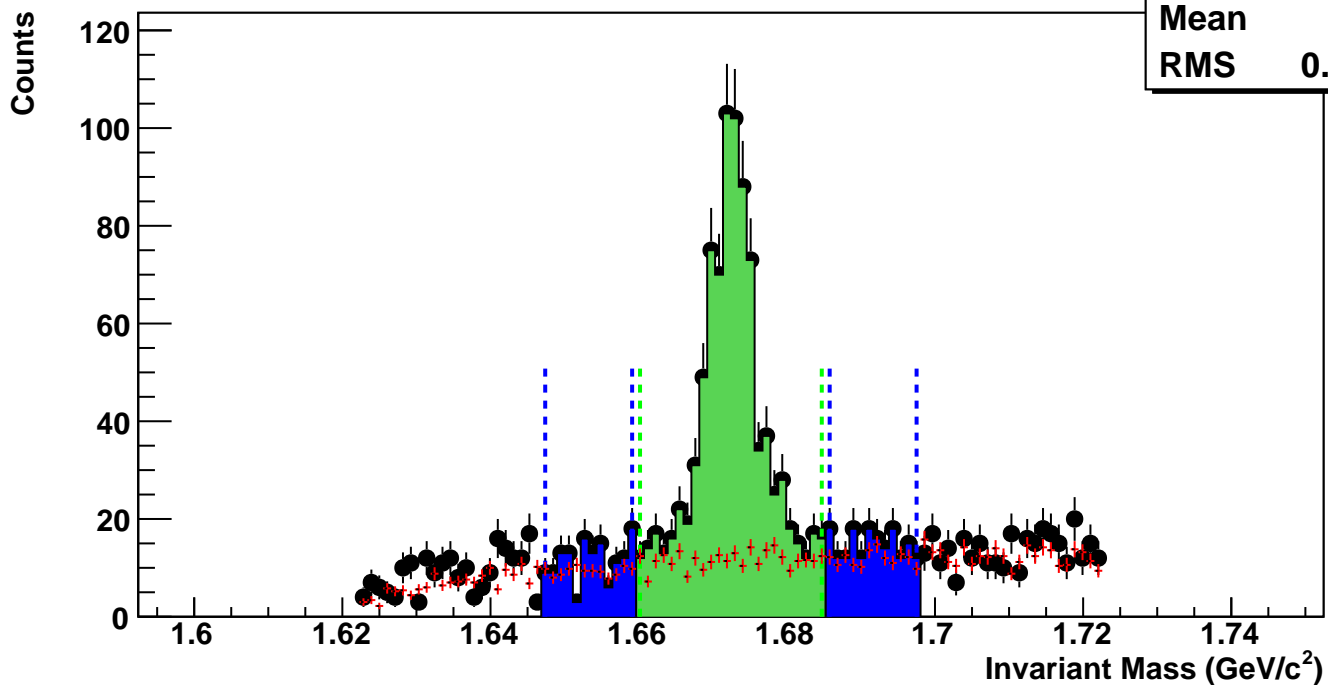
$\Omega^+$ , Au+Au 39 GeV, 20-40%,  $p_T$  2.4-2.8 GeV/c

hmlInvMassBgCent2Pt7	
Entries	54
Mean	1.679
RMS	0.02688



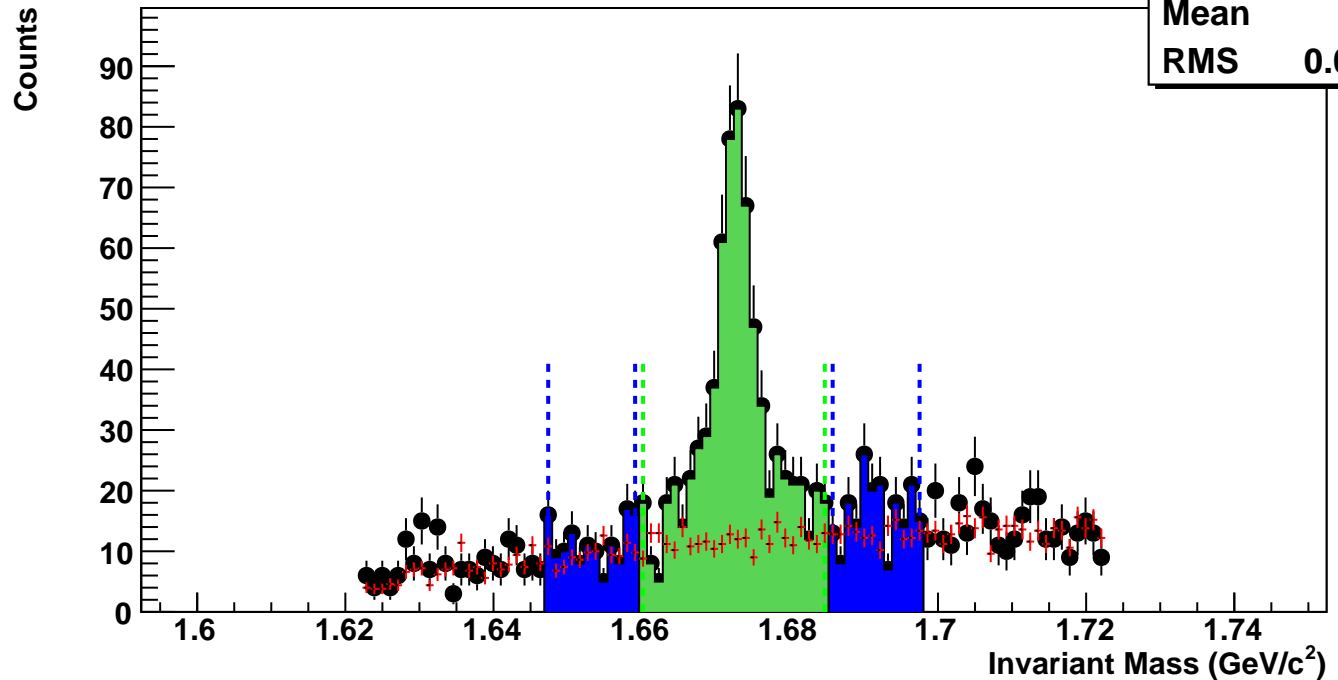
$\Omega^+$ , Au+Au 39 GeV, 10-20%,  $p_T$  2.4-2.8 GeV/c

hmlInvMassBgCent3Pt7	
Entries	118
Mean	1.678
RMS	0.02684



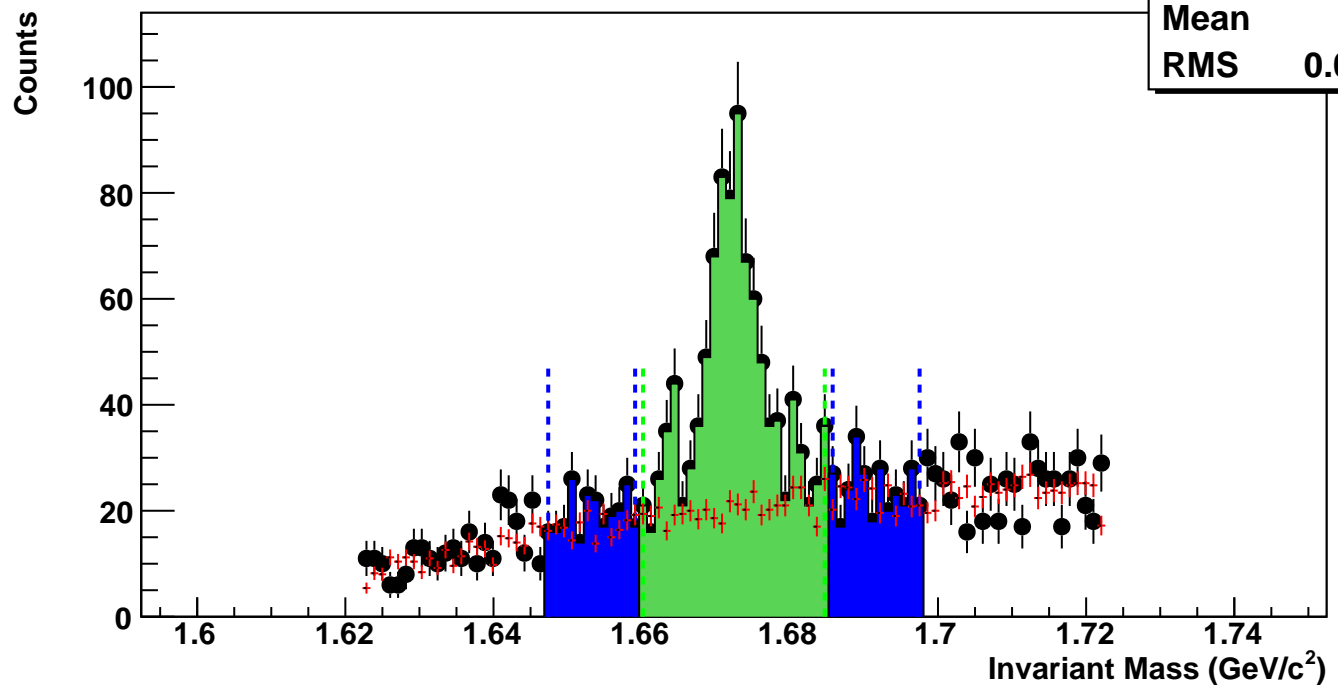
$\Omega^+$ , Au+Au 39 GeV, 5-10%,  $p_T$  2.4-2.8 GeV/c

hmlInvMassBgCent4Pt7	
Entries	124
Mean	1.679
RMS	0.02697



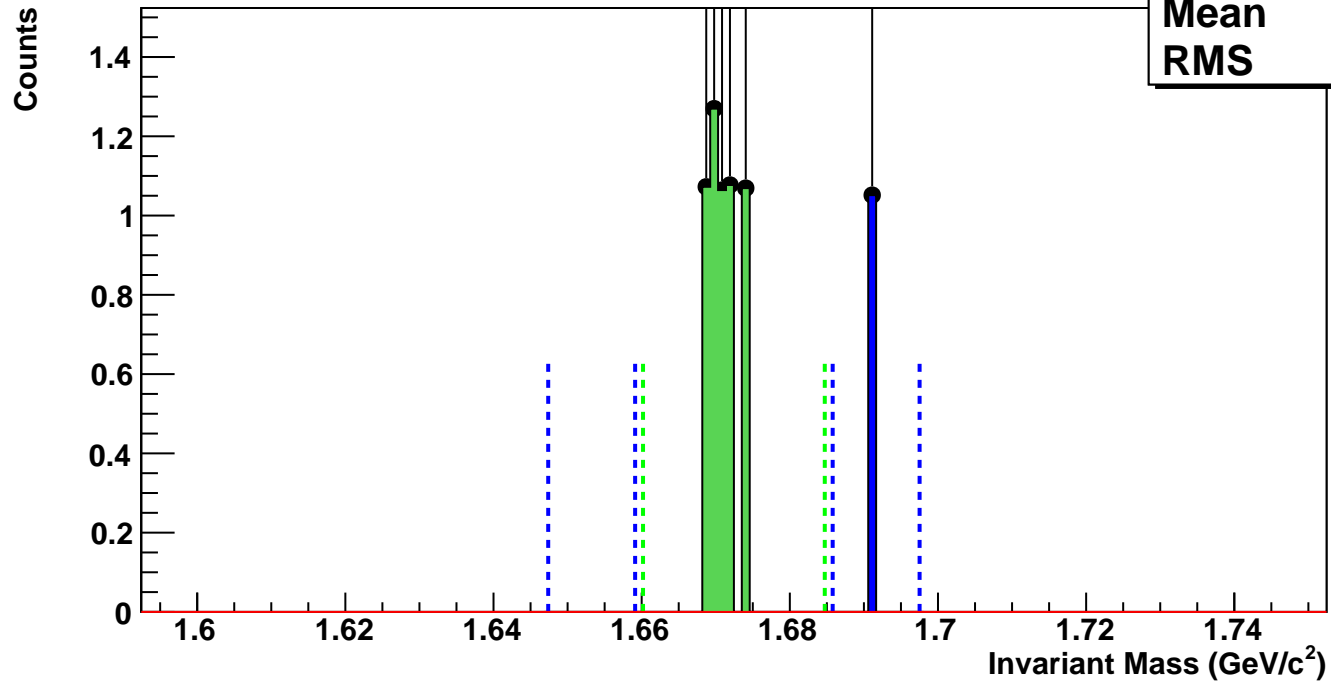
$\Omega^+$ , Au+Au 39 GeV, 0-5%,  $p_T$  2.4-2.8 GeV/c

hmlInvMassBgCent5Pt7	
Entries	216
Mean	1.679
RMS	0.02704



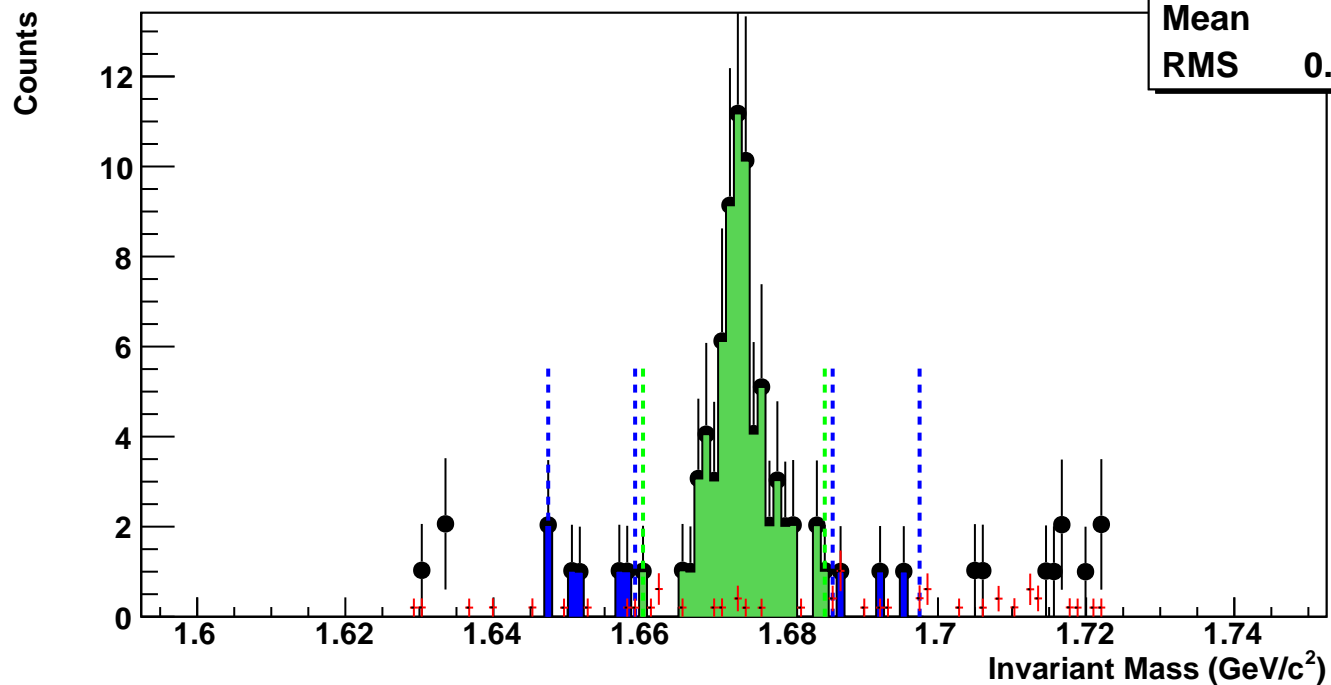
$\Omega^+$ , Au+Au 39 GeV, 60-80%,  $p_T$  2.8-3.2 GeV/c

hmlInvMassBgCent0Pt8	
Entries	0
Mean	0
RMS	0



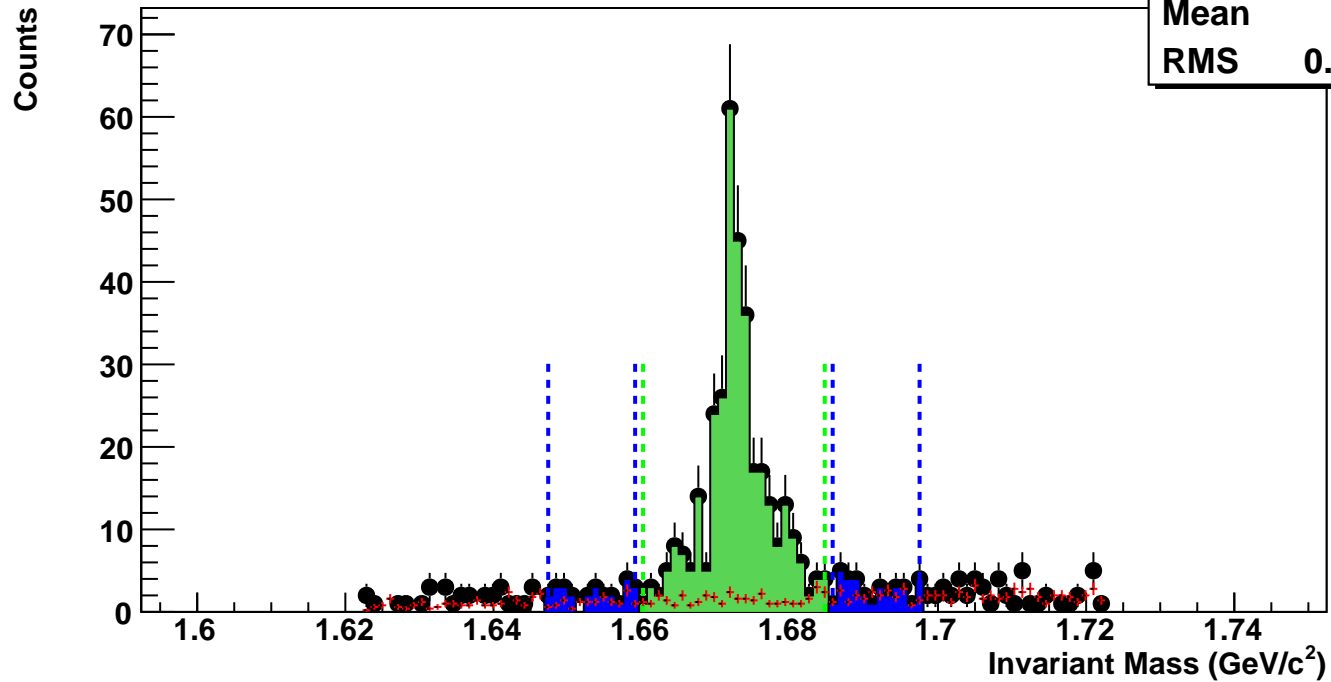
$\Omega^+$ , Au+Au 39 GeV, 40-60%,  $p_T$  2.8-3.2 GeV/c

hmlInvMassBgCent1Pt8	
Entries	1
Mean	1.684
RMS	0.02506



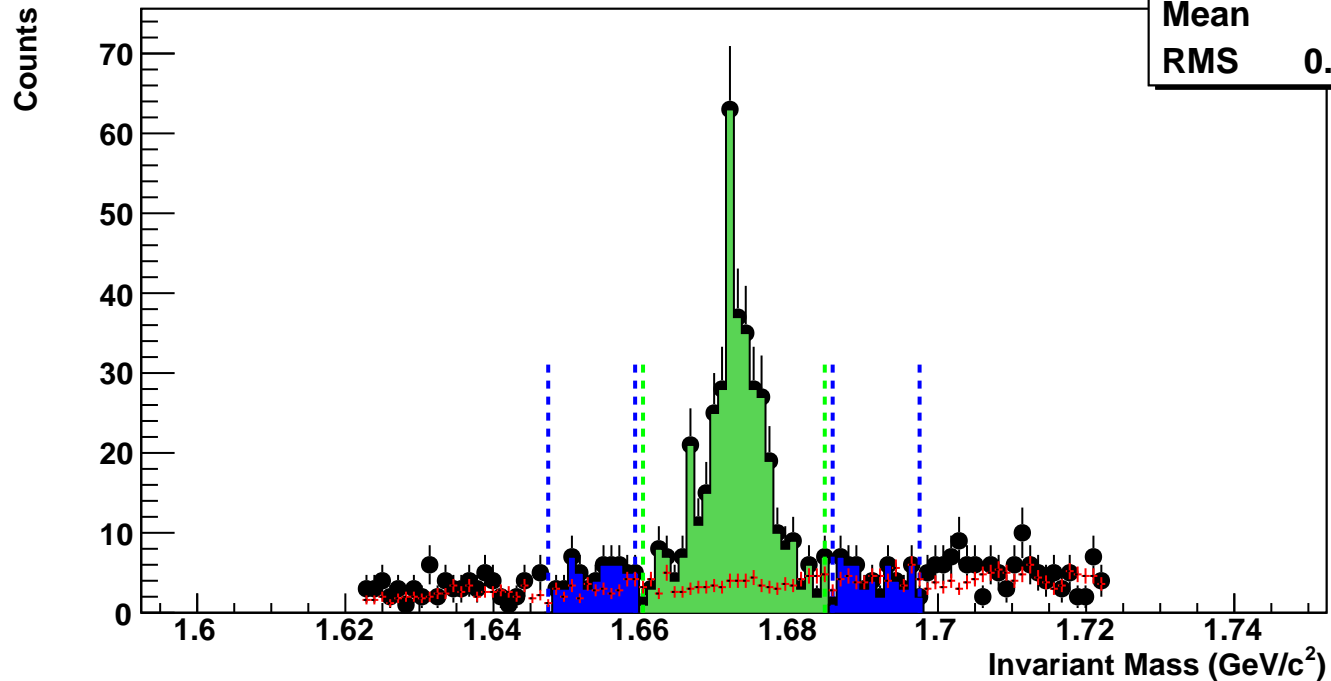
$\Omega^+$ , Au+Au 39 GeV, 20-40%,  $p_T$  2.8-3.2 GeV/c

hmlInvMassBgCent2Pt8	
Entries	17
Mean	1.68
RMS	0.02718



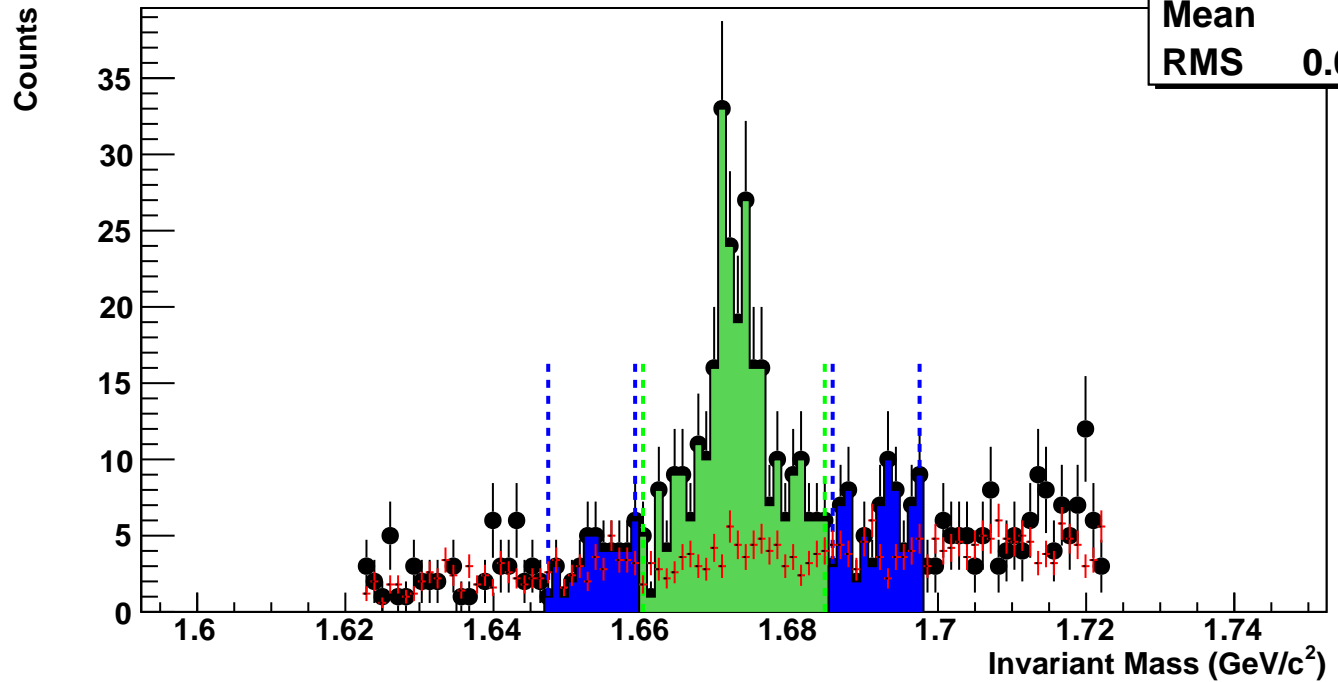
$\Omega^+$ , Au+Au 39 GeV, 10-20%,  $p_T$  2.8-3.2 GeV/c

hmlInvMassBgCent3Pt8	
Entries	39
Mean	1.679
RMS	0.02742



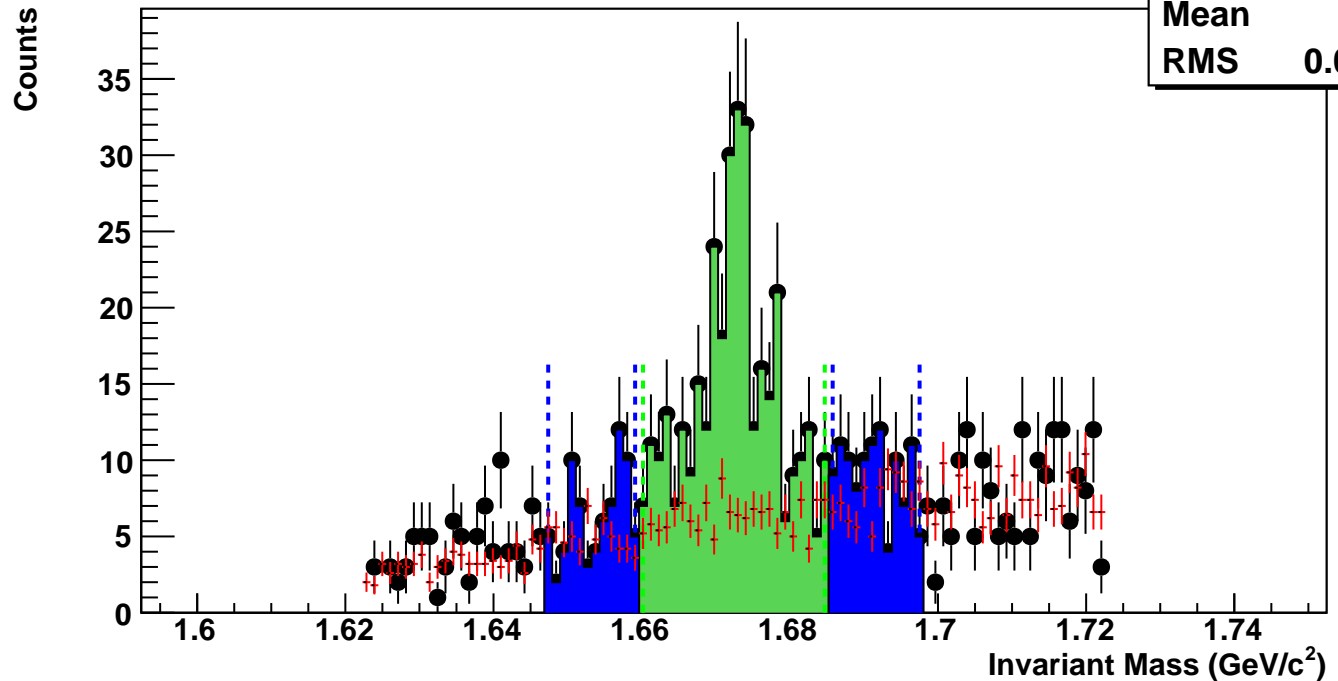
$\Omega^+$ , Au+Au 39 GeV, 5-10%,  $p_T$  2.8-3.2 GeV/c

hmlInvMassBgCent4Pt8	
Entries	38
Mean	1.68
RMS	0.02711



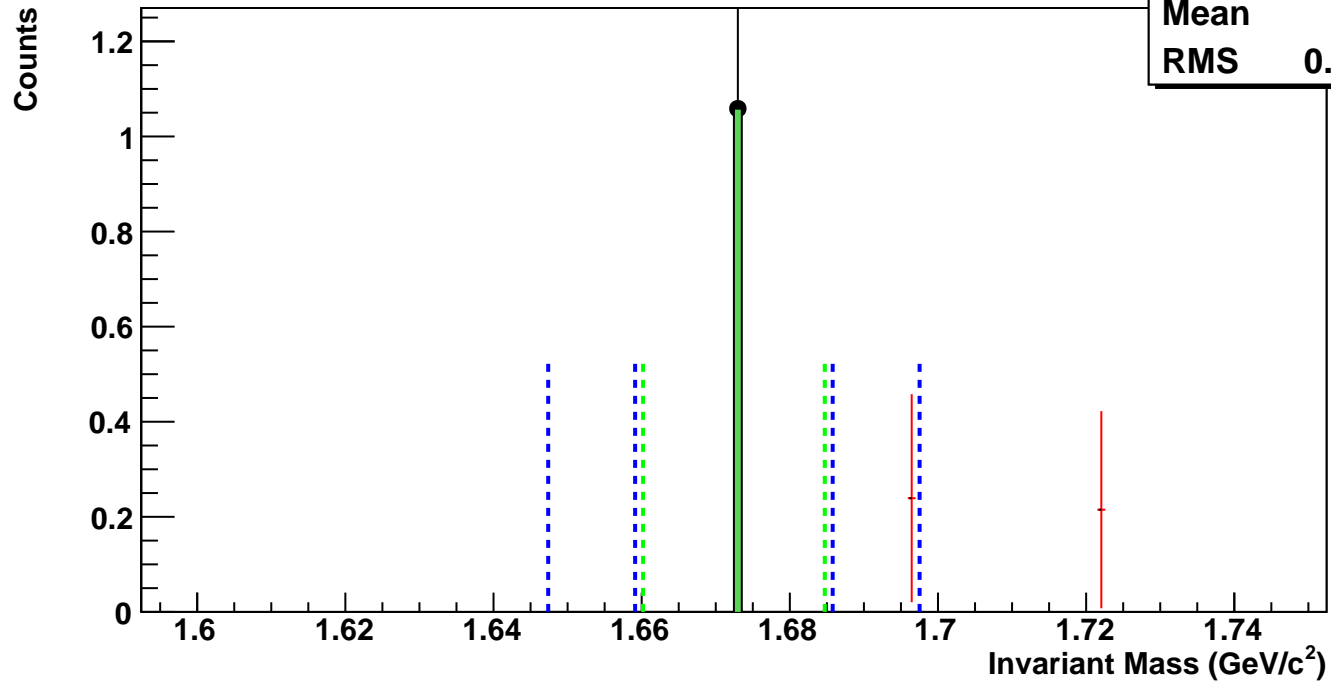
$\Omega^+$ , Au+Au 39 GeV, 0-5%,  $p_T$  2.8-3.2 GeV/c

hmlInvMassBgCent5Pt8	
Entries	67
Mean	1.681
RMS	0.02687



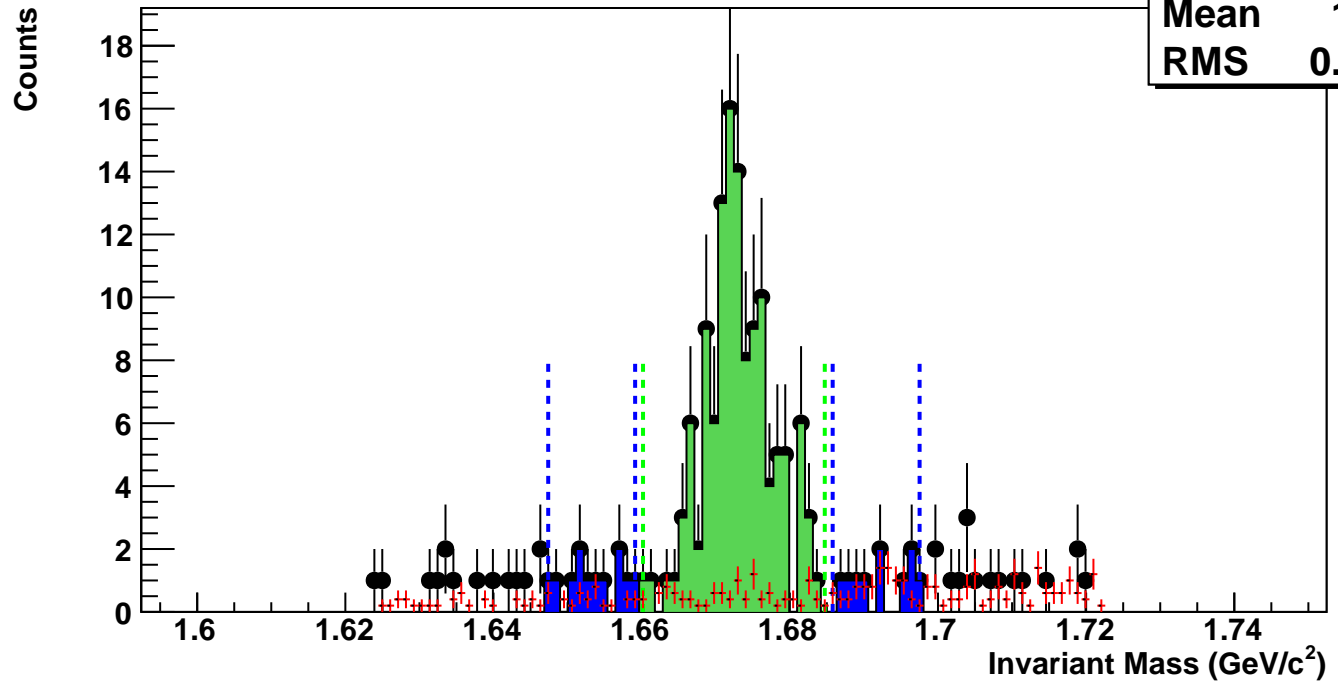
$\Omega^+$ , Au+Au 39 GeV, 60-80%,  $p_T$  3.2-3.6 GeV/c

hmlInvMassBgCent0Pt9	
Entries	0
Mean	1.709
RMS	0.01278



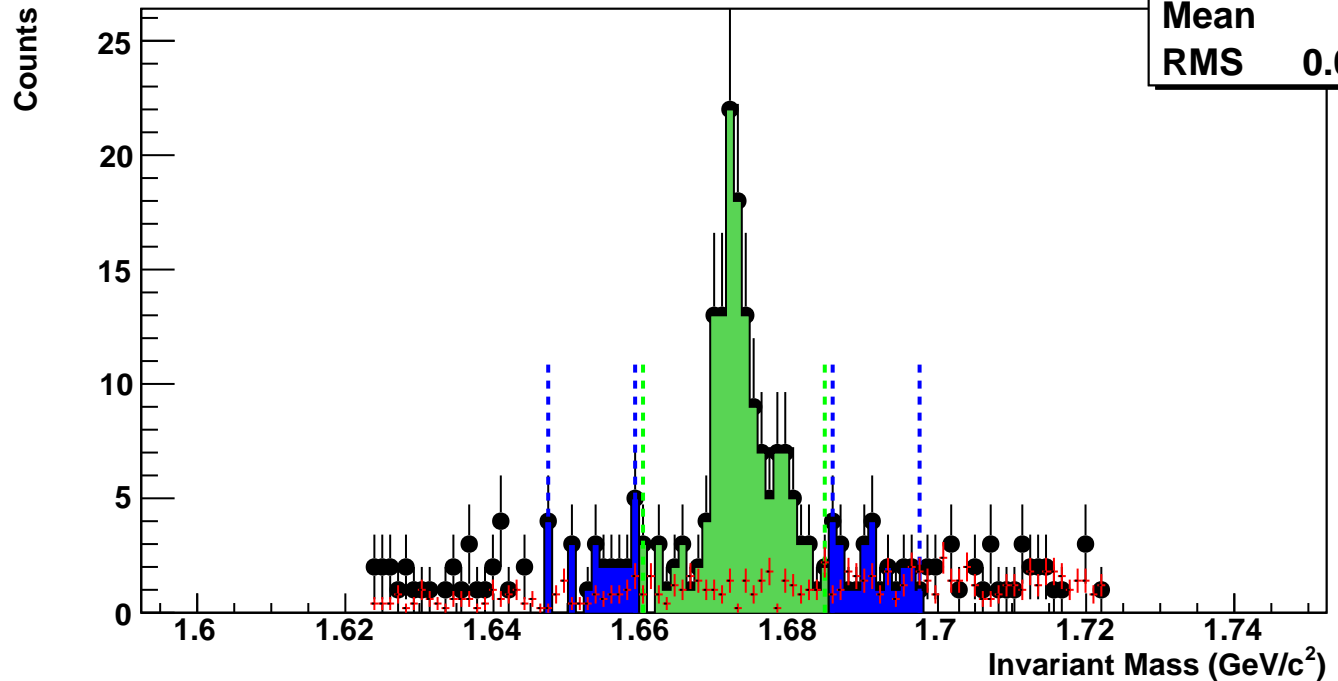
$\Omega^+$ , Au+Au 39 GeV, 20-40%,  $p_T$  3.2-3.6 GeV/c

hmlInvMassBgCent2Pt9
Entries 5
Mean 1.683
RMS 0.0259



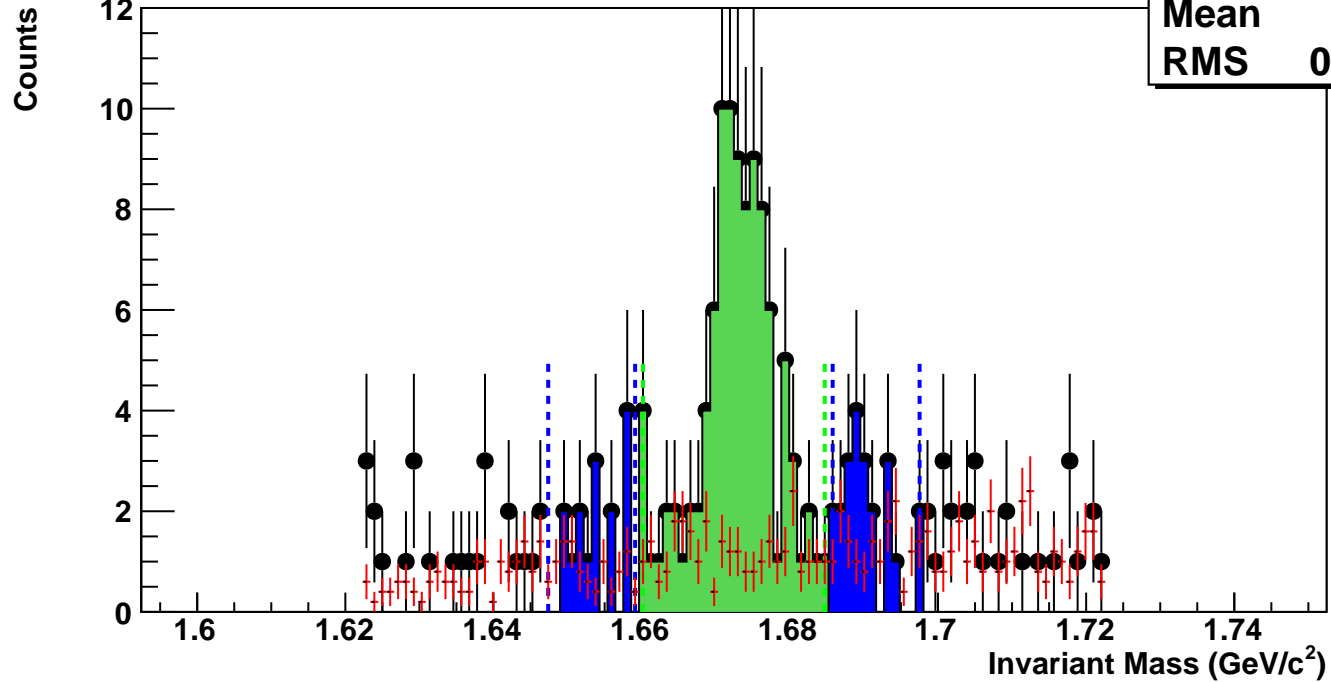
$\Omega^+$ , Au+Au 39 GeV, 10-20%,  $p_T$  3.2-3.6 GeV/c

hmlInvMassBgCent3Pt9
Entries 11
Mean 1.682
RMS 0.02611



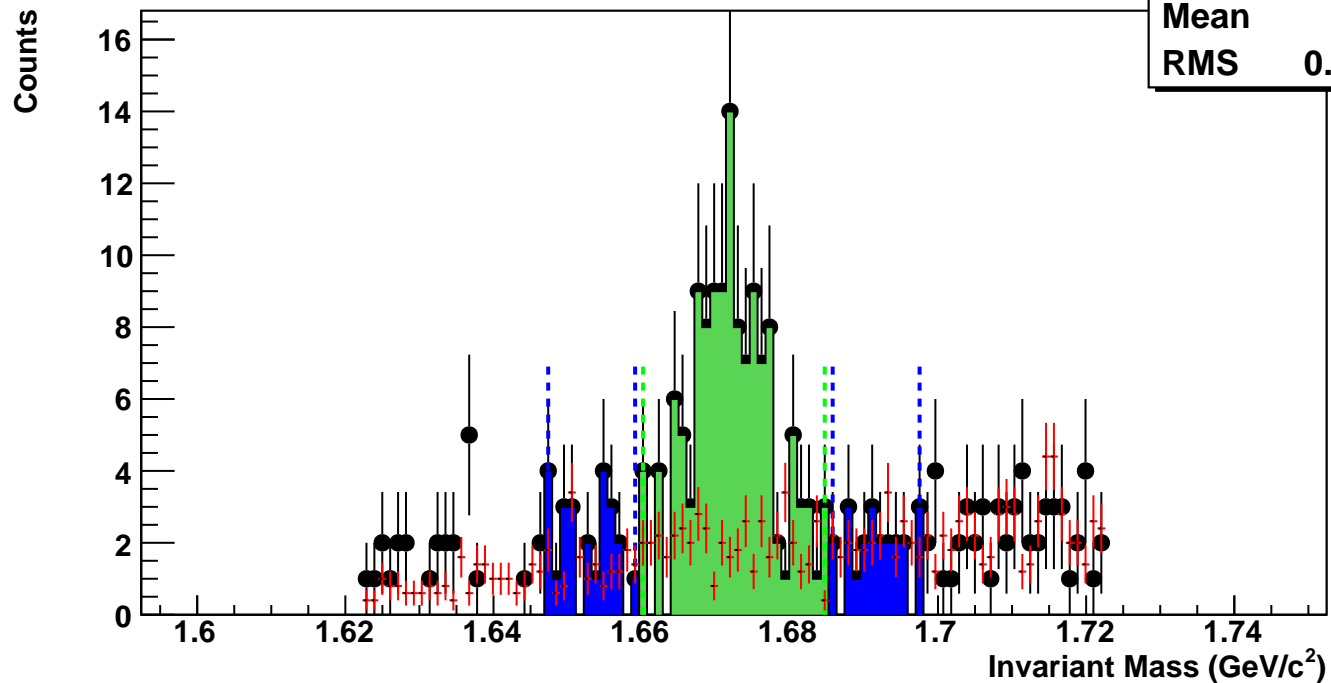
$\bar{\Omega}^+$ , Au+Au 39 GeV, 5-10%,  $p_T$  3.2-3.6 GeV/c

hmlInvMassBgCent4Pt9	
Entries	12
Mean	1.679
RMS	0.0266

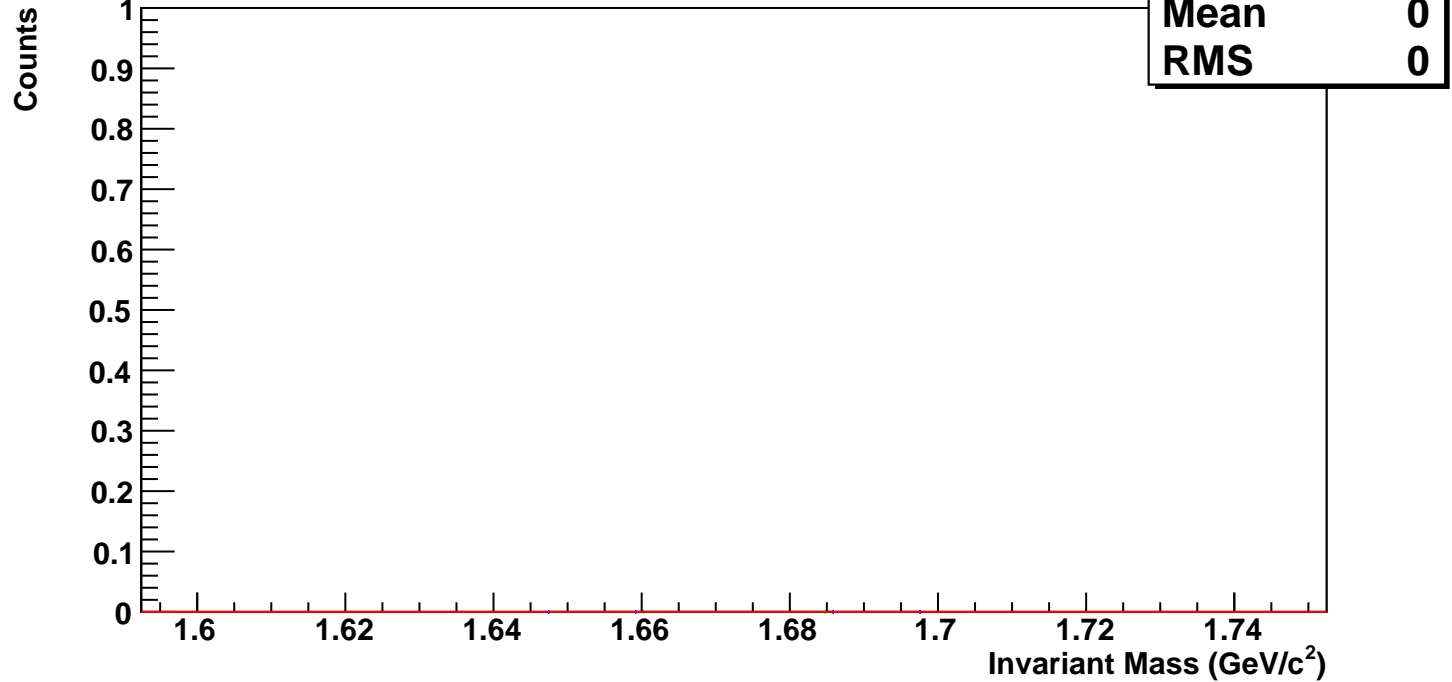


$\bar{\Omega}^+$ , Au+Au 39 GeV, 0-5%,  $p_T$  3.2-3.6 GeV/c

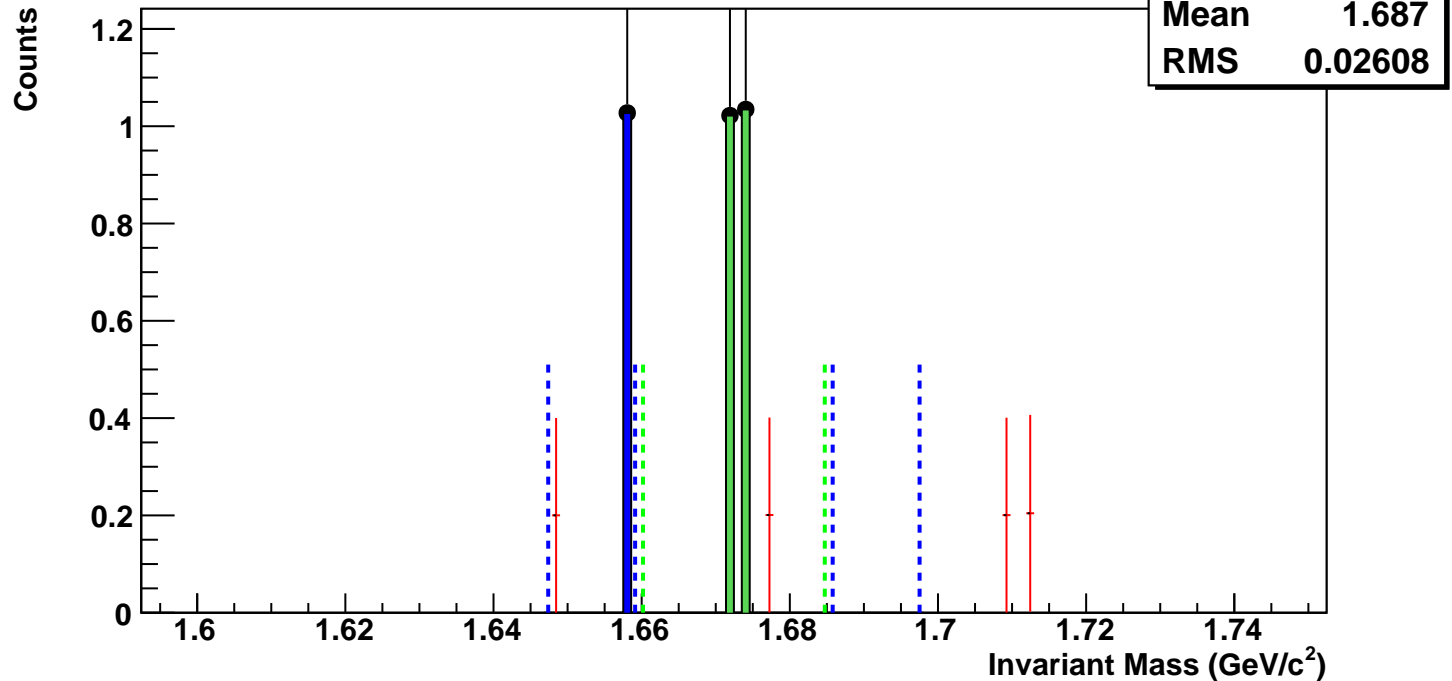
hmlInvMassBgCent5Pt9	
Entries	20
Mean	1.682
RMS	0.02652



$\Omega^+$ , Au+Au 39 GeV, 60-80%,  $p_T$  3.6-4.0 GeV/c

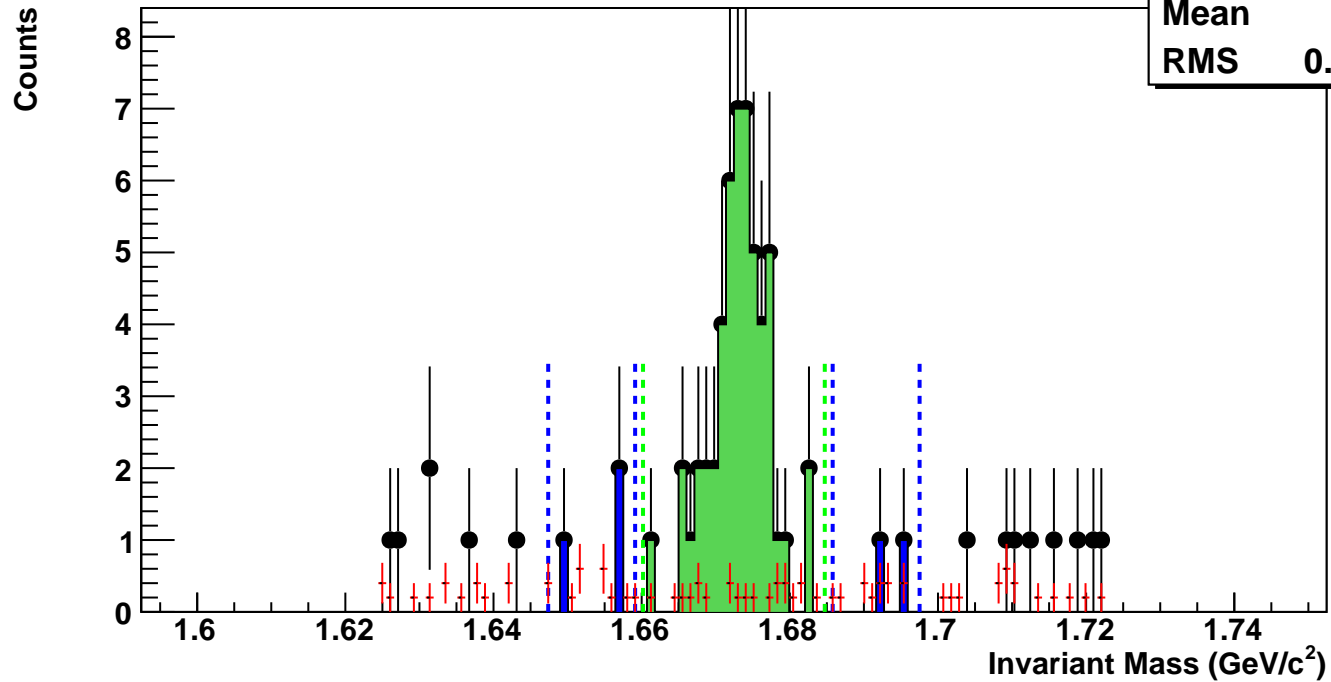


$\Omega^+$ , Au+Au 39 GeV, 40-60%,  $p_T$  3.6-4.0 GeV/c



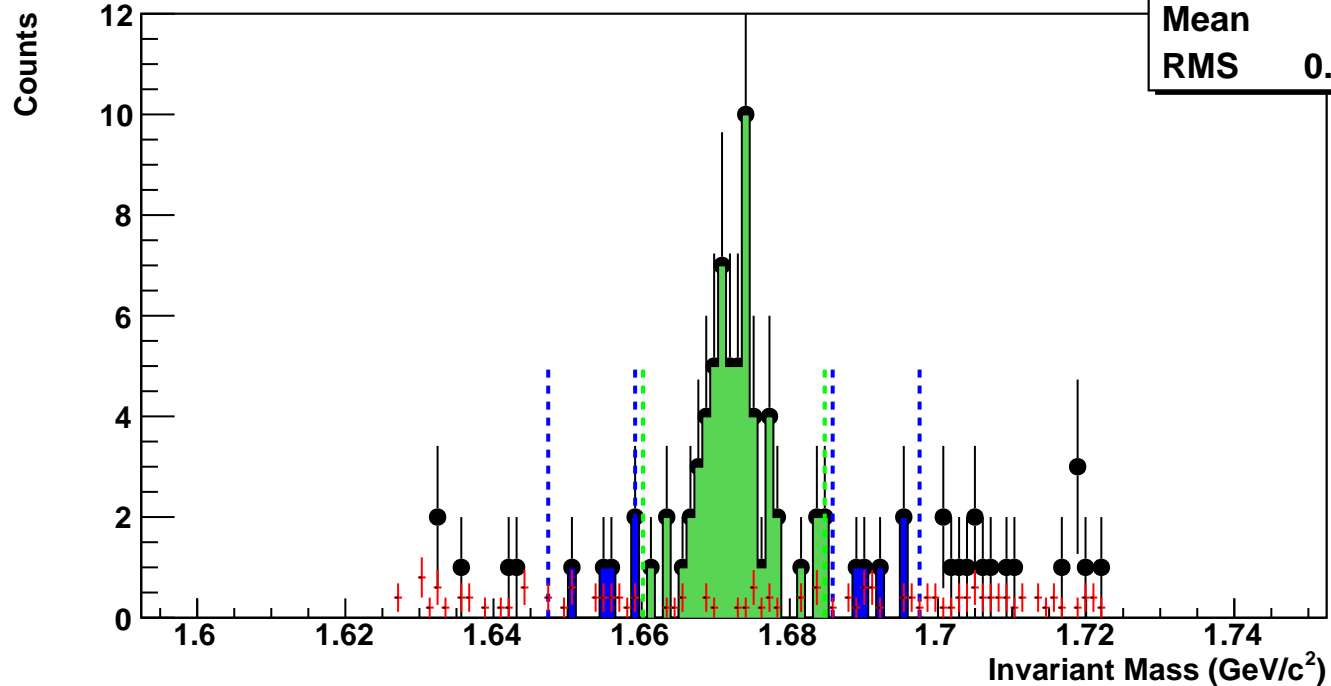
$\Omega^+$ , Au+Au 39 GeV, 20-40%,  $p_T$  3.6-4.0 GeV/c

hmlInvMassBgCent2Pt10	
Entries	2
Mean	1.673
RMS	0.02684



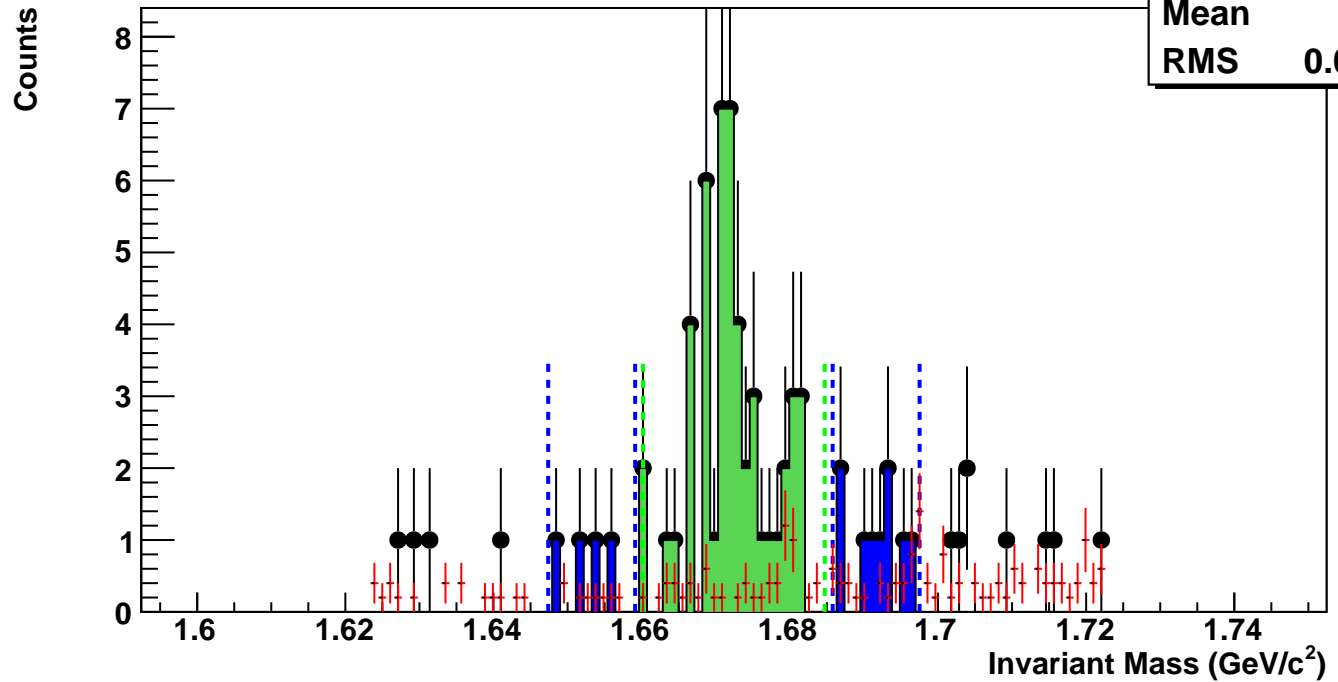
$\Omega^+$ , Au+Au 39 GeV, 10-20%,  $p_T$  3.6-4.0 GeV/c

hmlInvMassBgCent3Pt10	
Entries	3
Mean	1.678
RMS	0.02859



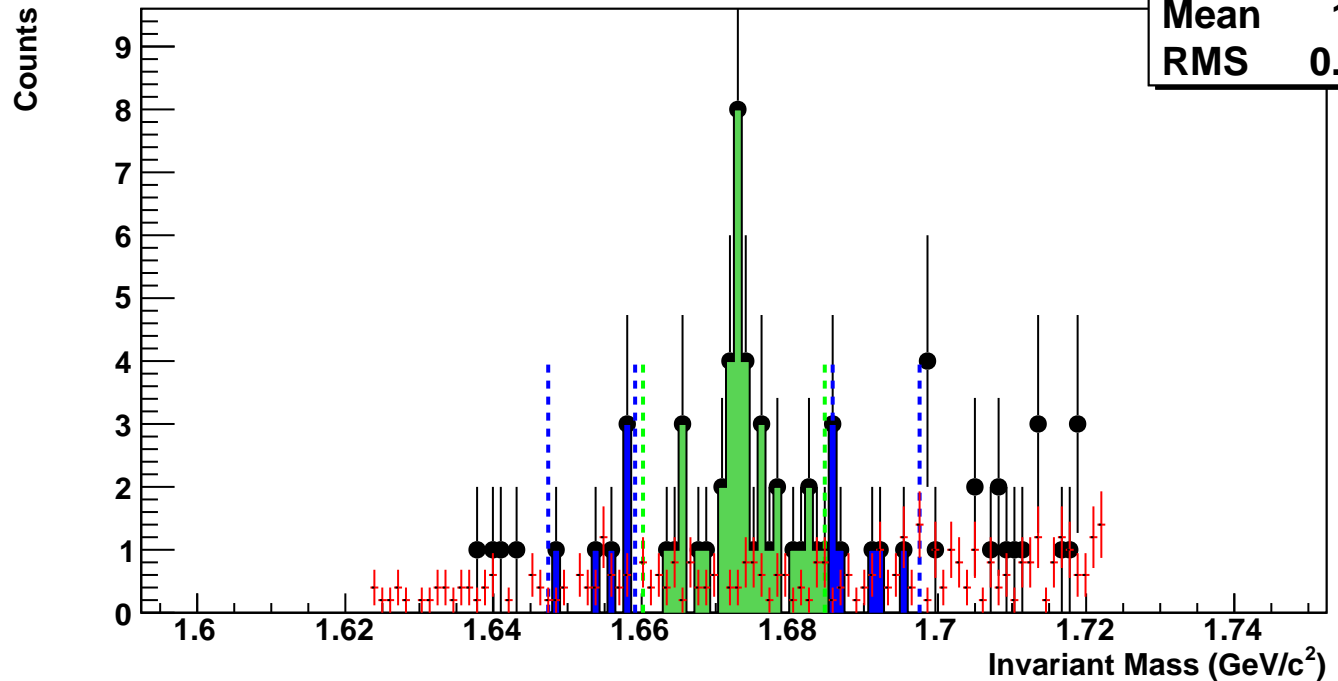
$\Omega^+$ , Au+Au 39 GeV, 5-10%,  $p_T$  3.6-4.0 GeV/c

hmlInvMassBgCent4Pt10	
Entries	3
Mean	1.684
RMS	0.02665

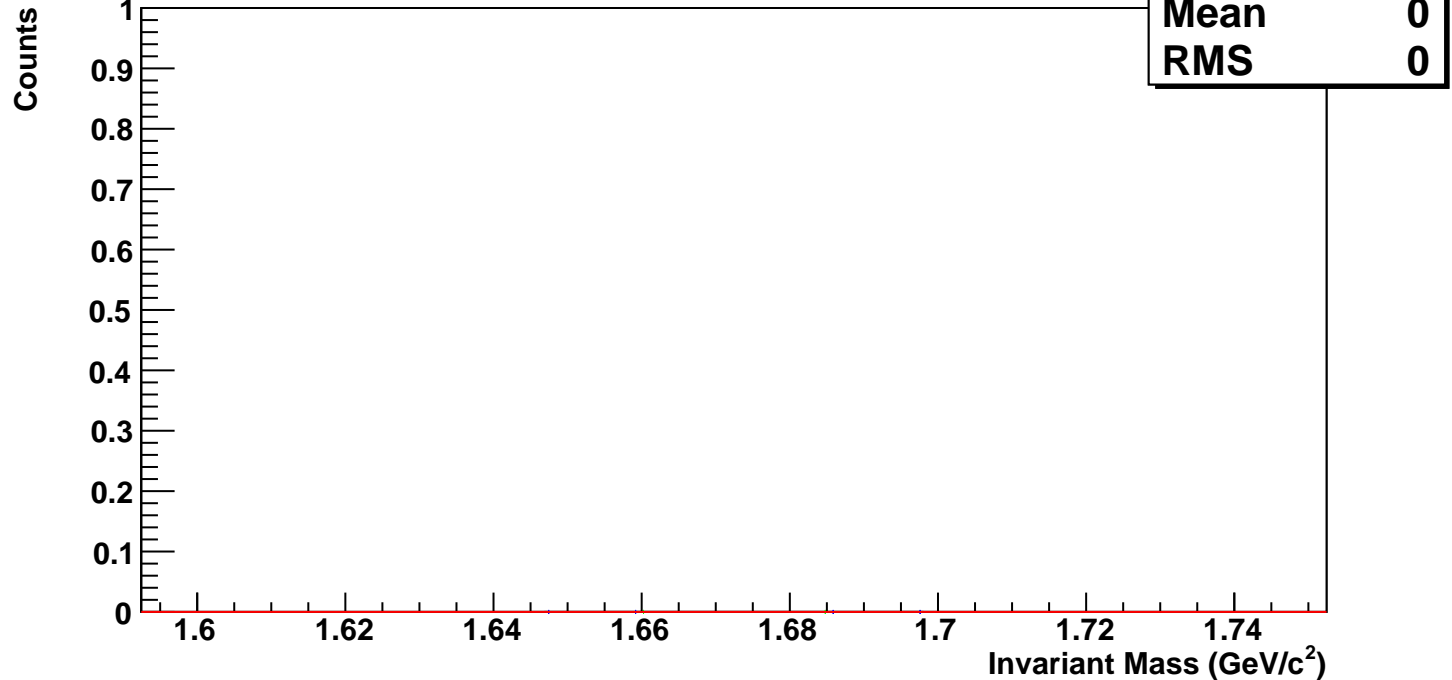


$\Omega^+$ , Au+Au 39 GeV, 0-5%,  $p_T$  3.6-4.0 GeV/c

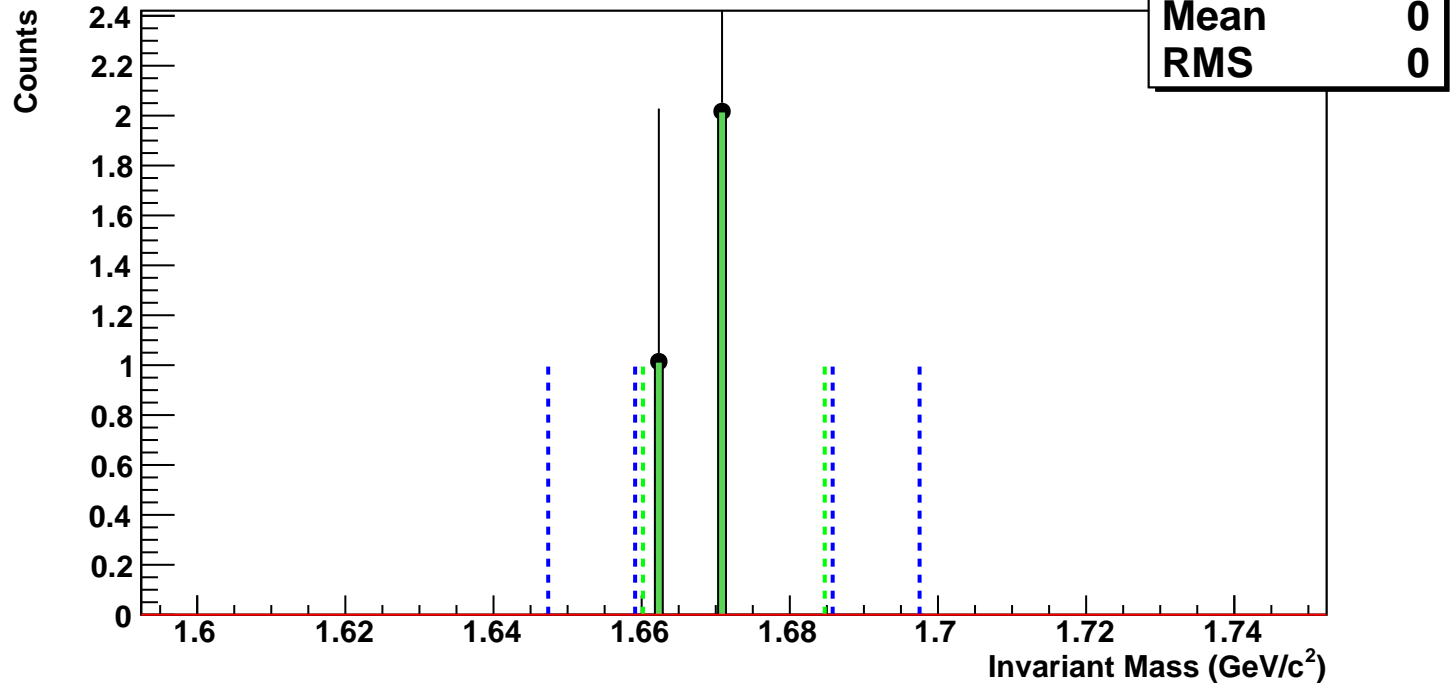
hmlInvMassBgCent5Pt10	
Entries	6
Mean	1.683
RMS	0.0275



$\Omega^+$ , Au+Au 39 GeV, 60-80%,  $p_T$  4.0-5.0 GeV/c

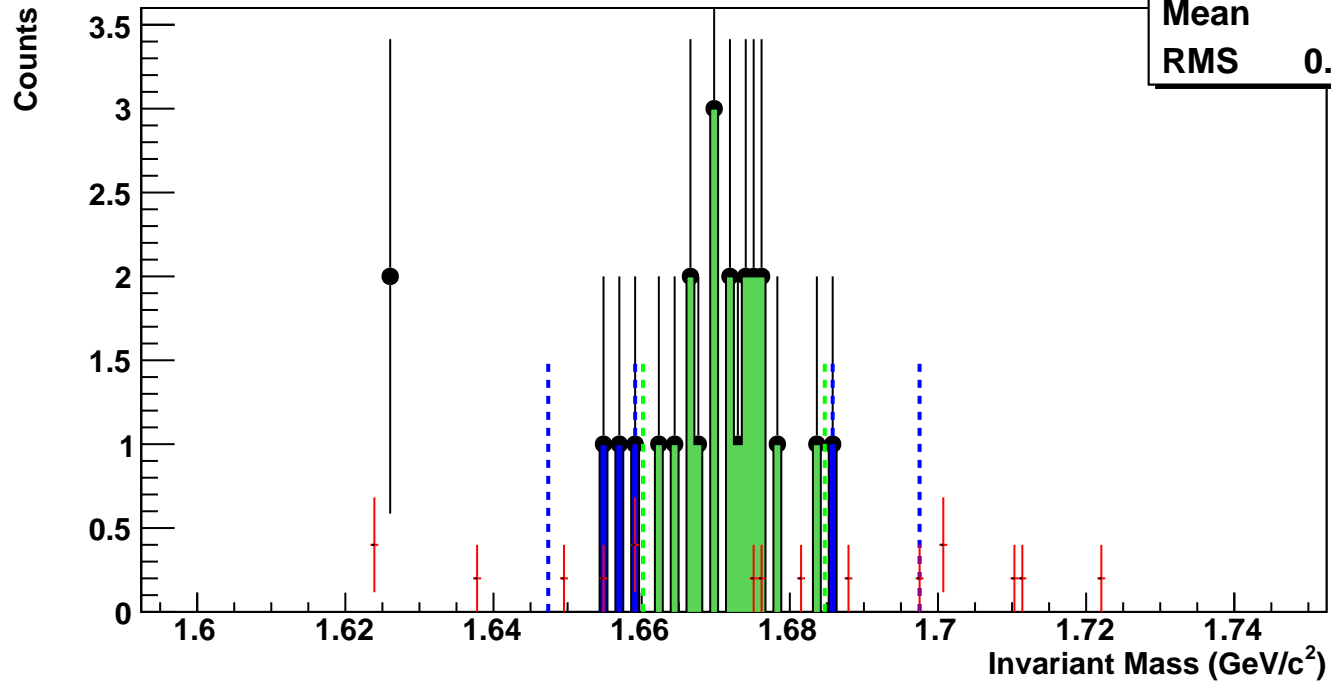


$\Omega^+$ , Au+Au 39 GeV, 40-60%,  $p_T$  4.0-5.0 GeV/c



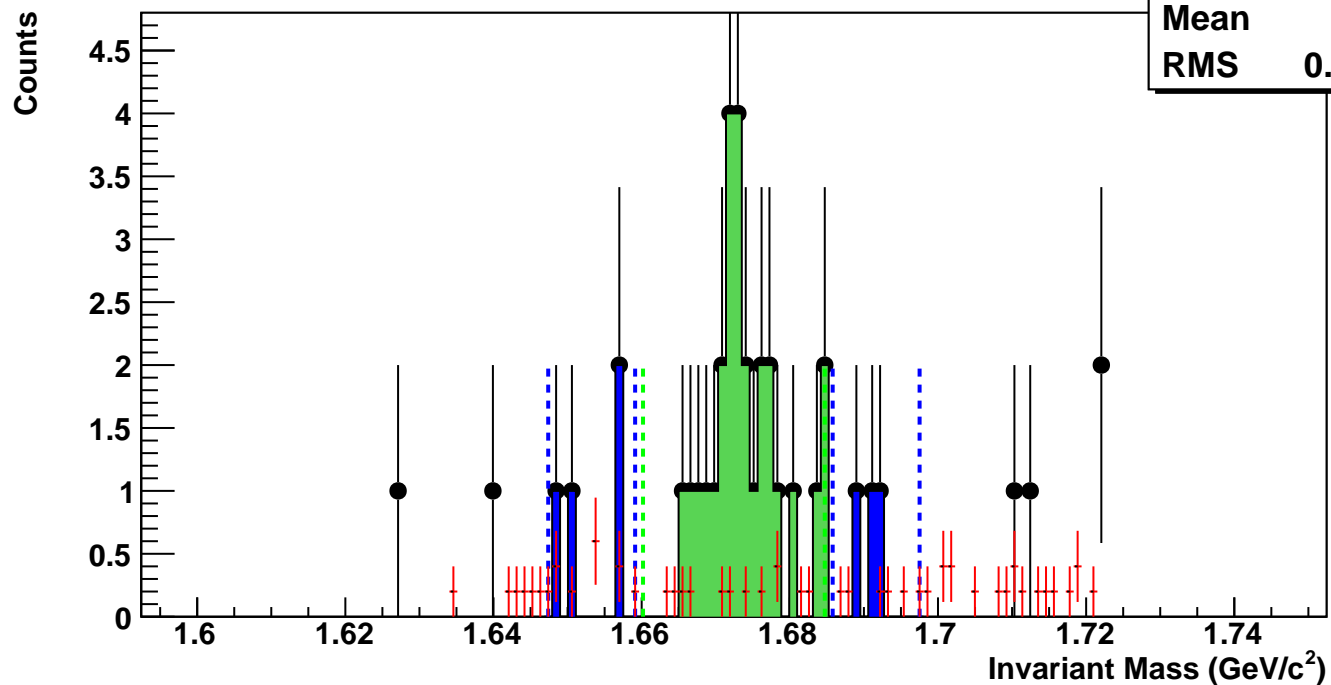
$\bar{\Omega}^+$ , Au+Au 39 GeV, 20-40%,  $p_T$  4.0-5.0 GeV/c

hmlInvMassBgCent2Pt11	
Entries	0
Mean	1.675
RMS	0.02969



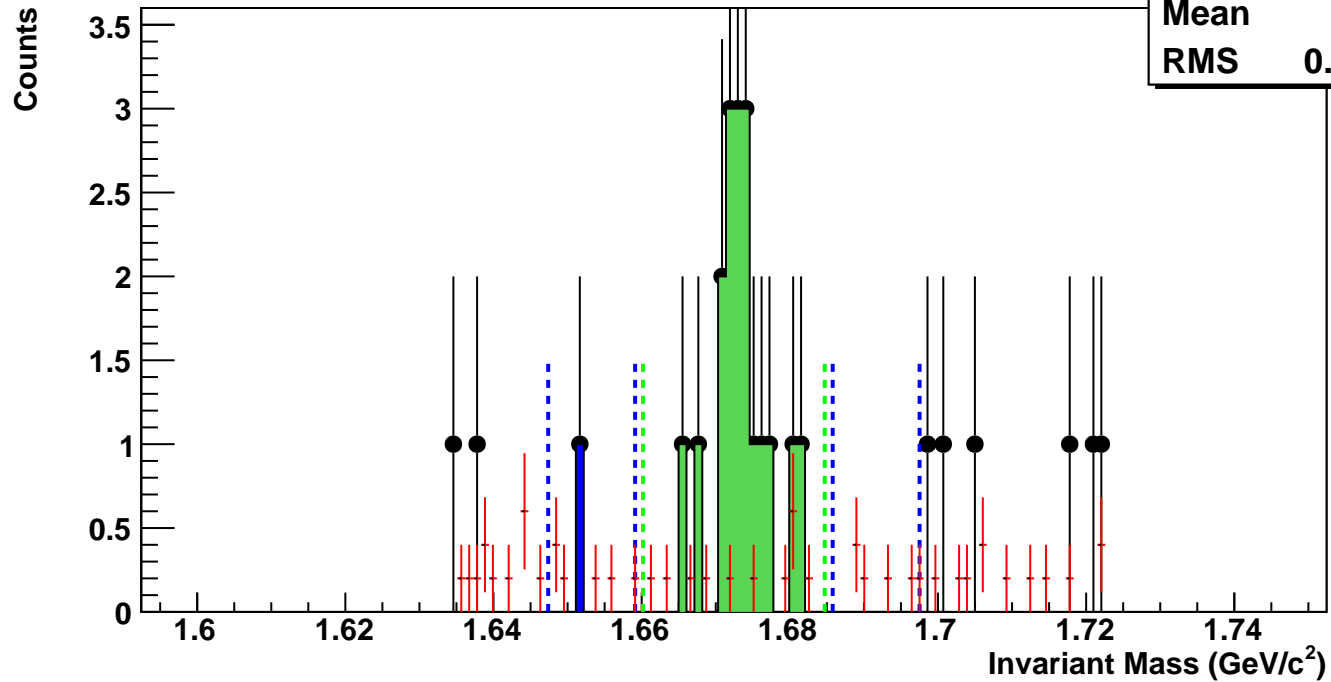
$\bar{\Omega}^+$ , Au+Au 39 GeV, 10-20%,  $p_T$  4.0-5.0 GeV/c

hmlInvMassBgCent3Pt11	
Entries	1
Mean	1.681
RMS	0.02595



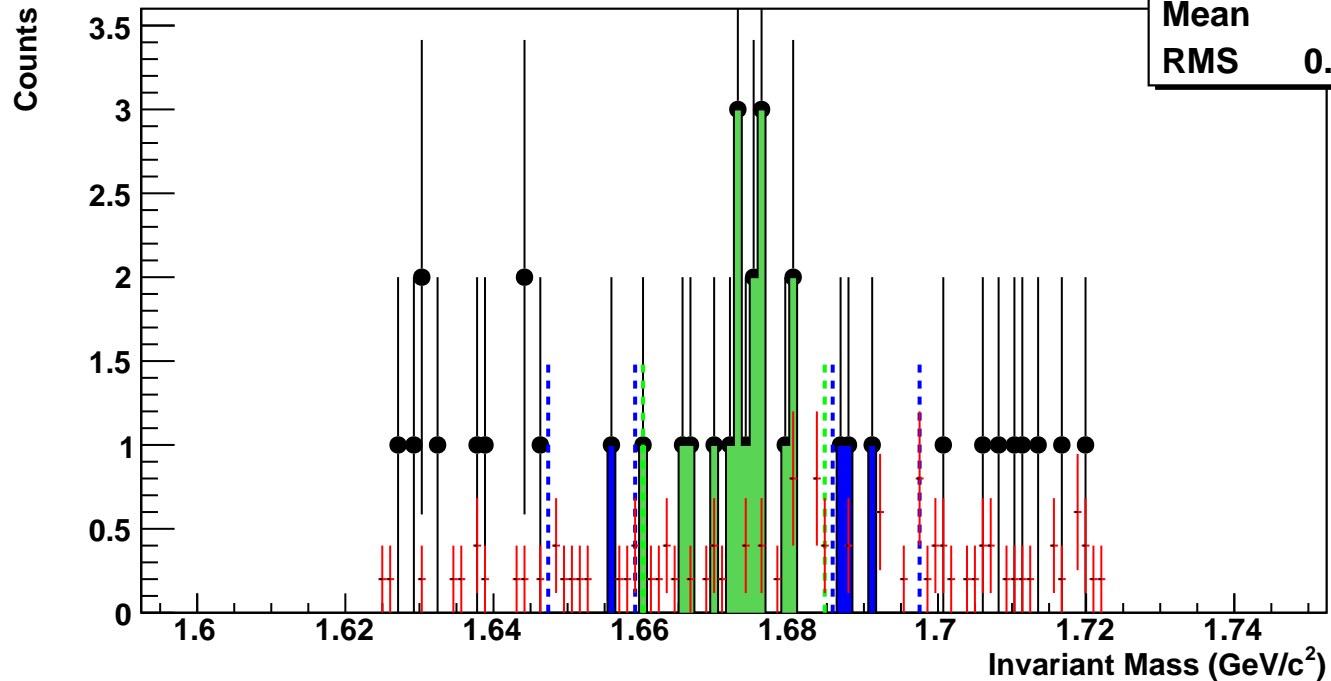
$\Omega^+$ , Au+Au 39 GeV, 5-10%,  $p_T$  4.0-5.0 GeV/c

hmlInvMassBgCent4Pt11	
Entries	1
Mean	1.674
RMS	0.02716

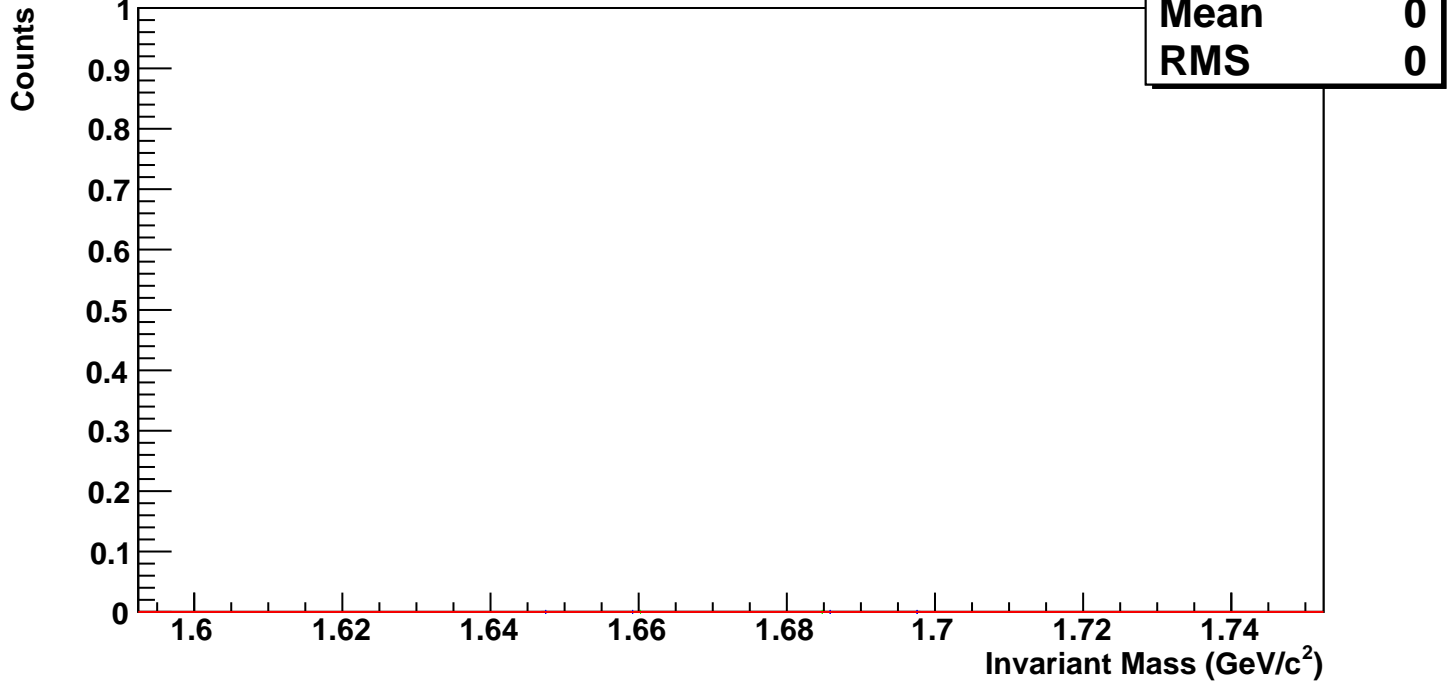


$\Omega^+$ , Au+Au 39 GeV, 0-5%,  $p_T$  4.0-5.0 GeV/c

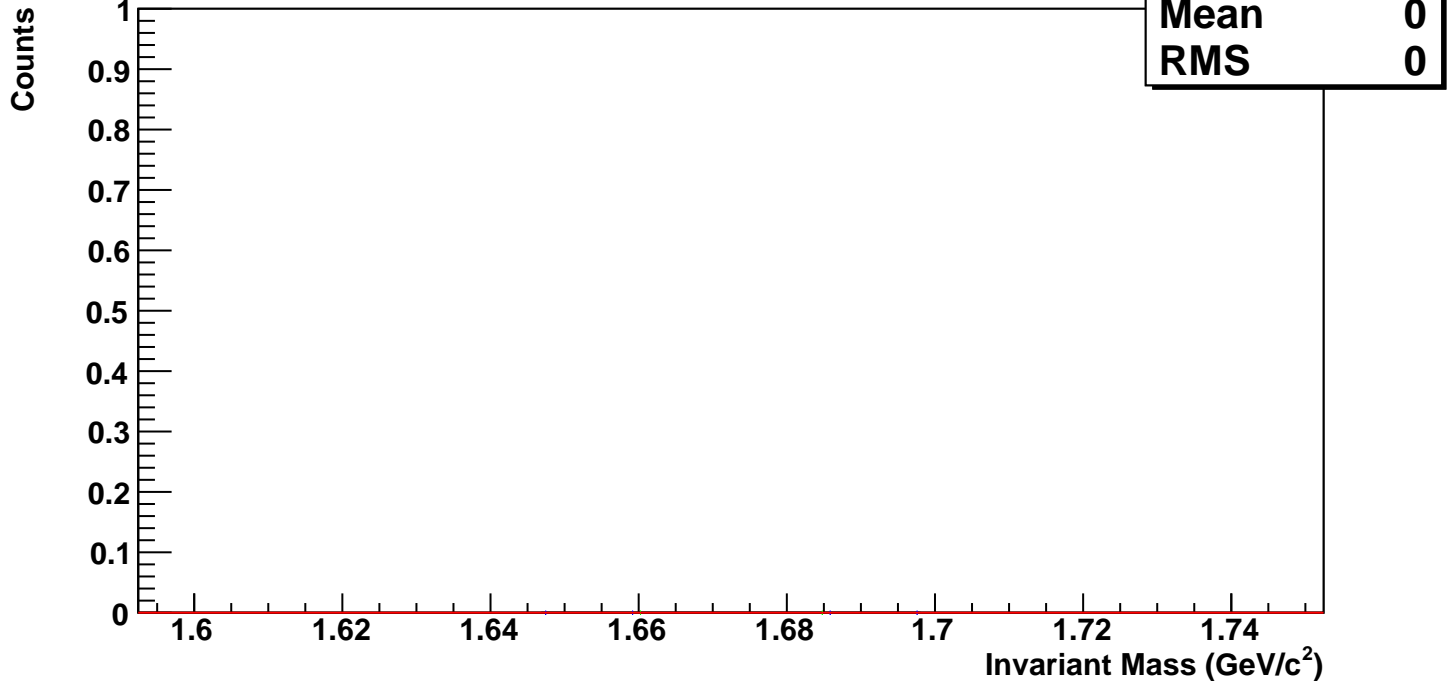
hmlInvMassBgCent5Pt11	
Entries	2
Mean	1.681
RMS	0.02666



$\bar{\Omega}^+$ , Au+Au 39 GeV, 60-80%,  $p_T$  5.0-7.0 GeV/c

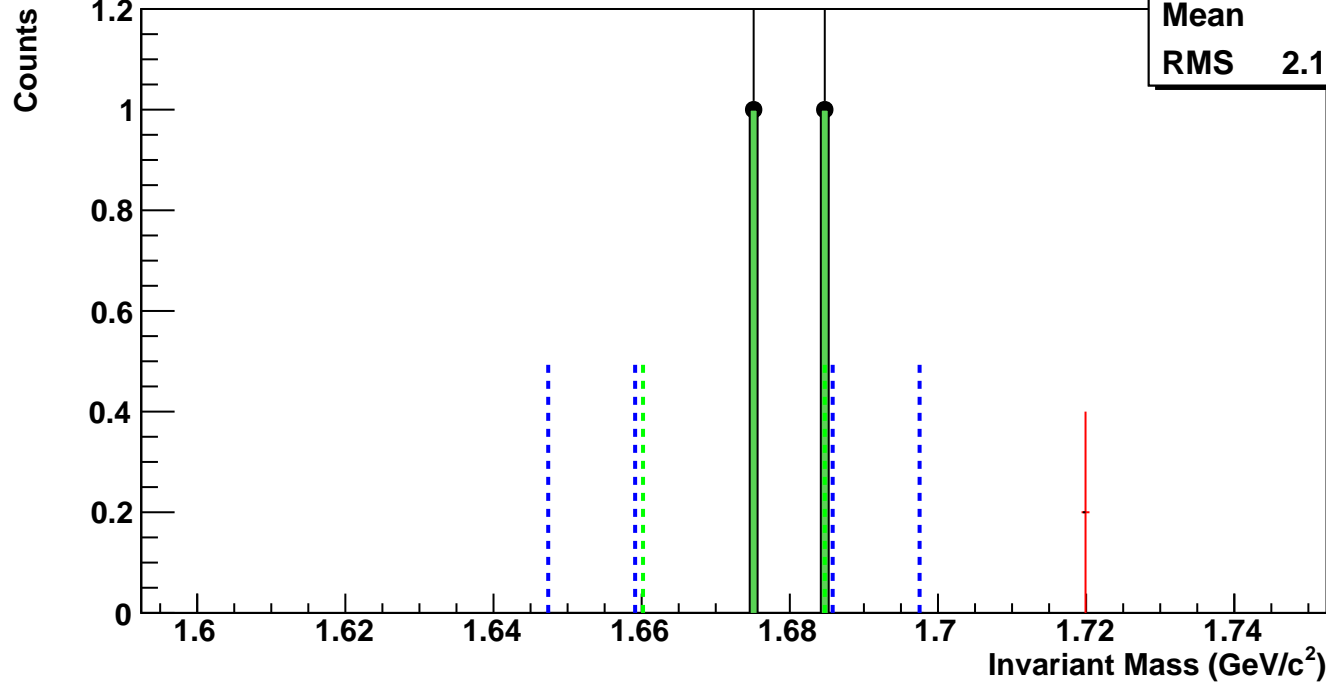


$\bar{\Omega}^+$ , Au+Au 39 GeV, 40-60%,  $p_T$  5.0-7.0 GeV/c



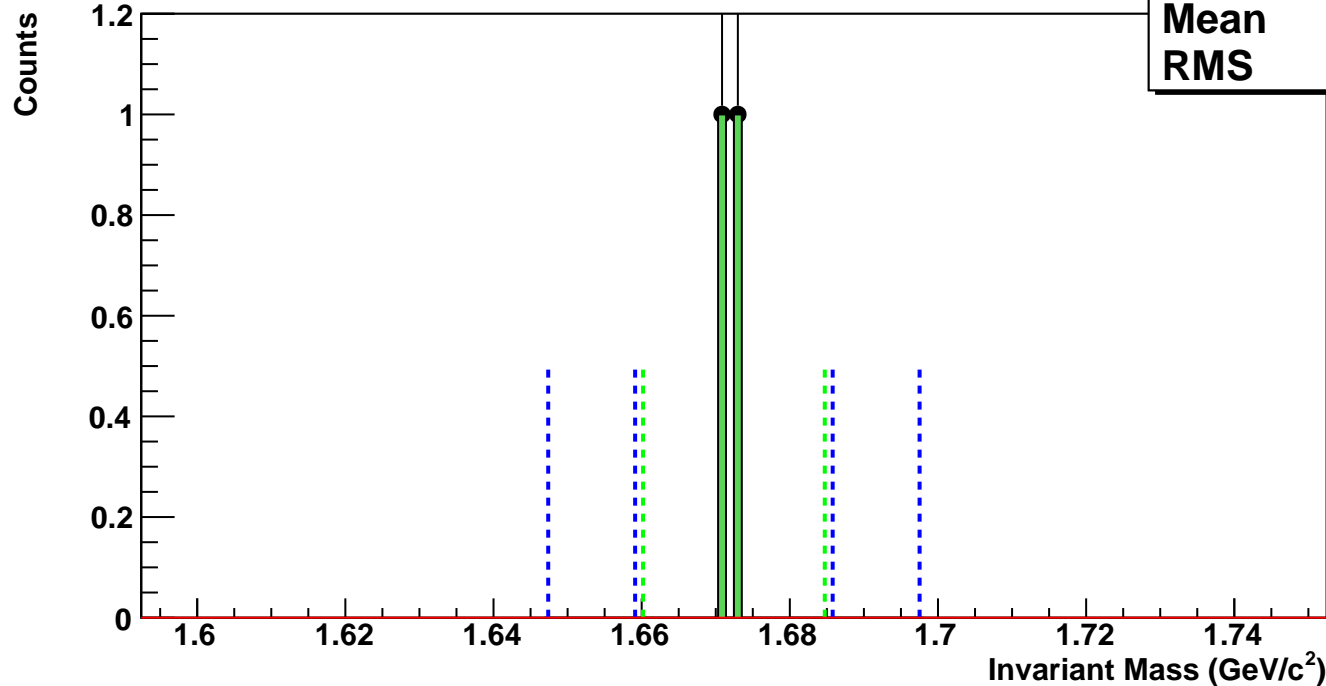
$\Omega^+$ , Au+Au 39 GeV, 20-40%,  $p_T$  5.0-7.0 GeV/c

hmlInvMassBgCent2Pt12	
Entries	0
Mean	1.72
RMS	2.107e-08



$\Omega^+$ , Au+Au 39 GeV, 10-20%,  $p_T$  5.0-7.0 GeV/c

hmlInvMassBgCent3Pt12	
Entries	0
Mean	0
RMS	0



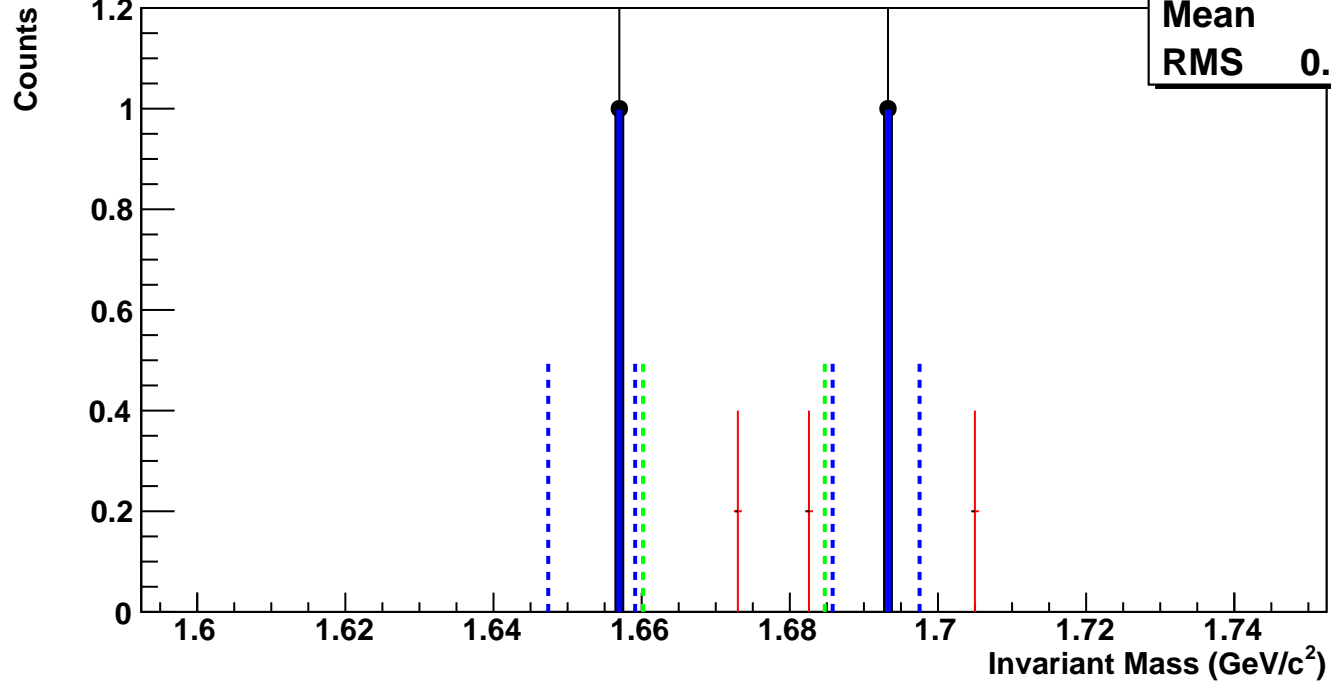
$\Omega^+$ , Au+Au 39 GeV, 5-10%,  $p_T$  5.0-7.0 GeV/c

hmlInvMassBgCent4Pt12

Entries 0

Mean 1.687

RMS 0.01341



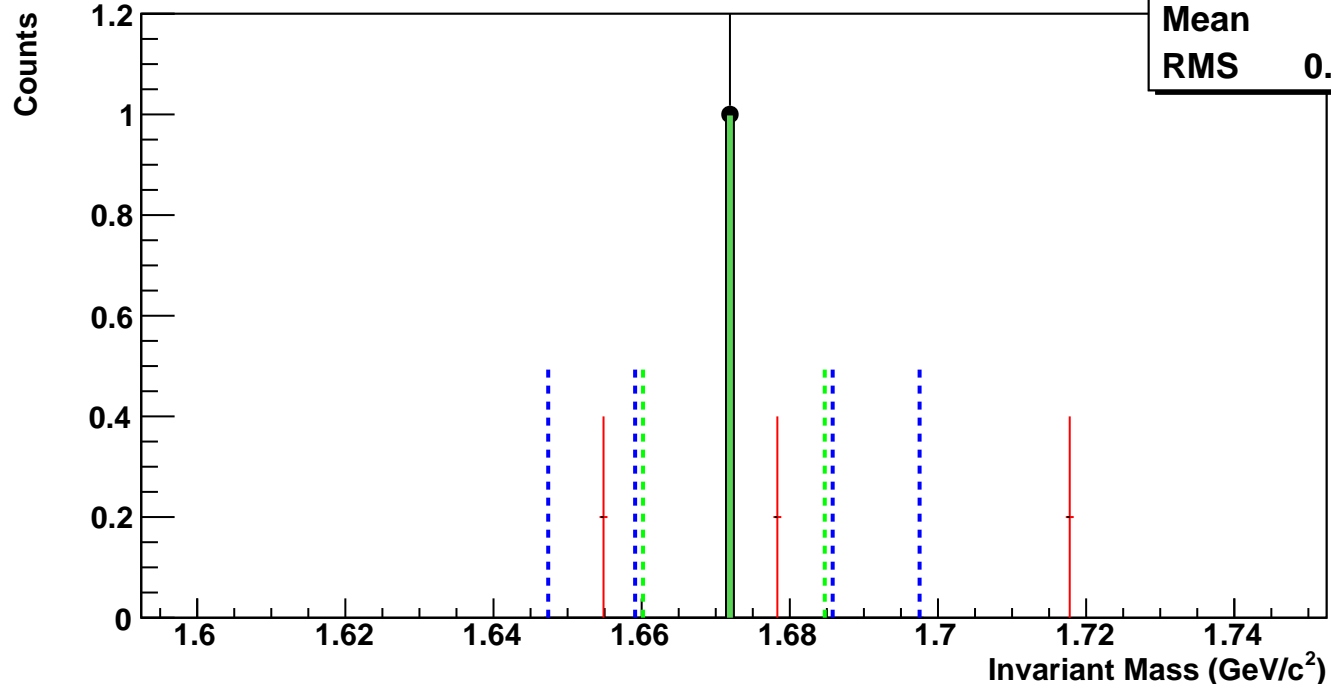
$\Omega^+$ , Au+Au 39 GeV, 0-5%,  $p_T$  5.0-7.0 GeV/c

hmlInvMassBgCent5Pt12

Entries 0

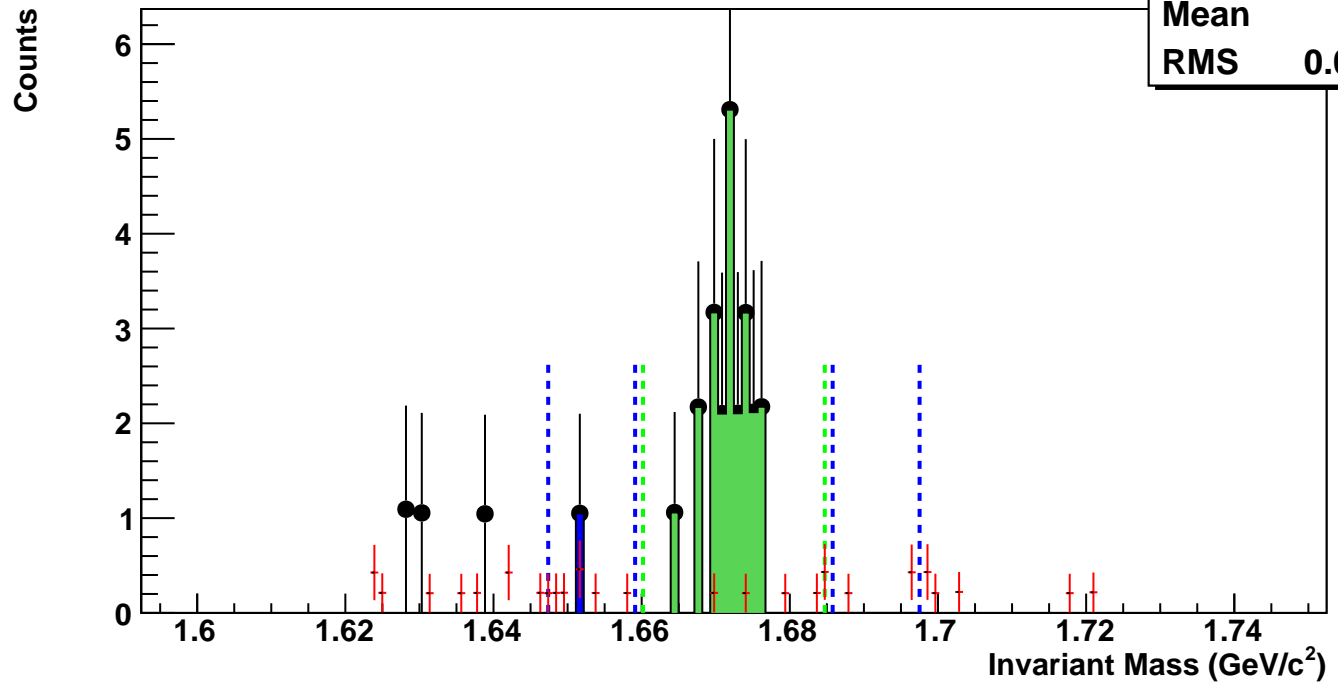
Mean 1.684

RMS 0.02597



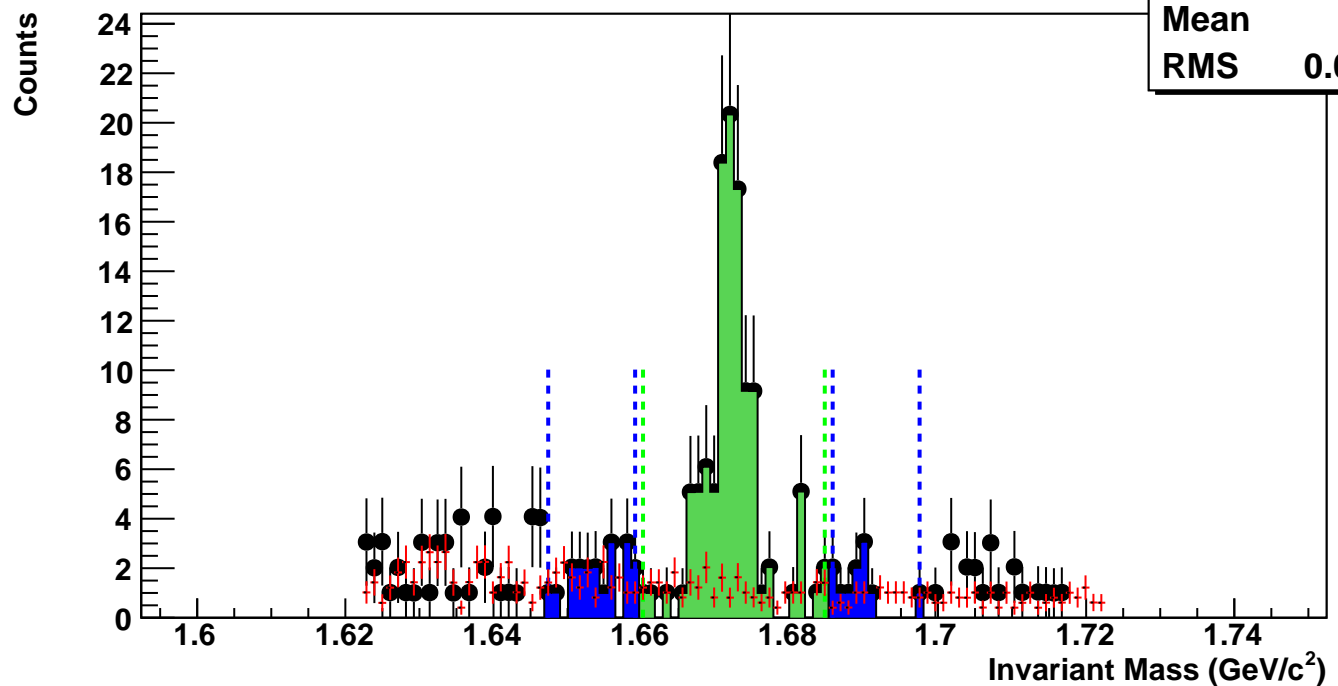
$\Omega^-$ , Au+Au 27 GeV, 60-80%,  $p_T$  0.8-1.2 GeV/c

hmlInvMassBgCent0Pt0	
Entries	1
Mean	1.667
RMS	0.02847



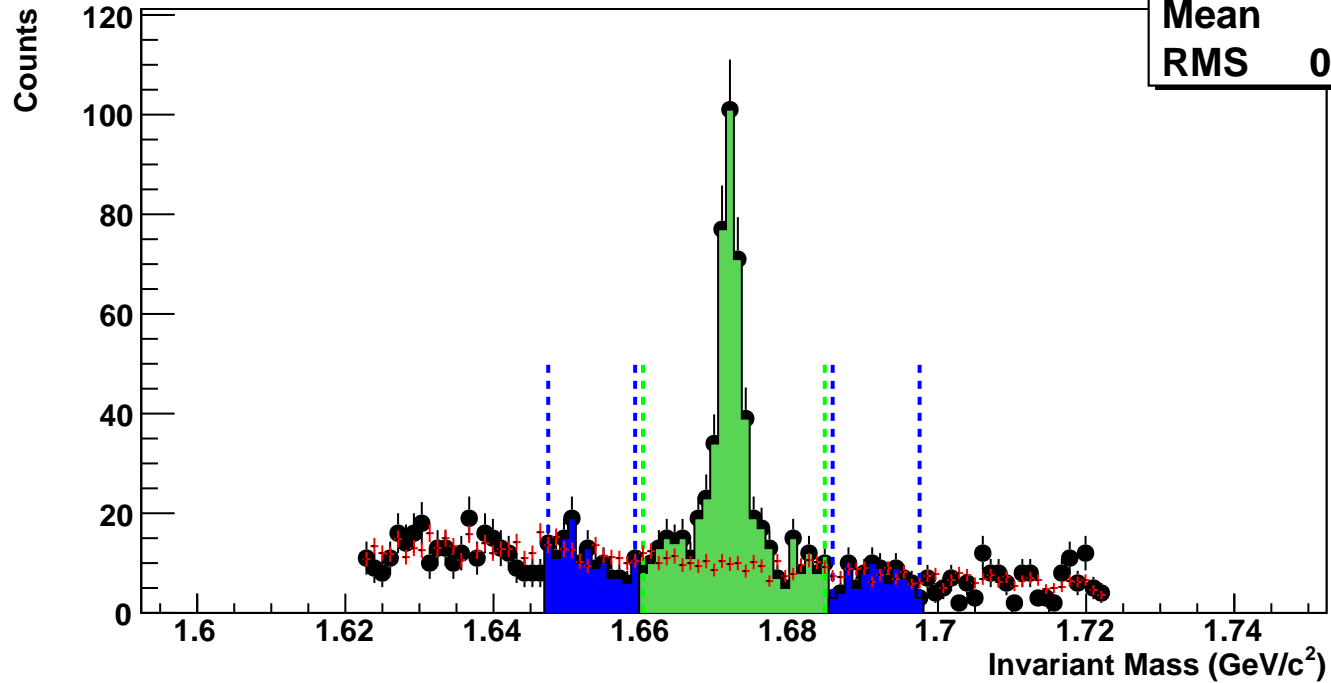
$\Omega^-$ , Au+Au 27 GeV, 40-60%,  $p_T$  0.8-1.2 GeV/c

hmlInvMassBgCent1Pt0	
Entries	13
Mean	1.664
RMS	0.02798



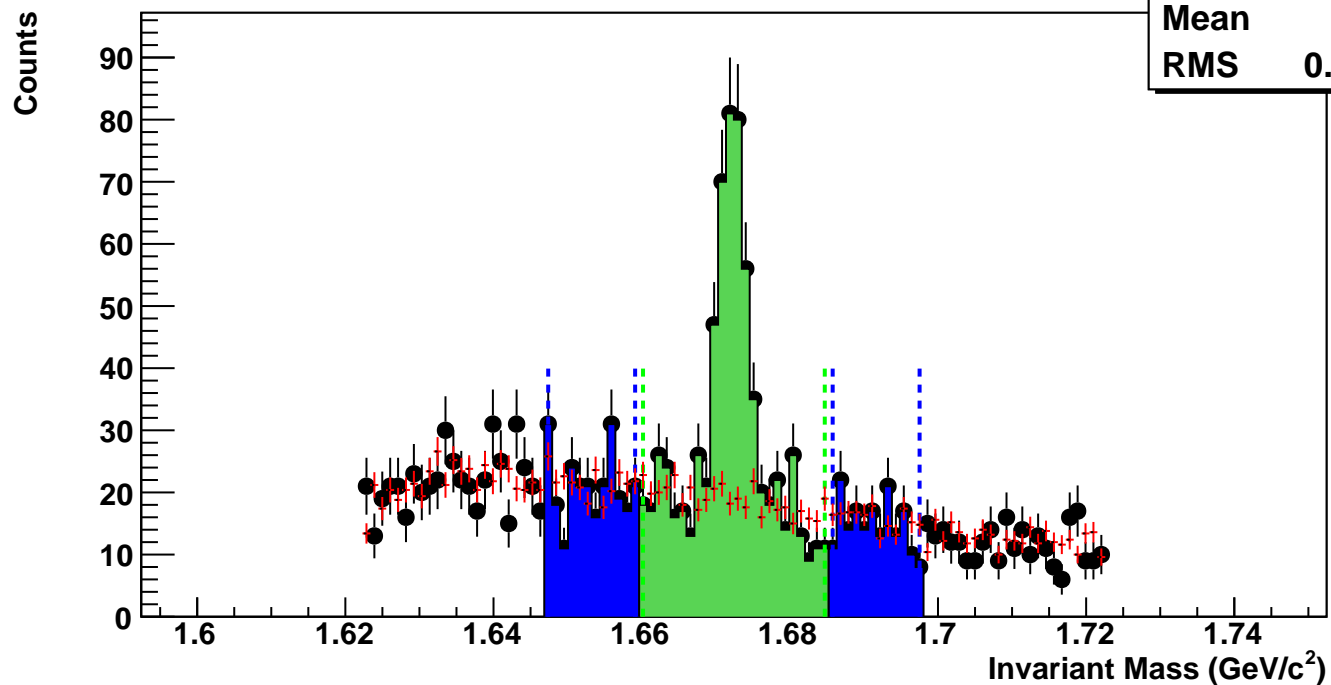
$\Omega^-$ , Au+Au 27 GeV, 20-40%,  $p_T$  0.8-1.2 GeV/c

hmlInvMassBgCent2Pt0  
Entries 111  
Mean 1.665  
RMS 0.0276



$\Omega^-$ , Au+Au 27 GeV, 10-20%,  $p_T$  0.8-1.2 GeV/c

hmlInvMassBgCent3Pt0  
Entries 205  
Mean 1.667  
RMS 0.02762



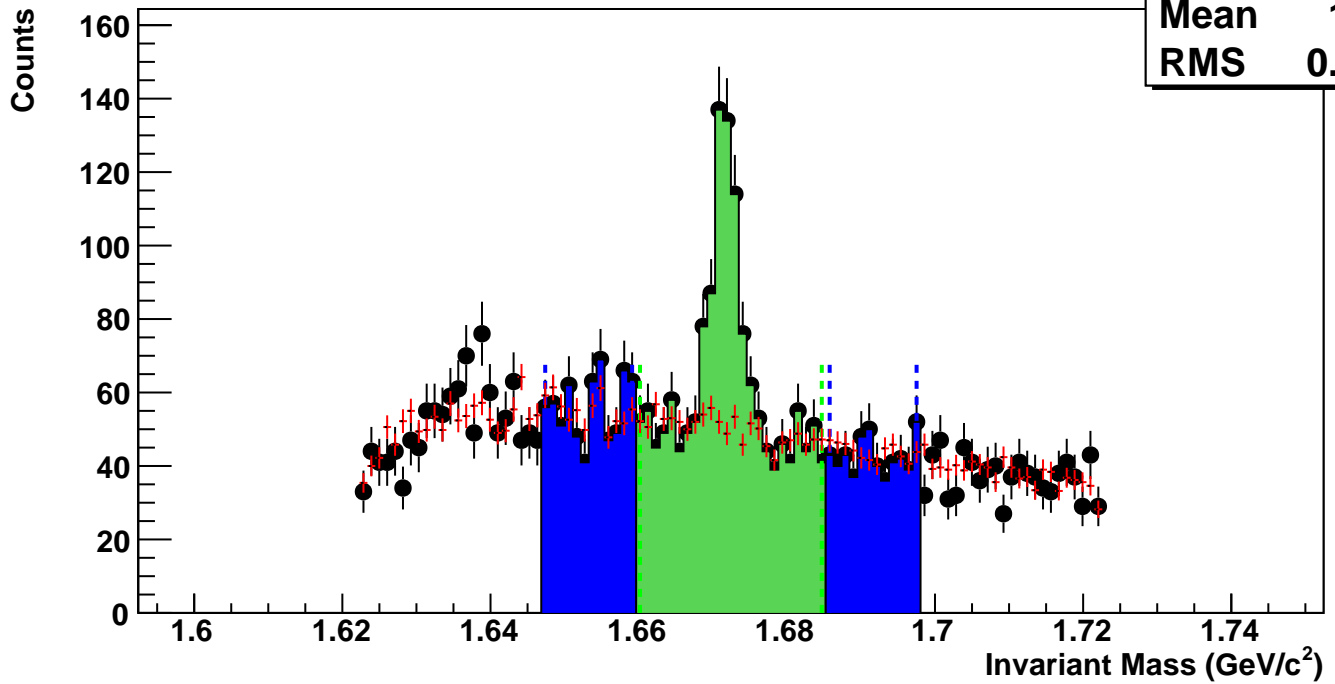
$\Omega^-$ , Au+Au 27 GeV, 0-10%,  $p_T$  0.8-1.2 GeV/c

hmlnvMassBgCent4Pt0

Entries 541

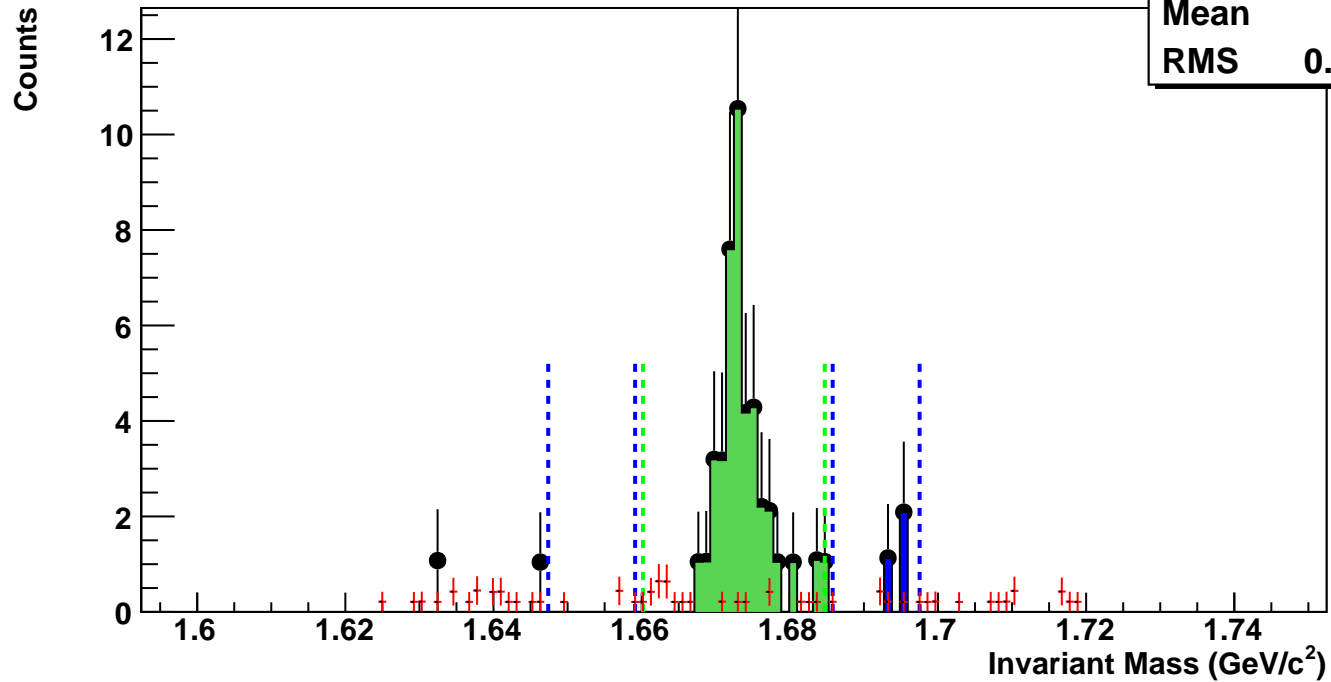
Mean 1.669

RMS 0.0278



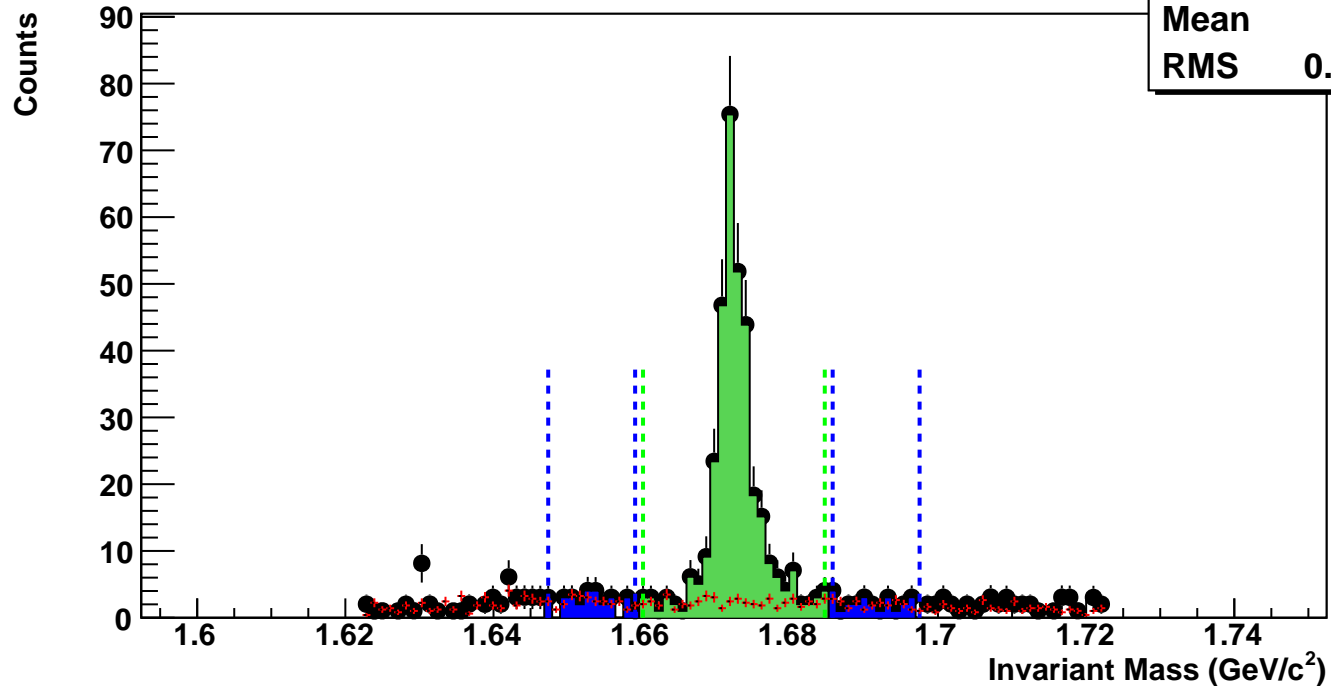
$\Omega^-$ , Au+Au 27 GeV, 60-80%,  $p_T$  1.2-1.6 GeV/c

hmlInvMassBgCent0Pt1	
Entries	1
Mean	1.67
RMS	0.02712



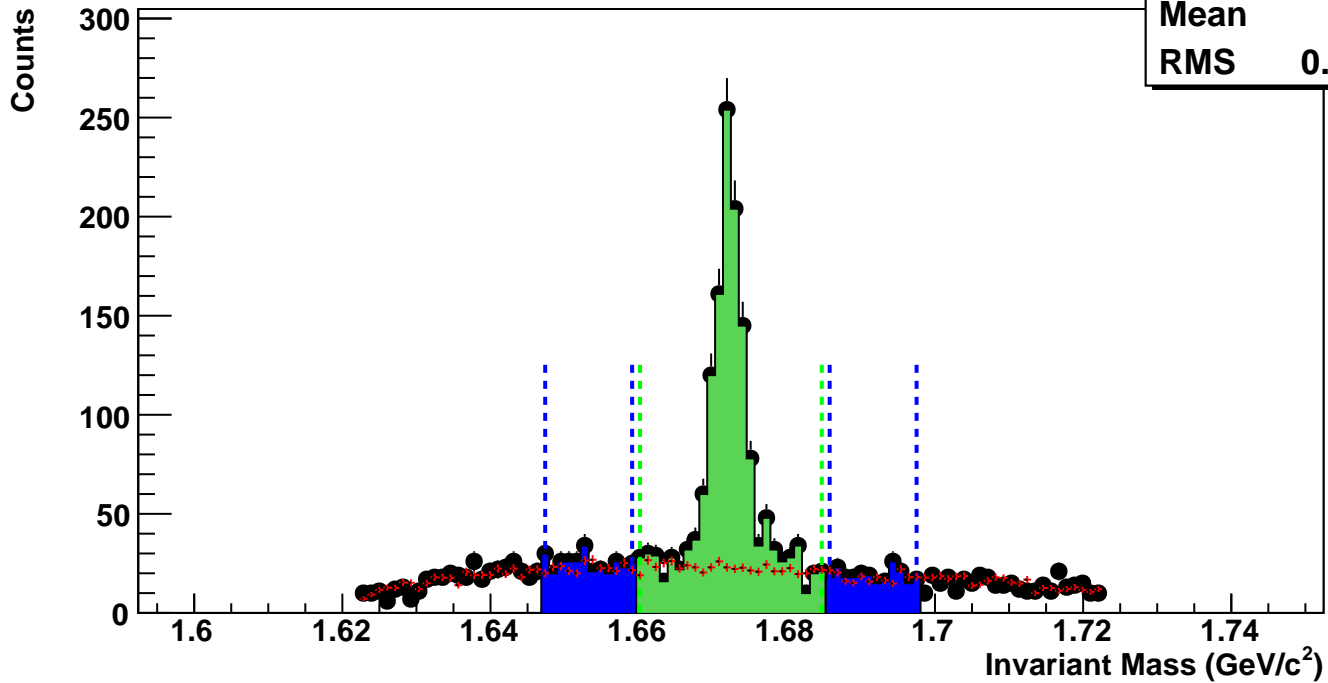
$\Omega^-$ , Au+Au 27 GeV, 40-60%,  $p_T$  1.2-1.6 GeV/c

hmlInvMassBgCent1Pt1	
Entries	22
Mean	1.669
RMS	0.02607



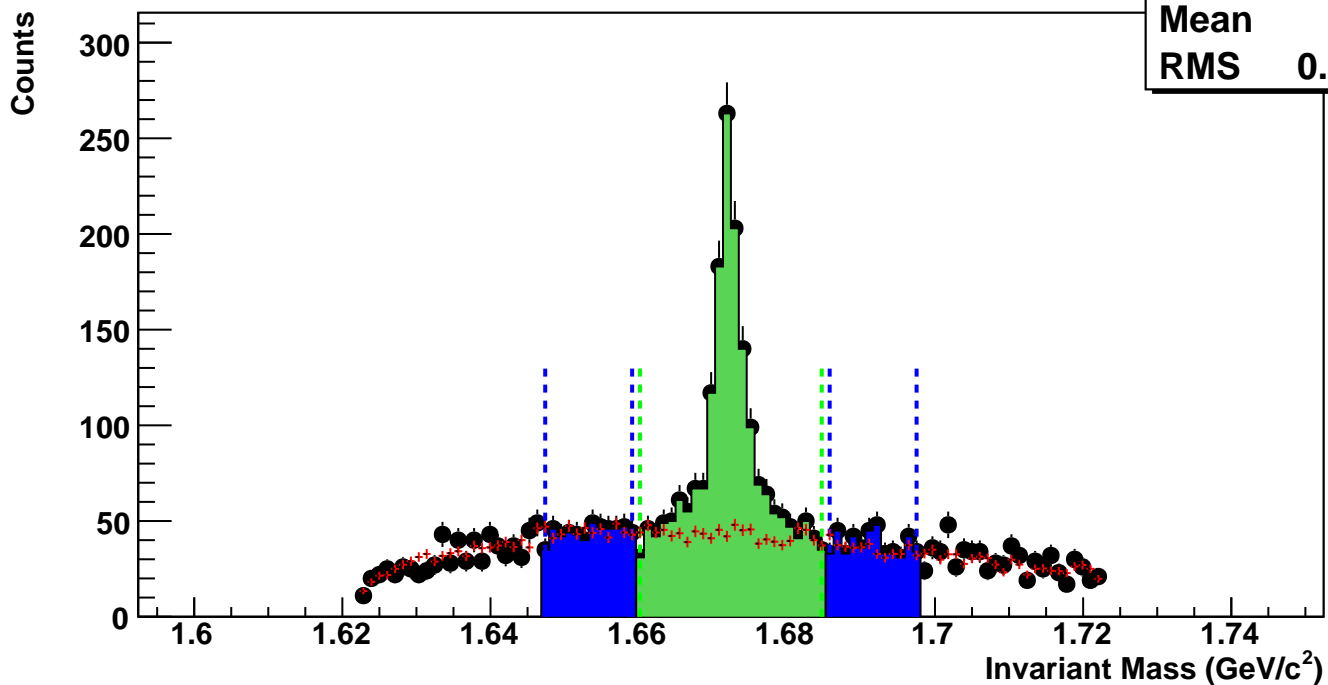
$\Omega^-$ , Au+Au 27 GeV, 20-40%,  $p_T$  1.2-1.6 GeV/c

hmlInvMassBgCent2Pt1	
Entries	214
Mean	1.671
RMS	0.02624



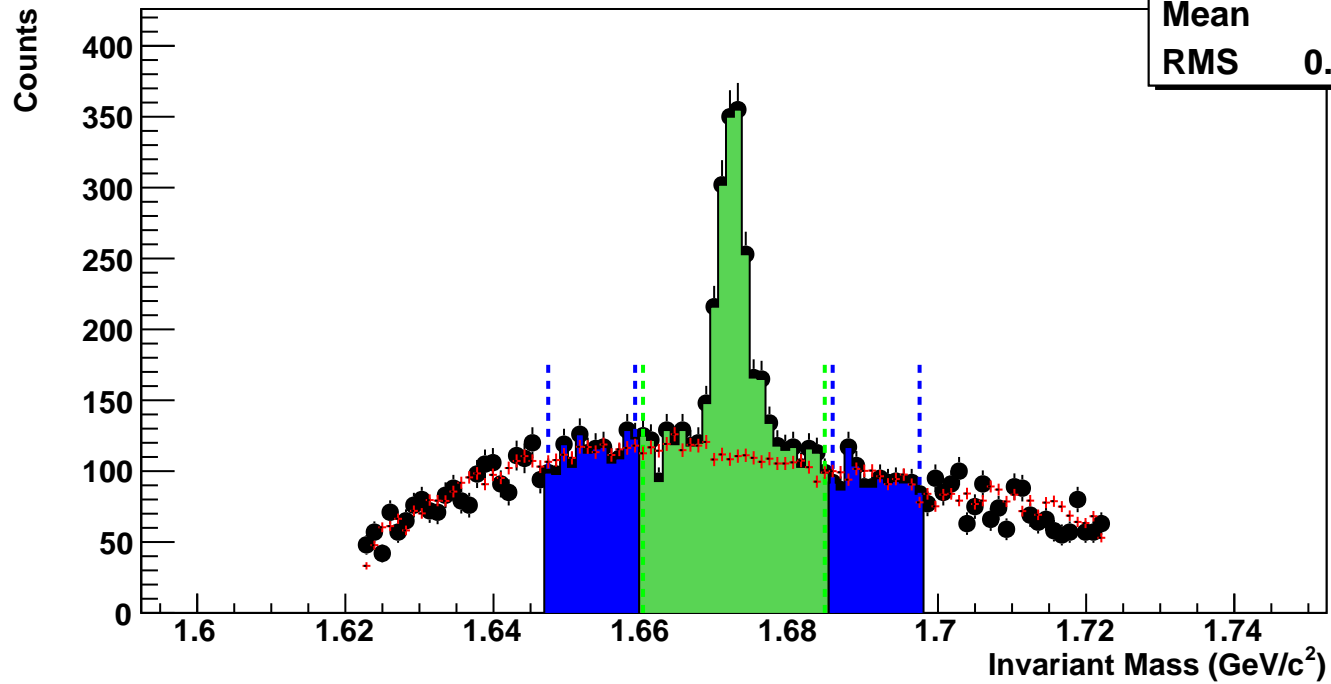
$\Omega^-$ , Au+Au 27 GeV, 10-20%,  $p_T$  1.2-1.6 GeV/c

hmlInvMassBgCent3Pt1	
Entries	407
Mean	1.671
RMS	0.02621



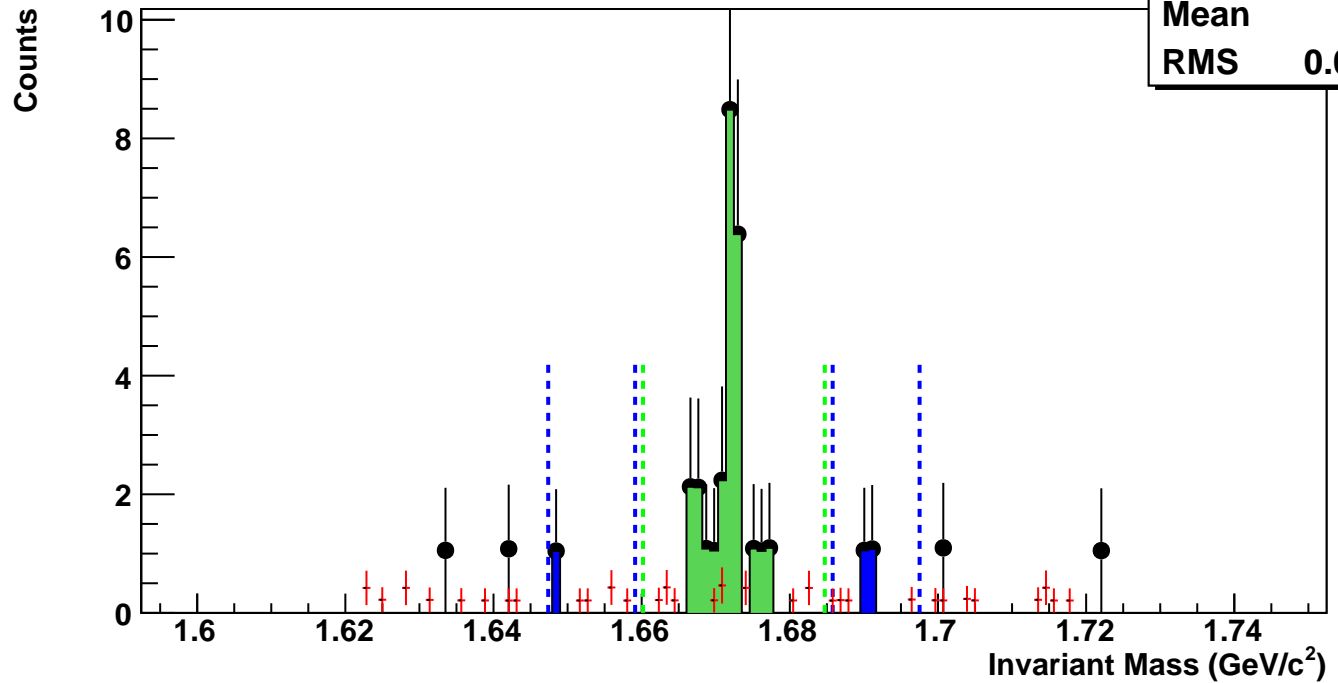
$\Omega^-$ , Au+Au 27 GeV, 0-10%,  $p_T$  1.2-1.6 GeV/c

hmlInvMassBgCent4Pt1
Entries 1074
Mean 1.671
RMS 0.02646



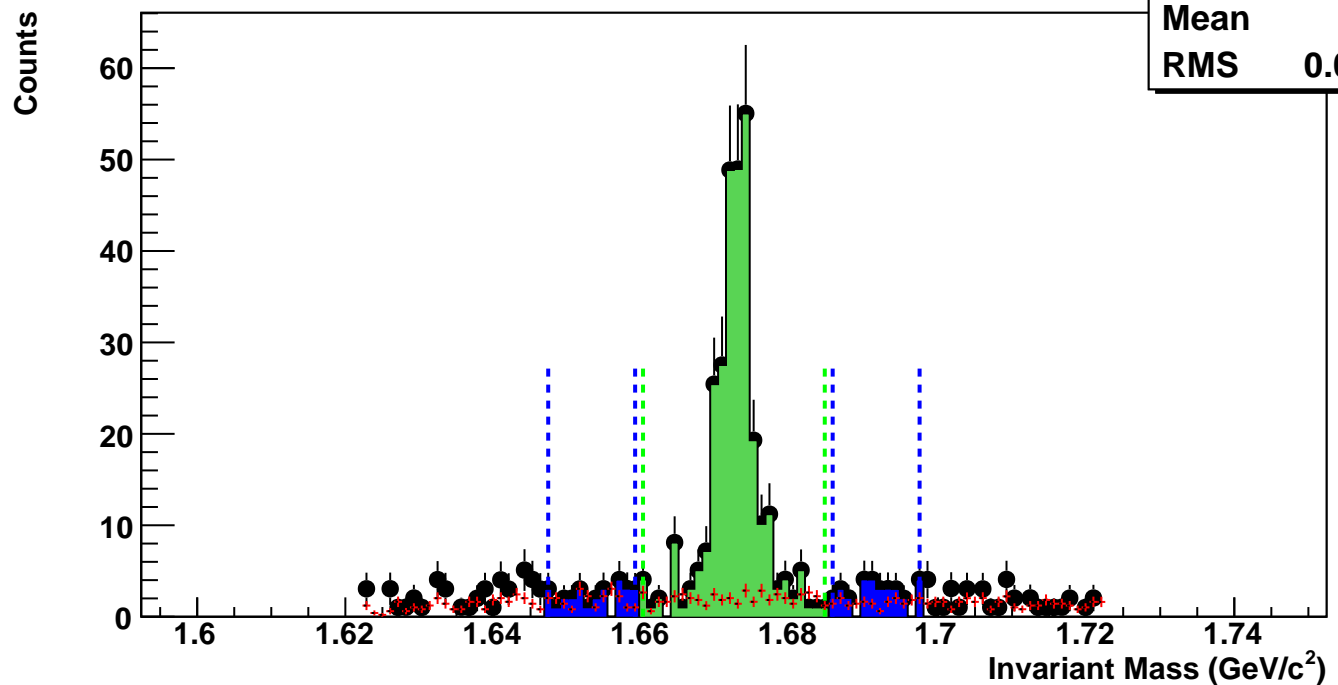
$\Omega^-$ , Au+Au 27 GeV, 60-80%,  $p_T$  1.6-2.0 GeV/c

hmlInvMassBgCent0Pt2	
Entries	1
Mean	1.67
RMS	0.02866



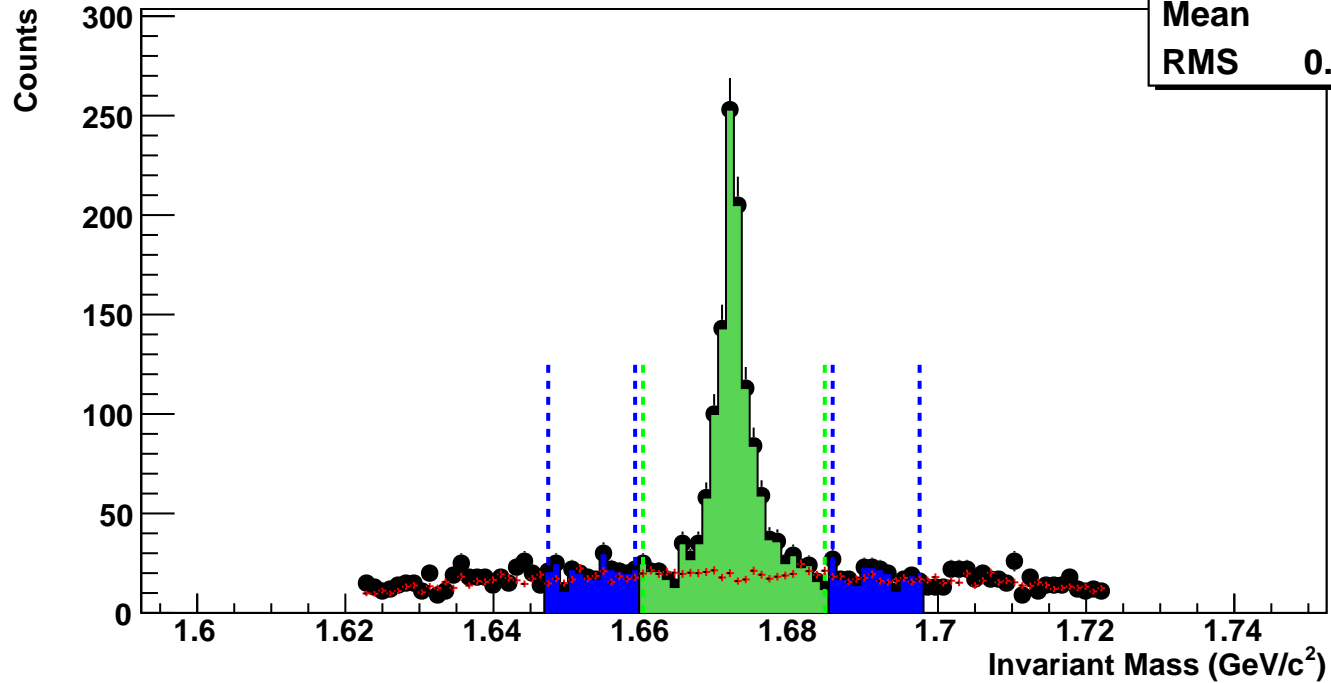
$\Omega^-$ , Au+Au 27 GeV, 40-60%,  $p_T$  1.6-2.0 GeV/c

hmlInvMassBgCent1Pt2	
Entries	18
Mean	1.673
RMS	0.02642



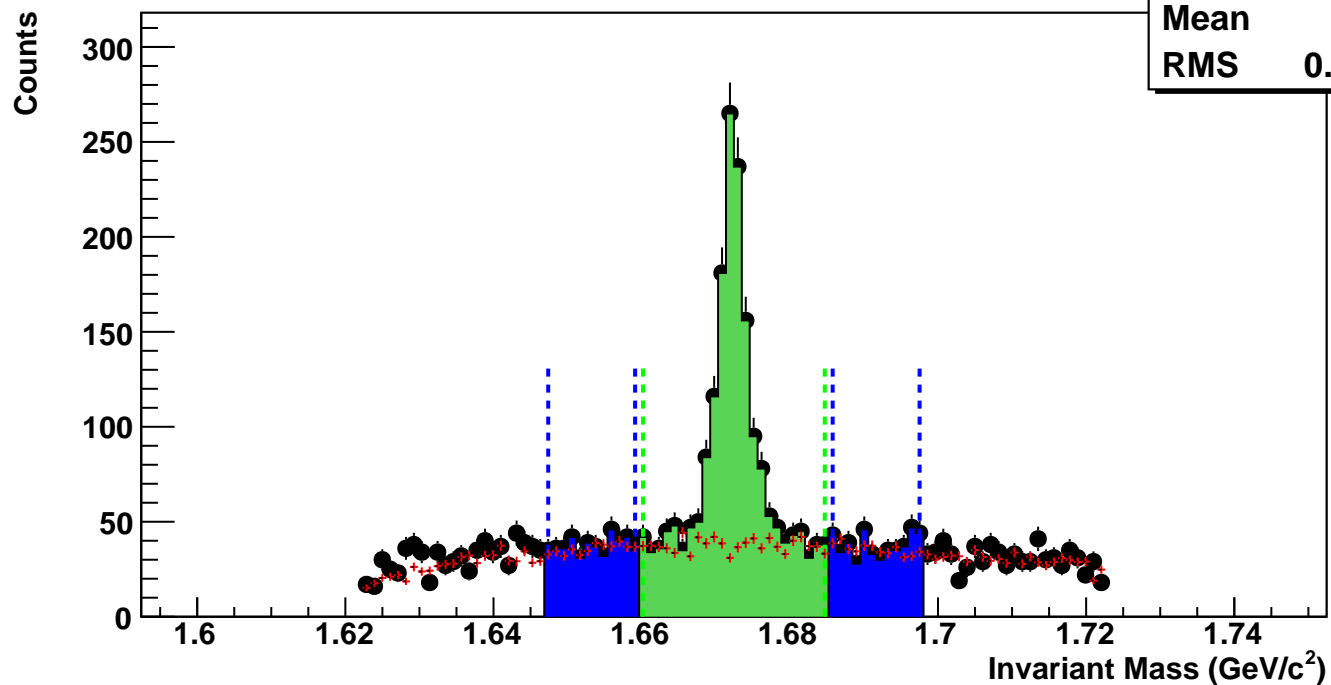
$\Omega^-$ , Au+Au 27 GeV, 20-40%,  $p_T$  1.6-2.0 GeV/c

hmlInvMassBgCent2Pt2	
Entries	190
Mean	1.673
RMS	0.02684



$\Omega^-$ , Au+Au 27 GeV, 10-20%,  $p_T$  1.6-2.0 GeV/c

hmlInvMassBgCent3Pt2	
Entries	372
Mean	1.673
RMS	0.02688



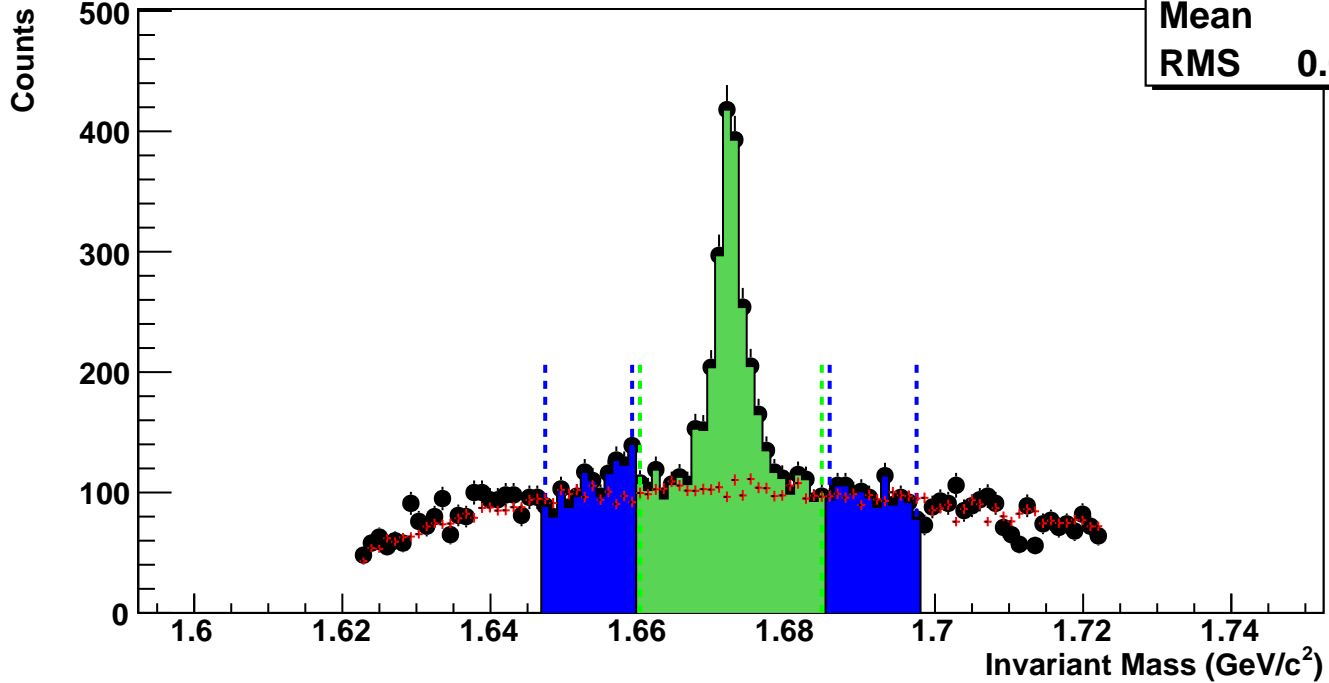
$\Omega^-$ , Au+Au 27 GeV, 0-10%,  $p_T$  1.6-2.0 GeV/c

hmlInvMassBgCent4Pt2

Entries 1018

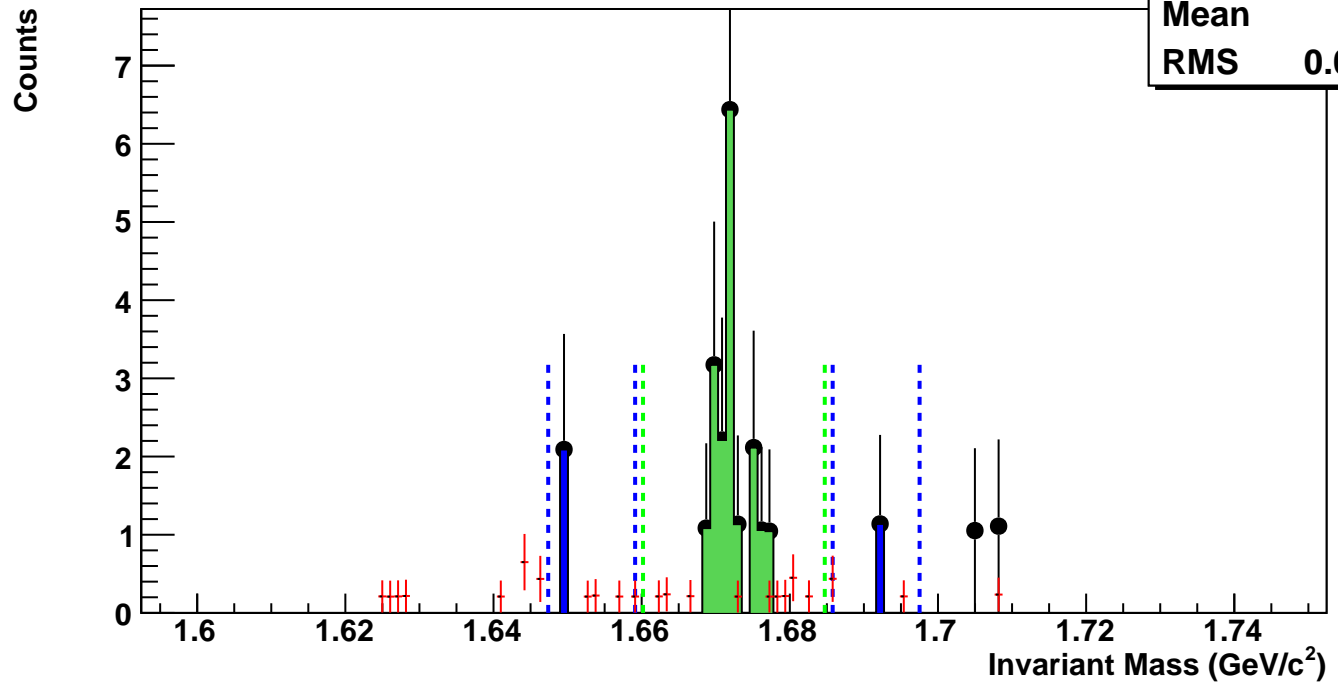
Mean 1.673

RMS 0.02701



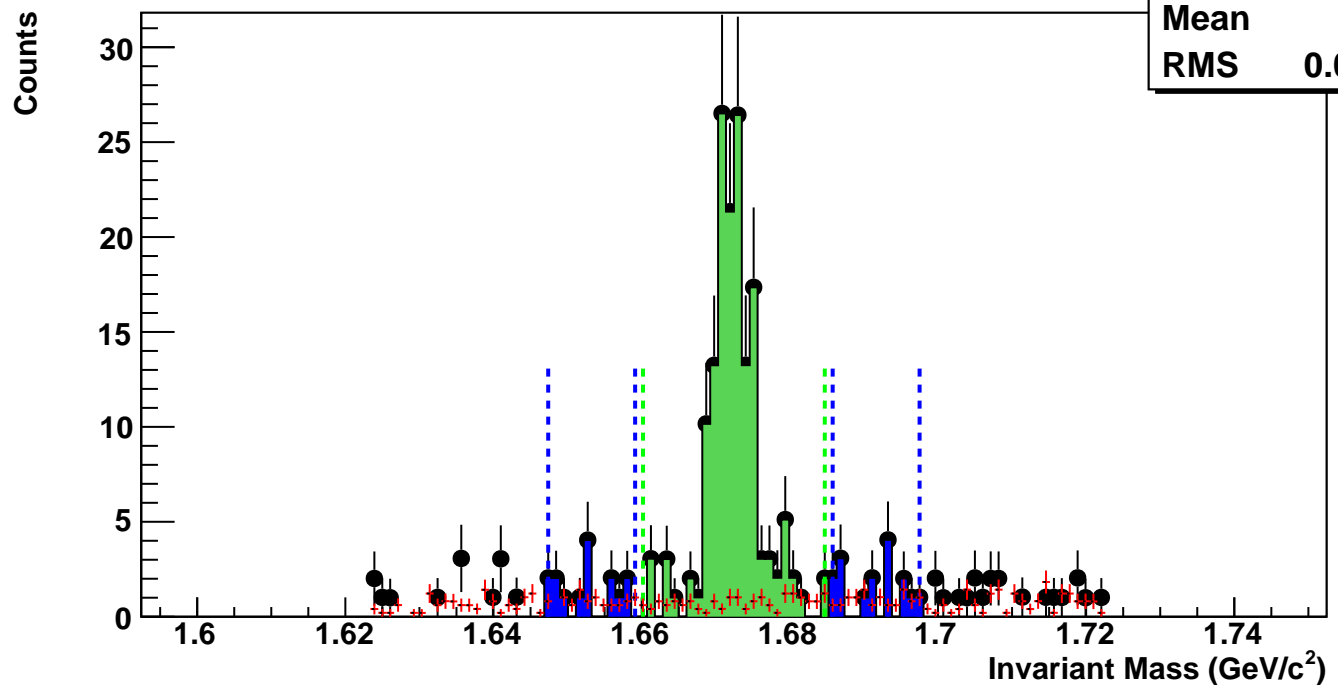
$\Omega^-$ , Au+Au 27 GeV, 60-80%,  $p_T$  2.0-2.4 GeV/c

hmlInvMassBgCent0Pt3	
Entries	1
Mean	1.661
RMS	0.02203



$\Omega^-$ , Au+Au 27 GeV, 40-60%,  $p_T$  2.0-2.4 GeV/c

hmlInvMassBgCent1Pt3	
Entries	8
Mean	1.676
RMS	0.02743



$\Omega^-$ , Au+Au 27 GeV, 20-40%,  $p_T$  2.0-2.4 GeV/c

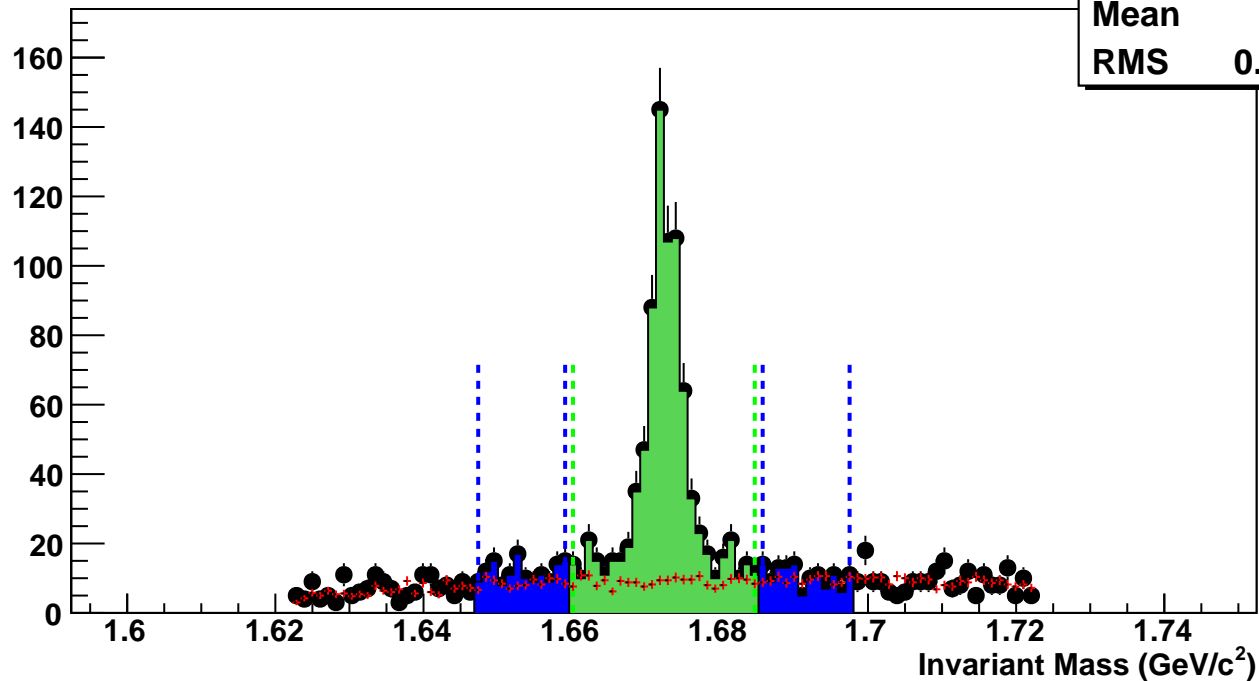
hmlInvMassBgCent2Pt3

Entries 95

Mean 1.676

RMS 0.02734

Counts



$\Omega^-$ , Au+Au 27 GeV, 10-20%,  $p_T$  2.0-2.4 GeV/c

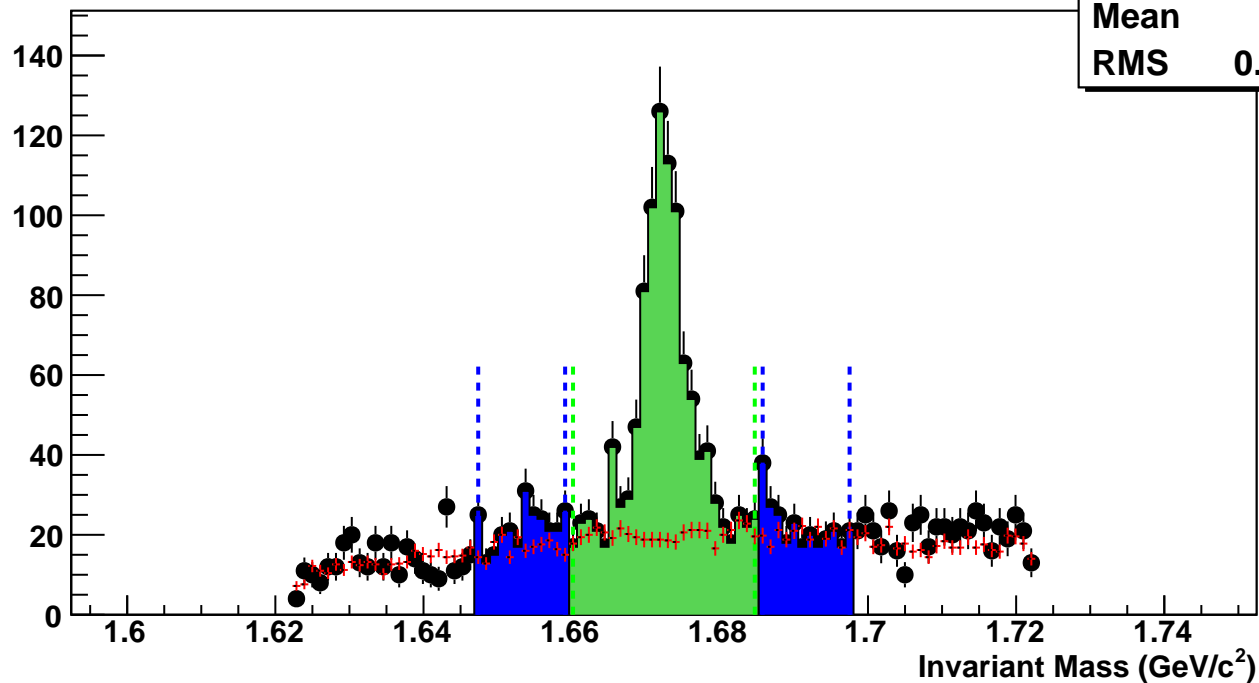
hmlInvMassBgCent3Pt3

Entries 197

Mean 1.676

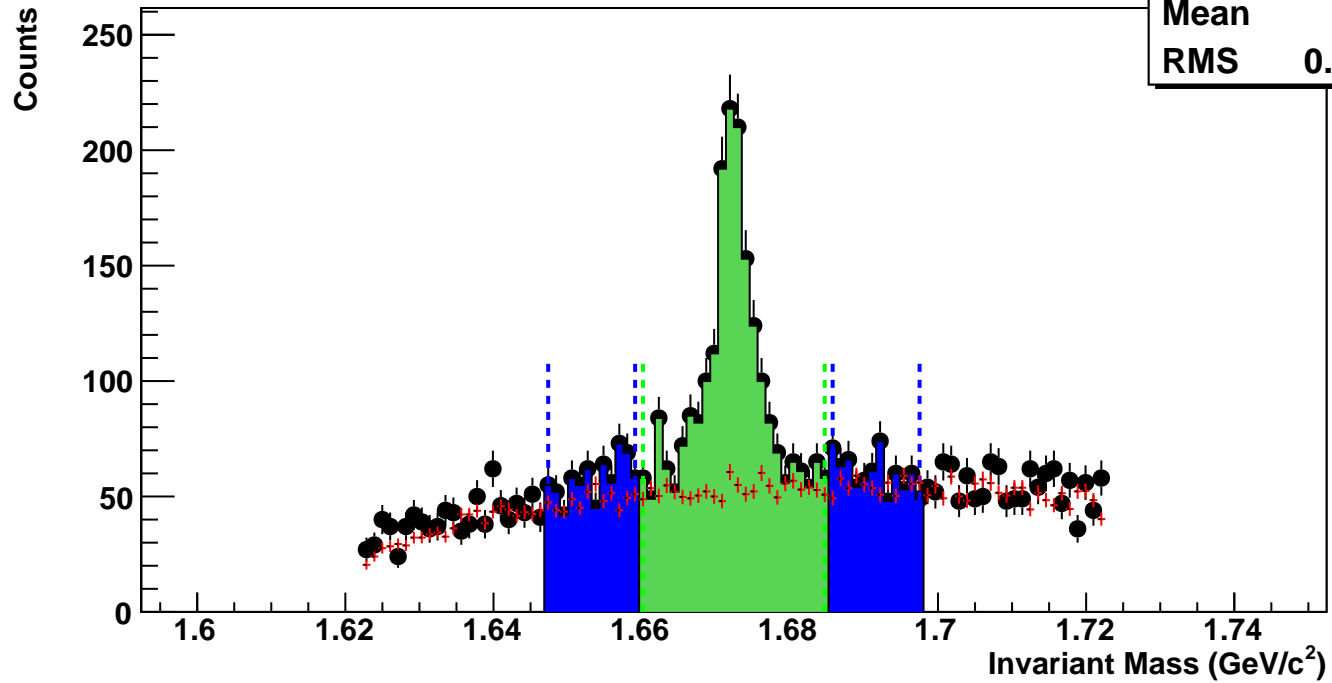
RMS 0.02703

Counts



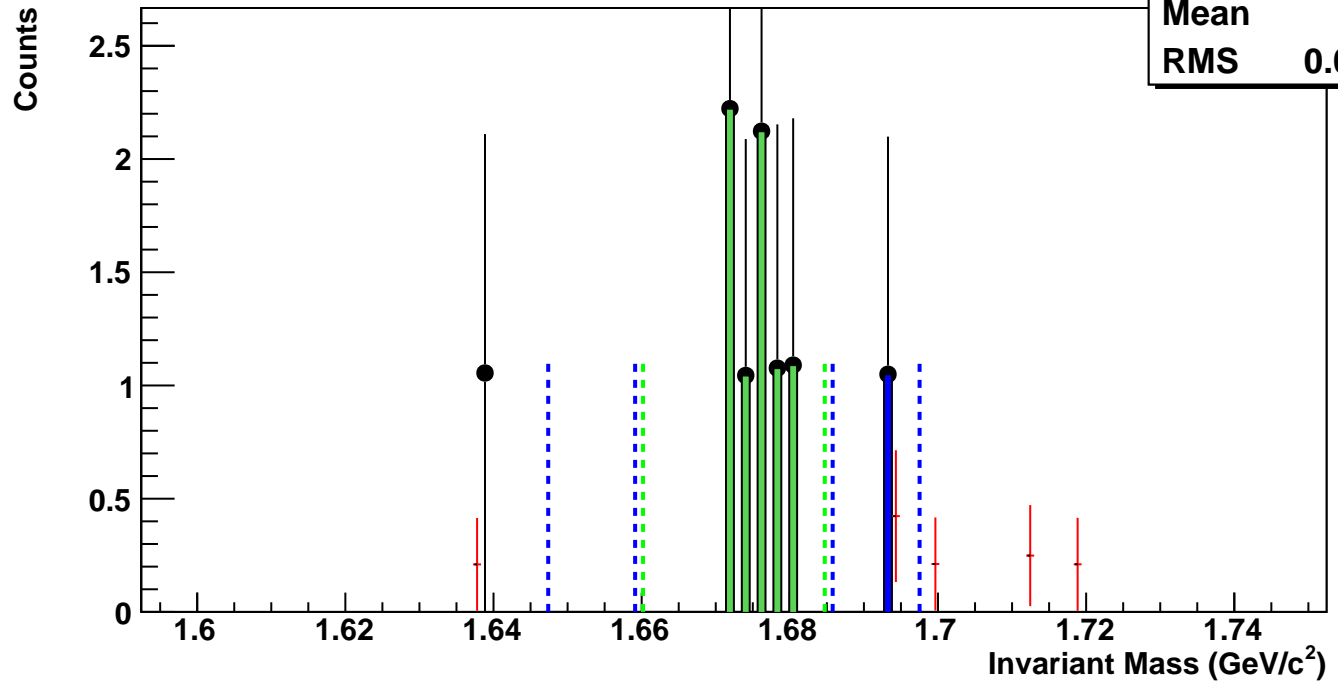
$\Omega^-$ , Au+Au 27 GeV, 0-10%,  $p_T$  2.0-2.4 GeV/c

hmlInvMassBgCent4Pt3	
Entries	549
Mean	1.676
RMS	0.02725



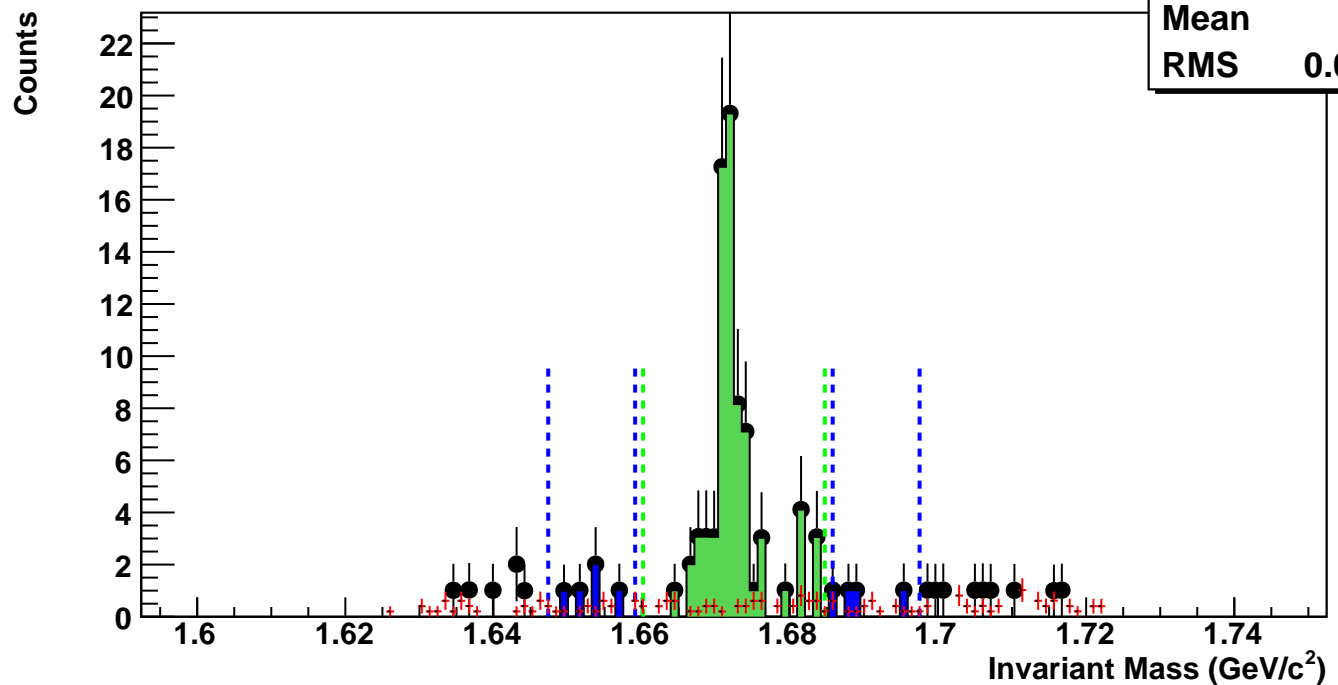
$\Omega^-$ , Au+Au 27 GeV, 60-80%,  $p_T$  2.4-2.8 GeV/c

hmlInvMassBgCent0Pt4	
Entries	0
Mean	1.693
RMS	0.02605



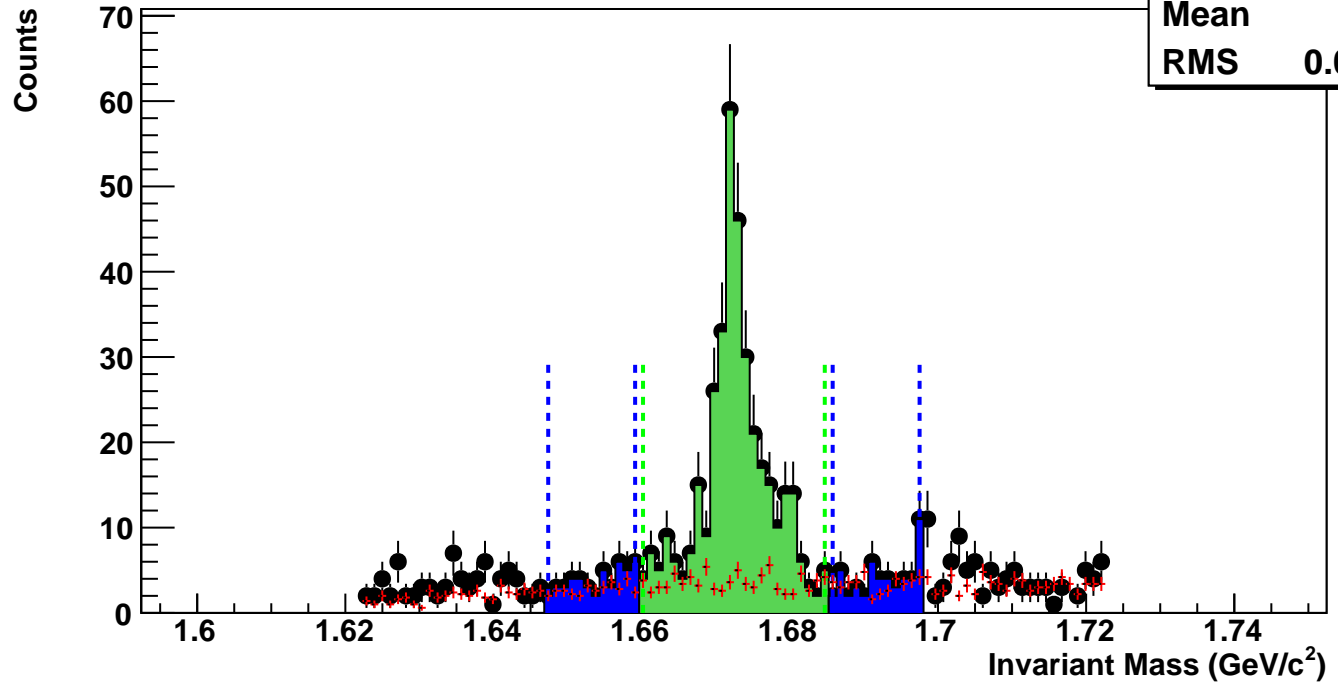
$\Omega^-$ , Au+Au 27 GeV, 40-60%,  $p_T$  2.4-2.8 GeV/c

hmlInvMassBgCent1Pt4	
Entries	3
Mean	1.677
RMS	0.02653



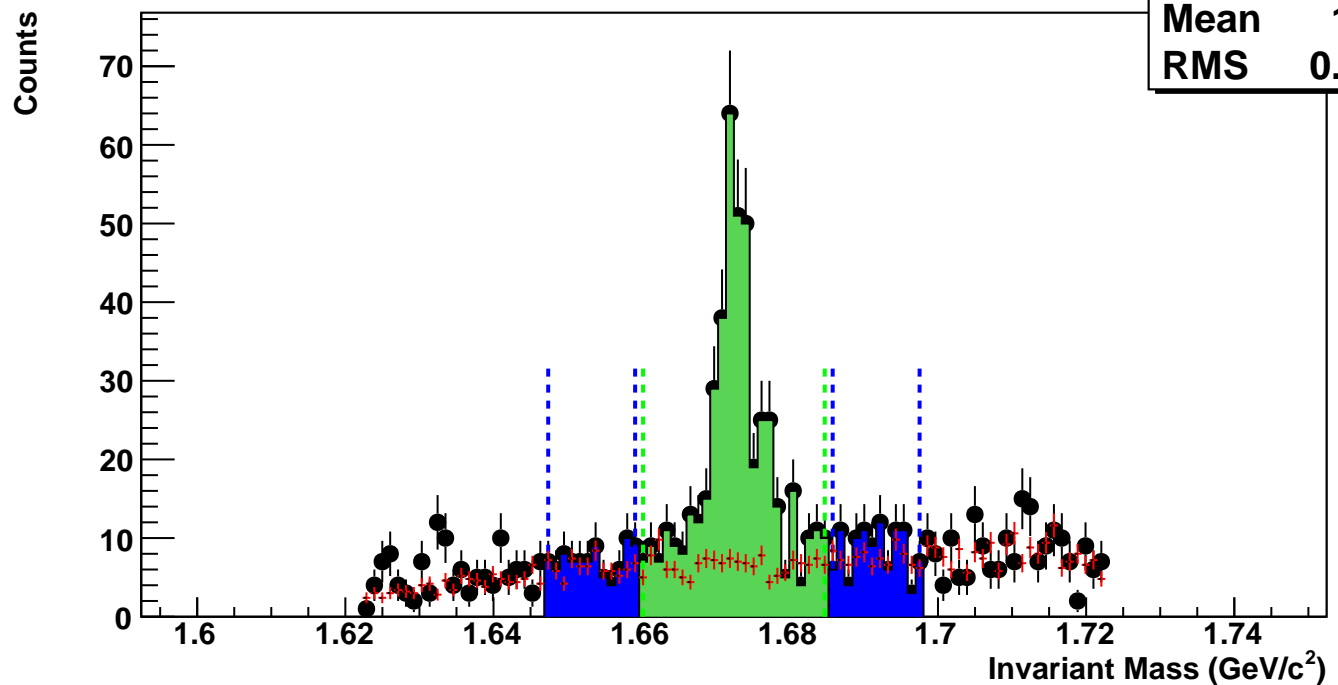
$\Omega^-$ , Au+Au 27 GeV, 20-40%,  $p_T$  2.4-2.8 GeV/c

hmlInvMassBgCent2Pt4	
Entries	34
Mean	1.677
RMS	0.02666



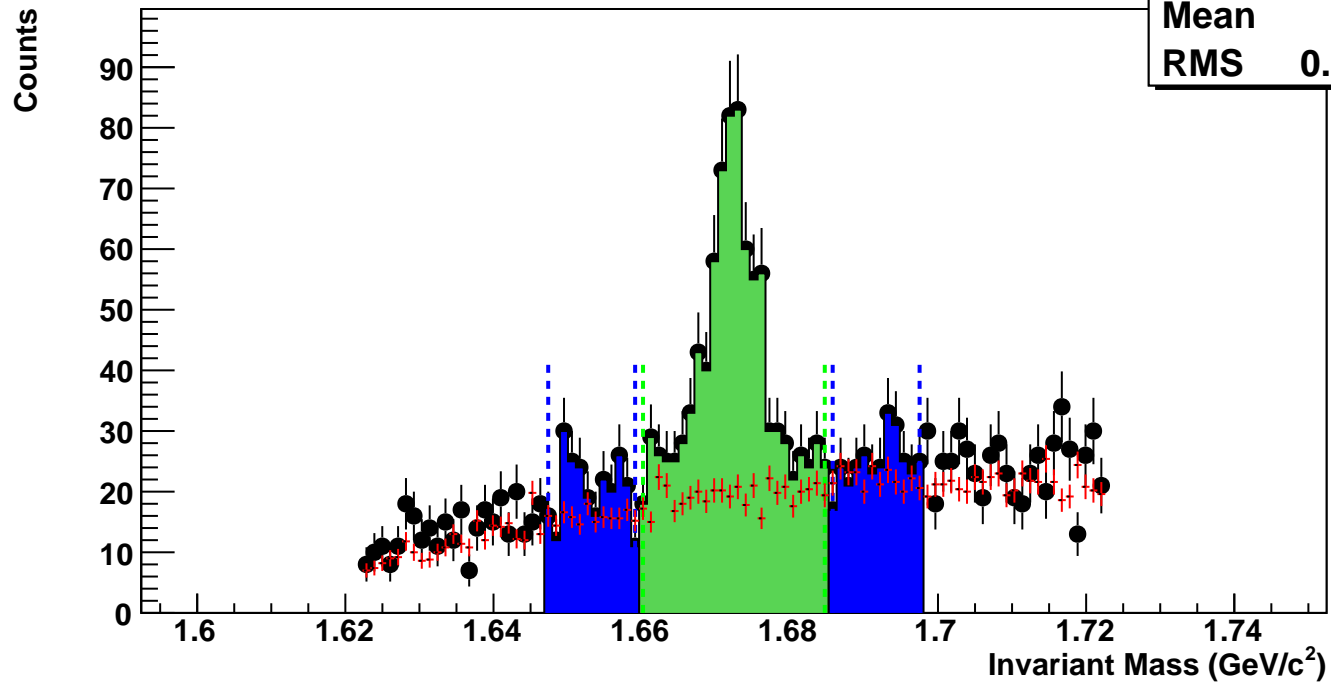
$\Omega^-$ , Au+Au 27 GeV, 10-20%,  $p_T$  2.4-2.8 GeV/c

hmlInvMassBgCent3Pt4	
Entries	73
Mean	1.679
RMS	0.0272



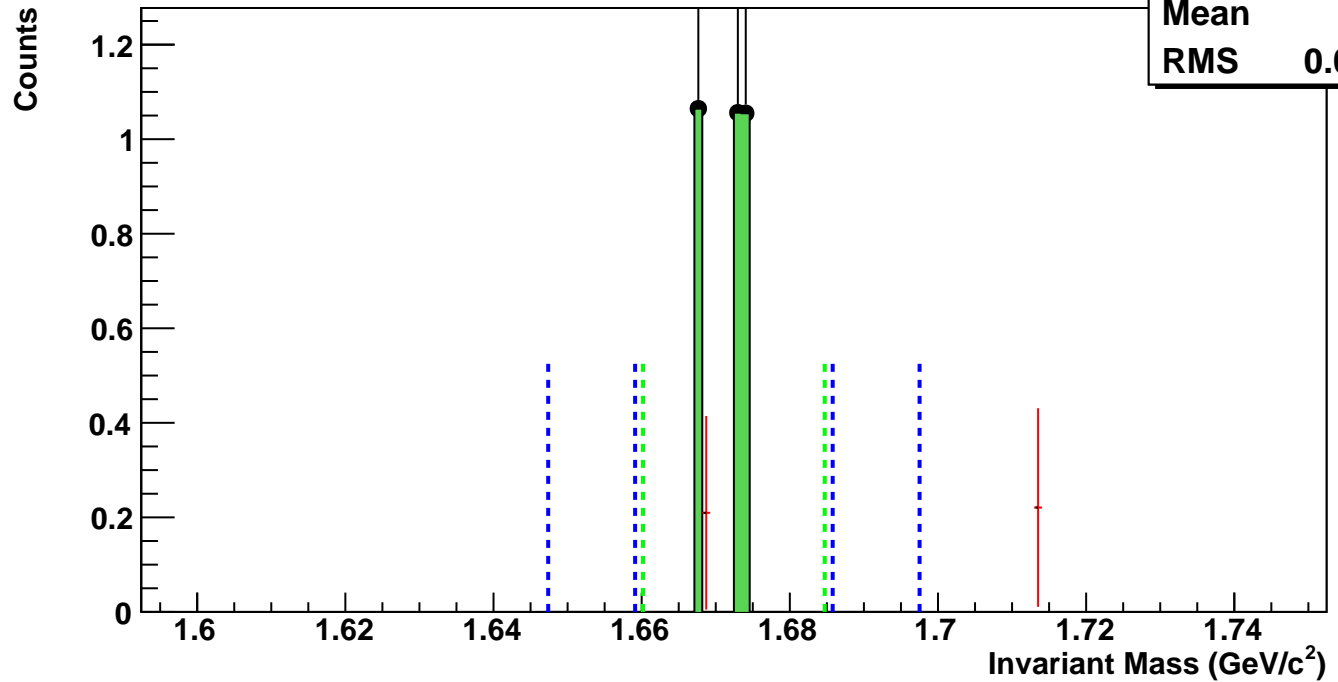
$\Omega^-$ , Au+Au 27 GeV, 0-10%,  $p_T$  2.4-2.8 GeV/c

hmlInvMassBgCent4Pt4  
Entries 204  
Mean 1.679  
RMS 0.02701



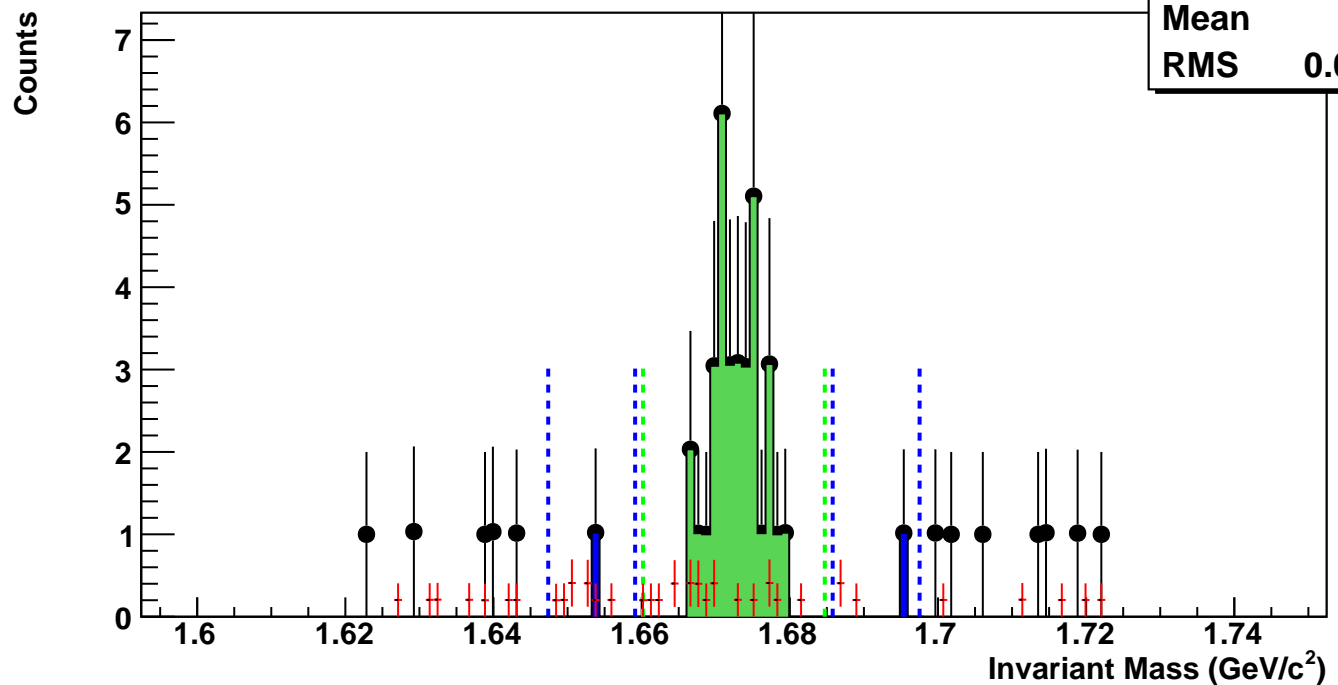
$\Omega^-$ , Au+Au 27 GeV, 60-80%,  $p_T$  2.8-3.6 GeV/c

hmlInvMassBgCent0Pt5	
Entries	0
Mean	1.692
RMS	0.02239



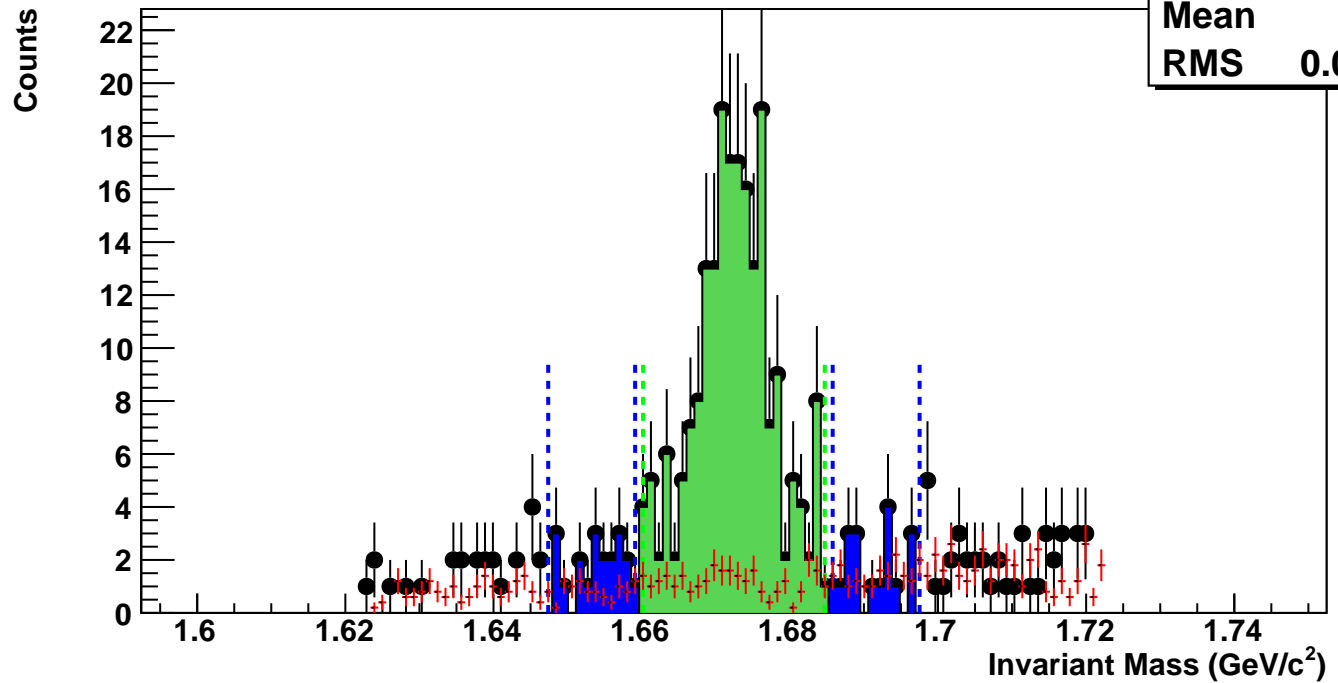
$\Omega^-$ , Au+Au 27 GeV, 40-60%,  $p_T$  2.8-3.6 GeV/c

hmlInvMassBgCent1Pt5	
Entries	1
Mean	1.667
RMS	0.02336



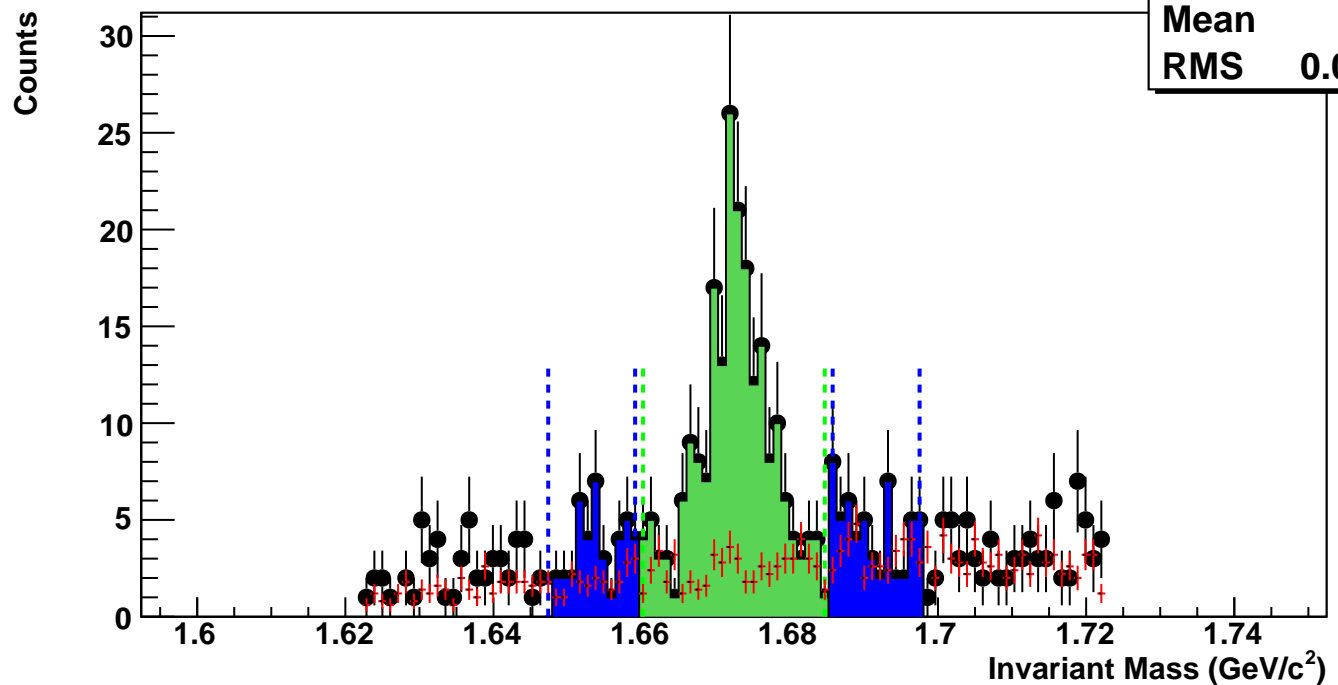
$\Omega^-$ , Au+Au 27 GeV, 20-40%,  $p_T$  2.8-3.6 GeV/c

hmlInvMassBgCent2Pt5	
Entries	13
Mean	1.68
RMS	0.02701



$\Omega^-$ , Au+Au 27 GeV, 10-20%,  $p_T$  2.8-3.6 GeV/c

hmlInvMassBgCent3Pt5	
Entries	26
Mean	1.68
RMS	0.02641



$\Omega^-$ , Au+Au 27 GeV, 0-10%,  $p_T$  2.8-3.6 GeV/c

hmlInvMassBgCent4Pt5

Entries 77

Mean 1.68

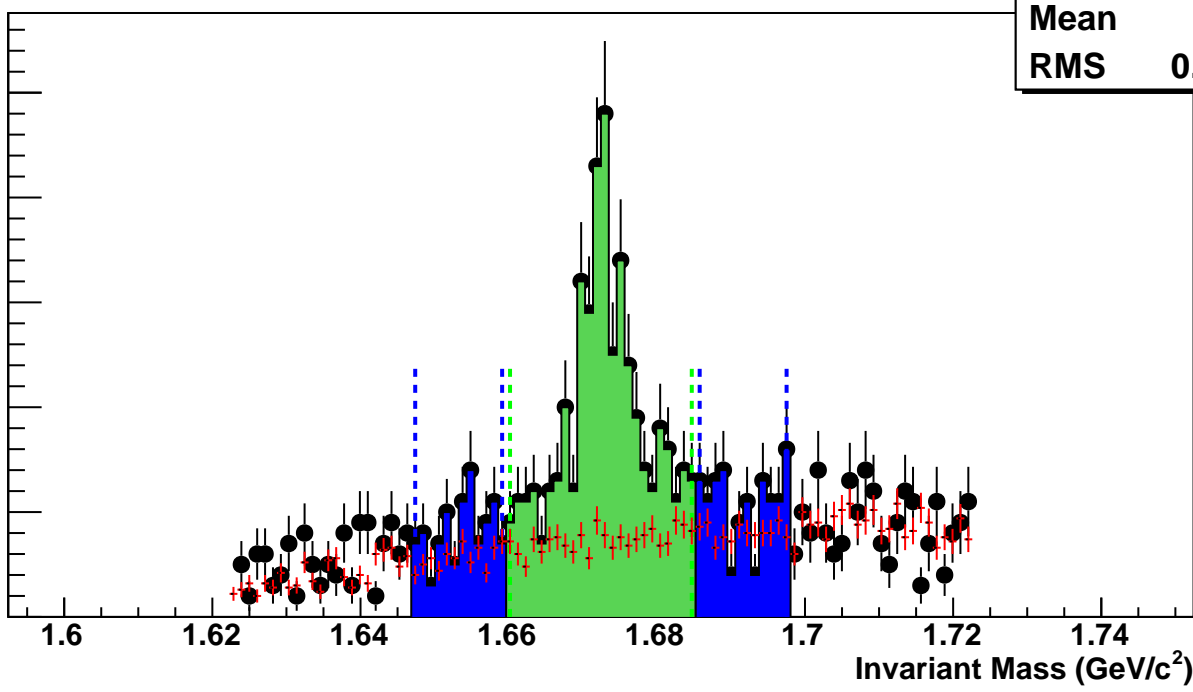
RMS 0.02672

Counts

50  
40  
30  
20  
10  
0

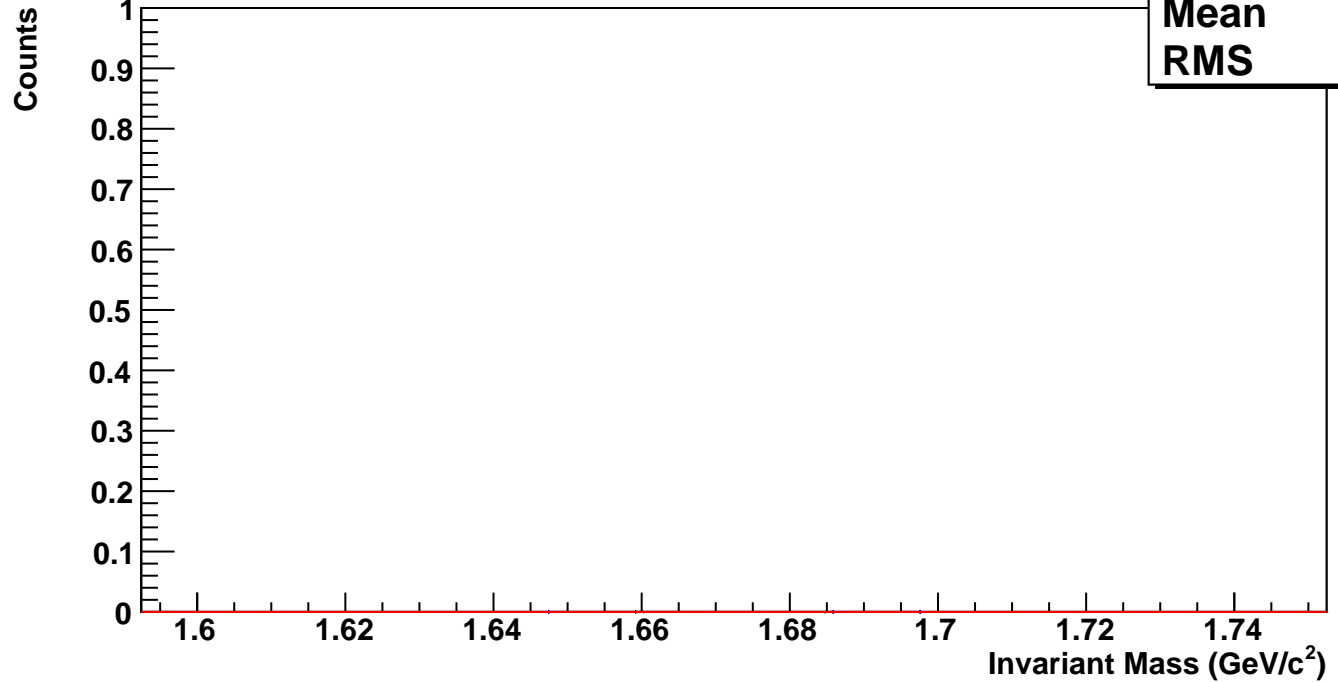
1.6 1.62 1.64 1.66 1.68 1.7 1.72 1.74

Invariant Mass (GeV/c<sup>2</sup>)



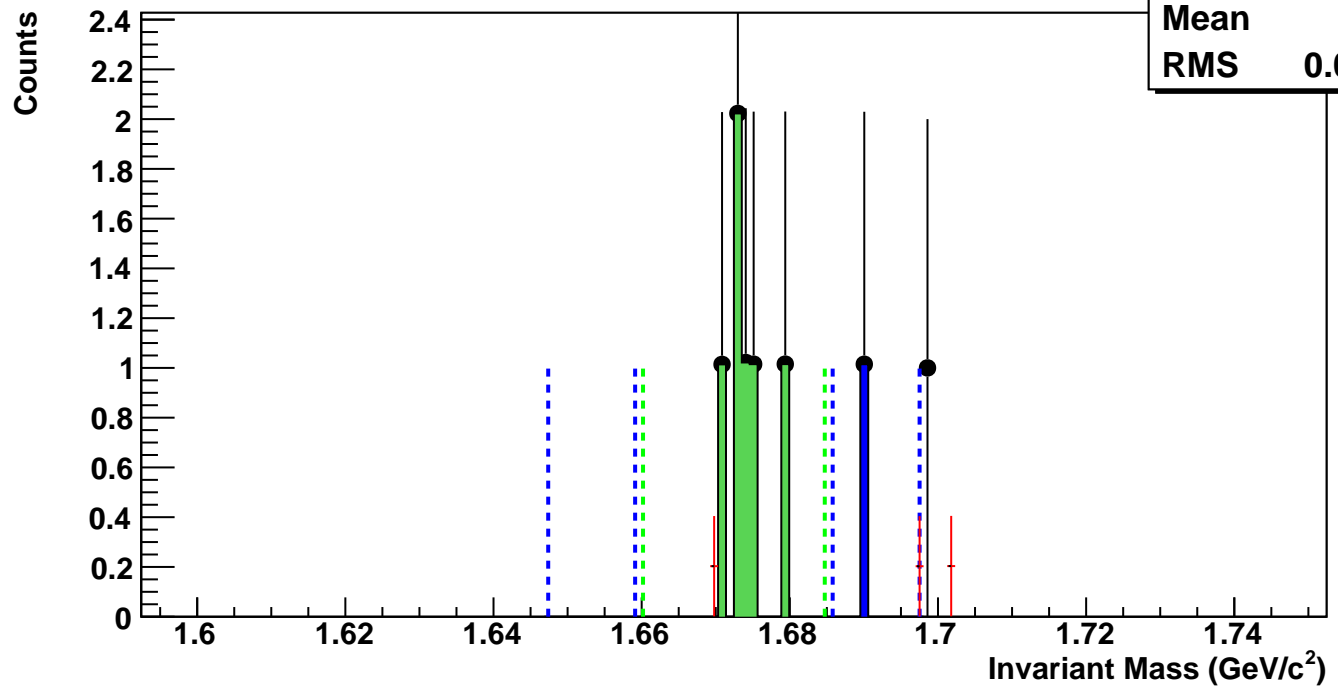
$\Omega^-$ , Au+Au 27 GeV, 60-80%,  $p_T$  3.6-5.0 GeV/c

hmlInvMassBgCent0Pt6	
Entries	0
Mean	0
RMS	0



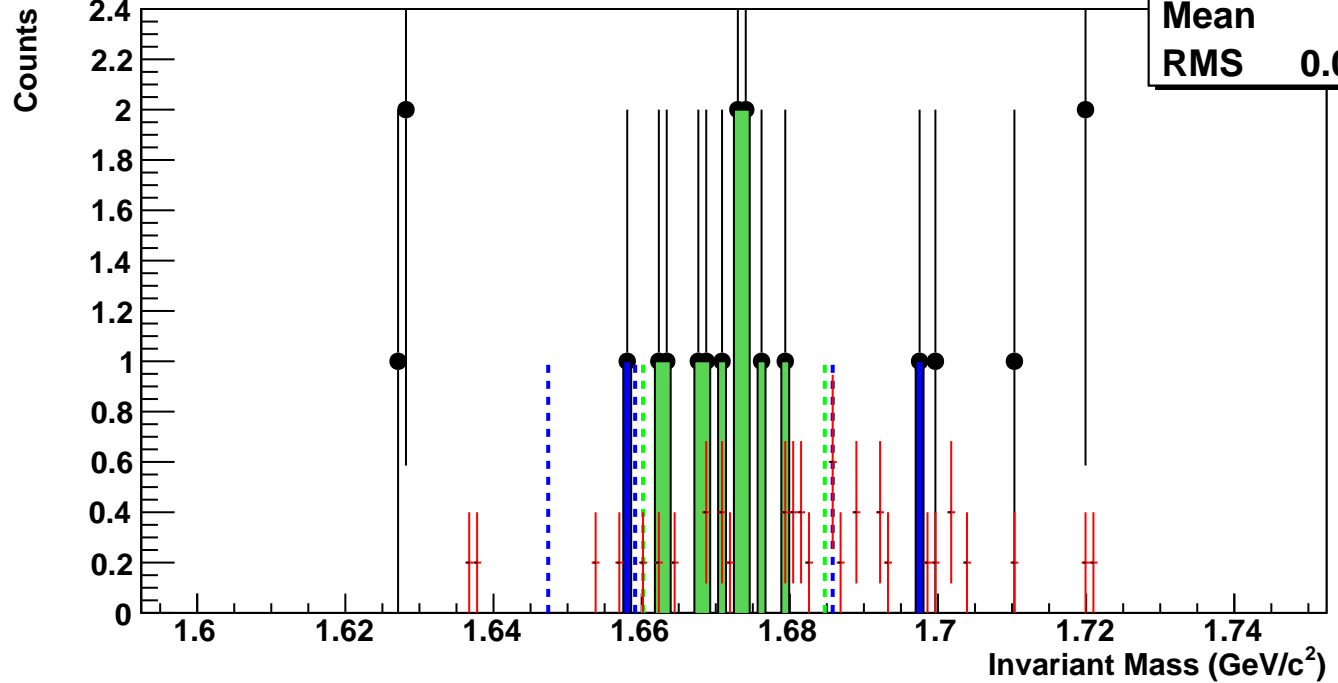
$\Omega^-$ , Au+Au 27 GeV, 40-60%,  $p_T$  3.6-5.0 GeV/c

hmlInvMassBgCent1Pt6	
Entries	0
Mean	1.69
RMS	0.01419



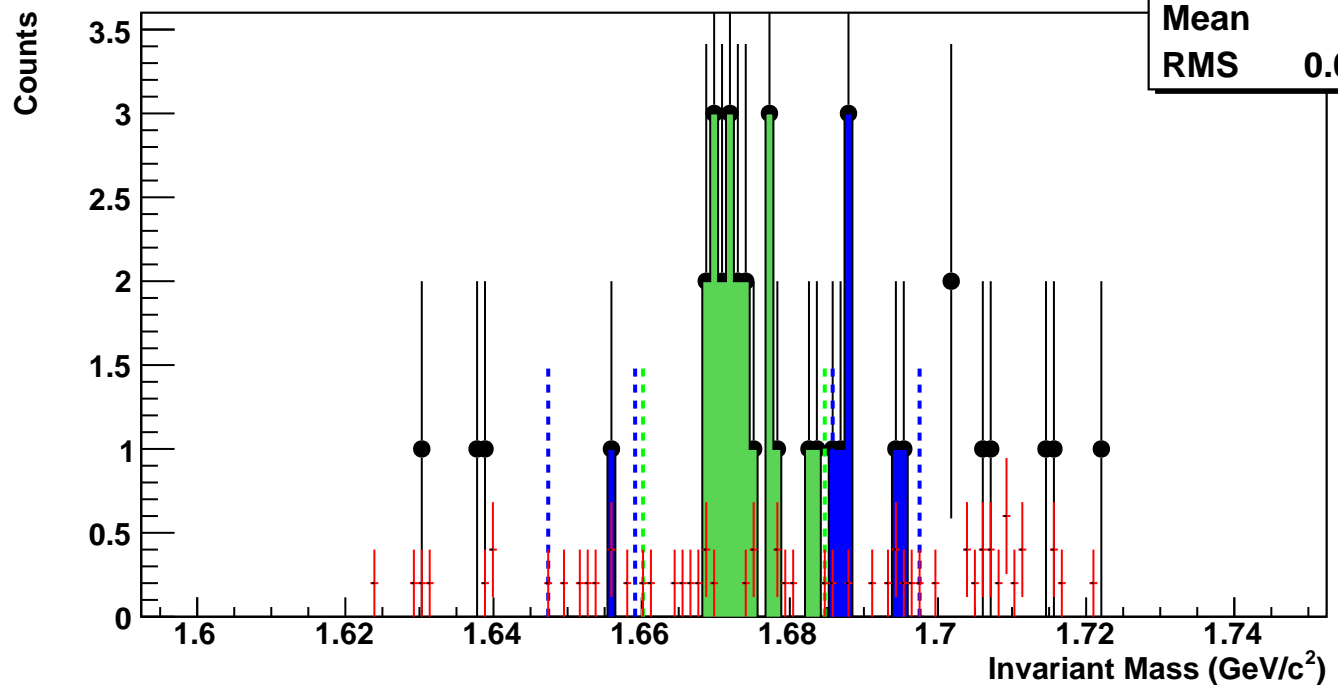
$\Omega^-$ , Au+Au 27 GeV, 20-40%,  $p_T$  3.6-5.0 GeV/c

hmlInvMassBgCent2Pt6	
Entries	1
Mean	1.682
RMS	0.01931



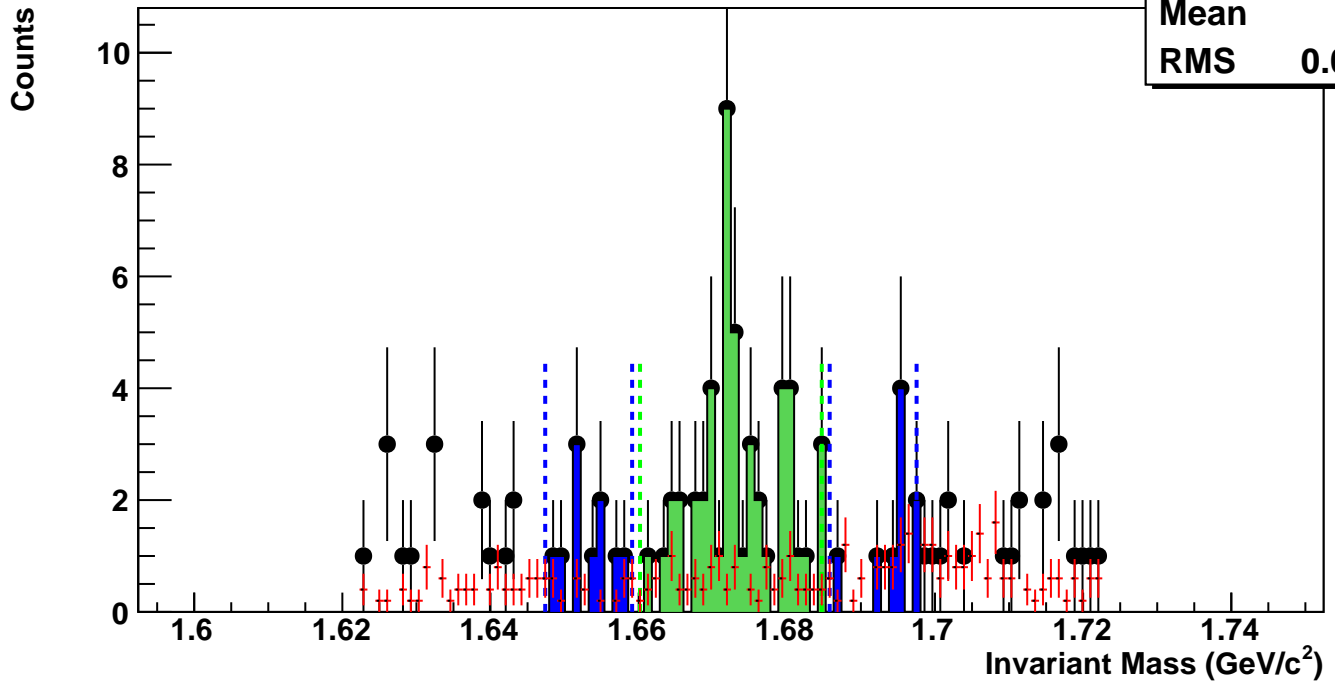
$\Omega^-$ , Au+Au 27 GeV, 10-20%,  $p_T$  3.6-5.0 GeV/c

hmlInvMassBgCent3Pt6	
Entries	1
Mean	1.68
RMS	0.02638



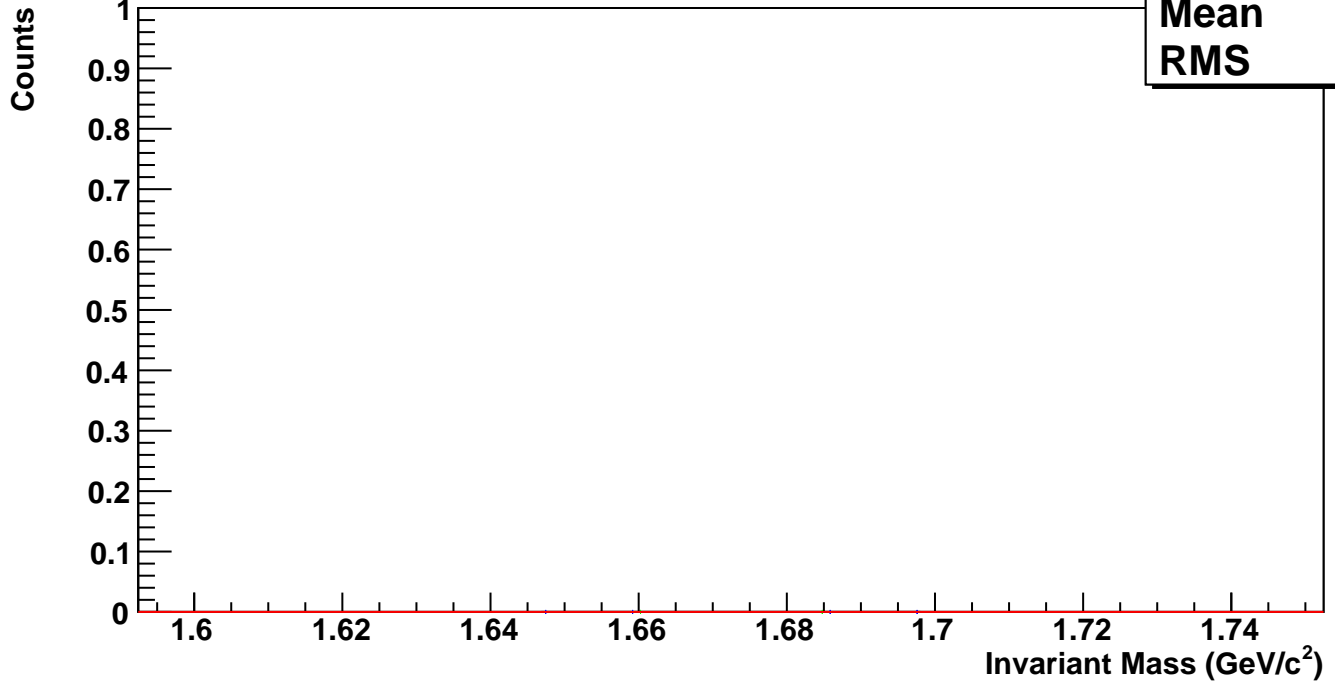
$\Omega^-$ , Au+Au 27 GeV, 0-10%,  $p_T$  3.6-5.0 GeV/c

hmlInvMassBgCent4Pt6	
Entries	6
Mean	1.68
RMS	0.02669



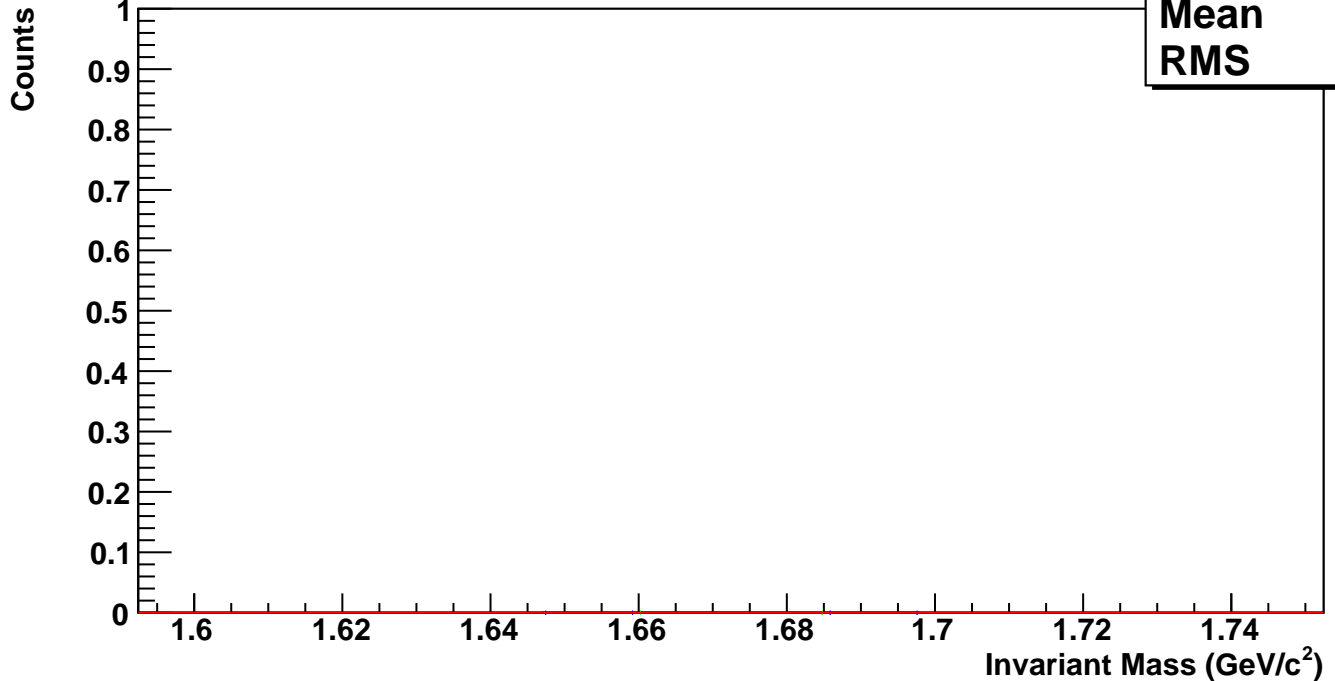
$\Omega^-$ , Au+Au 27 GeV, 60-80%,  $p_T$  5.0-7.0 GeV/c

hmlInvMassBgCent0Pt7	
Entries	0
Mean	0
RMS	0



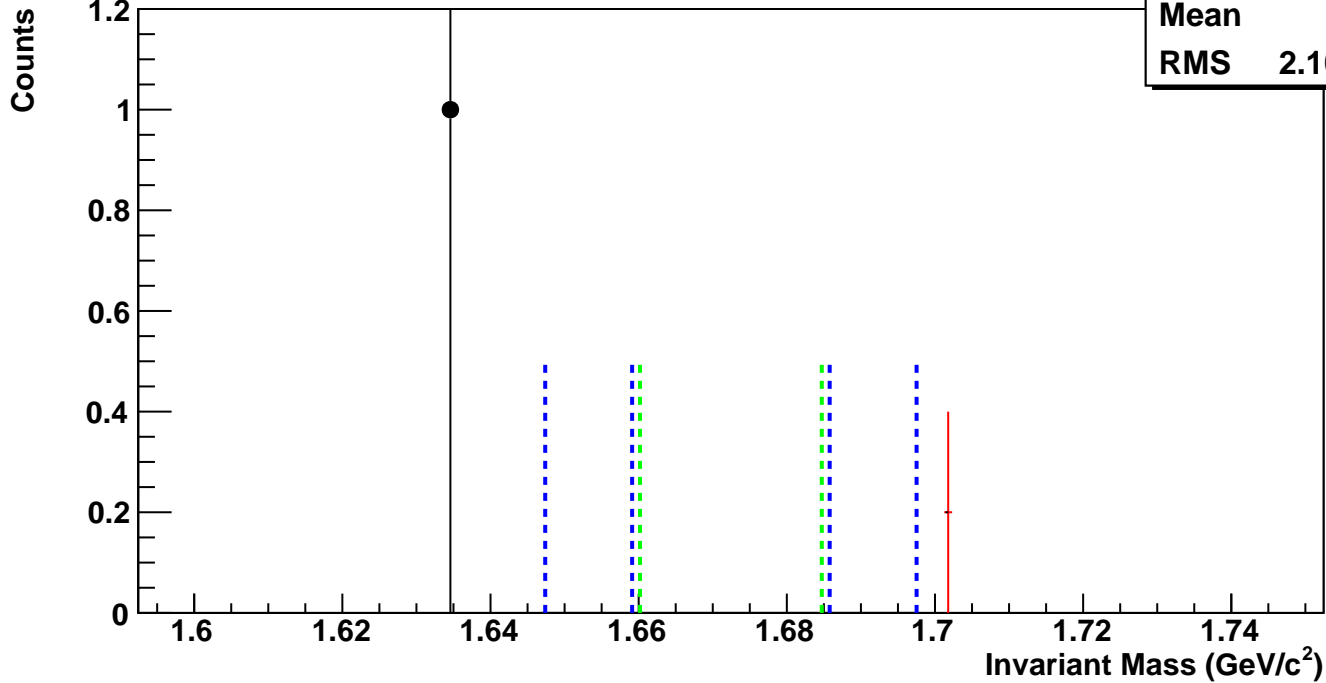
$\Omega^-$ , Au+Au 27 GeV, 40-60%,  $p_T$  5.0-7.0 GeV/c

hmlInvMassBgCent1Pt7	
Entries	0
Mean	0
RMS	0



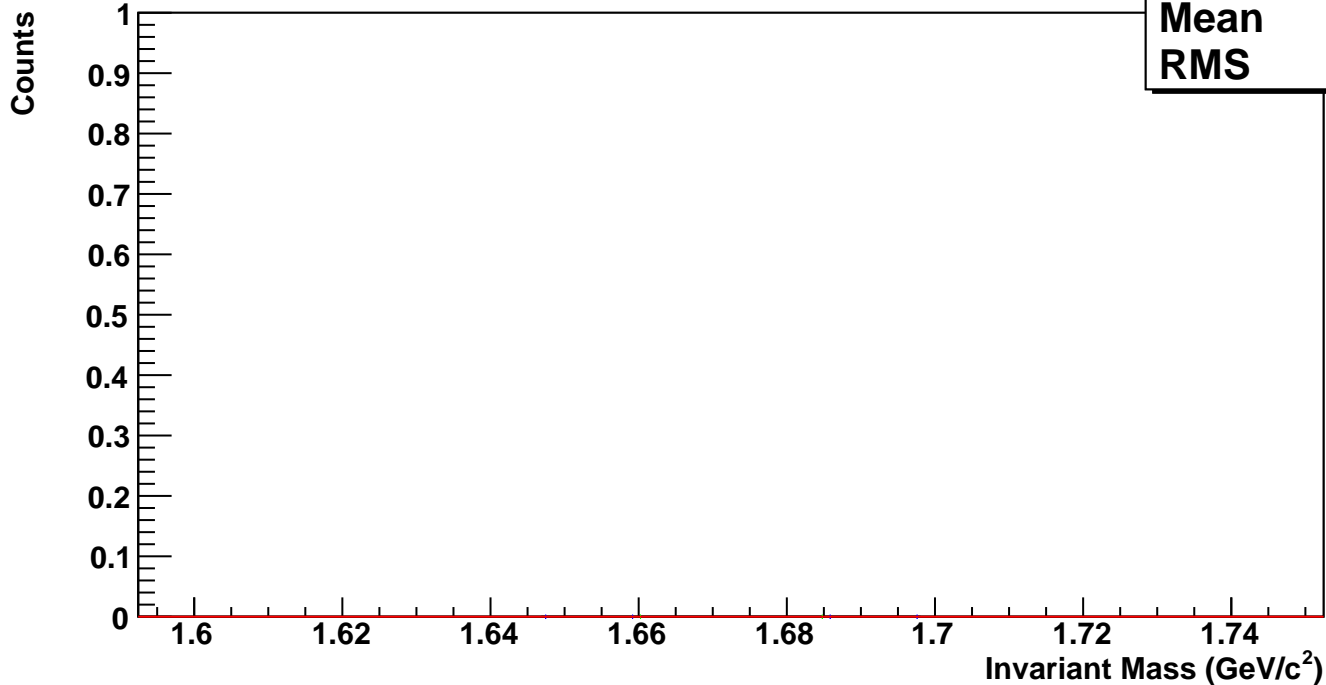
$\Omega^-$ , Au+Au 27 GeV, 20-40%,  $p_T$  5.0-7.0 GeV/c

hmlInvMassBgCent2Pt7	
Entries	0
Mean	1.702
RMS	2.107e-08



$\Omega^-$ , Au+Au 27 GeV, 10-20%,  $p_T$  5.0-7.0 GeV/c

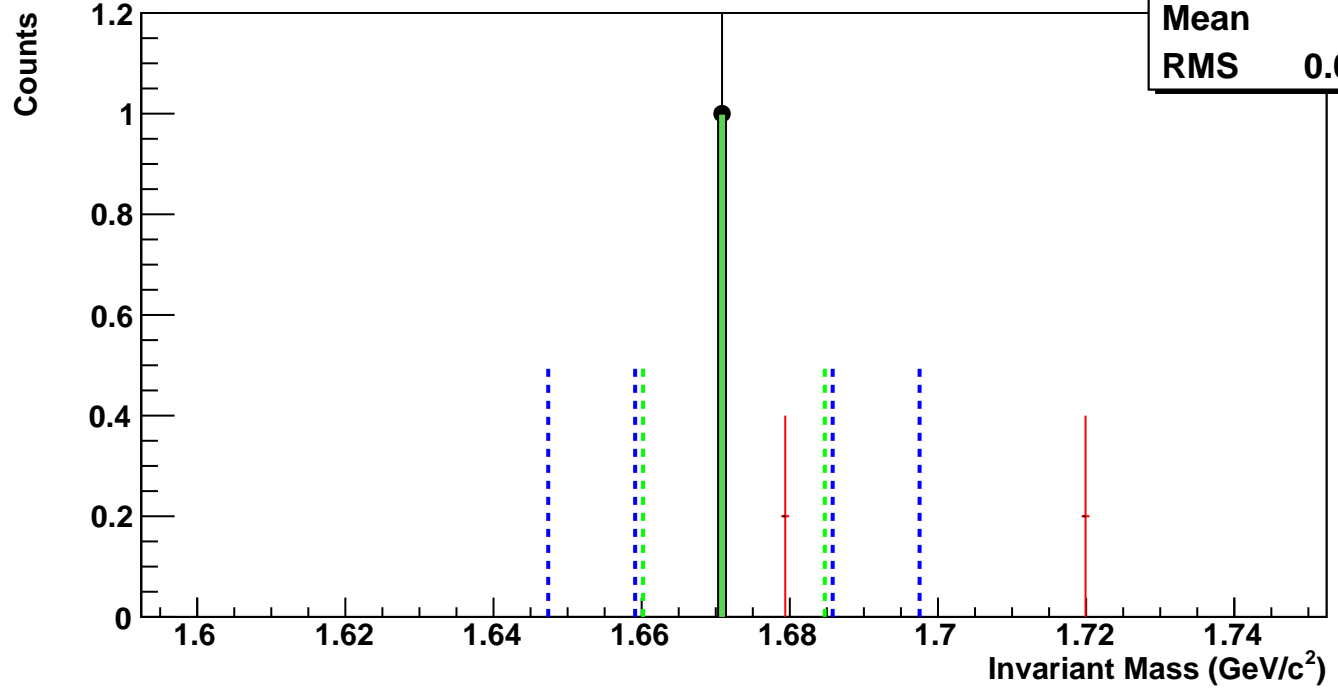
hmlInvMassBgCent3Pt7	
Entries	0
Mean	0
RMS	0



$\Omega^-$ , Au+Au 27 GeV, 0-10%,  $p_T$  5.0-7.0 GeV/c

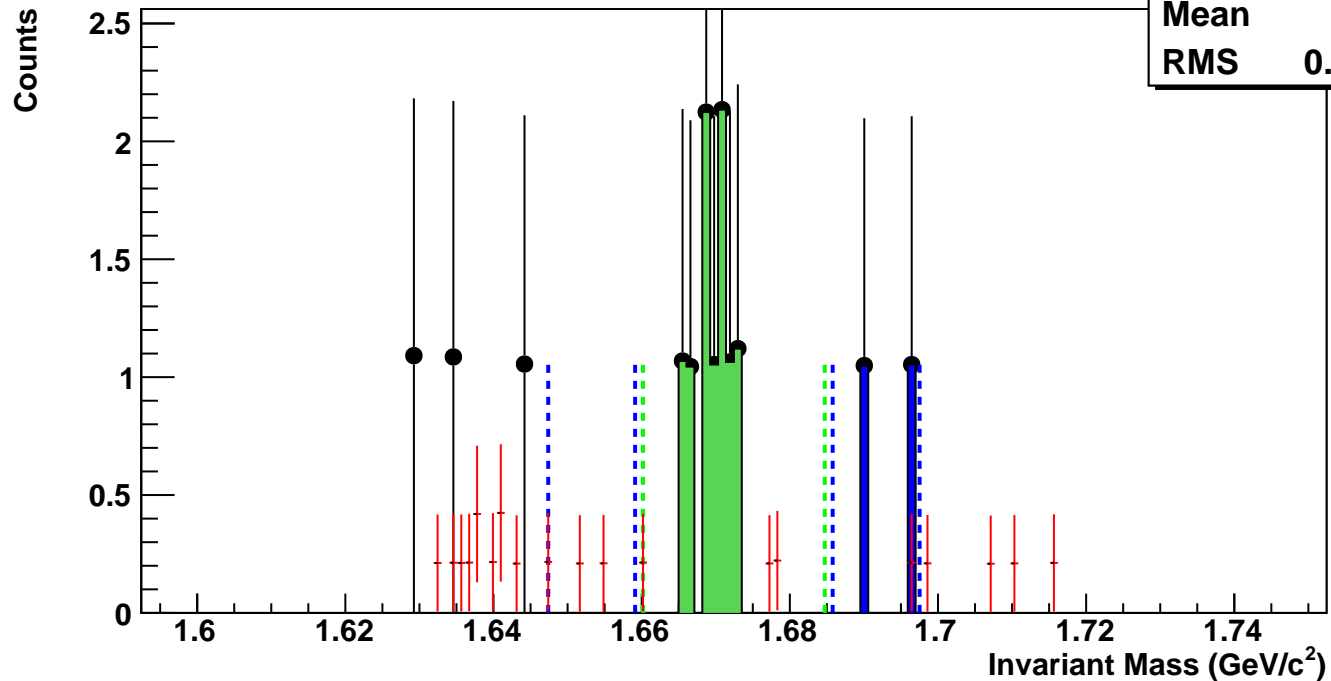
hmlnvMassBgCent4Pt7

Entries	0
Mean	1.7
RMS	0.02027



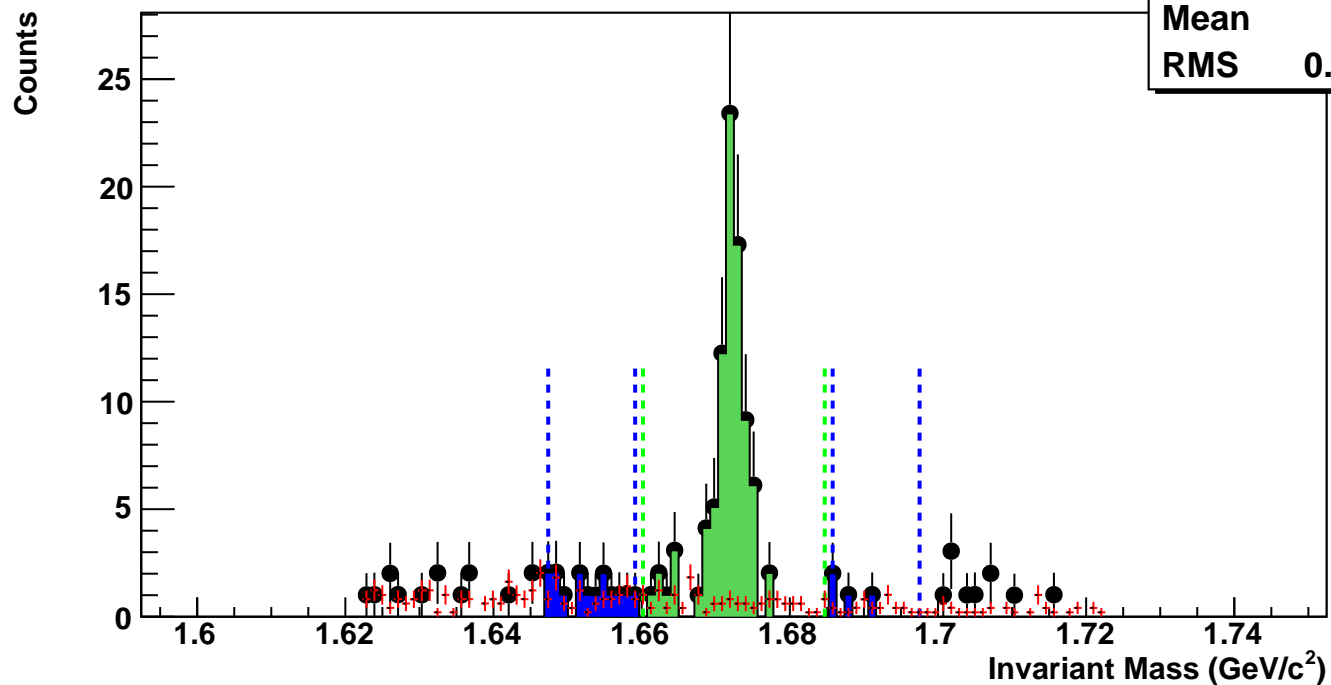
$\Omega^+$ , Au+Au 27 GeV, 60-80%,  $p_T$  0.8-1.2 GeV/c

hmlInvMassBgCent0Pt0	
Entries	1
Mean	1.661
RMS	0.02797



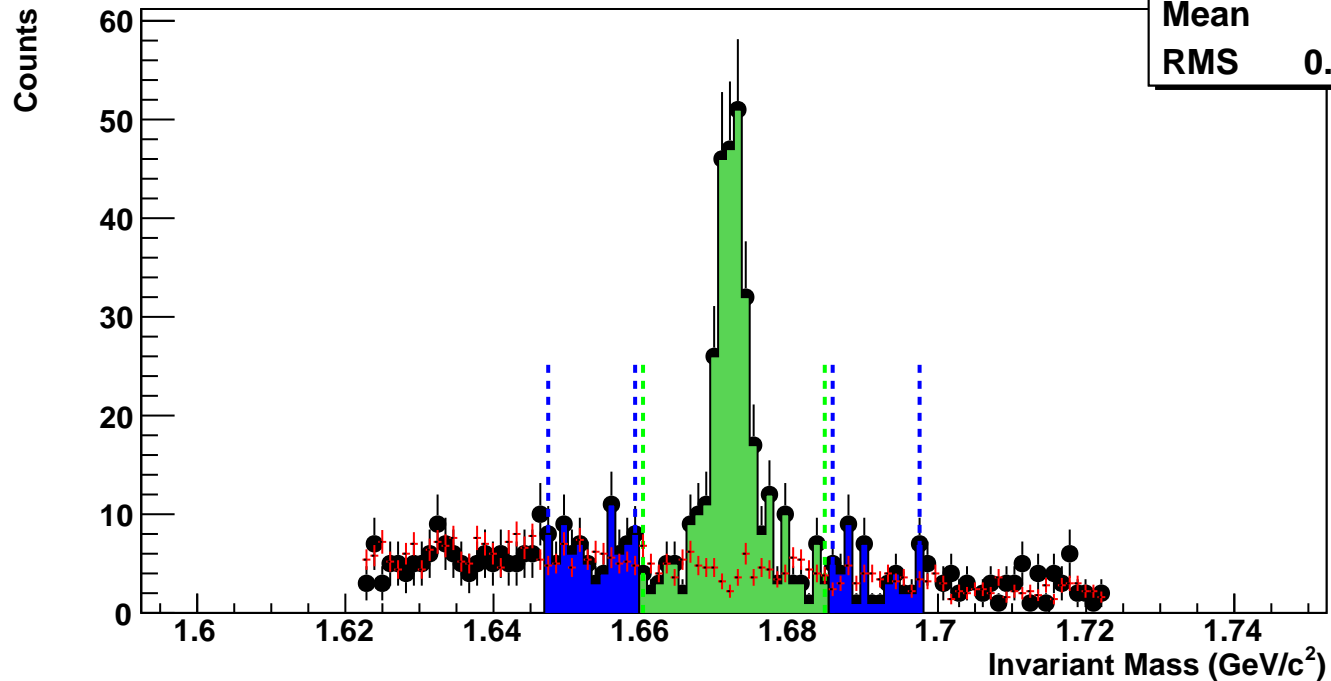
$\Omega^+$ , Au+Au 27 GeV, 40-60%,  $p_T$  0.8-1.2 GeV/c

hmlInvMassBgCent1Pt0	
Entries	7
Mean	1.662
RMS	0.02544



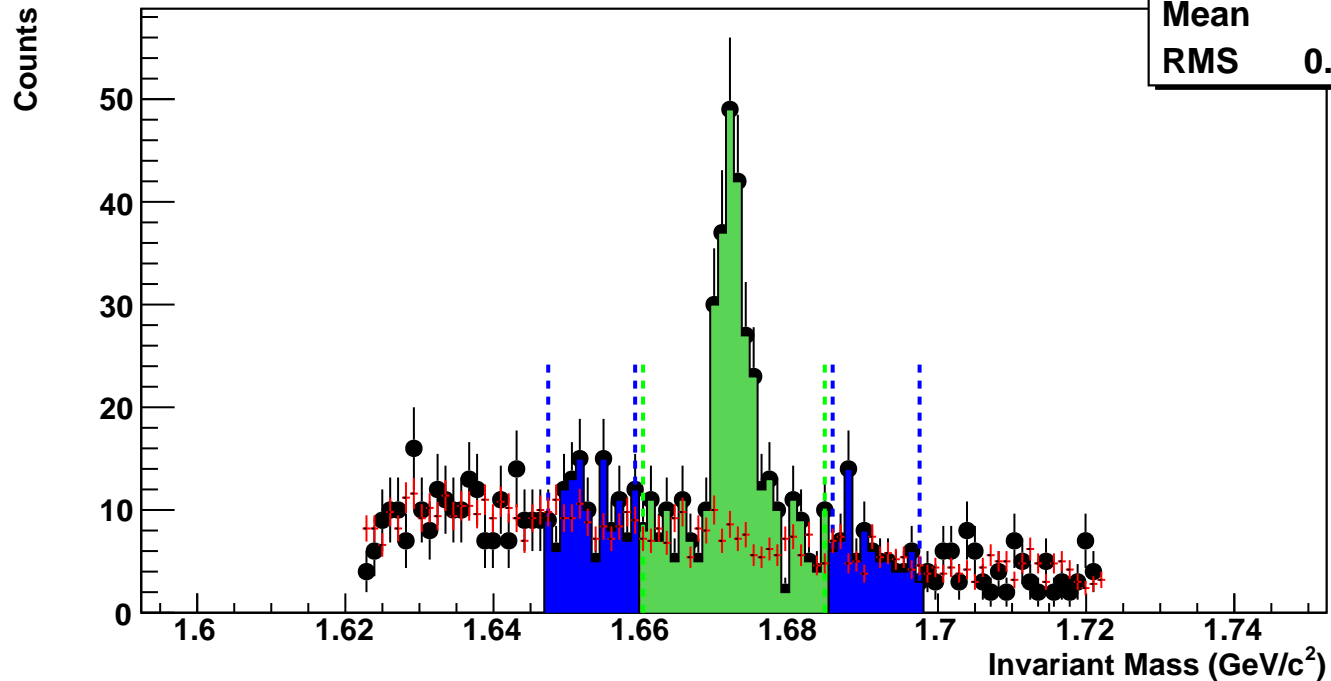
$\Omega^+$ , Au+Au 27 GeV, 20-40%,  $p_T$  0.8-1.2 GeV/c

hmlInvMassBgCent2Pt0	
Entries	51
Mean	1.663
RMS	0.02688



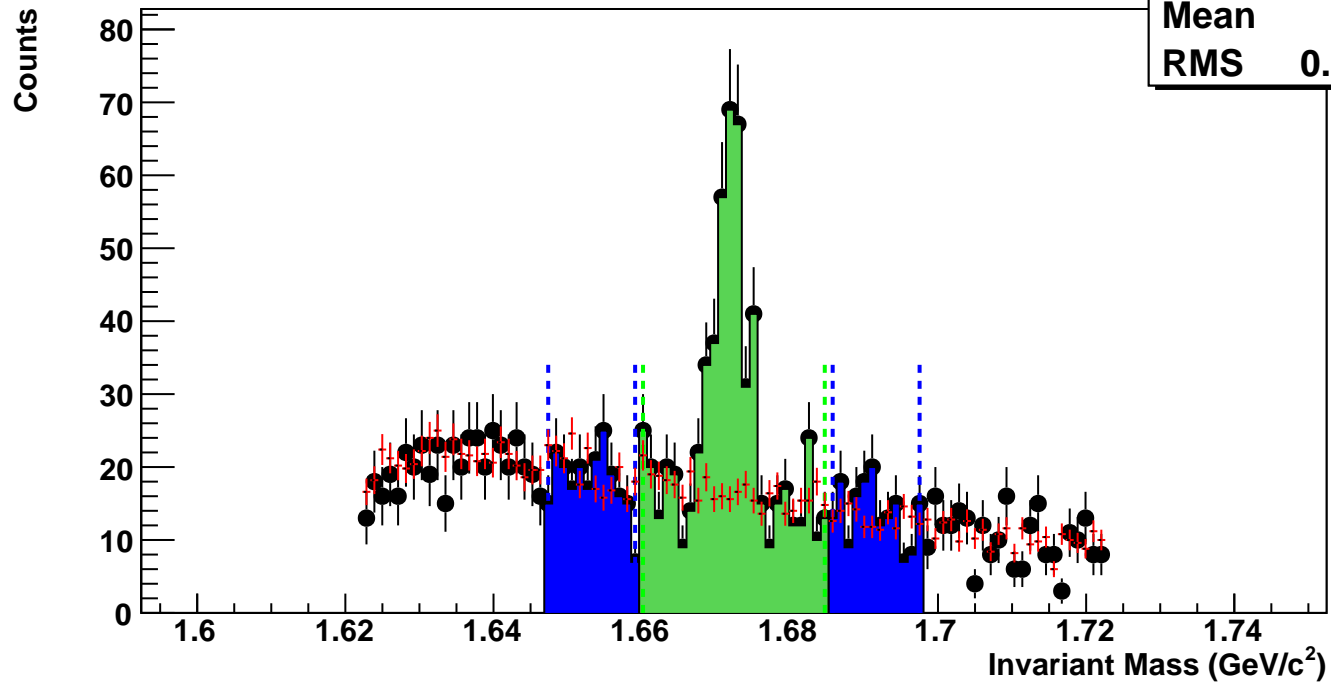
$\Omega^+$ , Au+Au 27 GeV, 10-20%,  $p_T$  0.8-1.2 GeV/c

hmlInvMassBgCent3Pt0	
Entries	80
Mean	1.664
RMS	0.02714



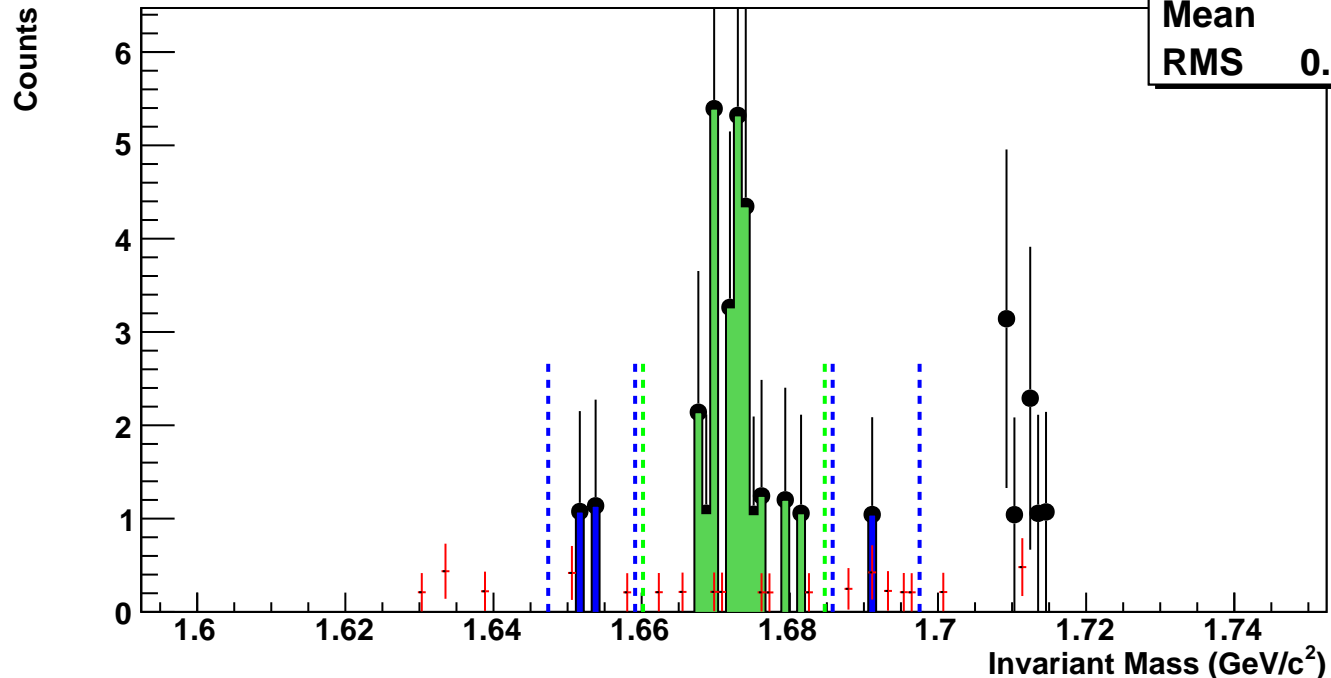
$\Omega^+$ , Au+Au 27 GeV, 0-10%,  $p_T$  0.8-1.2 GeV/c

hmlnvMassBgCent4Pt0  
Entries 185  
Mean 1.665  
RMS 0.02761



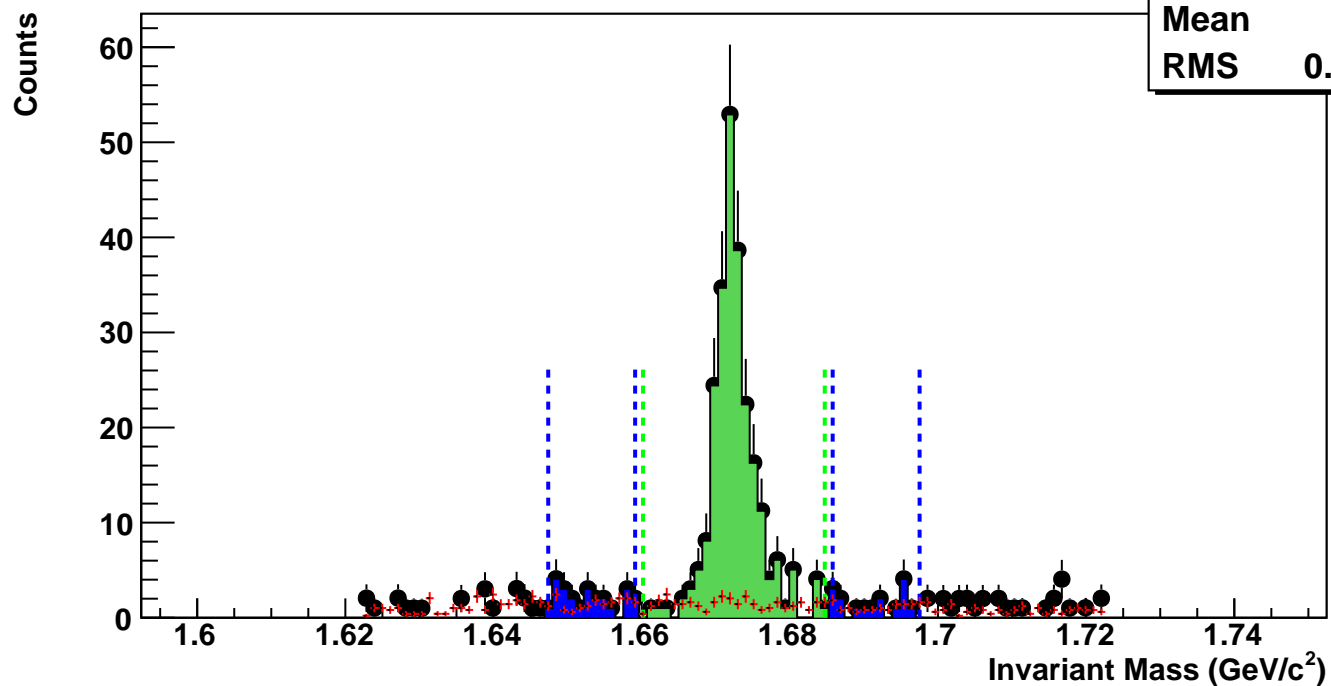
$\bar{\Omega}^+$ , Au+Au 27 GeV, 60-80%,  $p_T$  1.2-1.6 GeV/c

hmlInvMassBgCent0Pt1	
Entries	1
Mean	1.673
RMS	0.02461



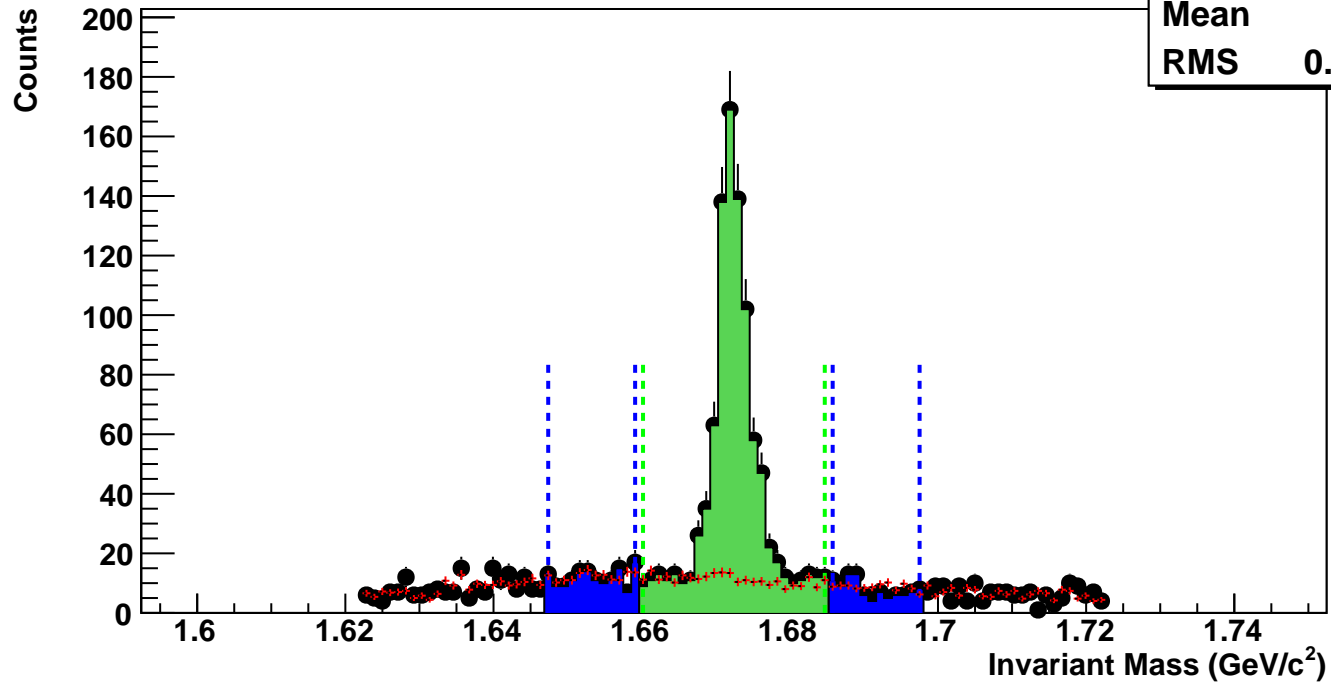
$\bar{\Omega}^+$ , Au+Au 27 GeV, 40-60%,  $p_T$  1.2-1.6 GeV/c

hmlInvMassBgCent1Pt1	
Entries	13
Mean	1.669
RMS	0.02568



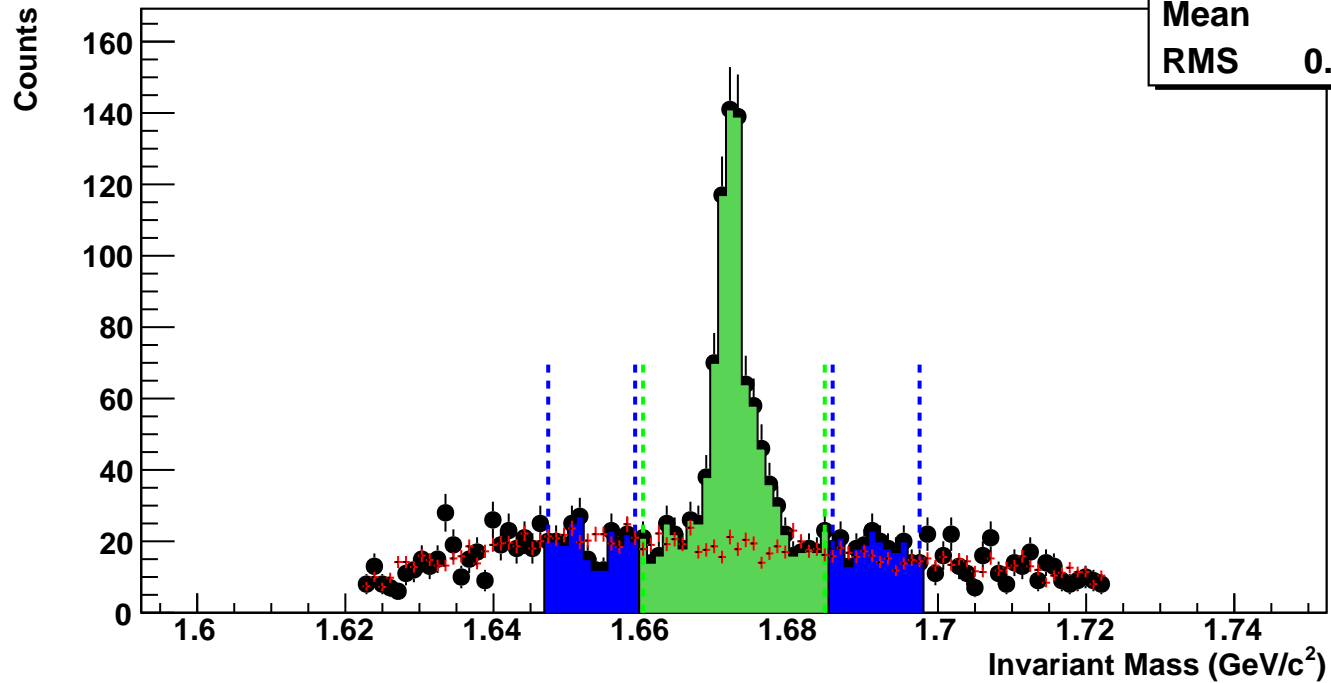
$\Omega^+$ , Au+Au 27 GeV, 20-40%,  $p_T$  1.2-1.6 GeV/c

hmlInvMassBgCent2Pt1
Entries 105
Mean 1.669
RMS 0.02592



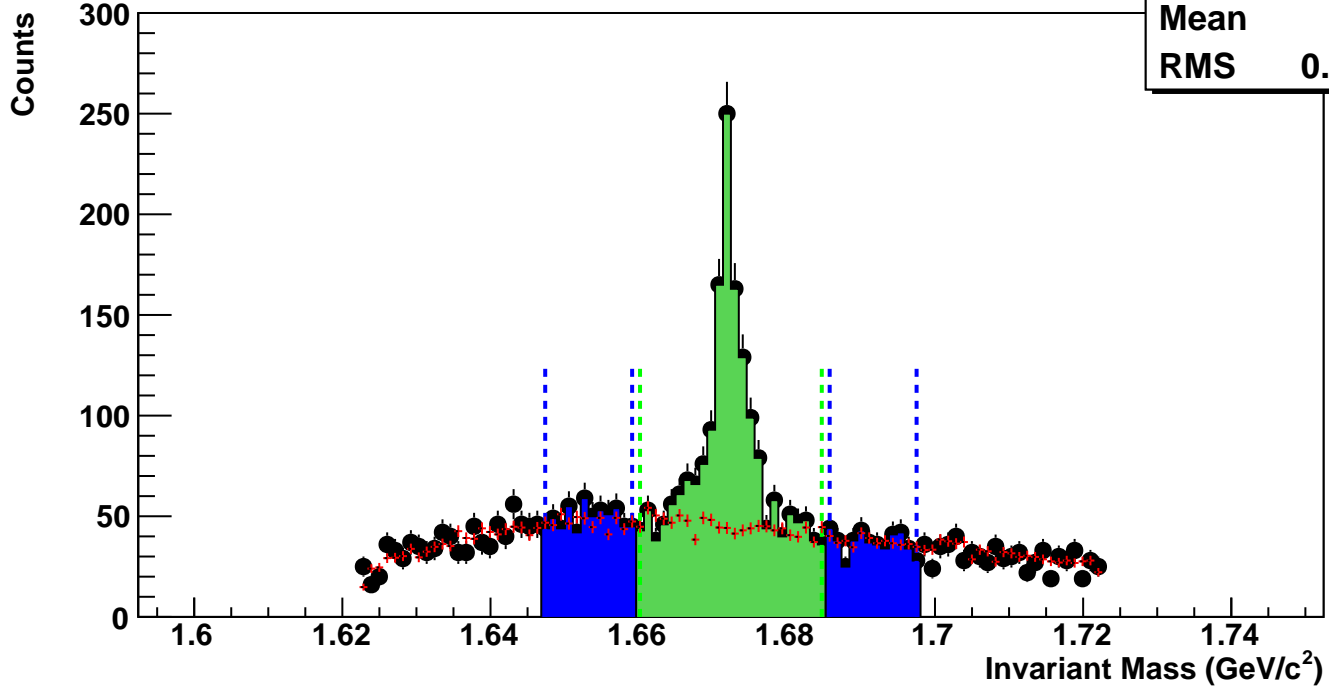
$\Omega^+$ , Au+Au 27 GeV, 10-20%,  $p_T$  1.2-1.6 GeV/c

hmlInvMassBgCent3Pt1
Entries 186
Mean 1.67
RMS 0.02643



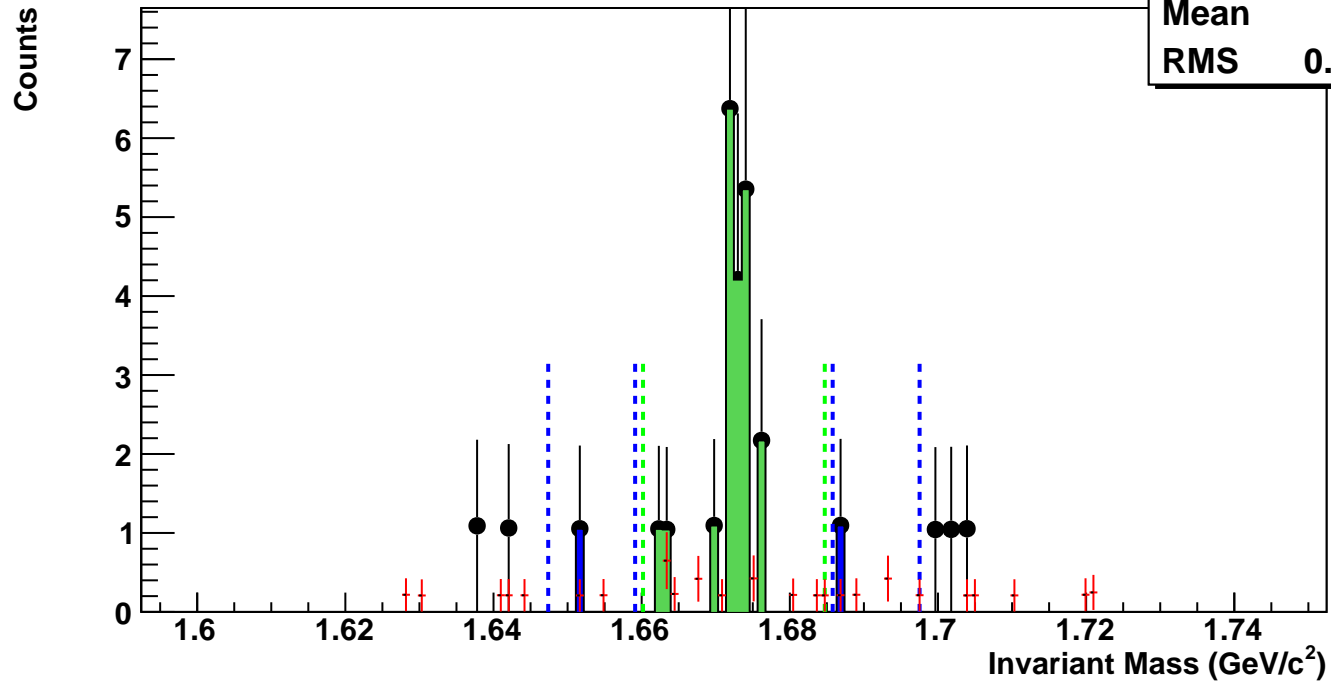
$\Omega^+$ , Au+Au 27 GeV, 0-10%,  $p_T$  1.2-1.6 GeV/c

hmlInvMassBgCent4Pt1
Entries 441
Mean 1.671
RMS 0.02665



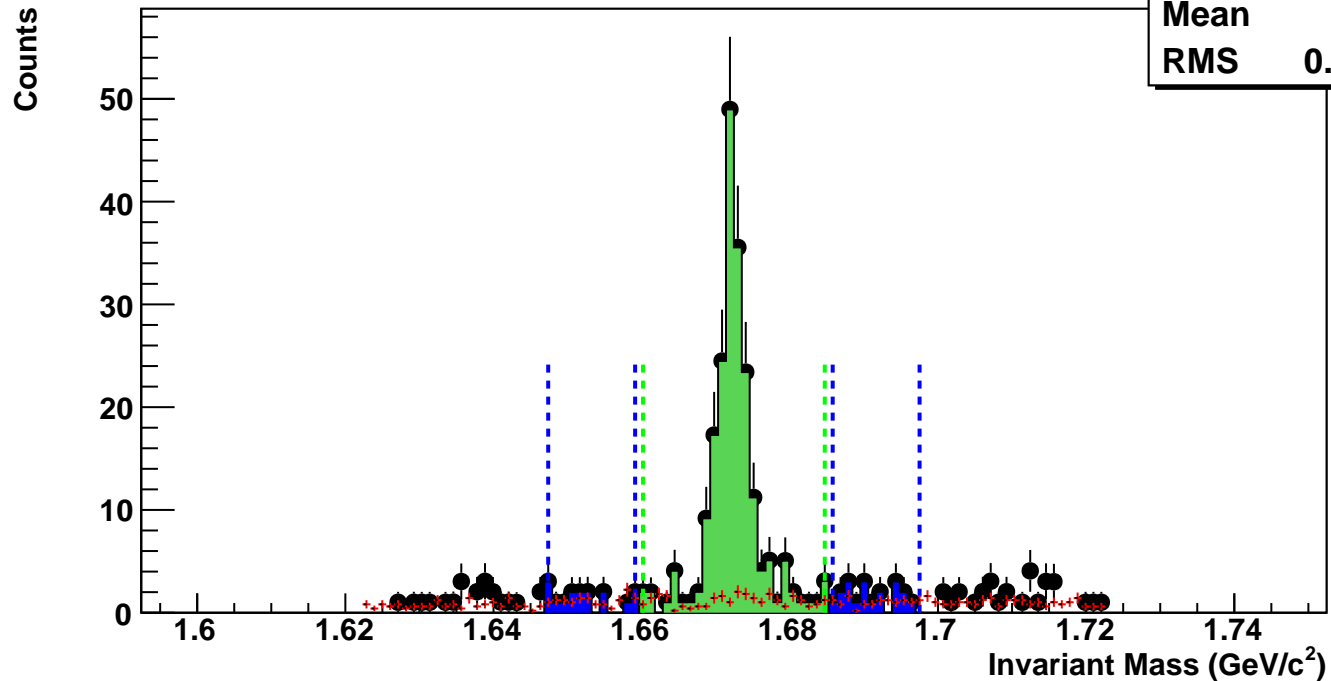
$\bar{\Omega}^+$ , Au+Au 27 GeV, 60-80%,  $p_T$  1.6-2.0 GeV/c

hmlInvMassBgCent0Pt2	
Entries	1
Mean	1.675
RMS	0.02492



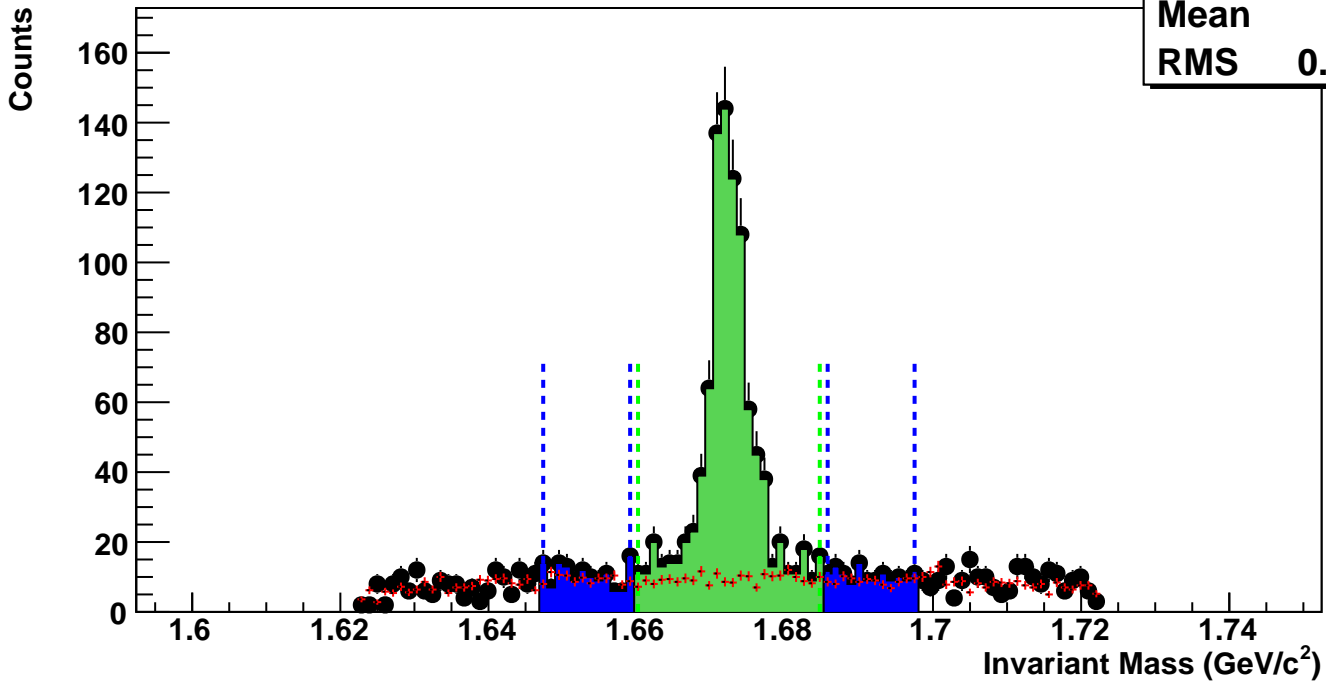
$\bar{\Omega}^+$ , Au+Au 27 GeV, 40-60%,  $p_T$  1.6-2.0 GeV/c

hmlInvMassBgCent1Pt2	
Entries	11
Mean	1.674
RMS	0.02693



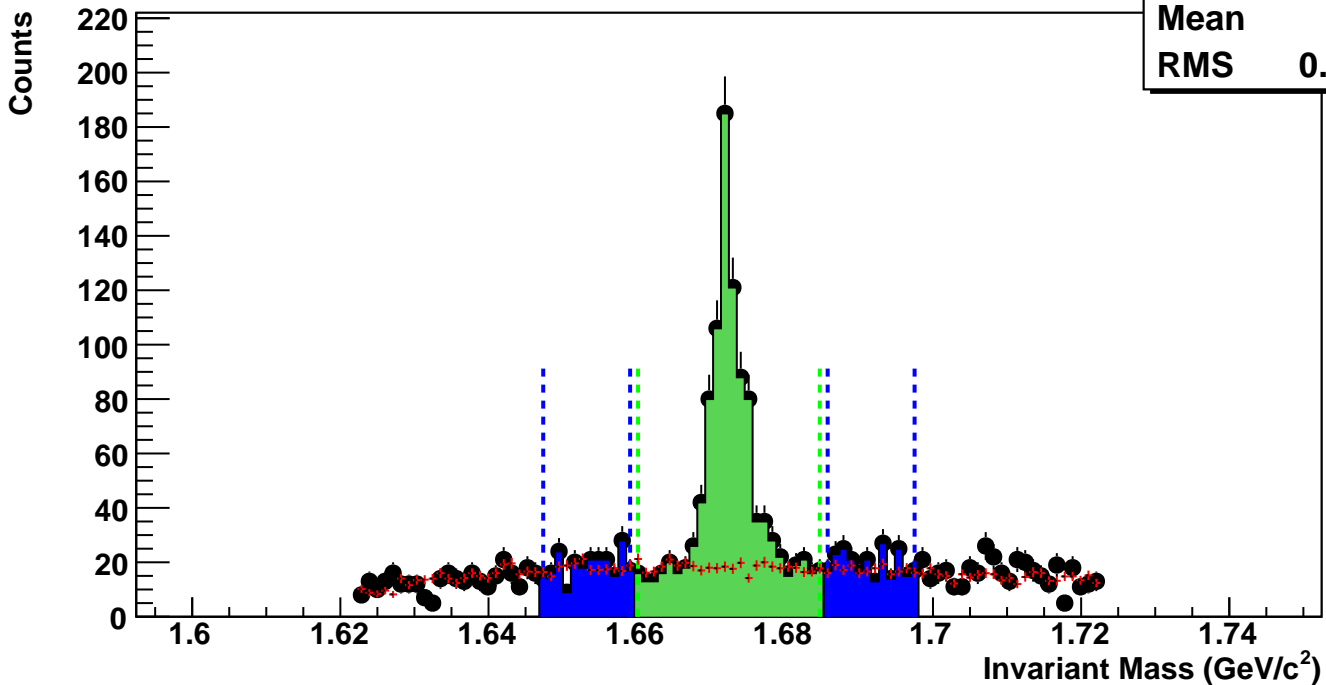
$\Omega^+$ , Au+Au 27 GeV, 20-40%,  $p_T$  1.6-2.0 GeV/c

hmlInvMassBgCent2Pt2	
Entries	97
Mean	1.673
RMS	0.02711



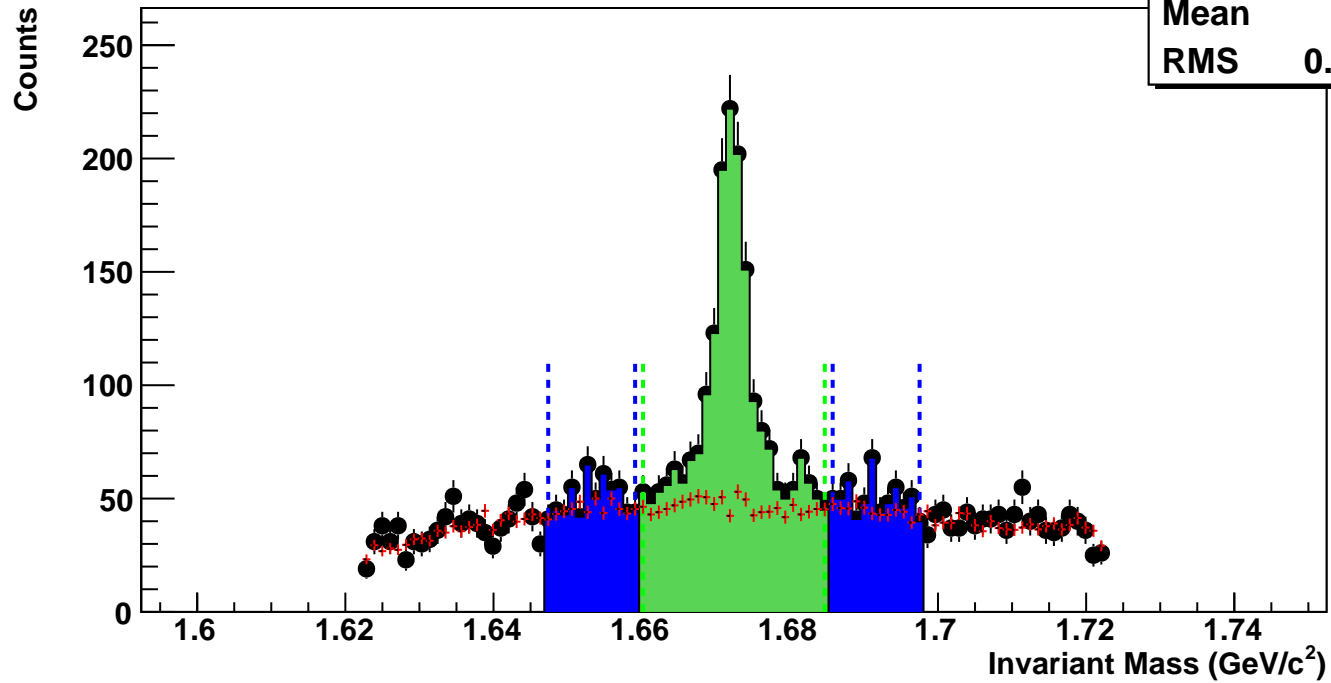
$\Omega^+$ , Au+Au 27 GeV, 10-20%,  $p_T$  1.6-2.0 GeV/c

hmlInvMassBgCent3Pt2	
Entries	184
Mean	1.673
RMS	0.02715



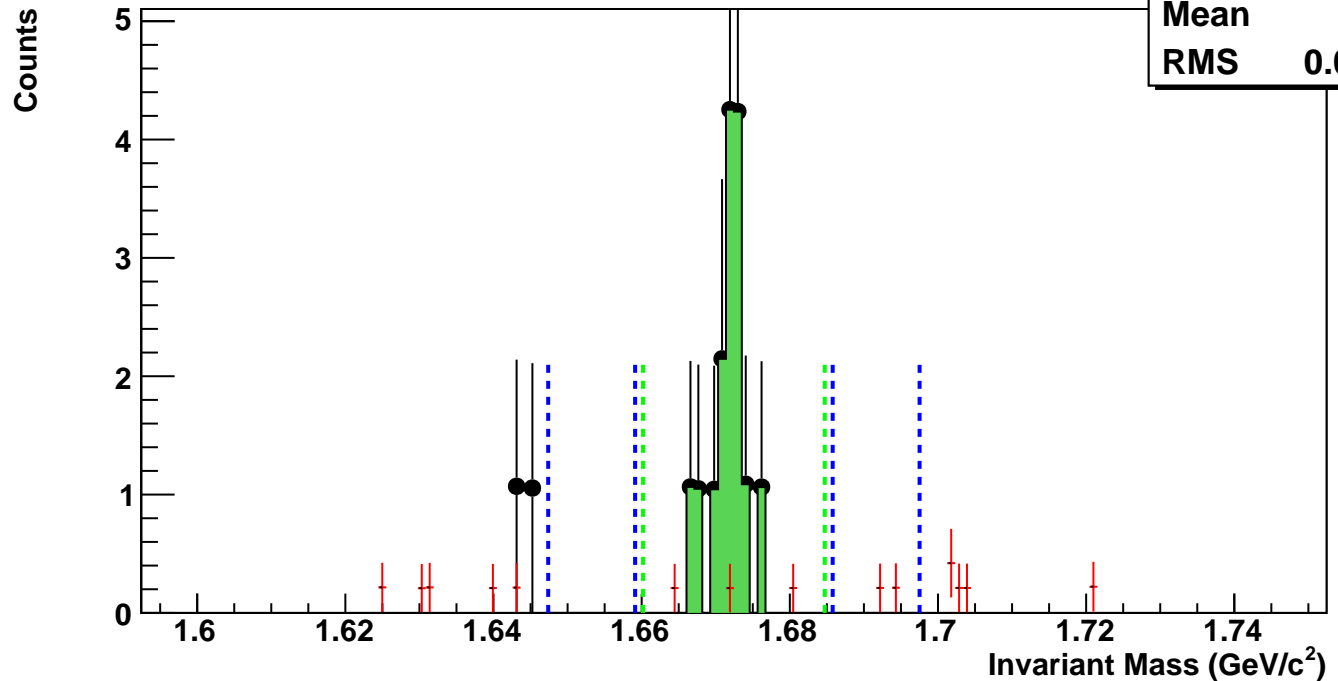
$\Omega^+$ , Au+Au 27 GeV, 0-10%,  $p_T$  1.6-2.0 GeV/c

hmlnvMassBgCent4Pt2	
Entries	473
Mean	1.673
RMS	0.02725



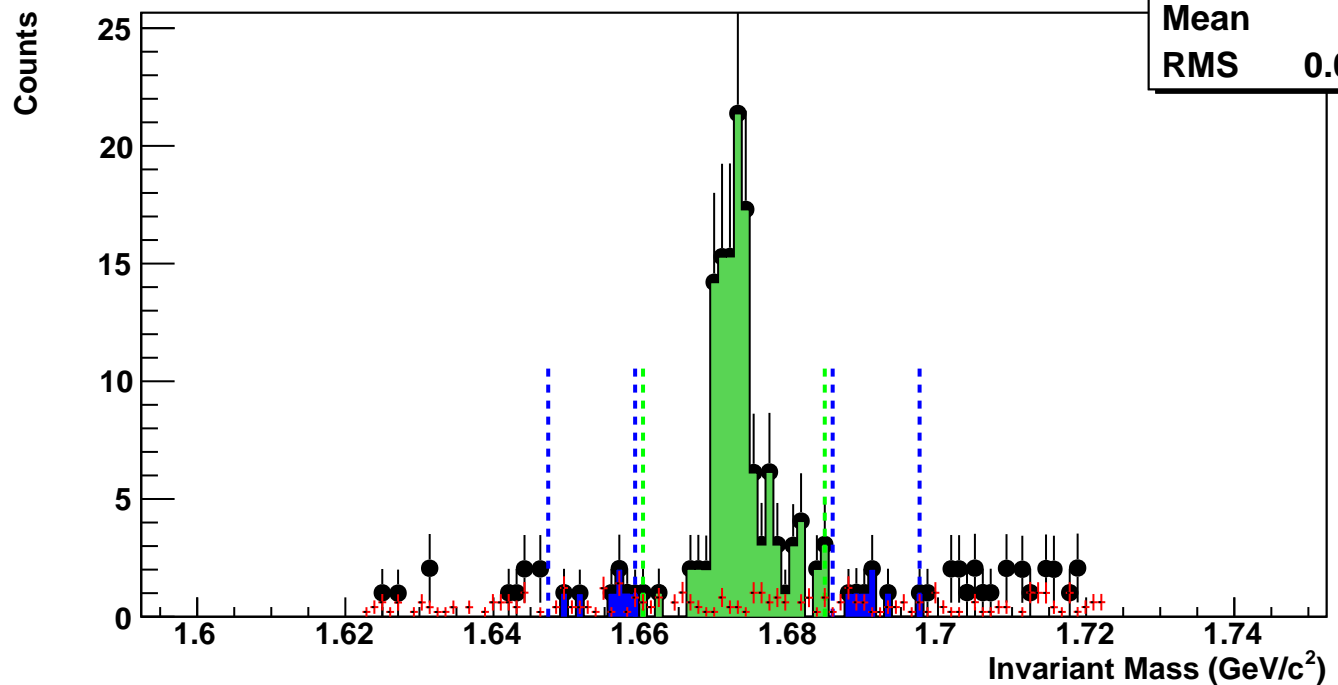
$\Omega^+$ , Au+Au 27 GeV, 60-80%,  $p_T$  2.0-2.4 GeV/c

hmlInvMassBgCent0Pt3	
Entries	0
Mean	1.674
RMS	0.03132



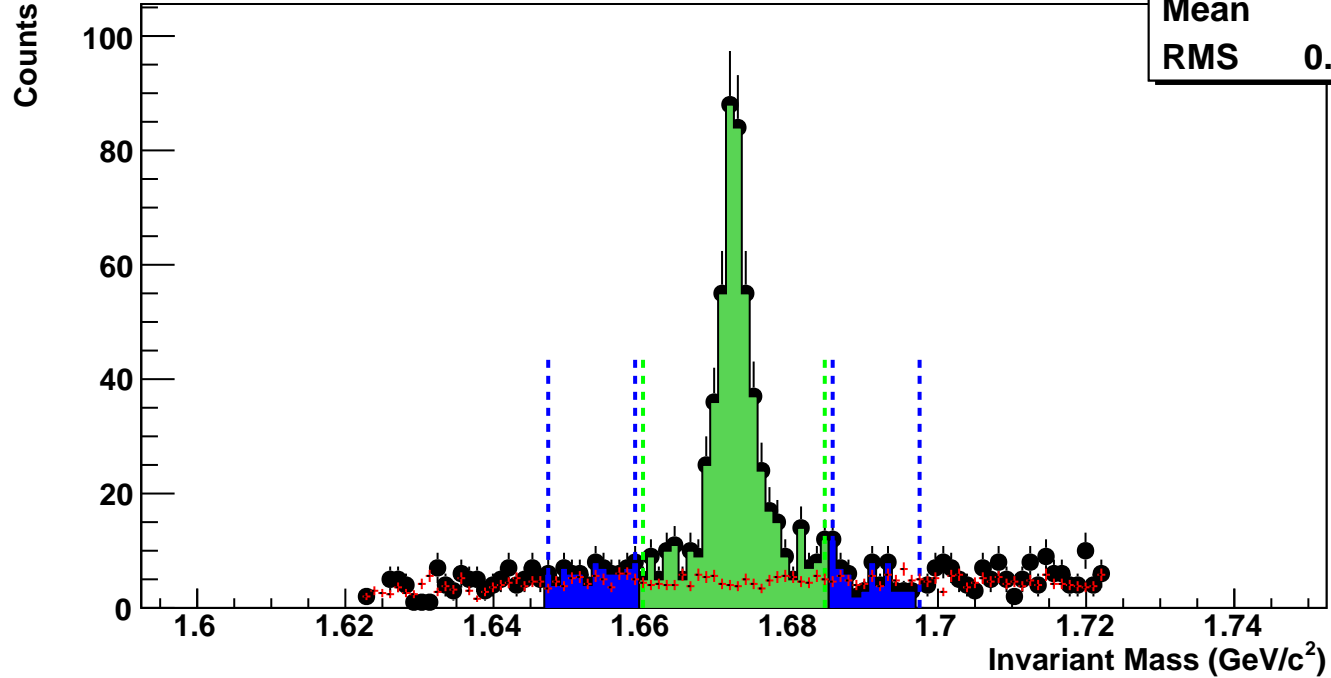
$\Omega^+$ , Au+Au 27 GeV, 40-60%,  $p_T$  2.0-2.4 GeV/c

hmlInvMassBgCent1Pt3	
Entries	5
Mean	1.675
RMS	0.02742



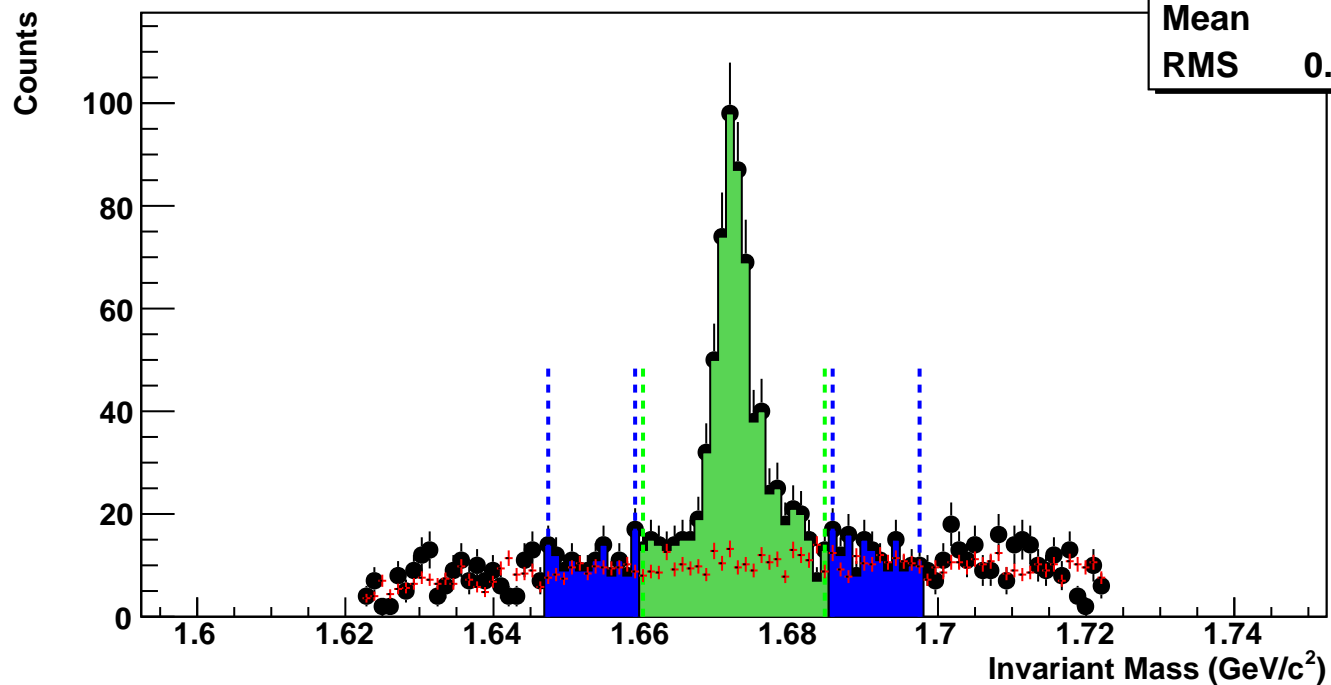
$\Omega^+$ , Au+Au 27 GeV, 20-40%,  $p_T$  2.0-2.4 GeV/c

hmlnvMassBgCent2Pt3	
Entries	51
Mean	1.675
RMS	0.02752



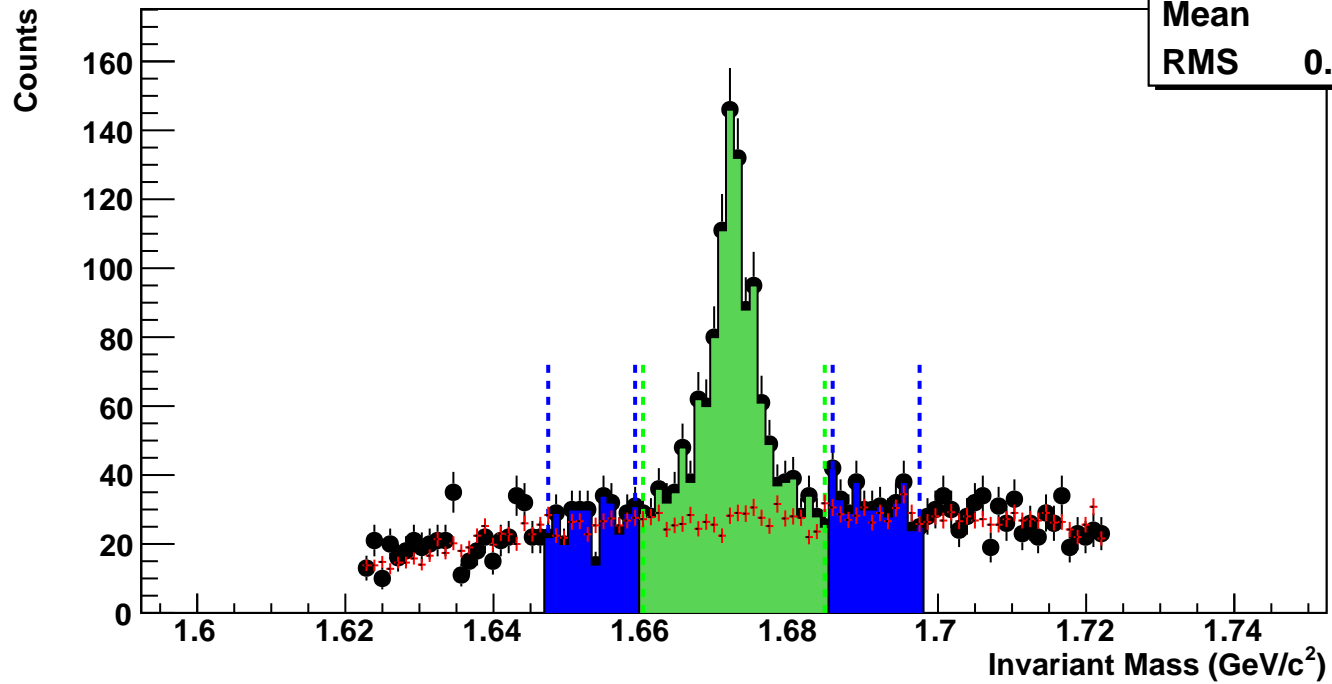
$\Omega^+$ , Au+Au 27 GeV, 10-20%,  $p_T$  2.0-2.4 GeV/c

hmlnvMassBgCent3Pt3	
Entries	105
Mean	1.676
RMS	0.02716



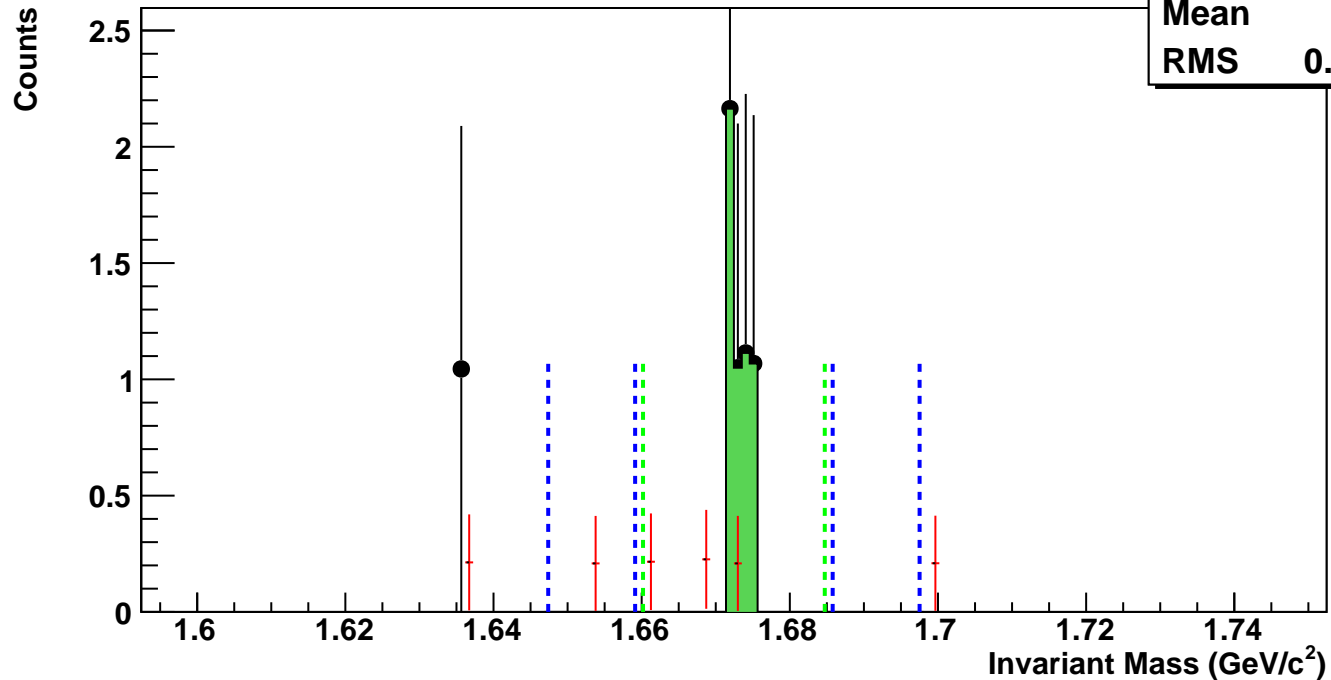
$\Omega^+$ , Au+Au 27 GeV, 0-10%,  $p_T$  2.0-2.4 GeV/c

hmlnvMassBgCent4Pt3	
Entries	287
Mean	1.676
RMS	0.02734



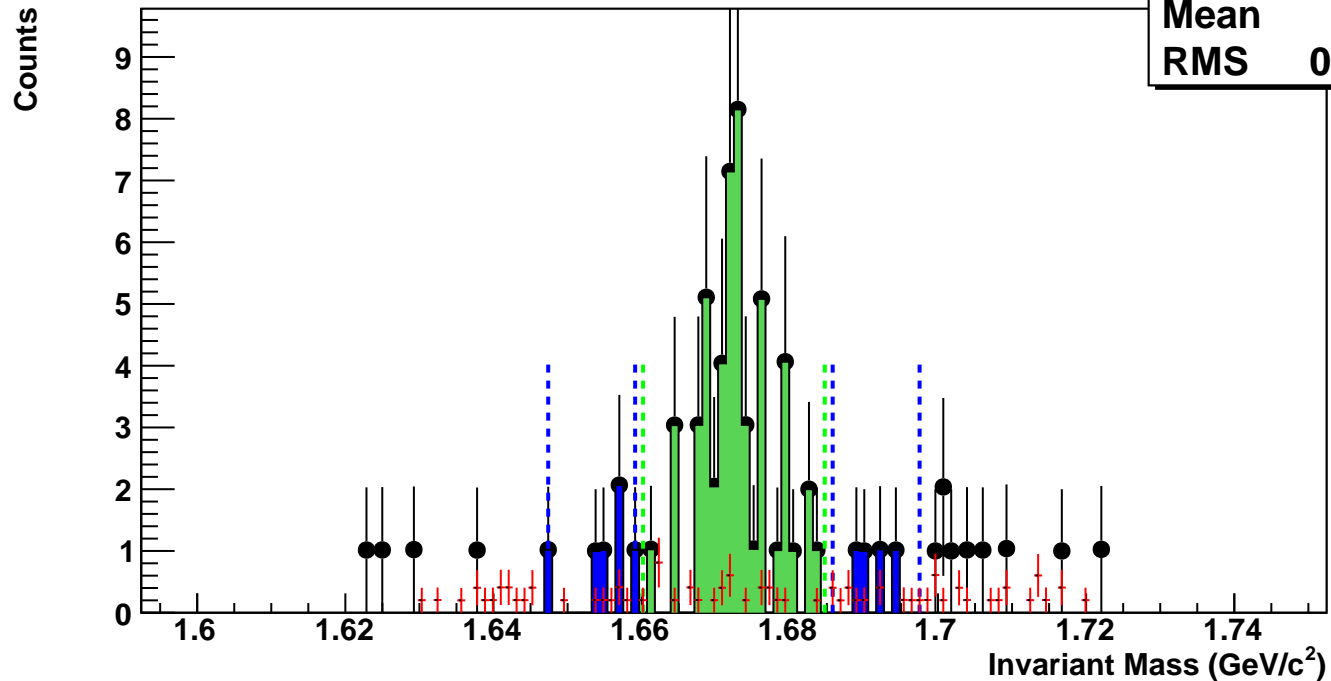
$\Omega^+$ , Au+Au 27 GeV, 60-80%,  $p_T$  2.4-2.8 GeV/c

hmlInvMassBgCent0Pt4	
Entries	0
Mean	1.665
RMS	0.01909



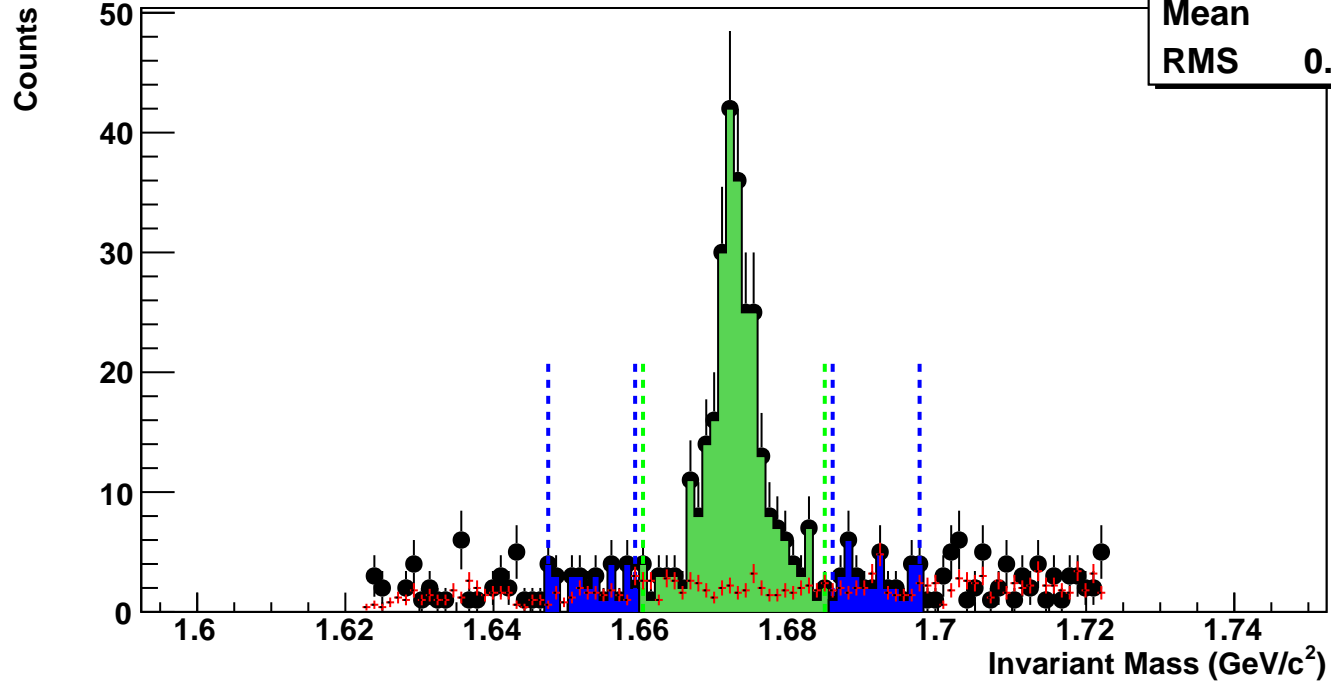
$\Omega^+$ , Au+Au 27 GeV, 40-60%,  $p_T$  2.4-2.8 GeV/c

hmlInvMassBgCent1Pt4	
Entries	2
Mean	1.676
RMS	0.0252



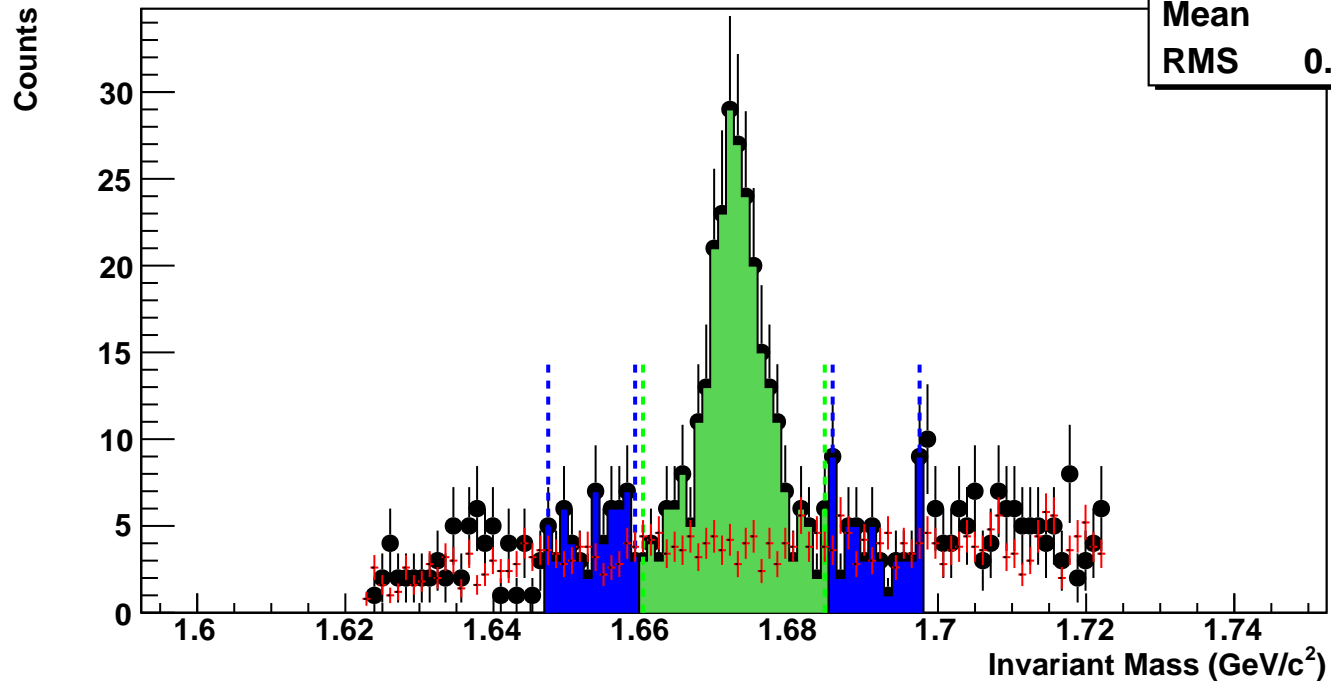
$\Omega^+$ , Au+Au 27 GeV, 20-40%,  $p_T$  2.4-2.8 GeV/c

hmlInvMassBgCent2Pt4	
Entries	21
Mean	1.679
RMS	0.02733



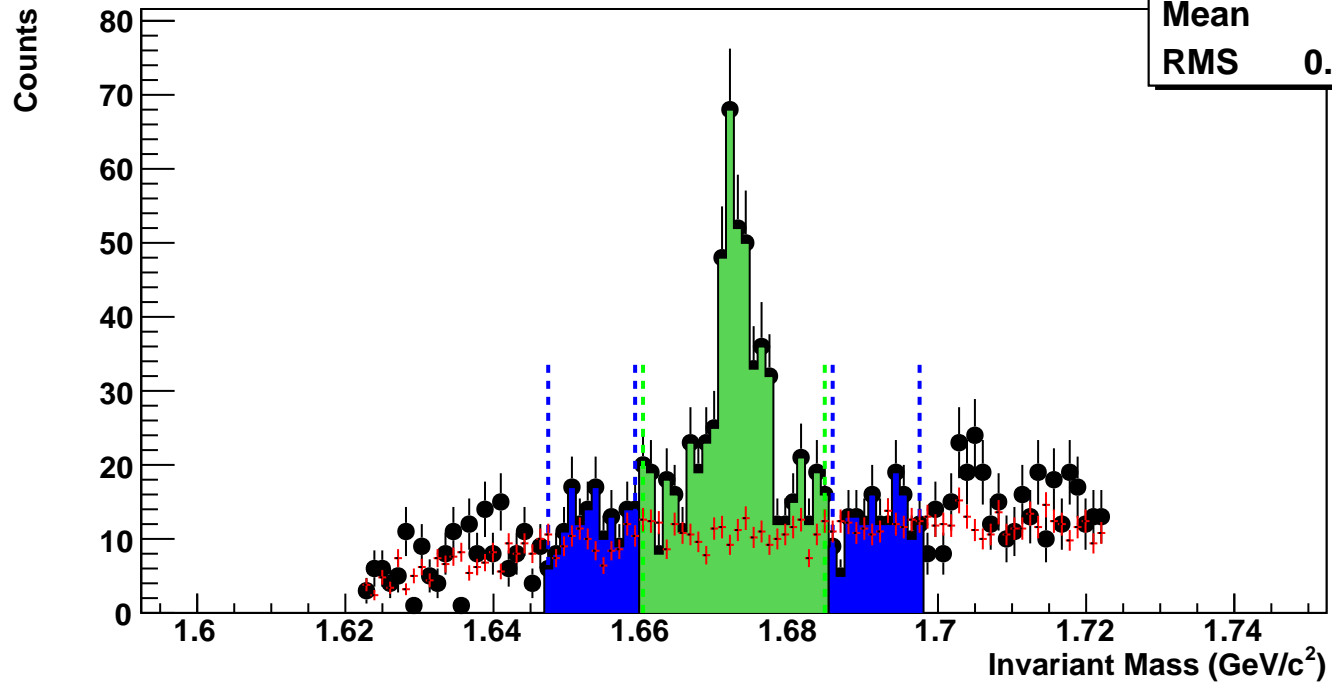
$\Omega^+$ , Au+Au 27 GeV, 10-20%,  $p_T$  2.4-2.8 GeV/c

hmlInvMassBgCent3Pt4	
Entries	40
Mean	1.677
RMS	0.02713

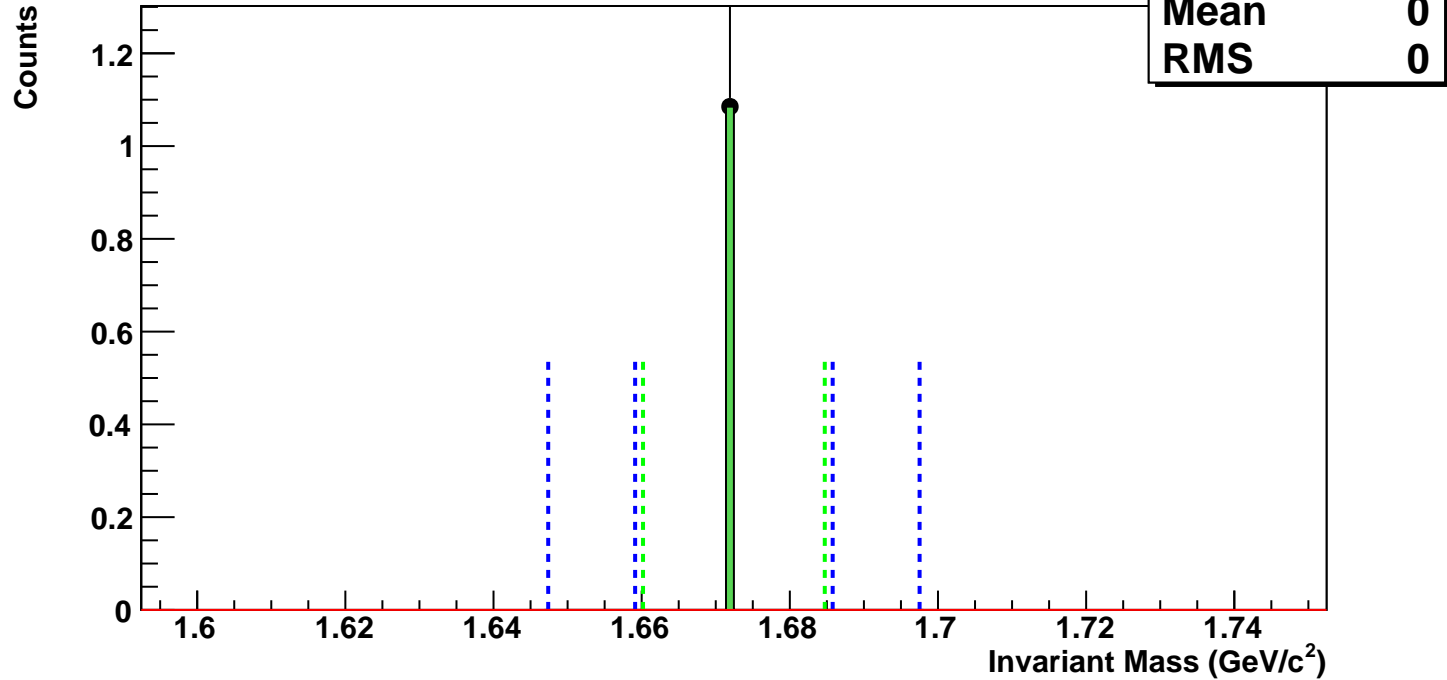


$\Omega^+$ , Au+Au 27 GeV, 0-10%,  $p_T$  2.4-2.8 GeV/c

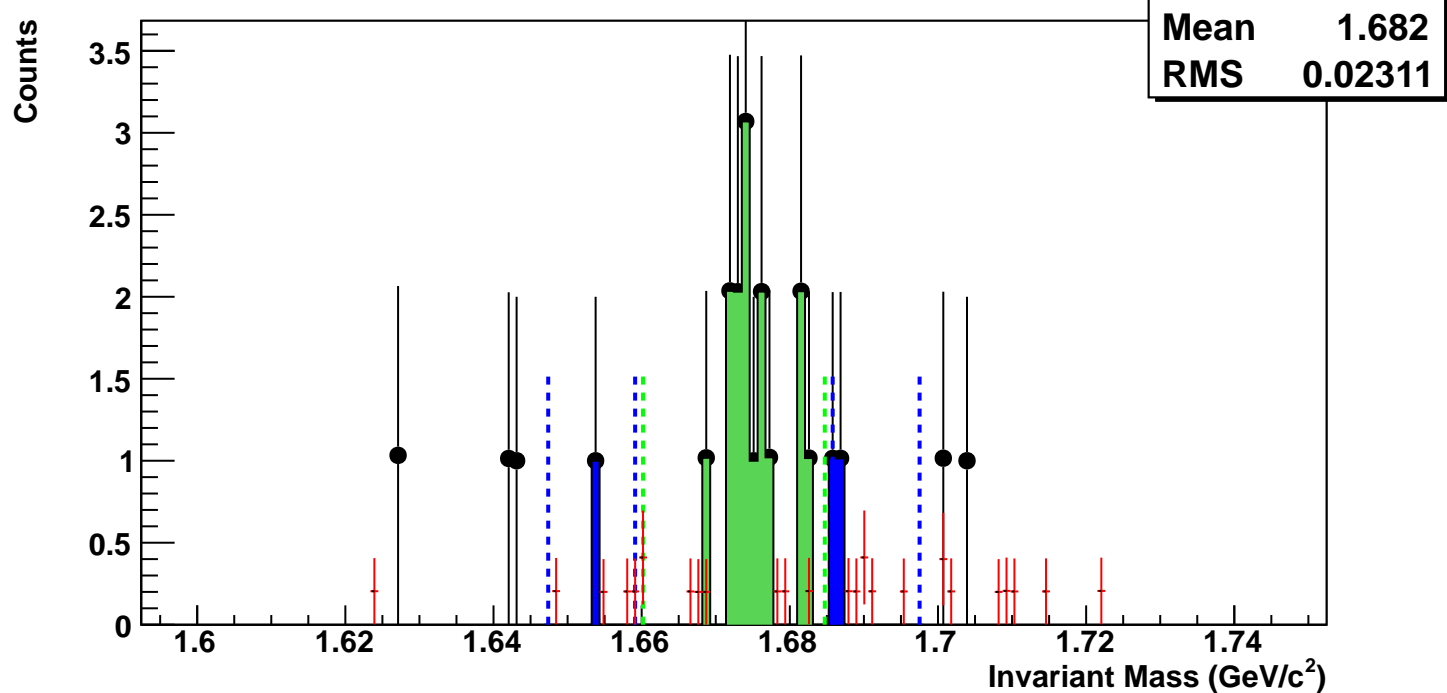
hmlInvMassBgCent4Pt4  
Entries 114  
Mean 1.678  
RMS 0.02696



$\bar{\Omega}^+$ , Au+Au 27 GeV, 60-80%,  $p_T$  2.8-3.6 GeV/c

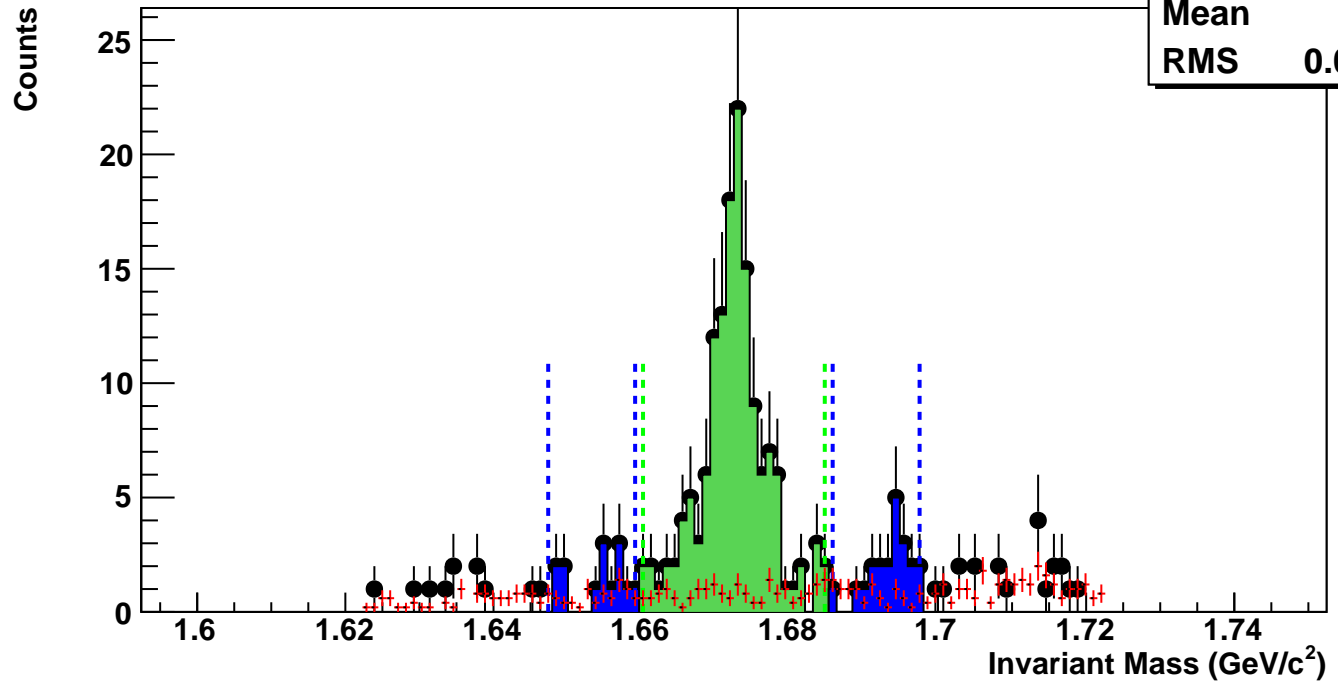


$\bar{\Omega}^+$ , Au+Au 27 GeV, 40-60%,  $p_T$  2.8-3.6 GeV/c



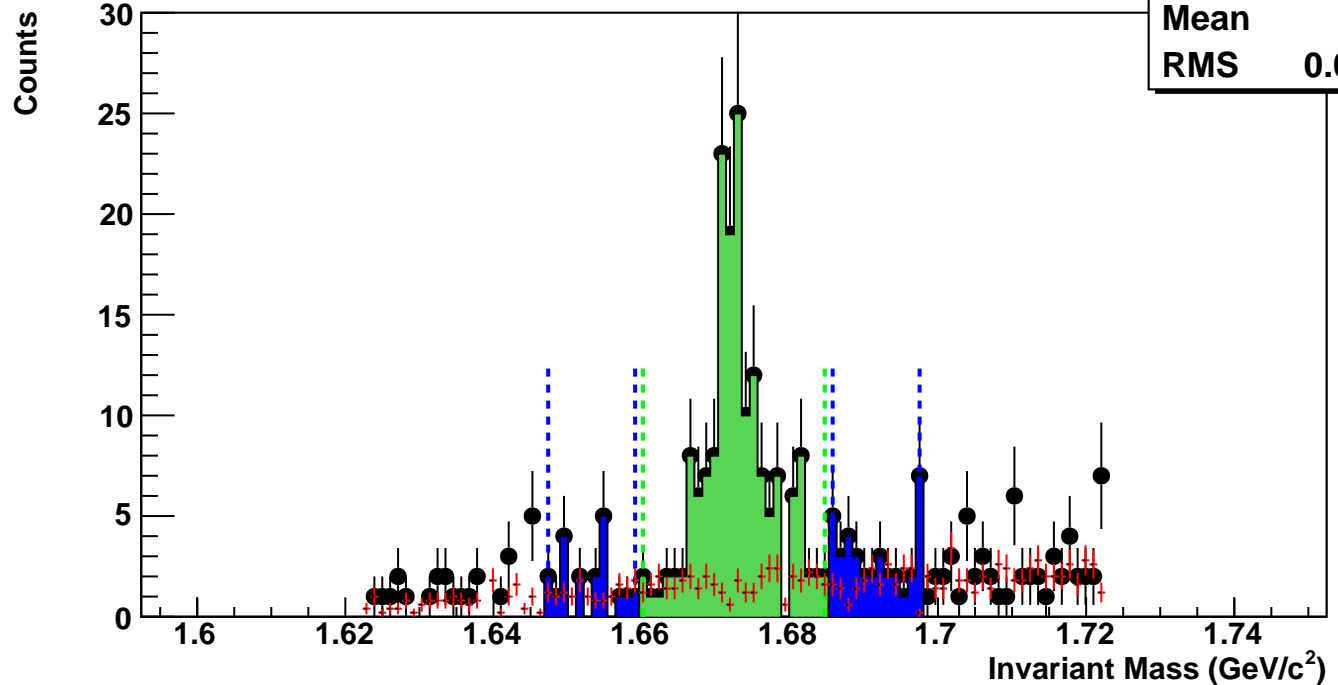
$\bar{\Omega}^+$ , Au+Au 27 GeV, 20-40%,  $p_T$  2.8-3.6 GeV/c

hmlInvMassBgCent2Pt5	
Entries	9
Mean	1.681
RMS	0.02717



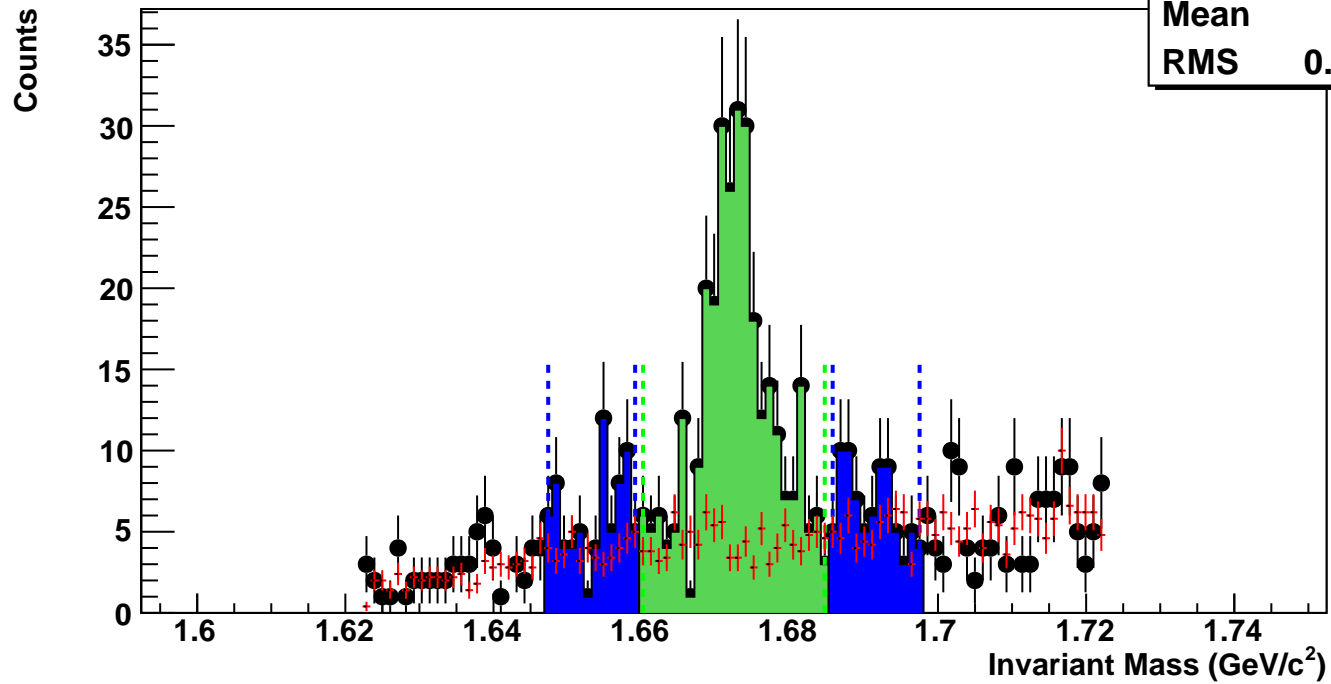
$\bar{\Omega}^+$ , Au+Au 27 GeV, 10-20%,  $p_T$  2.8-3.6 GeV/c

hmlInvMassBgCent3Pt5	
Entries	17
Mean	1.682
RMS	0.02639

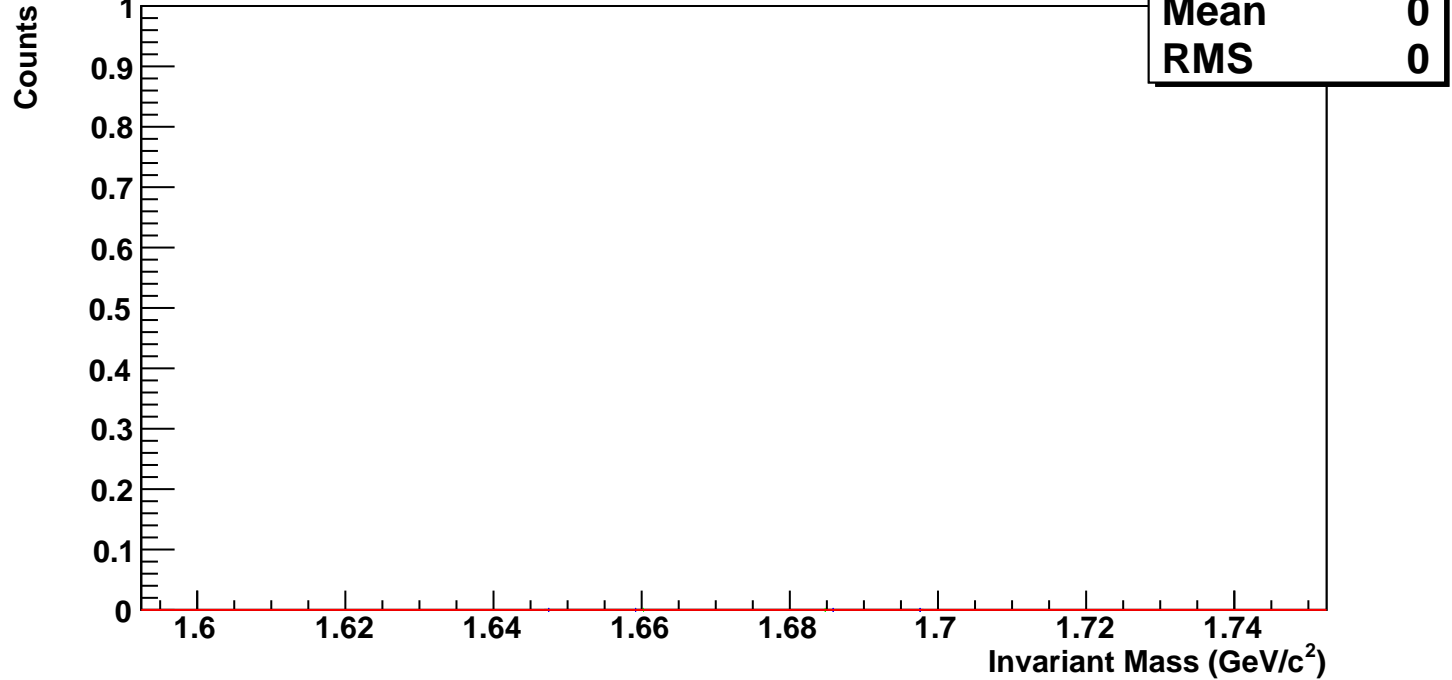


$\Omega^+$ , Au+Au 27 GeV, 0-10%,  $p_T$  2.8-3.6 GeV/c

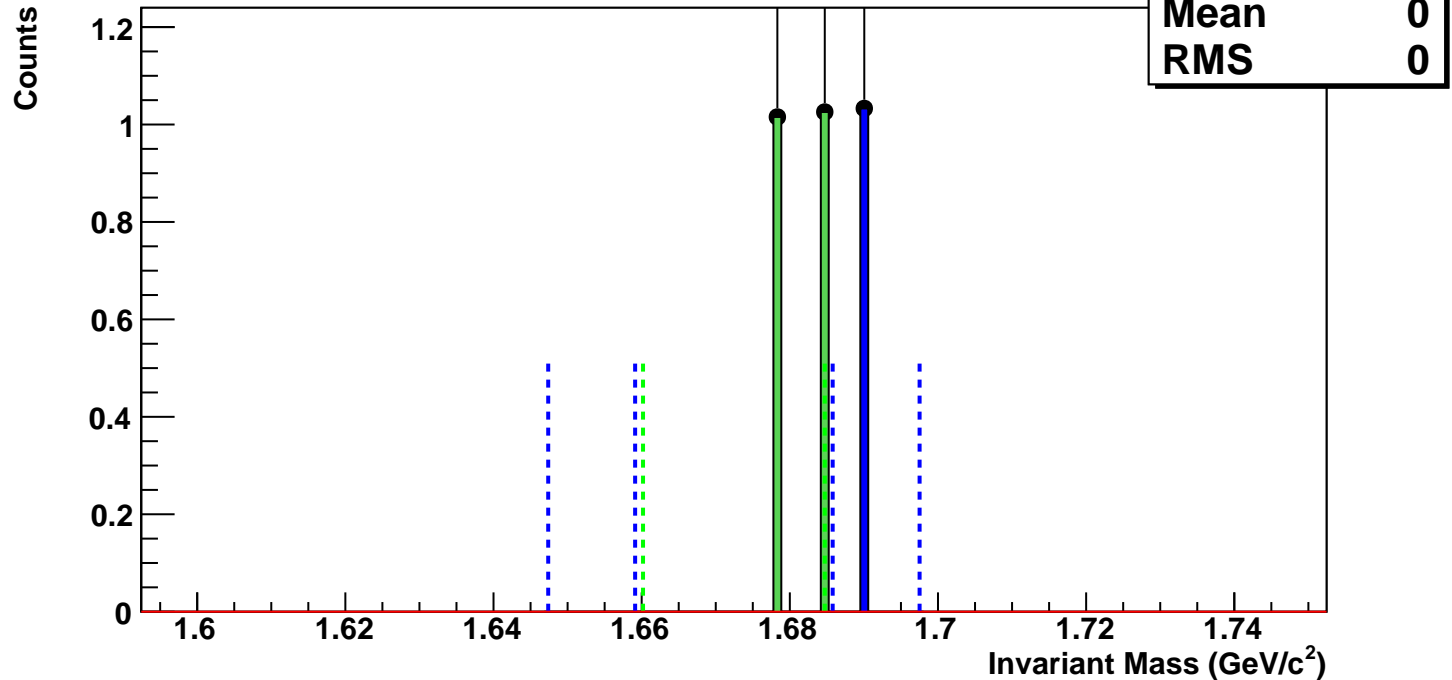
hmlnvMassBgCent4Pt5	
Entries	48
Mean	1.681
RMS	0.02694



$\Omega^+$ , Au+Au 27 GeV, 60-80%,  $p_T$  3.6-5.0 GeV/c

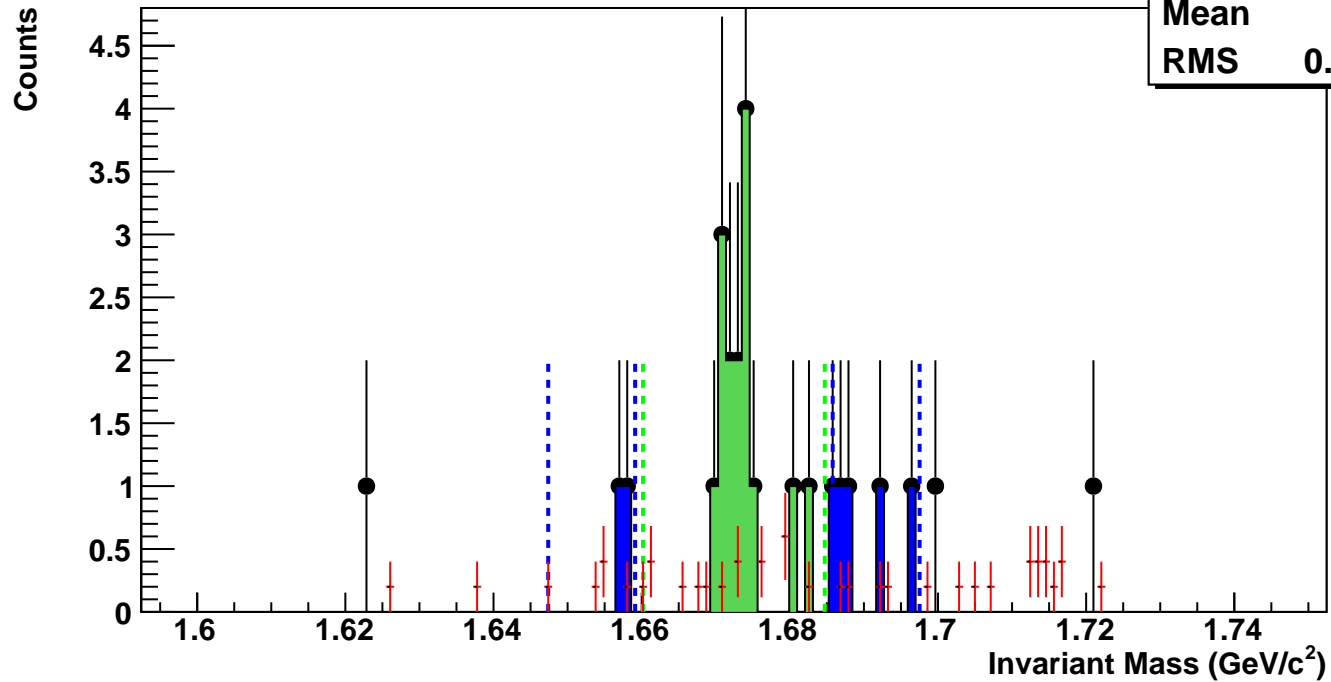


$\Omega^+$ , Au+Au 27 GeV, 40-60%,  $p_T$  3.6-5.0 GeV/c



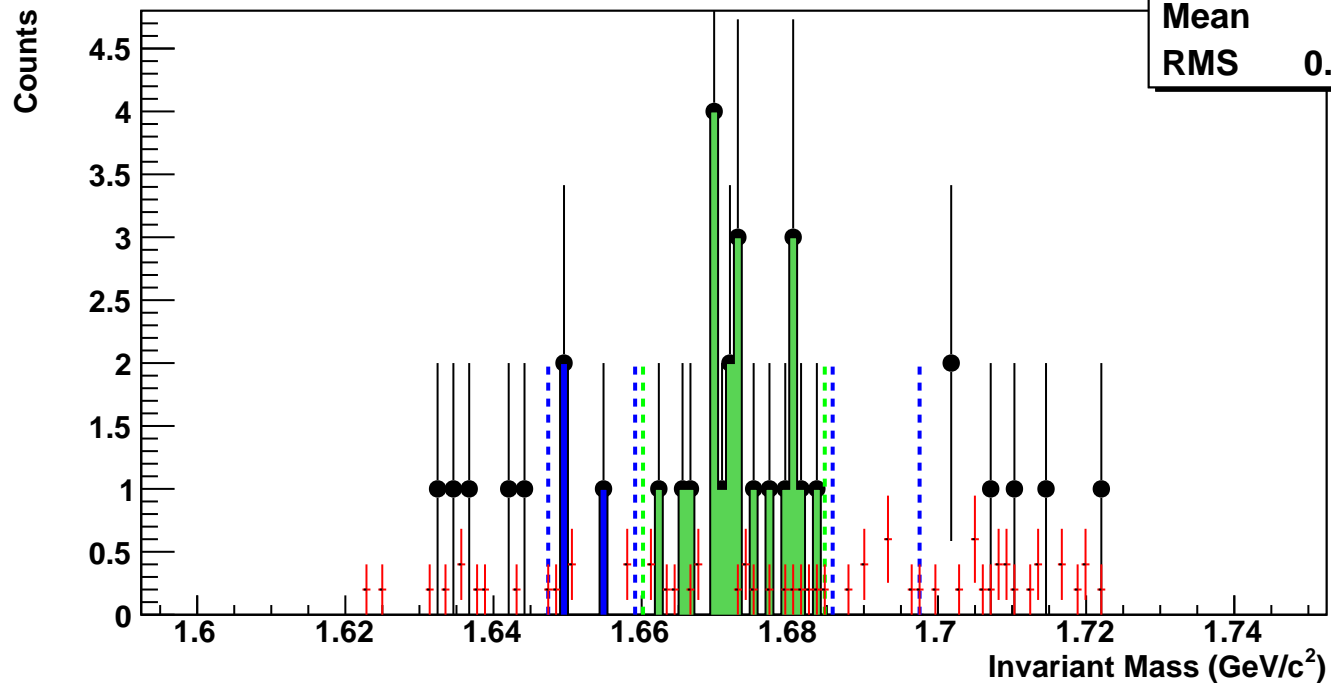
$\Omega^+$ , Au+Au 27 GeV, 20-40%,  $p_T$  3.6-5.0 GeV/c

hmlInvMassBgCent2Pt6	
Entries	1
Mean	1.683
RMS	0.02485



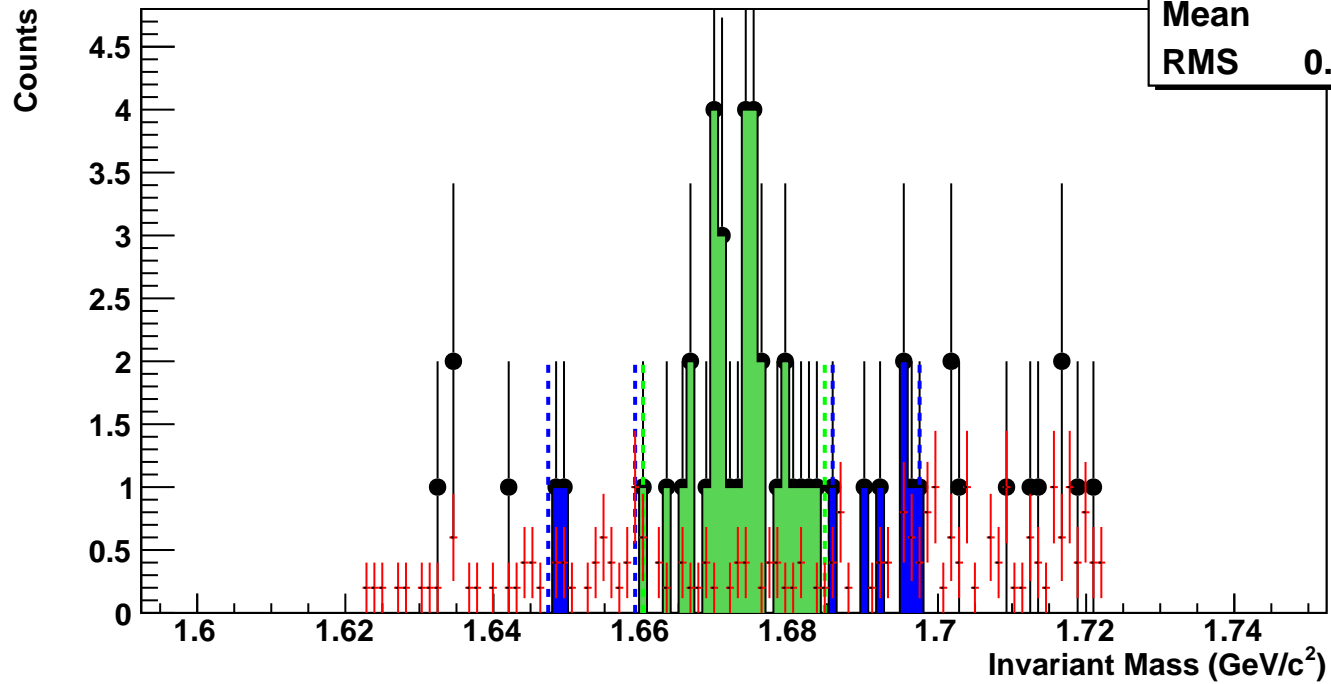
$\Omega^+$ , Au+Au 27 GeV, 10-20%,  $p_T$  3.6-5.0 GeV/c

hmlInvMassBgCent3Pt6	
Entries	2
Mean	1.681
RMS	0.02795



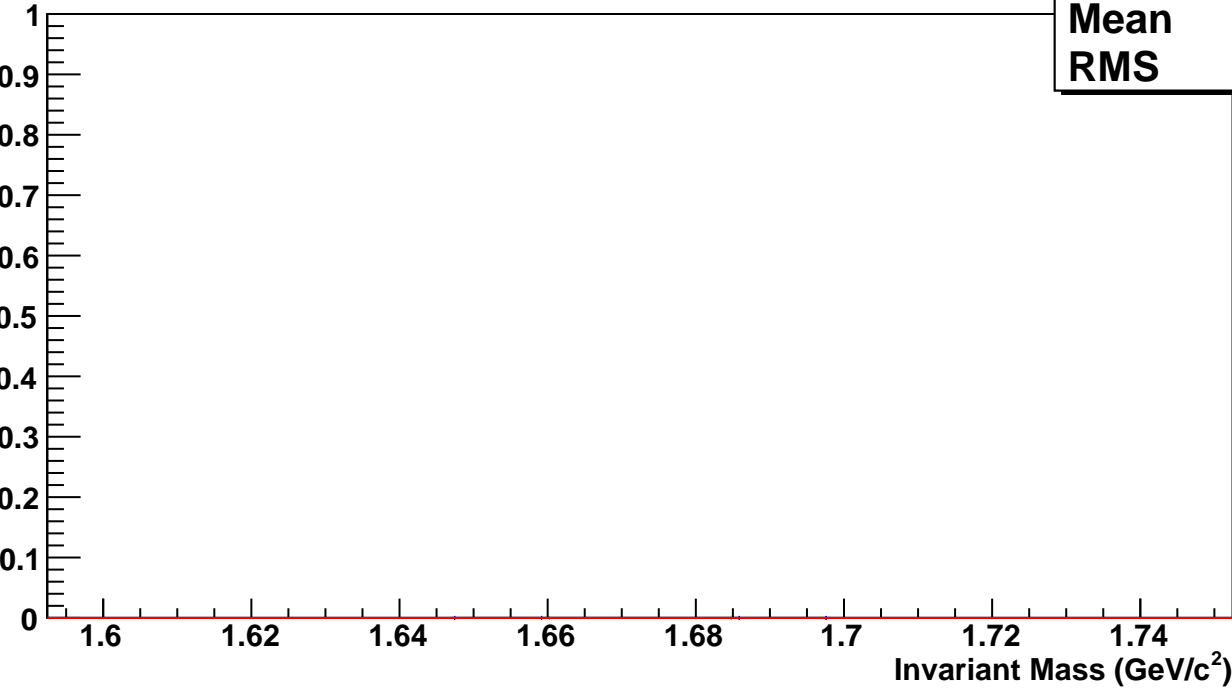
$\Omega^+$ , Au+Au 27 GeV, 0-10%,  $p_T$  3.6-5.0 GeV/c

hmlnvMassBgCent4Pt6	
Entries	4
Mean	1.683
RMS	0.02812



$\Omega^+$ , Au+Au 27 GeV, 60-80%,  $p_T$  5.0-7.0 GeV/c

Counts

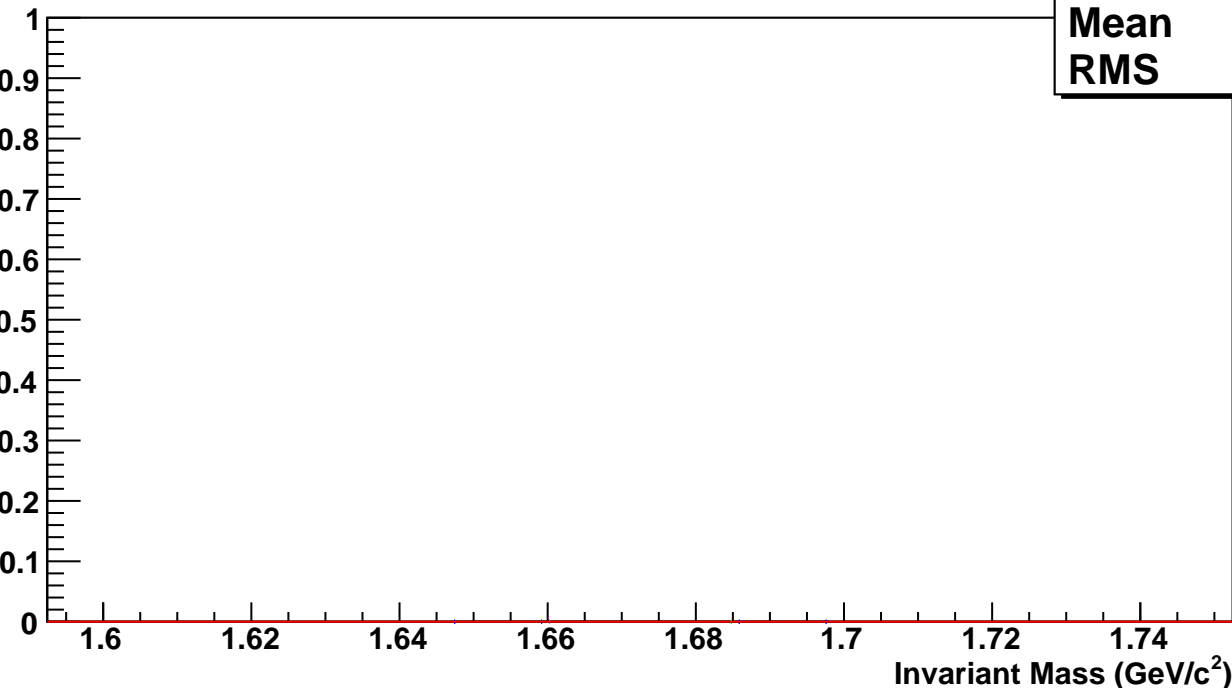


hmlInvMassBgCent0Pt7

Entries	0
Mean	0
RMS	0

$\Omega^+$ , Au+Au 27 GeV, 40-60%,  $p_T$  5.0-7.0 GeV/c

Counts

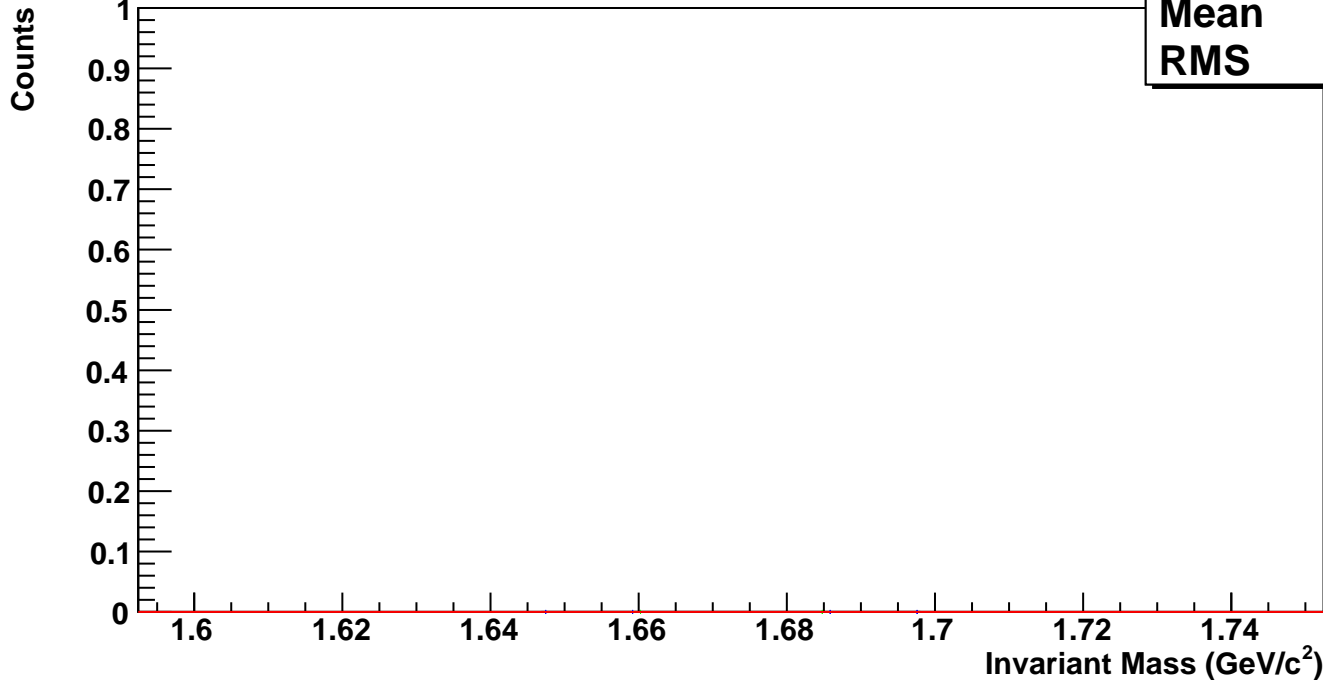


hmlInvMassBgCent1Pt7

Entries	0
Mean	0
RMS	0

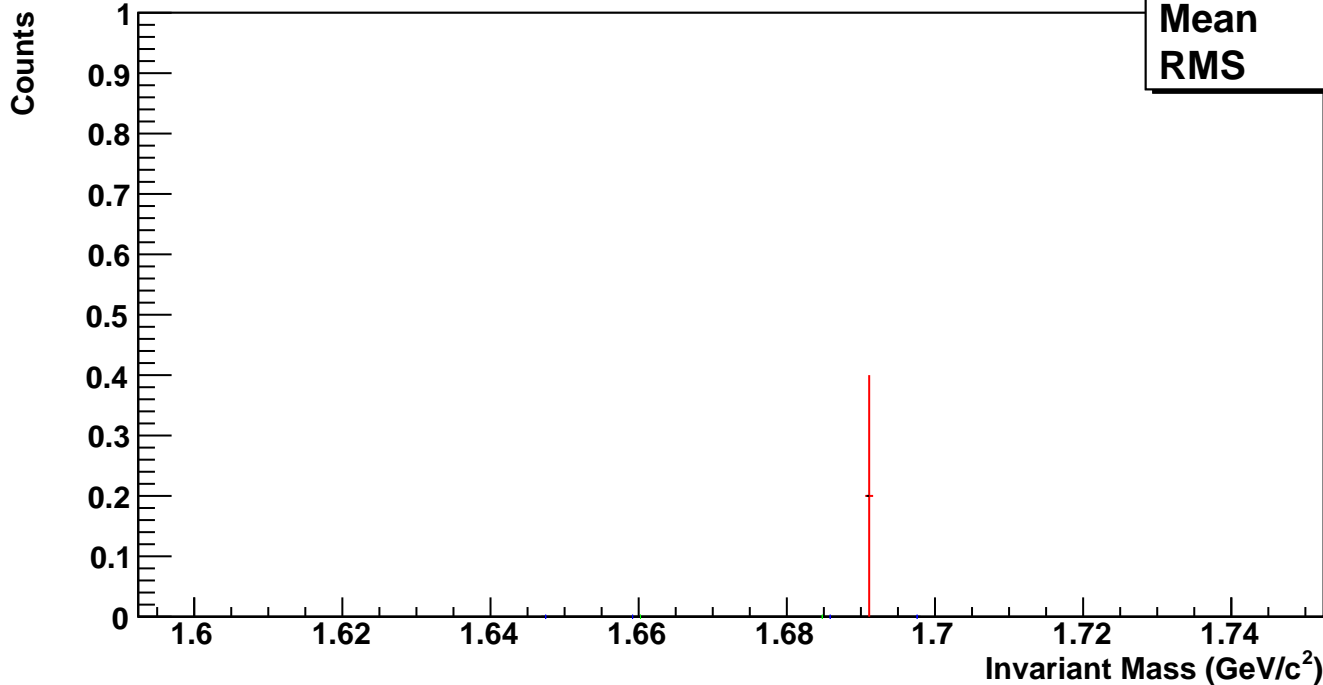
$\bar{\Omega}^+$ , Au+Au 27 GeV, 20-40%,  $p_T$  5.0-7.0 GeV/c

hmlInvMassBgCent2Pt7	
Entries	0
Mean	0
RMS	0



$\bar{\Omega}^+$ , Au+Au 27 GeV, 10-20%,  $p_T$  5.0-7.0 GeV/c

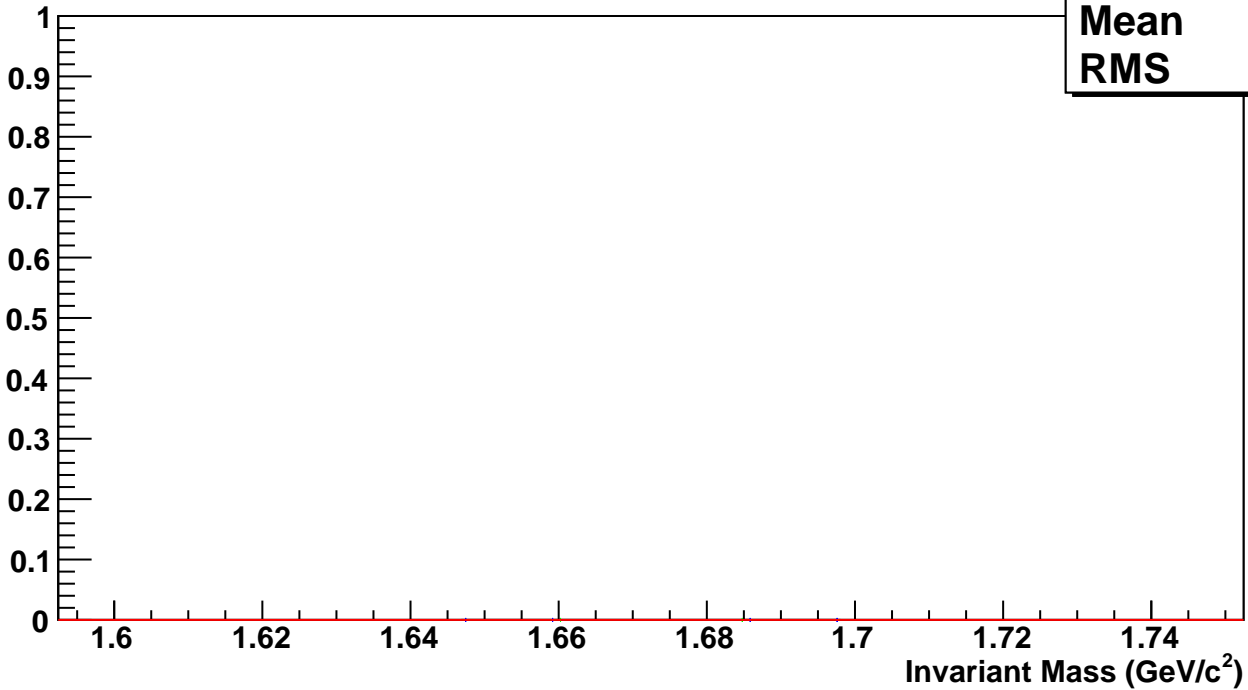
hmlInvMassBgCent3Pt7	
Entries	0
Mean	1.691
RMS	0



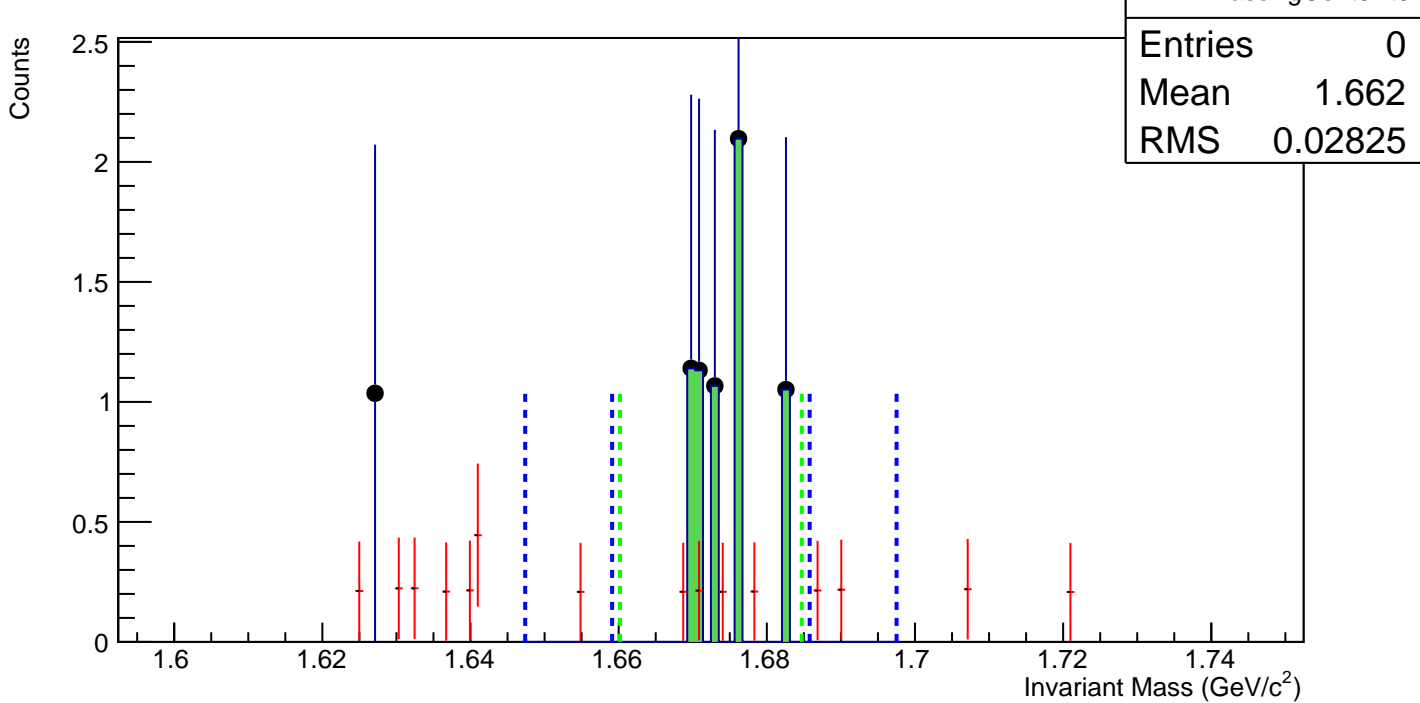
$\Omega^+$ , Au+Au 27 GeV, 0-10%,  $p_T$  5.0-7.0 GeV/c

hmlInvMassBgCent4Pt7	
Entries	0
Mean	0
RMS	0

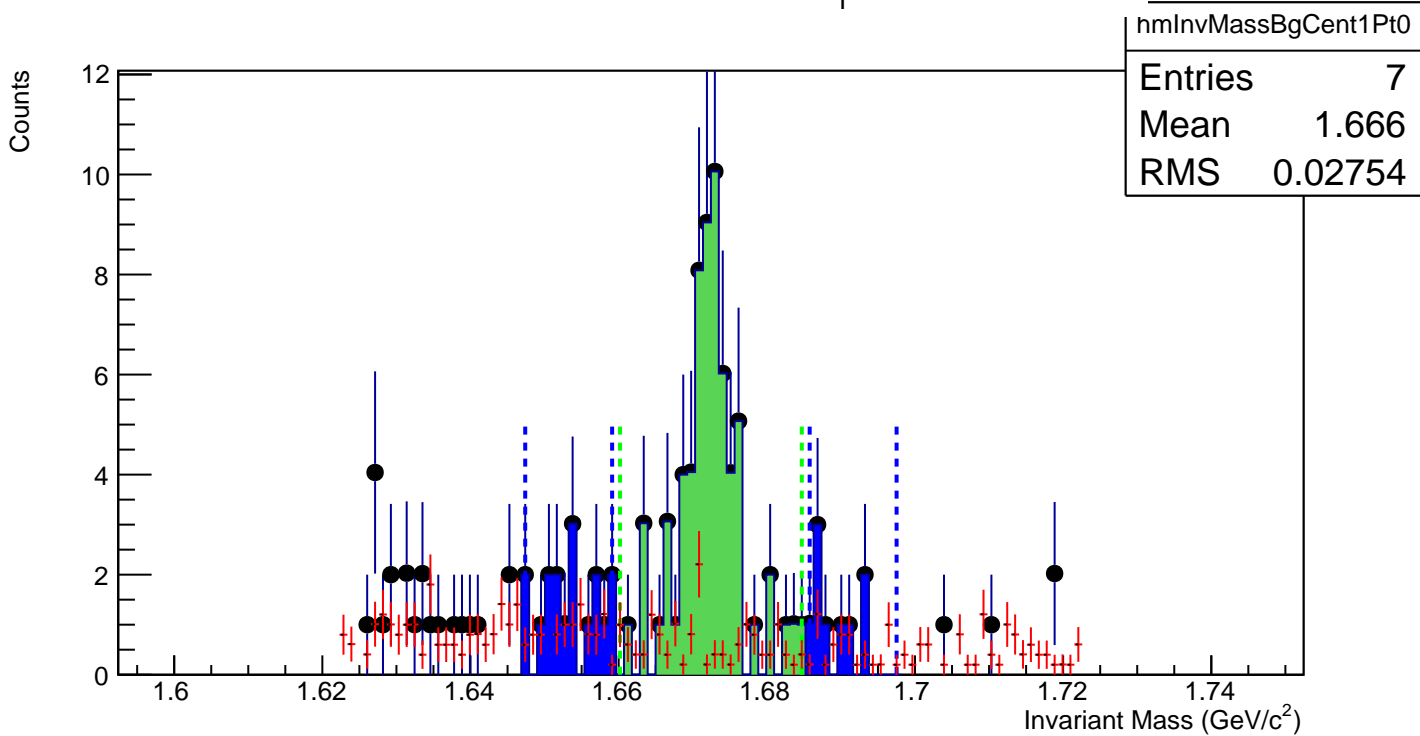
Counts



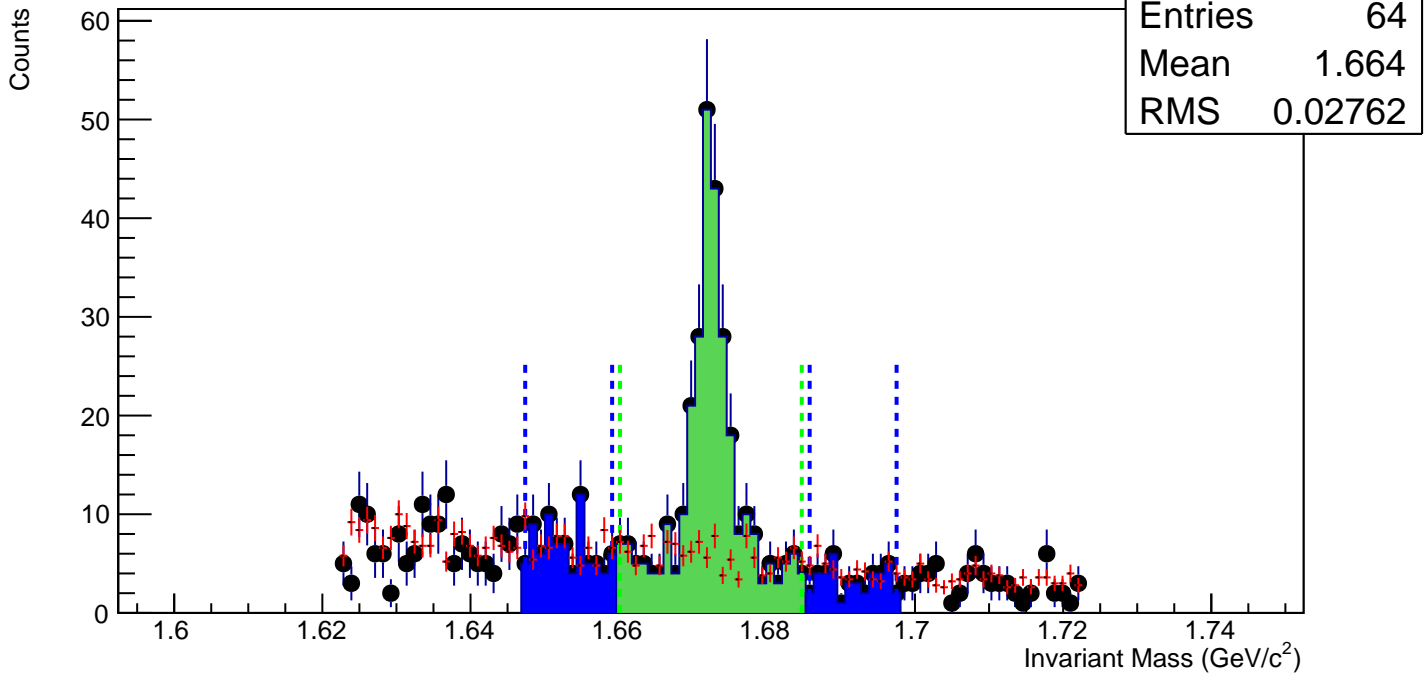
$\Omega^-$ , Au+Au 19 GeV, 60-80%,  $p_T$  0.8-1.2 GeV/c



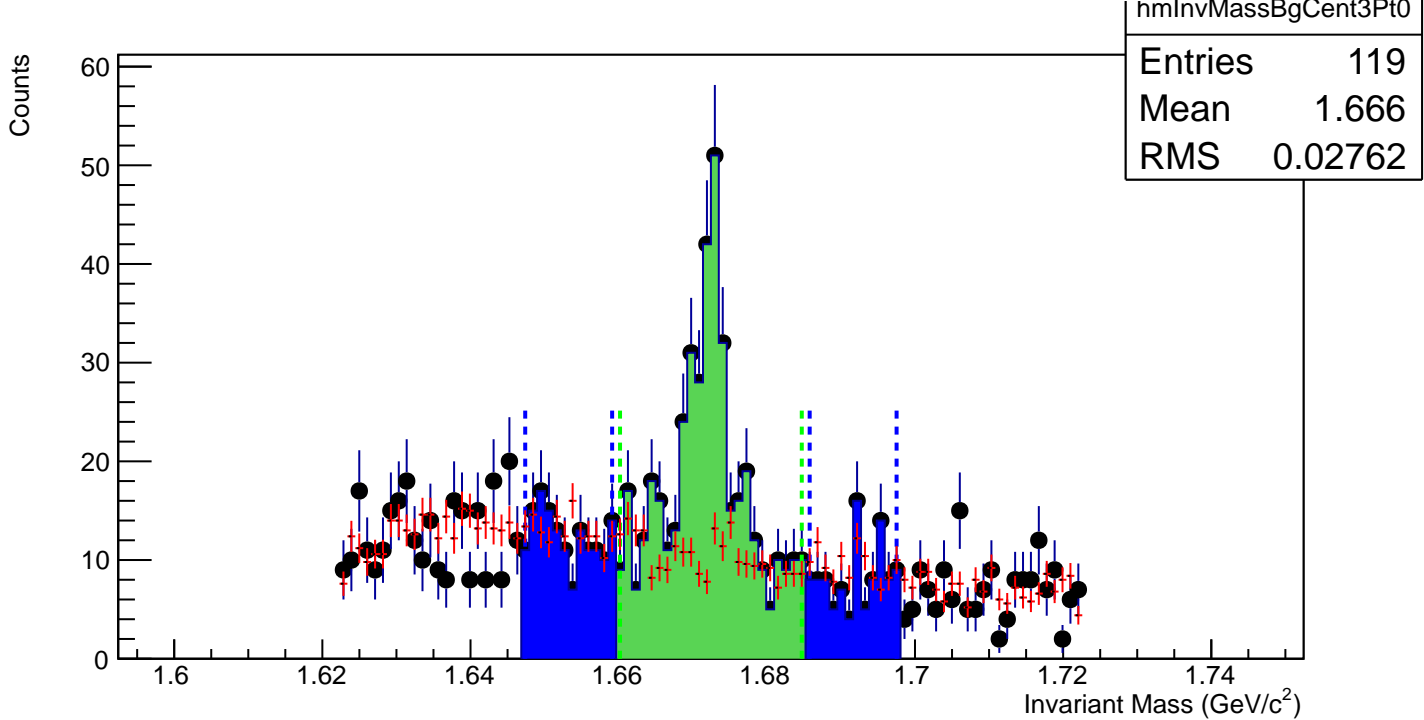
$\Omega^-$ , Au+Au 19 GeV, 40-60%,  $p_T$  0.8-1.2 GeV/c



$\Omega^-$ , Au+Au 19 GeV, 20-40%,  $p_T$  0.8-1.2 GeV/c

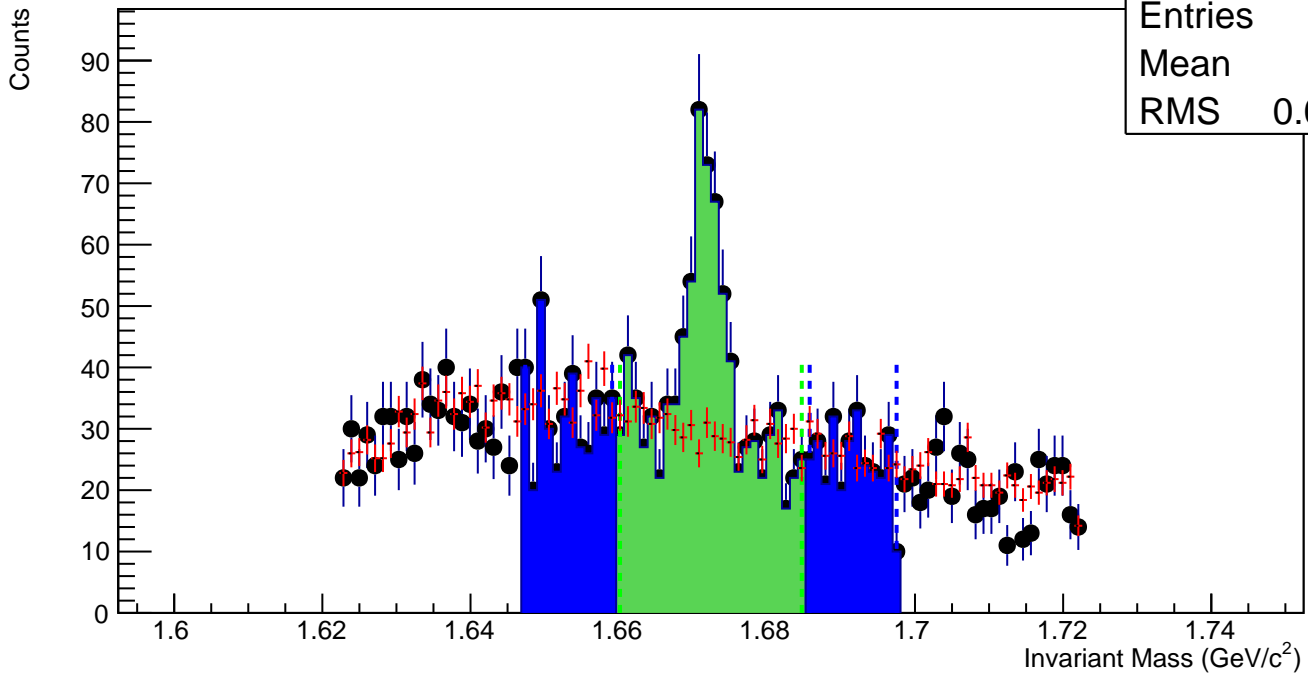


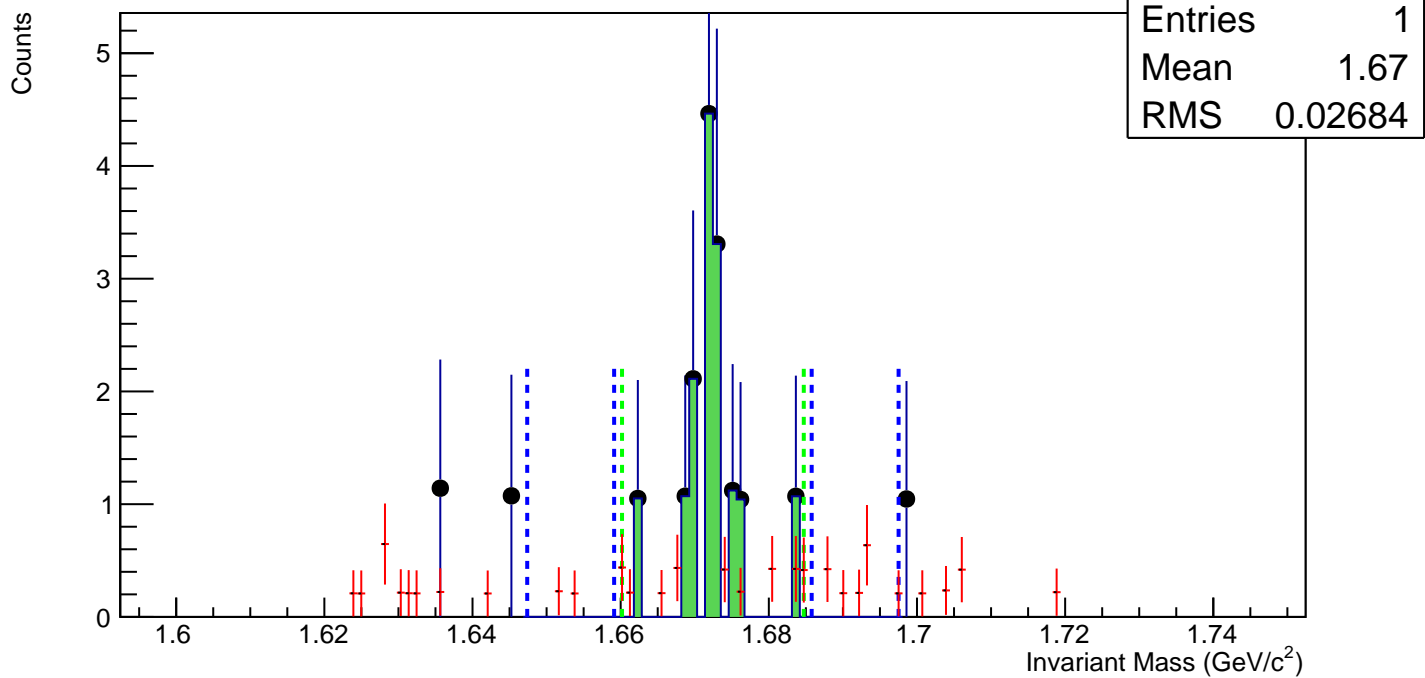
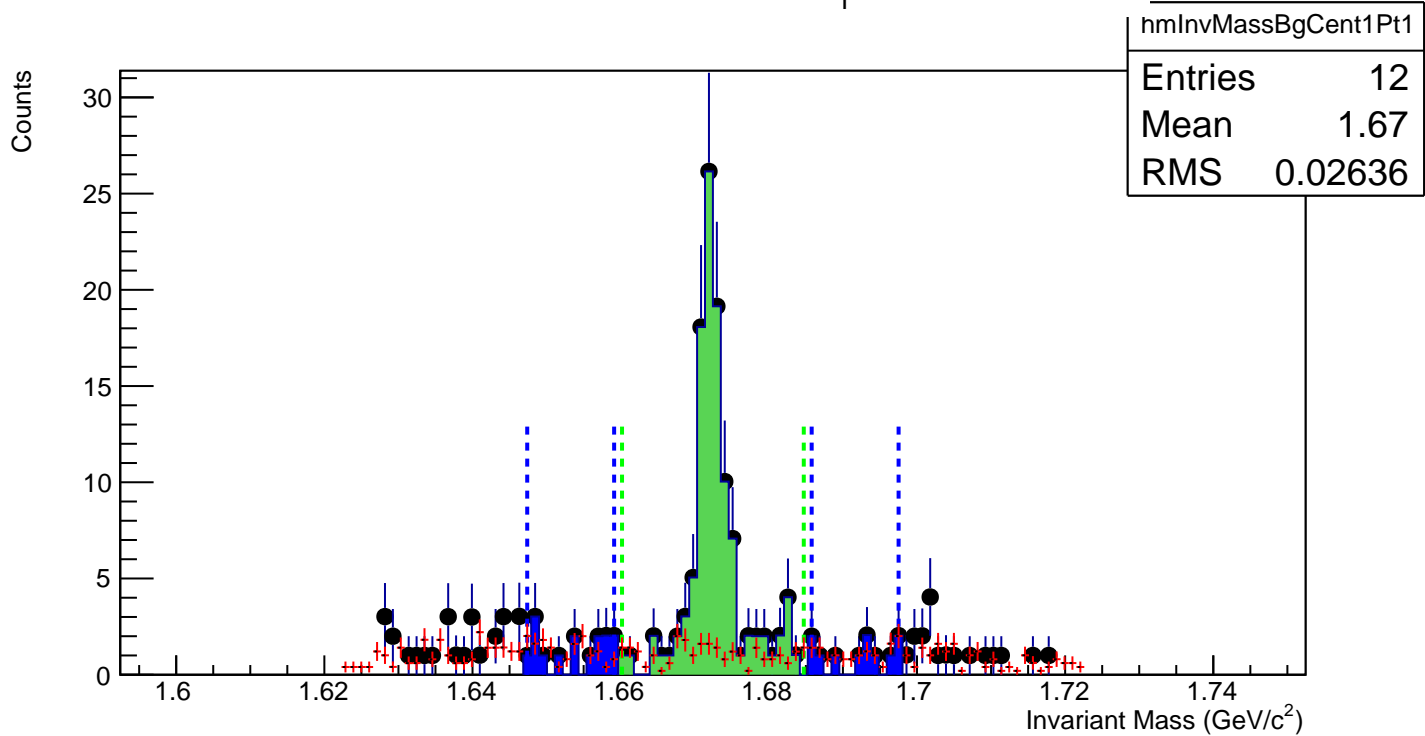
$\Omega^-$ , Au+Au 19 GeV, 10-20%,  $p_T$  0.8-1.2 GeV/c



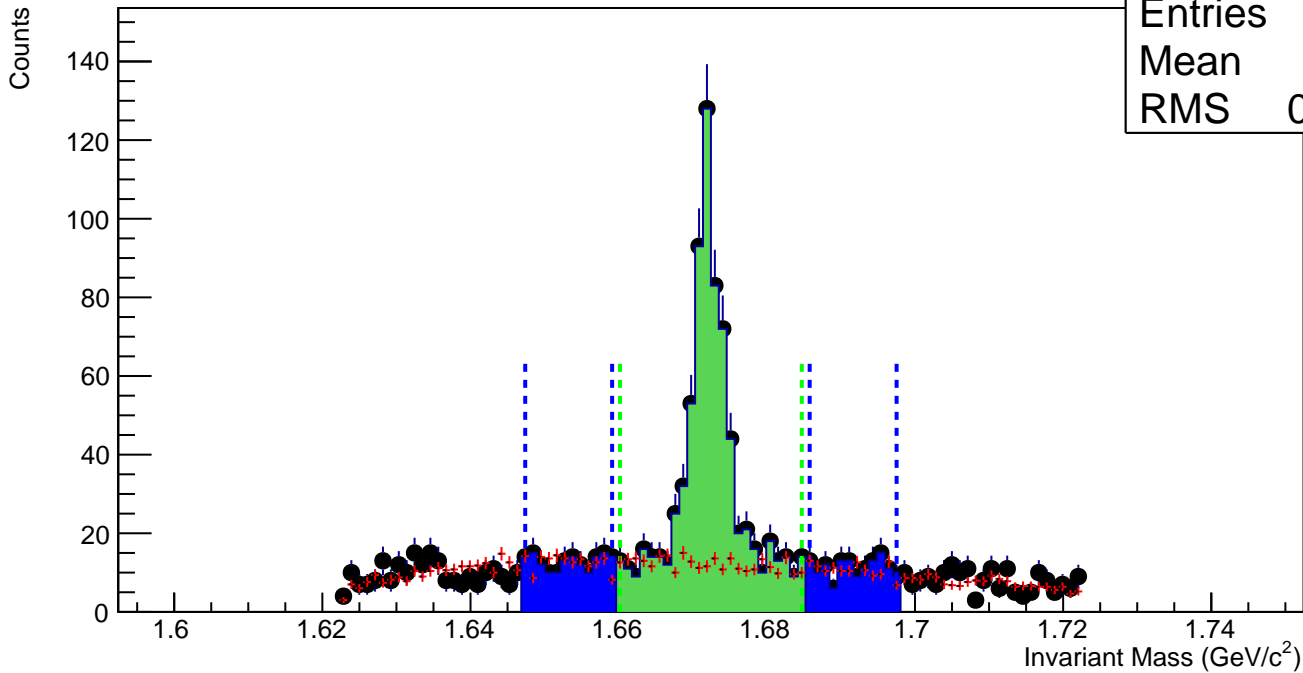
$\Omega^-$ , Au+Au 19 GeV, 0-10%,  $p_T$  0.8-1.2 GeV/c

hmlInvMassBgCent4Pt0
Entries 324
Mean 1.668
RMS 0.02757

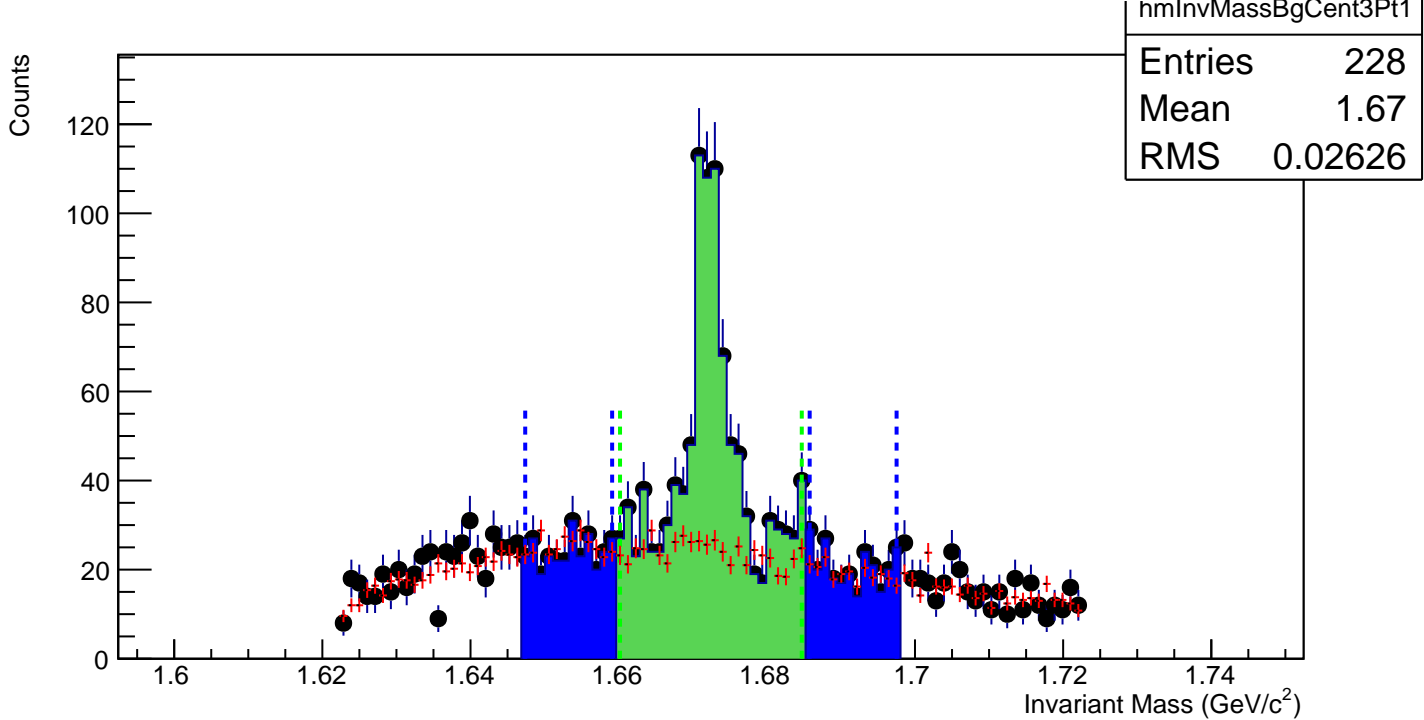


$\Omega^-$ , Au+Au 19 GeV, 60-80%,  $p_T$  1.2-1.6 GeV/c $\Omega^-$ , Au+Au 19 GeV, 40-60%,  $p_T$  1.2-1.6 GeV/c

$\Omega^-$ , Au+Au 19 GeV, 20-40%,  $p_T$  1.2-1.6 GeV/c

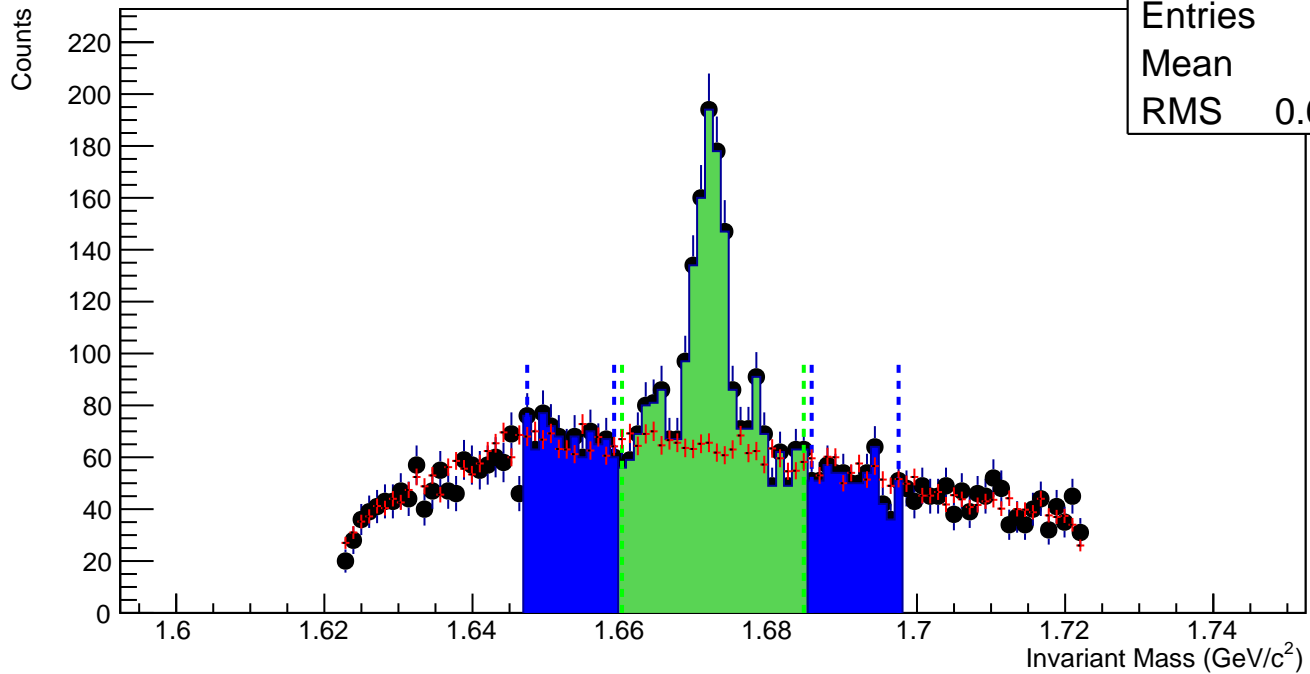


$\Omega^-$ , Au+Au 19 GeV, 10-20%,  $p_T$  1.2-1.6 GeV/c

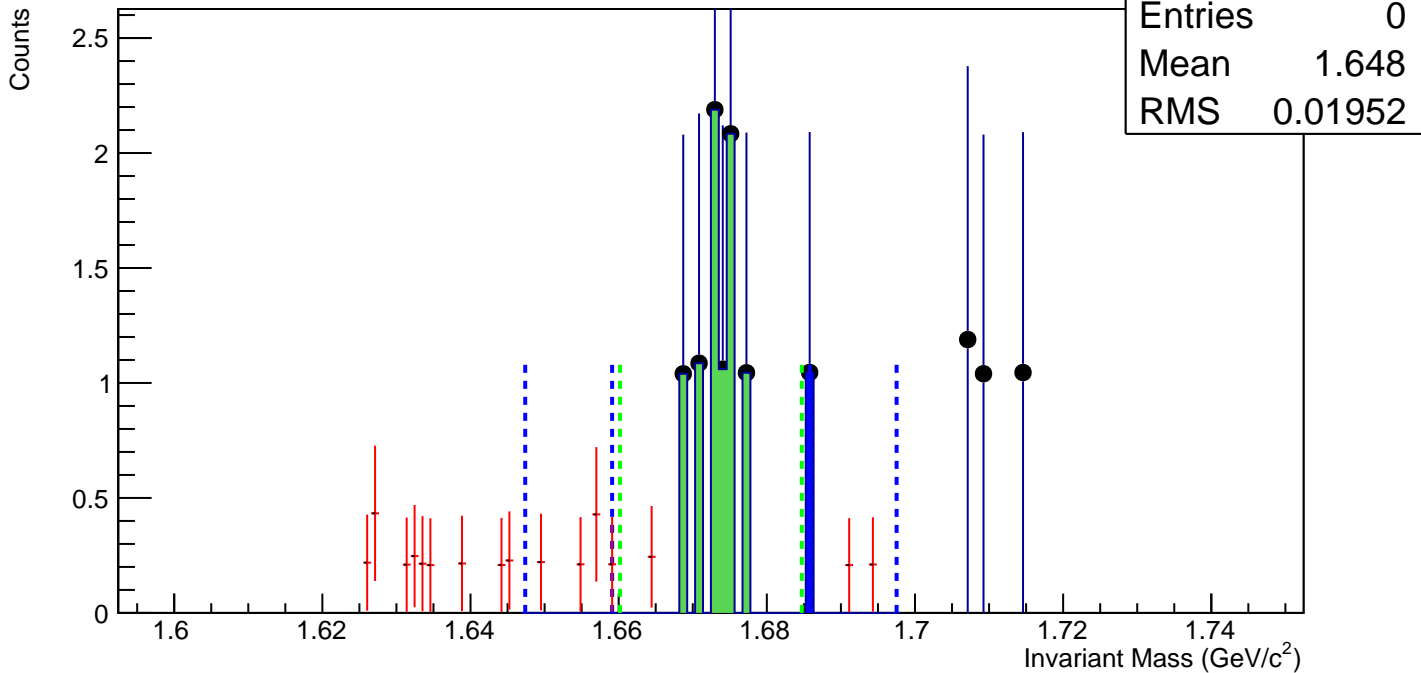


$\Omega^-$ , Au+Au 19 GeV, 0-10%,  $p_T$  1.2-1.6 GeV/c

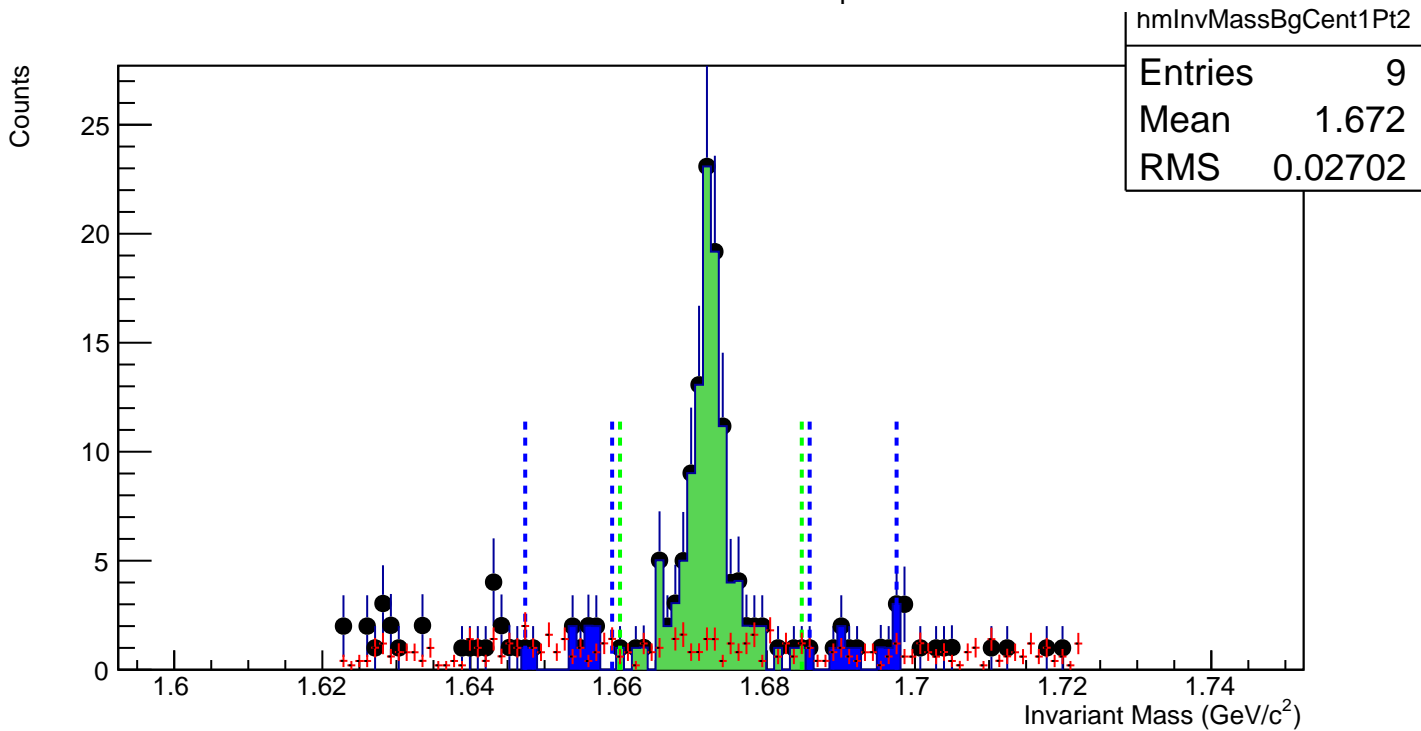
hmlInvMassBgCent4Pt1
Entries 619
Mean 1.671
RMS 0.02647

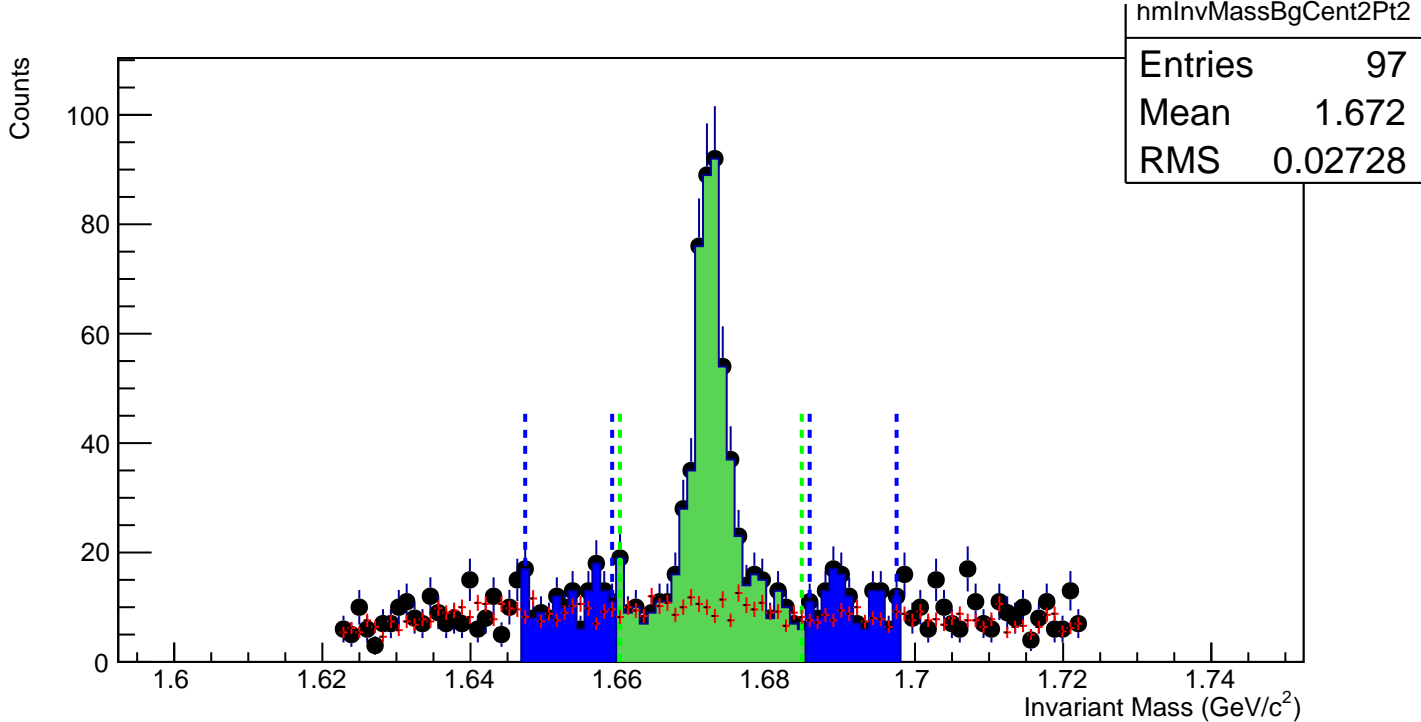
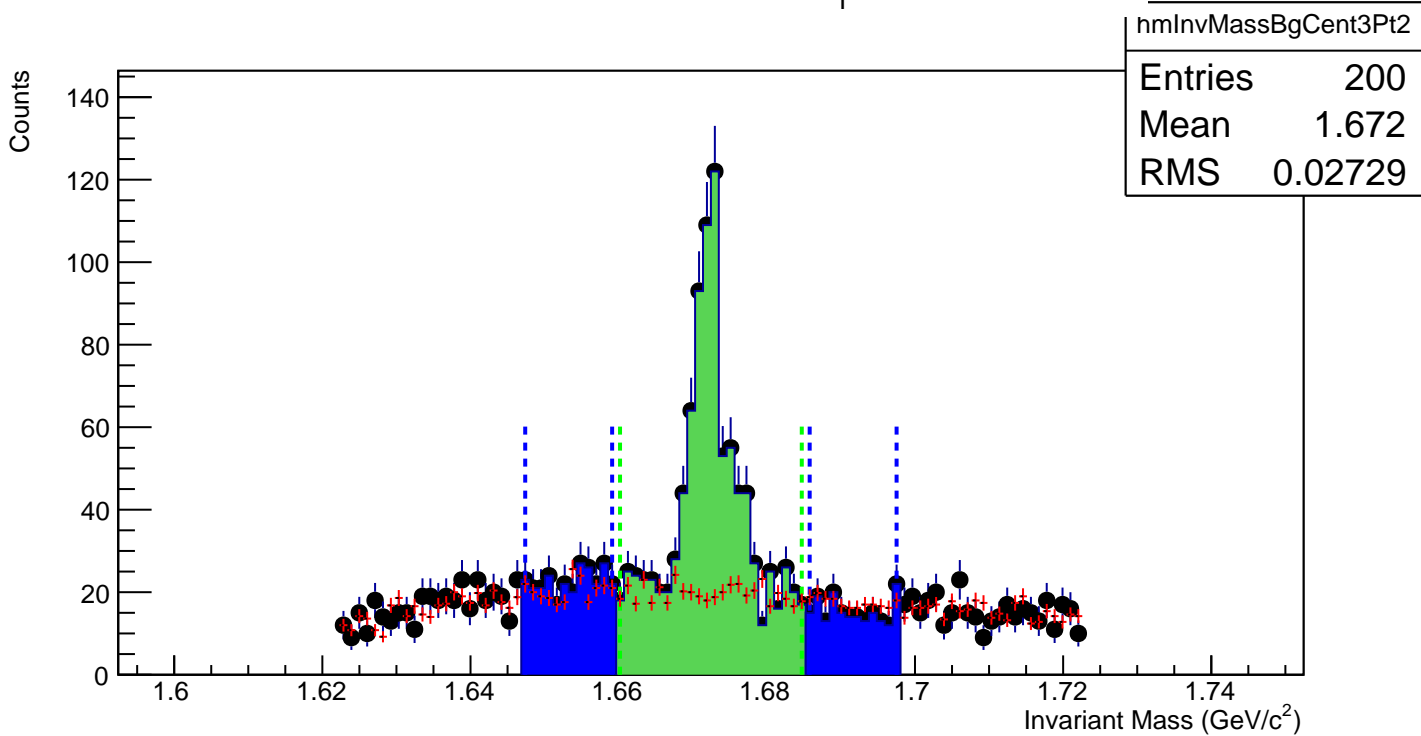


$\Omega^-$ , Au+Au 19 GeV, 60-80%,  $p_T$  1.6-2.0 GeV/c

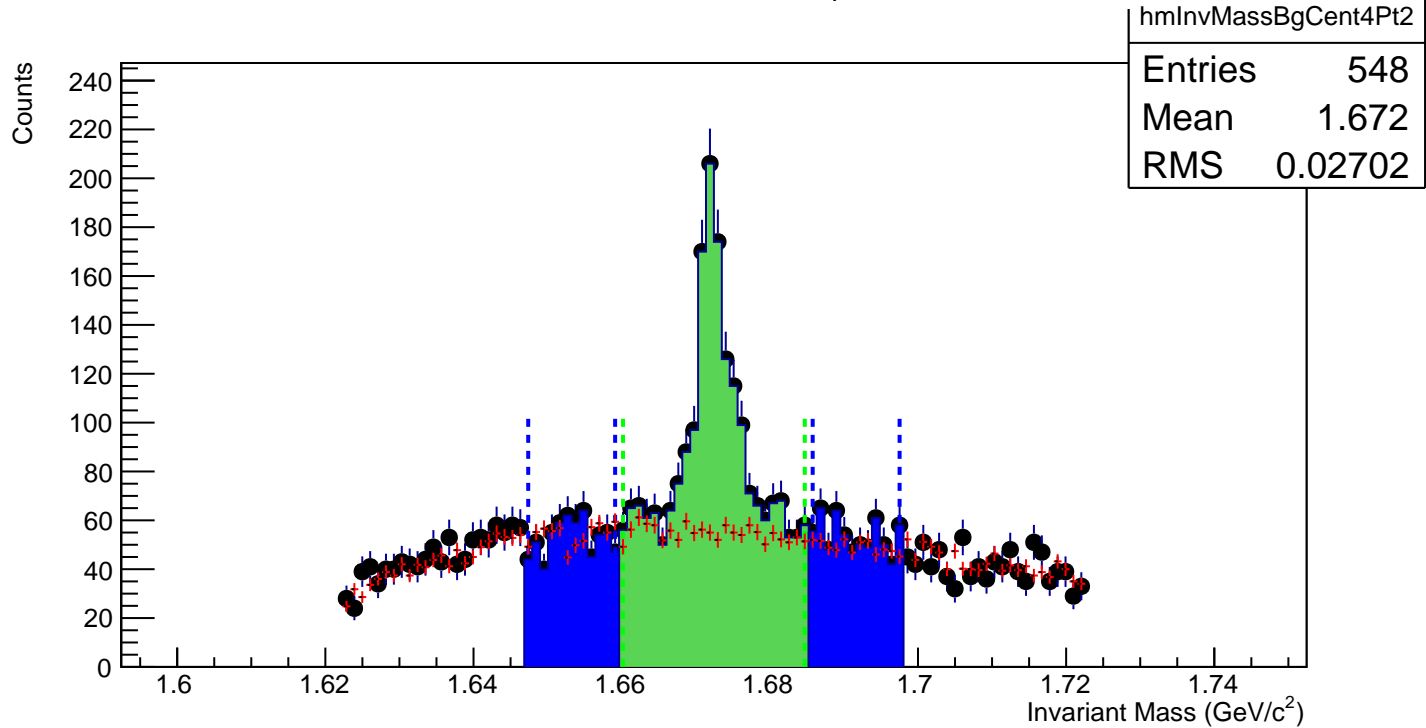


$\Omega^-$ , Au+Au 19 GeV, 40-60%,  $p_T$  1.6-2.0 GeV/c

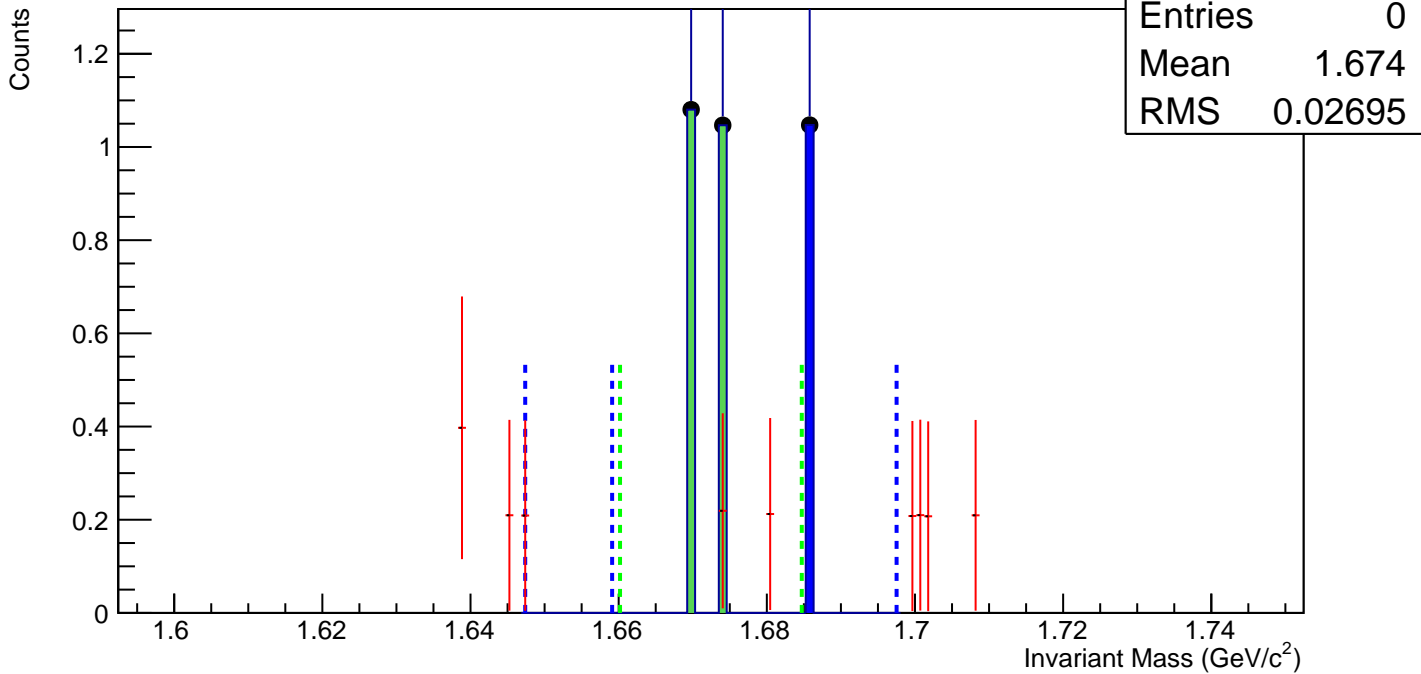


$\Omega^-$ , Au+Au 19 GeV, 20-40%,  $p_T$  1.6-2.0 GeV/c $\Omega^-$ , Au+Au 19 GeV, 10-20%,  $p_T$  1.6-2.0 GeV/c

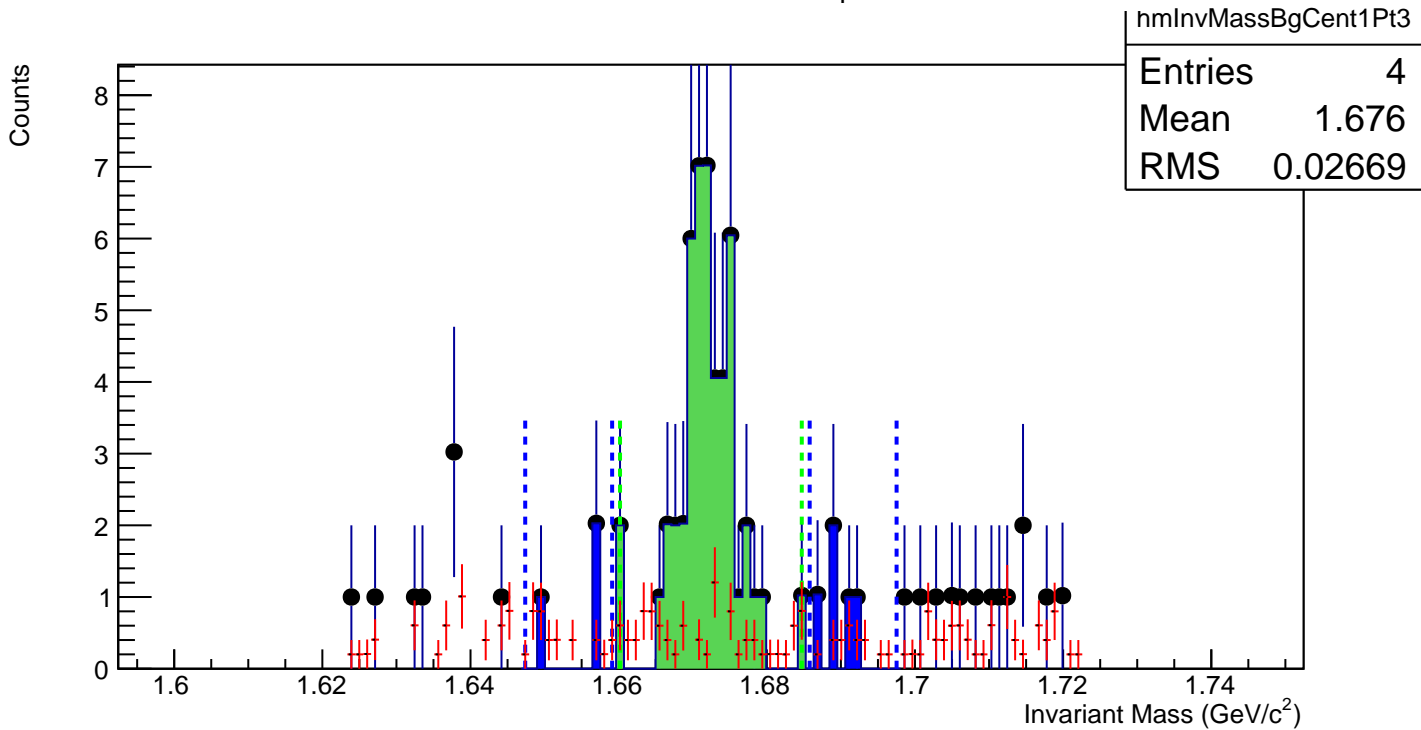
$\Omega^-$ , Au+Au 19 GeV, 0-10%,  $p_T$  1.6-2.0 GeV/c



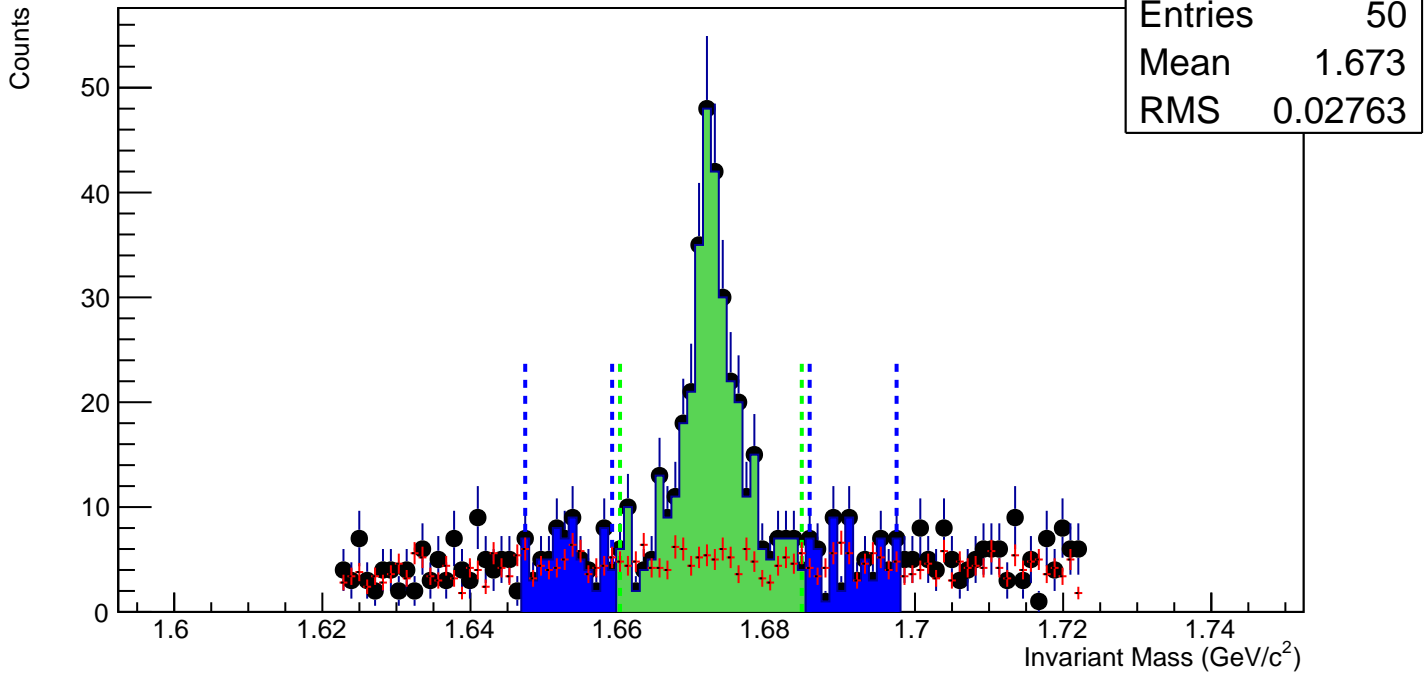
$\Omega^-$ , Au+Au 19 GeV, 60-80%,  $p_T$  2.0-2.4 GeV/c



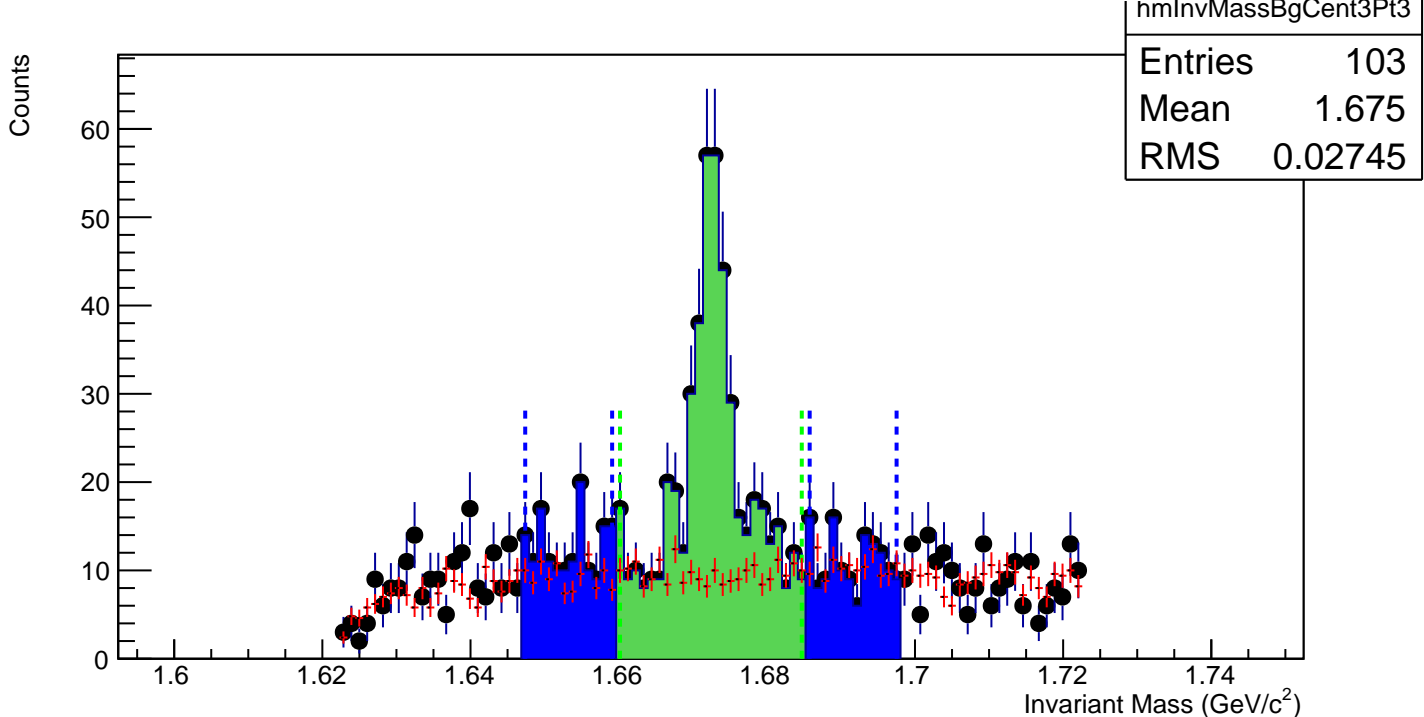
$\Omega^-$ , Au+Au 19 GeV, 40-60%,  $p_T$  2.0-2.4 GeV/c



$\Omega^-$ , Au+Au 19 GeV, 20-40%,  $p_T$  2.0-2.4 GeV/c

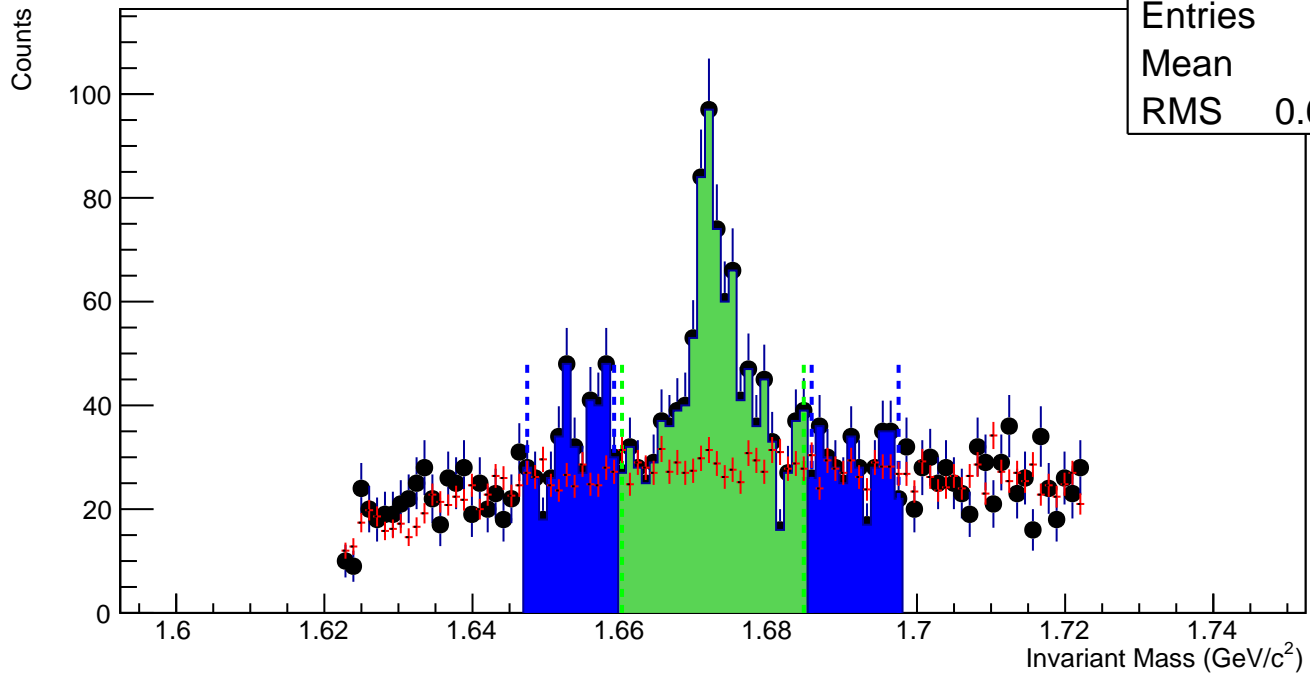


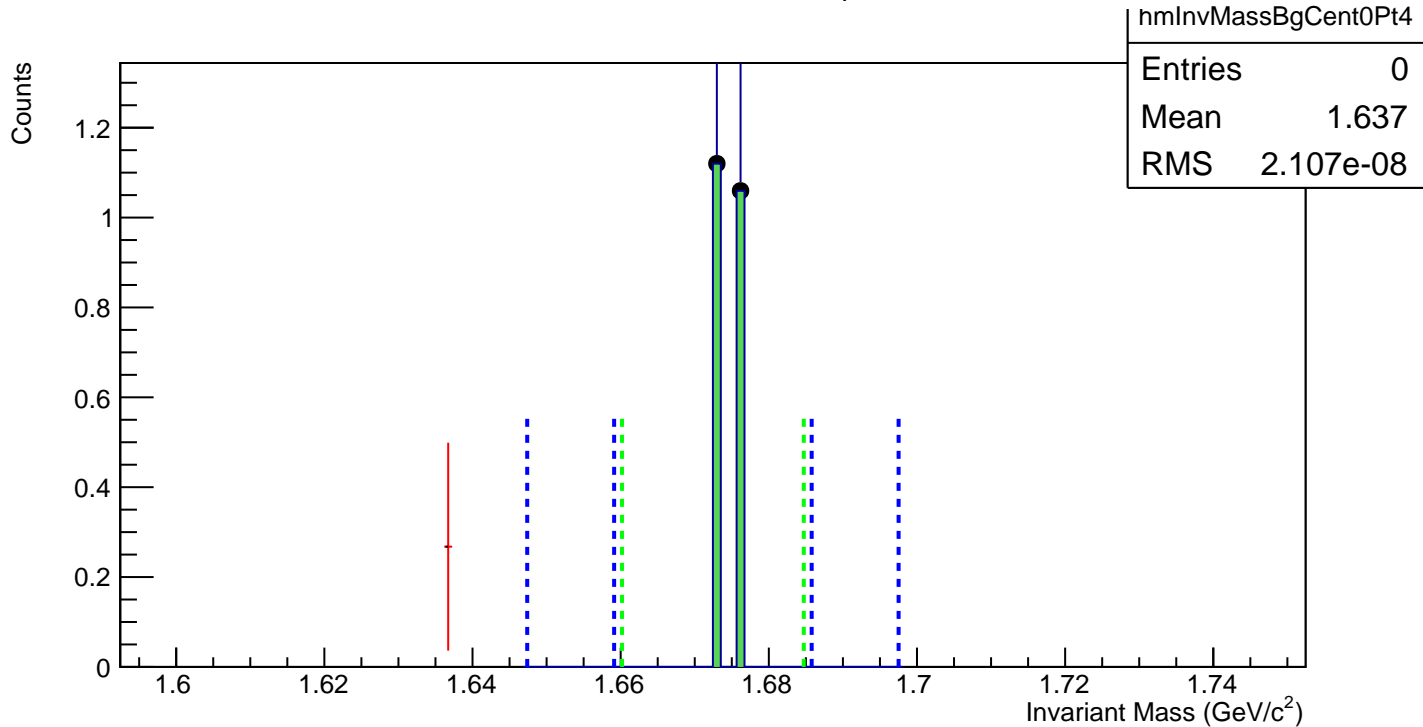
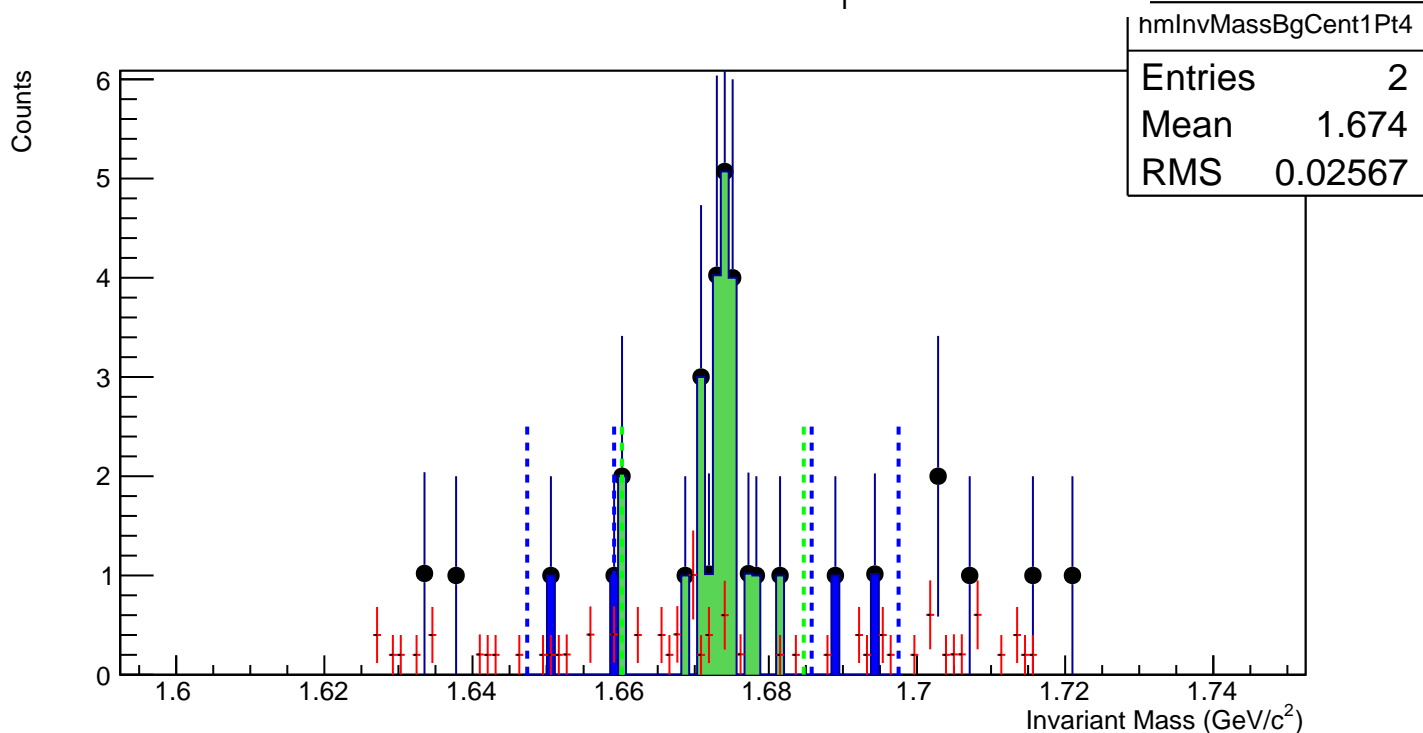
$\Omega^-$ , Au+Au 19 GeV, 10-20%,  $p_T$  2.0-2.4 GeV/c

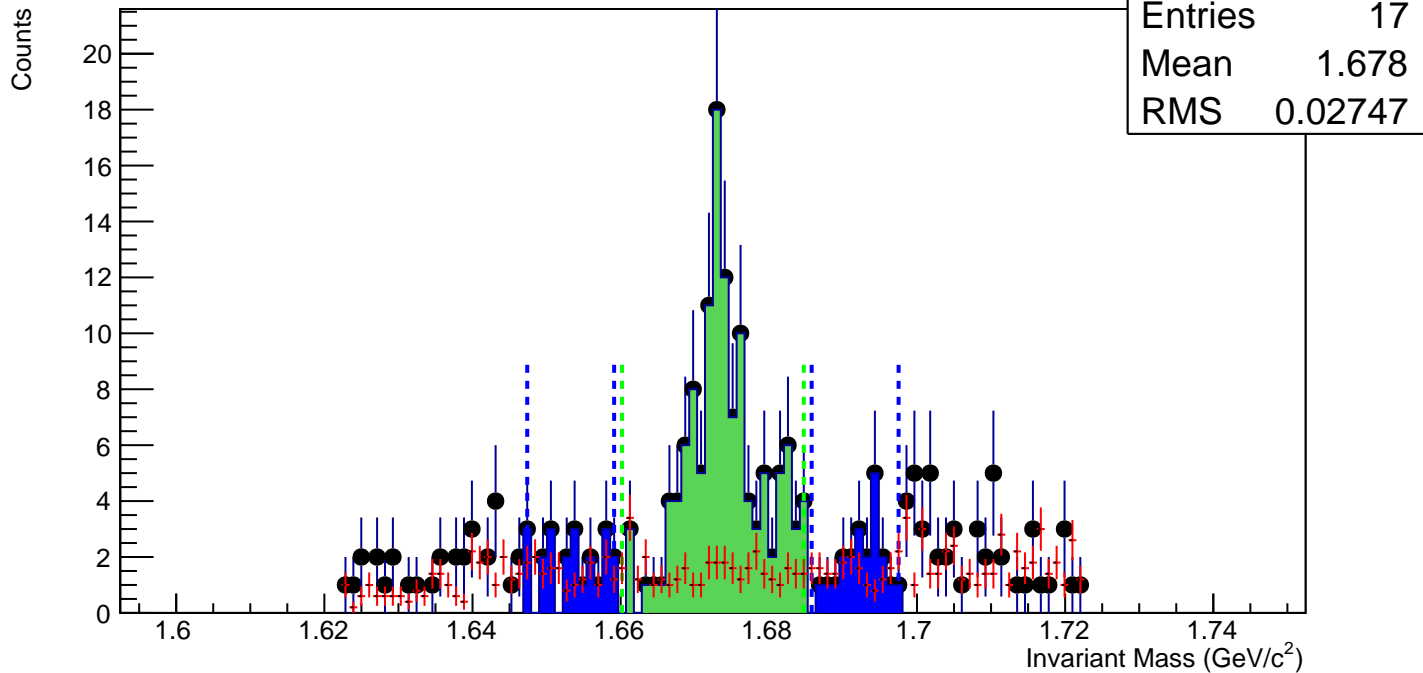
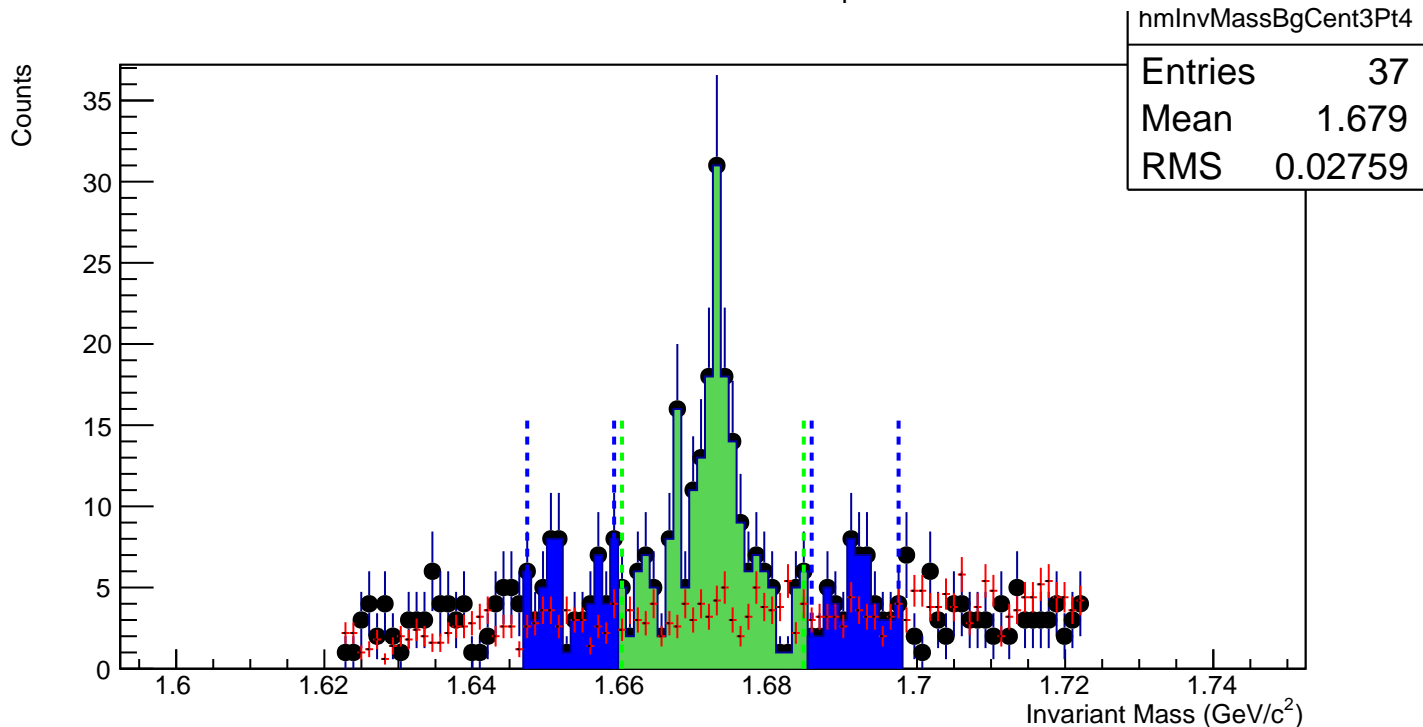


$\Omega^-$ , Au+Au 19 GeV, 0-10%,  $p_T$  2.0-2.4 GeV/c

hmlInvMassBgCent4Pt3
Entries 290
Mean 1.675
RMS 0.02732

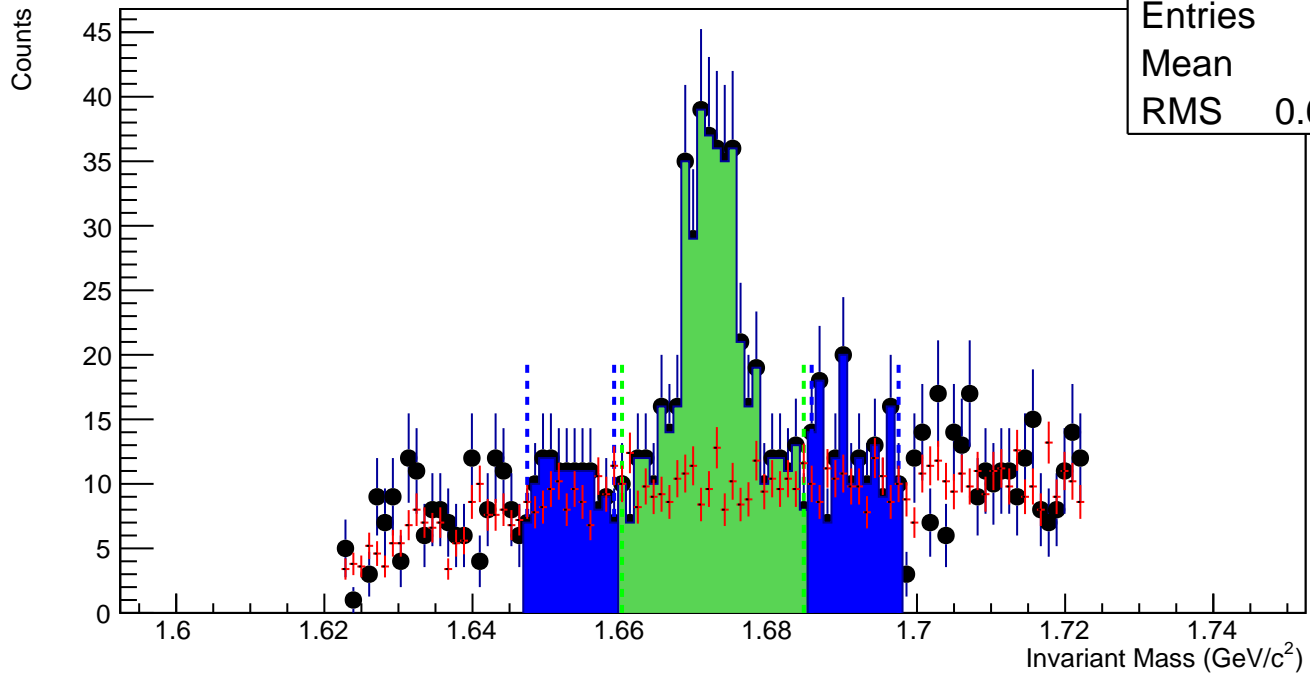


$\Omega^-$ , Au+Au 19 GeV, 60-80%,  $p_T$  2.4-2.8 GeV/c $\Omega^-$ , Au+Au 19 GeV, 40-60%,  $p_T$  2.4-2.8 GeV/c

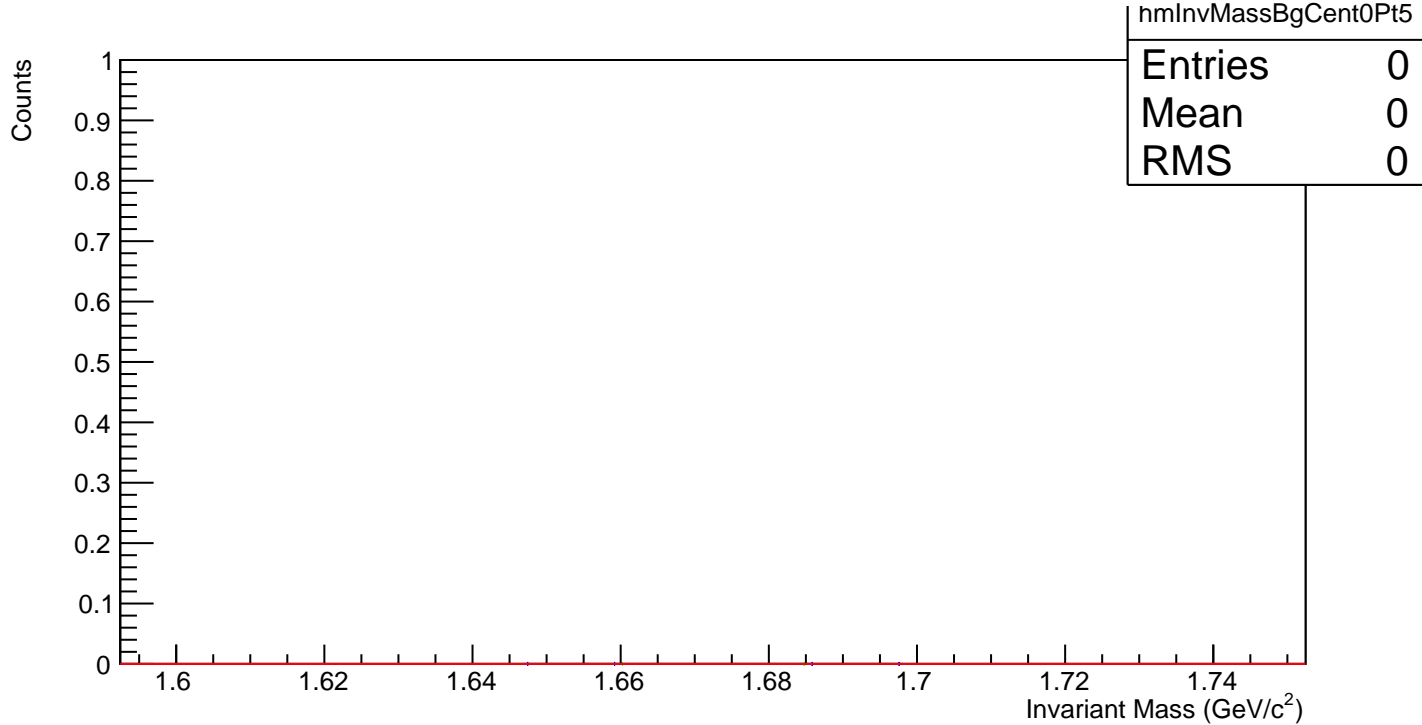
$\Omega^-, \text{Au+Au } 19 \text{ GeV, 20-40\%, } p_T \text{ 2.4-2.8 GeV/c}$  $\Omega^-, \text{Au+Au } 19 \text{ GeV, 10-20\%, } p_T \text{ 2.4-2.8 GeV/c}$ 

$\Omega^-$ , Au+Au 19 GeV, 0-10%,  $p_T$  2.4-2.8 GeV/c

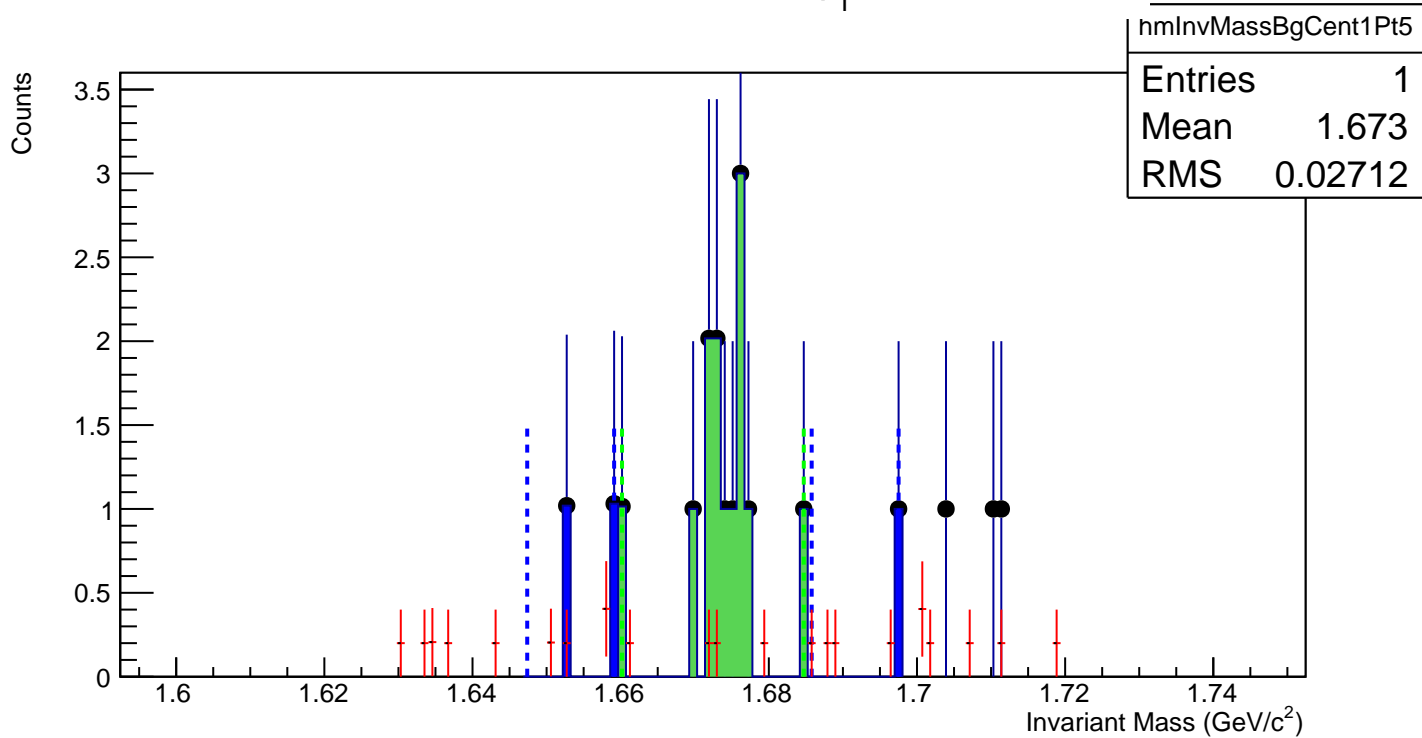
hmlInvMassBgCent4Pt4
Entries 103
Mean 1.677
RMS 0.02716



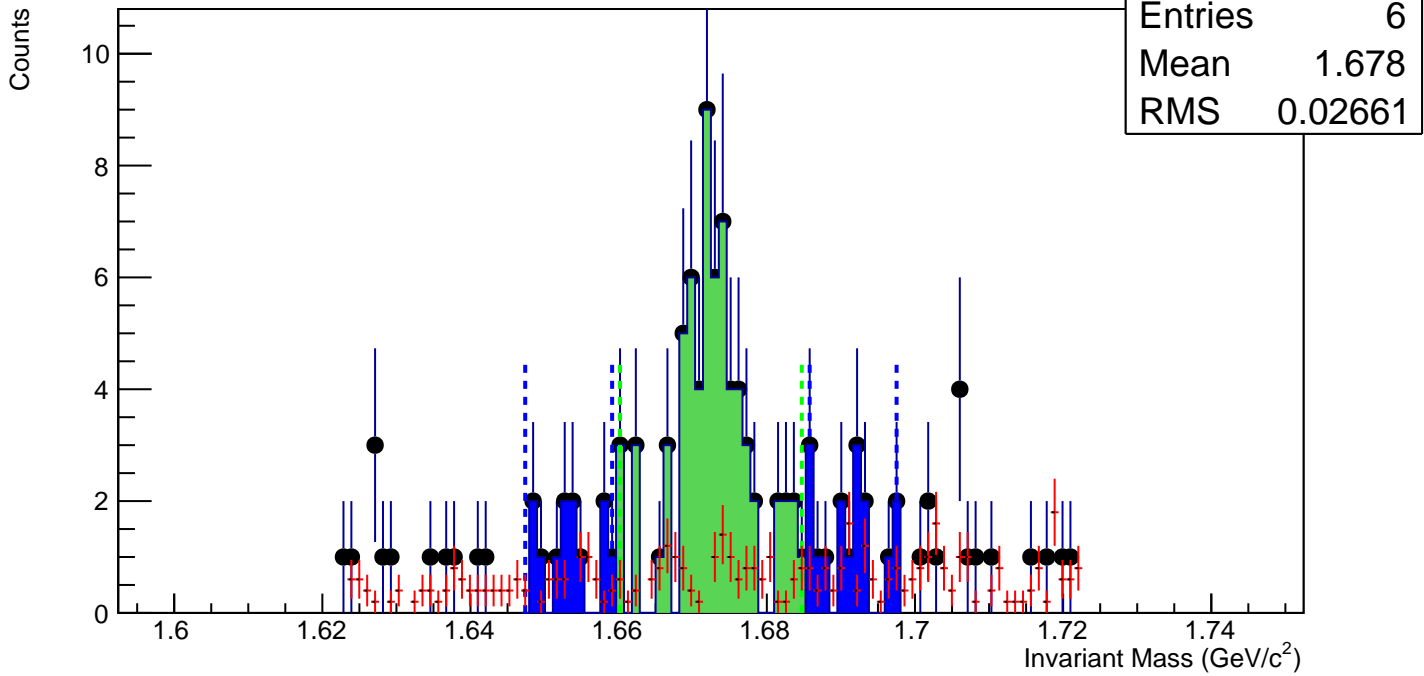
$\Omega^-$ , Au+Au 19 GeV, 60-80%,  $p_T$  2.8-3.6 GeV/c



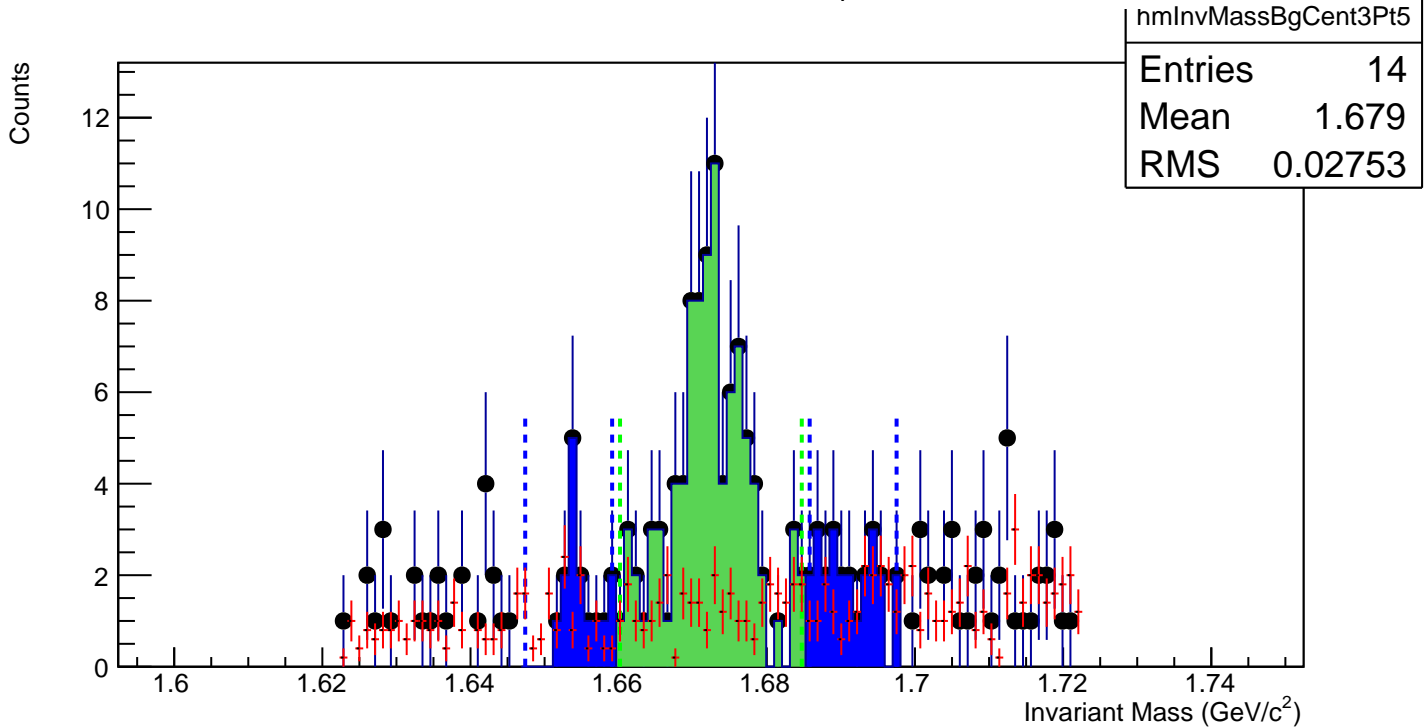
$\Omega^-$ , Au+Au 19 GeV, 40-60%,  $p_T$  2.8-3.6 GeV/c



$\Omega^-$ , Au+Au 19 GeV, 20-40%,  $p_T$  2.8-3.6 GeV/c

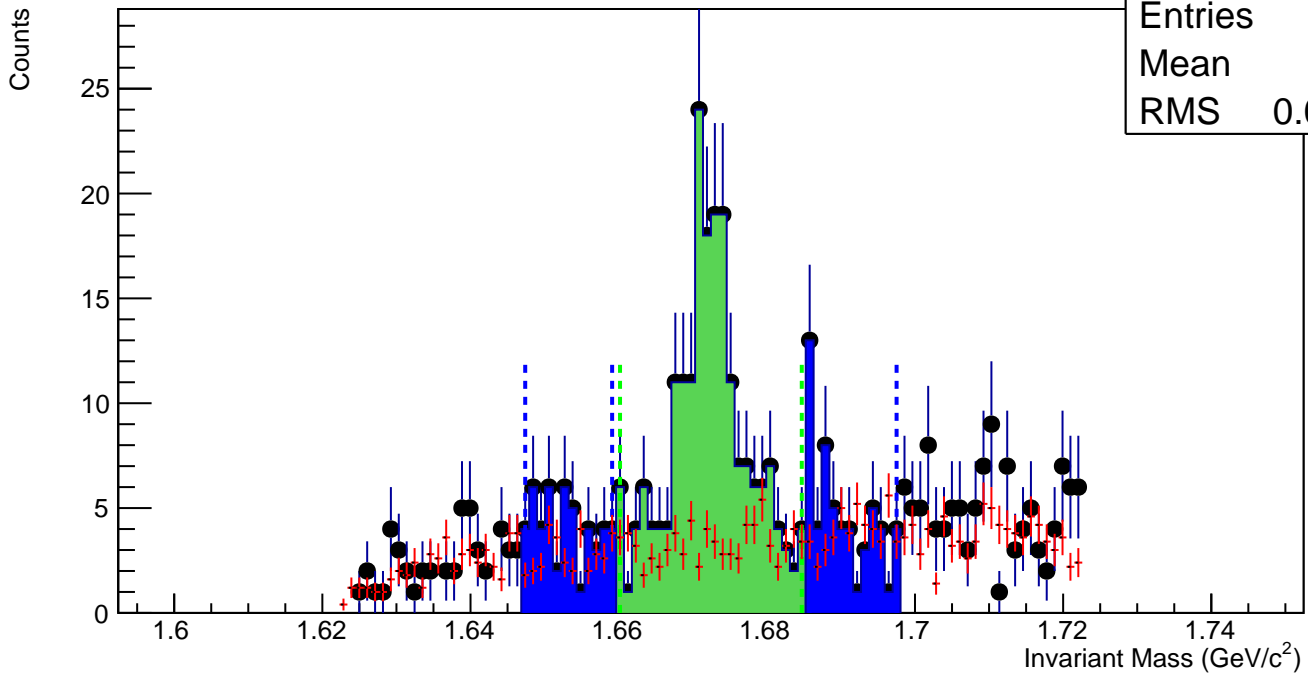


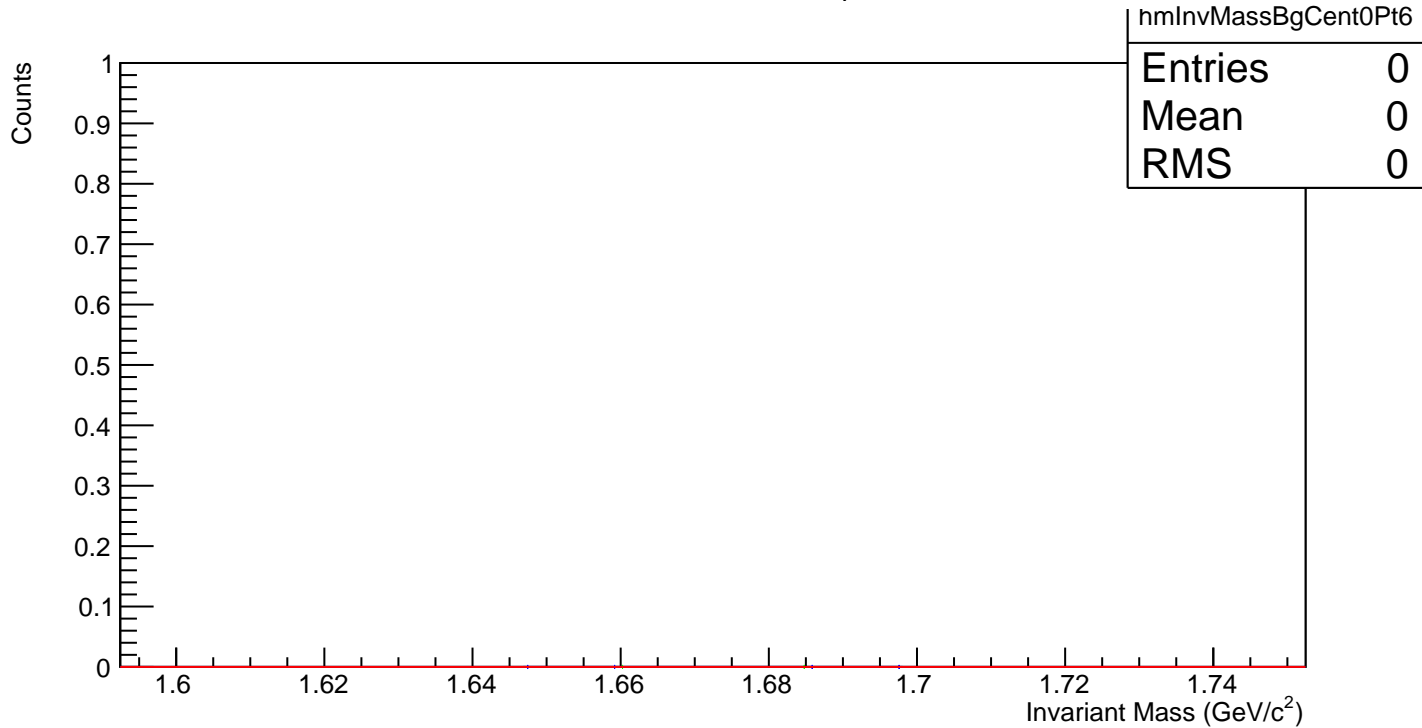
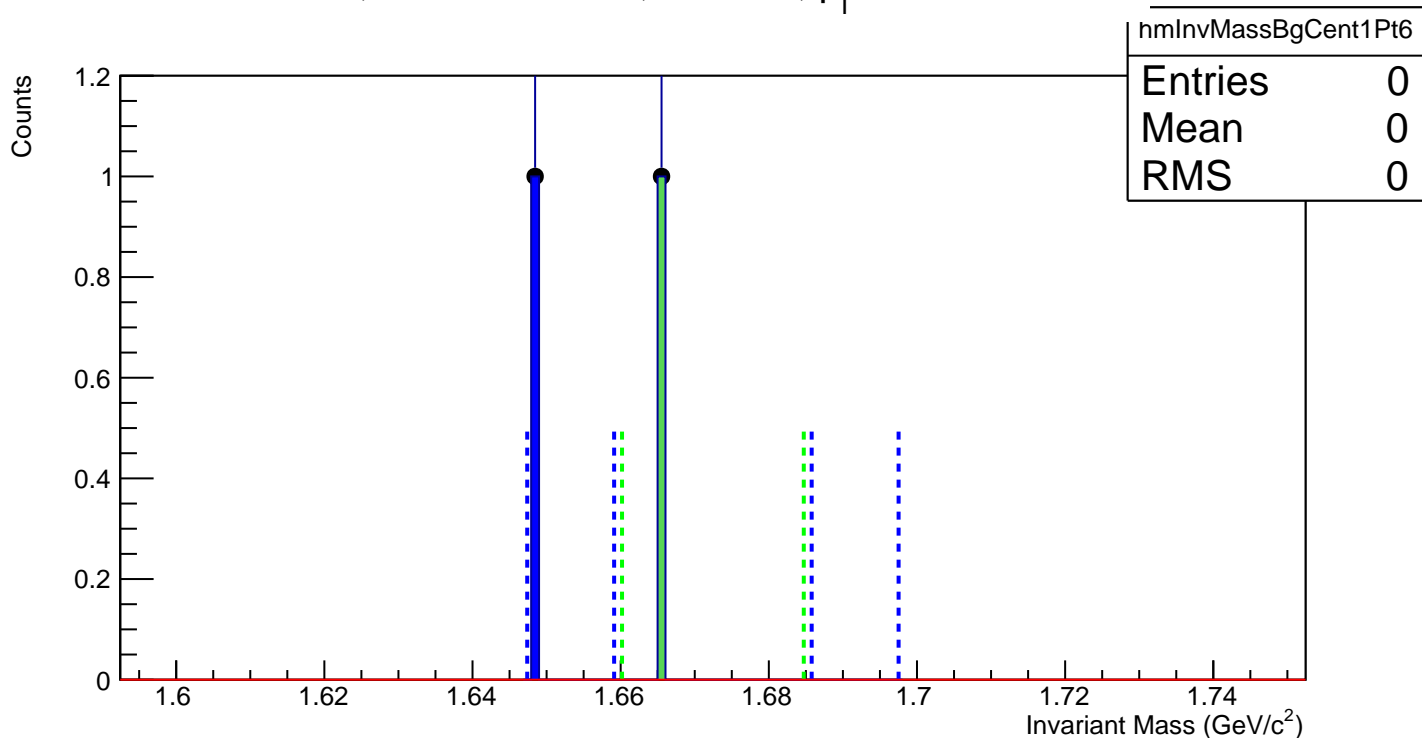
$\Omega^-$ , Au+Au 19 GeV, 10-20%,  $p_T$  2.8-3.6 GeV/c



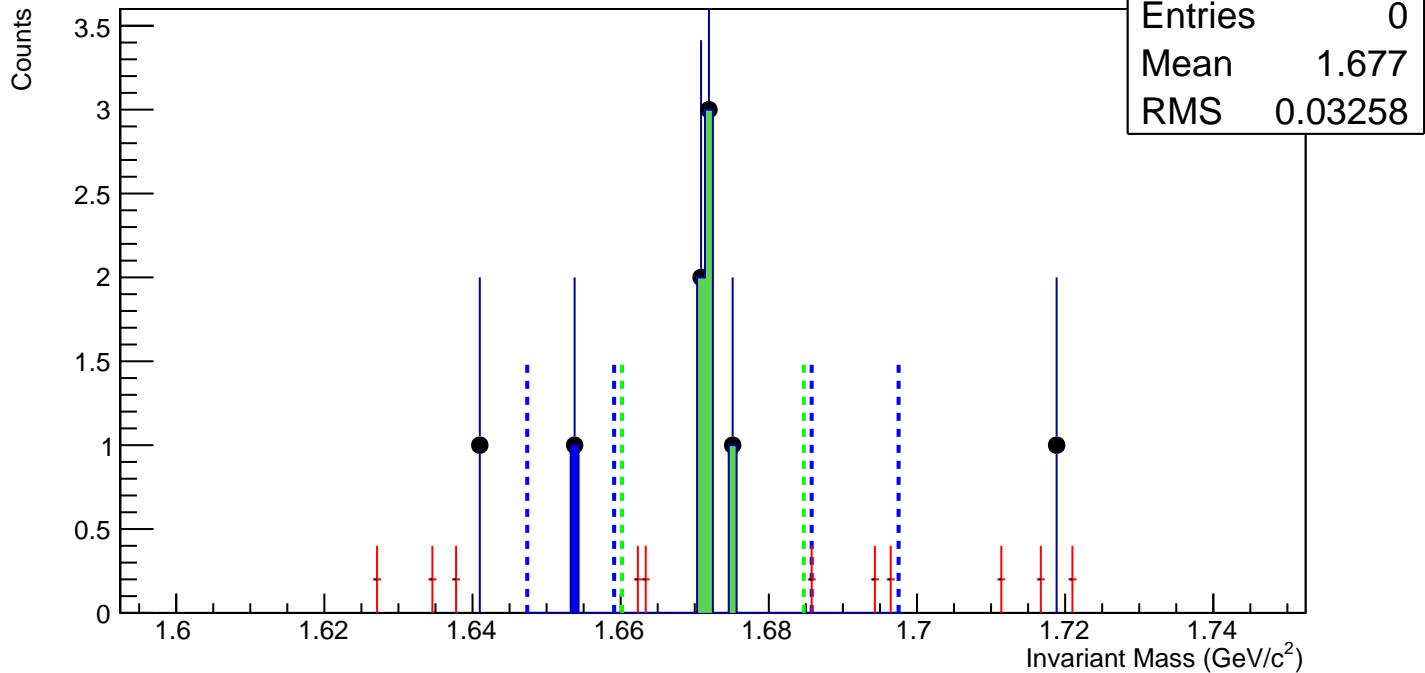
$\Omega^-$ , Au+Au 19 GeV, 0-10%,  $p_T$  2.8-3.6 GeV/c

hmlInvMassBgCent4Pt5
Entries 35
Mean 1.678
RMS 0.02685

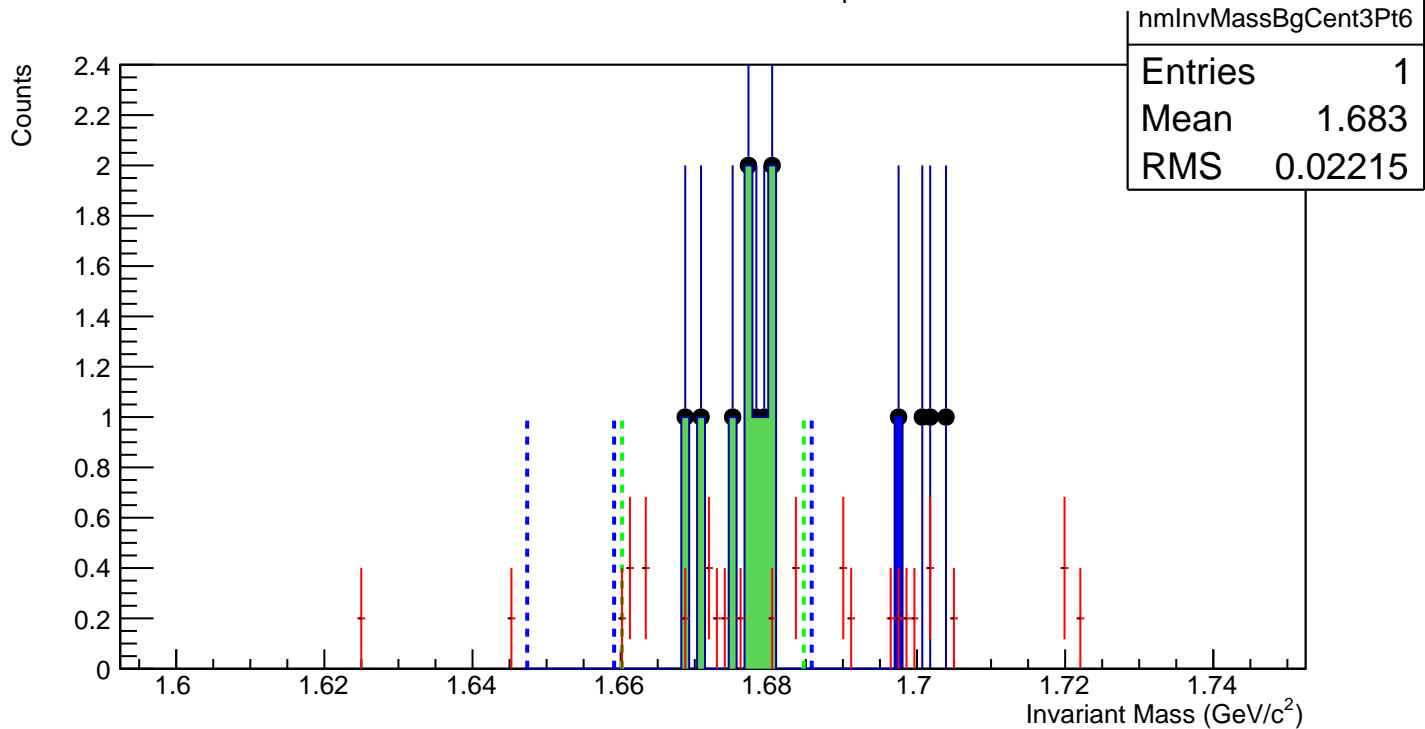


$\Omega^-$ , Au+Au 19 GeV, 60-80%,  $p_T$  3.6-5.0 GeV/c $\Omega^-$ , Au+Au 19 GeV, 40-60%,  $p_T$  3.6-5.0 GeV/c

$\Omega^-$ , Au+Au 19 GeV, 20-40%,  $p_T$  3.6-5.0 GeV/c

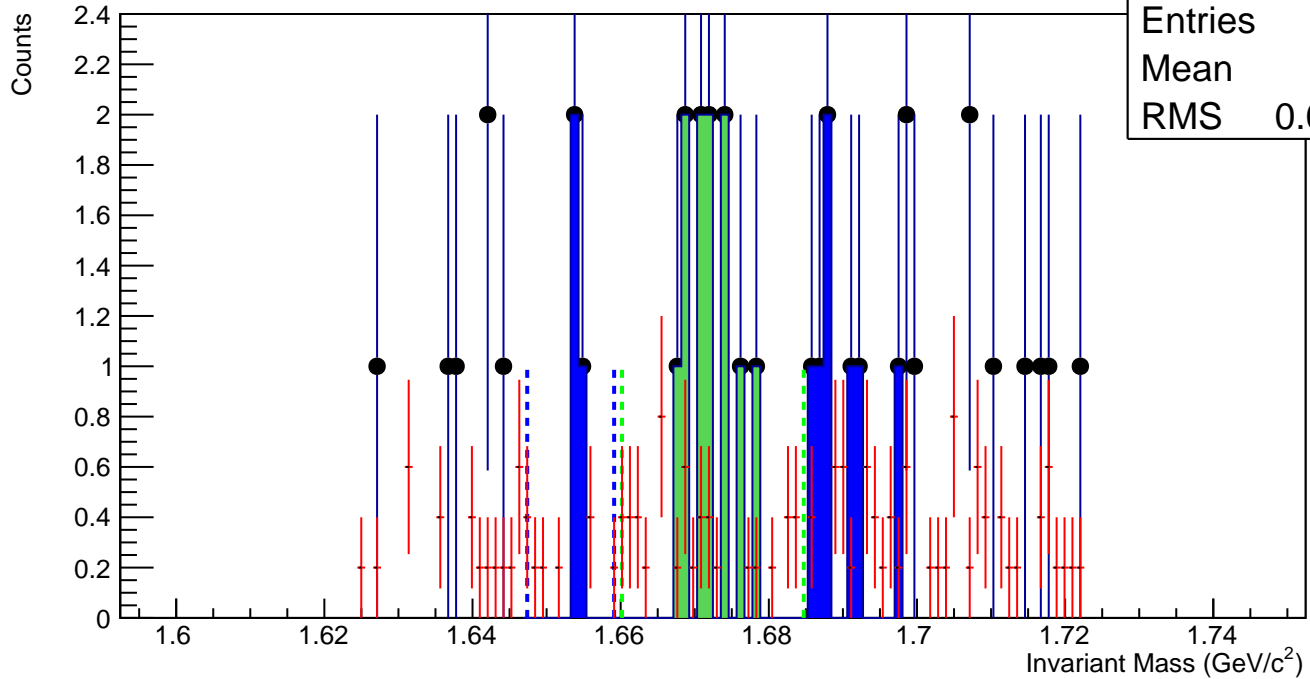


$\Omega^-$ , Au+Au 19 GeV, 10-20%,  $p_T$  3.6-5.0 GeV/c

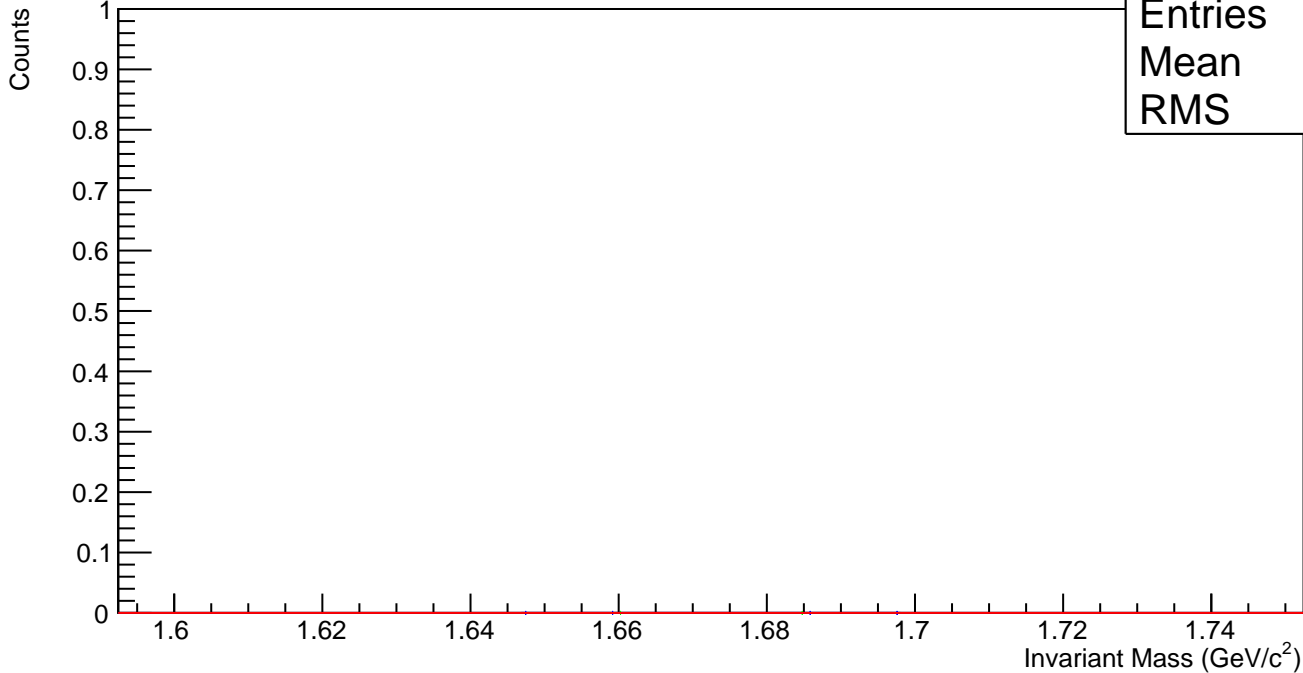


$\Omega^-$ , Au+Au 19 GeV, 0-10%,  $p_T$  3.6-5.0 GeV/c

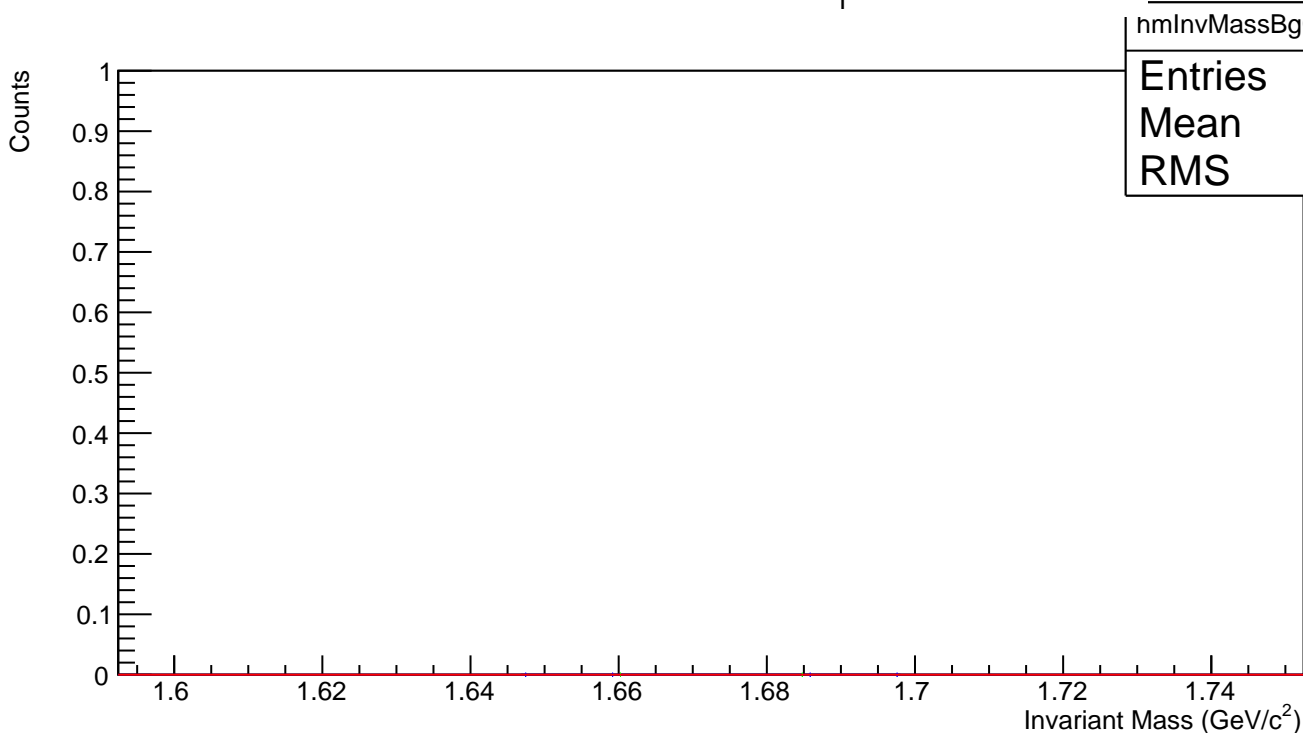
hmlInvMassBgCent4Pt6
Entries 2
Mean 1.679
RMS 0.02668



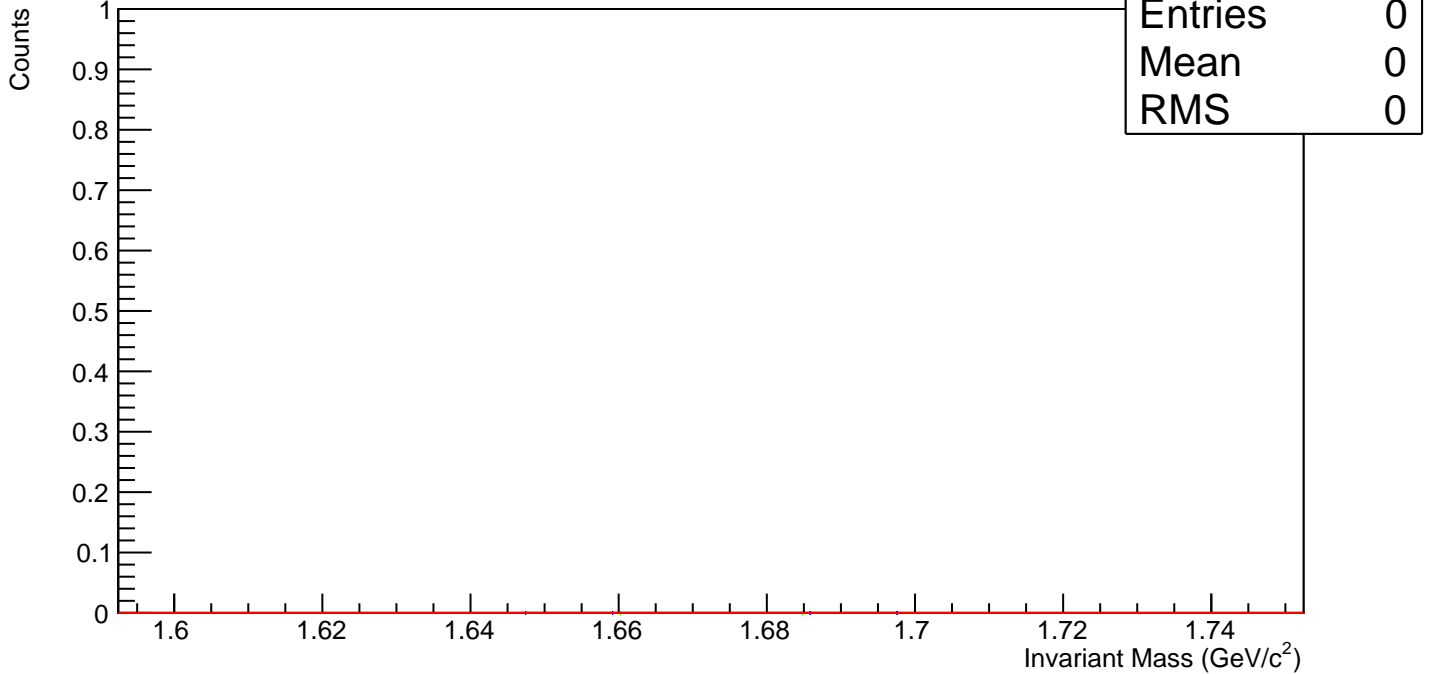
$\Omega^-$ , Au+Au 19 GeV, 60-80%,  $p_T$  5.0-7.0 GeV/c



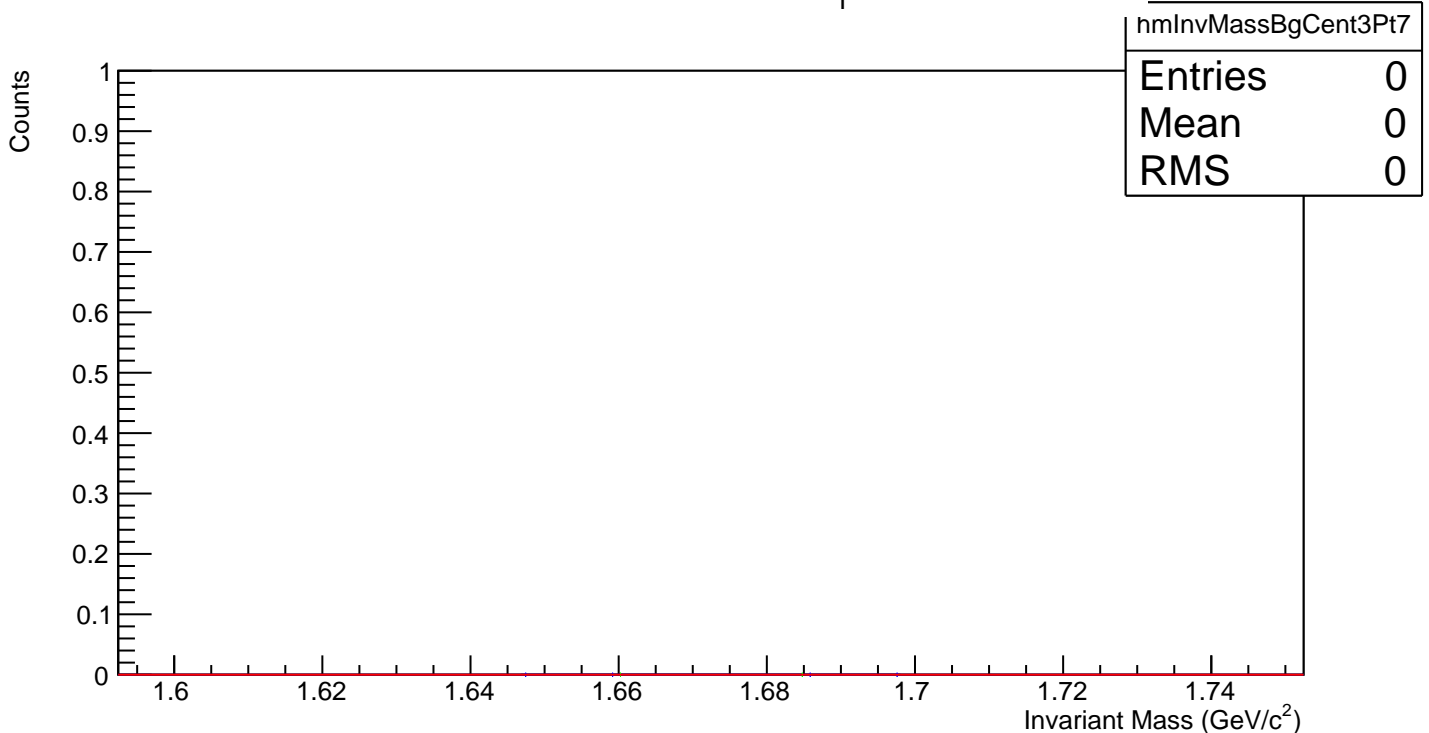
$\Omega^-$ , Au+Au 19 GeV, 40-60%,  $p_T$  5.0-7.0 GeV/c



$\Omega^-$ , Au+Au 19 GeV, 20-40%,  $p_T$  5.0-7.0 GeV/c



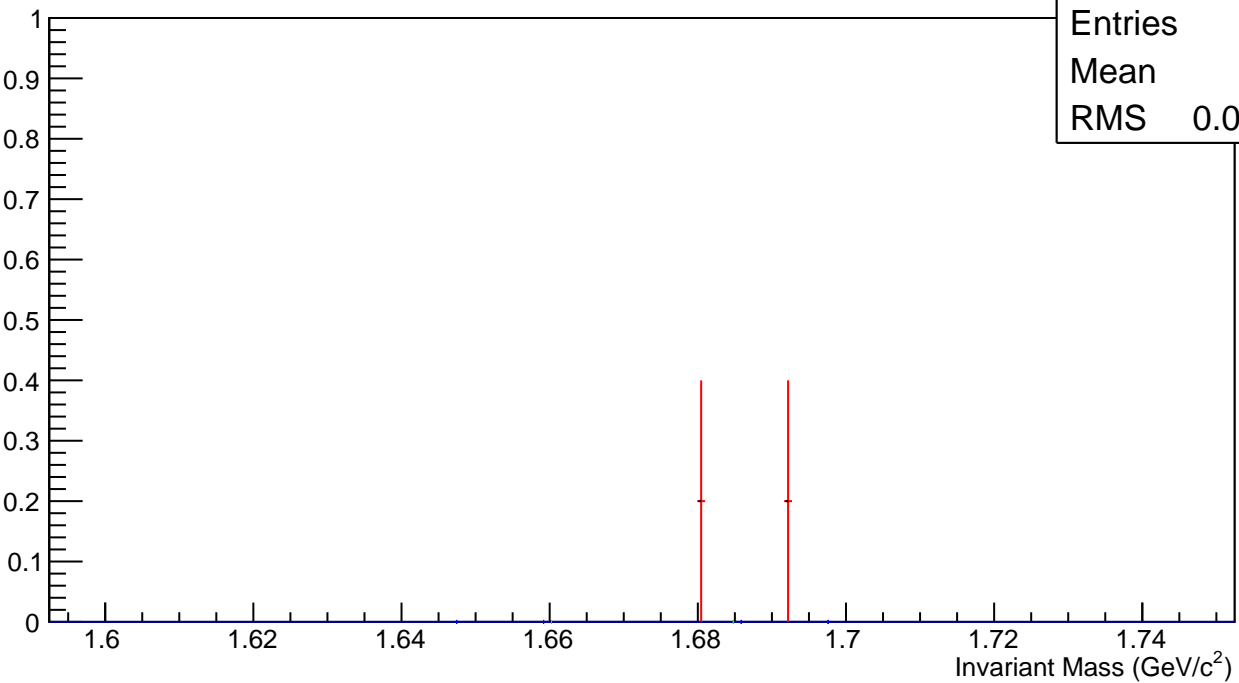
$\Omega^-$ , Au+Au 19 GeV, 10-20%,  $p_T$  5.0-7.0 GeV/c



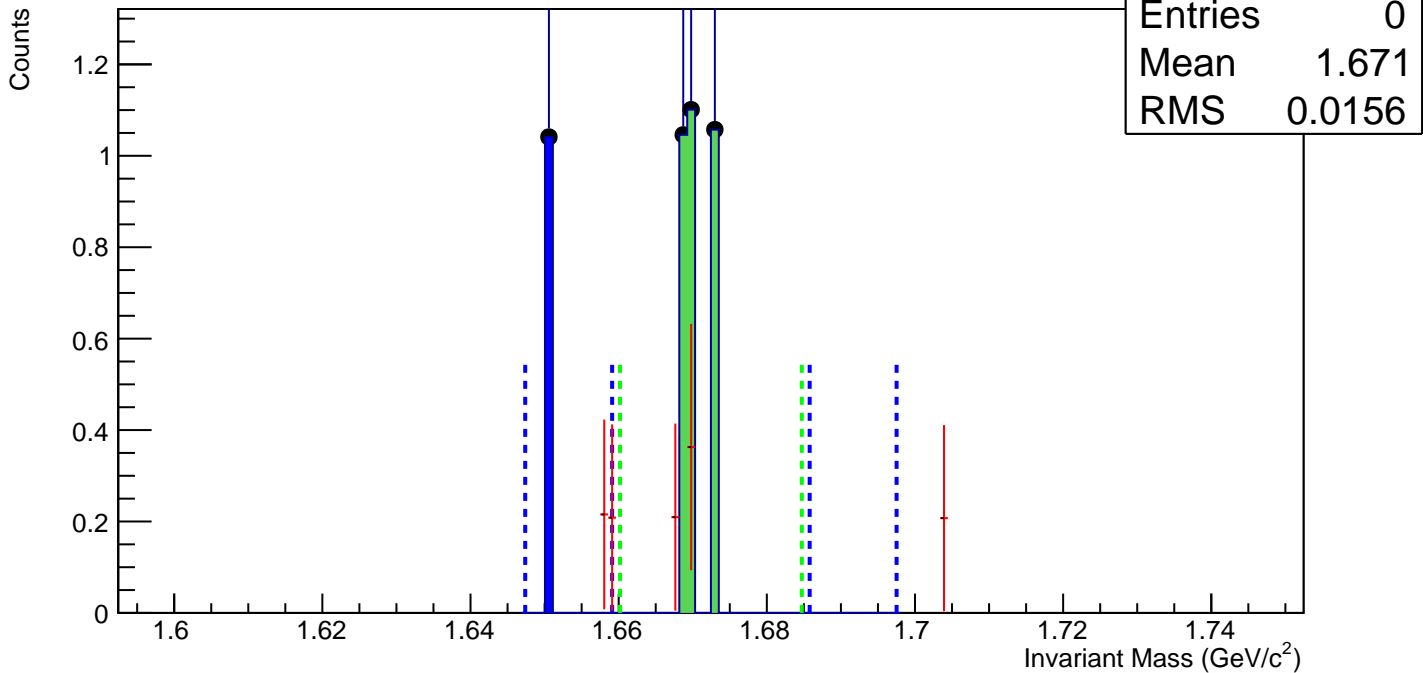
$\Omega^-$ , Au+Au 19 GeV, 0-10%,  $p_T$  5.0-7.0 GeV/c

Counts

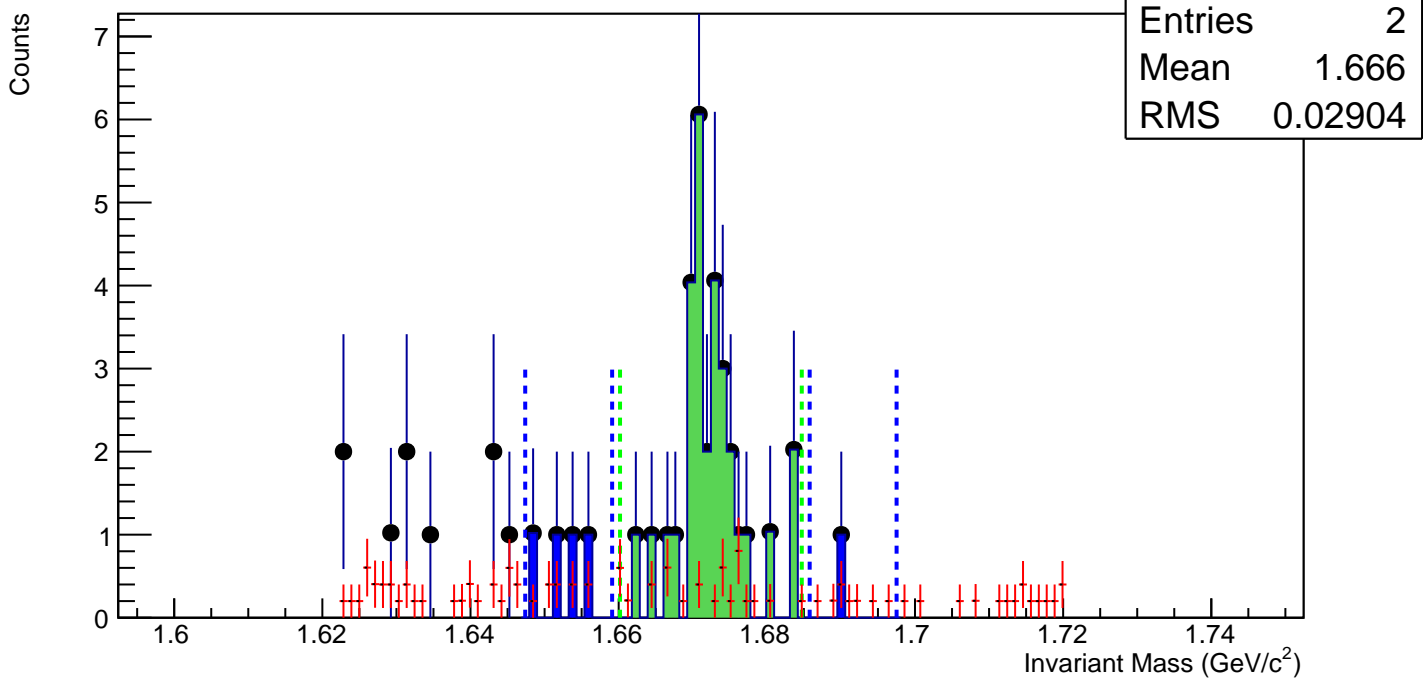
hmlInvMassBgCent4Pt7	
Entries	0
Mean	1.686
RMS	0.005867



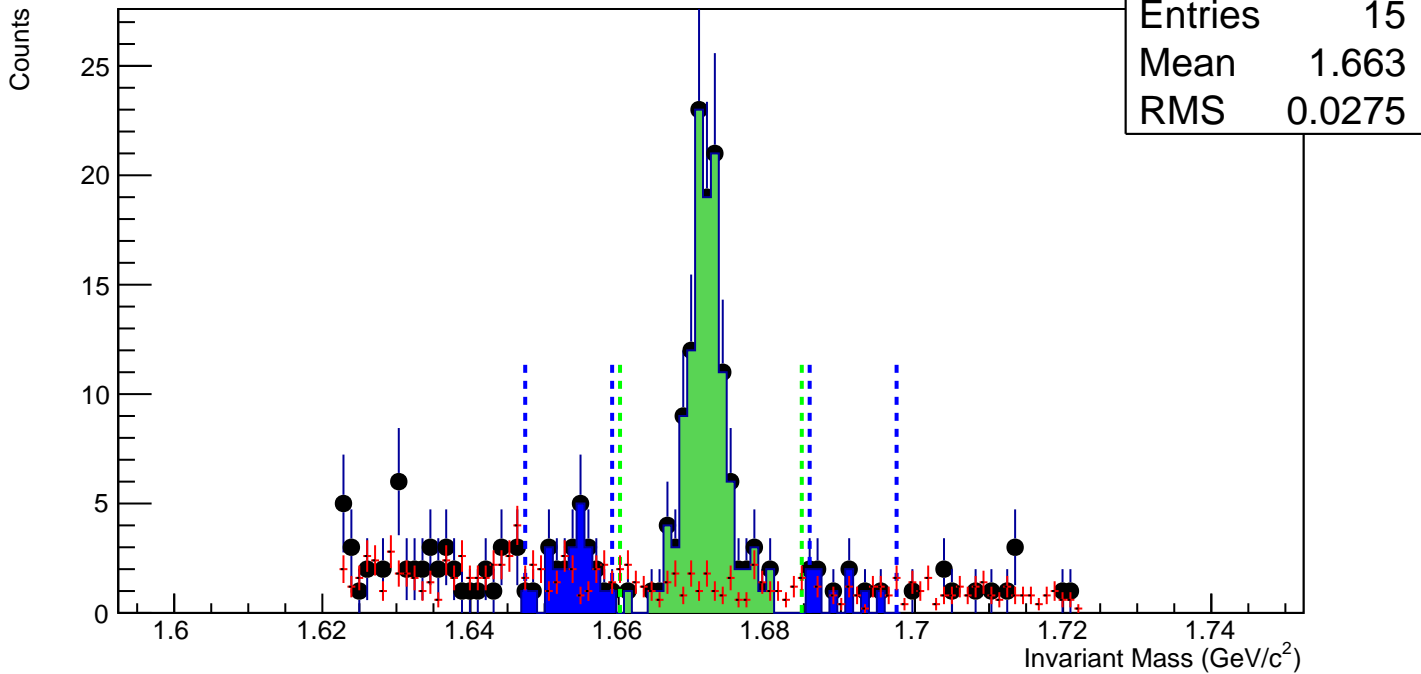
$\Omega^+$ , Au+Au 19 GeV, 60-80%,  $p_T$  0.8-1.2 GeV/c



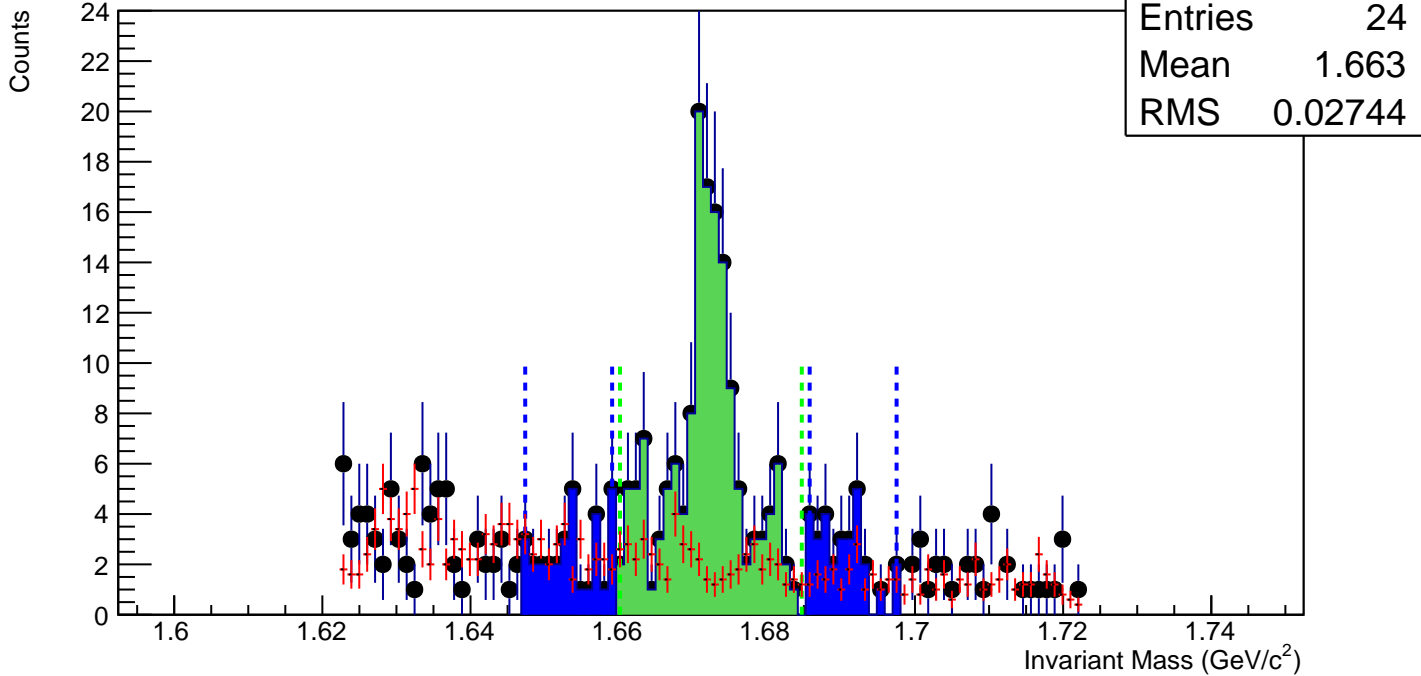
$\Omega^+$ , Au+Au 19 GeV, 40-60%,  $p_T$  0.8-1.2 GeV/c



$\Omega^+$ , Au+Au 19 GeV, 20-40%,  $p_T$  0.8-1.2 GeV/c

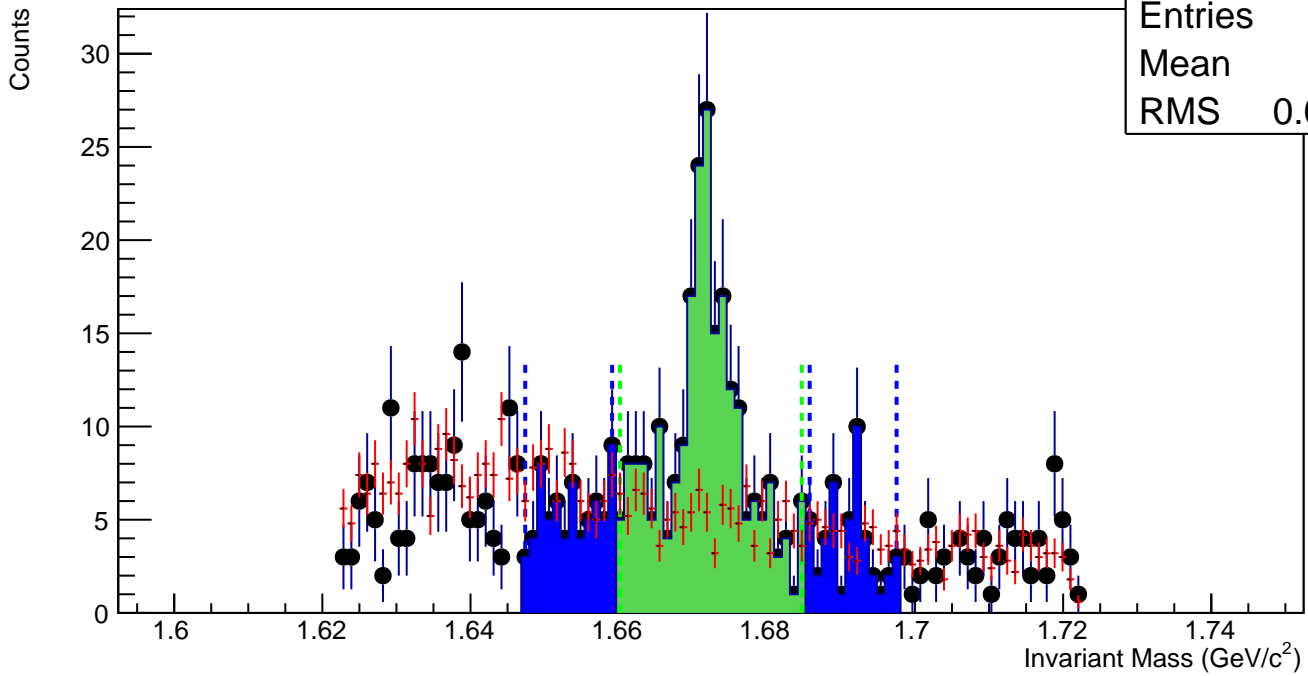


$\Omega^+$ , Au+Au 19 GeV, 10-20%,  $p_T$  0.8-1.2 GeV/c

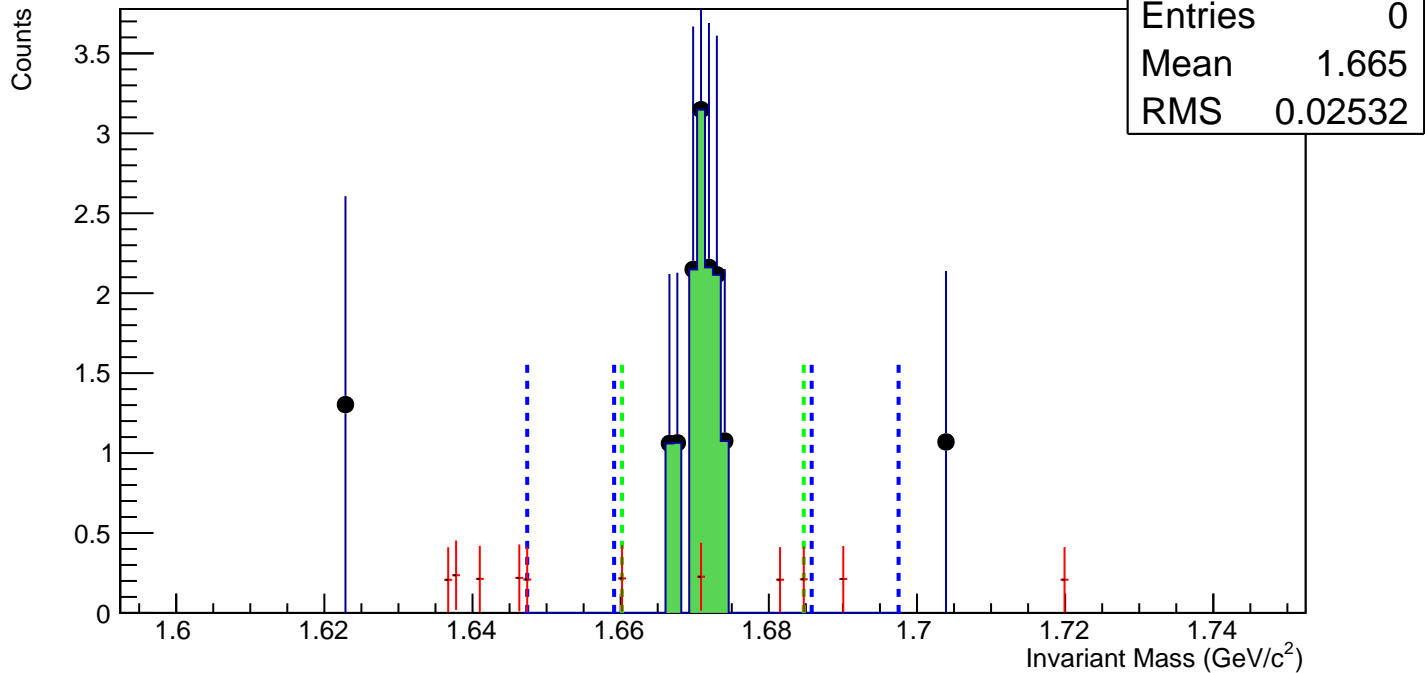


$\Omega^+$ , Au+Au 19 GeV, 0-10%,  $p_T$  0.8-1.2 GeV/c

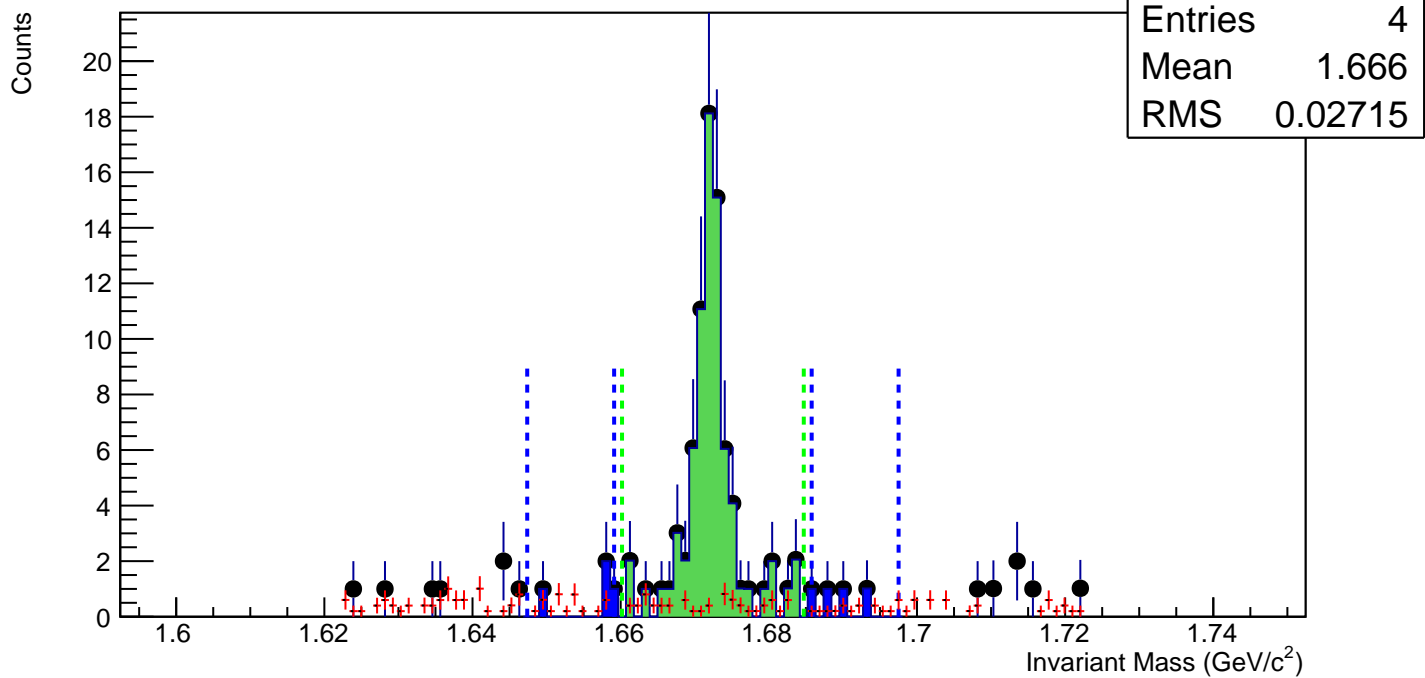
hmlInvMassBgCent4Pt0
Entries 61
Mean 1.663
RMS 0.02706



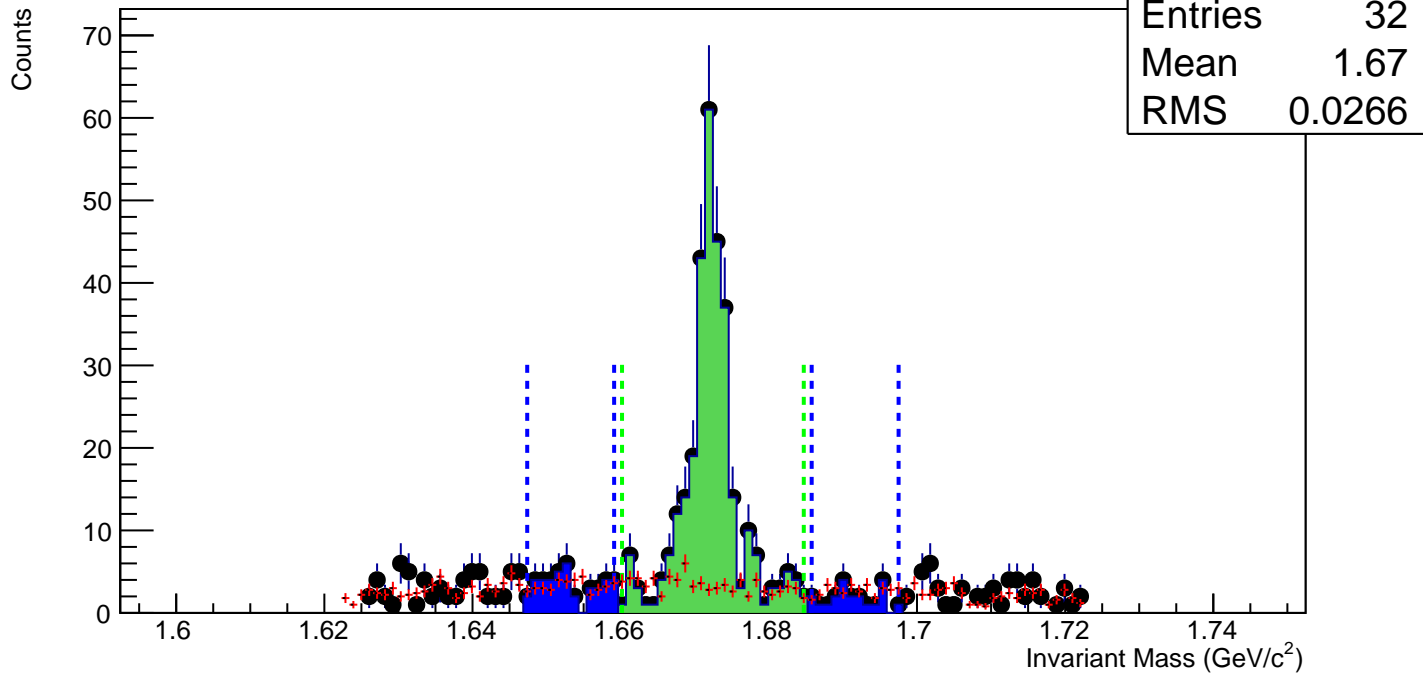
$\Omega^+$ , Au+Au 19 GeV, 60-80%,  $p_T$  1.2-1.6 GeV/c



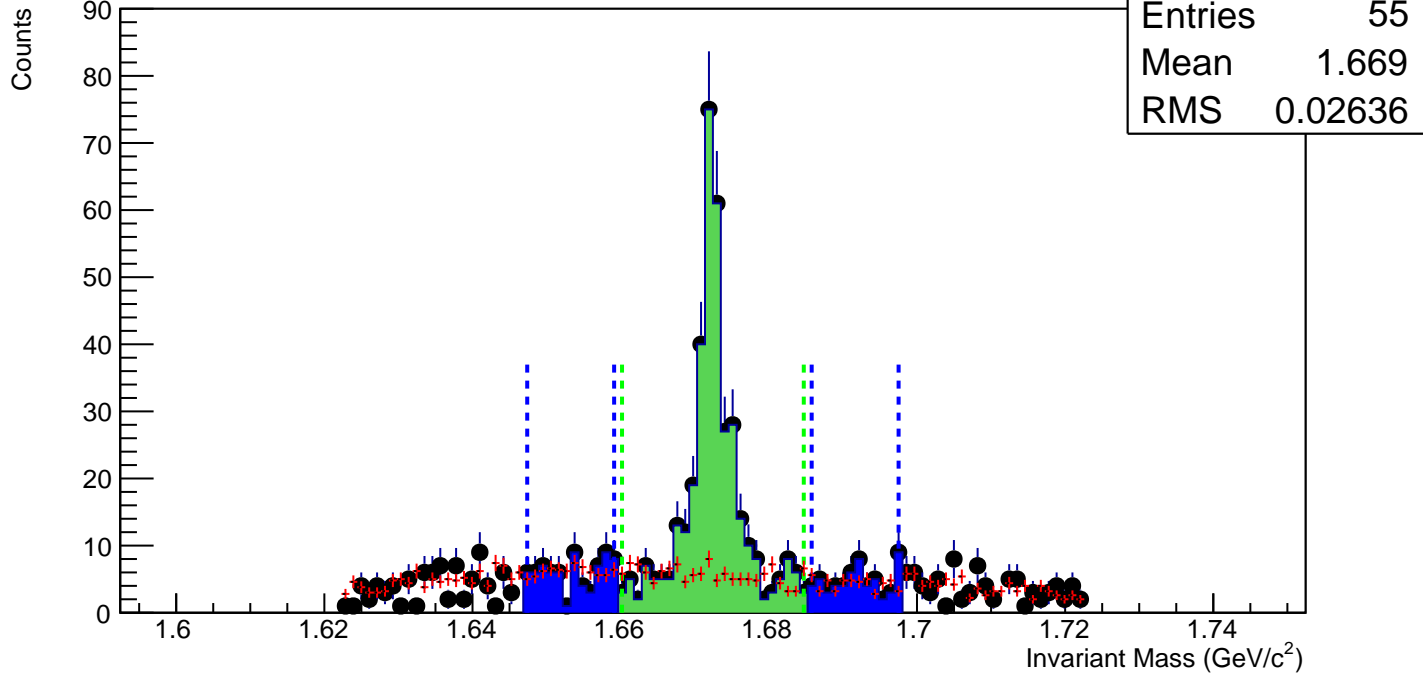
$\Omega^+$ , Au+Au 19 GeV, 40-60%,  $p_T$  1.2-1.6 GeV/c



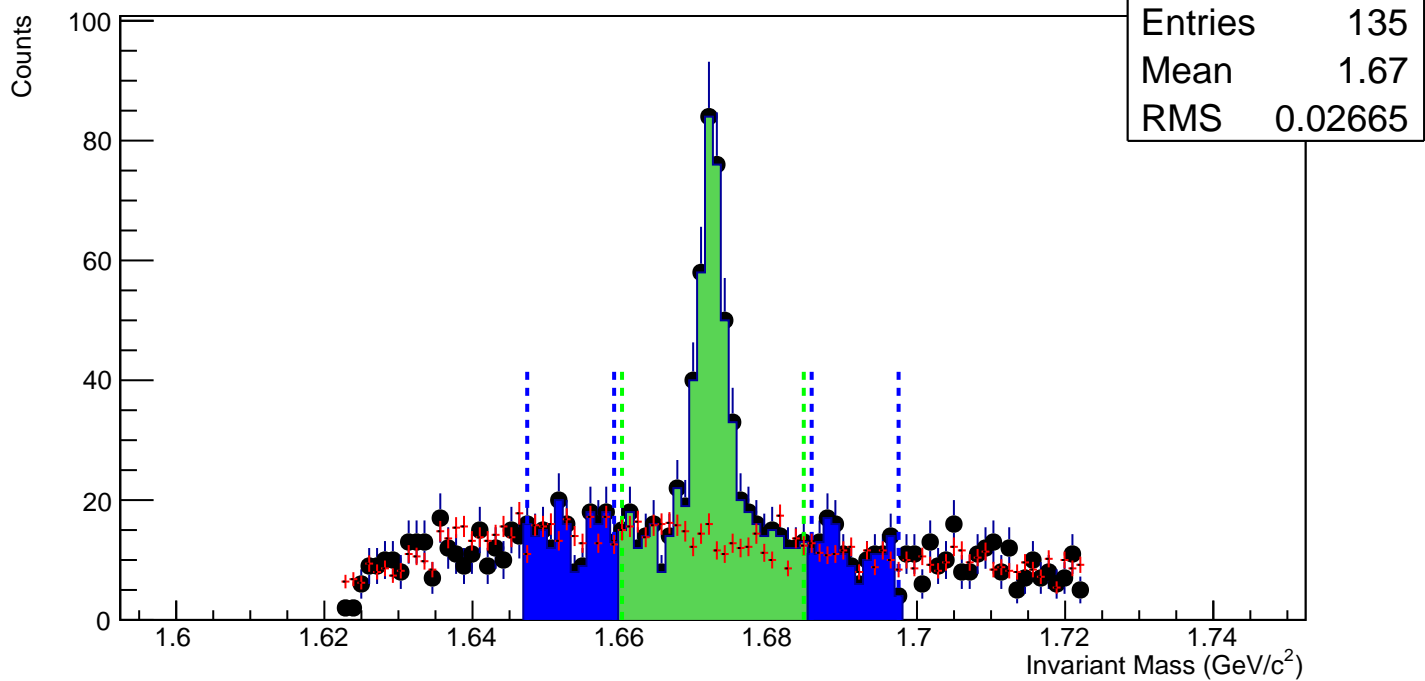
$\Omega^+$ , Au+Au 19 GeV, 20-40%,  $p_T$  1.2-1.6 GeV/c



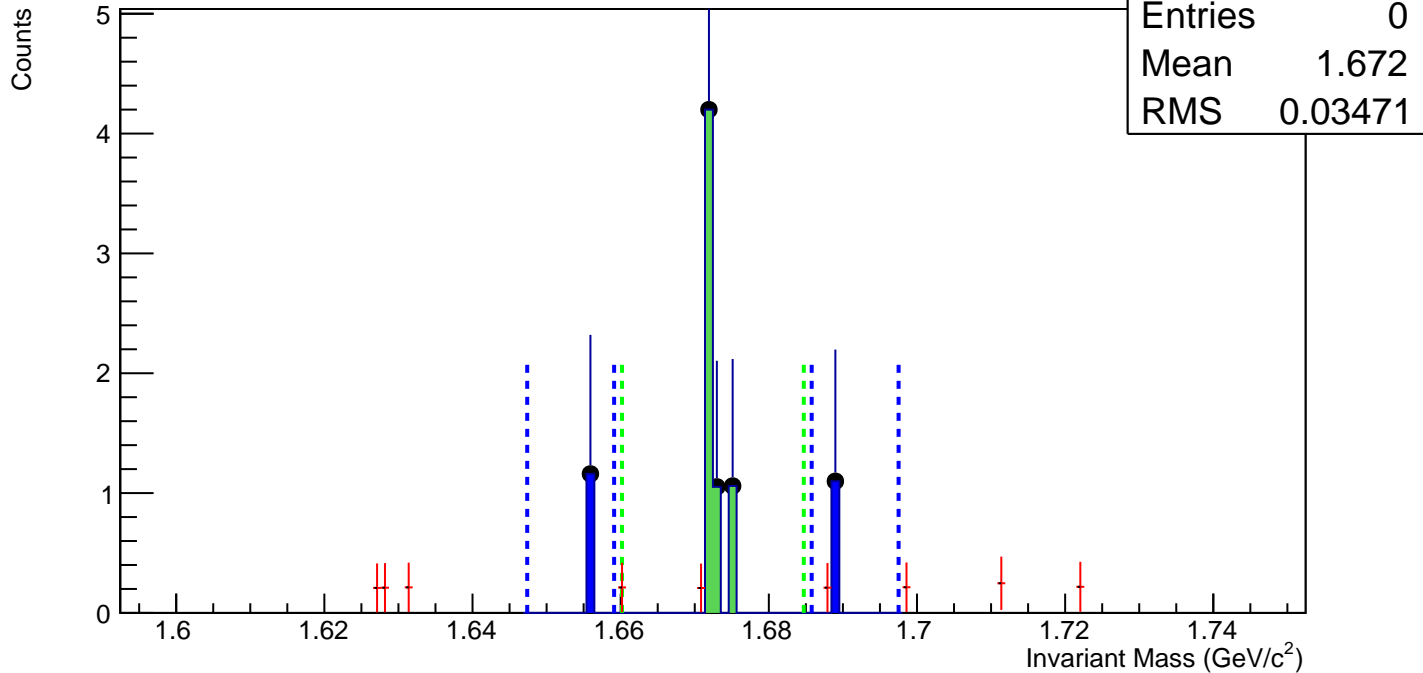
$\Omega^+$ , Au+Au 19 GeV, 10-20%,  $p_T$  1.2-1.6 GeV/c



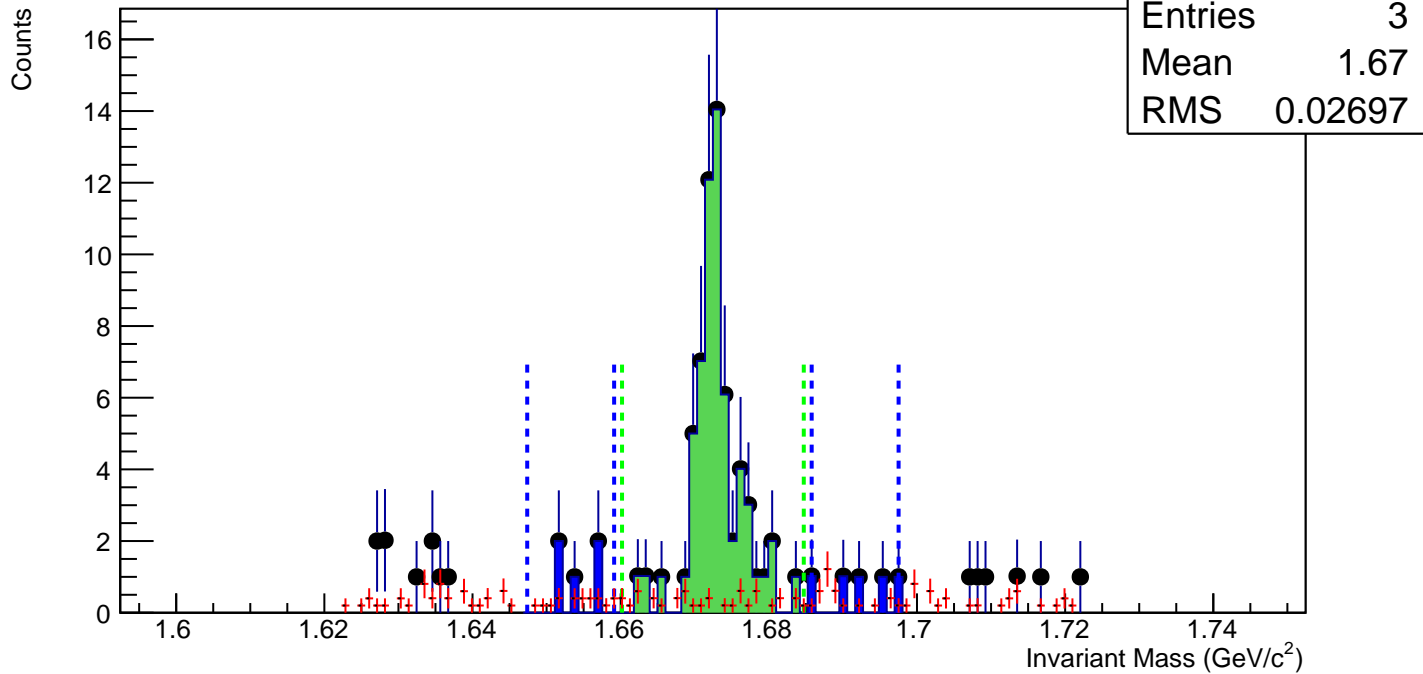
$\Omega^+$ , Au+Au 19 GeV, 0-10%,  $p_T$  1.2-1.6 GeV/c



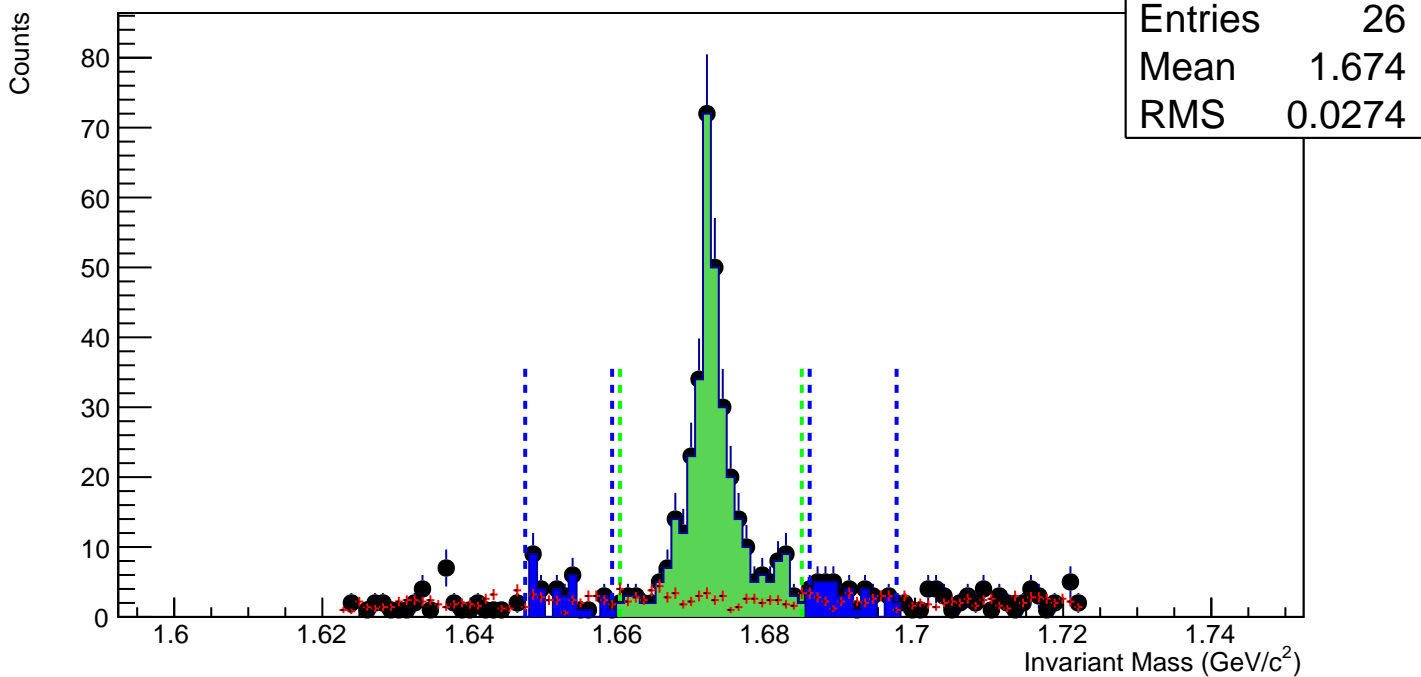
$\Omega^+$ , Au+Au 19 GeV, 60-80%,  $p_T$  1.6-2.0 GeV/c



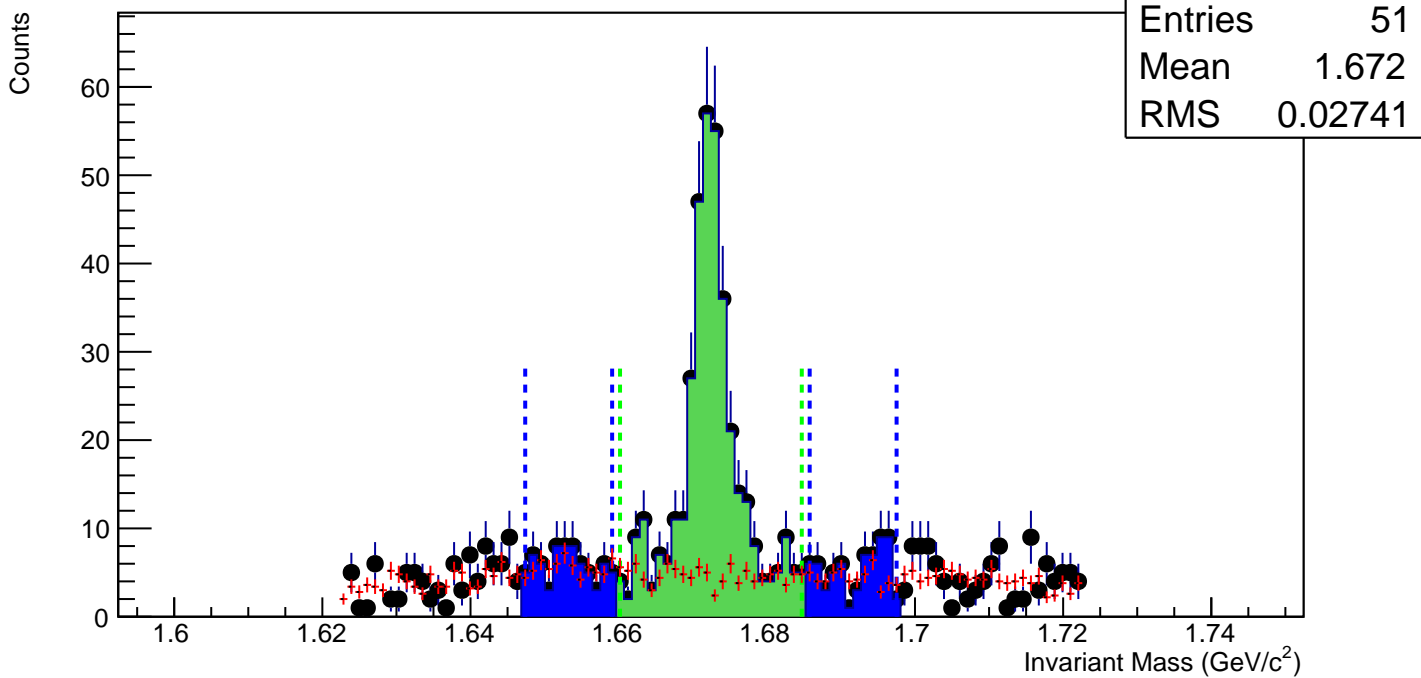
$\Omega^+$ , Au+Au 19 GeV, 40-60%,  $p_T$  1.6-2.0 GeV/c



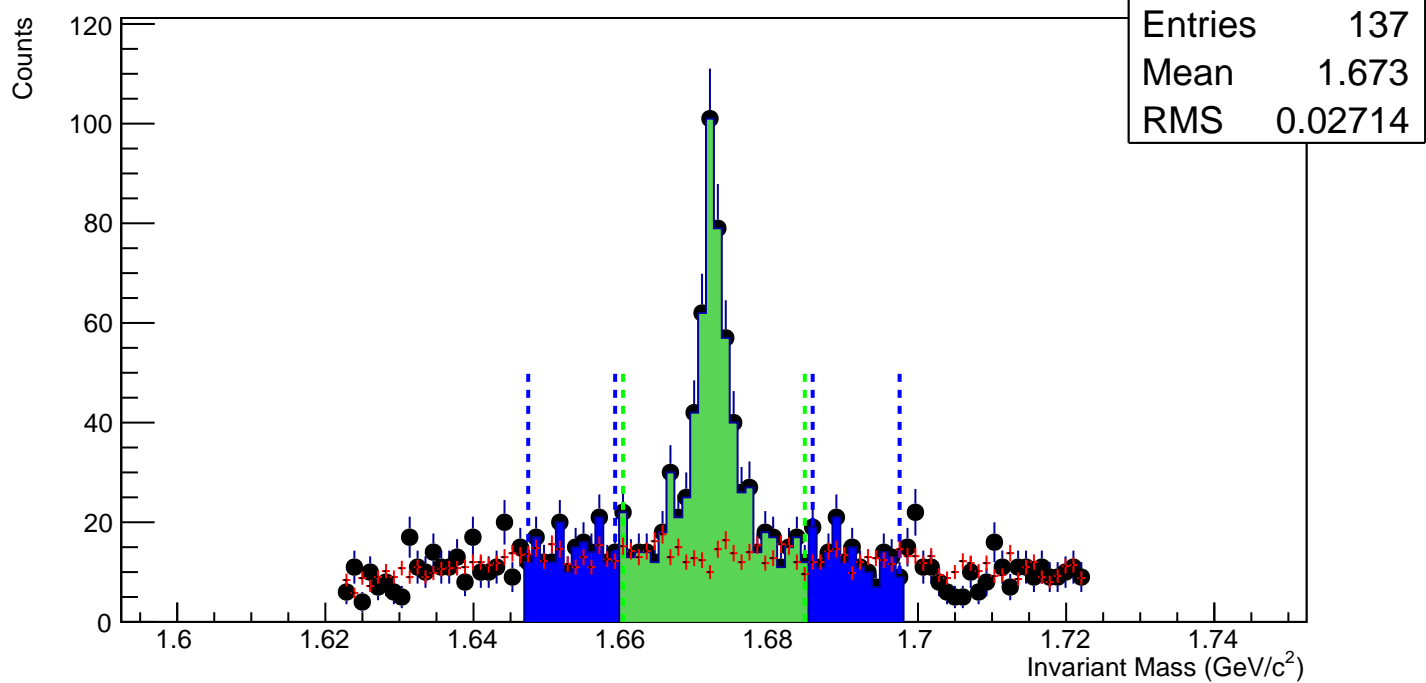
$\bar{\Omega}^+$ , Au+Au 19 GeV, 20-40%,  $p_T$  1.6-2.0 GeV/c



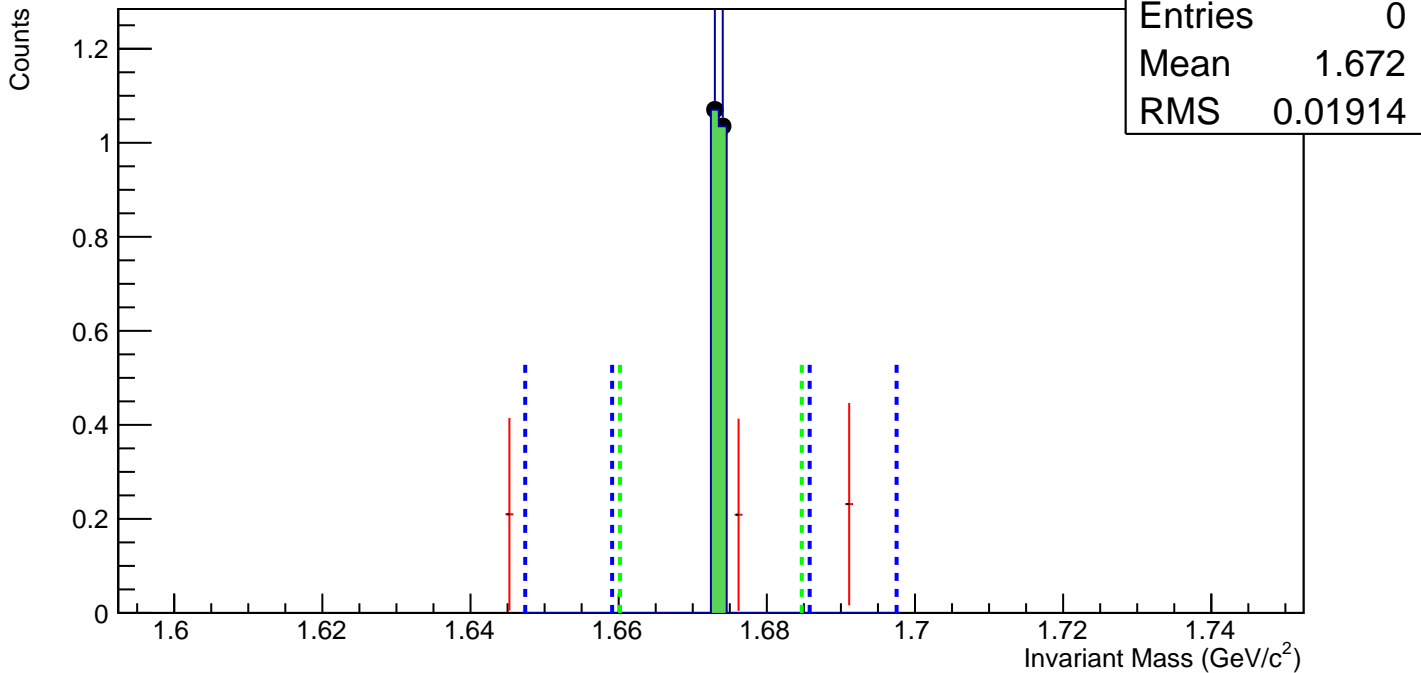
$\bar{\Omega}^+$ , Au+Au 19 GeV, 10-20%,  $p_T$  1.6-2.0 GeV/c



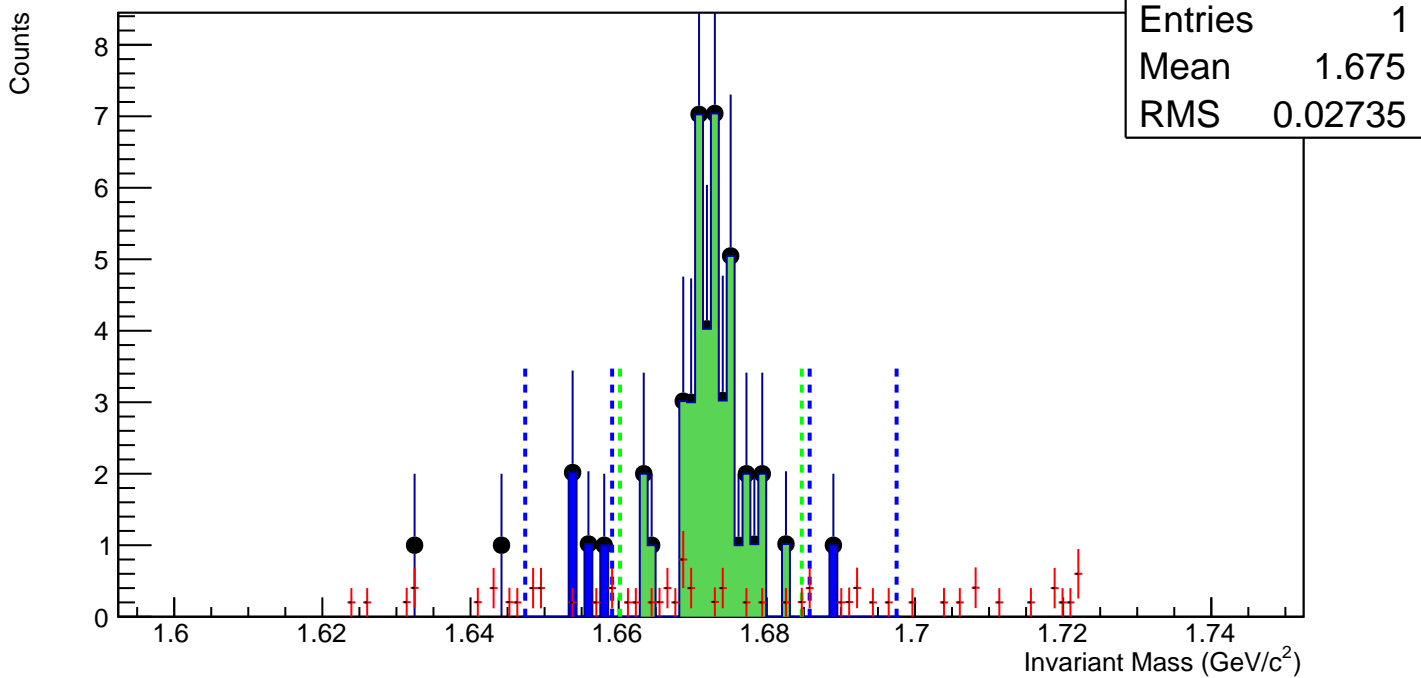
$\Omega^+$ , Au+Au 19 GeV, 0-10%,  $p_T$  1.6-2.0 GeV/c



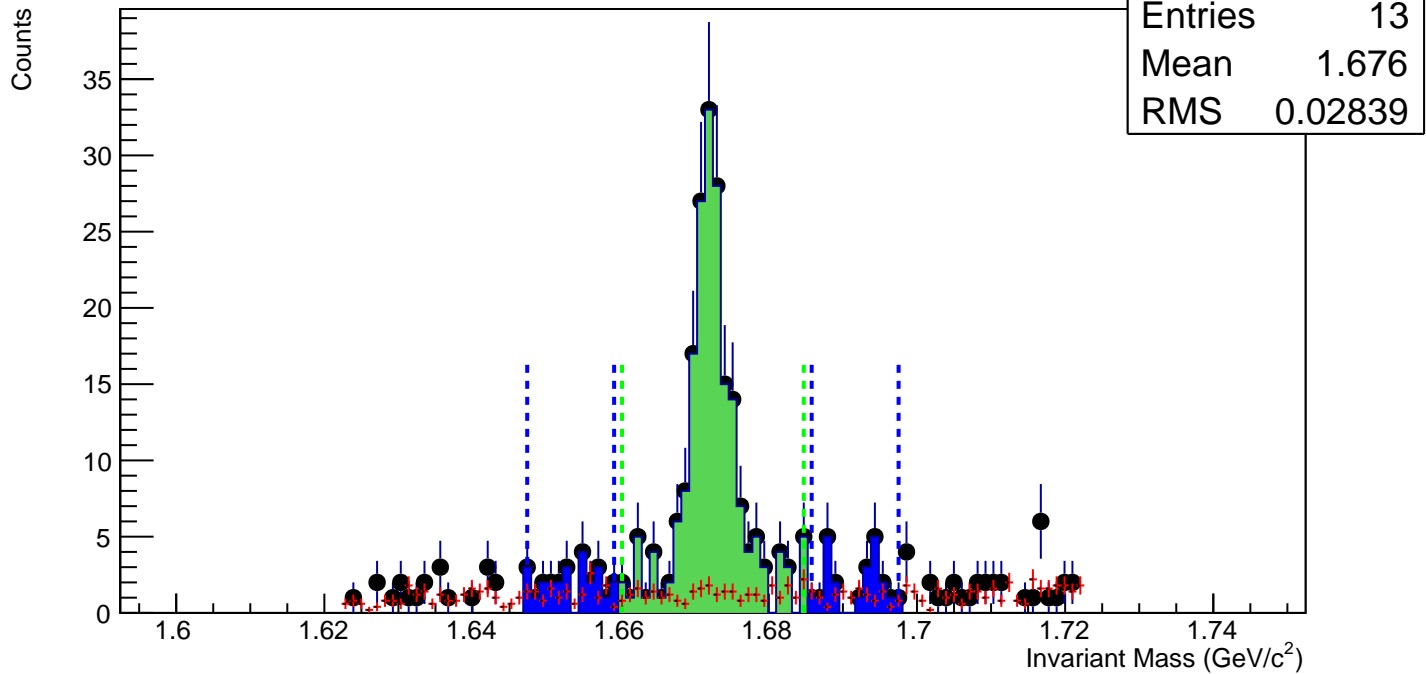
$\Omega^+$ , Au+Au 19 GeV, 60-80%,  $p_T$  2.0-2.4 GeV/c



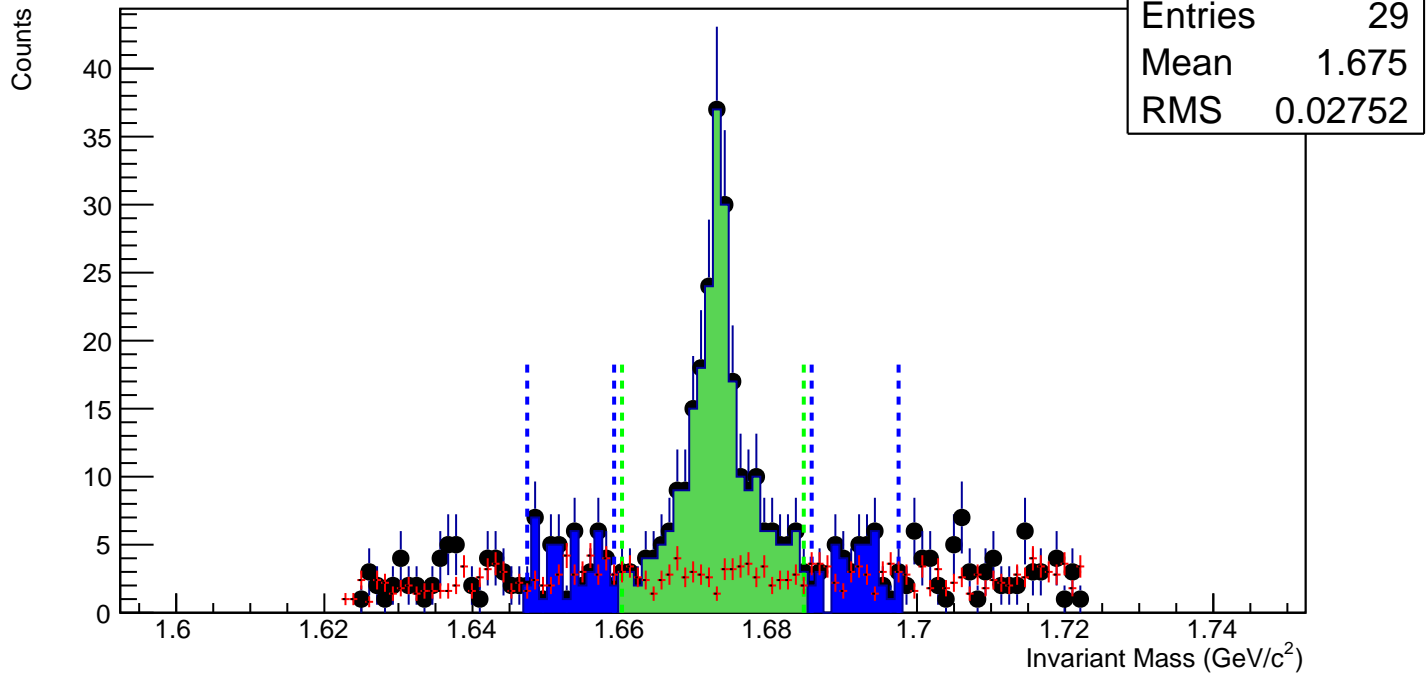
$\Omega^+$ , Au+Au 19 GeV, 40-60%,  $p_T$  2.0-2.4 GeV/c



$\Omega^+$ , Au+Au 19 GeV, 20-40%,  $p_T$  2.0-2.4 GeV/c



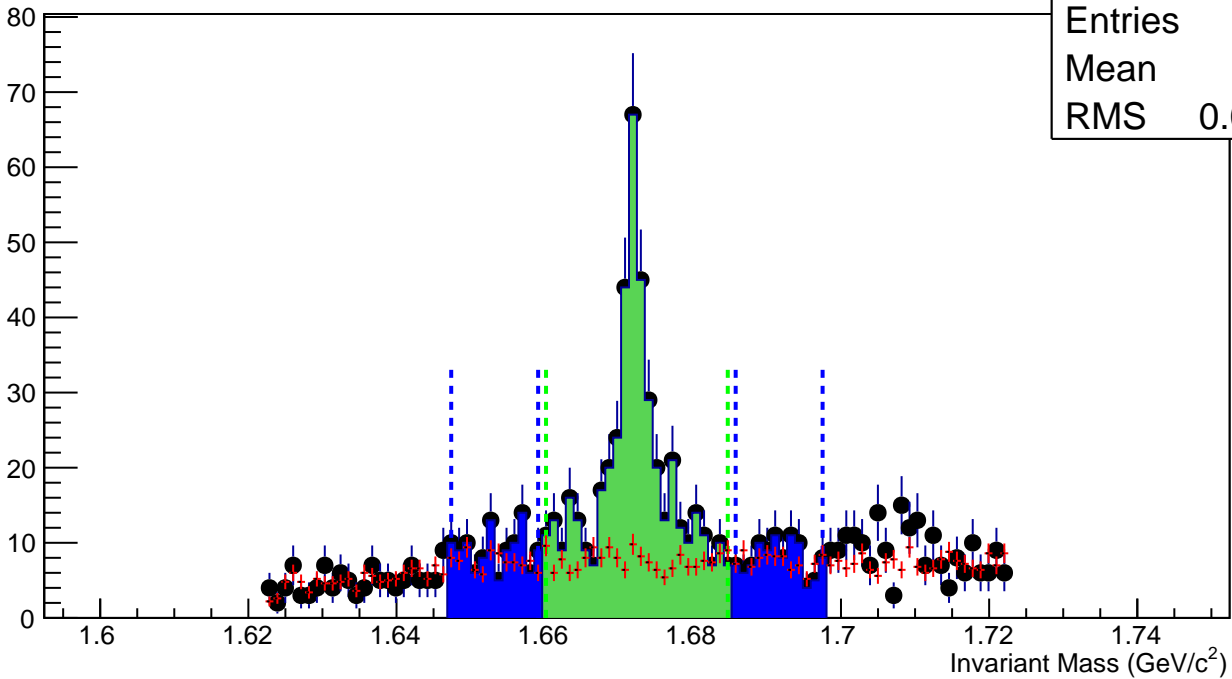
$\Omega^+$ , Au+Au 19 GeV, 10-20%,  $p_T$  2.0-2.4 GeV/c



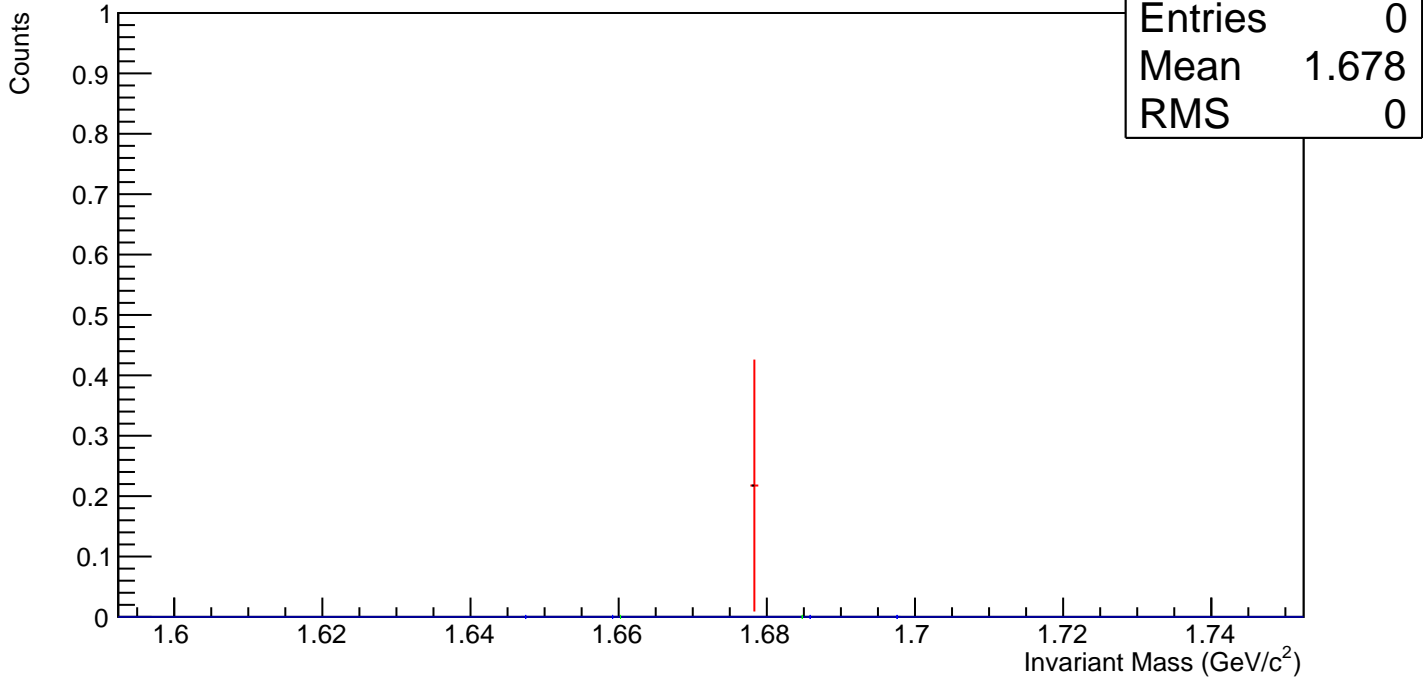
$\Omega^+$ , Au+Au 19 GeV, 0-10%,  $p_T$  2.0-2.4 GeV/c

Counts

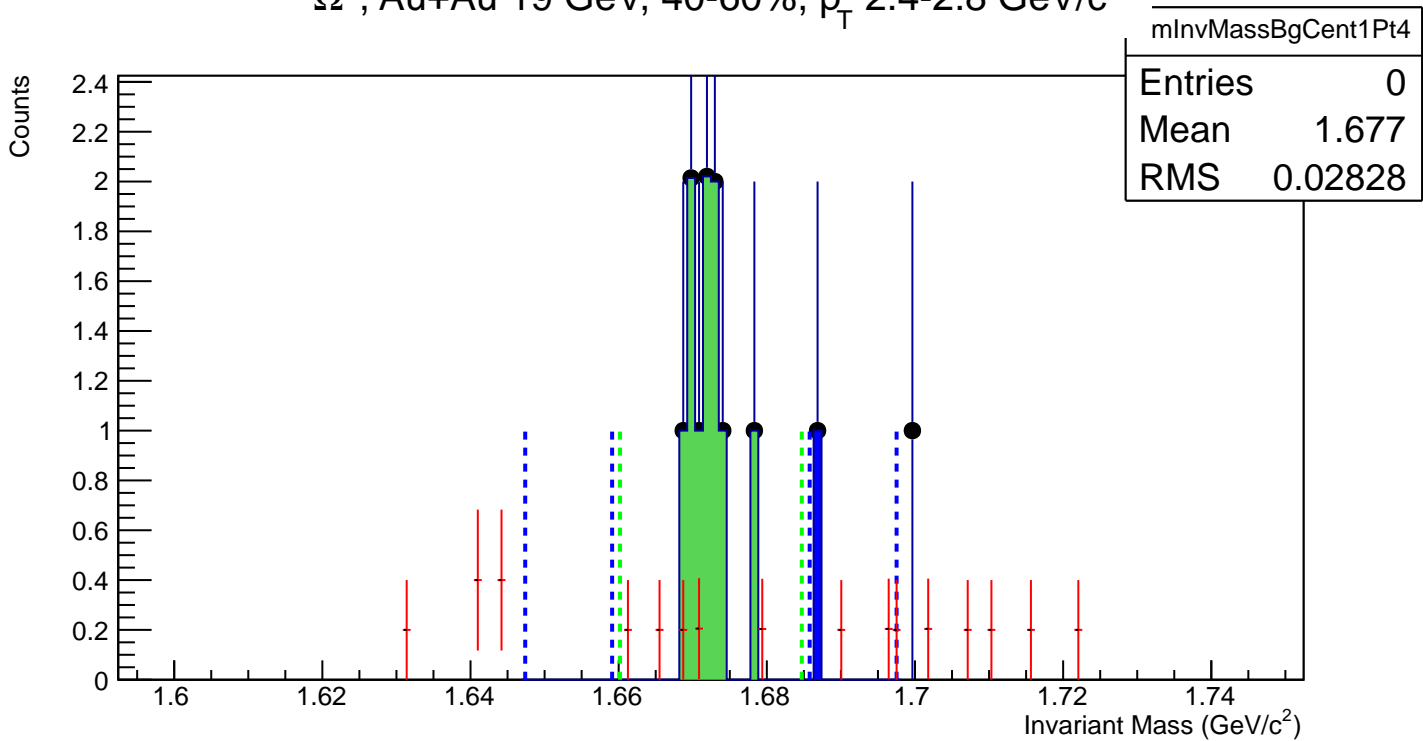
hmlInvMassBgCent4Pt3
Entries 79
Mean 1.676
RMS 0.02738



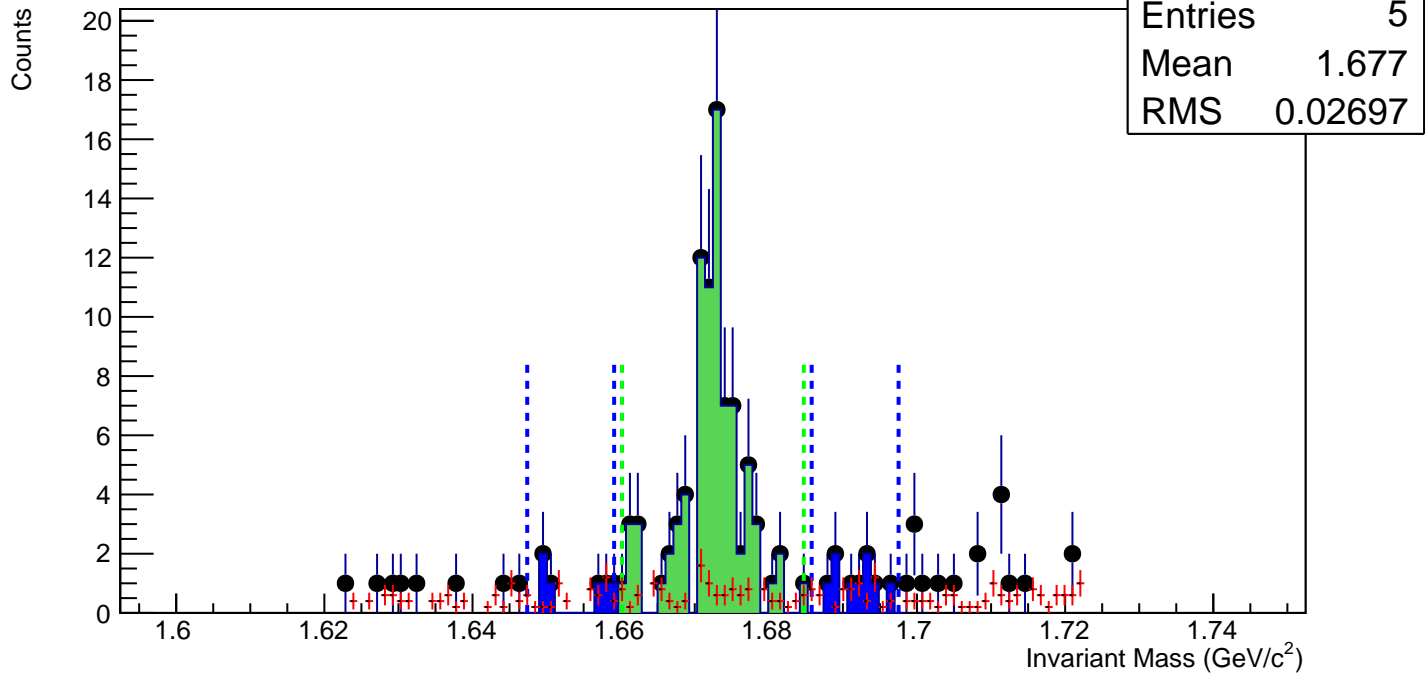
$\Omega^+$ , Au+Au 19 GeV, 60-80%,  $p_T$  2.4-2.8 GeV/c



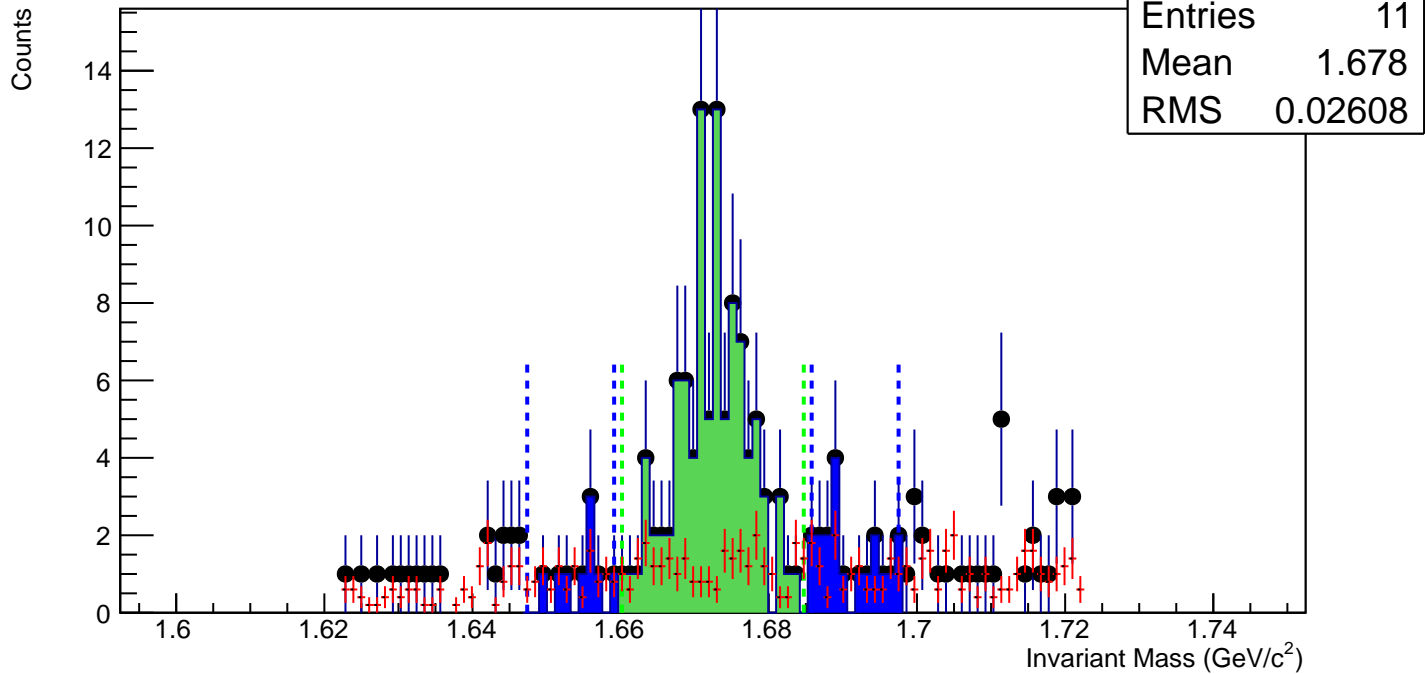
$\Omega^+$ , Au+Au 19 GeV, 40-60%,  $p_T$  2.4-2.8 GeV/c



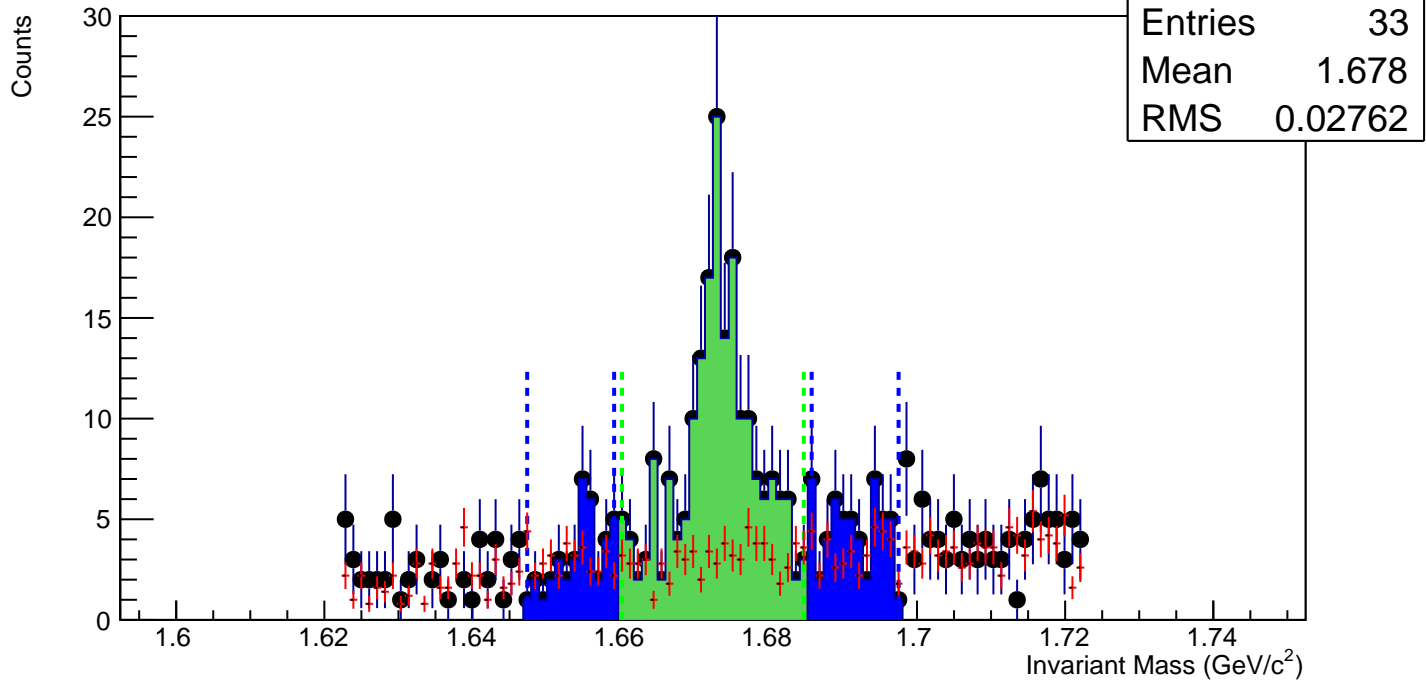
$\Omega^+$ , Au+Au 19 GeV, 20-40%,  $p_T$  2.4-2.8 GeV/c



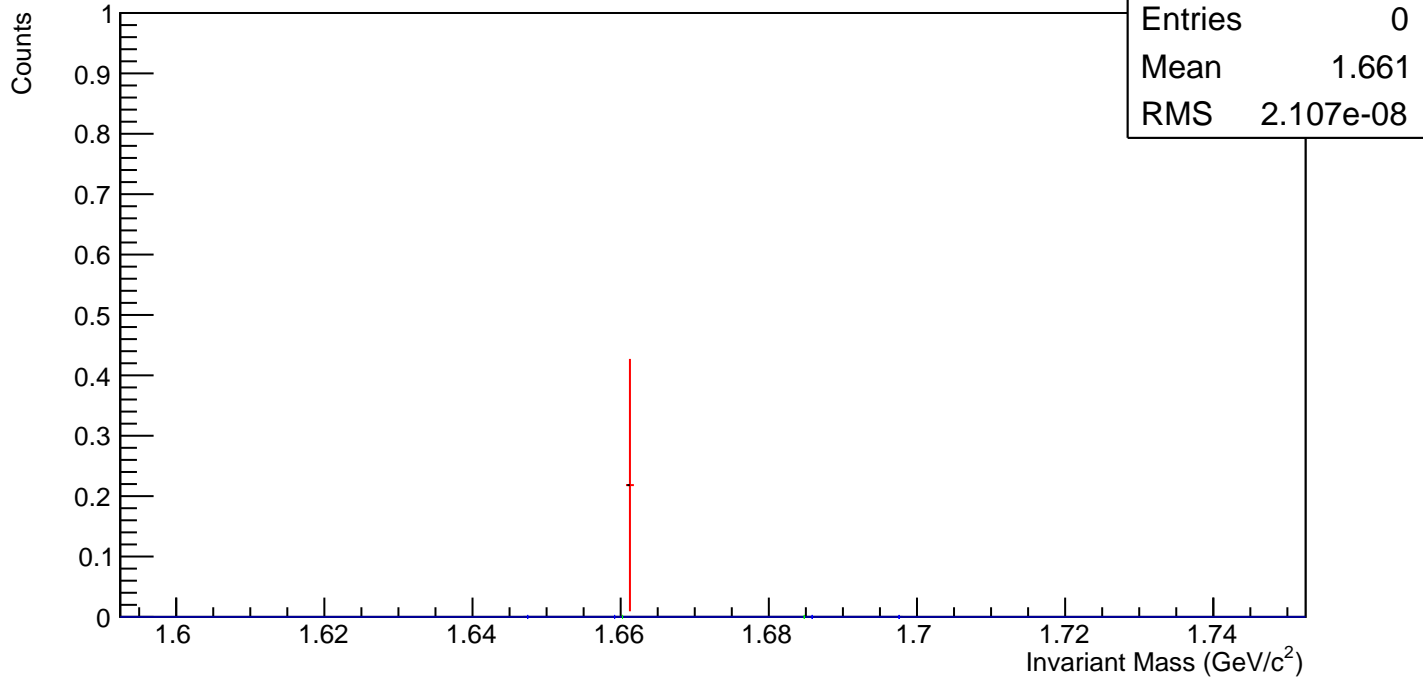
$\Omega^+$ , Au+Au 19 GeV, 10-20%,  $p_T$  2.4-2.8 GeV/c



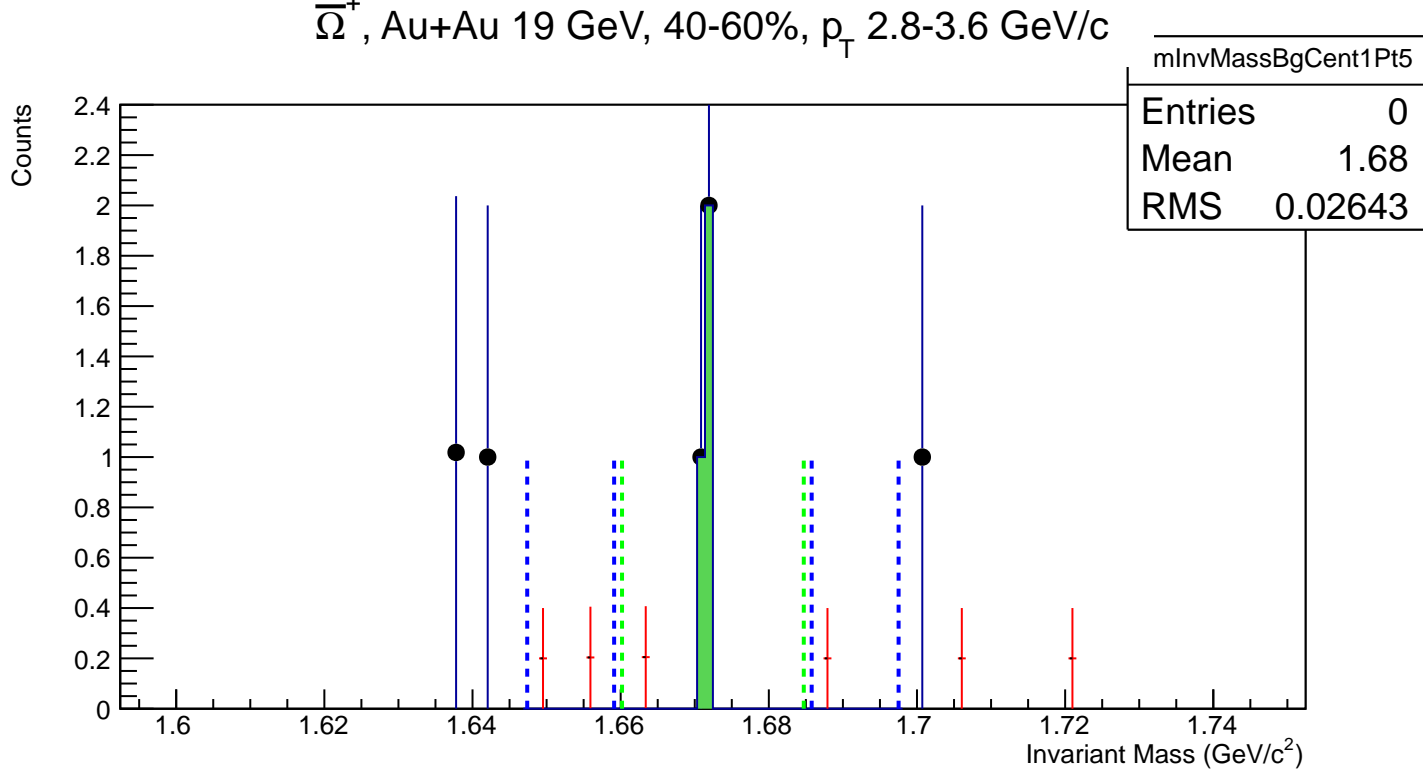
$\Omega^+$ , Au+Au 19 GeV, 0-10%,  $p_T$  2.4-2.8 GeV/c



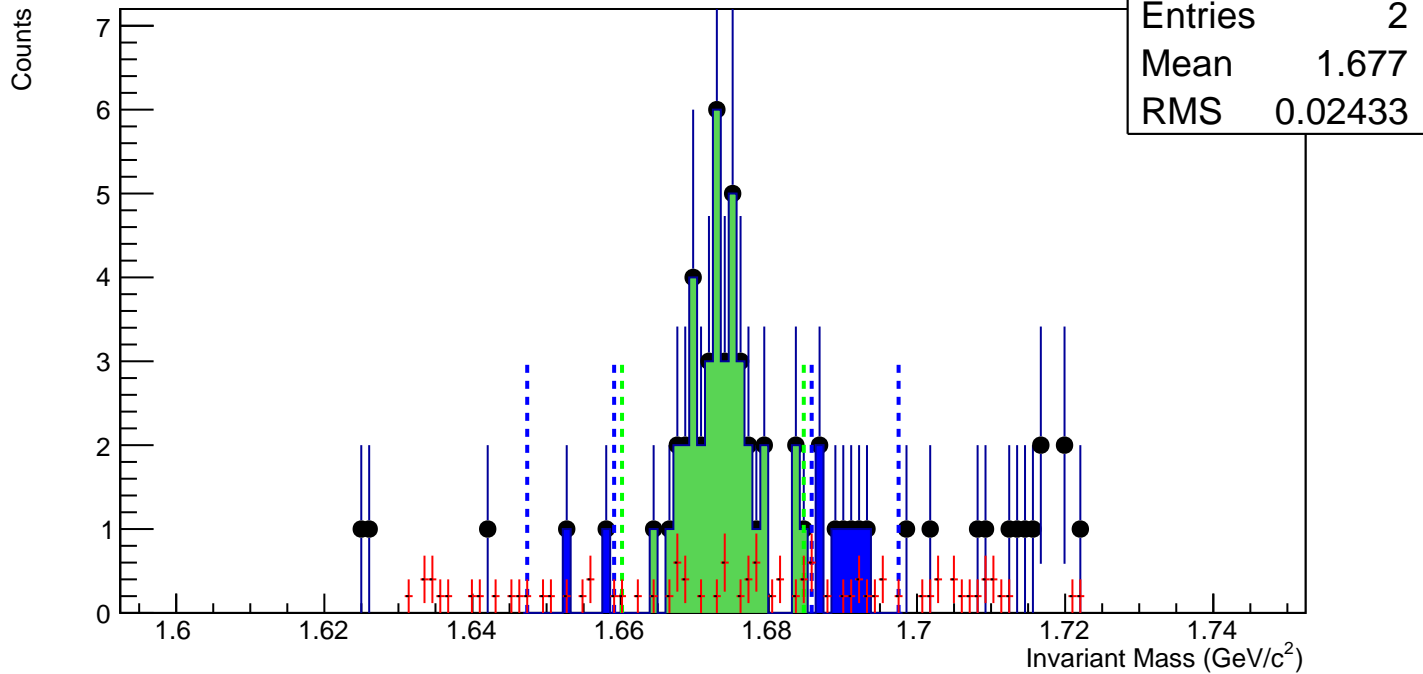
$\Omega^+$ , Au+Au 19 GeV, 60-80%,  $p_T$  2.8-3.6 GeV/c



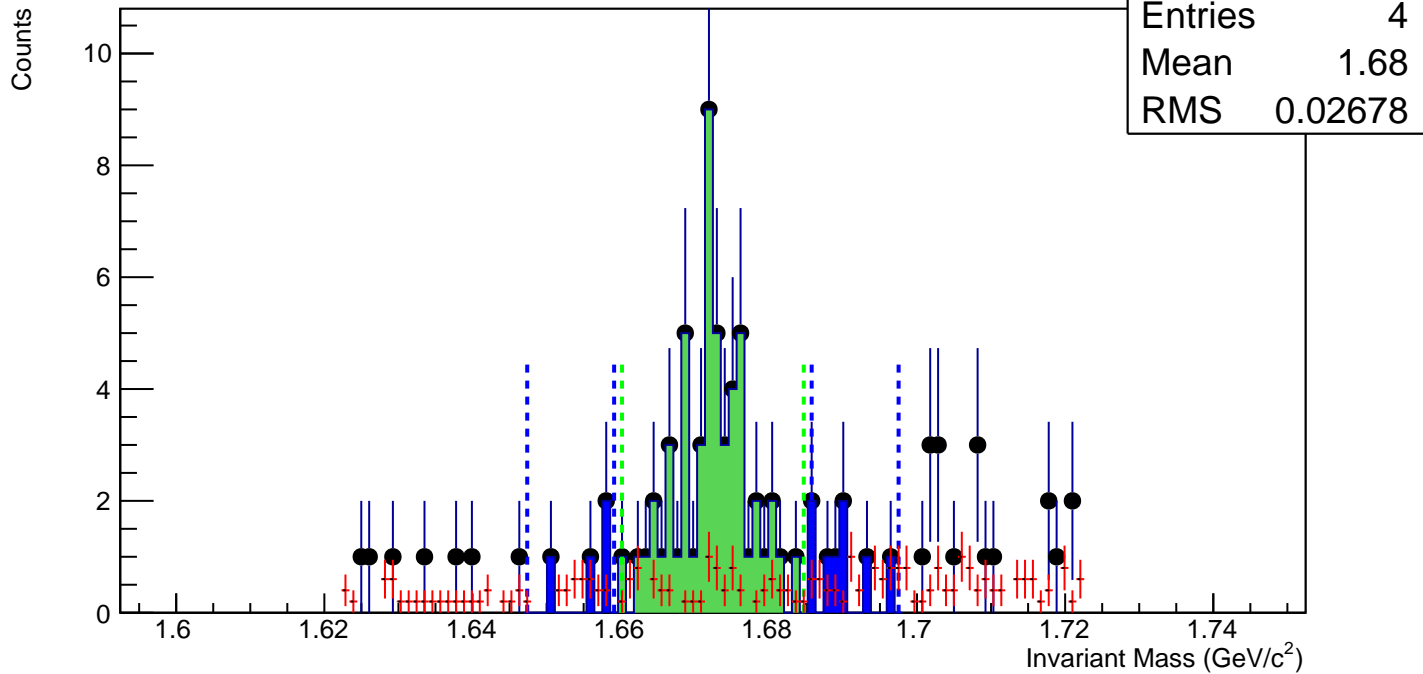
$\Omega^+$ , Au+Au 19 GeV, 40-60%,  $p_T$  2.8-3.6 GeV/c



$\Omega^+$ , Au+Au 19 GeV, 20-40%,  $p_T$  2.8-3.6 GeV/c

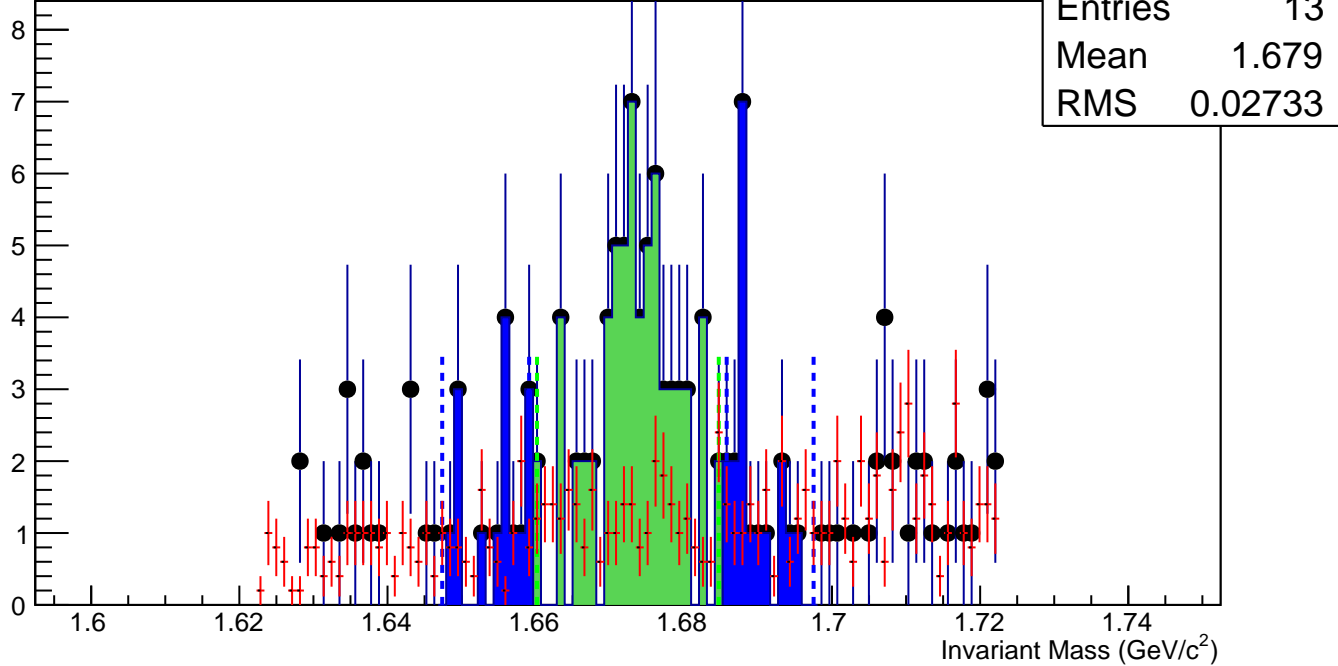


$\Omega^+$ , Au+Au 19 GeV, 10-20%,  $p_T$  2.8-3.6 GeV/c

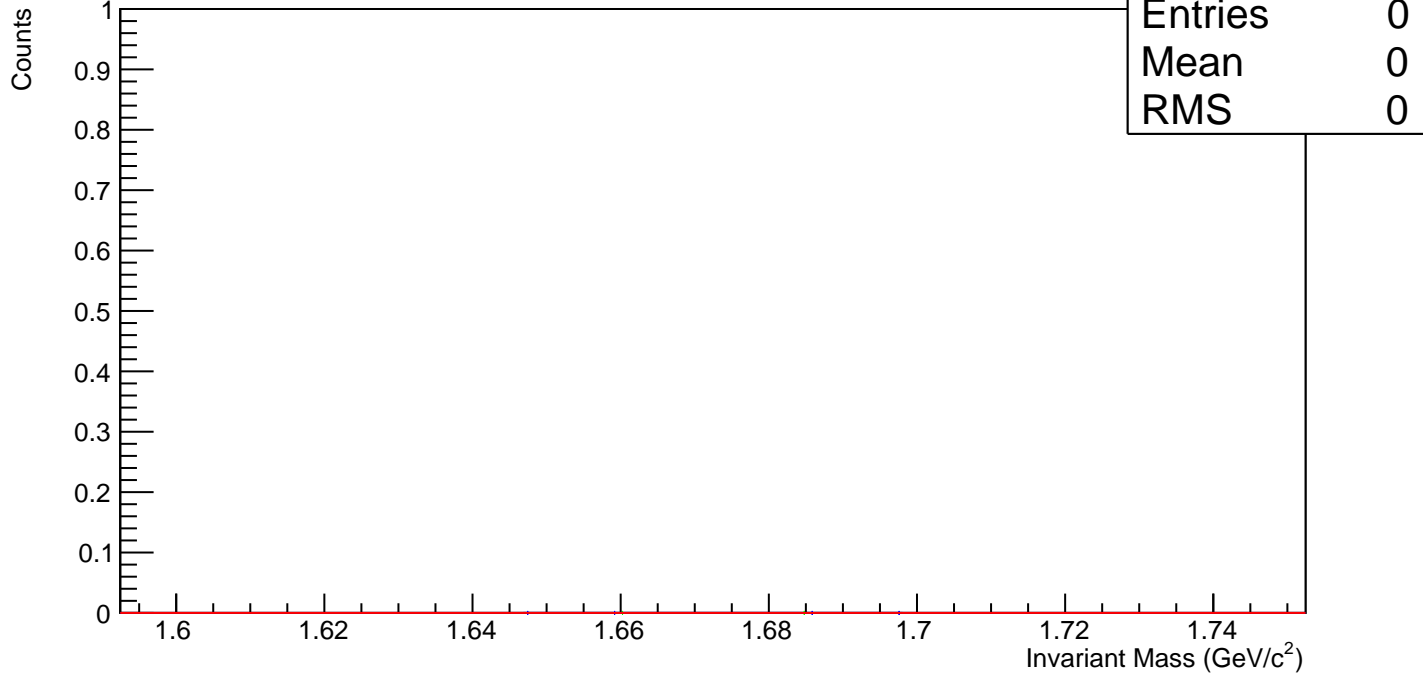


$\Omega^+$ , Au+Au 19 GeV, 0-10%,  $p_T$  2.8-3.6 GeV/c

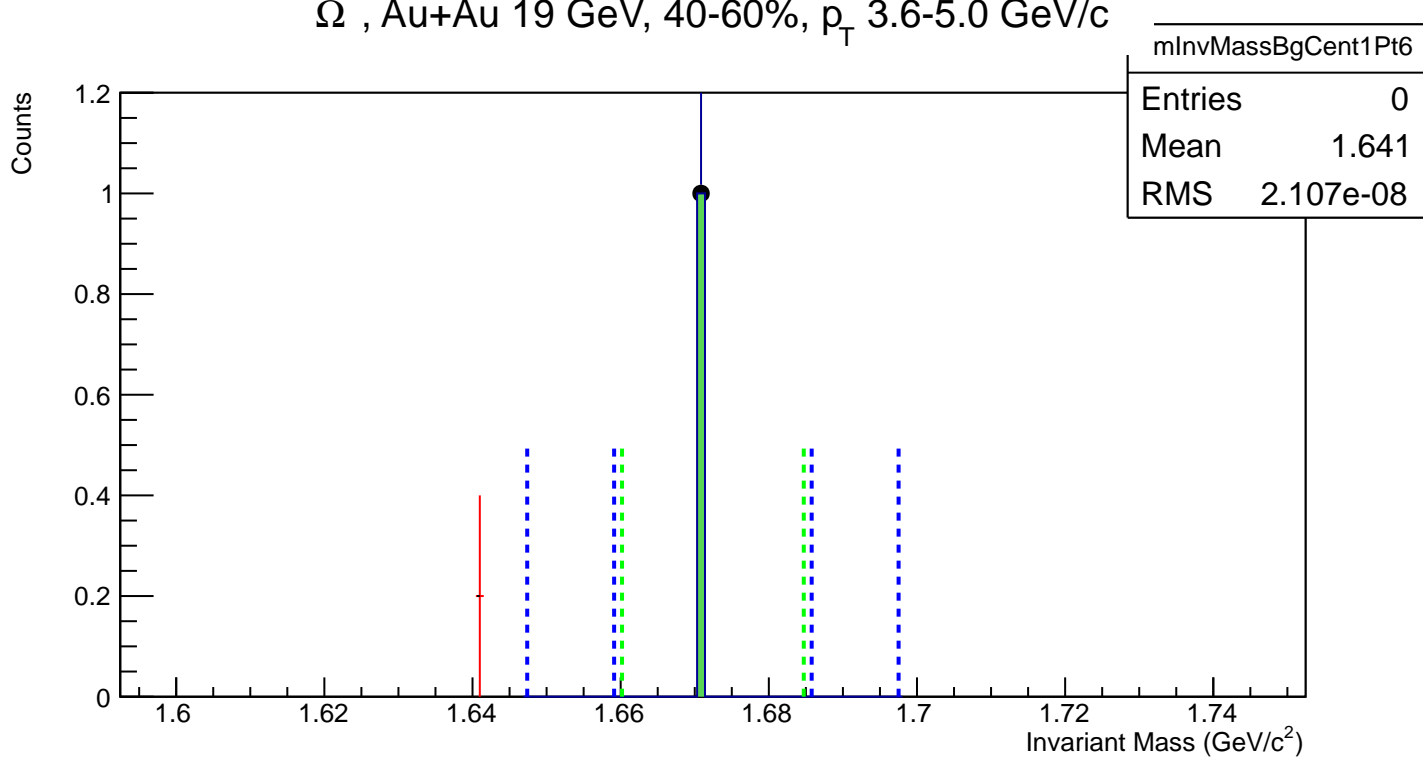
Counts



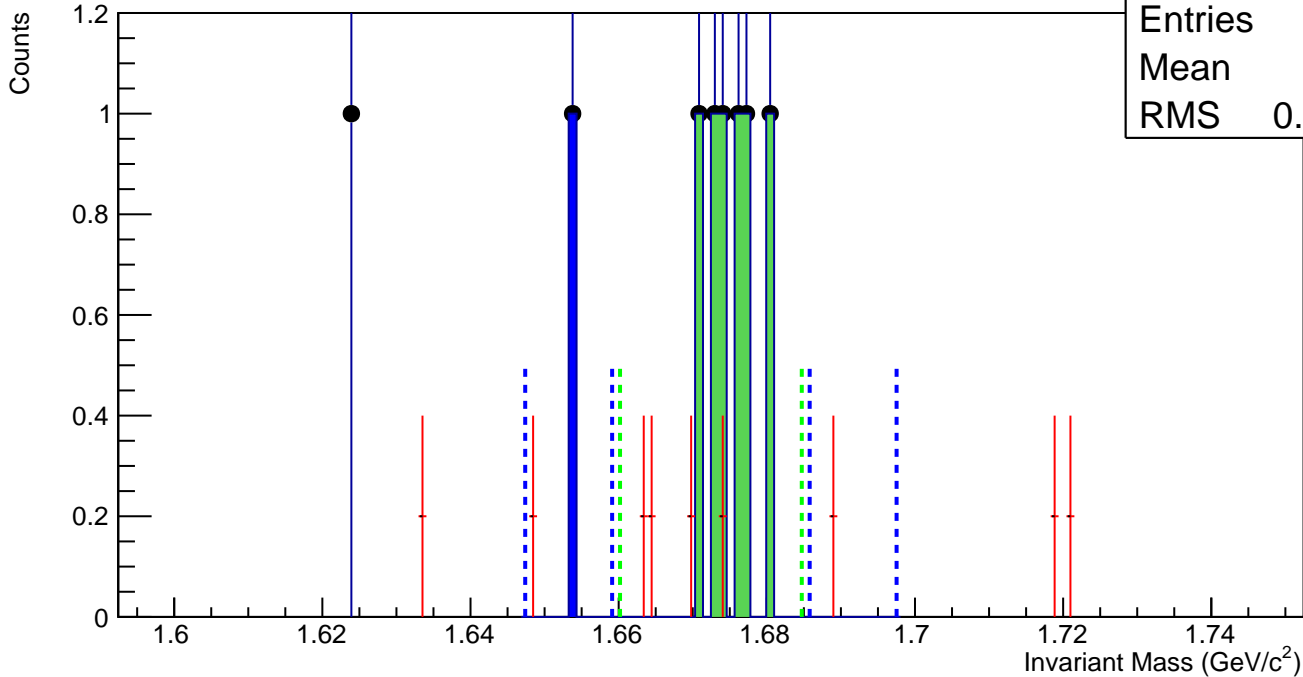
$\Omega^+$ , Au+Au 19 GeV, 60-80%,  $p_T$  3.6-5.0 GeV/c



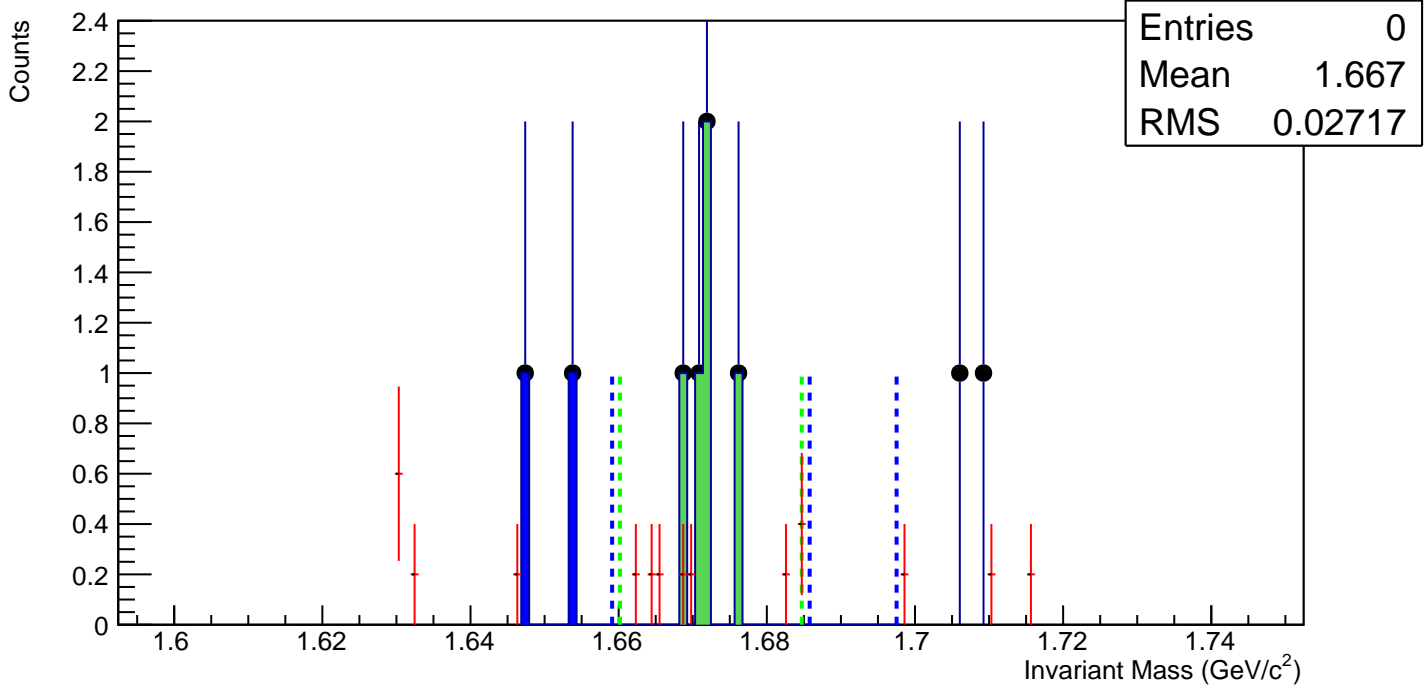
$\Omega^+$ , Au+Au 19 GeV, 40-60%,  $p_T$  3.6-5.0 GeV/c



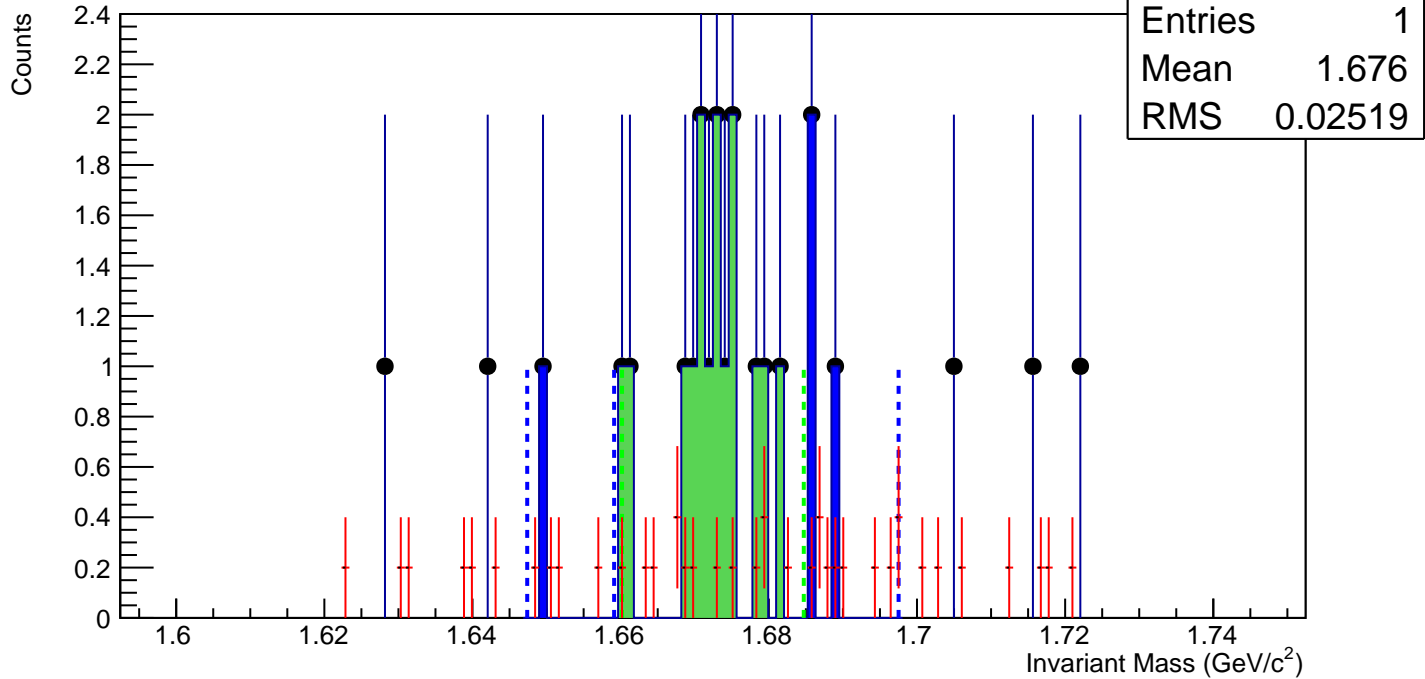
$\Omega^+$ , Au+Au 19 GeV, 20-40%,  $p_T$  3.6-5.0 GeV/c



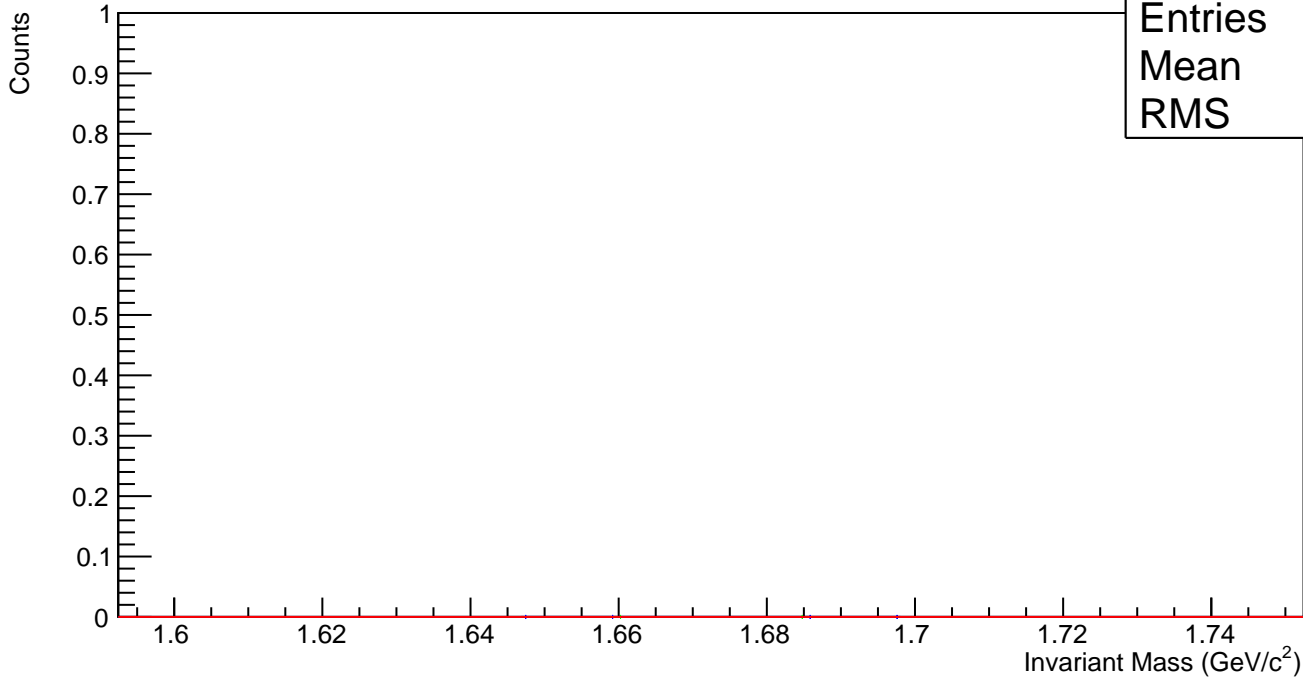
$\Omega^+$ , Au+Au 19 GeV, 10-20%,  $p_T$  3.6-5.0 GeV/c



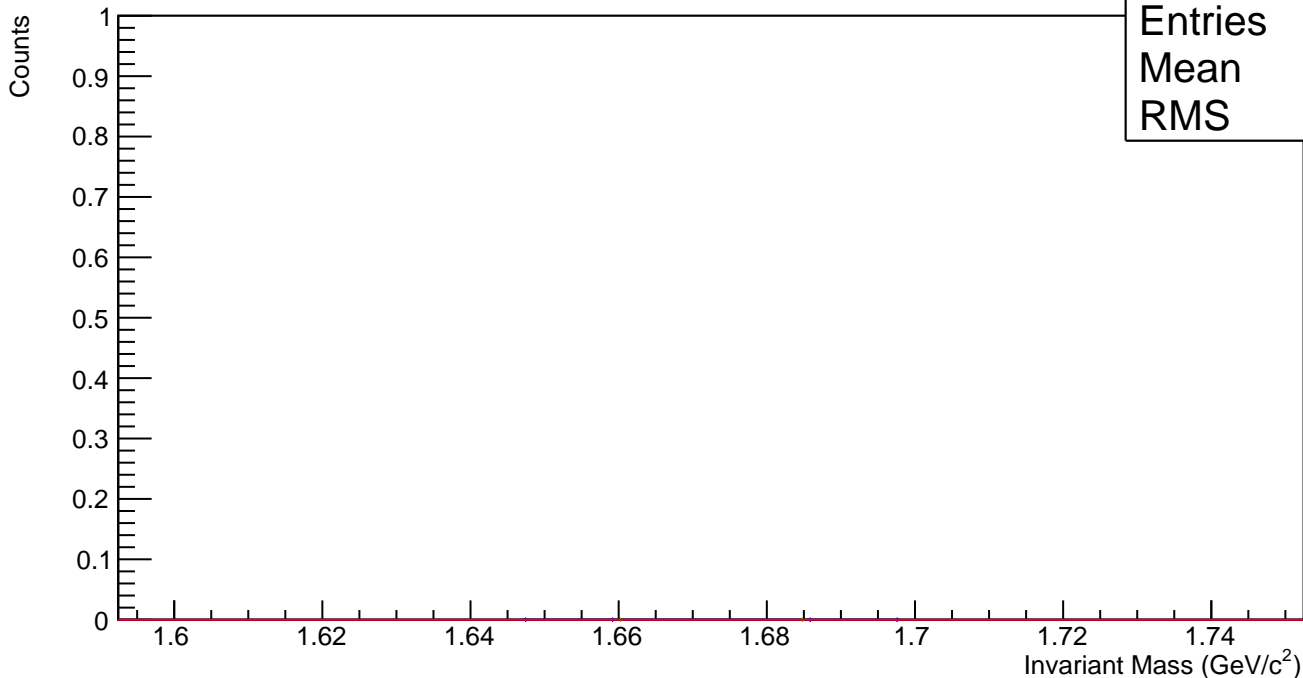
$\Omega^+$ , Au+Au 19 GeV, 0-10%,  $p_T$  3.6-5.0 GeV/c



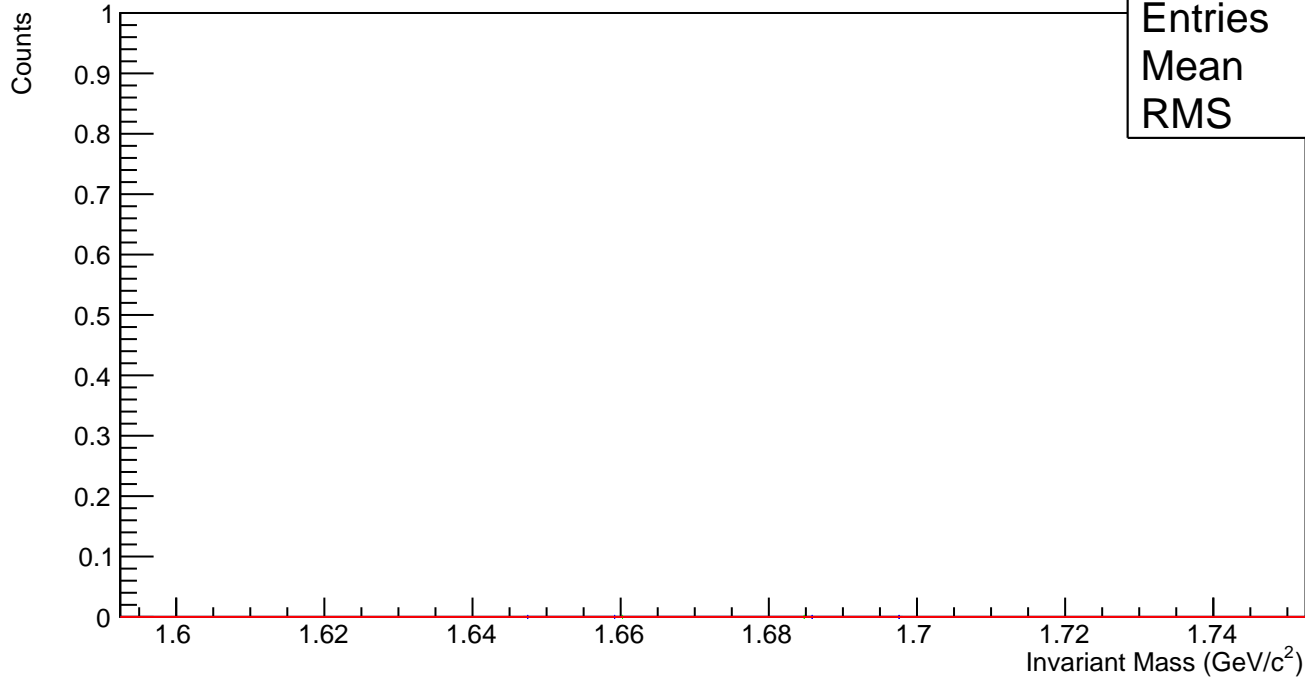
$\bar{\Omega}^+$ , Au+Au 19 GeV, 60-80%,  $p_T$  5.0-7.0 GeV/c



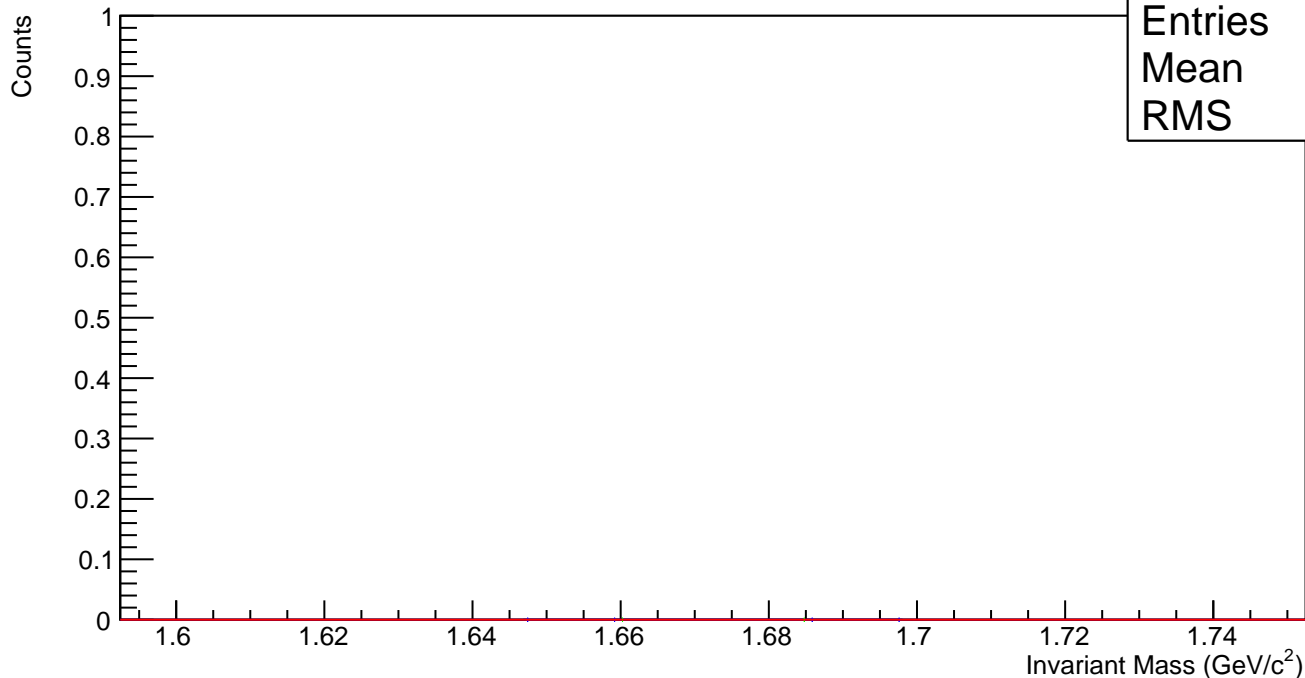
$\bar{\Omega}^+$ , Au+Au 19 GeV, 40-60%,  $p_T$  5.0-7.0 GeV/c



$\bar{\Omega}^+$ , Au+Au 19 GeV, 20-40%,  $p_T$  5.0-7.0 GeV/c



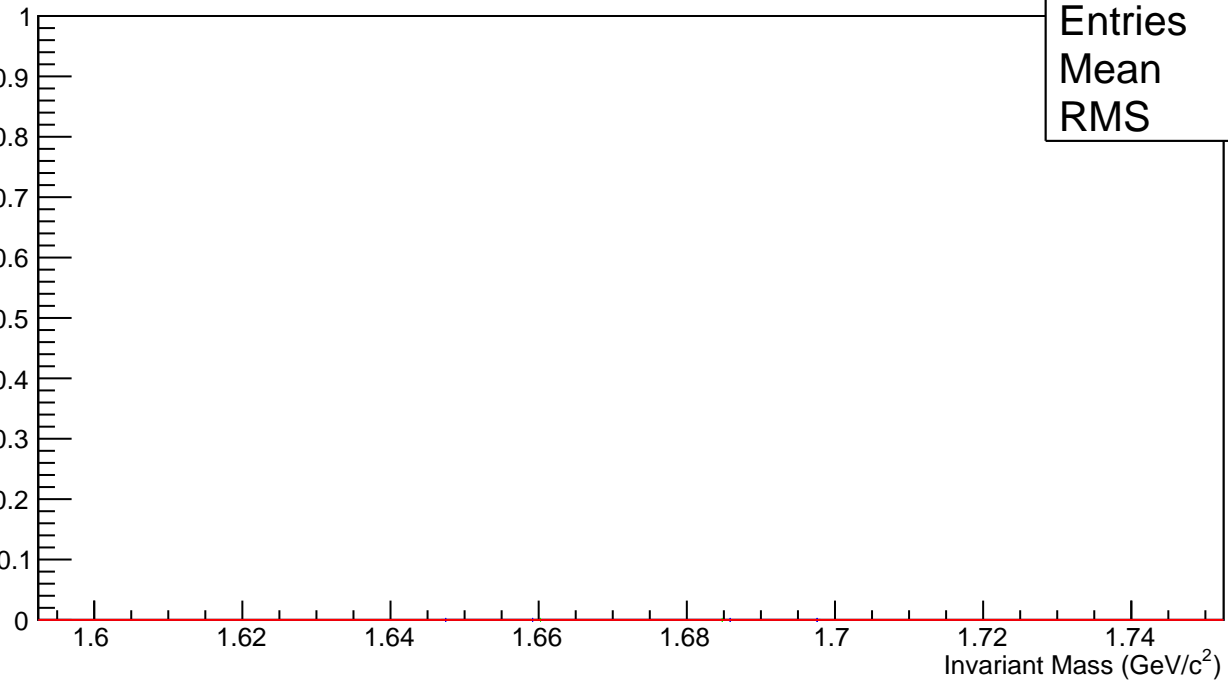
$\bar{\Omega}^+$ , Au+Au 19 GeV, 10-20%,  $p_T$  5.0-7.0 GeV/c



$\Omega^+$ , Au+Au 19 GeV, 0-10%,  $p_T$  5.0-7.0 GeV/c

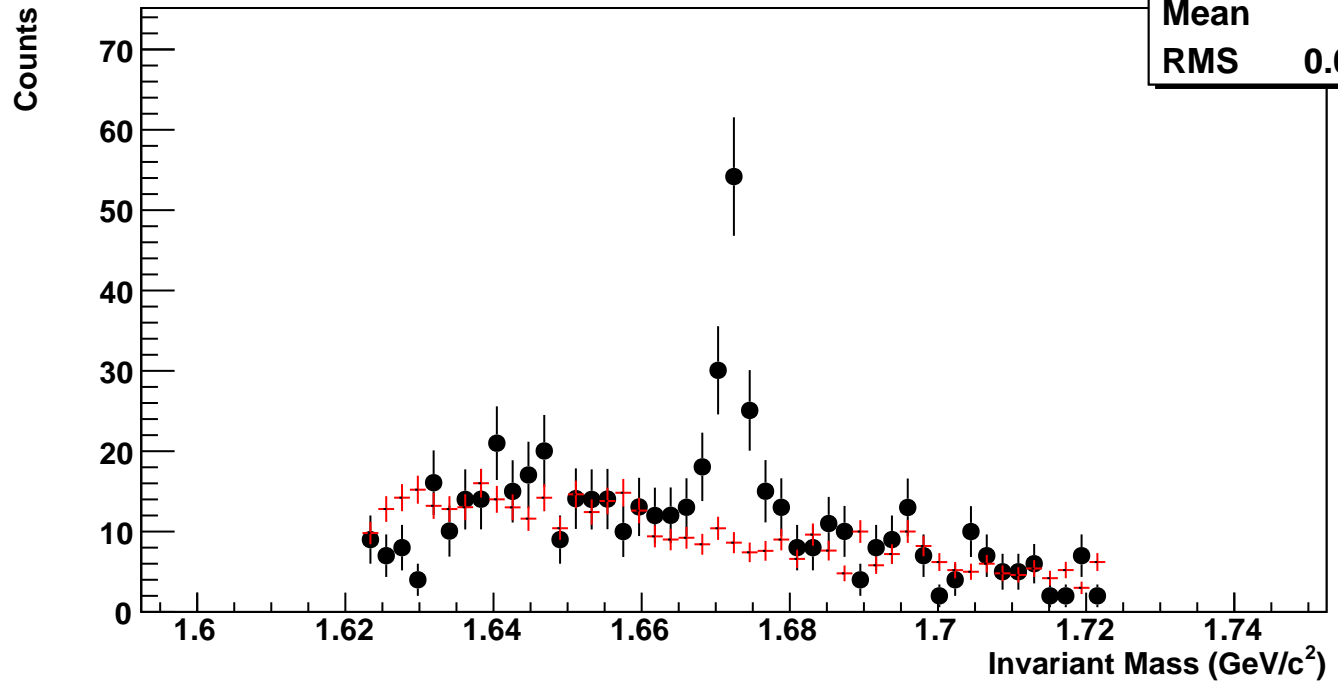
Counts

hmlInvMassBgCent4Pt7	
Entries	0
Mean	0
RMS	0



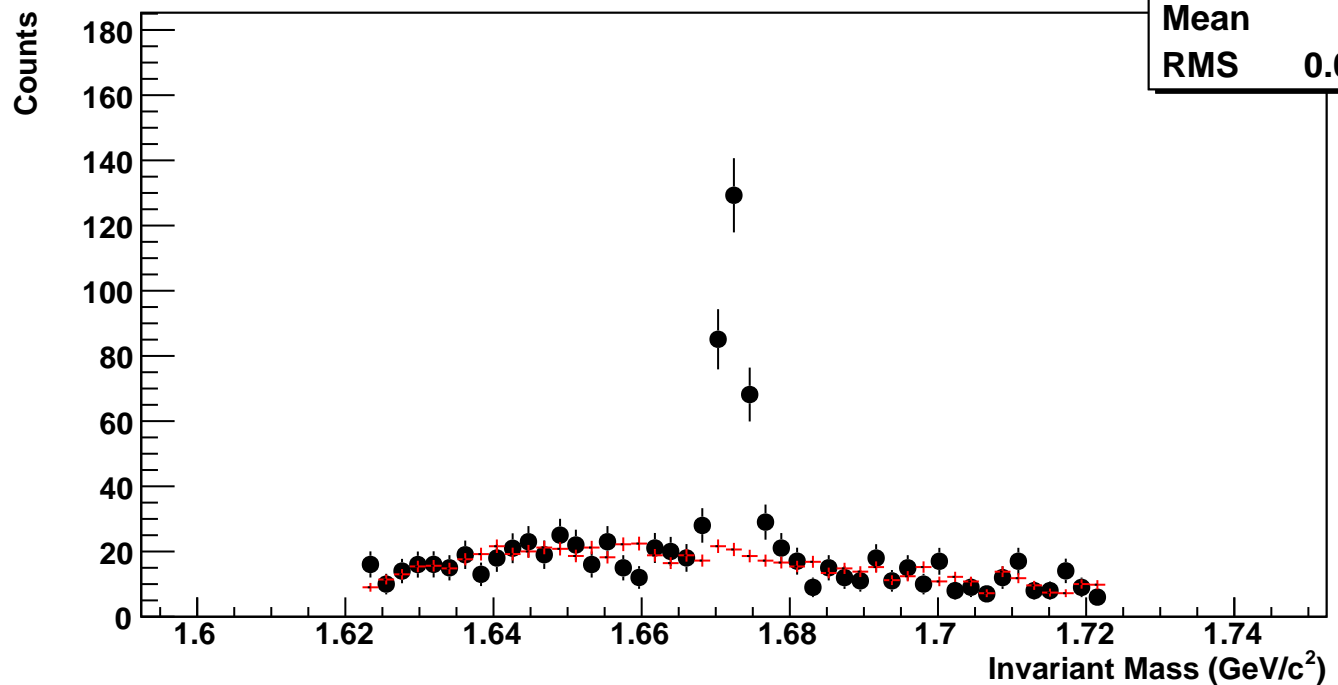
$\Omega^-$ , Au+Au 11 GeV, 10-60%,  $p_T$  0.8-1.2 GeV/c

hmlInvMassBgCent0Pt0	
Entries	54
Mean	1.663
RMS	0.02702



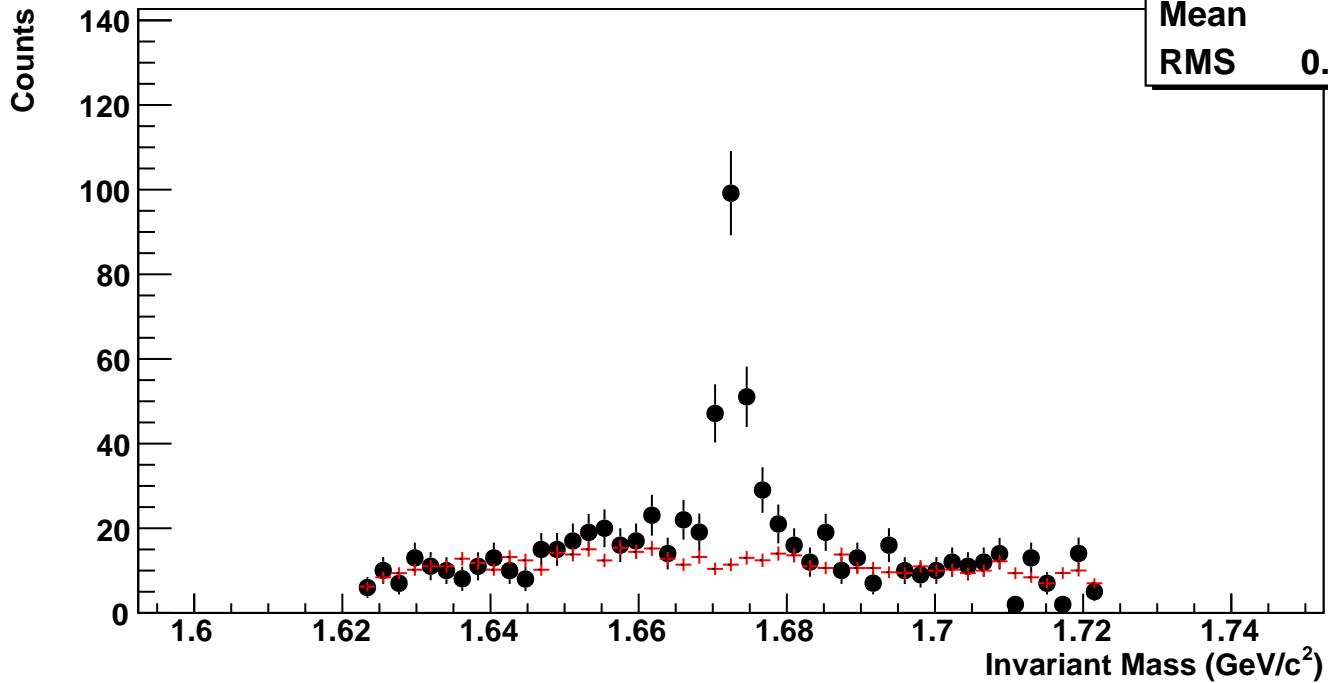
$\Omega^-$ , Au+Au 11 GeV, 10-60%,  $p_T$  1.2-1.6 GeV/c

hmlInvMassBgCent0Pt1	
Entries	89
Mean	1.668
RMS	0.02618



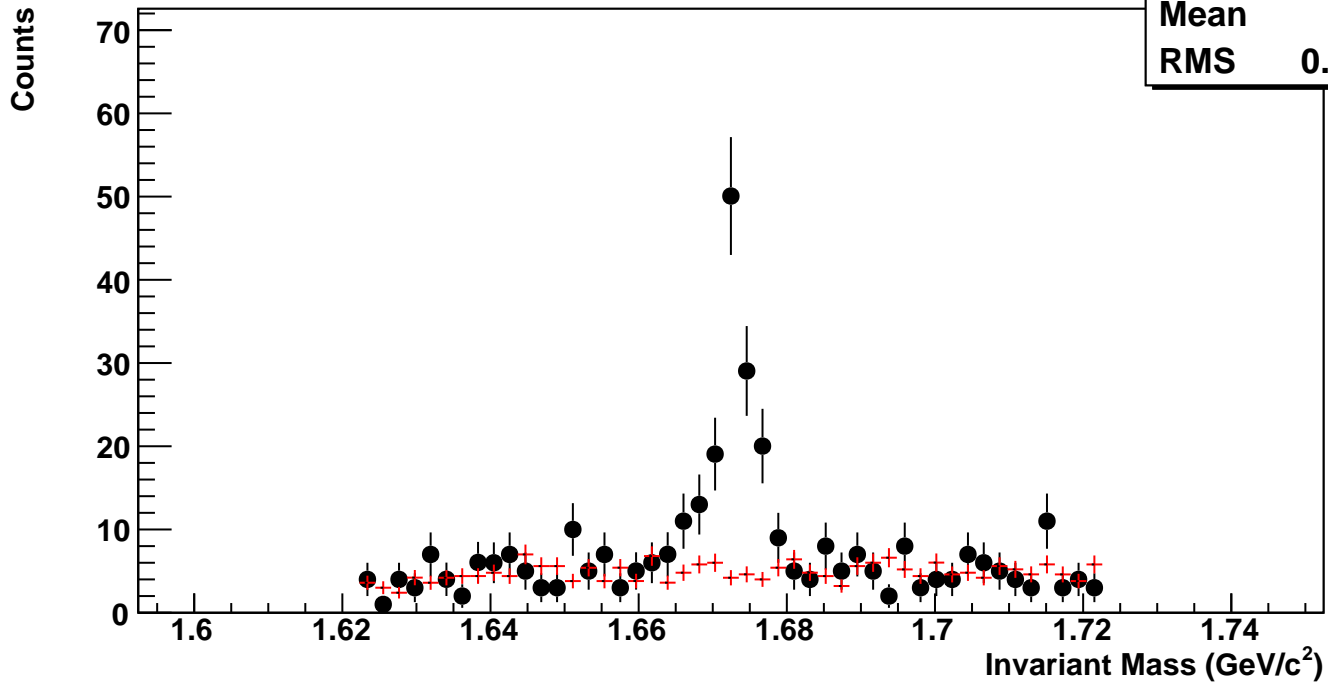
$\Omega^-$ , Au+Au 11 GeV, 10-60%,  $p_T$  1.6-2.0 GeV/c

hmlInvMassBgCent0Pt2	
Entries	65
Mean	1.671
RMS	0.02714



$\Omega^-$ , Au+Au 11 GeV, 10-60%,  $p_T$  2.0-2.4 GeV/c

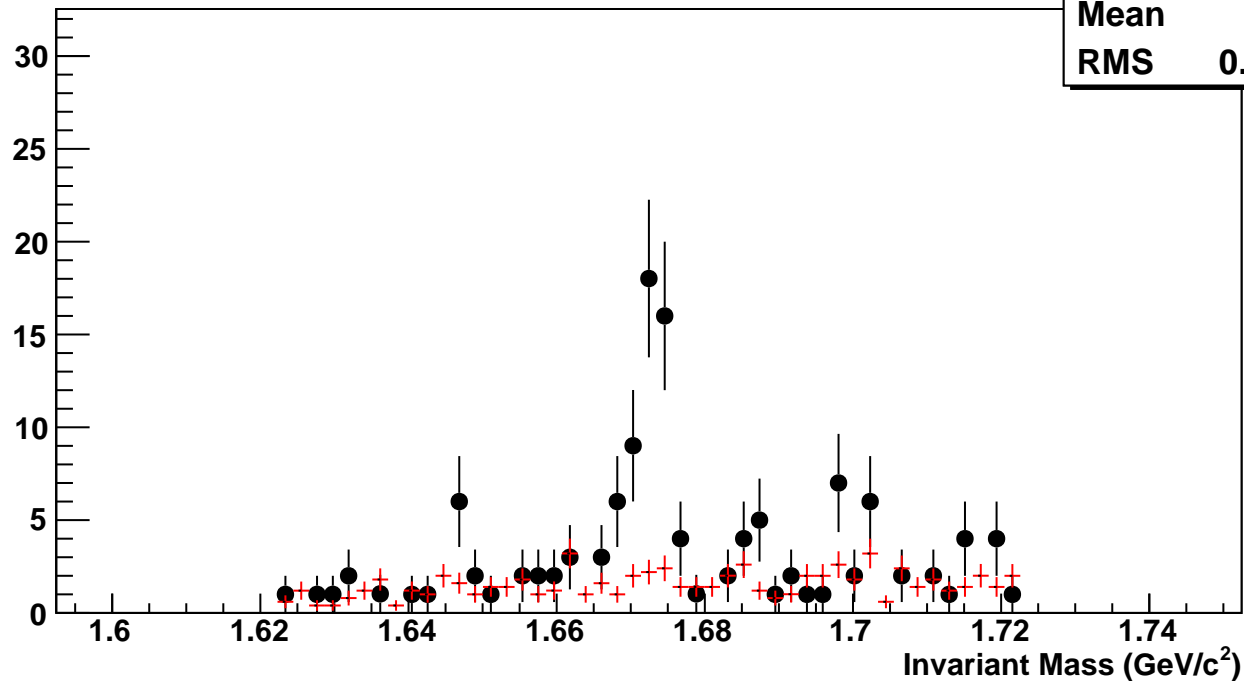
hmlInvMassBgCent0Pt3	
Entries	28
Mean	1.674
RMS	0.02799



$\Omega^-$ , Au+Au 11 GeV, 10-60%,  $p_T$  2.4-2.8 GeV/c

hmlInvMassBgCent0Pt4	
Entries	9
Mean	1.678
RMS	0.02678

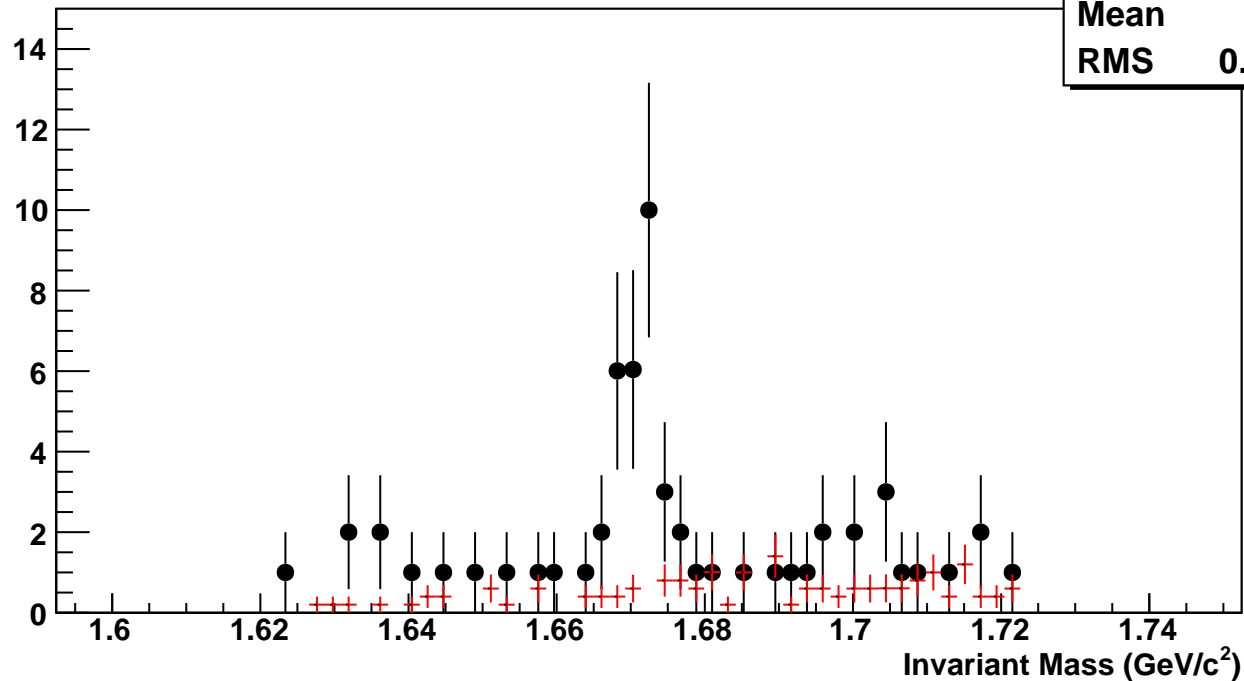
Counts



$\Omega^-$ , Au+Au 11 GeV, 10-60%,  $p_T$  2.8-3.6 GeV/c

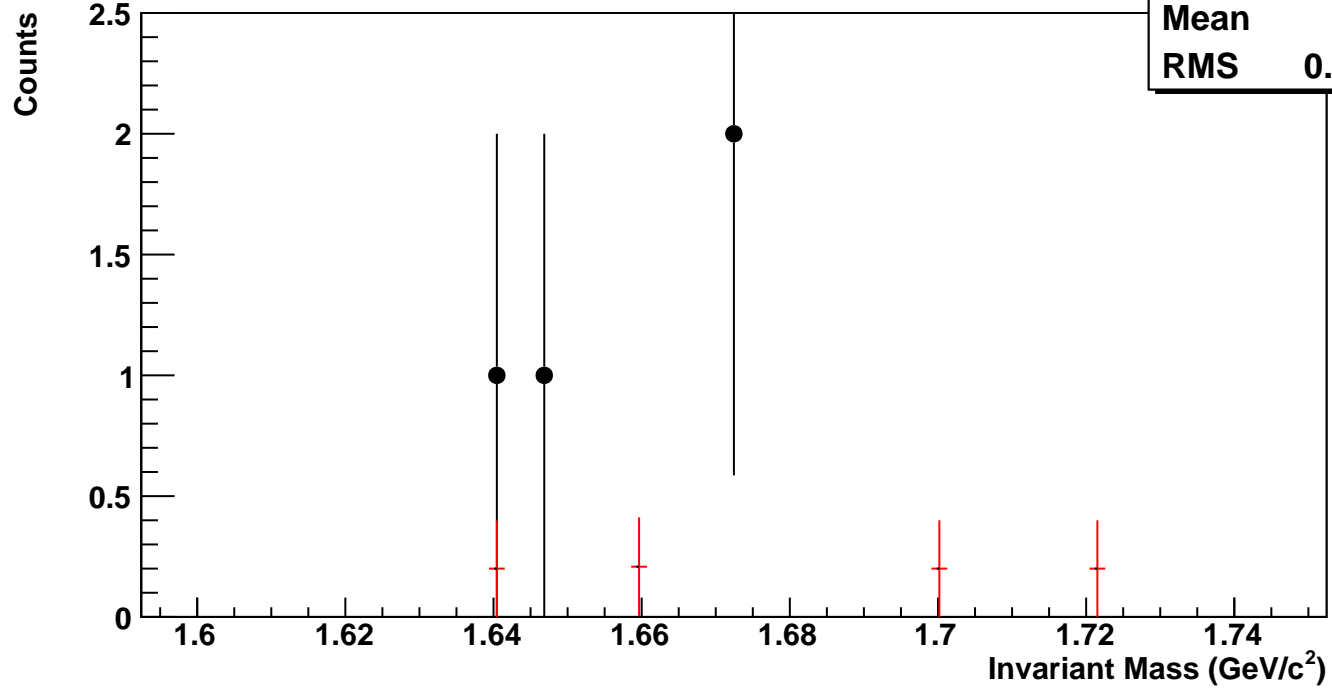
hmlInvMassBgCent0Pt5	
Entries	2
Mean	1.686
RMS	0.02395

Counts



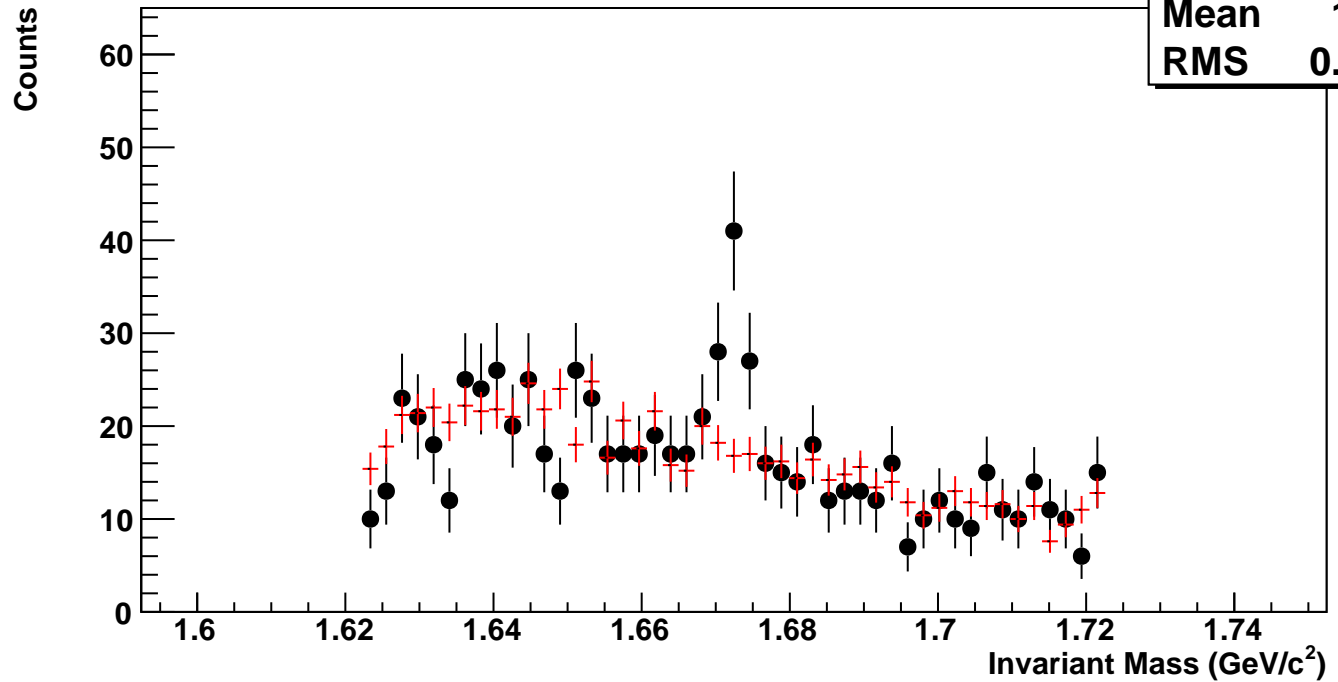
$\Omega^-$ , Au+Au 11 GeV, 10-60%,  $p_T$  3.6-5.0 GeV/c

hmlnvMassBgCent0Pt6	
Entries	0
Mean	1.68
RMS	0.03213



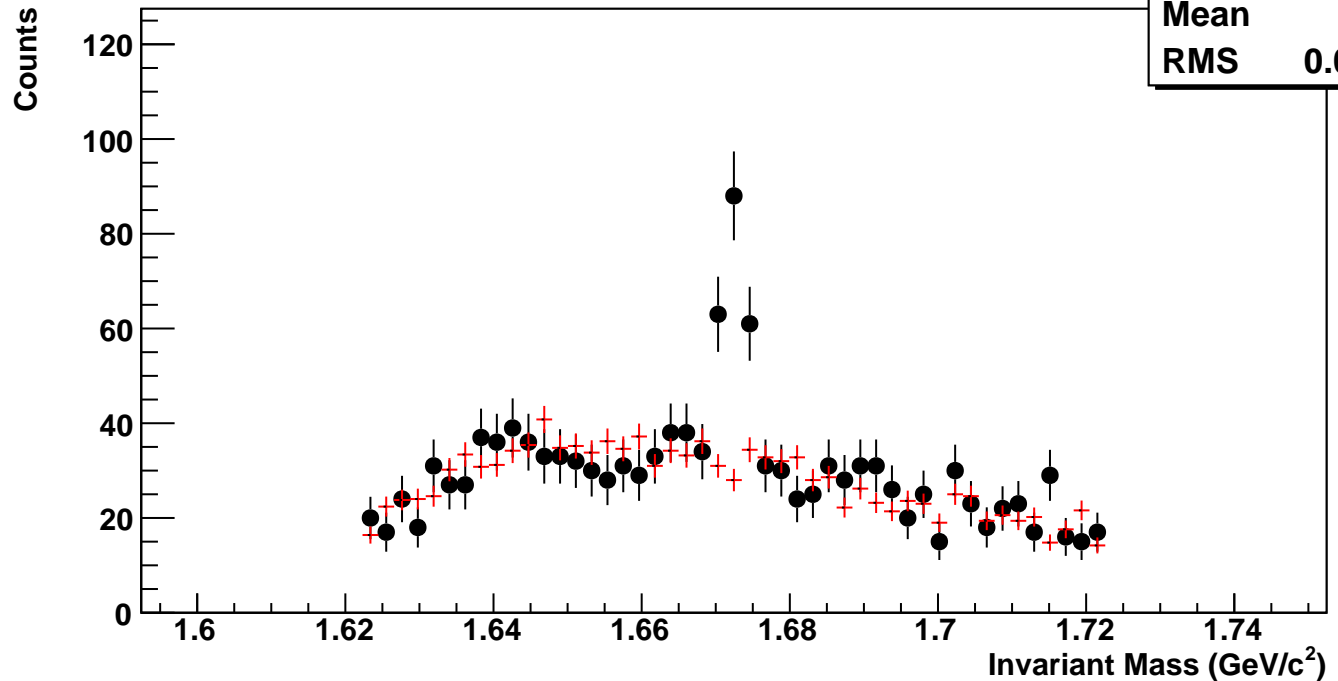
$\Omega^-$ , Au+Au 11 GeV, 0-10%,  $p_T$  0.8-1.2 GeV/c

hmlInvMassBgCent1Pt0  
Entries 95  
Mean 1.666  
RMS 0.0275



$\Omega^-$ , Au+Au 11 GeV, 0-10%,  $p_T$  1.2-1.6 GeV/c

hmlInvMassBgCent1Pt1  
Entries 158  
Mean 1.669  
RMS 0.02652



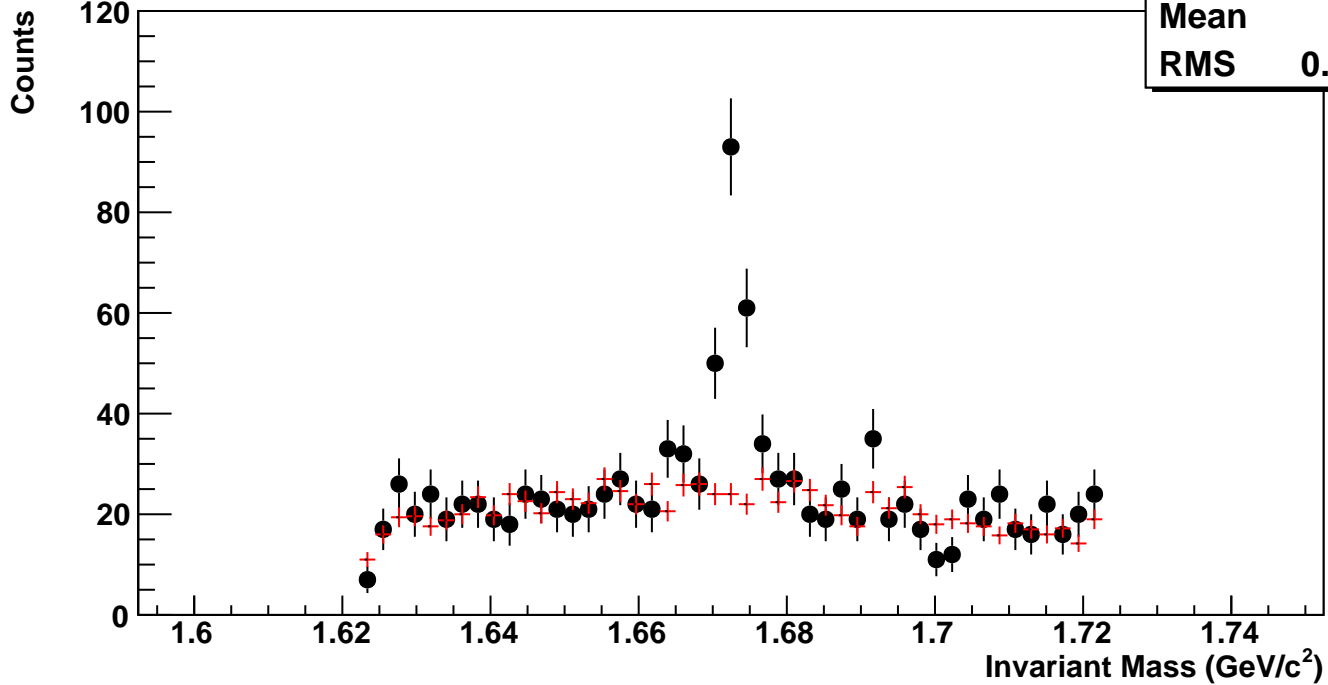
$\Omega^-$ , Au+Au 11 GeV, 0-10%,  $p_T$  1.6-2.0 GeV/c

hmlInvMassBgCent1Pt2

Entries 120

Mean 1.672

RMS 0.02712



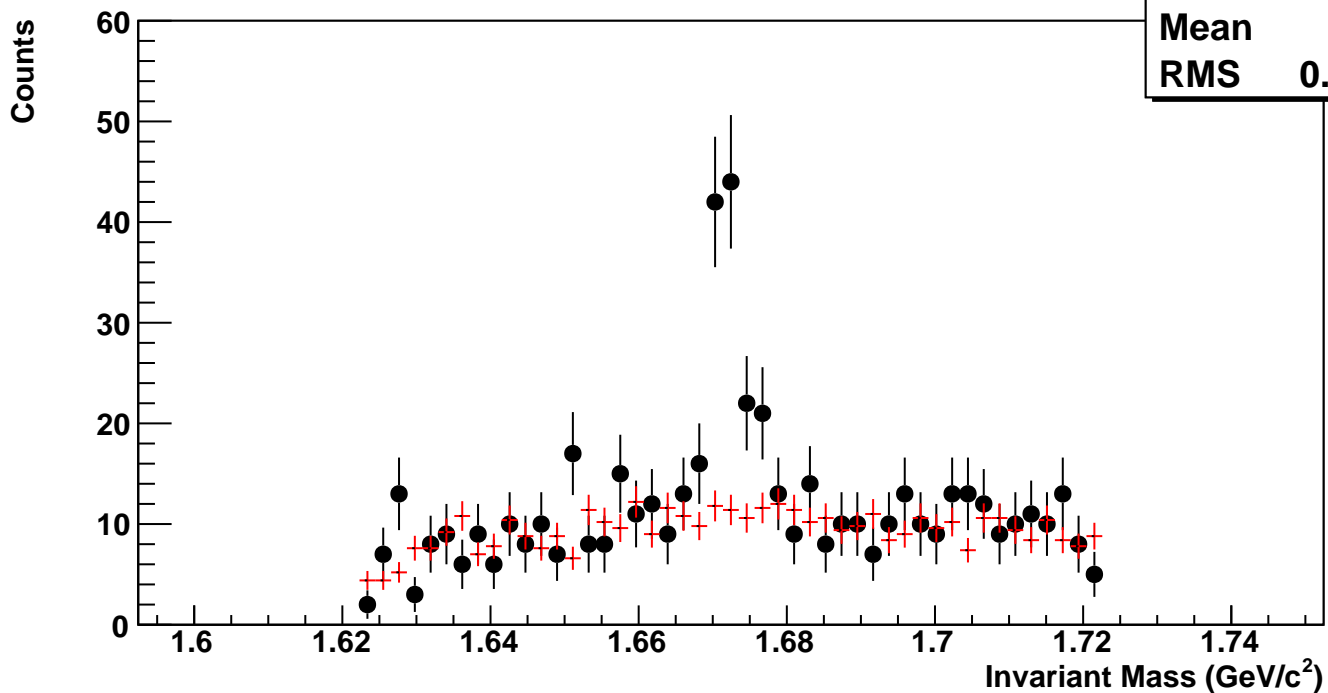
$\Omega^-$ , Au+Au 11 GeV, 0-10%,  $p_T$  2.0-2.4 GeV/c

hmlInvMassBgCent1Pt3

Entries 54

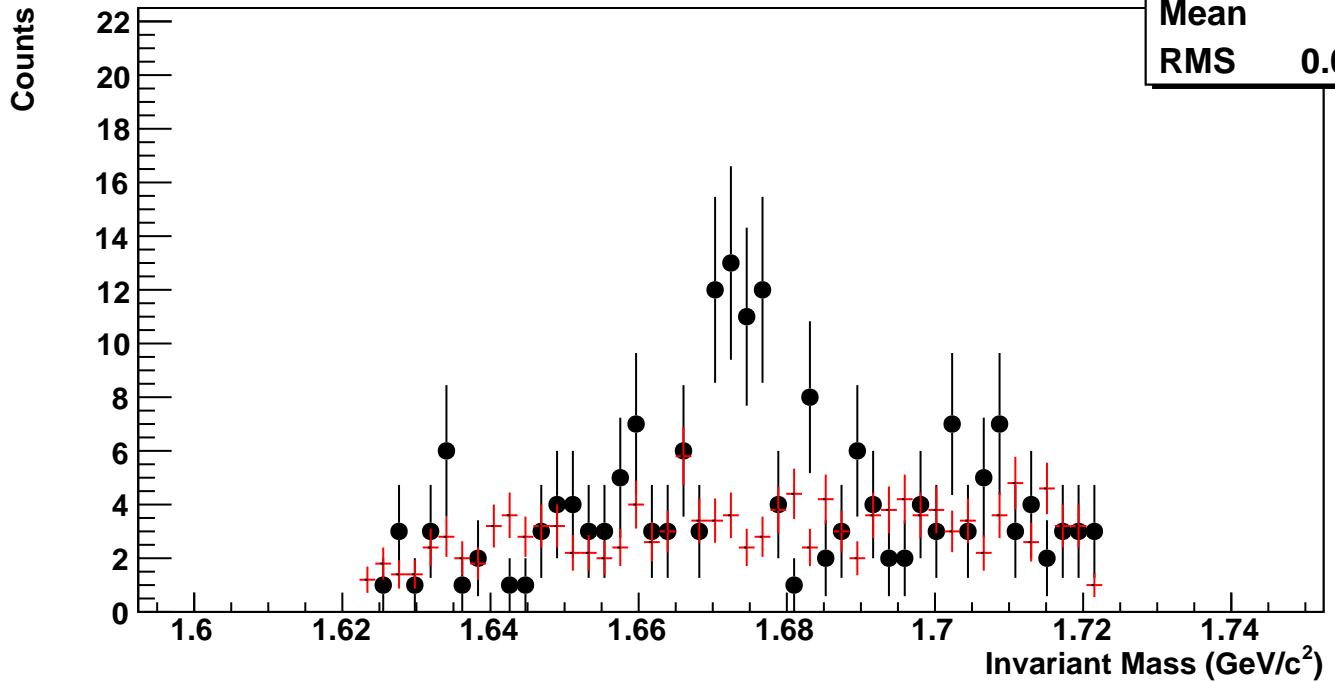
Mean 1.675

RMS 0.02711



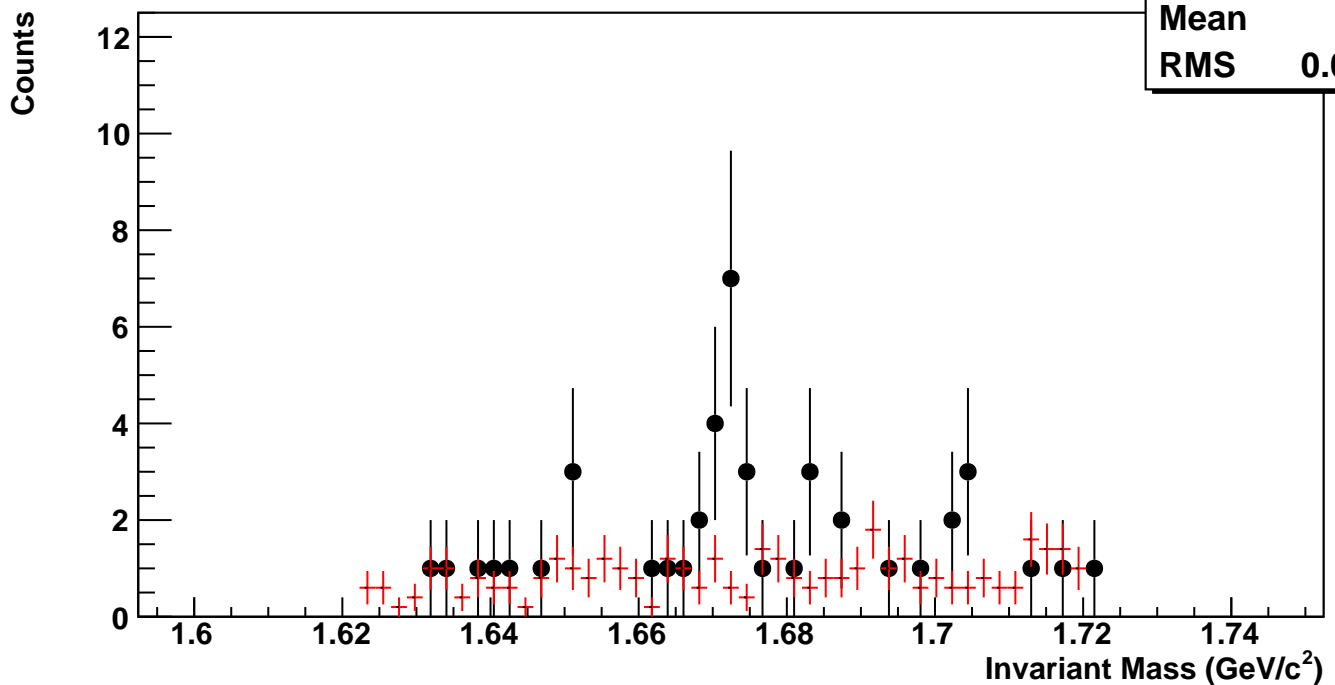
$\Omega^-$ , Au+Au 11 GeV, 0-10%,  $p_T$  2.4-2.8 GeV/c

hmlInvMassBgCent1Pt4	
Entries	17
Mean	1.676
RMS	0.02695



$\Omega^-$ , Au+Au 11 GeV, 0-10%,  $p_T$  2.8-3.6 GeV/c

hmlInvMassBgCent1Pt5	
Entries	5
Mean	1.676
RMS	0.02762



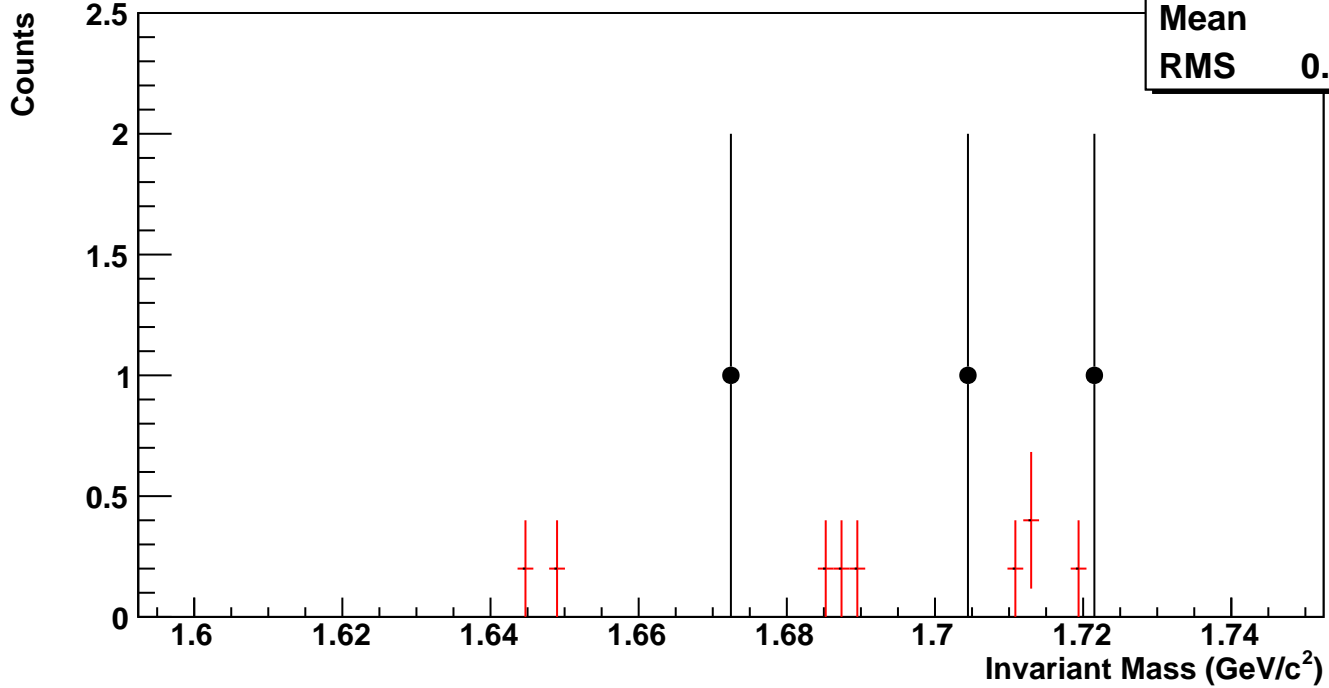
$\Omega^-$ , Au+Au 11 GeV, 0-10%,  $p_T$  3.6-5.0 GeV/c

hmlInvMassBgCent1Pt6

Entries 0

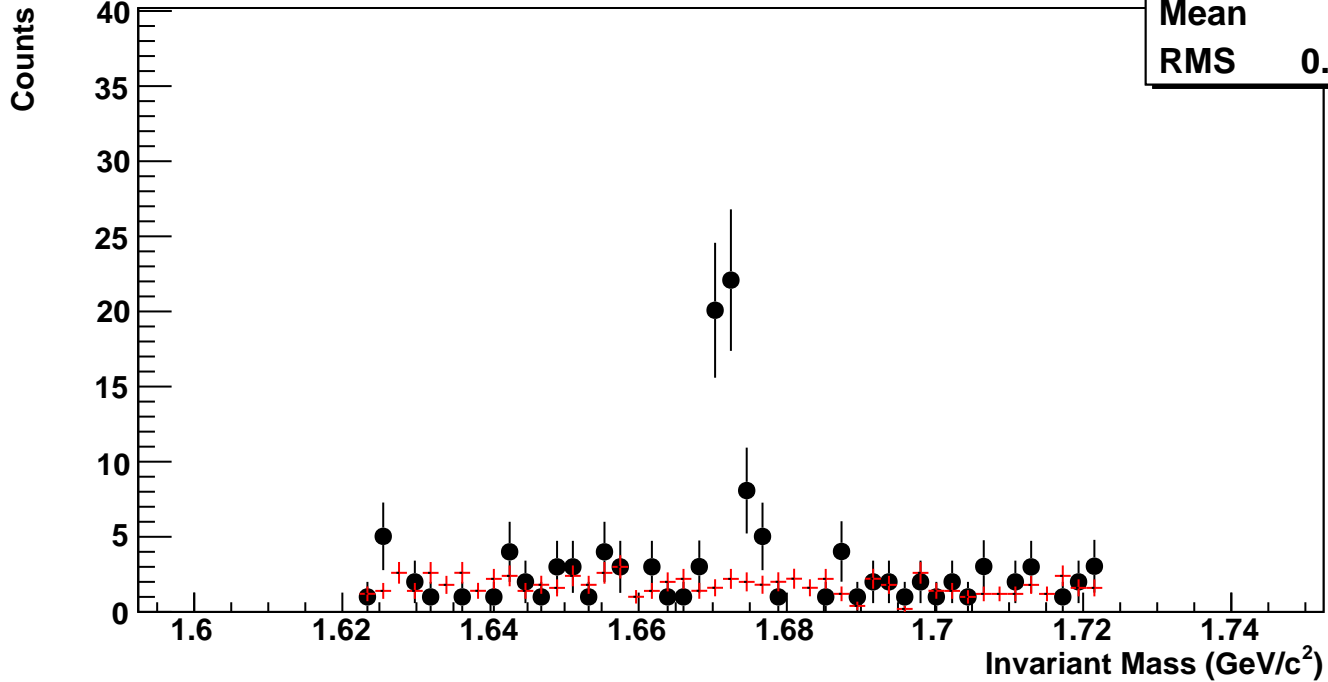
Mean 1.69

RMS 0.02614



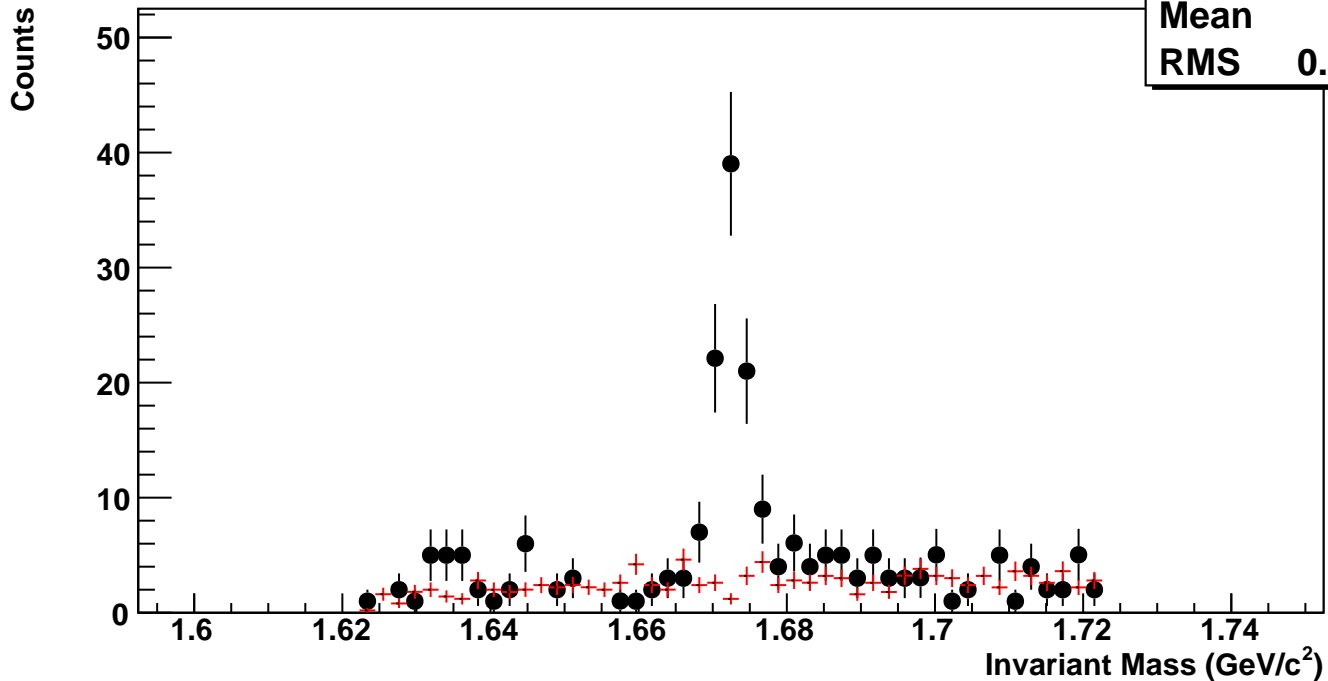
$\Omega^+$ , Au+Au 11 GeV, 10-60%,  $p_T$  0.8-1.2 GeV/c

hmlInvMassBgCent0Pt0	
Entries	10
Mean	1.67
RMS	0.02839



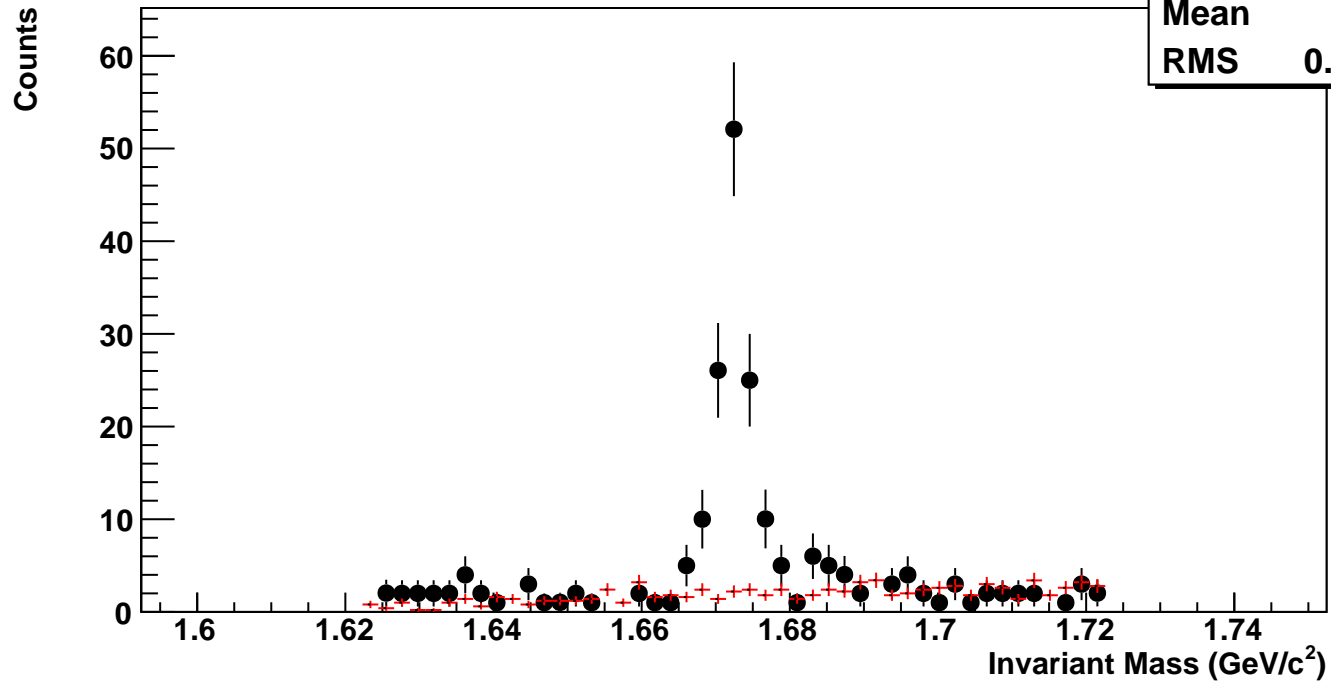
$\Omega^+$ , Au+Au 11 GeV, 10-60%,  $p_T$  1.2-1.6 GeV/c

hmlInvMassBgCent0Pt1	
Entries	14
Mean	1.678
RMS	0.02691



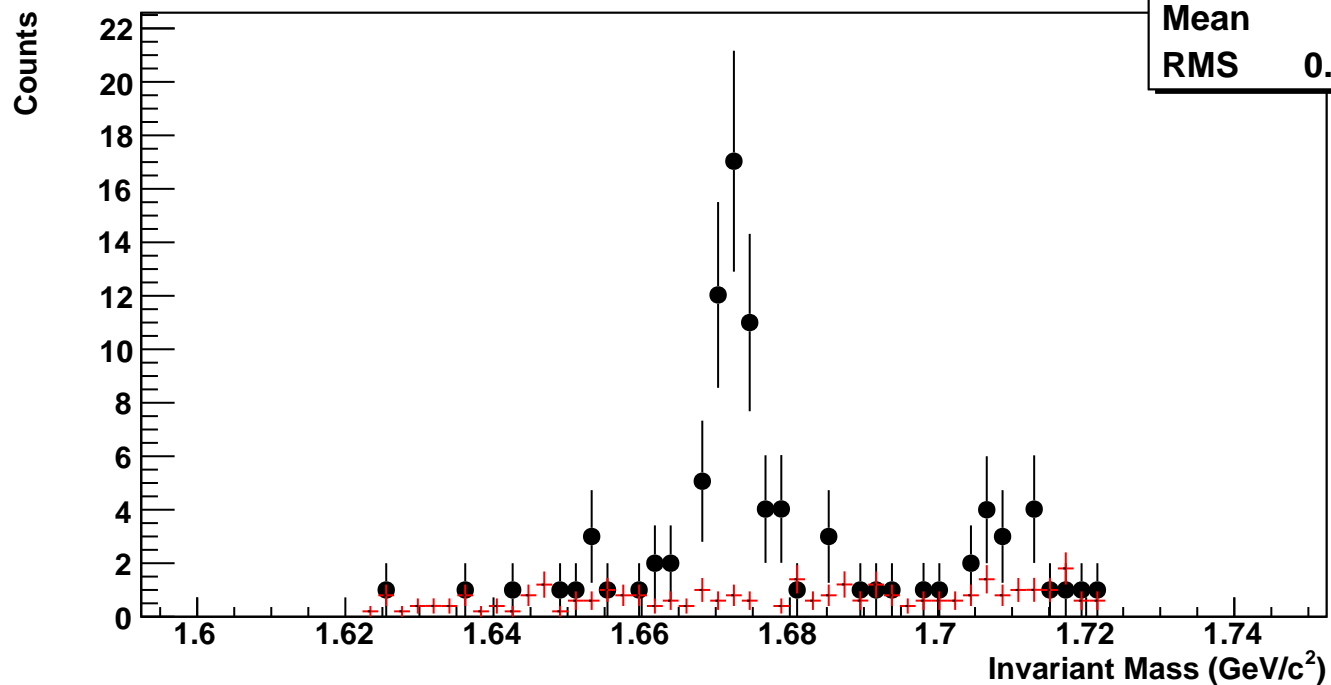
$\Omega^+$ , Au+Au 11 GeV, 10-60%,  $p_T$  1.6-2.0 GeV/c

hmlnvMassBgCent0Pt2	
Entries	11
Mean	1.682
RMS	0.02604



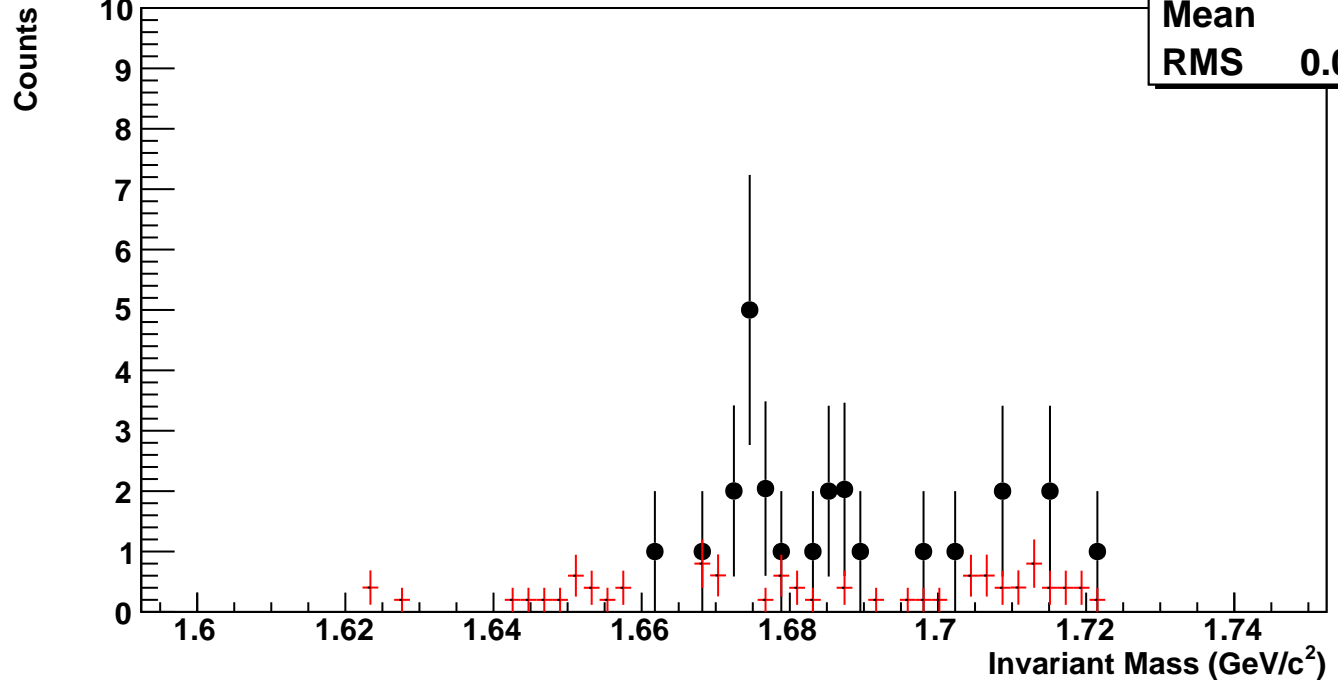
$\Omega^+$ , Au+Au 11 GeV, 10-60%,  $p_T$  2.0-2.4 GeV/c

hmlnvMassBgCent0Pt3	
Entries	4
Mean	1.679
RMS	0.02806



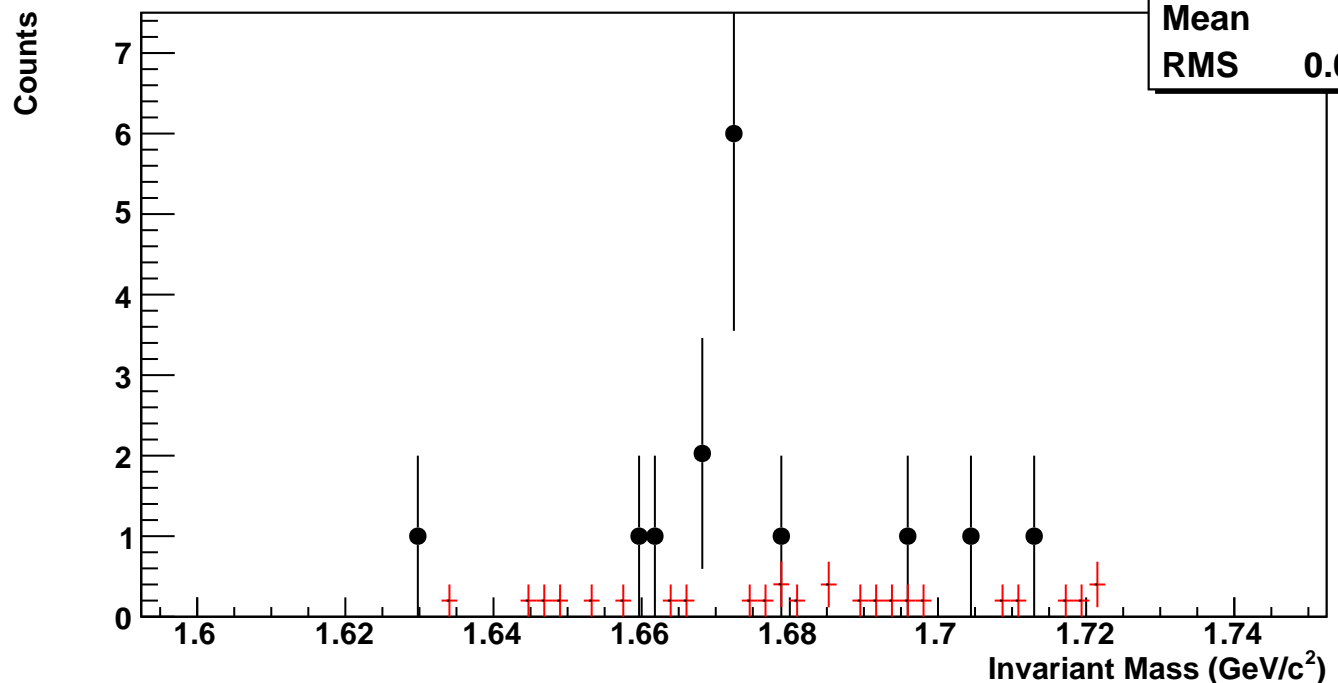
$\Omega^+$ , Au+Au 11 GeV, 10-60%,  $p_T$  2.4-2.8 GeV/c

hmlInvMassBgCent0Pt4	
Entries	1
Mean	1.683
RMS	0.02771



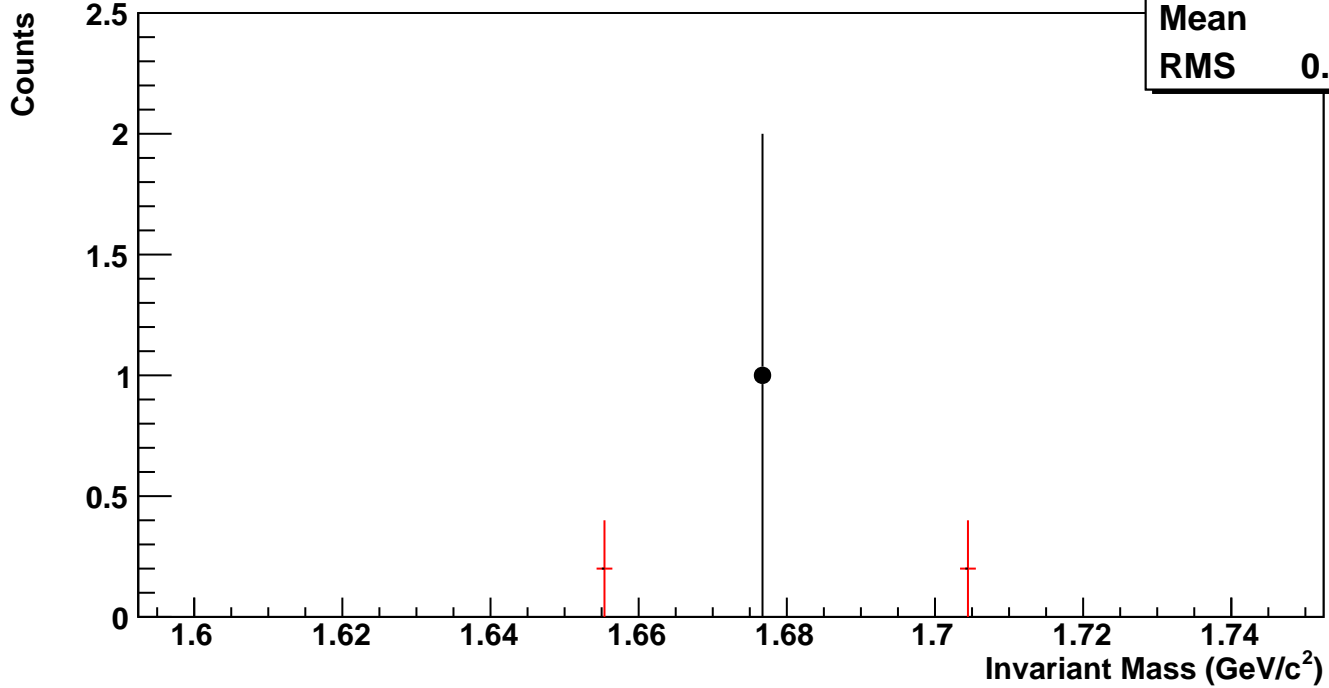
$\Omega^+$ , Au+Au 11 GeV, 10-60%,  $p_T$  2.8-3.6 GeV/c

hmlInvMassBgCent0Pt5	
Entries	1
Mean	1.682
RMS	0.02487



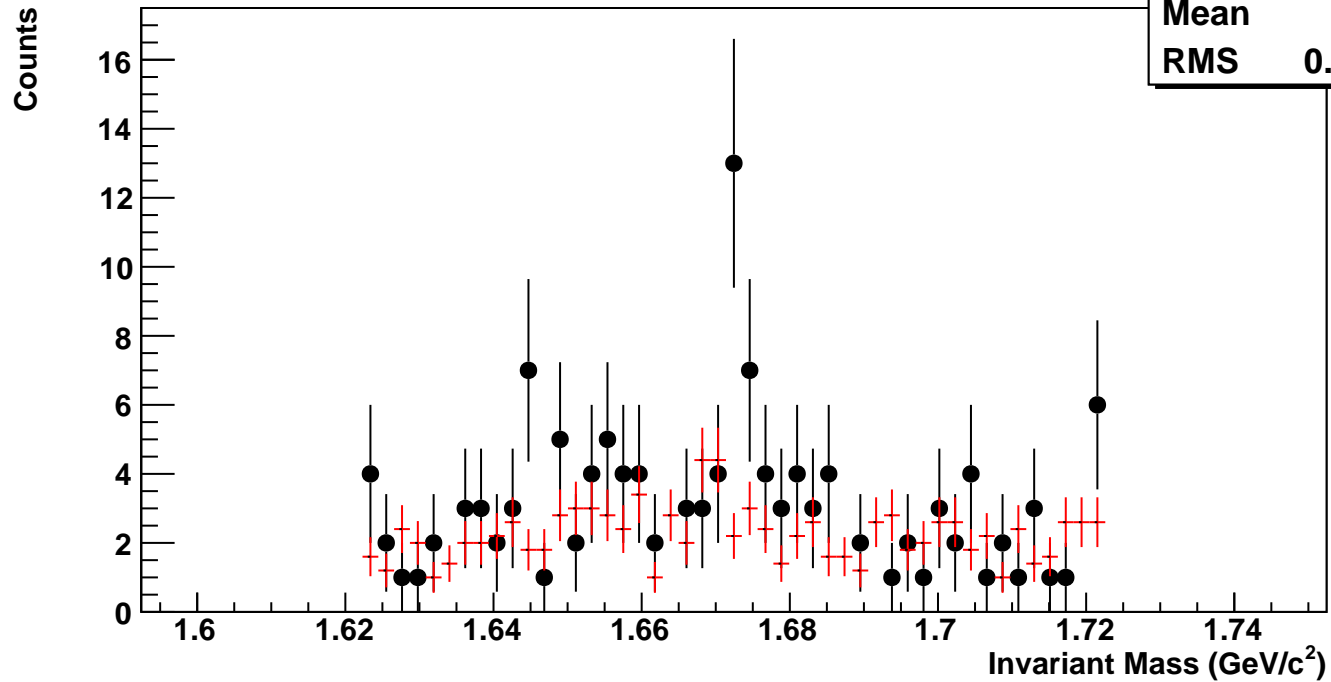
$\Omega^+$ , Au+Au 11 GeV, 10-60%,  $p_T$  3.6-5.0 GeV/c

hmlnvMassBgCent0Pt6	
Entries	0
Mean	1.68
RMS	0.02453



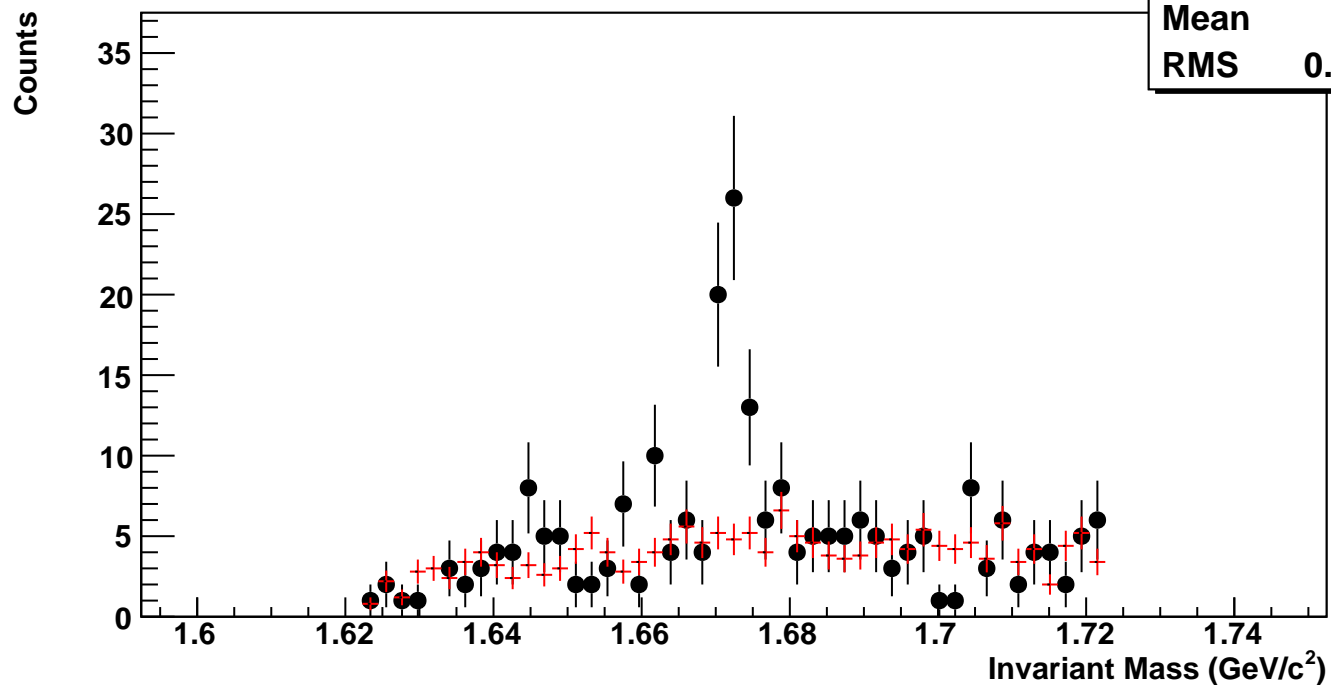
$\bar{\Omega}^+$ , Au+Au 11 GeV, 0-10%,  $p_T$  0.8-1.2 GeV/c

hmlInvMassBgCent1Pt0	
Entries	13
Mean	1.673
RMS	0.02744



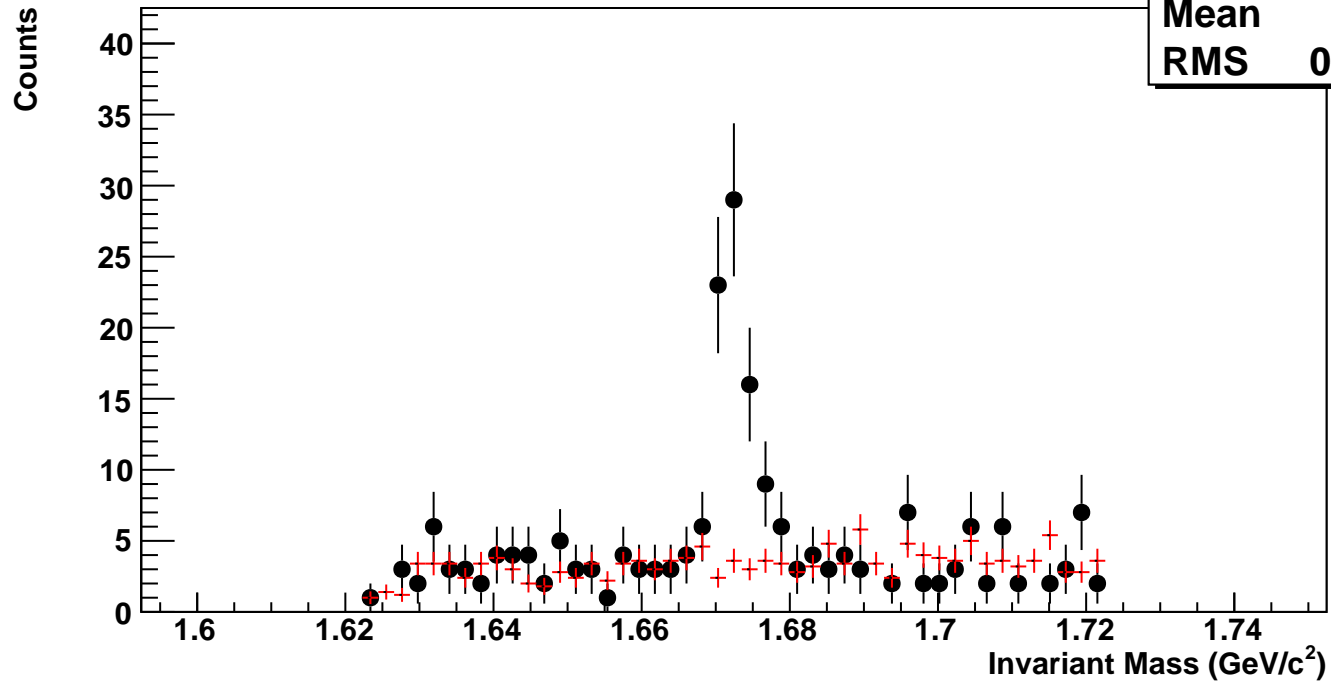
$\bar{\Omega}^+$ , Au+Au 11 GeV, 0-10%,  $p_T$  1.2-1.6 GeV/c

hmlInvMassBgCent1Pt1	
Entries	22
Mean	1.677
RMS	0.02643



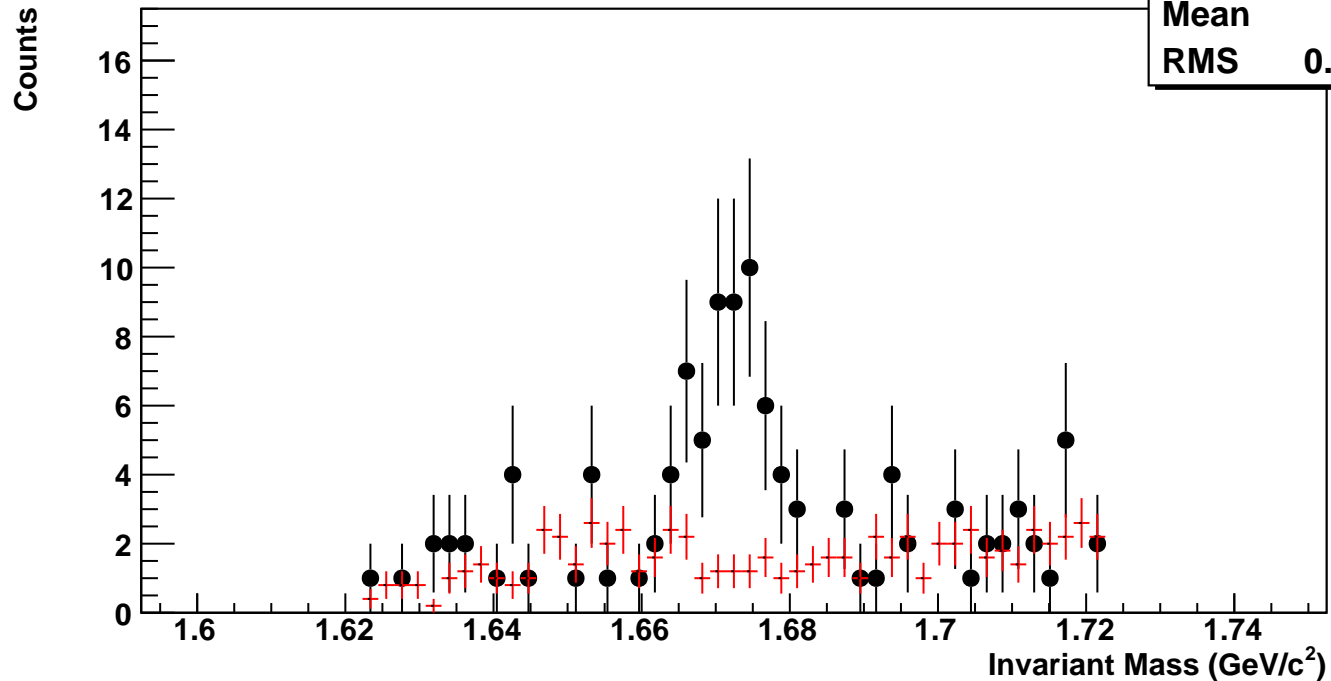
$\Omega^+$ , Au+Au 11 GeV, 0-10%,  $p_T$  1.6-2.0 GeV/c

hmlInvMassBgCent1Pt2	19
Entries	19
Mean	1.677
RMS	0.0276



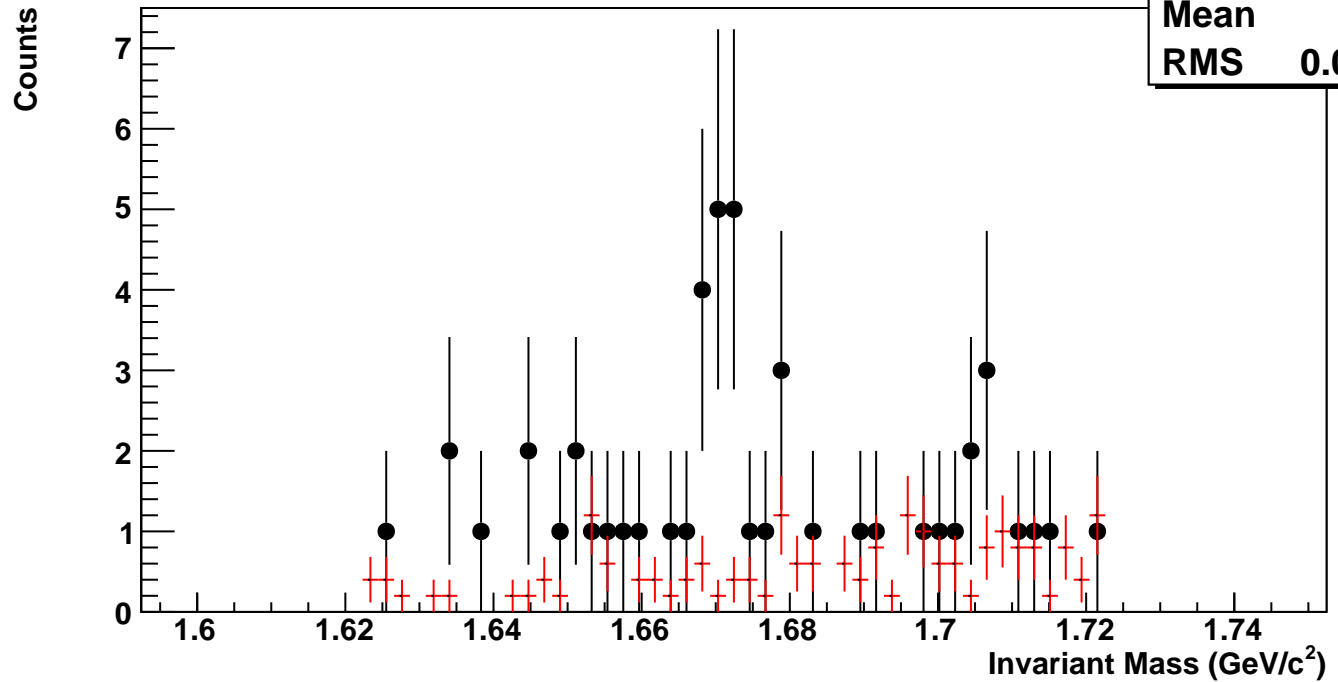
$\Omega^+$ , Au+Au 11 GeV, 0-10%,  $p_T$  2.0-2.4 GeV/c

hmlInvMassBgCent1Pt3	9
Entries	9
Mean	1.679
RMS	0.02776



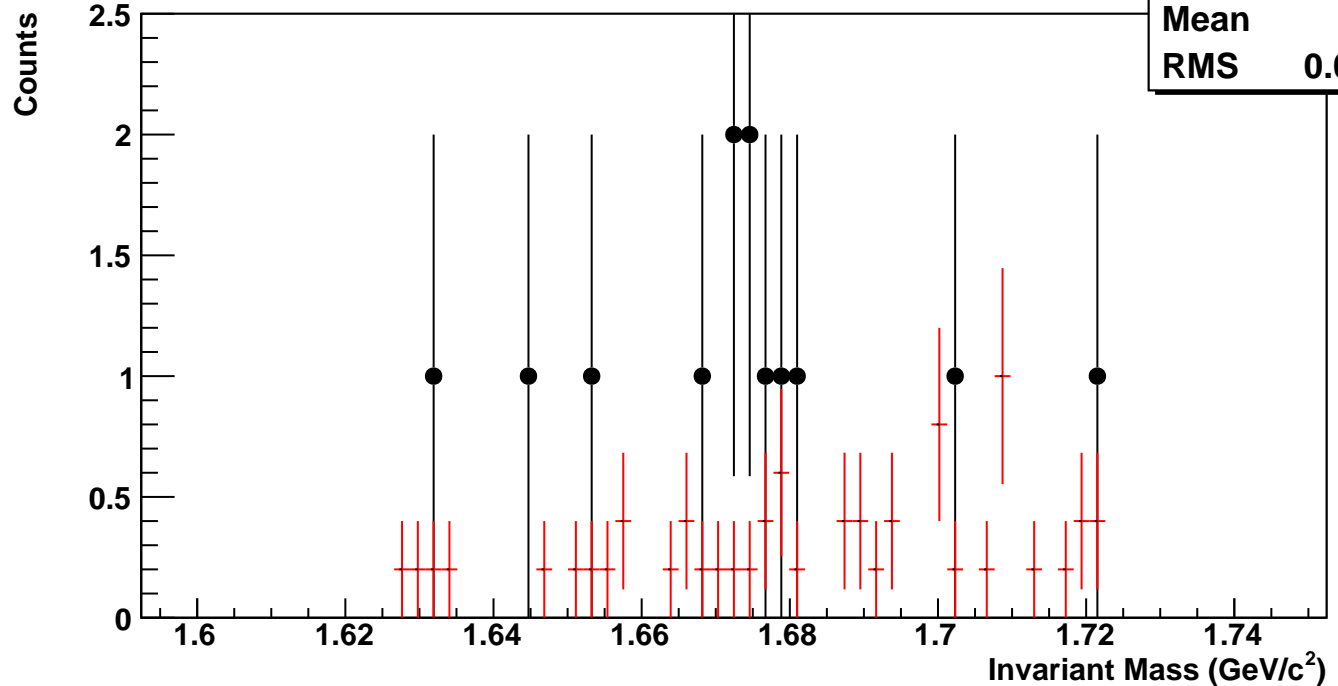
$\Omega^+$ , Au+Au 11 GeV, 0-10%,  $p_T$  2.4-2.8 GeV/c

hmlInvMassBgCent1Pt4	
Entries	3
Mean	1.685
RMS	0.02651



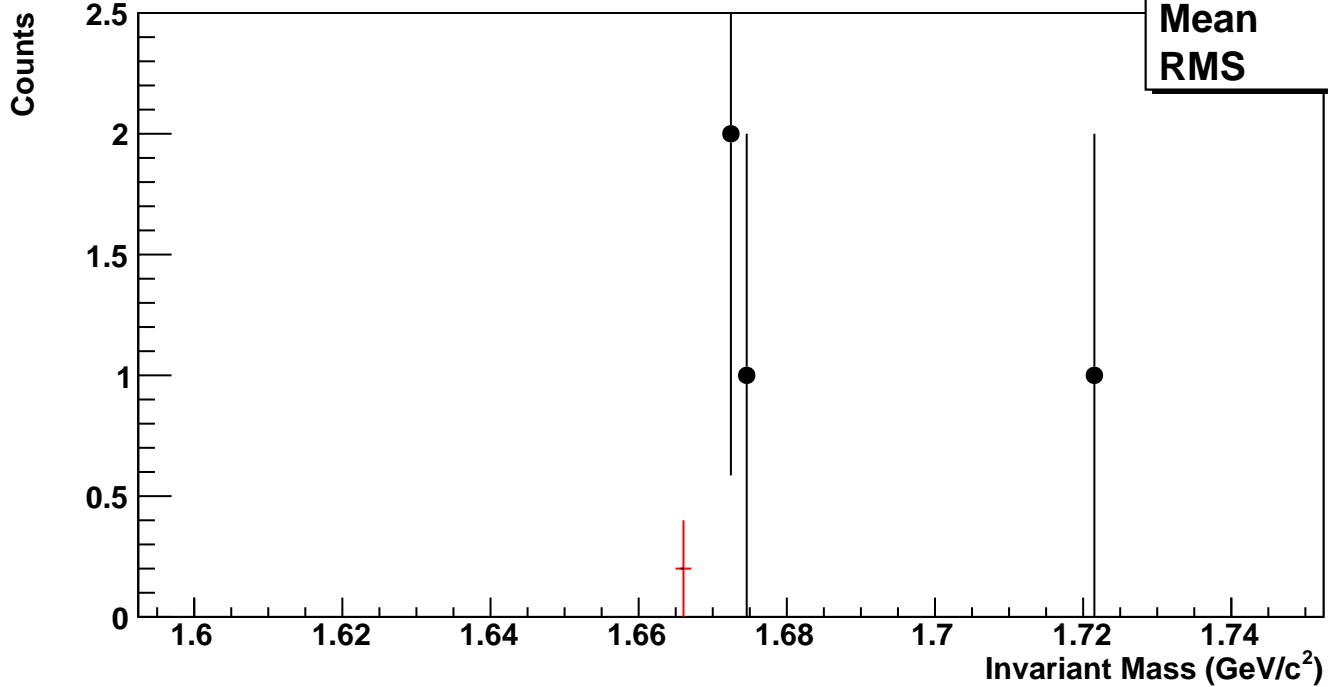
$\Omega^+$ , Au+Au 11 GeV, 0-10%,  $p_T$  2.8-3.6 GeV/c

hmlInvMassBgCent1Pt5	
Entries	1
Mean	1.683
RMS	0.02583



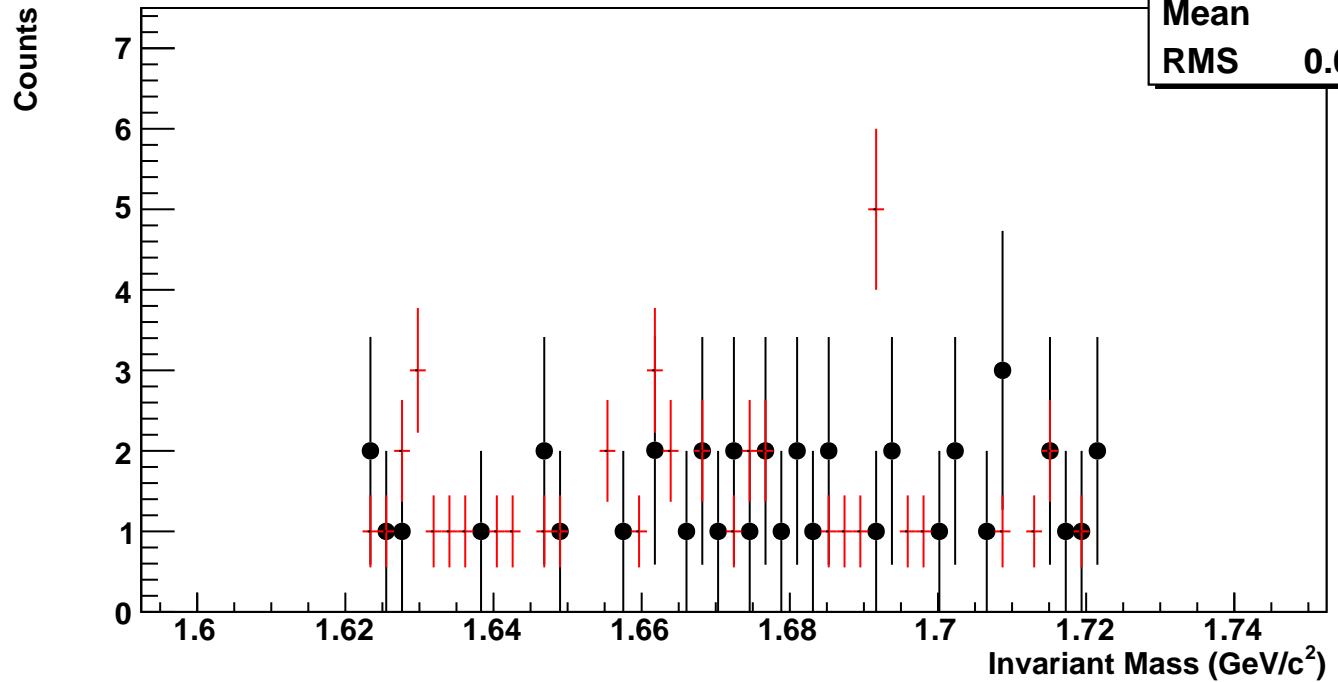
$\Omega^+$ , Au+Au 11 GeV, 0-10%,  $p_T$  3.6-5.0 GeV/c

hmlInvMassBgCent1Pt6	
Entries	0
Mean	1.667
RMS	0



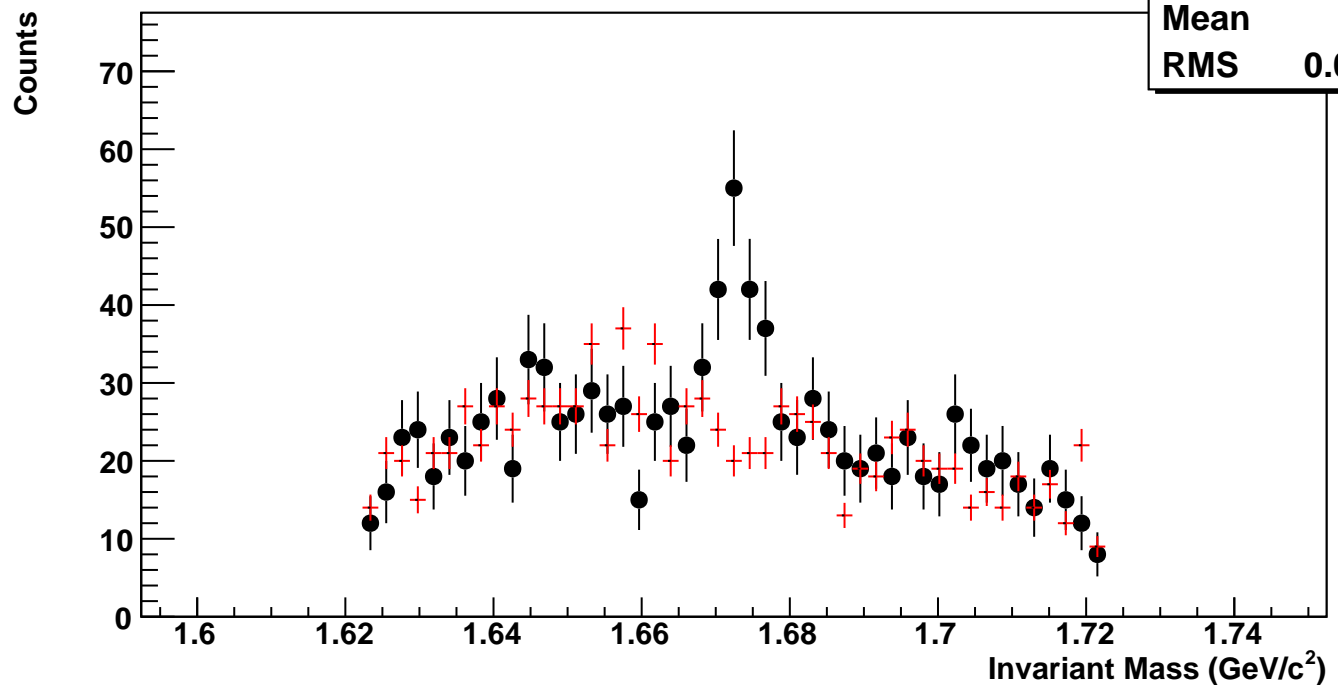
$\Omega^-$ , Au+Au 7 GeV, 0-60%,  $p_T$  0.4-0.7 GeV/c

hmlInvMassBgCent0Pt0	
Entries	44
Mean	1.667
RMS	0.02785



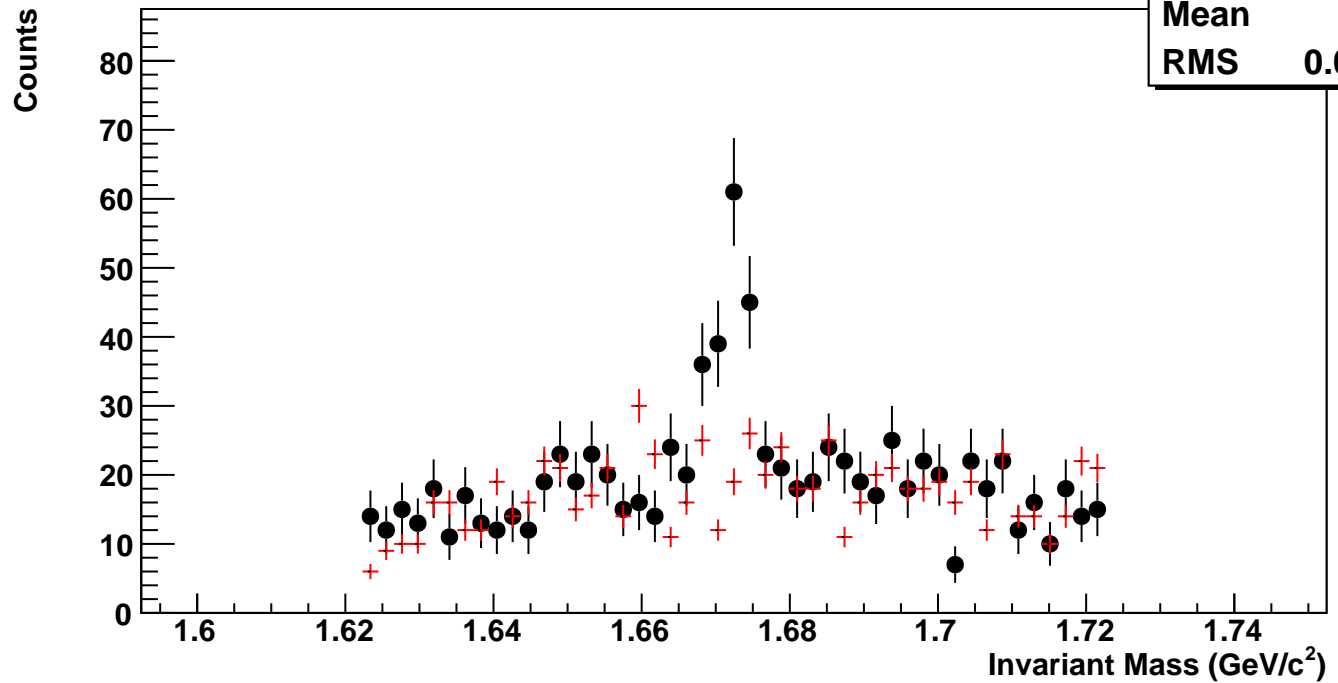
$\Omega^-$ , Au+Au 7 GeV, 0-60%,  $p_T$  0.7-1.3 GeV/c

hmlInvMassBgCent0Pt1	
Entries	1027
Mean	1.669
RMS	0.02674



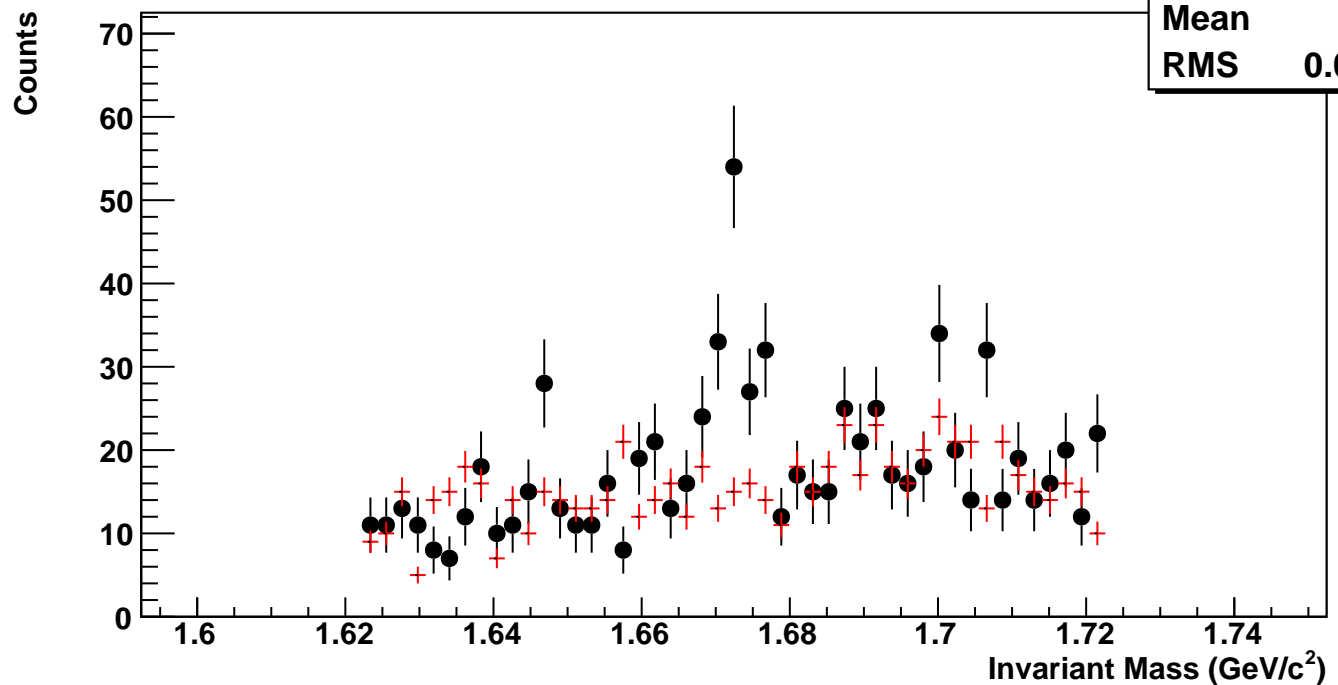
$\Omega^-$ , Au+Au 7 GeV, 0-60%,  $p_T$  1.3-1.6 GeV/c

hmlInvMassBgCent0Pt2	
Entries	805
Mean	1.675
RMS	0.02698



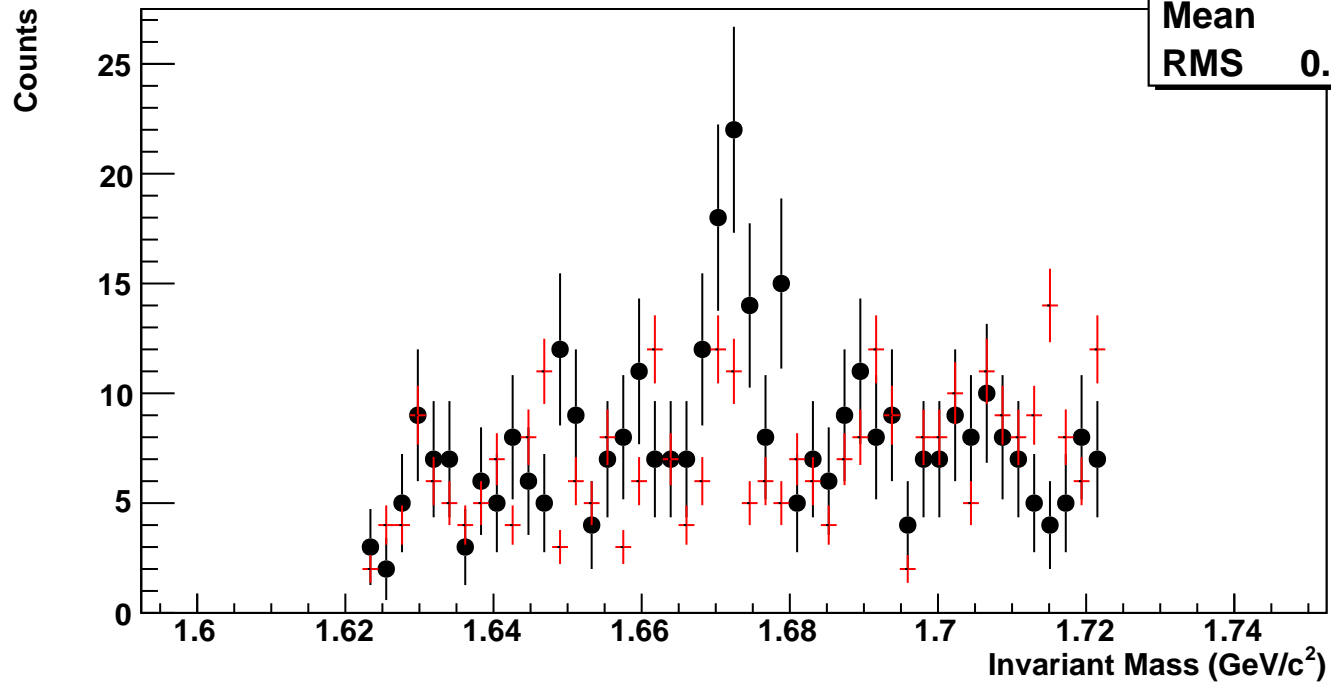
$\Omega^-$ , Au+Au 7 GeV, 0-60%,  $p_T$  1.6-2.0 GeV/c

hmlInvMassBgCent0Pt3	
Entries	719
Mean	1.676
RMS	0.02774



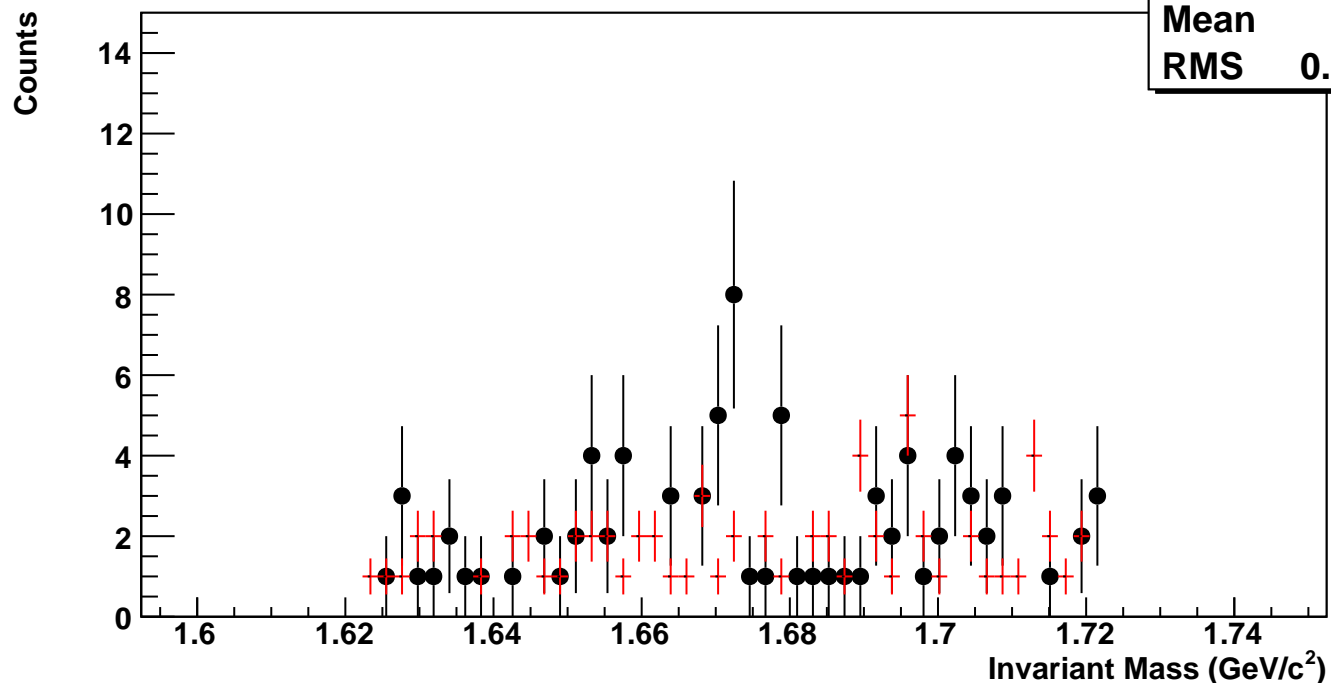
$\Omega^-$ , Au+Au 7 GeV, 0-60%,  $p_T$  2.0-2.5 GeV/c

hmlInvMassBgCent0Pt4  
Entries 331  
Mean 1.678  
RMS 0.02851



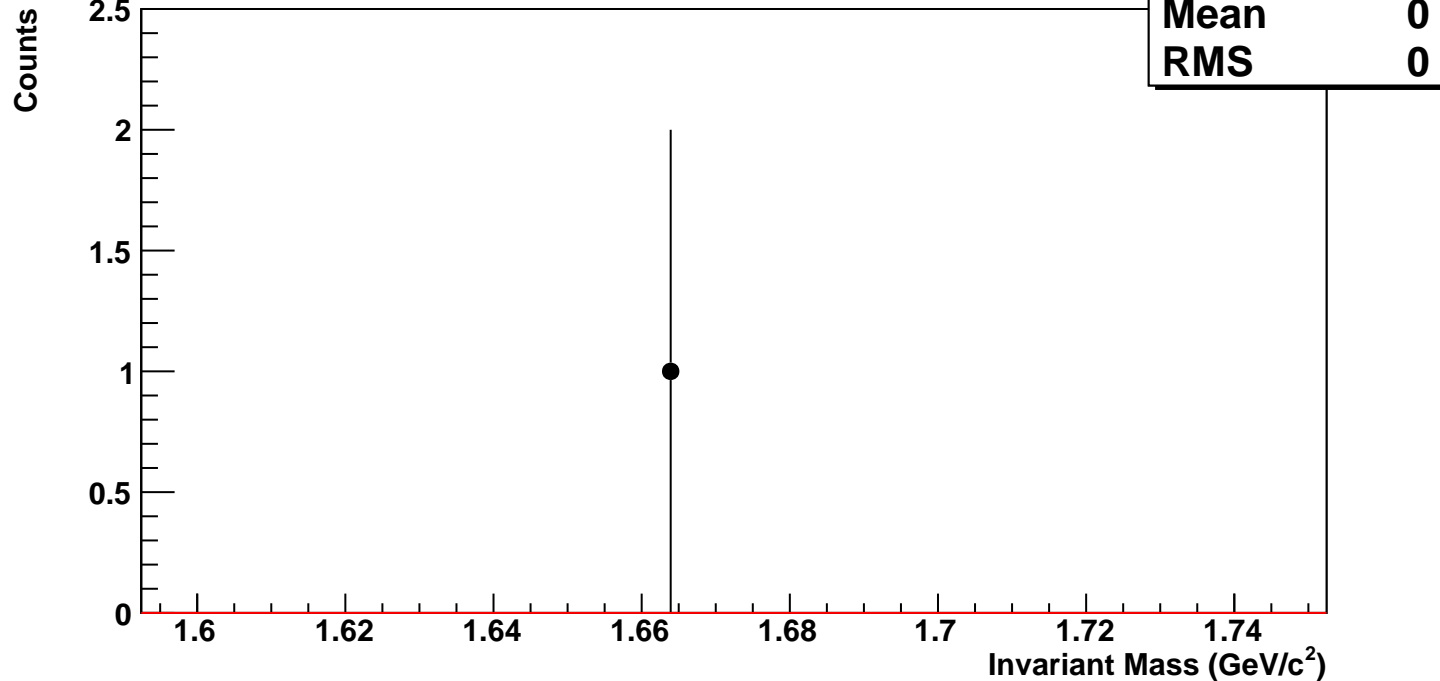
$\Omega^-$ , Au+Au 7 GeV, 0-60%,  $p_T$  2.5-3.5 GeV/c

hmlInvMassBgCent0Pt5  
Entries 70  
Mean 1.676  
RMS 0.02741



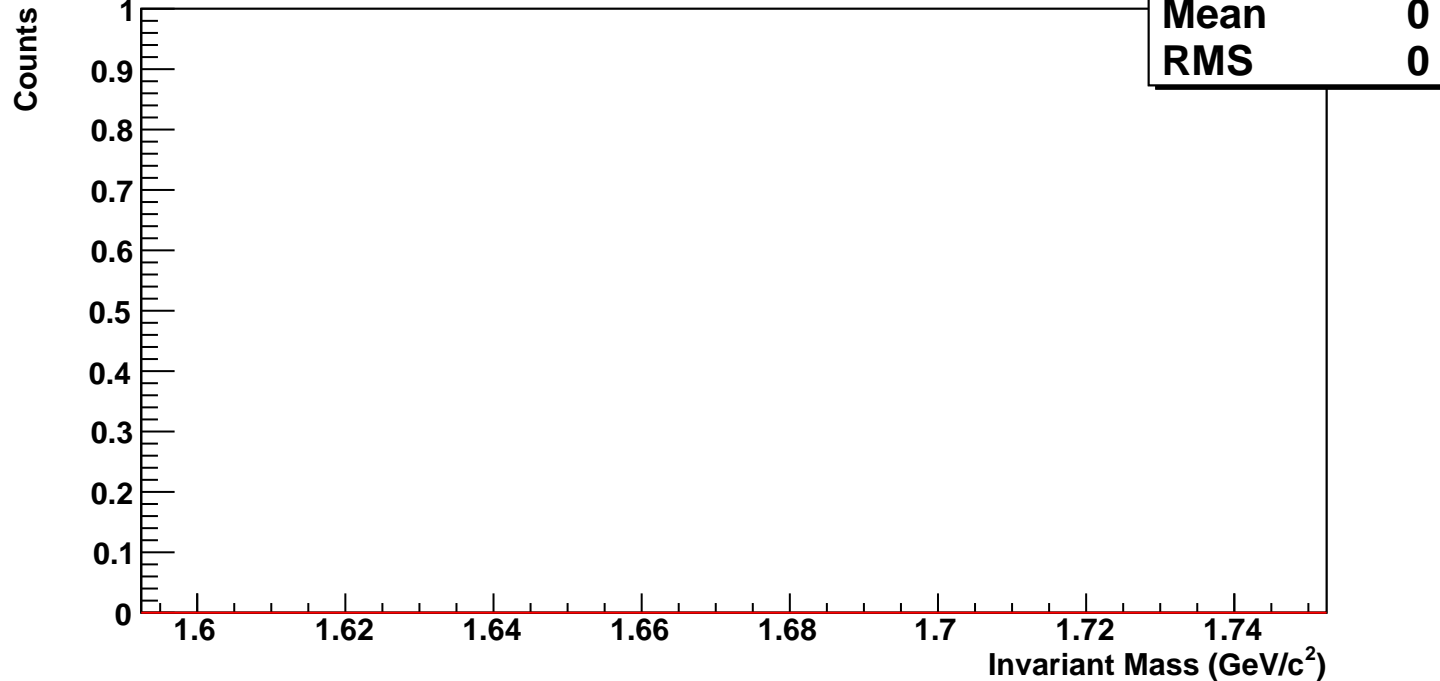
$\Omega^-$ , Au+Au 7 GeV, 0-60%,  $p_T$  3.5-5.0 GeV/c

hmlInvMassBgCent0Pt6



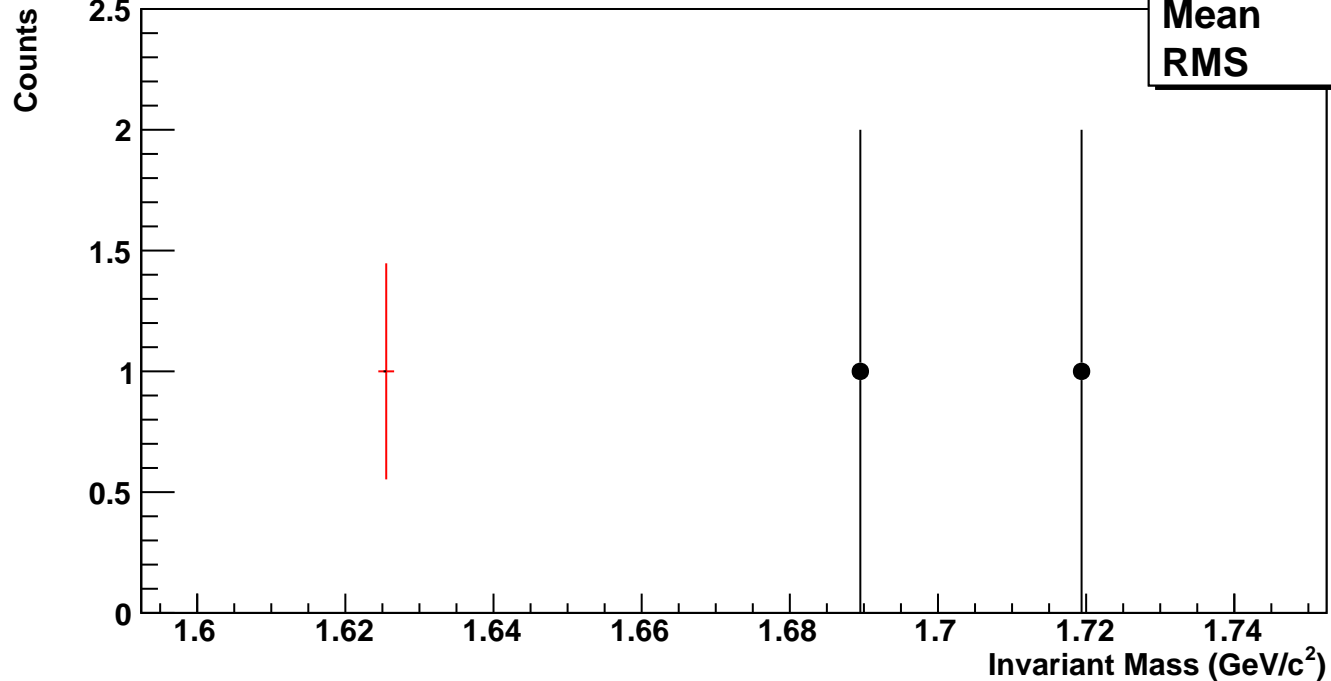
$\Omega^-$ , Au+Au 7 GeV, 0-60%,  $p_T$  5.0-8.0 GeV/c

hmlInvMassBgCent0Pt7



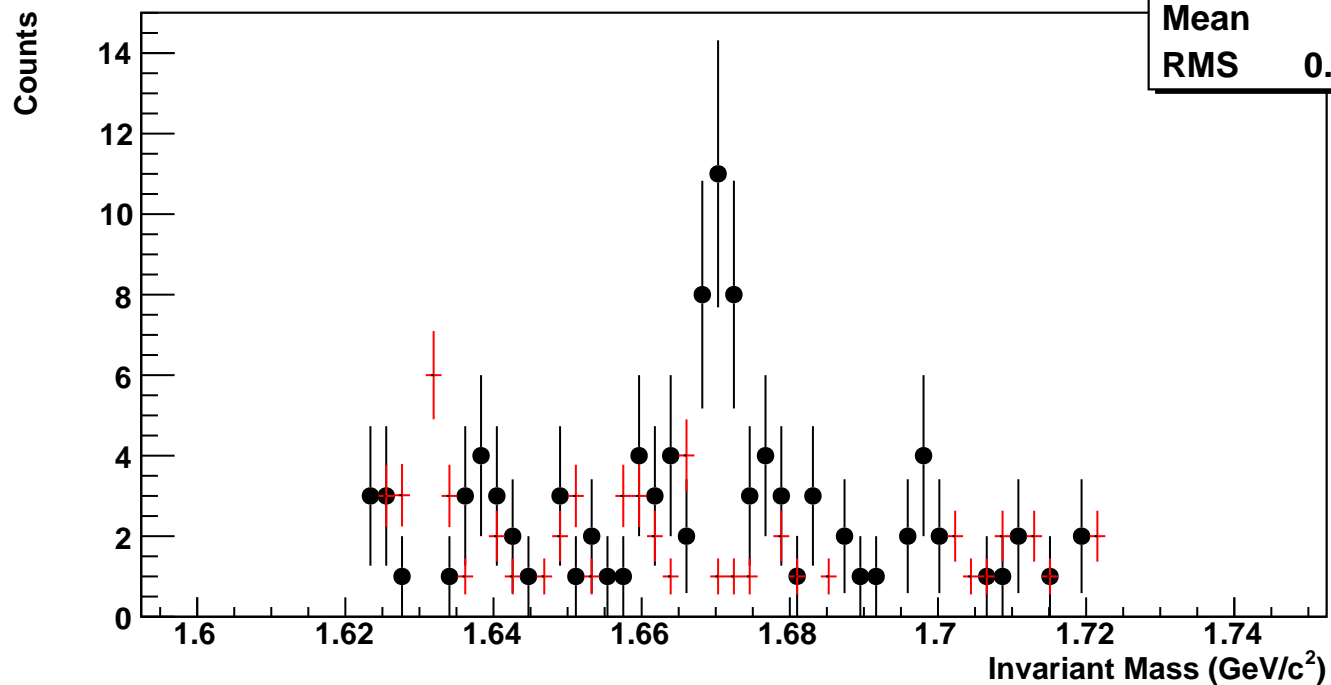
$\bar{\Omega}^+$ , Au+Au 7 GeV, 0-60%,  $p_T$  0.4-0.7 GeV/c

hmlInvMassBgCent0Pt0	
Entries	1
Mean	1.625
RMS	0



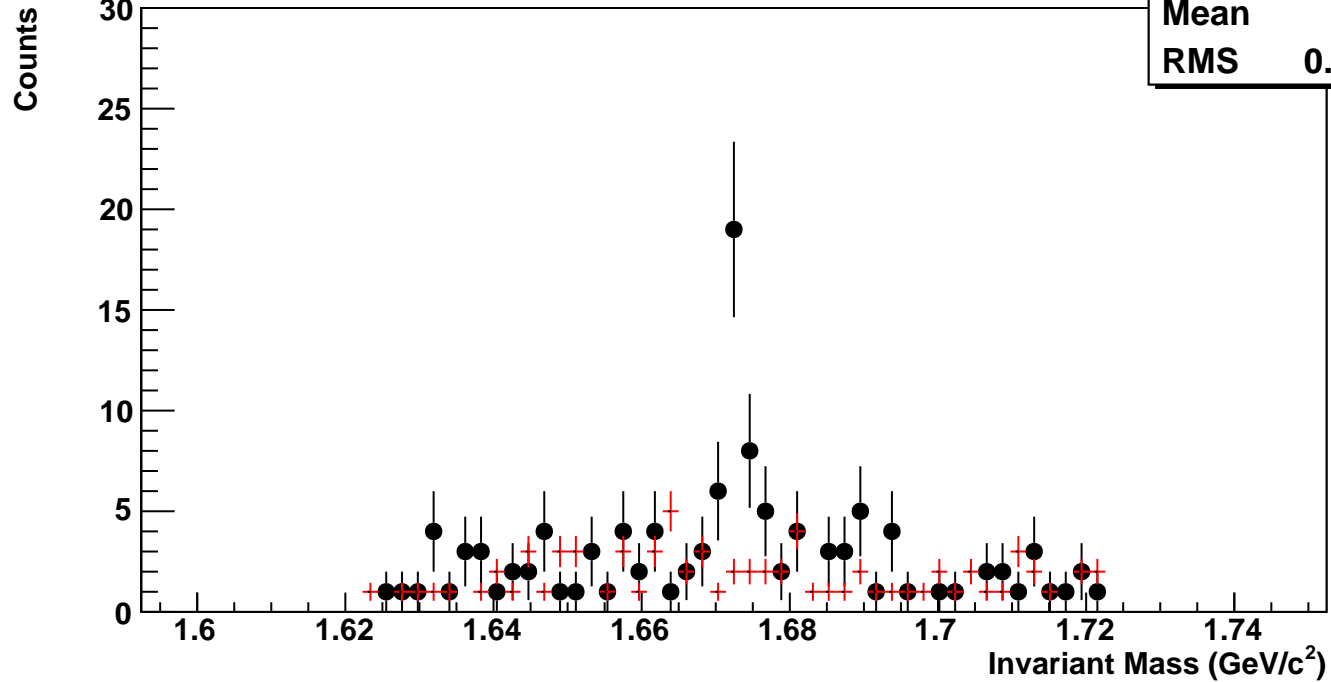
$\bar{\Omega}^+$ , Au+Au 7 GeV, 0-60%,  $p_T$  0.7-1.3 GeV/c

hmlInvMassBgCent0Pt1	
Entries	57
Mean	1.662
RMS	0.02877



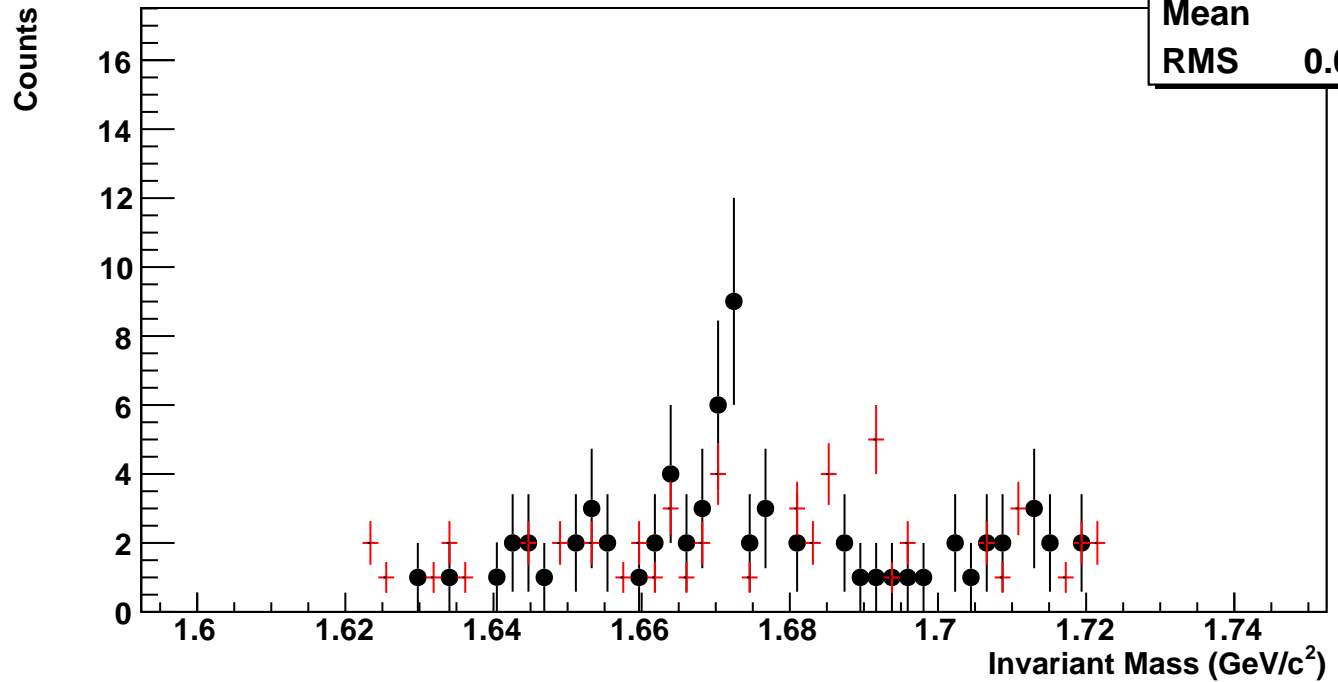
$\bar{\Omega}^+$ , Au+Au 7 GeV, 0-60%,  $p_T$  1.3-1.6 GeV/c

hmlInvMassBgCent0Pt2	
Entries	76
Mean	1.674
RMS	0.02582



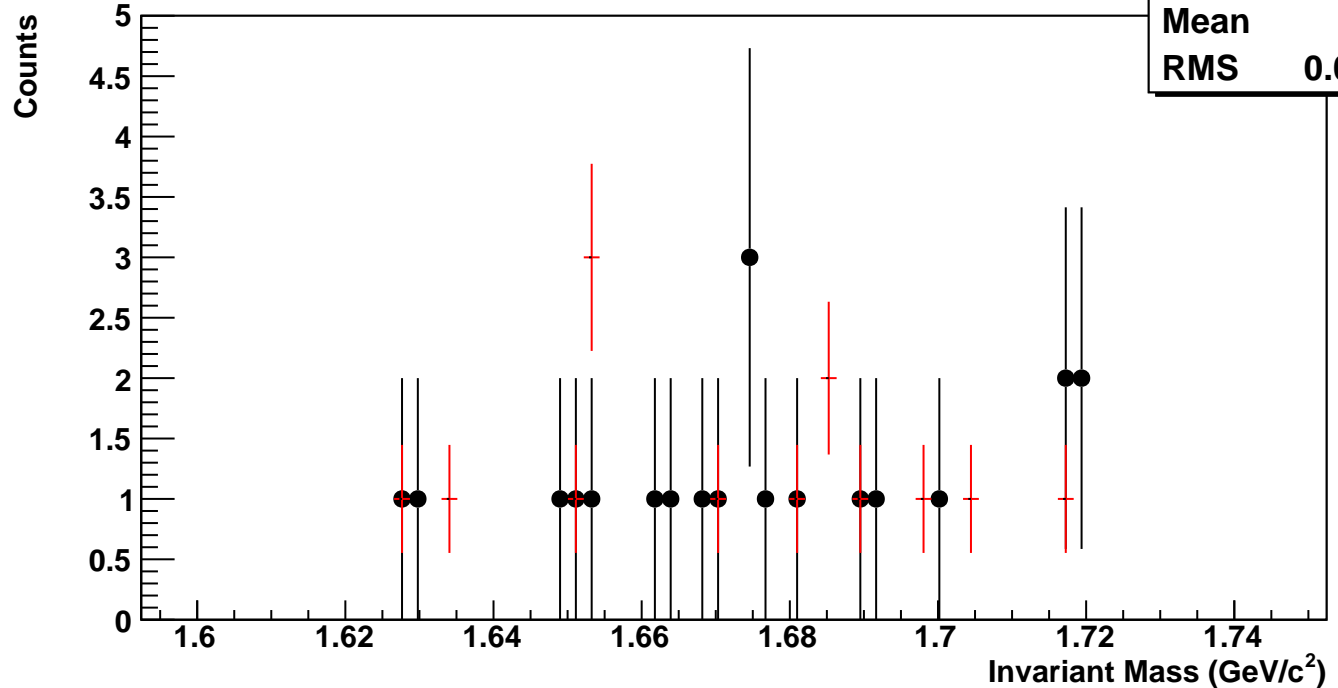
$\Omega^+$ , Au+Au 7 GeV, 0-60%,  $p_T$  2.0-2.5 GeV/c

hmlInvMassBgCent0Pt4	
Entries	56
Mean	1.676
RMS	0.02695

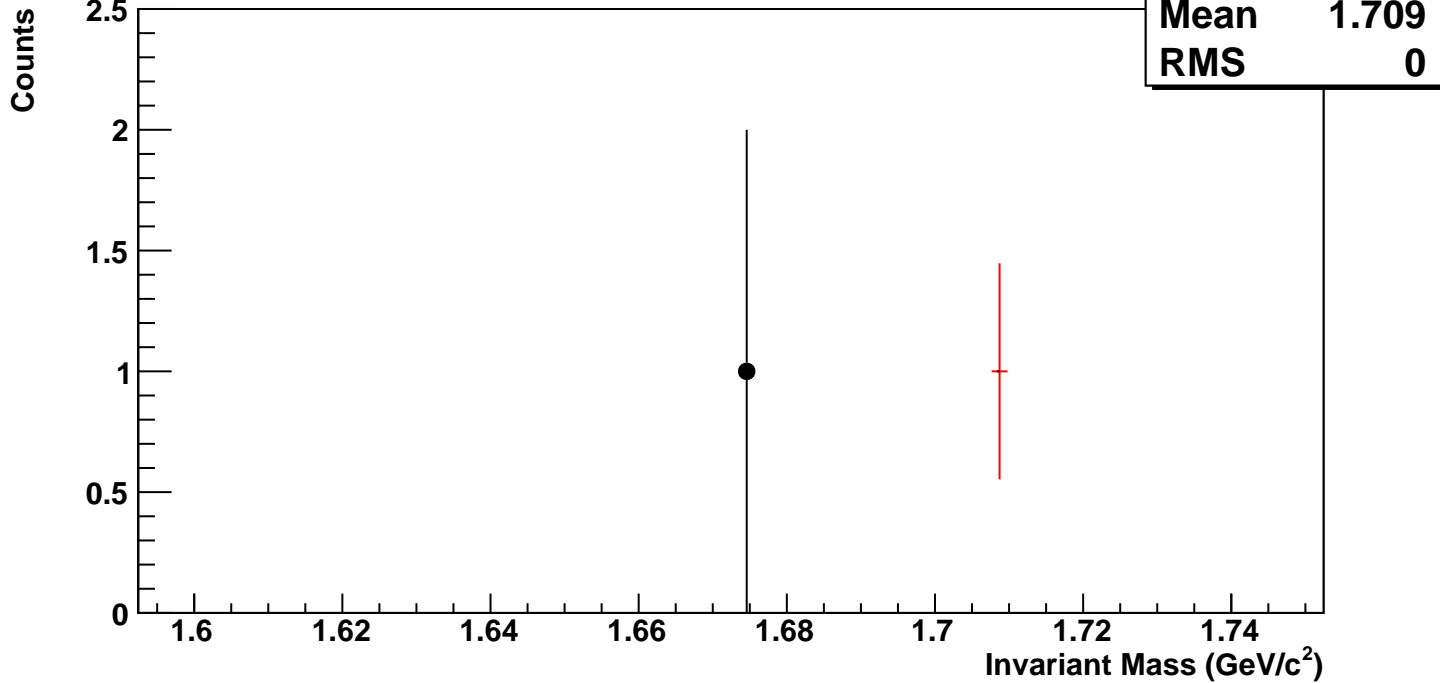


$\Omega^+$ , Au+Au 7 GeV, 0-60%,  $p_T$  2.5-3.5 GeV/c

hmlInvMassBgCent0Pt5	
Entries	14
Mean	1.672
RMS	0.02572



$\Omega^+$ , Au+Au 7 GeV, 0-60%,  $p_T$  3.5-5.0 GeV/c



$\Omega^+$ , Au+Au 7 GeV, 0-60%,  $p_T$  5.0-8.0 GeV/c

